Advanced Materials Series

ADVANCED BIOELECTRONIC MATERIALS

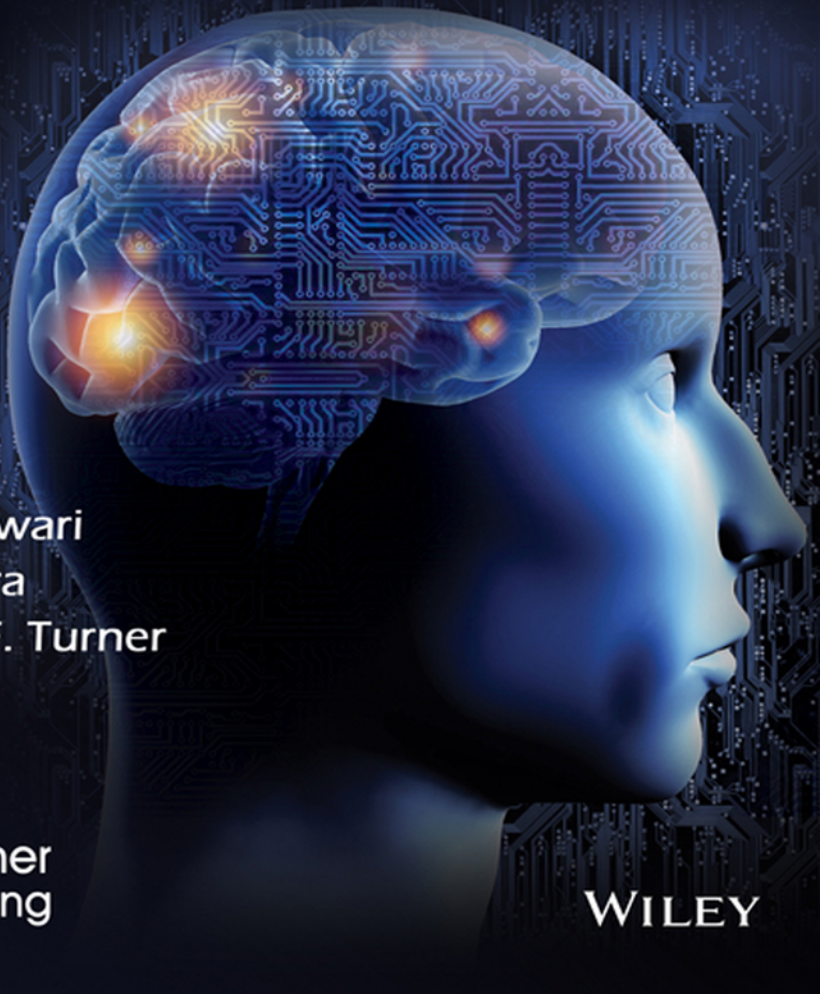

Edited by
Ashutosh Tiwari
Hirak K. Patra
Anthony P.F. Turner

Scrivener Publishing

WILEY

Advanced Bioelectronic Materials

Scrivener Publishing
100 Cummings Center, Suite 541J
Beverly, MA 01915-6106

Advanced Materials Series

The Advanced Materials Series provides recent advancements of the fascinating field of advanced materials science and technology, particularly in the area of structure, synthesis and processing, characterization, advanced-state properties, and applications. The volumes will cover theoretical and experimental approaches of molecular device materials, biomimetic materials, hybrid-type composite materials, functionalized polymers, supramolecular systems, information- and energy-transfer materials, biobased and biodegradable or environmental friendly materials. Each volume will be devoted to one broad subject and the multidisciplinary aspects will be drawn out in full.

Series Editor: Dr. Ashutosh Tiwari
Biosensors and Bioelectronics Centre
Linköping University
SE-581 83 Linköping
Sweden
E-mail: ashutosh.tiwari@liu.se

Managing Editors: Revuri Vishnu and Sudheesh K. Shukla

Publishers at Scrivener
Martin Scrivener(martin@scrivenerpublishing.com)
Phillip Carmical (pcarmical@scrivenerpublishing.com)

Advanced Bioelectronic Materials

Edited by

Ashutosh Tiwari, Hirak K. Patra and Anthony P.F. Turner

WILEY

Co-published by John Wiley & Sons, Inc. Hoboken, New Jersey, and Scrivener Publishing LLC, Salem, Massachusetts.
Published simultaneously in Canada.

Cover design by Russell Richardson

Library of Congress Cataloging-in-Publication Data:

ISBN 978-1-118-99830-4

Printed in the United States of America

10 9 8 7 6 5 4 3 2 1

We dedicate this book to Prof. Anthony P. F. Turner on the occasion of his 65th birthday. It is because of his persistence, foresight and proficiency in establishing biosensor principles that millions of patients worldwide are benefiting.

To Tony for
fathering biosensors and bioelectronics
&
for every kid
who walks with him.

Ashu
Hirak

Contents

Preface

The interface between electronics and medicine has resulted in extraordinary benefits for recent generations in clinical practice. The development of electrocardiography nearly a century ago can be considered a key milestone for chronicling the electrical activity of the heart, thus providing one of the defining moments in the field of cardiology. A similarly important advance was the development of the heart pacemaker, which has transformed the lives of millions of people and continues to serve an ever-aging population. The legacy of biomedical research at the interface between electrical engineering and human physiology has empowered these discoveries.

In recent times, however, "bioelectronics" has diversified into a multifarious and cross-disciplinary field. In this book, a selection of leading scientists and technology experts describe advances in nanoscale electronics and how they mesh with the bioengineering community to deliver specific applications. The contributors chronicle a wide span of opportunities, possibilities and challenges for this diverse interdisciplinary field. The principal themes of this volume on advanced bioelectronic materials are: miniaturization of bioelectronics, smart biosensing, and a systemic approach for the development of bioelectronics. The machinery and procedures that will facilitate these areas will also have a significant impact on other areas such as advanced security systems, forensics and environmental monitoring. The evolution of all these segments entails innovations in cross-cutting disciplines ranging from fabrication to application.

We hope that this collection of articles will help convince stakeholders from academia, government and industry to cooperate in developing a comprehensive bioelectronics roadmap to accelerate the commercialization of bioelectronic materials for novel biomedical devices. This work provides a comprehensive description of some of the emerging opportunities in bioelectronics facilitated by the development of novel materials. While it is challenging to evaluate the exact economic benefits from this technology at the current stage, a clear sense of the magnitude of the benefits to mankind and society are apparent.

In order to reflect the promise of bioelectronics at this time, we have endeavored to include research that crosses several disciplines, including electronics, materials science, human physiology, chemistry and physics. It is intended for a wide spectrum of readers, offering perspectives on aspects of both fundamental and advanced materials of the field and covering:

- Molecular-electronic interfaces;
- Stimuli-responsive (mechanical, electrical, chemical and thermal) materials;
- Real-time monitoring of essential parameters to assess the state of biomolecules; and
- Smart biosensing.

The successful translation of this multidisciplinary research to commercial reality needs a deep understanding at a very early stage of the interface between electronics and biology. This book addresses researchers in a range of sectors and disciplines who do not necessarily speak with the same 'language,' but who are willing to commit to a collaborative effort in areas such as this, where interdisciplinary contributions are key for success.

The Editors
August 22, 2015
Ashutosh Tiwari
Hirak K. Patra
Anthony PF Turner

Part 1

RECENT ADVANCES IN BIOELECTRONICS

1

Micro- and Nanoelectrodes in Protein-Based Electrochemical Biosensors for Nanomedicine and Other Applications

Niina J. Ronkainen*

Department of Chemistry and Biochemistry, Benedictine University, Lisle, IL, USA

Abstract

Electrochemical biosensors have gradually decreased in size from devices containing electrodes with micrometer critical dimension to nanoelectrodes over the past 35 years. Nanoelectrodes are now also being used both *in vivo* and *in vitro*, in the quantification of various analytes of biological interest such as dopamine, serotonin, glutamate, lactate, glucose, and cancer biomarkers. Their small size is an advantage, allowing the study of biological analytes in small intracellular and extracellular environments to be less invasive, compared to larger electrodes. Micro- and nanoelectrodes have been used in applications such as single-cell or single-molecule studies, point-of-care clinical analysis, coordinated biosensor development, and fabrication of microchips. Indeed, biosensor applications in medicine utilizing nanoelectrodes and nanoelectrode arrays are a rapidly developing research area due to significant advancements in materials science, more cost-effective and reproducible nanomaterial fabrication methods. The electrochemistry, common applications as well as integration of the electronic transducer, and the biological recognition components into the appropriate biosensors will be described.

***Keywords*:** Biosensors, electroanalytical methods, microelectrodes, nanoelectrodes, nanomaterials, voltammetry, amperometry, clinical analysis

**Corresponding author*: NRonkainen@ben.edu

Ashutosh Tiwari, Hirak K. Patra and Anthony P.F. Turner (eds.) Advanced Bioelectronic Materials, (3–34)

1.1 Introduction

Electrochemical biosensors may be divided into biocatalytic devices such as enzyme electrodes and affinity biosensors based on a highly specific immunochemical reaction between an antibody and an antigen. Over the past 35 years, electrochemical biosensors have gradually decreased in size from devices containing electrodes with micrometer critical dimension to nanoelectrodes. In addition, since single micro- or nanoelectrodes generate rather small currents that can be difficult to distinguish from background noise using standard electrochemical equipment, electrode arrays and ensembles which amplify the measured current are an active area of research. Furthermore, the fabrication of electrodes and biosensors that incorporate nanomaterials as well as their characterization once prepared have also been studied extensively. Indeed, the integration of electronic transducers and the biological recognition components into biosensors is critical in the development of highly sensitive, nanobiosensors suitable for clinical analysis.

Many nanobiosensors for clinically relevant analytes, to which nanomaterials have been incorporated, have shown significantly improved electrochemical performance when utilizing electroanalytical methods such as voltammetry and amperometry. Specifically, the incorporation of highly conductive nanomaterials such as carbon nanotubes (CNTs) and metal nanoparticles into electrochemical biosensors has led to increased signal-to-noise (S/N) ratios and significantly lower limits of detection. These properties are the result of significant changes in diffusion profiles and mass transfer of redox-active species at electrodes with small dimensions. The transition from mass transport by primarily linear diffusion at larger electrodes to the domination of radial diffusion at micro- and nanoelectrodes will be described in this chapter. Another reason for the amplified sensitivity in biosensor devices is the high loading of the biological protein components (i.e., enzymes or antibodies) on the large, often three-dimensional surface areas of nanomaterials. A number of key nanoscale biosensor applications which utilize biocatalytic and bioaffinity sensors will be described in detail. The main concerns with the use of nanotechnology in the fabrication of the clinical devices include the biocompatibility and toxicity of some nanomaterials which is currently an area of research. These concerns are important because many nanomaterial-based electrodes are being considered for implantable devices to be used for real-time diagnosis, management and monitoring of certain disease states. For instance, cancer diagnosis and management are one of the most common applications for affinity biosensors, while glucose monitoring remains the largest

and most profitable catalytic biosensor application. In addition, biosensor applications also exist for cardiovascular, infectious, autoimmune, psychiatric, and neurogenerative diseases. However, there remain challenges in the fabrication of protein-based nanobiosensors for clinical applications such as the low concentrations of analyte molecules in relatively complex biological sample matrix (e.g., blood), the requirement of ultralow detection limits (DLs) (nM and below) for certain analytes, the biocompatibility and safety of the nanobiosensors, a need for multiplexing capabilities, practical detection times, sample size requirements, selectivity of *in vivo* biosensors in the presence of multiple similar molecules as well as various interfering species, ease of use, the ability to scale up developed prototypes into mass production, and the storage stability of the biological components of nanobiosensors such as enzymes and antibodies. Some of these challenges will also be discussed.

Many well-established methods used in clinical analysis are based on spectrophotometric detection which often requires bulky light sources, monochromators, sample cells with fixed path lengths, and complex detectors to obtain adequate sensitivity. These methods usually require a fair amount of the sample and cannot be performed in colored, turbid, or complex sample matrices (such as blood) without sample preparation. Therefore, these methods are not amenable to *in vivo* studies of biological systems. Electrochemical detection methods, which are based on interfacial phenomenon, are better suited for detection in ultralow volumes (with samples from microliters to as low as nanoliters) because the sensitivity of these methods is independent of the sample volume [1]. The analyte molecules usually investigated in electroanalytical experiments are either freely diffusing in aqueous solution or have adsorbed or been attached to an electrode surface or a membrane. The main focus in this chapter will be on freely diffusing redox-active species in aqueous solution environments.

Oxidation and reduction reactions consist of a series of fast chemical and physical steps that take place at very small length scales. First, the analyte molecules are transported from the bulk sample solution to the electrode surface through a depletion layer (a 0.01–100 μm thick interfacial zone) where the composition of the solution has been affected by an electrochemical reaction. Then, transfer of an electron between the electrode surface and a redox-active analyte occurs over a distance of 2 nm or less in an interfacial region which contains adsorbed ions and solvent molecules.

Since the electrochemical oxidation or reduction of the analyte species occurs at the interface of the electrode(s) and the transducer(s), the analyte molecules must be transported from the solution to the electrode surface in order to be detected. This movement between an electrochemical

detection cell and the electrode surface is called mass transport. There are three modes of mass transport that are of significance in electroanalytical techniques. These are migration, hydrodynamic mass transport, and diffusion. Migration is the movement of charges particles due to their interaction with an electric field such as that which occurs in the vicinity of electrodes. For example, anions are attracted by a positively charged electrode and repelled by a negatively charged electrode. An inert, supporting electrolyte, which decreases the field strength near an electrode, can be added to most electroanalytical techniques in order to minimize migration effects. Hydrodynamic mass transport, as implied by its name, is caused by the movement of the sample solution due to rotating the electrode, stirring the solution, or flowing the solution through the detection cell. The solution itself continuously transports redox-active reactants to the electrode surface and also carries away the electrogenerated product. Diffusion, which is a key factor in virtually every type of electrochemical measurement, is the simplest and best understood process influencing electrochemistry. Certain mathematical relationships and differences in diffusion profiles of electrodes with differing dimensions, shapes, and configurations will be addressed in this chapter.

Miniaturized electrochemical probes can even be implanted in living systems due to biocompatibility of the materials used as well as the minimal damage caused by these devices to surrounding cells or tissues. Furthermore, interference from sample components, such as ascorbic acid or acetaminophen, can be eliminated by carefully choosing the detection potential in methods such as amperometry. Additionally, most electroanalytical detection methods require little or no sample preparation prior to analysis. Finally, high-sensitive nanosized electroanalytical methods have become popular in clinical and biosensor applications because commonly used biomarkers for diagnosing, managing, and monitoring diseases are in the nanomolar range.

Nanoelectrodes have also allowed significant advancements to be made in electroanalytical chemistry, for example, by making experiments in the microsecond or even in the nanosecond scale possible under favorable conditions by minimizing problematic double-layer charging and resistance effects, ultimately making reliable measurements of fast electron transfer reactions possible. Nanoelectrodes have also significantly increased the spatial resolution of electrochemical experiments performed with the scanning electrochemical microscope (SECM). Advances and applications of micro- and nanoelectrodes in SECM will be described later in the chapter.

1.2 Microelectrodes

Wightman, Fleischmann, and co-workers are considered the pioneers of microelectrode use in electroanalytical chemistry [2,3]. Although the transition from macroelectrode-based detection to microelectrodes for various electroanalytical applications such as sensing inside a living brain to quantify the dynamic concentrations of neurotransmitters began in the early 1980s [2–4], microelectrodes had been used by physiologists in amperometry to measure oxygen concentrations in biological tissue as early as the 1940s [5]. The main driving force for the transition to smaller electrochemical probes was the need for portable, sensitive, *in vivo* sensing devices capable of quantifying trace levels of analytes in very small sample volumes and spaces [6]. Although advancements in materials science and electrode fabrication methods have led to the production of electrochemical transducers with significantly smaller dimensions and a variety of geometric shapes in the past decade, voltammetric electrodes with dimensions capable of probing chemical events inside single biological cells or membrane pores were already being produced in 1990 [7]. The multiple, well-known advantages of microelectrodes over larger electrodes may largely be attributed to reduced ohmic resistance and enhanced mass transport of the redox-active species to the microelectrode surface due primarily to radial diffusion in solution. This ultimately results in higher current densities and improved S/N ratios. It was hypothesized that these positive effects due to small dimensions that were observed in microelectrodes, microelectrode arrays, and later in ultramicroelectrodes (an electrode having at least one dimension <25 microns) would be further enhanced in nanosized electrodes. Of note, nanosized electrodes are generally smaller than the diffusion layer where electrochemical reactions occur between the electrode and analyte [8]. In addition, microelectrodes have allowed electrochemical studies of even single molecules in a variety of chemical media such as nonaqueous solvents, ice, and air [8]. The electrochemistry, properties, and advantages of microelectrodes over conventional macroelectrodes will be described in the next section.

1.2.1 Electrochemistry and Advantages of Microelectrodes

Microelectrodes have several important advantages over macroelectrodes (which have dimensions in the millimeter scale) and allow the development of several approaches to investigating electrochemical phenomena and monitoring living biological systems. Individual microelectrodes with

various geometries, such as inlaid ring disks, bands, cylinders, cones, inlaid disks, and hemispheres as well as arrays of closely spaced microelectrodes have been constructed [6,8]. Microelectrodes with bands or ring geometries may be prepared using lithography or foils and films. Disk- or cylinder-shaped microelectrodes are prepared using gold and platinum microwires as well as carbon fibers among others. Metal disk electrodes encapsulated in glass have been very popular due to their ease of fabrication [8].

Most electroanalytical detection techniques measure current, potential, or impedance. These techniques can be divided into four main categories: voltammetry, amperometry, potentiometry, and coulometry. Voltammetry and amperometry are popular electroanalytical detection methods that are commonly performed using micro- and nanoelectrodes. In amperometry, a constant potential (mV) is applied to the sample, while changes in current Δi (A) are detected. In voltammetry, the potential is varied over time, while changes in current Δi (A) are measured. In coulometry, which measures charge (C), the amount of an electroactive analyte can be quantified based on measurement of the total coulombs of electricity needed to completely oxidize or reduce the analyte. Potentiometry does not involve an oxidation–reduction process and measures the cell potential, E_{membrane} (V or mV) across a thin, selectively permeable membrane. A more detailed description of various electroanalytical techniques and their use in electrochemical immunosensors may be found in a recent review paper [9].

Electrochemical detection cells (Figure 1.1) typically consist of two or three electrodes. A two-electrode system consists of working and reference electrodes, whereas a three-electrode system consists of working, reference, and auxiliary electrodes. Three-electrode setups tend to be more commonly used in voltammetry and amperometry. The working electrode (a.k.a. indicator electrode) is usually made of a solid, conductive material such as gold, platinum, or glassy carbon. In the three-electrode system, the charge from electrolysis passes through the auxiliary electrode (a.k.a. the counter electrode) instead of the reference electrode, thereby protecting the reference electrode from changing its half-cell potential against which electrochemical processes are measured over time. A reference electrode is a known half-cell such as silver/silver chloride (Ag/AgCl) or saturated calomel electrode (SCE) that is reversible, insensitive to the sample solution, obeys the Nernst equation, provides constant potential throughout an analysis, and returns to its original potential after an analysis. Using electrochemical detection, measurements may also be made in very small sample volumes such as drops as opposed to more traditional sample cells with milliliter volumes.

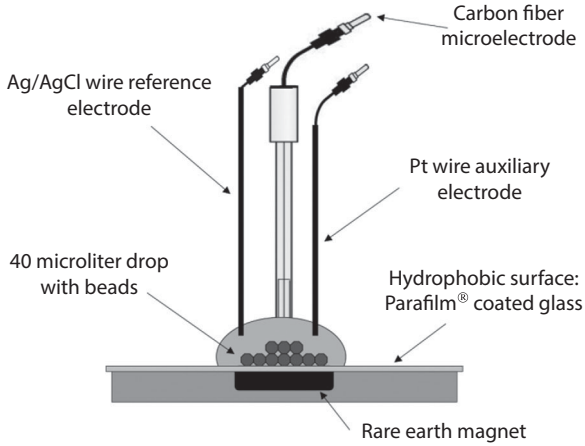

Figure 1.1 A simple electrochemical detection cell consisting of three electrodes that can be used in bead-based sandwich immunoassay detection step. The working electrode, a carbon fiber microelectrode, is lowered into the sample drop that beads on a hydrophobic surface along with Ag/AgCl wire reference electrode and a Pt wire auxiliary electrode. A rare earth magnet is used to gather the gold nanoparticles that contain all the biological components of the immunoassay (antibodies, antigens, and enzyme labels).

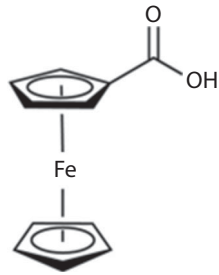

Figure 1.2 Structure of FCA, a common model species used in bioelectrochemistry.

Three bioelectrochemical redox species of significance in biosensors and assays that are commonly used in studying the performance of newly prepared electrodes and new electroanalytical detection methods include hydrogen peroxide (H_2O_2), 4-aminophenol (PAP), and ferrocene carboxylic acid (FCA, $C_{11}H_{10}FeO_2$).

Ferrocene molecules are metallocenes that have a sandwich structure with a redox-active iron (III) ion at their center (the structure of FCA is shown in Figure 1.2). FCA (Fe^{3+} at the center) undergoes a reversible single-electron oxidation to ferricene (Fe^{2+}). In an electrochemical cell, the forward (oxidation) reaction is favored at potentials positive of the E_0

resulting in a positive current. The reverse (reduction) reaction is favored at potentials negative of the E_0 for the redox couple giving a negative current. When a redox reaction is 100% reversible, the oxidation and reduction peak currents are equal. Since the electrochemistry of these species is well known, it is possible to characterize and compare the performance of electroanalytical probes with different sizes, arrangements, and geometries.

Enzyme-coupled electrochemical biosensors, also known as enzyme electrodes, are commercially the most successful biosensors and function based on the detection of hydrogen peroxide. These clinically significant biosensors are based on the detection of an electric signal produced by an electroactive species, either produced or depleted by an enzymatic reaction. The relatively simple layout consists of a biorecognition layer of enzymes attached to a working electrode, a transducer [10]. The enzyme has high biological affinity for a specific substrate molecule which provides the selectivity for the biosensor [11]. The activity of the immobilized enzyme depends on solution parameters and electrode design. The product of the enzymatic reaction is typically electroactive and can be directly monitored using amperometry, in which the produced current is measured in response to an applied voltage. Enzyme electrodes are routinely used in biomedical applications such as glucose monitoring and as stated earlier are commercially available [10,12]. The use of enzyme electrodes as biosensors will continue to increase because they are simple and inexpensive to construct, they provide rapid analysis, they can easily regenerate, and they are reusable. However, enzymes are relatively short-lived biorecognition molecules because they gradually loose activity, which also determines the lifespan of the biosensor.

Electrodes coated with glucose oxidase (GOx, also commonly abbreviated as GOD) have been widely used in the detection of glucose due to the pioneering work of Clark and Lyons [13]. GOx is highly specific for β-D-glucose [14,15], which can be detected via the following reactions:

$$\beta\text{-D-glucose} + \text{GOx-FAD} \longrightarrow \text{GOx-FADH}_2 + \delta\text{-D-gluconolactone} \quad (1.1)$$

$$\text{GOx-FADH}_2 + \text{O}_2 \longrightarrow \text{GOx-FAD} + \text{H}_2\text{O}_2 \quad (1.2)$$

The two-electron transfer during the oxidation of H_2O_2, generated in Equation 1.2, results in the current response of the enzyme electrode [16]. GOx exists as a dimeric protein with a molecular weight of 160,000 Da [14]. A single molecule of flavin adenine dinucleotide (FAD) is tightly bound to each monomer of GOx [15]. GOx, obtained from the fungus *Aspergillus niger*, is an ideal enzyme for glucose biosensors due to its high specificity, high stability, high turnover, resistance to proteolysis, and low cost [17].

The reversible, two-electron oxidation reaction of another well-characterized redox couple, PAP to 4-quinone imine (PQI) shown in Equation 1.3, and reduction back to PAP can easily be detected using an electroanalytical method called cyclic voltammetry (CV). PAP electrochemistry will be used as an example throughout this chapter.

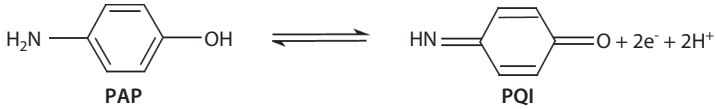

(1.3)

A CV setup typically includes a potentiostat and a three-electrode cell. In CV, the potential is linearly swept (i.e., voltage is varied) between two fixed values E_1 and E_2 (Figure 1.3) at a fixed rate known as the scan rate (v). The rate of change of potential with time at a given the scan rate (v), has units of mV/s. When the voltage reaches E_2 (the switching potential) at time T_1, the scan is reversed and the voltage is swept back to E_1 (the final potential) producing a triangular shape on a voltage versus time plot for one full cycle in CV. The first potential sweep typically results in oxidation of the redox-active analyte species with a loss of one or two electrodes followed by reduction back to its original state.

The potential applied, E, controls the concentration of the two redox forms of the analyte in accordance with the Nernst equation (Equation 1.4).

$$E = E^0 + (RT/nF) \ln[Ox]/[Red] \quad (1.4)$$

in which E^0 is the standard cell potential, R is the universal gas constant, T is the absolute temperature, F is the Faraday constant, n is the electron

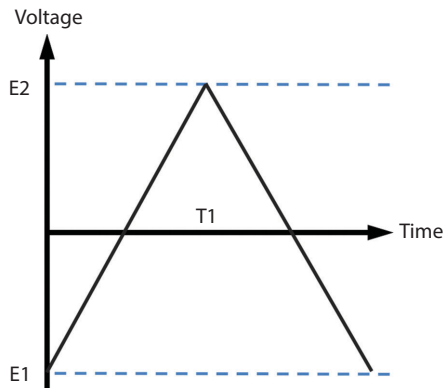

Figure 1.3 Voltage versus time plot for one cycle in CV measurements, where T_1 is the switching time, E_1 is the initial and final applied potential, and E_2 is the switching potential.

stoichiometry, Ox is the concentration of the oxidized species, and Red is the concentration of the reduced species.

In addition to quantification of redox-active analytes, CV is commonly used to characterize newly prepared electrochemical probes. The shape of voltammetric wave observed in cyclic voltammograms obtained using microsized electrodes differs significantly from those obtained with conventional macroelectrodes which have diameters in the millimeter range. A sigmoidal CV response that retraces on the return sweep is characteristic of microelectrodes [18,19], whereas conventional macroelectrodes give a "duck"-shaped response with separate well-defined oxidation and reduction peaks [20,21]. A "duck"-shaped voltammogram recorded for a reversible two-electron transfer reaction upon oxidation of PAP to PQI is shown in Figure 1.4. Oxidation reaction of PAP to PQI is favored at potentials positive of the E^0 for the redox couple (i.e., the lower wave or lower part of the "duck"). The sweep toward more positive potentials produces a current response where the current begins to flow and eventually reaches a peak before dropping. When the scan is reversed, we move back through the equilibrium positions toward more negative potentials gradually converting the electrolysis product back to reactant. The current now flows from the solution species back to the electrode in the opposite direction to the initial sweep forming the head of the "duck".

There are noticeable differences in voltammogram shapes which depend on the working electrode dimensions and are the result of different mass

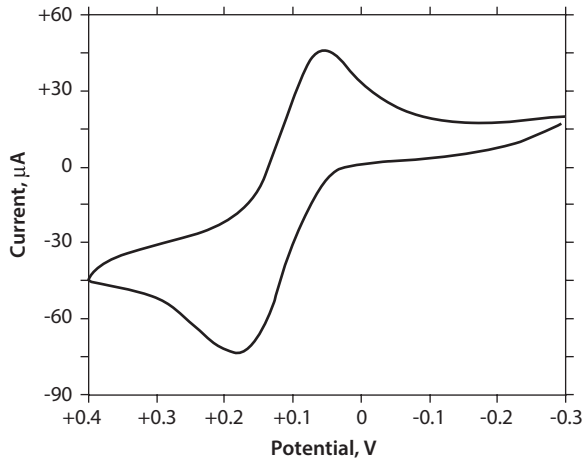

Figure 1.4 A cyclic voltammogram of 4 µM PAP in 10µM $MgCl_2$, 0.1 M PBS buffer done at scan rate of 50 mV/s with a platinum macroelectrode (d=1.6 mm) against Ag wire quasi-reference electrode.

transport rates within the diffusion layer (i.e., the solution region in the vicinity of the working electrode surface) where the redox reaction takes place [18–21]. Mass transport at microelectrodes is hemispherical and three dimensional due to radial diffusion fields. Ultimately, this leads to much greater flux under diffusion-controlled detection conditions such as those found in unstirred samples. In comparison in macroelectrodes, most mass transport occurs perpendicular to the electrode surface as planar diffusion (also known as linear diffusion). Radial diffusion is known to significantly enhance the mass transport to/from the microelectrode surface [18,22]. However, it should be noted that different diffusion equations are used to describe diffusion as the primary mode of mass transport in microelectrode experiments with differing electrode geometries [6]. The difference in the diffusion layer profiles between cylindrical micro- and macroelectrodes is shown in Figure 1.5 [23]. These commercially available electrodes are primarily used to determine the concentrations of electroactive analyte species via use of standard calibration methods. The insulating material surrounding the electrodes (typically glass or plastic) makes them less delicate, easier to handle and set up, but at the same time may limit their use in small spaces.

The smaller area and proportionately lower capacitance of microelectrodes also allow their use at shorter time scales than conventional voltammetric electrodes [6]. Of note, radial diffusion is favored when using slow scan rates, whereas planar diffusion is dominant with fast scan rates as is utilized in high-speed CV [18,22,24]. In addition, the current density at

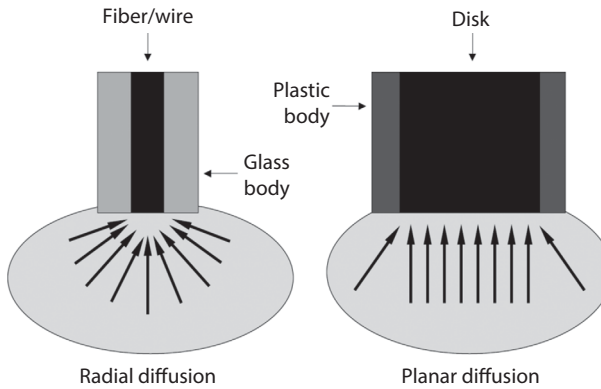

Figure 1.5 Diffusion layer profiles within a sample as indicated by arrows for three-dimensional radial diffusion at a commercially sold disk-shaped microelectrode (left) and for planar diffusion (a.k.a. linear diffusion) at a macroelectrode surface (right).

a microelectrode with radial diffusion is much higher than that at a macroelectrode with planar diffusion giving rise to many of the advantages of microelectrodes. Furthermore, the higher current density at the microelectrode results in a significantly smaller background/charging current [6,18]. This reduction is significant because the charging current may mask the desired faradaic current in certain electroanalytical detection methods, such as pulsed voltammetric methods. Also, the charging current decreases in proportion to the surface area of the electrode, whereas the faradaic current decreases in proportion to the radius under steady-state conditions [6]. This means that the ratio of the faradaic current to the charging current is improved as the electrode size decreases which results in enhanced S/N ratios during the detection step. Scan rates also affect the diffusion profile at the electrode.

The CV of a common bioelectrochemical redox species, PAP with a slight hysteresis (i.e., a gap in the sigmoidal forward versus reverse segments of the voltammogram) is shown in Figure 1.6. This may be an indication that there is a poor seal between the insulator and metal wire of the microelectrode. A similar separation between the segments is sometimes seen when the scan rate in CV is too fast [8]. The CV below was obtained using an 11 μm diameter (d) disk-shaped carbon fiber microelectrode versus an Ag wire quasi-reference electrode to detect deoxygenated 4 μM PAP in 800 μL sample including 10 μM $MgCl_2$ and 1 μM Tris buffer at a slow scan rate of 50 mV/s.

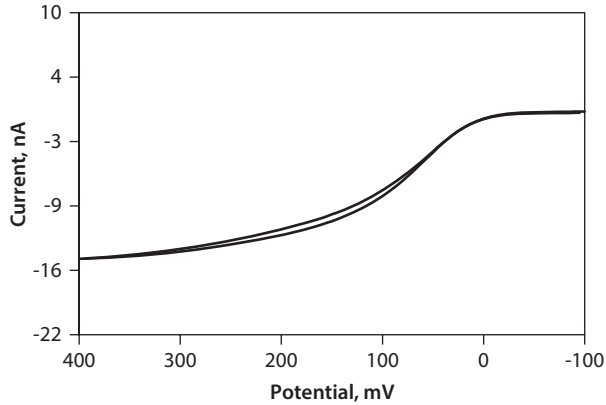

Figure 1.6 Cyclic voltammogram of deoxygenated 4 μM PAP in 10 μM $MgCl_2$, 1 μM tris buffer using a disk-shaped (d=11 μm) carbon fiber microelectrode versus Ag wire quasi-reference electrode at a slow scan rate of 50 mV/s.

Given the continuous emphasis in literature on decreasing individual electrode sizes to molecular-level scales, it is easy to forget that the electrode geometry and that of its insulating surroundings are just as important to consider because they significantly impact mass transport of redox-active species to the electrode surface. A perfect hemisphere surrounded by a flat shroud at the level of the hemisphere's rim is perhaps the ideal shape of micro- and nanoelectrodes because there is a uniform flux of mass transport of redox-active reactants to the electrode surface as well as a uniform current density across the electrode/electrolyte interface [25]. A cross section of an individual hemispherical nanoelectrode is shown in Figure 1.7.

As stated earlier, the current at a microelectrode/electrolyte interface depends on its geometry. The limiting plateau current, i_{lim} (in A), from steady-state voltammetry (SSV) such as is obtained via CV for a disk-shaped microelectrode, is given by Equation 1.5 [4].

$$i_{lim} = 4nFrDC^b \tag{1.5}$$

in which F is the Faraday constant, r is the electrode disk radius (in cm), D is the diffusion coefficient (in cm^2/s), n is the number of electrons, and C^b is the bulk concentration of the electroactive species [4].

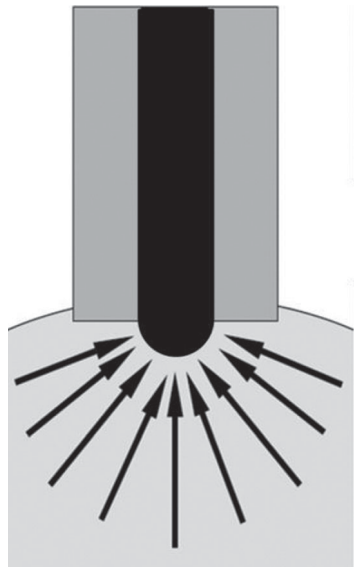

Figure 1.7 Cross section of an individual hemispherical micro- or nanoelectrode with rapid radial mass transport of redox-active analyte from sample solution.

In comparison, the limiting plateau current, i_{lim} (in A), from SSV for a hemisphere-shaped microelectrode, is given by Equation 1.6:

$$i_{lim} = 2\pi nFr_0DC^b \tag{1.6}$$

in which F is the Faraday constant, r_0 is the radius of the hemisphere, D is the diffusion coefficient (in cm^2/s), n is the electron stoichiometry, and C^b is the bulk concentration of the electroactive species [4].

Steady-state response is obtained quickly with hemispherical microelectrodes as diffusion lines converge on the electrode surface from all directions. Therefore, the volume of the sample solution providing redox-active species to the electrode is very large in comparison to the exposed electrode surface area.

However, with planar or linear diffusion dominating at macroelectrodes, the current is proportional to electrode area, but is independent of their geometry. The Randles–Sevcik equation (Equation 1.7) describes the peak current, i_p (in A), for a reversible redox process at a macroelectrode [26]. A is the electrode area (in cm^2), and v corresponds with scan rate (in V/s).

$$i_p = (2.69 \times 10^5)n^{3/2}AD^{1/2}Cv^{1/2} \tag{1.7}$$

In addition to the geometry and the size of a working electrode, the material used to fabricate the electrode also affects its performance. Cyclic voltammograms obtained using conventional gold (Au), glassy carbon (GC), and platinum (Pt) macroelectrodes are shown in Figure 1.8. All of the macroelectrode materials noted earlier exhibit well-defined oxidation waves; therefore, any of the electrodes would be suitable for quantification of PAP. However, the gold electrode exhibits the most reversible electron transfer and the highest current response as determined by the shape of the voltammogram. In addition, the voltage separation (potential difference) between the anodic and cathodic peak currents is smaller in the CV obtained using an Au electrode. Also, the ratio of the anodic to cathodic peak currents is closer to the ideal of one with an Au electrode.

1.2.2 Applications, Cleaning, and Performance of Microelectrodes

In addition to monitoring biological systems such as cells or pores, microelectrodes have proven to be invaluable detection probes for quantification of low-concentration analytes in other applications involving small sample volumes [6]. For example, microelectrode detection has been used extensively in small-volume liquid chromatographic separation to increase peak resolution in columns with internal diameters in micrometers [27,28], in

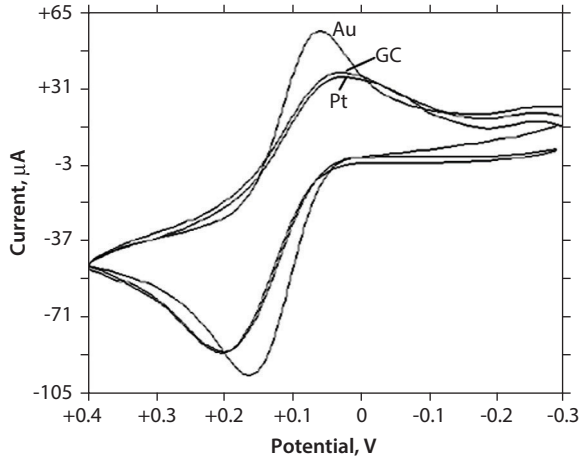

Figure 1.8 Cyclic voltammogram of the oxidation of 4 μM PAP to PQI followed by its reduction back to PAP. Gold (Au), glassy carbon (GC), and platinum (Pt) electrodes (3 mm diameter) were used as the working electrodes.

scanning electrochemical microscopy (SECM) [29–31], in detection of bead-based immunoassays [32,33], in resistive solvents [34], and in microfluidic devices with flowing solution [35,36].

SECM is the electrochemical equivalent of scanning tunneling microscopy, since in both techniques a very small probe tip is scanned over the surface undergoing imaging. In scanning probe techniques like SECM, the small electrode tip must be brought in close proximity to the cell or material undergoing a chemical change in order to examine the surface chemistry with very high resolution and then slowly scanned across a small area. This is possible when the electrode probe has a radius ≤10 μm [8]. Current generated by electrolysis of solution species at the electrode tip on the surface of interest is plotted as a function of position to give dimensional redox information. SECM can be used for imaging electrochemical or biochemical activity on surfaces with resolution in nm range. SECM has been used to investigate Ab immobilization and nonspecific binding (NSB) in immunoassays and immunosensors [37–39]. In addition, SECM and other related methods have great potential in miniaturized immunoassays [38].

SECM may also be used to characterize newly fabricated electrodes along with scanning electron microscopy (SEM) and SSV. SEM is useful for examining the seal between the metal or fiber and the insulating material as well as estimating their radii. SSV can be used to estimate the radius of the electrode in addition to demonstrating that the newly prepared electrode response obeys the applicable microelectrode electrochemical

theories. Well-characterized aqueous systems that are suitable for the aforementioned studies in SSV include the oxidation of ferrocene methanol, the oxidation of ferrocyanide, the reduction of ferricyanide, and the reduction of ruthenium hexamine [8].

Since electrochemical detection methods are based on interfacial phenomenon, careful cleaning of working electrode surfaces is essential to obtaining reproducible signal responses. With macroelectrodes, physical polishing of the electrode surface is done using abrasive material such as slurry of alumina particles or diamond paste. These polishing methods cannot be used with electrodes with a total structural diameter of < 1 μm due to electrode tips being very fragile [8]. Therefore, other electrode cleaning methods such as pulse techniques (e.g., pulsed amperometric detection) have been used to activate, clean, and rejuvenate microelectrode surfaces when replacing the entire electrode is not possible [8]. In pulsed amperometric detection, first a large anodic pulse helps with desorption of any bound species from the electrode surface followed by the formation of a thin oxide layer. Later, a cathodic pulse results in the dissolution of the oxide film and reactivation of the electrode surface. Finally, the potential can then be switched to a detection potential for the redox-active analyte of interest.

Although various nanoelectrodes have been prepared, studied, and described in literature, sturdy and/or disposable microelectrodes with well-defined geometries, reproducible electrochemical responses and reproducible fabrication outcome are still used in many physiological and electroanalytical detection applications. The next section will describe more recently prepared nanoelectrodes and their use.

1.3 Nanoelectrodes

Nanoelectrodes also known as nanodes have been defined as electrodes having a critical dimension, the dimension which controls the electrochemical response (i.e., the radius of a hemisphere- or disk-shaped electrode or the width for a band electrode), in the nanometer scale (<100 nm). Nanoelectrodes have been of great interest in bioelectrochemistry for over two decades. Preparation, characterization, and applications of a wide variety of nanoparticles and nanoelectrodes have resulted from synthetic advances and improvements in their fabrication methods. One of the driving forces for nanoelectrode development has been the need to prepare electrodes whose critical dimension is similar to molecular

dimensions that are capable of single-molecule detection [40]. The size, shape, and chemical composition of newly prepared nanomaterials must be thoroughly determined prior to their use in biosensors and other applications because their electrochemical properties are highly sensitive to the slightest variation in electrode geometry. For example, the steady-state limiting current of a recessed nanoelectrode is smaller than that of a disk-shaped nanoelectrode with the same size because of additional mass transport resistance [41]. Once the nanoelectrodes are well-characterized and relatively uniform, it is possible to probe how unique properties such as electron transfer and spectroscopic responses depend on size, geometry, composition, and surface characteristics.

Smaller electrodes are increasingly in demand as many aspects of modern chemistry and molecular science overall operate in the 1–1000 nanometer range. Also, their nanosized scale makes nanoelectrodes amendable to implantation in living systems and in some cases allows real-time, long-term *in vivo* monitoring of systems such as the animal brain [42].

Other benefits of nanoelectrodes based on their size are well understood in theory and have been observed experimentally. These advantages include enhanced mass transport, greater S/N ratios, increased sensitivity, and being more immune to hydrodynamic perturbations [40–45]. For example, the very high rate of radial mass transport or diffusion of redox-active species at nanoelectrode surfaces enables kinetic measurements under steady-state conditions rather than under dynamic sample conditions. These extremely small electrodes may also allow studying of faster biochemical, electrochemical, and chemical reactions because the electron transfer process is not limited by mass transport of reactants to the electrode surface [40]. When performing electroanalytical measurements, it has been noted that increased mass transport at the nanoelectrodes (which ultimately results in shorter transducer response times) to freely diffusing analyte species in the sample solution results in a shorter time needed to achieve a maximum signal. For example, this is useful in amperometry where a constant applied potential is used or in stripping voltammetry experiments where shorter deposition times are desired. The electrode response time varies as a function of the electrode size [42]. However, methods for nanoelectrode fabrication, characterization of nanoelectrode geometry as well as the electrochemical performance of nanoelectrodes after they are fabricated are problems which must be overcome before nanoelectrodes become widely used. Still, single nanoelectrodes as well as collections of individual nanodes that are arranged in an organized array or randomly dispersed throughout an inert matrix can be prepared. In

addition to possessing an increased and easily detectable signal response, large arrays containing multiple nanoelectrodes have the advantage of signal redundancy thereby increasing their statistical reliability.

Nanoelectrodes have been fabricated using several approaches. Nanoband electrodes, the first type of nanoelectrode fabricated by White et al. in the late 1980s, may be prepared using sputtered or evaporated metal films [46,47]. The edge of these electrodes is in contact with the sample solution. In another method, thin wires are carefully etched chemically or electrochemically to a cone shape prior to photoresisting or insulating all but the tip of the cone with another material such as polyimide [48] or Teflon [49]. Other nanoelectrode preparation methods include electrophoretic point deposition [50–53], the use of single- (SWCNTs) or multiwalled CNTs [54,55], glass encapsulation [56–58], micropipette pulling [59], and others. Nanoelectrode arrays (NEA) or nanoelectrode ensembles (NEE) may be prepared by deposition of metallic layers through nanoporous polymeric membranes. *In vivo* voltammetry and electrochemical imaging applications require disk or hemisphere-shaped nanoelectrodes. The preparation of hemispherical nanoelectrodes, such as the one depicted in Figure 1.7, with ≥1 nm radii via electrochemical etching of Pt or PtIr alloy microwires followed by insulating all but the tip of the tapered cone was first described by Penner et al. [57].

Nanosized materials have been used to modify or interact with the transducer surface that comes in contact with the sample in various enzyme-based biosensors, genosensors, and immunosensors. The transducer is ultimately responsible for measuring and transmitting the signal generated in the presence of the analyte of interest. Commonly used nanomaterials include graphene, nanowires, CNTs, magnetic nanoparticles, and quantum dots (QDs). Nanomaterials can be classified as biological, inorganic, or organic. Biological nanomaterials that are responsible for recognizing and interacting with the analyte in a biosensor include macromolecules such as antibodies and DNA as well as artificial, synthetic molecular recognition elements called aptamers. A common role of organic and inorganic nanomaterials, such as nanoparticles or nanowires, in biosensors is to amplify the analyte binding event by using some measurable change in a property such as the electrical conductivity of a nanowire. Furthermore, the use of nanomaterials has helped increase charge and electron transfer in electrochemical biosensors. In addition, nanomaterial-modified sensing surfaces have improved electrochemical properties as a result of low background current and higher S/N ratios. These and other advantageous properties of nanomaterial-based electrodes will be described in the next section.

1.3.1 Electrochemistry and Advantages of Nanoelectrodes

Nanowires are nanosized structures with diameters in 10^{-9} m scale and no restriction in length. Nanowires as long as 1 mm have been synthesized, but a typical length is about 1 μm. Due to their length being several orders of magnitude greater than their width, these nanostructures are often viewed as being one dimensional (1-D). The small sizes and 1-D structures of nanowires result in unique physical properties when compared to conventional three-dimensional wires. Nanowire conductance can be carefully controlled by preparing the wire from different substrates. Nanowires have been synthesized from metals (such as Au, Ni, Cu, and Pt), metal oxides (such as ZnO, SnO_2, and Fe_2O_3), silicon/indium/gallium semiconductors, and silicon/titanium oxide insulators. As one may expect, metallic nanowires are the most conductive.

Advances in fabrication methods for nanoelectrode preparation, synthesis of nanomaterials, and related nanotechnology as well as in analytical instrumentation have resulted in rapid expansion of this field. When nanoelectrodes and nanoelectrodes arrays were first produced in the late 1980s, imaging methods such as SEM were not capable of visualizing these nanostructures. As a result, researchers measured the dimensions of nanoelectrodes surfaces based on their electrochemical responses [40]. Since individual nanoscale electrodes produced very small currents, orderly NEA and NEE with signal amplification capabilities, became commonplace. When each nanoelectrode is sufficiently far away from neighboring nanoelectrodes, each electrode in the nanoelectrode collective has its individual diffusion regime with three-dimensional, radial diffusion dominating in sample solution (Figure 1.9, top). When the spacing of the nanoelectrodes is not sufficient, the electrodes in a higher-density NEE have overlapping diffusion regimes with 1-D, planar diffusion being most dominant (Figure 1.9, bottom) [40]. It is important to recall, however, that time scale (i.e., scan rate in voltammetry) also affects the shape of the diffusion profile and ultimately the shape of the voltammogram. For example, at slow scan rates (longer times), the diffusion regimes of individual nanoelectrodes overlap resulting in classic duck-shaped voltammograms. At intermediate and fast scan rates (shorter times), radial diffusion to each nanoelectrodes results in sigmoidal, steady-state voltammograms. Therefore, specific scan rates and timescales where diffusion behavior changes from planar and to radial and vice versa depend on the size of the nanostructures in the NEE and the average spacing of the electrodes.

Another important consideration in the electrochemistry of NEAs and NEEs is the background or charging current (similar to what was

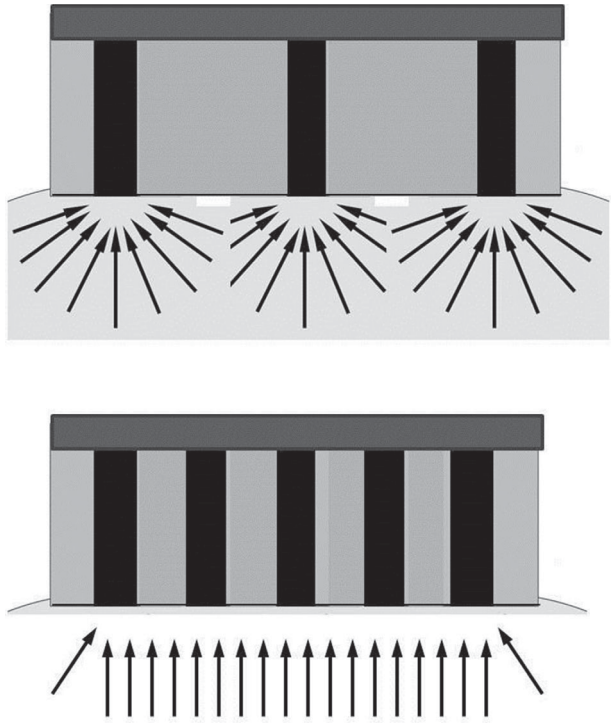

Figure 1.9 Diffusion layer profiles at nanoelectrodes array with individual diffusion regimes (top) and at nanoelectrodes ensemble with overlapping diffusion regimes (bottom) resulting in primarily 1-D, planar diffusion.

previously described in microelectrode detection). The observed charging current, which is proportional to the total geometric area of the individual electrode elements, should be as low as possible relative to Faradaic current in order to obtain high S/N ratio. When the nanoelectrodes are closely spaced and the diffusion regimes of neighboring electrodes in a NEA or a NEE overlap, the Faradaic current will be proportional to the total surface area (including both active nanoelectrode surfaces and interelectrode insulation) and results in an enhanced signal. In turn, this should result in lower DLs and allow the quantification of trace level analytes. For example, Martin et al. described DLs of 1.6 nM for CV of redox-active species using 10 nm diameter gold disk NEEs as opposed to DL of 1.6 μM (three orders of magnitude worse) for conventional working electrode with a mm-sized disk [60]. This was attributed to lower charging currents relative to Faradaic currents at the Au NEEs. Other notable improvements in S/N ratio, sensitivity, and other performance-related characteristics of merit in

a broad range of applications for NEAs and NEEs as well as individual nanoelectrodes, will be discussed in the next section.

1.3.2 Applications and Performance of Nanoelectrodes

In vivo detection of neurotransmitter release and determining the real-time concentrations of dopamine and serotonin in living systems by implantable nanoelectrodes has implications in the study of various neurological and neurodegenerative diseases such as Parkinson disease, epilepsy, schizophrenia, and obsessive-compulsive disorder [61–65]. Differential pulse voltammetry using carbon nanofiber nanoelectrodes that have been integrated into the Wireless Instantaneous Neurotransmitter Concentration Sensing System (WINCS) is a suitable method for real-time monitoring of neurotransmitter release *in vivo*. Zhang et al. demonstrated that such a system can be biocompatible as well as highly selective and sensitive for quantification of dopamine down to 50 nM and serotonin to 100 nM [42]. These nanoelectrodes have significantly higher S/N ratio and ultimately superior sensitivity when compared to macroelectrodes. Carbon nanofiber-based nanoelectrodes could be used to simultaneously detect and resolve these individual neurotransmitters in a complex sample mixture containing interfering agents such as ascorbic acid [42]. Adsorption kinetics studies and isopropyl alcohol treatments were done to investigate the properties on carbon nanofiber electrodes using fast-scan CV with WINCS as compared with results obtained previously using well-characterized carbon fiber microelectrodes [42]. It was found that carbon nanofiber electrodes had faster response times resulting in faster detection when compared to carbon fiber microelectrodes.

Claussen et al. prepared two nanomaterial-based biosensors for glutamate incorporating SWCNTs modified with either Pt nanospheres or Pd nanocubes and evaluated their performance in a side-by-side comparative study using amperometry and CV [66]. The authors first grew low-density arrays of SWCNTs on the biosensor surface followed by electrodeposition of Pd nanocubes (d=150 nm) and Pt nanospheres (d=150 nm) along individual SWCNTs with an average spacing of 366 nm. Then equal aliquots of glutamate oxidase enzyme were drop-coated on the modified surface and immobilized by cross-linking with glutaraldehyde. Of note, glutamate is an important excitatory neurotransmitter that is involved in locomotion, learning, and synaptic plasticity. Real-time sensing of glutamate levels is important in neurological research such as in diagnosing and treating neurological diseases like Parkinson's disease, Alzheimer's disease, schizophrenia, and epilepsy.

Sultana et al. recently investigated the performance of a 50 nm thick, relatively simple, nanoband electrode structure which formed an array of nanoscale electrodes for bioelectrochemical applications [67]. The nanoband electrode was used to detect three common bioelectrochemical redox species: hydrogen peroxide (H_2O_2), FCA, and PAP with DLs of 2, 89, and 36×10^{-9} mol dm^{-3}, respectively [67]. These results indicated an increase in sensitivity of the nanoelectrode system compared to larger electrodes, with DLs of about three orders of magnitude lower for each redox species. The DL of H_2O_2 was comparable to those previously obtained by using nanowires and modified electrodes. Furthermore, the nanoband electrode was capable of being used with short and fast modes of interrogation (e.g., fast-scan cyclic voltammetric) with detection of up to 10 V s^{-1} which yielded higher measurement certainty, while being relatively insensitive to hydrodynamic perturbations [67].

As with microelectrodes, the use of nanoelectrodes has extended to SECM techniques. Nanoscale electrodes in SECM have enabled greater resolution of probed surfaces because the nanoelectrodes moving across the surface being studied must be of comparable size to that surface. Nanosized surface features on a membrane or a corroding surface, for example, can be studied using a nanosized electrochemical probe [40,68–71]. Takahashi et al. described voltage-switching mode scanning electrochemical microscopy (VSM-SECM), in which a single SECM tip electrode consisting of pyrolytic carbon nanoelectrodes (radii=6.5–100 nm), were used to simultaneously acquire high-quality topographical and electrochemical images of living cells [72]. The electrodes with the largest radii reached a steady-state current in <20 ms, while the smaller electrodes were even faster. Furthermore, the group-performed VSM-SECM to visualize membrane proteins on A431 cells as well as to detect neurotransmitters from PC12 cells. In addition to physiological and biology applications that were demonstrated, VSM-SECM is likely to open new opportunities in nanoscale chemical mapping at interfaces.

Bard and Fan achieved what had been the ultimate driving force of ultramicro- and nanoelectrode development in electroanalytical chemistry for years by observing the electrochemical behavior of a single, isolated molecule in an SECM experiment [73]. Small, nm range SECM tips and other nanoelectrodes are generally capable of measurements of very small currents, in the picoamp or smaller range. The authors isolated a small, dilute solution segment by pushing a soft protruding wax shroud surrounding an electrode tip against a flat electrode substrate, thereby forming a pocket that acts as a collector–generator surrounded by an insulating film. The experimental setup used by Bard and Fan is shown in Figure 1.10. The

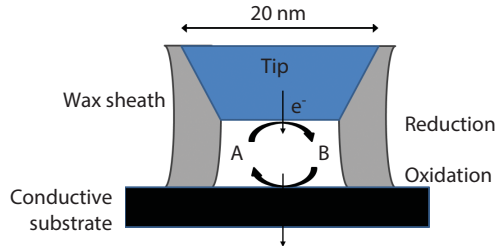

Figure 1.10 Single-molecule detection strategy with the SECM. Redox-active molecule A is trapped between the tip and a flat conductive substrate surface.

detectable current was produced inside a SECM collector–generator from the entrapment of a single molecule (A being reduced to B by accepting an electron). The molecule in a positive-feedback process has repeated collisions and electron transfers inside the pocket and thereby the current gets amplified by repeated cycling between oxidation states of the analyte molecule back and forth between the 20 nm radius electrode tip and substrate increasing the produced current to a readily detectable level. The redox cycling of the molecule resulted in about 10 million-fold current amplification and the estimated average single-molecule current of 1.6 pA [73]. The authors utilized a water soluble ferrocene derivative as the model species oxidized at the SECM tip to produce the ferrocenium form that is then reduced at the indium tin oxide substrate back to ferrocene form.

Fan and Bard also later reported the current-potential curve at a smaller 2.8 nm radius electrode immersed in a solution containing micromolar concentrations of [(trimethylammonio)methyl] ferrocene (Cp_2FeTMA^+), showing discrete steps (a coulomb staircase) representing single electron-transfer events [74].

A large number of single molecule, single biomolecule such as enzyme or hemoglobin, and single nanoparticles studies have also been done since mid-1990s using spectroscopy [75–80] and with spectroelectrochemistry [81,82]. Some progress has also been made toward single-enzyme molecule electrochemistry that has become a possibility using nanoelectrodes which are capable of detecting at millisecond time scale using protein film voltammetry [83,84]. Single-enzyme molecule studies are of great interest in molecular biology and biochemistry as they allow observing whether there are temporal variations in the enzyme activity; does the enzyme turn on and off in the course of the biochemical reaction or if there are variations in enzyme activity that can be accounted for by its conformational changes [84]. These kinds of effects may only be explored by single-enzyme

molecule studies as they would be averaged out in an ensemble of enzymes or even a small number of enzyme molecules.

1.4 Integration of the Electronic Transducer, Electrode, and Biological Recognition Components (such as Enzymes) in Nanoscale-Sized Biosensors and Their Clinical Applications

Integration of an electronic transducer, electrode, and biological recognition components (e.g., enzymes) in biosensors is critical in order to develop highly sensitive, nanoscale-sized biosensors suitable for clinical analysis. Direct electrochemistry of redox enzymes using conventional electrodes made of glassy carbon, platinum or gold is quite challenging because the active sites and redox centers of these enzymes, are buried deep inside a hydrophobic polypeptide chain which is electrically insulated, and therefore inaccessible to these types of electrode surfaces. Thus, even if electron transfer between these enzymes and conventional electrodes takes place, it is slow at best.

For many decades, enzyme electrodes relied heavily on synthetic mediators (i.e., electron shuttle molecules) in their design in order to avoid dependence on dissolved O_2 in the production of H_2O_2, which was a major limitation in first generation glucose sensors. In the case of GOx, direct electron transfer is not possible without including an electron-transfer mediator because its FAD redox center is buried inside a thick protein layer, resulting in kinetically slow electron transfers [85]. The oxidized form of an electron-transfer mediator typically regenerates the redox center of the biorecognition enzyme (in the case of GOx, FAD) via simultaneous self-reduction. Later, the mediator reverts to its original reduced form at the electrode surface, resulting in a detectable electric signal. Ideal electron-transfer mediators react quickly with the reduced enzyme. In addition, they are nontoxic, chemically stable in both reduced and oxidized forms and possess low solubility in an aqueous sample environment. Ideal electron-transfer mediators also have a low detection potential. The electron-transfer mediator can be dissolved in an electrolyte solution to facilitate its mass transport between the electrode surface and the enzyme active site. In glucose biosensors, electron-transfer mediators such as poly(vinylimidazole) and poly(vinylpyridine) are linked with osmium-complex electron relays which are in close proximity to the redox center

of the polymers and the FAD redox center of the enzymes. This arrangement results in rapid biosensor response and high current output. Of note, carefully chosen electron-transfer mediators may be readily regenerated at lower applied voltages, eliminating the background signal from interfering species. However, leaching of soluble, synthetic electron-transfer mediators from biosensors over time has been a problem with many enzyme-based biosensors. Therefore, soluble electron-transfer mediators cannot be used in biosensors designed for *in vivo* use.

Nanomaterials such as CNTs have been found to significantly promote direct electrochemistry of enzymes. This has stimulated great interest in redesigning enzyme-based biosensors with conductive nanomaterials to replace the current electron-transfer mediators in use.

Furthermore, conjugating proteins onto CNTs has resulted in plethora of new applications in biosensors, imaging and cellular delivery. Joshi et al. demonstrated that CNTs may be used to mediate the selective deactivation of proteins *in situ* by photochemical effects upon being exposed to near-infrared irradiation by designing CNT–peptide conjugates which selectively destroyed anthrax toxin [86]. Such nanotube-assisted protein deactivation will likely find increased application in the selective destruction of other similar toxins or pathogens. It has also been suggested that composites of CNTs and polymers may potentially act as hosts for specific enzymes and ultimately help prevent fouling due to protein adsorption on the surfaces of medical devices and in other applications [87]. Fouling, the nonspecific adsorption of proteins on surfaces, is a major problem with implantable biosensors as well as medical implants, such as cardiovascular stents. The resulting biofilms significantly reduce the performance of implantable devices with eventual loss of activity or function upon the complete encapsulation of these devices.

1.5 Conclusion

Many of the exceptional properties of microelectrodes, such as rapid mass transport and radial diffusion, have been experimentally demonstrated in nanoelectrodes where they are usually even more pronounced because of their nanoscale sizes. Nanoelectrodes are also capable of monitoring experiments in the microsecond or even in the nanosecond scale allowing single-enzyme electrochemical studies and many other exciting applications. Although advances in materials science and nanofabrication techniques have made the use of nanoelectrodes in bioanalytical and medical

measurements possible and more common, several practical challenges remain. These challenges, which limit the experimental realization of some of the well-known theoretical benefits, include not being able to produce robust electrochemical probes that are characterized by precise and reproducible experimental performance. Furthermore, surface-fouling by non-electroactive sample components found in the complex biological sample matrices where nanoelectrodes and NEE are utilized, adversely affects voltammetric responses at electrode surfaces.

Acknowledgment

Dr. Stanley Okon is acknowledged for assisting with manuscript proofreading.

References

1. N.J. Ronkainen, H.B. Halsall, and W.R. Heineman, Electrochemical biosensors. *Chemical Society Reviews*, 39, pp. 1747–1763, 2010.
2. M.A. Dayton, J.C. Brown, K.J. Stutts, and R.M. Wightman, Faradaic electrochemistry at microvoltammetric electrodes. *Analytical Chemistry*, 52, pp. 946–950, 1980.
3. M. Fleischmann and S. Pons, The behavior of microelectrodes. *Analytical Chemistry,* 59(24), pp. 1391A–1399A, 1987.
4. R.M. Wightman, Voltammetry with microscopic electrodes in the new domains. *Science*, 240, pp. 415–420, 1988.
5. P.W. Davies and F. Brink, Microelectrodes for measuring local oxygen tension in animal tissues. *Review of Scientific Instruments,* 13, pp. 524–533, 1942.
6. A.C. Michael and R.M. Wightman, Microelectrodes, Chapter 12 in *Laboratory Techniques in Electroanalytical Chemistry*, P. Kissinger and W.R. Heineman (Eds.), Marcel Dekker, New York, pp. 367–402, 1999.
7. J.B. Chien, R.A. Wallingford, and A.G. Ewing, Estimation of free dopamine in the cytoplasm of the giant dopamine cell of *Planorbis corneus* by voltammetry and capillary electrophoresis. *Journal of Neurochemistry,* 54, pp. 633–638, 1990.
8. C.G. Zoski, Ultramicroelectrodes: design, fabrication, and characterization. *Electroanalysis*, 14(15–16), pp. 1041–1051, 2002.
9. N.J. Ronkainen and S.L. Okon, Nanomaterial-based electrochemical immunosensors and immunoassays for clinically significant biomarkers. *Materials*, 7(6), pp. 4669–4709, 2014.
10. L.X. Tang and P. Vadgama, Optimization of enzyme electrodes. *Medical & Biological Engineering & Computing,* 28, pp. B18–24, 1990.

11. J. Wang, Electroanalysis and biosensors. *Analytical Chemistry*, 67, pp. 487–492, 1995.
12. J. Wang, Glucose biosensors: 40 years of advances and challenges. *Electroanalysis*, 13(12), pp. 983–988, 2001.
13. L.C. Clark and C. Lyons, Electrode systems for continuous monitoring in cardiovascular surgery. *Annals of the New York Academy of Sciences,* 102, pp. 29–45, 1962.
14. J.J. O'Malley and J.L. Weaver, Subunit structure of glucose oxidase from *Aspergillus niger*. *Biochemistry*, 11, pp. 3527–3532, 1972.
15. H. Tsuge, O. Natsuaki, and K. Ohashi, Purification, properties and molecular features of glucose oxidase from *Aspergillus niger*. *The Journal of Biochemistry*, 78, pp. 835–843, 1975.
16. C. Tlili, K. Reybier, A. Géloën, L. Ponsonnet, C. Martelet, H. Ben Ouada, M. Lagarde, and N. Jaffrezic-Renault, Fibroblast cells: a sensing bioelement for glucose detection by impedance spectroscopy. *Analytical Chemistry*, 75(14), pp. 3340–3344, 2003.
17. R. Wilson and A.P.F. Turner, Glucose oxidase: an ideal enzyme. *Biosensors Bioelectronics,* 7, pp. 165–185, 1992.
18. S. Pons and M. Fleischmann, The behavior of microelectrodes. *Analytical Chemistry*, 59, pp. 1391A, 1987.
19. S. Ching, R. Dudek, and E. Tabet, Cyclic voltammetry with ultramicroelectrodes. *Journal of Chemical Education*, 71, pp. 602–605, 1994.
20. P.T. Kissinger and W.R. Heineman, Cyclic voltammetry. *Journal of Chemical Education,* 60(9), pp. 702–706, 1983.
21. W.R. Heineman and P.T. Kissinger, Cyclic voltammetry: the electrochemical equivalent of spectroscopy. *Current Separations*, 9(1–2), pp. 15–18, 1989.
22. R.M. Wightman and D.O. Wipf, *Electroanalytical Chemistry*, A.J. Bard (Ed.), Marcel Dekker, New York, Vol. 15, p. 267, 1989.
23. J. Heinze, Electrochemistry with ultramicrooelectrodes. *Angewandte Chemie International Edition in English,* 32, pp. 1268–1288, 1993.
24. R.M. Wightman and D.O. Wipf, High-speed cyclic voltammetry. *Accounts of Chemical Research*, 23(3), pp. 64–70, 1990.
25. R.W. Murray, Nanoelectrochemistry: metal nanoparticles, nanoelectrodes, and nanopores. *Chemical Reviews*, 108(7), pp. 2688–2720, 2008.
26. P.T. Kissinger and W.R. Heineman (Editors), *Laboratory Techniques in Electroanalytical Chemistry*, Marcel Dekker, New York, 1996.
27. J.G. White and J.W. Jorgensen, Improvements in scanning voltammetric detection for open-tubular liquid chromatography. *Analytical Chemistry,* 58, pp. 2992–2995, 1986.
28. L.J. Magee, Jr. and J. Osteryoung, Dynamic and steady-state response of electrochemical detectors based on arrays of small electrodes. *Analytical Chemistry,* 62, pp. 2625–2631, 1990.
29. R.C. Engstrom and C.N. Pharr, Scanning electrochemical microscopy. *Analytical Chemistry,* 61, pp. 1099A–1104A, 1989.

30. C. Lee, J. Kwak, and A.J. Bard, Application of scanning electrochemical microscopy to biological samples. *Proceedings of the National Academy of Sciences*, 87(5), pp. 1740–1743, 1990.
31. C.A. Wijayawardhana, N.J. Ronkainen-Matsuno, S. Farrell, G. Wittstock, H.B. Halsall, and W.R. Heineman, Microspot enzyme assays with scanning electrochemical microscopy. *Analytical Sciences*, 17, pp. 535–538, 2001.
32. S. Farrell, N.J. Ronkainen-Matsuno, H.B. Halsall, and W.R. Heineman, Bead-based immunoassays with microelectrode detection. *Analytical and Bioanalytical Chemistry,* 379, pp. 358–367, 2004.
33. J.H. Thomas, N.J. Ronkainen-Matsuno, S. Farrell, H.B. Halsall, and W.R. Heineman, Microdrop analysis of a bead-based immunoassay. *Microchemical Journal*, 74, pp. 267–276, 2003.
34. A.M. Bond, M. Fleischmann, and J. Robinson, Electrochemistry in organic solvents without supporting electrolyte using platinum microelectrodes. *Journal of Electroanalytical Chemistry and Interfacial Electrochemistry*, 168(1), pp. 299–312, 1984.
35. S. Metz, R. Holzer, and P. Renaud, Polyimide-based microfluidic devices. *Lab on a Chip*, 1(1), pp. 29–34, 2001.
36. S. Choi and J.K. Park, Microfluidic system for dielectrophoretic separation based on a trapezoidal electrode array. *Lab on a Chip*, 5(10), pp. 1161–1167, 2005.
37. G. Wittstock, K. Yu, H.B. Halsall, T.H. Ridgway, and W.R. Heineman, Imaging of immobilized antibody layers with scanning electrochemical microscopy. *Analytical Chemistry,* 67, pp. 3578–3582, 1995.
38. C.A. Wijayawardhana, G. Wittstock, H.B. Halsall, and W.R. Heineman, Spatially addressed deposition and imaging of biochemically active bead microstructures by scanning electrochemical microscopy. *Analytical Chemistry,* 72, pp. 333–338, 2000.
39. C.A. Wijayawardhana, G. Wittstock, H.B. Halsall, and W.R. Heineman, Electrochemical immunoassay with microscopic immunomagnetic bead domains and scanning electrochemical microscopy. *Electroanalysis,* 12, p. 640, 2000.
40. D.W. Arrigan, Nanoelectrodes, nanoelectrode arrays and their applications. *Analyst*, 129(12), pp. 1157–1165, 2004.
41. J.T. Cox and B. Zhang, Nanoelectrodes: recent advances and new directions. *Annual Review of Analytical Chemistry*, 5, pp. 253–272, 2012.
42. D.A. Zhang, E. Rand, M. Marsh, R.J. Andrews, K.H. Lee, M. Meyyappan, and J.E. Koehne, Carbon nanofiber electrode for neurochemical monitoring. *Molecular Neurobiology*, 48(2), pp. 380–385, 2013.
43. N. Godino, X. Borrise, F.X. Munoz, F.J. del Campo, and R.G. Compton, Mass transport to nanoelectrode arrays and limitations of the diffusion domain approach: theory and experiment. *The Journal of Physical Chemistry C*, 113(25), pp. 11119–11125, 2009.

44. D. Grieshaber, R. MacKenzie, J. Voeroes, and E. Reimhult, Electrochemical biosensors-sensor principles and architectures. *Sensors*, 8(3), pp. 1400–1458, 2008.
45. C. Amatore, C. Pebay, L. Thouin, A. Wang, and J.S. Warkocz, Difference between ultramicroelectrodes and microelectrodes: influence of natural convection. *Analytical Chemistry*, 82(16), pp. 6933–6939, 2010.
46. R.B. Morris, D.J. Franta, and H.S. White, Electrochemistry at platinum bane electrodes of width approaching molecular dimensions: breakdown of transport equations at very small electrodes. *Journal of Physical Chemistry*, 91(13), pp. 3559–3564, 1987.
47. J.D. Seibold, E.R. Scott, and H.S. White, Diffusional transport to nanoscopic band electrodes. *Journal of Electroanalytical Chemistry and Interfacial Electrochemistry*, 264(1), pp. 281–289, 1989.
48. P. Sun, Z. Zhang, J. Guo, and Y. Shao, Fabrication of nanometer-sized electrodes and tips for scanning electrochemical microscopy. *Analytical Chemistry*, 73(21), pp. 5346–5351, 2001.
49. B. Liu, J.P. Rolland, J.M. DeSimone, and A.J. Bard, Fabrication of ultramicroelectrodes using A "Teflon-like" coating material. *Analytical Chemistry*, 77(9), pp. 3013–3017, 2005.
50. S. Chenand and A. Kucernak, Fabrication of carbon microelectrodes with an effective radius of 1 nm. *Electrochemistry Communications*, 4(1), pp. 80–85, 2002.
51. J.J. Watkins, J. Chen, H.S. White, H.D. Abruña, E. Maisonhaute, and C. Amatore, Zeptomole voltammetric detection and electron-transfer rate measurements using platinum electrodes of nanometer dimensions. *Analytical Chemistry*, 75(16), pp. 3962–3971, 2003.
52. B.K. Jena, S.J. Percival, and B. Zhang, Au disk nanoelectrode by electrochemical deposition in a nanopore. *Analytical Chemistry*, 82(15), pp. 6737–6743, 2010.
53. J.J. Watkins and H.S. White, The role of the electrical double layer and ion pairing on the electrochemical oxidation of hexachloroiridate (III) at Pt electrodes of nanometer dimensions. *Langmuir*, 20(13), pp. 5474–5483, 2004.
54. J.K. Campbell, L. Sun, and R.M. Crooks, Electrochemistry using single carbon nanotubes. *Journal of the American Chemical Society*, 121(15), pp. 3779–3780, 1999.
55. B.M. Quinn and S.G. Lemay, Single-walled carbon nanotubes as templates and interconnects for nanoelectrodes. *Advanced Materials*, 18(7), pp. 855–859, 2006.
56. K. Dawson, J. Strutwolf, G. Herzog, D. Arrigan, A. Quinn, and A.J. O'Riordan, Nanofabrication of robust nanoelectrodes for electrochemical applications. *ECS Transactions*, 28(34), pp. 29–37, 2010.
57. R. Penner, M. Heben, T. Longin, and N. Lewis, Fabrication and use of nanometer-sized electrodes in electrochemistry. *Science*, 250(4984), pp. 1118–1121, 1990.

58. B. Zhang, J. Galusha, P.G. Shiozawa, G. Wang, A.J. Bergren, R.M. Jones, R.J. White, E.N. Ervin, C.C. Cauley, and H.S. White, Bench-top method for fabricating glass-sealed nanodisk electrodes, glass nanopore electrodes, and glass nanopore membranes of controlled size. *Analytical Chemistry*, 79(13), pp. 4778–4787, 2007.
59. Y. Shao, M.V. Mirkin, G. Fish, S. Kokotov, D. Palanker, and A. Lewis, Nanometer-sized electrochemical sensors. *Analytical Chemistry*, 69(8), pp. 1627–1634, 1997.
60. V.P. Menon and C.R. Martin, Fabrication and evaluation of nanoelectrode ensembles. *Analytical Chemistry*, 67(13), pp. 1920–1928, 1995.
61. C.C. McIntyre, M. Savasta, B.L. Walter, and J.L. Vitek, How does deep brain stimulation work? Present understanding and future questions. *Journal of Clinical Neurophysiology*, 21(1), pp. 40–50, 2004.
62. H.S. Mayberg, A.M. Lozano, V. Voon, H.E. McNeely, D. Seminowicz, C. Hamani, J.M. Schwalb, and S.H. Kennedy, Deep brain stimulation for treatment-resistant depression. *Neuron,* 45(5), pp. 651–660, 2005.
63. W.H. Theodore and R.S. Fisher, Brain stimulation for epilepsy. *The Lancet Neurology*, 3(2), pp. 111–118, 2004.
64. S. Kapur and G. Remington, Serotonin-dopamine interaction and its relevance to schizophrenia. *American Journal of Psychiatry*, 153(4), pp. 466–476, 1996.
65. D.L. Robinson, A. Hermans, A.T. Seipel, and R.M. Wightman, Monitoring rapid chemical communication in the brain. *Chemical Reviews*, 108(7), pp. 2554–2584, 2008.
66. J.C. Claussen, M.S. Artiles, E.S. McLamore, S. Mohanty, J. Shi, J.L. Rickus, T.S. Fisher, and D.M. Porterfield, Electrochemical glutamate biosensing with nanocube and nanosphere augmented single-walled carbon nanotube networks: a comparative study. *Journal of Materials Chemistry*, 21(30), pp. 11224–11231, 2011.
67. R. Sultana, N. Reza, N.J. Kay, I. Schmueser, A.J. Walton, J.G. Terry, A.R. Mount, and N.J. Freeman, Practical implications of using nanoelectrodes for bioanalytical measurements. *Electrochimica Acta*, 126, pp. 98–103, 2014.
68. N.J. Gray and P.R. Unwin, Simple procedure for the fabrication of silver/silver chloride potentiometric electrodes with micrometre and smaller dimensions: application to scanning electrochemical microscopy. *Analyst*, 125(5), pp. 889–893, 2000.
69. C.J. Slevin, N.J. Gray, J.V. Macpherson, M.A. Webb, and P.R. Unwin, Fabrication and characterisation of nanometre-sized platinum electrodes for voltammetric analysis and imaging. *Electrochemistry Communications*, 1(7), pp. 282–288, 1999.
70. K.B. Ballesteros, A. Schulte, and W. Schuhmann, Constant-distance mode scanning electrochemical microscopy. Part II: high-resolution SECM imaging employing Pt nanoelectrodes as miniaturized scanning probes. *Electroanalysis*, 16(1–2), pp. 60–65, 2004.

71. A. Lugstein, E. Bertagnolli, C. Kranz, and B. Mizaikoff, Fabrication of a ring nanoelectrode in an AFM tip: novel approach towards simultaneous electrochemical and topographical imaging. *Surface and Interface Analysis*, 33(2), pp. 146–150, 2002.
72. Y. Takahashi, A.I. Shevchuk, P. Novak, B. Babakinejad, J. Macpherson, P.R. Unwin, H. Shiku, J. Gorelik, D. Klenerman, Y.E. Korchev, and T.Matsue, Topographical and electrochemical nanoscale imaging of living cells using voltage-switching mode scanning electrochemical microscopy. *Proceedings of the National Academy of Sciences*, 109(29), pp. 11540–11545, 2012.
73. A.J. Bard and F.-R.F. Fan, Electrochemical detection of single molecules. *Accounts of Chemical Research*, 29(12), pp. 572–578, 1996.
74. F.-R.F. Fan and A.J. Bard, An electrochemical coulomb staircase: detection of single electron-transfer events at nanometer electrodes. *Science*, 277(5333), pp. 1791–1793, 1997.
75. S. Nie and S.R. Emory, Probing single molecules and single nanoparticles by surface-enhanced Raman scattering. *Science*, 275(5303), pp. 1102–1106, 1997.
76. J. Jiang, K. Bosnick, M. Maillard, and L. Brus, Single molecule Raman spectroscopy at the junctions of large Ag nanocrystals. *The Journal of Physical Chemistry B*, 107(37), pp. 9964–9972, 2003.
77. S. Weiss, Fluorescence spectroscopy of single biomolecules. *Science*, 283(5408), pp. 1676–1683, 1999.
78. H. Xu, E.J. Bjerneld, M. Käll, and L. Börjesson, Spectroscopy of single hemoglobin molecules by surface enhanced Raman scattering. *Physical Review Letters*, 83(21), pp. 4357, 1999.
79. B. Schuler, E.A. Lipman, and W.A. Eaton, Probing the free-energy surface for protein folding with single-molecule fluorescence spectroscopy. *Nature*, 419(6908), pp. 743–747, 2002.
80. T. Ha, A.Y. Ting, J. Liang, W.B. Caldwell, A.A. Deniz, D.S. Chemla, P.G. Schultz, and S. Weiss, Single-molecule fluorescence spectroscopy of enzyme conformational dynamics and cleavage mechanism. *Proceedings of the National Academy of Sciences*, 96(3), pp. 893–898, 1999.
81. R.E. Palacios, F.-R.F. Fan, A.J. Bard, and P.F. Barbara, Single-molecule spectroelectrochemistry (SMS-EC). *Journal of the American Chemical Society*, 128, pp. 9028–9029, 2006.
82. Y.-L. Chang, R.E. Palacios, F.-R.F. Fan, A.J. Bard, and P.F. Barbara, Electrogenerated chemiluminescence of single conjugated polymer nanoparticles. *Journal of the American Chemical Society*, 130, pp. 8906–8907, 2008.
83. F.J. Hoeben, F.S. Meijer, C. Dekker, S.P. Albracht, H.A. Heering, and S.G. Lemay, Toward single-enzyme molecule electrochemistry: [NiFe]-hydrogenase protein film voltammetry at nanoelectrodes. *ACS Nano*, 2(12), pp. 2497–2504, 2008.
84. A.J. Bard, Toward single enzyme molecule electrochemistry. *ACS Nano*, 2(12), pp. 2437–2440, 2008.

85. W. Putzbach and N.J. Ronkainen, Immobilization techniques in the fabrication of nanomaterial-based electrochemical biosensors: a review. *Sensors*, 13(4), pp. 4811–4840, 2013.
86. J. Amit, S. Punyani, S.S. Bale, H. Yang, T. Borca-Tasciuc, and R.S. Kane, Nanotube-assisted protein deactivation. *Nature Nanotechnology*, 3, pp. 41–45, 2008.
87. P.B. Messersmith and M. Textor, Nanomaterials: enzymes on nanotubes thwart fouling. *Nature Nanotechnology*, 2(3), pp. 138–139, 2007.

2

Radio-Frequency Biosensors for Label-Free Detection of Biomolecular Binding Systems

Hee-Jo Lee*[1], Sang-Gyu Kim[2], and Jong-Gwan Yook*[3]

[1]*Department of Physics Education, Daegu University, Gyeongsan, South Korea*
[2]*LG Electronics, Seoul, South Korea*
[3]*School of Electrical and Electronic Engineering, Yonsei University, Seoul, South Korea*

Abstract

In this topic, we focus on the label-free biosensing using resonators at microwave frequencies. Specifically, we investigate a carbon nanotube (CNT) resonator and split-ring resonator as the radio-frequency (RF) biosensor schemes. The feasibility of the sensing devices is demonstrated with the biomolecular binding systems, biotin–streptavidin, deoxyribonucleic acid (DNA) hybridization, and so on. From the experimental data, we analyze in detail the electrical properties with the biomolecular binding via a RF circuit modeling. In addition, we introduce the recently developed sensing platform that can be associated with a RF active system. Finally, we suggest the prospect and direction for RF biosensor in the future.

***Keywords*:** Radio-frequency, biosensor, carbon nanotube, resonator, active circuits, sensing platform

2.1 Overview

This chapter covers label-free biosensing schemes and recent advances in biomolecular detection methods based on radio-frequency (RF) components and systems at microwave region. In particular, carbon

**Corresponding authors*: hjlee@daegu.ac.kr; jgyook@yonsei.ac.kr

Ashutosh Tiwari, Hirak K. Patra and Anthony P.F. Turner (eds.) Advanced Bioelectronic Materials, (35–54) © 2015 Scrivener Publishing LLC

nanotube-combined interdigital capacitors (IDCs) and asymmetric split-ring resonator (ASRR) as the RF biosensing schemes are introduced. The feasibility of the sensing devices is validated with the various biomolecular binding systems, such as biotin–streptavidin, deoxyribonucleic acid (DNA) hybridization, and so on. In addition, the recent RF biosensing platform that can be associated with an active system is also reviewed in detail and evaluated. Finally, the prospect and direction for RF biosensor in the future are discussed.

2.2 Introduction

In general, a biosensor is defined as an analytical device for the detection of an analyte that combines a biological component with a physicochemical detector [1]. It consists of a detecting, a transducing, and a signal conditioning part (Figure 2.1).

In particular, RF biosensor means that specific RF components, e.g., resonators [2–5], are used as a transducer for biomolecular detection. Here, RF is a rate of oscillation roughly in the range of around 3 kHz to 300 GHz, which corresponds to the frequency of radio waves, and the alternating current (AC) which carries radio signals. Then, binding or unbinding information can be recognized by an observed signal through microwave equipment, such as vector network analyzer (VNA), spectrum analyser, and so on.

During the past decade, the RF systems for biomedical applications have received a lot of attention due to their suitability for non-invasive, non-contact as well as non-destructive detection capabilities [6–8]. Various RF biosensing schemes [9–11] have been introduced for sensing of the antigen–antibody reaction as well as living cells. For examples, the biosensing devices utilizing coplanar waveguide (CPW) [12, 13], IDCs [14, 15], polymer-transmission line [16], and dielectric resonator (DR) [17] have been studied for the detection of label-free biomolecular interactions.

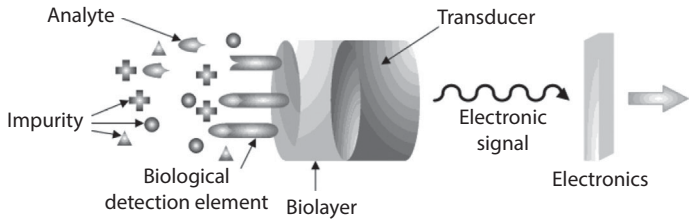

Figure 2.1 Schematic of biosensor.

In addition, the micro-electromechanical system (MEMS)-based RF biosensors for living cell detection have been also studied [18, 19]. These approaches reveal clear possibilities in RF biomolecular sensing, but they still bear several disadvantages, such as need of expensive equipment, complex measurement system, which is RF probe system associated with VNA, and sophisticated micro-fabrication process. In recent years, the RF biosensing platforms have been expansively investigated for the diverse healthcare applications in conjunction with wireless communication system including radio-frequency identification (RFID), wireless sensor node, and so on. In this chapter, a few RF biosensing schemes, such as carbon nanotube (CNT)-, resonator- as well as RF active system-based RF biosensors, for biomolecular detection are introduced, and these principles and performances are described.

2.3 Carbon Nanotube-Based RF Biosensor

2.3.1 Carbon Nanotube

CNTs have received considerable attention as chemical and biological sensors because of their high sensitivity and real-time detection capabilities [20–25] (Figure 2.2). In particular, the field-effect transistor (FET) structures with CNT conducting channel have been studied extensively. If biomolecules are bound onto the CNT surface, the threshold voltage is shifted and the direct current (DC) electrical conductance of the CNT transistors changes due to charge transfer between semiconducting CNTs and biomolecules. So far, most measurements of for FET sensors have been limited to DC electrical transport. However, since immobilization of

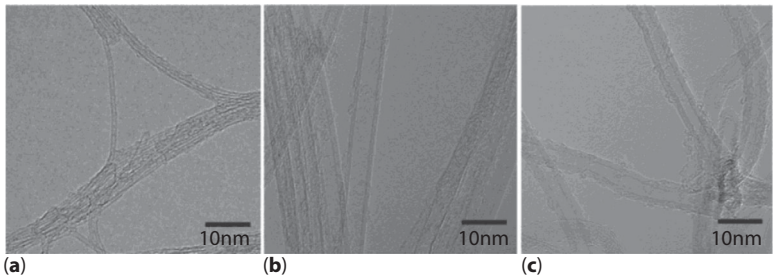

Figure 2.2 Transmission electron microscope (TEM) images of different types of CNTs. (a) Single-walled CNTs, (b) few-walled CNTs, and (c) multi-walled CNTs. Reproduced with permission from Y. Hou, J. Tang, H. Zhang, C. Qian, Y. Feng, and J. Liu, *ACS Nano*, 2009, 3, 5, 1057. © 2009, ACS [26].

biomolecules on the CNT surface leads to a change in the dielectric constant (and capacitance) of the CNTs, RF electrical measurements, particularly frequency-based measurements, can possibly be used for biosensing.

2.3.2 Fabrications of Interdigital Capacitors with Carbon Nanotube

In case of the CNT bridging the upper gap of the metal pad, it was fabricated by a patterned catalyst growth technique. First, cocatalyst islands were patterned on a SiO_2/Si substrate, and CNTs were grown by chemical vapor deposition (CVD) using a mixture of methane and argon as a carbon source at 900 °C. Next, the metal pad was formed to cover the catalyst islands. Finally, CNTs were grown in parallel with IDCs. Here, the Au pad (~0.1 μm thickness) as IDCs pattern and electrode was fabricated on heavily doped Si substrate with a 500 nm thick grown SiO_2 layer via photolithography and lift-off techniques (Figure 2.3a). Meanwhile, IDCs, which is a kind of RF passive element that produces capacitance at high frequencies, has long finger conductors to provide appropriate coupling effect between the input and output ports (Figure 2.3b). Since the conductors are mounted on a substrate, their height and dielectric constant affect the capacitors' performance. In addition, the thickness of the conductor and its resistivity also affect the electrical characteristics. For a capacitor element, its impedance behaves as would be expected from the specified capacitance

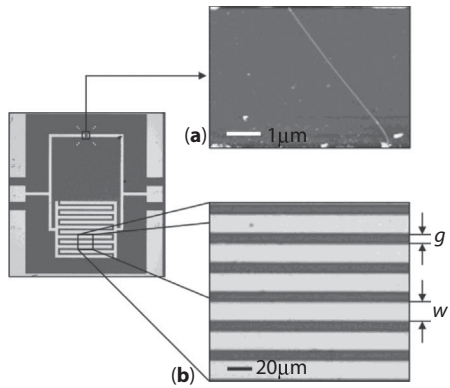

Figure 2.3 Photograph of the IDCs-based CNT biosensor. (a) Atomic force microscope (AFM) image of a CNT in the 5 um upper gap and (b) multiple finger periodic pattern in the IDCs (the gap between fingers and the width of finger are g=10 μm and w=20 μm, respectively). Reproduced with permission from H. J. Lee, H. S. Lee, H. H. Choi, K. H. Yoo and J. G. Yook, *IEEE Transactions on Nanotechnology*, 2010, 9, 6, 682. © 2010, IEEE [27].

at low frequencies. However, the capacitive and parasitic inductive impedance cancel each other out leaving only a resistive component at high frequencies. The critical frequency is so-called self-resonance frequency (SRF). Above this frequency, inductive reactance becomes dominant, as it becomes much larger than the capacitive and the resistive components.

In this work, IDCs have been designed at 10 GHz from the self-resonant formula as following:

$$f_r = \frac{1}{2\pi\sqrt{LC}} \tag{2.1}$$

where f_r is the resonant frequency, L is the parasitic inductance, and C is the designed capacitance. As a result, the IDCs-based CNT device itself can be regarded as a novel RF biosensor based on frequency change for biomolecular sensing at desired frequency.

2.3.3 Functionalization of Carbon Nanotube

To validate the performance of a CNT as a RF biosensor, CNT surface shown in Figure 2.4 has been immobilized by biomolecule as follows: first, the CNT device is placed in 6 μM 1-pyrenbutanoic acid succinimidyl ester (Aldrich) in dimethylformamide (DMF) for 1 hour under stirring and then washed with clean DMF, where 1-pyrenbutanoic acid succinimidyl ester is used as a linking molecule. The device is then immersed in phosphate-buffered saline (PBS) (Aldrich) overnight to fix the biotin molecules

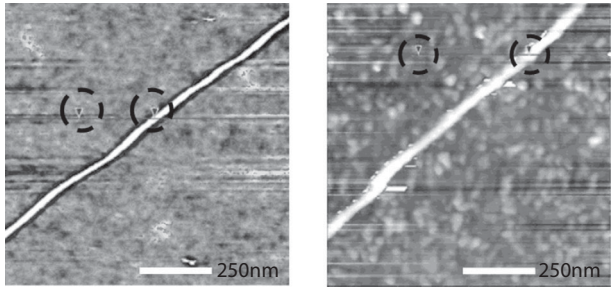

Figure 2.4 AFM image before and after immobilization onto the CNT. (a) Before immobilization and (b) after immobilization. Reproduced with permission from H. J. Lee, H. S. Lee, K. H. Yoo and J. G. Yook, *The Journal of Korean Institute of Electromagnetic Engineering and Science*, 2008, 19, 8, 1. © 2008, KIEES [28].

to the CNT surface. Finally, the freshly biotinylated device is immersed in 100 mg/ml streptavidin in PBS solution for 6 hours at room temperature. The streptavidin has been immobilized onto the CNT surface by strong intermolecular attraction with biotin.

2.3.4 Measurement and Results

Each sample was measured with an RF probe tip (40A-GSG-200-P, GGB) and a probe station system (PM5HF, Karl Suss) associated with a VNA (PNA, E8364A, Agilent). The power level is maintained at –17 dBm, and the intermediate frequency (IF) is set to 2 kHz for the VNA, and full two-port calibration has been executed with short-open-load-through calibration method using a calibration substrate (CS-5, GGB).

In this work, to validate performance of IDCs-based CNT RF biosensor, four configurations, IDCs alone, IDCs with CNT, a biotinylated CNT, and streptavidin-biotinylated CNT, have been considered and studied as follows: for the IDCs alone sample, the SRF is measured as about 10.02 GHz, and when a CNT is placed in the gap between the extended electrodes, the resonant frequency is shifted toward higher frequency of 11.02 GHz due to occurrence of an electrical short circuit. Consequently, the capacitance is very small. Thus, the resonance frequencies of the IDCs ($f_{\mathrm{Re}\,f}$) and the IDCs with CNT (f_{CNT}) are quite different and the difference ($\Delta f_{\mathrm{Re}\,f-CNT}$) is about 1 GHz. In case of the biotinylated CNT (Δf_B) and streptavidin-biotinylated CNT (Δf_S), the resonant frequency has been observed at 10.82 and 10.22 GHz, respectively. When biotin is immobilized onto CNT, the frequency is shifted by $\Delta f_{B-CNT} \approx 200$ MHz and streptavidin-biotinylated CNT, the frequency is further shifted by $\Delta f_{S-B} \approx 600$ MHz (Figure 2.5).

From the obtained results, the frequency changes can be modeled as a variation in the parasitic capacitance, inductance, and resistance over the CNT due to the two different nanosized biomolecular binding systems, which consist of a captured streptavidin layer over uniformly immobilized biotinylated onto the CNT surface.

2.4 Resonator-Based RF Biosensor

2.4.1 Resonator

In general, a resonator is a device that oscillates with the greatest amplitude at particular resonant frequencies. Therefore, it is employed to either generate waves of specific frequencies or to select specific frequencies from a signal. The resonator is a vital element in RF system because it can have

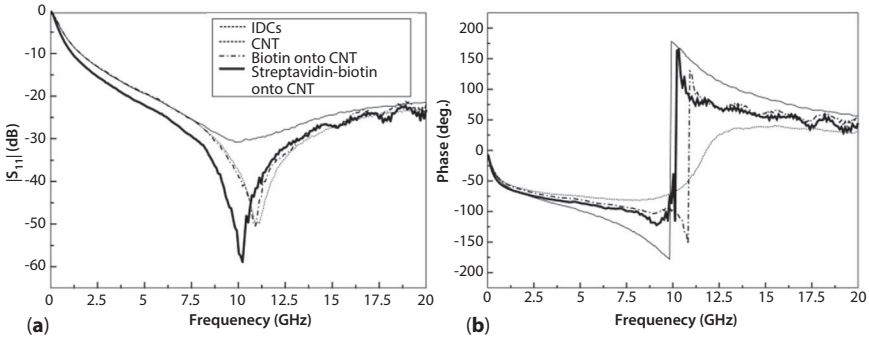

Figure 2.5 Frequency and phase response to the four configurations: IDCs (thin dot line), IDCs with CNT (thick dot line), biotinylated CNT (dot–dot line), and streptavidin-biotinylated CNT (thick solid line). (a) The change of self-resonant frequency of S11. (b) The corresponding phases. Reproduced with permission from H. J. Lee, H. S. Lee, H. H. Choi, K. H. Yoo, and J. G. Yook, *IEEE Transactions on Nanotechnology*, 2010, 9, 6, 682. ©2010, IEEE [27].

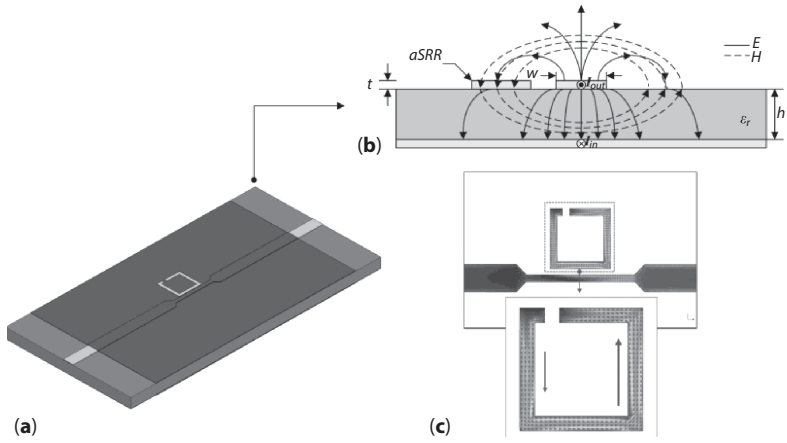

Figure 2.6 ASRR-based RF biosensor. (a) Schematic of the biosensor consisted of a resonator and a microstrip transmission line, signal line (~35 μm)/dielectric layer (0.76 mm)/ground plane (~35 μm), with a locally high-impedance line, (b) distribution of electric and magnetic fields with quasi-transverse electromagnetic mode (TEM), and (c) distribution of surface current of the resonator. Reproduced with permission from H. J. Lee, J. H. Lee, S. J. Choi, I. S. Jang, J. S. Choi, and H. I. Jung, *Applied Physics Letters*, 2013, 103, 5, 053702. © 2013, AIP [29].

characteristics to pass (or stop) want (or unwanted) signals in a frequency band. Also, the material properties can be characterized by using a high-Q resonator at microwave frequencies. With these characteristics, various resonators have been widely used as a transducer of RF biosensor. In this work, an ASRR has been received which is used for RF biosensing scheme (Figure 2.6).

In this device, an ASRR having a characteristic of high Q-factor as a biosensing transducer has been designed and, in addition, a high-impedance line (w=0.2 mm) with respect to 50 Ω matching line (w=0.72 mm) is partially used to increase the surface current intensity. The ASRR, i.e., an inductor-capacitor (LC) circuit, consisting of inductive and capacitive components, is mainly excited by time-varying magnetic field component generated by locally high-impedance line. The current mode induced by Faraday's law can occur a resonance at specific frequency due to the intrinsic ASRR structure.

2.4.2 Sample Preparation and Measurement

The sample for RF biosensor based on resonator was prepared as follows: first, photoresist (PR) is spin coated onto the surface of the substrate, and then the PR is exposed to UV through a mask. After development, the patterned substrate is etched with a wet printed circuit board (PCB) etchant, and finally, the remaining PR is removed using acetone/PR remover. Specifically, in order to use as a biosensing device, the completed copper pattern is coated with thin nickel (~3–5 μm thicknesses) as adhesion layer and finally, it is plated with gold (~0.03–0.07 μm thickness). A masking layer (~10–20 μm thicknesses) made of solder mask of PCB is also used for confinement of biomolecular binding to the surface of the target resonator, excluding the rest of the part of the resonator that is the active sensing circuit region and edge contact pads used for measurement.

2.4.3 Functionalization of Resonator

In order to functionalize the resonator, the bio-conjugation process has been performed as illustrated in Figure 2.7. First, ASRR surfaces of all samples are rinsed by pure PBS solution, and then they are immobilized with cysteine (cys) 3-mediated protein G for detection alpha-amylase biomarker. After binding between anti-α-amylase and cys3-linked protein G, bovine serum albumin (BSA) for blocking non-specific binding has been also treated. Finally, the direct reaction between α-amylase antibody and antigen was performed. All samples are rinsed three times with pure PBS to remove all the unbounded biomolecules and then dried.

Figure 2.8 shows the frequency shift due to the configuration of α-amylase concentrations, 100, 10, and 1 ng/ml. After immobilizing the cys3-mediated protein G and then accommodating α-amylase antibody, the binding surface is treated with BSA. With the BSA process, the resonant frequency is changed by approximately 32.30 MHz compared with

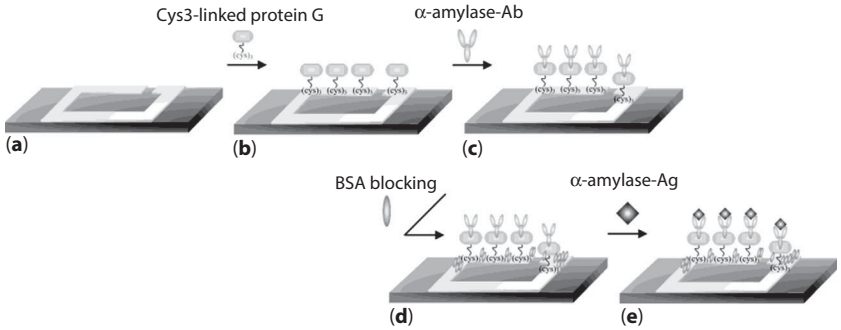

Figure 2.7 Bio-conjugation processes: (a) bare resonator, (b) cys3-linked protein G, (c) α-amylase antibody (Ab), (d) BSA blocking, and (e) α-amylase antigen (Ag). Reproduced with permission from H. J. Lee, J. H. Lee, S. J. Choi, I. S. Jang, J. S. Choi, and H. I. Jung, *Applied Physics Letters*, 2013, 103, 5, 053702. ©2013, AIP [29].

the bare sample. Finally, in case of the α-amylase antigen with different concentrations, i.e., 100, 10, and 1 ng/ml, the corresponding frequency shifts are approximately 65.38, 50.00, and 37.03 MHz, respectively. Here, the immobilized samples are measured by a test fixture system (Model 3680-20, Anritsu) associated with two-port VNA (E8364A, Agilent).

From the work, providing that the variation in the inductive and capacitive components of ASRR with the immobilization process is small, the frequency shift can be modeled with the LC-resonant formula. This phenomenon can be expressed as follows:

$$f = \frac{1}{2\pi\sqrt{LC}} \approx f_0 - \frac{f_0}{2}\left(\frac{\Delta C}{C_0} + \frac{\Delta L}{L_0}\right) = f_0 - \Delta f \tag{2.2}$$

where $L=L_0+\Delta L$ ($L0>>\Delta L$), $C=C_0+\Delta C$ ($C0>>\Delta C$), $f_0 = \frac{1}{2\pi\sqrt{L_0 C_0}}$, and $\Delta f = \frac{f_0}{2}\left(\frac{\Delta C}{C_0} + \frac{\Delta L}{L_0}\right)$. Here f_0, L_0, and C_0 are the resonant frequency, inductance, and capacitance of the bare resonator, respectively. Regarding interaction of the biomolecule with the resonator, as biomolecule is bound on the gold surface, the capacitive and inductive components of the resonator can be slightly changed and ultimately result in a resonance frequency variation. In particular, the phenomenon of frequency shift can be explained by an equivalent dielectric model of the biomolecular mono- and bilayers, namely cys3-mediated protein G with α-amylase-Ab (ε_{r1}^{err})

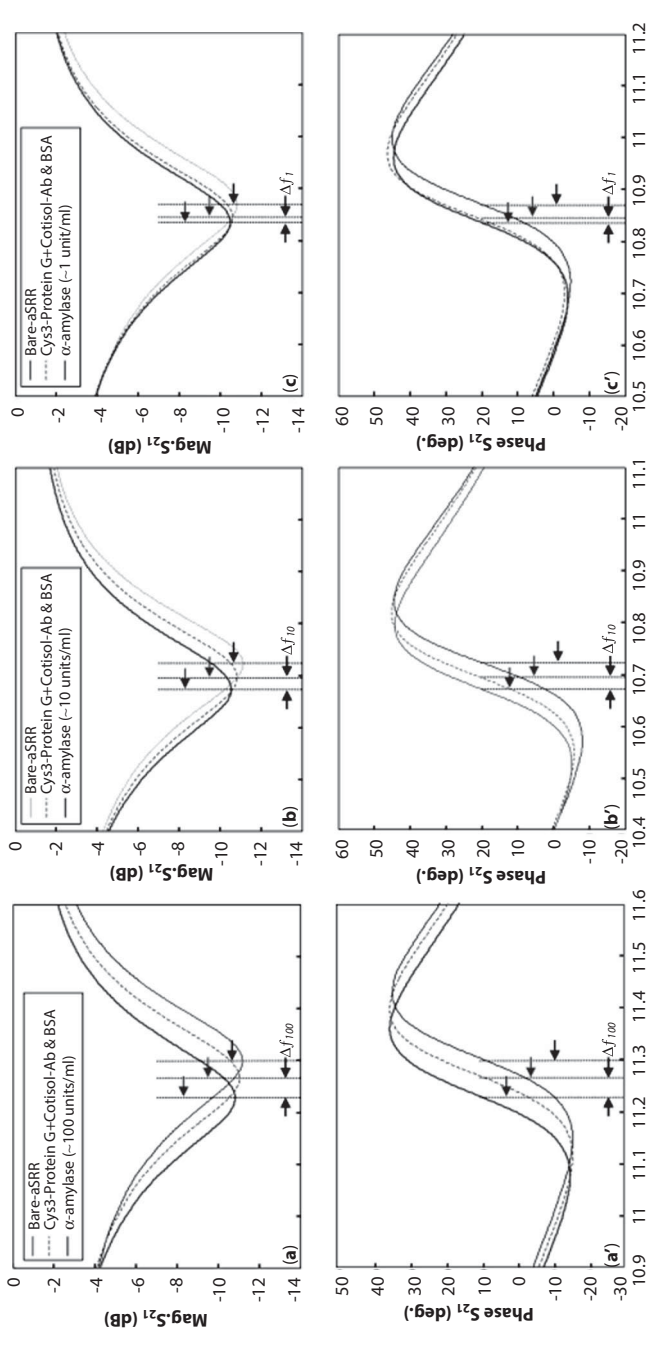

Figure 2.8 Frequency and phase response with three different concentrations. (a) Magnitude and (a′) phase of S_{21} to the 100 ng/ml, (b) magnitude and (b′) phase of S_{21} to the 10 ng/ml, and (c) magnitude and (c′) phase of S_{21} to the 1 ng/ml. Reproduced with permission from H. J. Lee, J. H. Lee, S. J. Choi, I. S. Jang, J. S. Choi, and H. I. Jung, *Applied Physics Letters*, 2013, 103, 5, 053702. ©2013, AIP [29].

and α-amylase-Ag (ε_{r2}^{err}), respectively, having different permittivity attributed to an increase in capacitance as well as in inductance of the resonator. Based on the results, the frequency as detection parameters of our device can be varied with biomolecular concentration as well as the binding and/or unbinding state.

2.5 Active System-Based RF Biosensor

2.5.1 Principle and Configuration of System

Figure 2.9a shows the operating principle of an active RF biosensing platform. The system consists of an oscillator, a surface acoustic wave (SAW) filter, and a power detector. The biosensing mechanism of the system is as follows: first, the oscillation frequency is changed by the impedance variation of the planar resonator due to the biomolecular immobilization. Here, the immobilization has an effect on the surface characteristics of the resonator, thus changing the resonator impedance components, such as resistive (R), inductive (L), and capacitive (C). Moreover, the resonator plays important roles in sensing as well as feedback component in the system. Since the target biomolecules are much smaller in size compare to the RF devices and almost weightless, the frequency deviation due to the immobilization is extremely small. As a result, with conventional circuit topologies, the detection capability was not sensitive enough for medical applications. To overcome this difficulty, a SAW filter is used at the oscillator output to increase the sensitivity of the system. Assuming that the impedance variation and resulting frequency deviation are in the locking range of the oscillator, the output amplitude of the SAW filter can be maximized in the skirt frequency region which is just outside of the pass band. As a result, even though the frequency deviation is small, the small variation can be transformed into a large voltage fluctuation and power detector is adapted at the output of the SAW filter to transform the frequency deviation of the oscillator to the variation of DC voltage. This signal can be easily digitized for additional digital signal processing. With this approach, the oscillation frequency deviation can be eventually used for biosensing. In particular, Figure 2.9b shows in detail the schematic diagram of the 2.4 GHz amplifier and cascade type resonator combined with an emitter follower-type buffer amplifier [30–32]. Here, the buffer amplifier of the emitter follower type is used to prevent a strong mutual interaction between the oscillator and the filter because the oscillation condition can be changed by the

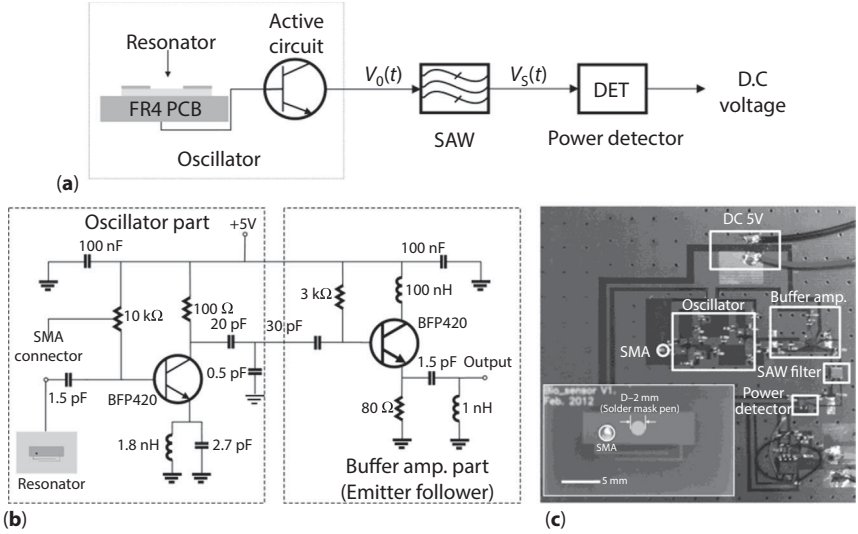

Figure 2.9 Schematic diagram of RF biosensing platform. (a) Schematic of the biosensing platform, (b) layout of fabricated resonator and system, and (c) schematic of oscillator and buffer amplifier. Reproduced with permission from S. G. Kim, H. J. Lee, J. H. Lee, H. I. Jung, and J. G. Yook, *Biosensors and Bioelectronics*, 2013, 50, 0, 362. © 2013, Elsevier [33].

rapid impedance variation at the skirt frequency range of the SAW filter. Figure 2.9c represents sample of active system with resonator, respectively.

2.5.2 Fabrication of RF Active System with Resonator

2.5.2.1 Functionalization of Resonator

In order to verify the feasibility of the biosensing device, the biotin–streptavidin and DNA hybridization are used. Figure 2.10 shows conceptual biological binding process for immobilization on gold surface. Here, thiols (–SH)-linked biotin and single-stranded deoxyribonucleic acid (ssDNA) is used because the thiols substrate can enhance the sensitivity as well as selectivity, and can specify chemically modified gold surface; thus, it has been widely used as a biological receptor of many gold-based biosensors [34–36]. In this work, the biological process is as follows: in case of biotin–streptavidin binding, first, all samples are simultaneously immobilized with 25 μg/ml concentration of biotinylated thiols in deionized (DI) water for about 1 hour. Next, to deactivate and block the excess reactive groups remaining on the surface, the devices are treated with BSA of 25 μg/ml concentration for about 1 hour. Finally, the biotin has been coupled with

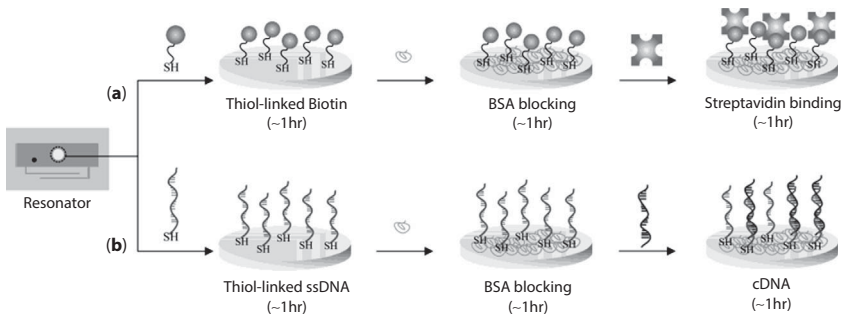

Figure 2.10 Bio-conjugation processes: (a) biotin–streptavidin: thiol-linked biotin (first step), BSA blocking (second step), and streptavidin binding (third step). (b) DNA hybridization: thiol-linked biotin (first step), BSA blocking (second step), and cDNA binding (third step). Reproduced with permission from S. G. Kim, H. J. Lee, J. H. Lee, H. I. Jung, and J. G. Yook, *Biosensors and Bioelectronics*, 2013, 50, 0, 362. © 2013, Elsevier [33].

different streptavidin concentration, i.e., 100, 10, and 1 ng/ml in DI water about 1 hour. Similarly, the biological process of DNA hybridization has been progressed with the same method as the biotin–streptavidin system. All samples are immobilized with 25 μg/ml concentration of thiol-linked ssDNA (5′-CTA gAA TTC TgC CAC TTT ATA CAT TCC-3′) in PBS water for about an hour. After treating with BSA, the ssDNA is coupled with three different complementary deoxyribonucleic acid (cDNA) (5′-ggA ATg TAT AAA gTg gCA gAA TTC TAg-3′) concentrations, i.e., 100, 10, and 1 ng/ml in PBS for about 1 hour. Finally, after washing with pure DI water or PBS, the samples are measured with the proposed measurement system.

2.5.3 Measurement and Result

Before starting the biological process, the effect of frequency deviation with DI solution on the resonator has been tested. Three samples are used, and each sample is measured five times for oscillation frequency deviation. After drying process, the measured samples show slight differences compared to bare samples. However, it is found that the DI solution causes minimal effect on oscillation frequency deviation. The other samples (15) have been also prepared for biological process, and each sample is measured five times for the variations of oscillation frequency, SAW filter output power, and the power detector output voltage for each biomolecule. Figure 2.11a–c shows the measured results of the aforementioned sensing parameters for thiols-linked biotin and streptavidin with different concentration levels of streptavidin and cDNA. Each sensing parameter

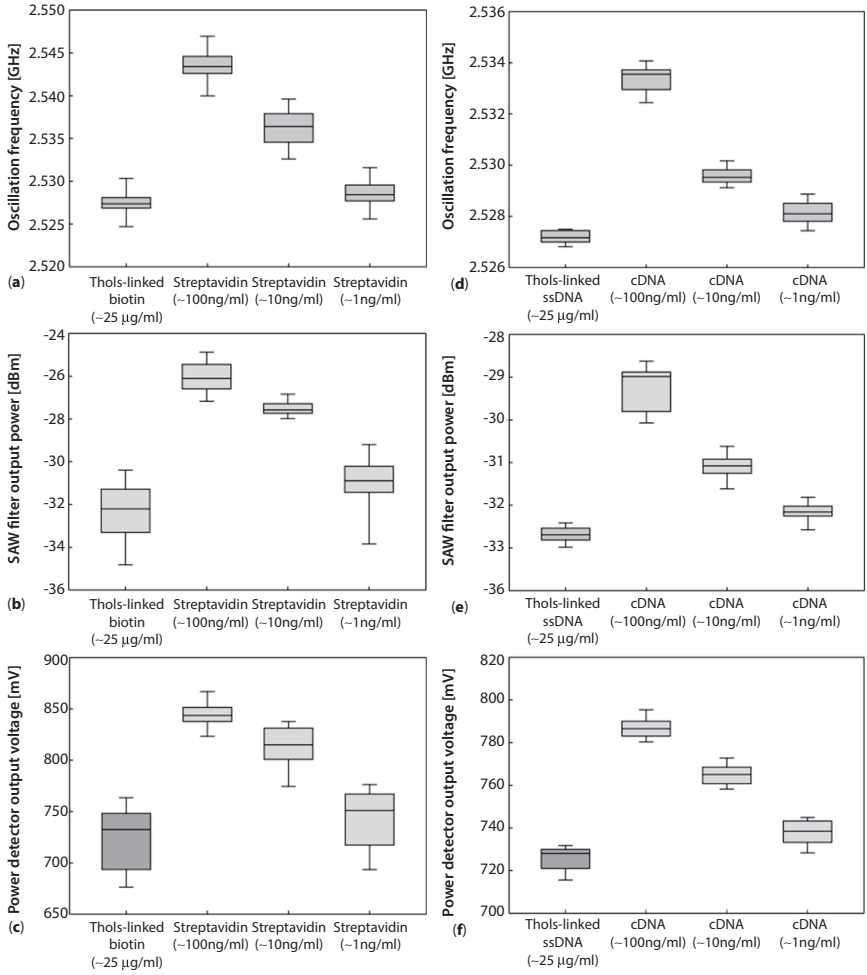

Figure 2.11 Frequency, amplitude, and voltage as the biomolecular immobilization. (a) Oscillation frequency deviation, (b) output power, and (c) power detector of the biotin–streptavidin binding system. (d) Oscillation frequency deviation, (e) output power, and (f) power detector of the DNA hybridization system. Reproduced with permission from S. G. Kim, H. J. Lee, J. H. Lee, H. I. Jung, and J. G. Yook, *Biosensors and Bioelectronics*, 2013, 50, 0, 362. © 2013, Elsevier [33].

of biotinylated thiols exhibits smaller variation compared to the streptavidin with different concentration levels, i.e., 100, 10, and 1 ng/ml. This is a reasonable result because biotin (~647 Da) (NanoScience, Inc.) is lower weight mass than streptavidin (~55 kDa) (Jackson ImmunoResearch Laboratories, Inc.). Meanwhile, Figure 2.11d–f also shows the measured results of the sensing parameters for thiols-linked ssDNA and cDNA with

different concentrations. Similarly, the thiols-linked ssDNA shows smaller variation compare to the sensing parameters of cDNA with different concentration levels.

In this work, ssDNA (~8.1 kDa) and cDNA (~8.4 kDa) (Bio Basic Canada, Inc.) for DNA hybridization have been used. In particular, even though the difference in weight mass between the ssDNA and cDNA is not large, the biosensing system clearly shows the discrimination for the DNA hybridization. From the obtained results, it is found that the sensing parameters exhibit approximately linear shifts in logarithm scale with three different streptavidin as well as cDNA concentration levels. Thus, it is clearly demonstrated that our system associated with oscillator is able to detect ng/ml concentration level (limit of detection ~1 ng/ml). The average variations of each sensing parameter for four different configurations, i.e., biotinylated, biotin–streptavidin, ssDNA and cDNA, are summarized in Table 2.1. According to Table 2.1, the biotinylated thiols and thiols-linked ssDNA with the same concentration (~25 μg/ml) show similar variation to three sensing parameters. This is due to the use of the same thiols substrate for two antibodies. In case of target biomolecules, i.e., streptavidin and cDNA, streptavidin shows the larger variation compared to the cDNA because of weight mass difference between two biomolecules.

2.6 Conclusions

Recent advances in the developing area of biomolecular detection using RF passive components as well as active systems have been summarized. In particular, for the CNT-IDCs component-based biosensor, the biomolecule-conjugated CNT is compatible for a biosensing configuration; however, it is very difficult in terms of fabrication and reproducibility of samples. Moreover, to detect a specific analyte, functionalize on CNT surface is necessary, and it is a time-consuming process, and high-priced equipment are required. Fortunately, although the resonator-based RF biosensor could reduce somewhat the above mentioned problems, it should be still required for high-Q resonators with high-priced equipment at microwave frequencies. In recent years, when the passive component, e.g., resonator, was associated with RF system, it is demonstrated that the sensitivity of the RF biosensor could be improved compared to the only resonator-based RF biosensor. Actually, the biosensing platform based on the RF active system having a low-Q resonator has been successfully demonstrated by using biotin–streptavidin and DNA hybridization binding systems. From the study, it is found that the sensitivity of RF

Table 2.1: Summary of experimental results.

Configurations		**Biotinylated thiols (~25 ug/ml)**	**Streptavidin, (100), (10), (1)**			**Thiols-linked ssDNA (~25ug/ml)**	**cDNA, (100), (10), (1)**		
Oscillation frequency deviation (MHz)	Max.	10.4	27.1	19.6	11.7	7.5	14.1	10.1	8.9
	Avg.	7.5	23.5	16.5	8.6	7.2	13.4	9.6	8.1
	Min.	4.5	19.8	12.6	5.4	6.8	12.4	9.1	7.4
SAW output power variation (dBm)	Max.	9.5	15.0	12.4	10.7	7.4	11.2	9.2	8.0
	Avg.	7.5	13.8	12.2	8.6	7.1	10.6	8.7	7.6
	Min.	4.9	12.6	11.8	5.7	6.9	9.7	8.4	7.3
Power detector voltage variation (mV)	Max.	184	288	258	197	152	216	193	165
	Avg.	144	264	235	165	146	207	185	158
	Min.	96	242	193	111	135	201	178	148

Reproduced with permission from S. G. Kim, H. J. Lee, J. H. Lee, H. I. Jung, and J. G. Yook, *Biosensors and Bioelectronics*, 2013, 50, 362. © 2013, Elsevier [33].

biosensing platform can be sufficiently improved under developing a novel active system as well as biosensing devices. According to the recent works of RF biosensor, it is expected that the system level biosensing device with various nanomaterials for enhancing performance can have been actively developed. It is clear that to realize a robust RF biosensing platform for biomedical, industrial, environmental applications, it still leaves lots of room for improvements, such as liquid sensing, real-time monitoring, extremely low detectable limit up to pg/ml level, and so on.

Abbreviations

AC	Alternating current
AFM	Atomic force microscope
ASRR	Asymmetric split-ring resonator
BSA	Bovine serum albumin
cDNA	complementary deoxyribonucleic acid
CNT	Carbon nanotube
CPW	Coplanar waveguide
CVD	Chemical vapor deposition
DC	Direct current
DI	Deionized
DMF	Dimethylformamide
DNA	Deoxyribonucleic acid
DR	Dielectric resonator
FET	Field-effect transistor
IDCs	Interdigital capacitors
IF	Intermediate frequency
MEMS	Micro-electromechanical system
PCB	Printed circuit board
PBS	Phosphate-buffered saline
PR	Photoresist
RF	Radio-frequency
RFID	Radio-frequency identification
SAW	Surface acoustic wave
ssDNA	Single-stranded deoxyribonucleic acid
SRF	Self-resonance frequency
TEM	Transmission electron microscope
VNA	Vector network analyzer

References

1. B. R. Eggins in *Biosensors: An Introduction*, John Wiley & Sons, New York, USA, 1996. [In English]
2. H. J. Lee and J. G. Yook, "Biosensing using split-ring resonators at microwave regime", *Applied Physics Letters*, 92(25), 254103, 2008.
3. H. J. Lee, H. S. Lee, K. H. Yoo and J. G. Yook, "DNA sensing using split-ring resonator alone at microwave regime", *Journal of Applied Physics*, 108(1), 014908.
4. H. J. Lee, J. H. Lee and H. I. Jung, "A symmetric metamaterial element-based RF biosensor for rapid and label-free detection", *Applied Physics Letters*, 99(16), 163703, 2011.
5. H. J. Lee, J. H. Lee, H. S. Moon, I. S. Jang, J. S. Choi, J. G. Yook and H. I. Jung, "A planar split-ring resonator-based microwave biosensor for label-free detection of biomolecules", *Sensors and Actuators B: Chemical*, 169(26), 2012.
6. R. Buchli, M. Saner, D. Meier, E. B. Boskamp and P. Boesiger, "Increased RF power absorption in MR imaging due to RF coupling between body coil and surface coil", *Magnetic Resonance in Medicine*, 9(1), 105, 1989.
7. G. X. Shen, F. E. Boada and K. R. Thulborn, "Dual-frequency, dual-quadrature, birdcage RF coil design with identical B1 pattern for sodium and proton imaging of the human brain at 1.5T", *Magnetic Resonance in Medicine*, 38(5), 717, 1997.
8. X. Zhang, K. Ugurbil and W. Chen, "Microstrip RF surface coil design for extremely high-field MRI and spectroscopy", *Magnetic Resonance in Medicine*, 46(3), 443, 2001.
9. R. H. Farahi, T. L. Ferrell, A. Guiseppi-Elie and P. Hansen, IEEE NIH Life Science Systems and Applications Workshop (LISA), pp. 27–30, 2007.
10. N. Sun, Y. Liu, H. Lee, R. Weissleder and D. H. Ham, "CMOS RF biosensor utilizing nuclear magnetic resonance", *IEEE Journal of Solid-State Circuits*, 44(5), 1629, 2009.
11. B. D. Malhotra and A. Chaubey, "Biosensors for clinical diagnostics industry", *Sensors and Actuators B: Chemical*, 91(1), 117, 2003.
12. Y. I. Kim, T. S. Park, J. H. Kang, M. C. Lee, J. T. Kim, J. H. Park and H. K. Baik, "Biosensors for label free detection based on RF and MEMS technology", *Sensors and Actuators B: Chemical*, 119(2), 592, 2006.
13. Q. Chen, D. Roitman and A. Knoesen, "Detection of biomolecular surface interactions by transit time measurement with a coplanar probe", *Sensors and Actuators A: Physical*, 152, 151, 2009.
14. J. H. Chien, P. H. Chen, L. S. Kuo, C. S. Lin and H. Wang, "Protein detection using a radio frequency biosensor with amplified gold nanoparticles", *Applied Physics Letters*, 91(14), 143901, 2007.
15. K. S. Saravan, O. Gul, H. Basaga, U. Sezerman and Y. Gurbuz, "Label-free biosensors for the detection and quantification of cardiovascular risk markers", *Sensor Letters*, 6(6), 873, 2008.

16. C. H. Yang, L. S. Kuo, P. H. Chen, C. R. Yang and Z. M. Tsai, "Development of a multilayered polymeric DNA biosensor using radio frequency technology with gold and magnetic nanoparticles", *Biosensors and Bioelectronics*, 31(1), 349, 2012.
17. J. Kim, A. Babajanyan, A. Hovsepyan, K. Lee and B. Friedman, "Microwave dielectric resonator biosensor for aqueous glucose solution", *Review of Scientific Instruments*, 79, 086107, 2009.
18. C. Dalmay, M. Cheray, A. Pothier, F. Lalloue, M. O. Jauberteau and P. Blondy, "Ultra sensitive biosensor based on impedance spectroscopy at microwave frequencies for cell scale analysis Ultra sensitive biosensor based on impedance spectroscopy at microwave frequencies for cell scale analysis", *Sensors and Actuators A: Physical*, 162(2), 189, 2010.
19. C. Dalmay, A. Pothier, M. Cheray, F. Lalloue, M. O. Jauberteau and P. Blondy, "Label-free RF biosensors for human cell dielectric spectroscopy", *International Journal of Microwave and Wireless Technologies*, 1(6), 497, 2010.
20. G. Gruner, "Carbon nanotube transistors for biosensing applications", *Analytical and Bioanalytical Chemistry*, 384(2), 322, 2006.
21. A. Star, E. Tu, J. Niemann, J. -C. P. Gabriel, C. S. Joiner and C. Valcke, "Label-free detection of DNA hybridization using carbon nanotube network field-effect transistors", *Proceedings of the National Academy of Sciences*, 103(00), 921, 2006.
22. C. -W. Wang, C. -Y. Pan, H. -C. Wu, P. -Y. Shi, C. -C. Tsai, K. -T. Liao, L. -L. Lu, W. -H. Hsieh, C. -D. Chen and Y. -T. Chen, "In situ detection of chromogranin a released from living neurons with a single-walled carbon-nanotube field-effect transistor", *Small*, 3(8), 1350, 2007.
23. K. Bestemann, J. -O. Lee, F. G. M. Wiertz, H. A. Heering and C. Dekker, "Enzyme-coated carbon nanotubes as single-molecule biosensors", *Nano Letters*, 3(6), 727, 2003.
24. R. J. Chen, H. C. Choi, S. Bansaruntip, E. Yenilmez, X. W. Tang, Q. Wang, Y. L. Chang and H. J. Dai, "An investigation of the mechanisms of electronic sensing of protein adsorption on carbon nanotube devices", *Journal of the American Chemical Society*, 126(5), 1563, 2004.
25. X. Tang, S. Bansaruntip, N. Nakayama, E. Yenilmez, Y. -I, Chang and Q. Wang, "Carbon nanotube DNA sensor and sensing mechanism", *Nano Letters*, 6(8), 1632, 2006.
26. Y. Hou, J. Tang, H. Zhang, C. Qian, Y. Feng and J. Liu, "Functionalized few-walled carbon nanotubes for mechanical reinforcement of polymeric composites", *ACS Nano*, 3(5), 1057, 2009.
27. H. J. Lee, H. S. Lee, H. H. Choi, K. H. Yoo and J. G. Yook, "An RF circuit model for interdigital capacitors-based carbon nanotube biosensors", *IEEE Transactions on Nanotechnology*, 9(6), 682, 2010.
28. H. J. Lee, H. S. Lee, K. H. Yoo and J. G. Yook, "A study on biomaterial detection using single-walled carbon nanotube based on interdigital capacitors", *The Journal of Korean Institute of Electromagnetic Engineering and Science*, 19(8), 1, 2008.

29. H. J. Lee, J. H. Lee, S. J. Choi, I. S. Jang, J. S. Choi, and H. I. Jung, "Asymmetric split-ring resonator-based biosensor for highly sensitive and label free stress biomarkers", *Applied Physics Letters*, 103(5), 053702, 2013.
30. M. Regis, O. Llopis and J. Graffeuil, "Nonlinear modeling and design of bipolar transistors ultra-low phase-noise dielectric-resonator oscillators", *IEEE Transactions on Microwave Theory and Techniques*, 46(10), 1589, 1998.
31. K. Grenier, D. Dubuc, P. E. Poleni, M. Jumemura, H. Toshiyochi, T. Fujii and H. Fujita, IEEE Radio and Wireless Symposium, pp. 523–526, 2010.
32. A. Takaoka and K. Ura, "Noise analysis of nonlinear feedback oscillator with AM-PM conversion coefficient", *IEEE Transactions on Microwave Theory and Techniques*, 28(6), 654, 1980.
33. S. G. Kim, H. J. Lee, J. H. Lee, H. I. Jung and J. G. Yook, "A highly sensitive and label free biosensing platform for wireless sensor node system", *Biosensors and Bioelectronics*, 50, 362, 2013.
34. M. Frasconi, F. Mazzei and T. Ferri, "Protein immobilization at gold–thiol surfaces and potential for biosensing", *Analytical and Bioanalytical Chemistry*, 398(4), 1545, 2010.
35. J. H. Seo, K. Adachi, B. K. Le, D. G. Kang, Y. K. Kim, K. R. Kim, H. Y. Lee. T. Kawai and H. J. Cha, "Facile and rapid direct gold surface immobilization with controlled orientation for carbohydrates", *Bioconjugate Chemistry*, 18(6), 2197, 2007.
36. G. Carpini, F. Lucarelli, G. Marrazza and M. Mascini, "Oligonucleotide-modified screen-printed gold electrodes for enzyme-amplified sensing of nucleic acids", *Biosensors and Bioelectronics*, 20(2), 167, 2004.

3

Affinity Biosensing: Recent Advances in Surface Plasmon Resonance for Molecular Diagnostics

S. Scarano, S. Mariani, and M. Minunni*

Dipartimento di Chimica "Ugo Schiff", Università degli Studi di Firenze, Sesto Fiorentino (FI), Italy

Abstract

Molecular diagnostics is defined as the use of biological markers, spanning from nucleic acids to proteins and small molecules, to test for specific states of health or diseases, possibly their progression, as well as the assessing of the risk of their development by a prognostic molecular profiling. Molecular diagnostics may eventually aid to finalize the best therapy for a given individual patient, that is, the ability to provide tailored therapies through the analysis of the patient's molecular specificity related to its disease. Biosensing represents at present an interesting tool for applications to molecular diagnostics. In particular, in the past years, many attempts have been devoted to apply different label-free transduction principles such as conventional surface plasmon resonance (SPR) and SPR imaging (SPRi) for the analysis of biomarkers in real matrices.

This chapter will deal with the main aspects to be considered in the development of innovative ultrasensitive, and label-free biosensors for molecular diagnostics. In particular, the identification/selection of the suitable bioreceptors and the signal sampling and management of the interaction between the biomarker (analyte) and the bioreceptors are two key aspects to take into account. The proper immobilization chemistry applied for biomolecules tethering on the sensing surface is an additional point, especially in order to reduce possible matrix effects in real samples and to allow the biosensor reuse. Finally, strategies for signal enhancement aimed to improve system sensitivity will be also considered in this chapter, and examples of some application to protein and DNA analysis in human specimens will be also provided.

**Corresponding author*: maria.minunni@unifi.it

Ashutosh Tiwari, Hirak K. Patra and Anthony P.F. Turner (eds.) Advanced Bioelectronic Materials, (55–88) © 2015 Scrivener Publishing LLC

***Keywords*:** Affinity biosensors, surface plasmon sesonance (SPR), surface plasmon resonance imaging, optical biosensors, molecular diagnostics, clinical analysis

3.1 Introduction

In 1991, the Pharmacia Biosensors AB, a Swedish company from Pharmacia AB, promoted the first surface plasmon resonance (SPR)-based commercial instrumentation, appearing at the global research world as novel exciting technology created by the efforts of many scientists (physicians, engineers, computer technicians, chemists, and biologists) who worked at the different aspects of the instrumental development as detection strategies, immobilization strategies, data analysis for kinetics aspects, and microfluidics and microsystems management.

Following SPR activity at their research laboratory in Uppsala, Sweden, at early 1990s where just few publications were available, mainly from the researchers developing the first Biacore instrument, it is particularly impressive for us to realize how far this technique went and how many applications to different fields have appeared during almost 25 years.

Since that beginning with few application examples in immunochemistry, a long trip started and many scientists joined the technology to test new applications, mainly in drug discovery and biochemistry/molecular biology. Up to now almost 80,000 publications are reported by ISI Web of Knowledge [v5.13.1], and if we analyze more in detail the distribution of the topics, the technology impacts most on chemistry, physics, biochemistry/molecular biology, engineering, and material science.

In parallel, new devices based on SPR were introduced on the market, eventually portable and more recently coupled to imaging technology [SPR imaging (SPRi)] allowing multi-analyte detection [1]. This allowed one to afford the SPR technology also with relatively low budgets, eventually facilitating its diffusion to a wider public of potential users.

Looking with the eye of an analytical chemist, we can say that, among papers dealing with SPR and SPRi-based sensing for the sensitive detection of pollutants in environmental, food, and pharmaceutical analysis, molecular diagnostics is the most explored and fertile application area. Molecular diagnostics exploits information inferred from biological markers, spanning from nucleic acids to proteins and small molecules, for diseases revealing or monitoring, patients' risk evaluation, and therapy choice for specific diagnosed diseases [2].

In this book chapter, we report and discuss the most recent advances in SPR-based biosensing (SPR and SPRi) for molecular diagnostics applications, focusing on the key points mandatory to set up effective detection strategies. Each issue includes a brief outline of the fundamental methods and approaches, to go deeper inside the most recent and challenging research on the issue. In particular, the first part of the chapter is focused on bioreceptors and their selection, including the most promising synthetic bioreceptors such as aptamers and plastic antibodies. Among emerging natural receptors, room is dedicated also to living cells, considered a very promising research area applied to optical biosensors.

First of all, depending on the analytical problem to be solved, i.e., the kind of analyte (small targets or macromolecules, proteins, or nucleic acids) and the matrix to be analyzed should be defined and the relative level of analyte concentration to design the best receptor (biological or biomimetic) to be used and the most suitable strategy (direct, sandwich, or competitive assay) for its detection. If necessary, a dedicated sample pretreatment should be considered if matrix effects could be present or if desired sensitivity difficult to be achieved.

Once identified the suitable bioreceptor for a purpose, the following key step is its immobilization on the biochip, and new bioreceptors require increasingly new strategy for their tethering on the substrate (typically a glass prism coated with a gold/silver thin layer). New emerging immobilization approaches for application to molecular diagnostics are reported, pointing out specific requirements of different classes of bioreceptors. Once selected the bioreceptor, it has to be properly immobilized on the surface, meaning with this that it has to retain its ability to recognize the analyte and to bind it, and at the same time, immobilization should prevent unspecific interaction with the gold surface to avoid unspecific contribution to the SPR signal.

The quality of the biochip preparation (proper selection of receptor combined with an effective immobilization chemistry) is undoubtedly the first step defining the limit of the analytical performance of the biosensor in terms of obtainable detection limit, specificity, and reproducibility of the result. As example, in the development of genosensors, the first key step is the selection of suitable and performing nucleotide sequences to assure the best biosensor analytical performances. Differently from immunobased approaches, in which the choice is confined to available antibodies, a genosensor can be highly personalized through the selection of the desired nucleic acid sequence. Thus is of key importance the evaluation of its characteristics during a pre-analytical study aimed to the selection of the best performing detecting sequence. We recently demonstrated that advantages

in terms of analytical performances can be addressed by applying a rational procedure for the selection of the DNA sequence to be used as primary receptor [3]. Further improvement of the analytical performances can be addressed by the rational sampling of the SPR signal [4–5], mainly in case of SPRi, and by playing with the use of additional detection strategies, such as the use of mass enhancers [i.e., sandwich-based assays, *in situ* DNA amplification by molecular architectures and enzymatic activity, use of functionalized nanoparticles (NPs), etc.]. Therefore, the second part of the chapter is centered on new methods for signal sampling and, finally, new tends for the enhancement of the SPR signal for molecular diagnostics purposes.

3.2 Artists of the Biorecognition: New Natural and Synthetic Receptors as Sensing Elements

Affinity biosensors can be defined as biosensors using as recognition element a receptor that binds the target analyte by an affinity interaction. In this category fall antibody–antigen interactions, hybridization between nucleic acids, (membrane or cellular) receptor-ligand binding, and more recently biomimetic or synthetic receptors, obtained by molecularly imprinted technology (MIP, or plastic antibodies), combinatorial selection (aptamers), and protein engineering (affibodies).

3.2.1 Antibodies and Their Mimetics

Immunosensors appeared in the early 1990s coupled to SPR transduction for a different variety of analytes of clinical interest thanks also to the contribution of worldwide groups involved in the development of new and performing monoclonal and polyclonal antibodies of clinical interest [6–8]. An antigen-specific antibody "fits" its unique antigen (or hapten molecule) in a highly specific manner. This unique property of antibodies is the key to their usefulness in immunosensors where only the specific analyte of interest, the target analyte, should bind the corresponding antibody-binding site. In contrast to classical immunoassays, like enzyme-linked immunosorbent assay (ELISA) and radio immunoassay (RIA), affinity-based SPR immunosensors display several advantages, spanning from the label-free and real-time detection of the analyte in few minutes, the reuse of the same receptor surface for many measurements, and the chance of monitoring up to tens of different interactions on the same biochip, which might imply an extremely important advantage of the immunosensor compared

to commercial kit immunoassays. One among the others, the possibility offered by real-time monitoring of the interaction to evaluate very easily the kinetic parameters of the interaction (association and dissociation rate constants (k_a and k_d), and form their ration the affinity constant (K_A and K_D) of the complex).

Generally, the approaches used in assays to develop affinity immunosensors both for small or high Molecular Weight (MW) analytes use essentially other heterogeneous phase immunoassays such as ELISA or RIA formats (direct, competitive, sandwich) but without using enzyme labeling. For high MW analytes, greater than 600 Daltons, direct assays can be applied by immobilizing the primary antibody (preferable monoclonal and tethered by exposing the specific Fab portion to the bulk) on the chip surface and by detecting the binding signal of the analyte after its injection in the system. This simple and direct approach may be coupled to a secondary suitable antibody able to bind the same target on a different epitope and enhance the SPR signal, i.e., the so-called sandwich strategy, in analogy to ELISA tests. In competitive assays, suitable for low MW analytes (below 600 Da), the analyte or its conjugate is immobilized on the chip and the bioreceptor, i.e., the specific antibody (primary receptor), added in solution, competing for the bound target molecule and the one (analyte) in the sample solution. In the perspective to enhance the sensor signals, molecular architectures can be built on the chip, by using affinity ligands able to recognize specifically molecules on the surface. This is the case of streptavidin alone or conjugated with gold NPs or with magnetic NPs, able to bind biotin with high affinity present eventually in biotinylated Ab. Also, anti-whole Ab, specific for the immunoglobulin source used (mouse, rabbit, IgG, etc.) as primary receptor can be used as secondary mass enhancers molecules, together with proteins A and G, this latter binding the Fc portion of the Ab. Eventually, Fab fragment (the recognizing portion of the Ab) has also been used in the development of immunosensors, but this fragment misses the Fc part thus mass enhancement cannot be performed in the aforementioned way (with protein A or G).

Thanks to advancements in molecular engineering and microbial expression, novel highly performing antibodies are now available, with improved binding properties (affinity, specificity, stability, etc.). Analytical systems for biomedical applications include a wide range of analytes commencing from small molecular substances such as glucose, neurotransmitters cofactors, and polypeptides (hormones) to high-molecular-weight proteins, DNA and RNA fragments and even alive virus or bacteria [9]. SPR immunosensors remain solid, actual, and fast evolving thanks to the development of ever new engineered antibodies for a huge number of emerging hapten

molecules (acting as biomarkers in molecular diagnostics). Nevertheless, in past decades, we assisted to the increasing appearance of mimetic synthetic receptors (bio- or not) that can be exploited in place of engineered antibodies. Among these, affibodies (developed and produced by Affibody AB, Sweden) are small synthetic peptides, considered antibody mimetics, applied both as alternative receptors and for diagnostics and therapeutics purposes [10]. By SPR-based biosensors, engineered variants of affibody molecules have proved their usefulness in understanding metal-binding and other properties of monomeric Aβ and Cu(II) under various physiological conditions [11], contributing to understand basic molecular mechanisms involved in Alzheimer's disease (AD) [12]. Multi-parametric affibody-based SPR biosensor using six bispecific affibody-based receptors was developed for the simultaneous detection of the two human epidermal growth factor (EGF) receptors, EGFR and HER2, respectively [13]. A so-called affitoxin, a novel class of HER2-specific cytotoxic molecules combining HER2-specific affibody molecule as a targeting moiety and a cell killing agent (PE38KDEL, a truncated version of *Pseudomonas* exotoxin A9) was recently reported, demonstrating that affitoxin could be an attractive candidate for treatment of HER2-positive tumors [14]. Synthetic binding sites of biological receptors are similarly exploited in SPR-based affinity biosensor, as the case of our recent work aimed to the comparison of the analytical performances of an antibody anti-human Hepcdin-25 and a short synthetic peptide mimicking the natural binding site of hepcidin on ferroportin [15].

Appeared in 1990s, aptamers are short DNA- and RNA-based nucleic sequences selected *in vitro* by SELEX (Systematic Evolution of Ligands by EXponential enrichment), which are still intensely selected and applied to biosensing for molecular diagnostics purposes [16, 17]. Their features make them intriguing and valid rivals of antibodies, since they possess several key advantages over their protein counterparts. Aptamers are self-refolding in the optimal binding conformation, so that binding activity is guaranteed; they are DNA or DNA single-chain sequences lacking the large hydrophobic cores of proteins and thus do not aggregate; they are redox insensitive and also tolerate (or recover from) pH and temperatures that proteins do not. They are easier and more economical to produce (especially at the affinity reagent scale) because are made through a well defined and highly reproducible chemical synthesis, which does not depend on bacteria, cell cultures or animals as for antibodies production. In contrast to antibodies, toxicity and low immunogenicity of particular antigens do not interfere with the aptamer selection. Further, highly custom or "orphaned" targets

can be addressed rapidly and cheaply. They can easily be modified chemically to yield improved, custom tailored properties.

Among pioneering aptamers for molecular diagnostics, undoubtedly aptamers selected for thrombin are one of the most successful case [18–21]. Recent advancements in applying aptamers for thrombin detection via SPR involve aptamer-based sandwich assays in which a primary aptamer acts as receptor (immobilized on the gold biochip) and, after its binding to the target molecule, the analytical performance of the instrumental response is gained by the binding of a secondary aptamer able to bind thrombin already captured by the primary receptor. The mass enhancement if further improved by the presence of gold NPs on the secondary aptamer (strategy here addressed in the dedicated paragraph), see Figure 3.1.

Other target molecules of clinical interest investigated by SPR aptasensors are immunoglobulin E [22], C-reactive protein [23], retinol binding protein 4, small molecules as adenosine, vascular endothelial growth factor (VEGF) [24], hemagglutinin (HA) of human influenza virus, nicotinamide phosphoribosyl transferase (Nampt [25]), eukaryotic initiation factor 4A (eIF4A) [26], and more [27–29].

After about two decades of research in field of molecular imprinting, MIP are nowadays a well-known product applied to a large variety of purposes, from solid-phase extraction in chromatography and electrophoresis [30], to drug delivery [31] and biosensing. For biosensing applications, MIP generally play the role of synthetic elements able to mimic natural recognition entities, such as antibodies and biological receptors. The key features of MIP as sensing elements alternative to antibodies have been extensively reviewed [32–34], also referred to SPR-based biosensing (35–40). Plastic antibodies for clinical applications (or related to) have been reported, by SPR-based sensing, for detection of sialic acid containing ganglioside GM1 in aqueous media [41], for the combined assay of theophylline, caffeine,

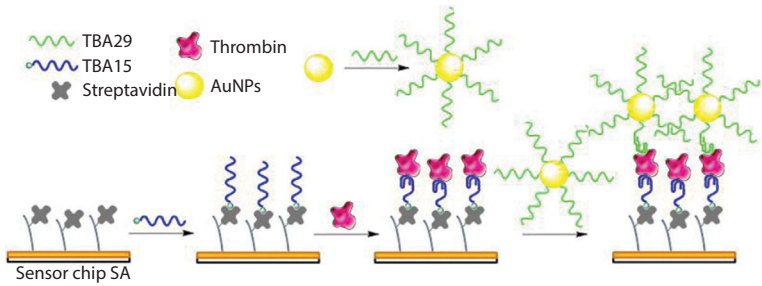

Figure 3.1 Schematic representation of AuNPs-enhanced SPR aptasensor for thrombin detection.

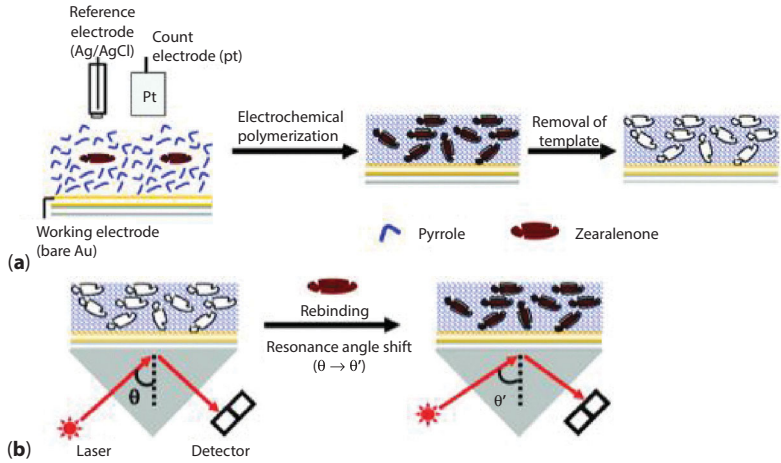

Figure 3.2 Schematic diagrams of the setup for electropolymerization and SPR for detecting zearalenone. (a) Preparation of molecularly imprinted polypyrrole on bare Au using a three-electrode electrochemical system. (b) The shift in resonance angle of the SPR sensor resulting from the rebinding of zearalenone to the MIPPy film.

and xanthine [42], domoic acid (veterinary interest [43]), lysozyme [44], ochratoxin A [45], and mycoestrogen zearalenone (Figure 3.2) [37]. The understanding of the mechanisms behind the polymer formation and recognition processes involved in molecular imprinting is continuously improving, together with increasingly efficient integration of the polymer materials with the transducer. As sensing elements, their robustness, porosity and flexibility, and signaling abilities of the material also need to be improved but MIPs promise to find good opportunities in the future in areas where other natural or synthetic receptors struggle to find reliable applications [40].

3.2.2 Nucleic Acids and Analogues

Nucleic acids and their analogues as bioreceptors are successfully and widely exploited for affinity-based SPR biosensors [46]. In particular, deoxyribonucleic acid (DNA), ribonucleic acid (RNA), peptide nucleic acid (PNA), and locked nucleic acid (LNA) are the classes of nucleic acids most exploited as oligonucleotide probes [47, 48]. Their application for clinical diagnostics spans from the detection of pathogenic microorganisms and other pathogenic agents like viruses to the traceability of genetic mutations and polymorphisms related to a large variety of diseases [49]. The recognition of the target part, i.e., a single-stranded (ss) DNA/RNA sequence, is based on its fully complementarity to the bioreceptor, i.e., the immobilized

probe. Respect to other bioreceptors (natural and synthetic), those based on nucleic acids display several advantages such as a high-stability, a low-cost, and *in vitro* production, the possibility of working on target DNAs after their amplification by PCR (Polymerase Chain Reaction) with consequent benefits in terms of detectability of samples at very low starting concentration. Moreover, by playing on tailored nucleotide sequences (3'/5' modifications, insertion/deletion of specific regions) and their combination with specific enzymatic activities (i.e., DNA polymerases, ligases [50], restrictions enzymes, etc.), nucleic acids bioreceptors allow the development of intriguing and effective *in situ* molecular mechanisms of great advantages in terms of sensitivity and selectivity. Among recent applications in this sense, DNA-based architectures similar to sandwich assays were set up by our research group for single nucleotide polymorphisms (SNPs) discrimination in human DNA. The goal was first achieved by optimizing the method [51] and then testing DNA samples after their amplification by whole genome amplification (WGA) [52] and lastly bypassing the amplification step (in preparation). Metallic NPs can be or not introduced as signal amplifiers via mass enhancement and/or plasmon coupling between the gold surface of the biochip and the localized plasmons of the NPs [53] (Figure 3.3).

A recently emerging *in situ* strategy is named "rolling circle amplification" (RCA) and has been applied to pathogenic microorganisms detection [54], cancer cells [55], VEGF [24], thrombin [55], and point mutations [56]. RCA is an isothermal, enzymatic process mediated by a DNA polymerase in which long ss-DNA molecules are synthesized on a short circular ssDNA exploited as template with the help of a single DNA primer [57]. An increasing number of RCA strategies are under fast development also for the production of repetitive sequences of DNA aptamers and DNAzymes as detection platforms for small molecules and proteins.

3.2.3 Living Cells

The increasing availability of new automated instruments for classical and imaging SPR has allowed to investigate other biological systems, such as membranes, viruses, and cells. Even if the use of cellular materials generates new issues, e.g., the introduction of proper CO_2 concentration in binding solution for mammalian cells and the use of specific anti-fouling treatments to avoid the contamination of tubing and other components in the instrument, by using proper precautions and immobilization strategies SPR can provide very valuable information. As for other biological elements, living cells can play the role of target analytes or sensing elements immobilized on the surface [58]. The latter case is the issue of this

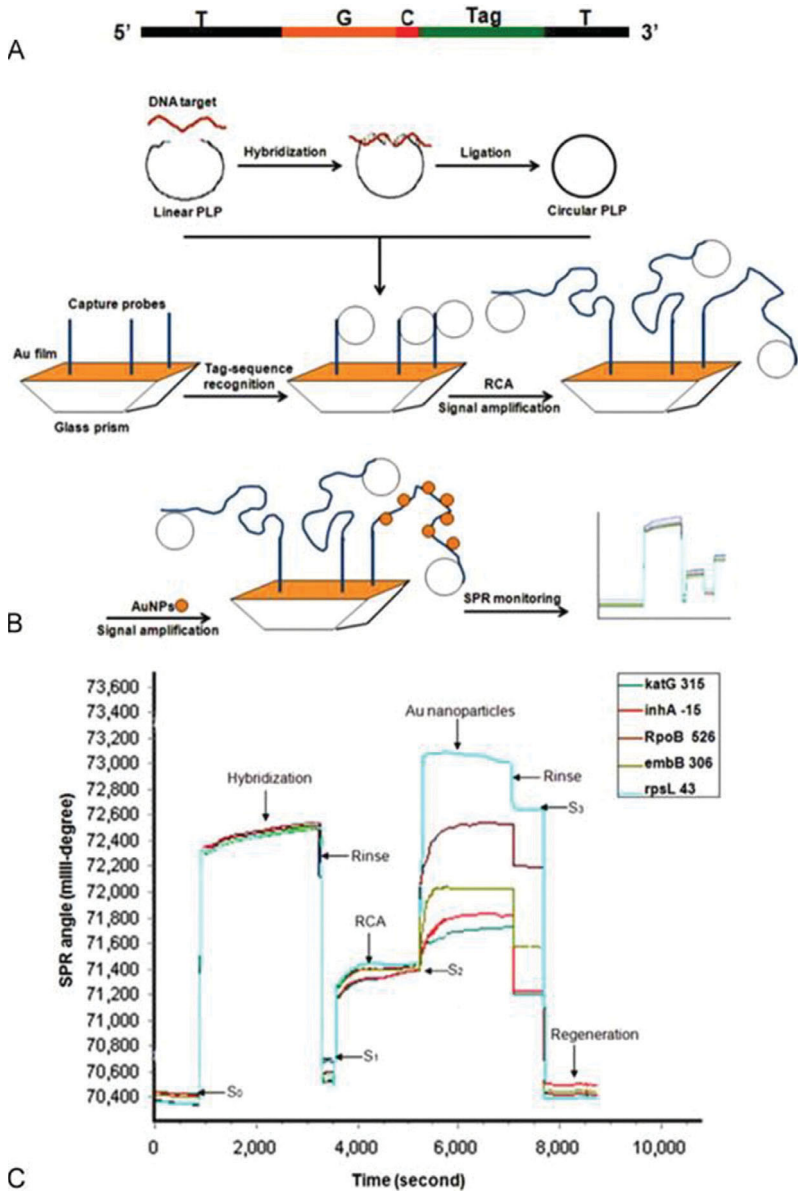

Figure 3.3 (A) PLP (Padlock Probe)design. The PLP contains target-complementary sequence (T), general sequence (G), and tag sequence (Tag). Tag sequence is unique for each PLP and complementary to the capture probe immobilized on the chip surface. The general sequence provides the repeats on the RCA products for AuNPs binding. "C" means the cutting site recognized by restriction endonuclease to remove the RCA products from the chip surface after the detection completed. (B) Schematic representation of the proposed detection strategy. (C) Real-time detection of multiple point mutations by SPR sensor.

paragraph and, actually, the most recent advancement in the use of living cells by SPR and SPRi technology. In the last 5 years, very innovative and exciting results have been obtained by this approach: SKOV-3 (human ovarian carcinoma cells immobilized on the sensor surface) were investigated for their secretion of VEGF by the direct recognition of the protein biomarker through specific antibodies [59]; Chinese hamster ovary (CHO) cells were seeded on the biochip surface, cultured, and then subjected to antigen and EGF by continuous and label-free monitoring of the SPR response in real time [60]; *Escherichia coli* cells immobilized on gold biochips modified with parylene-H film containing poly-l-lysine were exploited as sensor for the detection of CRP [61, 62]; B and T lymphocytes were grown on the sensor surface and distinguished using anti-IgM and anti-CD19 for identifying B lymphocytes, and anti-CD3 were used for T lymphocytes [63]; Horii et al. succeeded in achieving the reagent-less and real-time monitoring of the allergenic response of RBL-2H3 cells, immobilized on the chip, demonstrating that living cells give higher SPR signals than the corresponding immobilized antibodies (Figure 3.4) [64].

The aforementioned examples involve living cells as bioreceptors for SPR-based studies and demonstrate the fast growth of this research area. The ability to handle living cells directly on sensing surfaces with SPR technology lets imagine further and successful advancements in the understanding of cellular behavior and in other diagnostic relevant contexts.

3.3 Recent Trends in Bioreceptors Immobilization

Bioreceptors immobilization on the sensor surface is a key factor in for the biosensors sensitivity and selectivity. Many well-established immobilization chemistries were reported in literature for SPR- and SPRi-based biosensing such as physisorption, hydrophobic and electrostatic interactions, covalent binding through nucleophilic attack to carboxylic aldehydic or thiolic groups, and interactions between native and tagged molecules (e.g., avidin/biotin or Protein G and Fc) [65, 66]. The last two chemistries, i.e., covalent binding and noncovalent interactions between tagged and native molecules, are the most employed in SPR- and SPRi-based biosensing for their reproducibility, stability, and easiness of fulfillment, making them the most eligible methods for immuno-, aptamer-, and nucleic acids-based applications. However, the fast and continuous evolution of instrumental platforms and surface chemistries has stimulated the search of new immobilization strategies to improve the performances of traditional receptors and to address new emerging bioreceptors. For example, covalent attachment of sensing elements to graphene has the greatest potential for

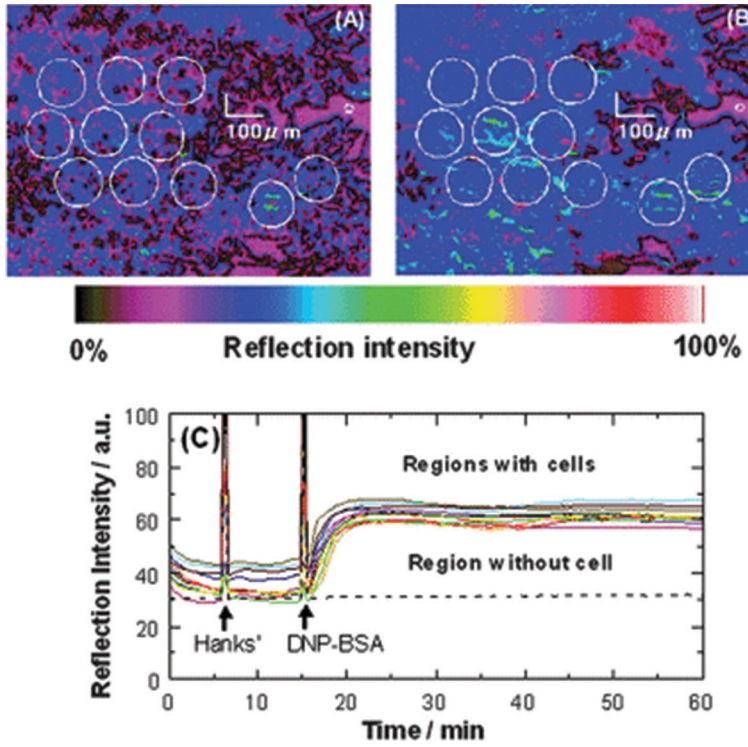

Figure 3.4 SPR images for cluster of RBL-2H3 cells before (A) and after (B) antigen stimulation [the final concentration of DNP (Dinitrophenyl)–bovine serum albumin (BSA) was 100 ng mL^{-1}]. (C) Reflection intensity change of several selected cell regions and cell-free region upon antigen stimulation. Solid line: Reflection intensity change of cell regions was monitored at the 11 large circular regions of cell clustered area in (A) and (B). Dashed line: The reflection intensity change of the cell-free region was monitored at the one small circular region in (A) and (B).

development of new high-performing graphene-based SPR sensing interfaces, owing to the stability of the resulting bond. Graphene and graphene oxide have already demonstrated their potential application as supports for biomolecules thanks to their features (i.e., large surface area up to 2630 m^2 g^{-1}, π-conjugation flat structure), and it is expected that important applications in the field of biosensors will be published soon. However, most of paper on this issue reported noncovalent approaches for bioreceptor immobilization, having the obvious advantage of being easy to perform (they are based on π–π stacking and van der Waals' interactions between graphene and aromatic moieties of biomolecules) and nondestructive for the extended π-conjugation of graphene (unlike covalent functionalization, which creates defects on the graphene sheets). On the other hand,

noncovalent immobilization of bioreceptors is highly undesirable for real application, due to its intrinsic unspecificity, i.e., other undesired aromatic-rich molecules present in the analyte solution could interfere with it in binding the sensing surface.

Therefore, despite the rapid progress made in the reproducible fabrication of graphene-based SPR interfaces, at present only a few advances in real-time biosensing have been achieved [67–71]. A recent paper dealing with a real application in this sense was reported by Wang *et al.* [69] for α-thrombin, obtaining sensitive and selective results. Dispersed graphene (GN), prepared by the chemical reduction of GO with hydrazine, is assembled on a positively charged SPR Au (p-Au) film *via* electrostatic interaction. Then, the α-thrombin aptamer (TBA) is adsorbed onto the GN layer through the strong noncovalent binding of GN with nucleobases. The binding between the aptamer and the target molecule will greatly disturb the interaction between the aptamer and GN. As a result, TBA is released from the SPR sensing surface and an obvious SPR angle decrease could be observed. In this application, the traditional approach of the SPR aptasensor (SPR signal increase after the analyte binding) is inverted, and the binding between TBA and thrombin generates a decrease of the signal *via* detachment of the TBA aptamer from the sensing surface due to the competition with the binding with the specific analyte (Figure 3.5). As proof of concept, a buffer BSA solution was tested as negative control, giving negligible difference in the SPR signal. Despite the novelty of the approach, there is the need to improve and standardize suitable immobilization protocols tailored for this emerging evolution of SPR biosensing.

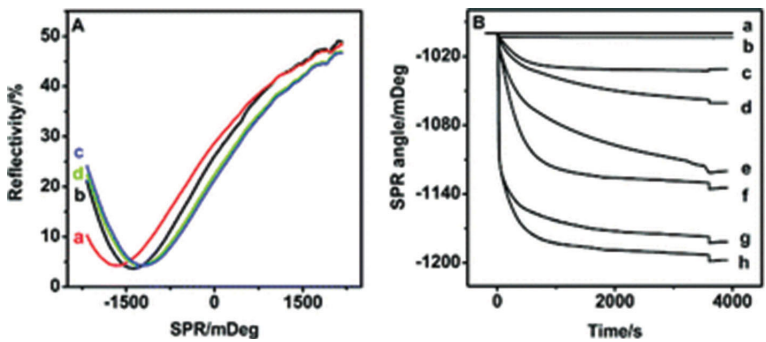

Figure 3.5 (A) The angle-resolved SPR curves during the different steps [p-Au film (a), GN (b), TBA (c), and treatment with 1 nM α-thrombin (d)] of the sensor immobilization. (B) SPR angle–time curves for the detection process between the TBA/GN/p-Au sensing interface with different concentrations of α-thrombin [(a) 0 nM, (b) 0.08 nM, (c) 0.4 nM, (d) 1 nM, (e) 20 nM, (f) 25 nM, (g) 100 nM, and (h) 150 nM].

The immobilization of proteins by retaining their functionally active form and by addressing their correct orientation once tethered on the biochip surface is pivotal for all protein–molecular interaction studies. In many cases, the oriented immobilization of protein bioreceptors (antibodies, peptides, proteins, antibody mimetics such as aptamers) can be addressed by introducing modifications (chemical groups, tails, small molecules) properly located on the side of the molecule which, once linked to the surface, leaves the bioreceptor able to bind the analyte. Among these, the most exploited modifications are biotin, His-tag [Ni(II)-mediated immobilization of His_6-tagged ligands], and nucleic acids-based (DNA and RNA) tails. The modification of the bioreceptor is then coupled to the proper chemical modification of the gold layer to obtain covalent or noncovalent bonding of the sensing element [72].

Among recent advancements of these established immobilization methods, some are devoted to adapt them to the needs of membrane-bound proteins [73]. Biochips conceived for membrane protein analysis can be obtained by building lipid layers [74], biomimetic membranes [75], vesicles, and nanopores [76] on existing gold SPR chips. Among the newest advancements, nanopores displayed good results, e.g., in obtaining the controlled and oriented immobilization of proteins by a puromycin-linker for cDNA display technology [76]. The utility and potential of this method were demonstrated by examining the interaction between the B domain of protein A and immunoglobulin G (IgG) by SPR.

Concerning nucleic acids-based bioreceptors, mainly immobilized via solid and well-established covalent binding to bare gold (thiol coupling) or three-dimensional hydrogels (biotinylated sequences), some optimized approach is reported to investigate small noncoding RNA (sRNA)–mRNA interactions [77]. Specifically, they ligated a biotinylated nucleotide to the 3′ end of RNA using T4 RNA ligase. Although this is a previously recognized approach, they optimized the method by the discovery that the incorporation of four or more adenine nucleotides at the 3′ end of the RNA (a poly-A-tail) is required in order to achieve high ligation efficiencies.

Livache's research group was pioneering in developing the *in situ* eletropolymerization of nucleotidic probe sequences [78] by the direct copolymerization of the probing biomolecule (modified with a pyrrole moiety) with pyrrole to obtain microarrays for SPRi. The same approach has been then successfully extended also for the fabrication of proteins [79], peptides [80], and oligosaccharides [81] arrays for biosensing applications spanning from cancer biomarkers [82] to humoral response against hepatitis C virus [83].

3.4 Trends for Improvements of Analytical Performances in Molecular Diagnostics

In the past years, many advancements were performed in SPR and based biosensing for the enhancement of analytical performances (e.g., sensitivity, specificity, and suitability for real matrices) [84, 85], and one of the most applied solutions was offered by the implementation of NPs to plasmonic sensing [86].

Recent researches about engineering of hybrid SPR interfaces such as oxide-based and nanocomposite films were examined by Gao et al. (2011), analyzing the optical properties and the suitable applications in sensing [87], while trends of NPs (i.e., AuNPs) embedding within the sensing plasmonic surface or as labeling molecules in SPR biosensor (2012) were reported by Bedford et al. (2012), where sensitivity increases and DLs decreases were described for a wide range of bioanalytes [88]. From a physical chemistry point of view when the plasmonic sensing surface is close to the NPs (e.g., AuNPs), the increase in sensitivity was explainable by two phenomena: the refractive index difference increase in the surface plasmon wave (SPW) as well as the optical coupling between the electric fields of localized surface plasmons (LSPs) and SPW, generating a strongly local electromagnetic fields enhancement [85]. Such change of resonance properties is key factor for the ultrasensitive detection of biomolecules, basic in molecular diagnostics where target are in complex matrices at a very low concentrations levels; in particular, for DNA sensing the NPs approach is useful to bypass PCR amplification steps (less time and reagent consumption) [89–91].

More recently (2013), Szunerits et al. collected the new trends of gold chip surface functionalization with graphene [71]. Although in literature were reported only few proof of concept applications of interest in molecular diagnostics (e.g., thrombin detection in standard solution by aptamer affinity interactions [69]), we are confident that the creation of hybrid gold/graphene interfaces might open new horizon for biomarker detection thanks to the high surface/volume ratio and the chance to adsorb bioreceptor by pi stacking interaction [71]. Other approaches, in addition to those based on NPs or graphene coupling to SPR, deal with innovative SPR engineering instrumental advances and implementations. The last forefront trends were collected by Abbas et al. (2011) and concerned: new optical configurations schemes of excitation; innovative microfluidics and microsystems for glass or poly(dimethylsiloxane) (PDMS) integrated chips; replacing of Cr or Ti in the adhesion gold layer with conducting metal zinc oxides (ZnO, ZnO/Au); advanced opto-electronic components

(light source and detector); hyphenated approaches with electrochemistry, scanning probe microscopy, mass spectrometry, Raman spectroscopy, and fluorescence [92].

After focusing on the last trends for the improvement of the SPR technology in bio-detection, we report their application in clinical diagnostics field for real bio-matrices first and for standard solution when in our opinion they represented a wide improvement of the current state of the art.

3.4.1 Coupling Nanotechnology to Biosensing

Among the different categories of NPs, gold NPs are the most widely employed and studied in biosensing and in molecular diagnostics taking advantage of their unique nanoscale properties for the increase of sensitivity, easiness of detection, and achievable implementation in portable instrumentation [93].

In this paragraph, we collect the most recent and significant NPs employment in molecular diagnostic with SPR- and SPRi-based optical transducer. Applications in real matrices have been mainly examined with a parallel analysis of the standard solution applications when they represent innovation compared to the current state of art. Different classes of bioanalyte detection have been review: hormones, cancer biomarker, and finally DNA samples.

Hormone analysis is an essential field and a major research thrust in molecular diagnostic and more recently in anti-doping controls [94]. Diagnosis of endocrine diseases may be difficult requiring ultrasensitive and real-time detection hormone in blood, serum, or urine. At this purpose, the employment of NPs enhancing strategies was reported in SPR-based detection to achieve the levels of required sensitivity [95].

A paradigmatic example of hormone detection mediated by gold NPs was reported by Jiang et al. with BIAcore X-100 system. They developed an inhibition immunoassay for the detectionestriol-16-glucuronidein urine samples, a hormone for the monitoring of ovarian function from nonpregnant and pregnant patients. The steroid hormone was immobilized by an ovalbumin conjugate using oligoethylene glycol (OEG) as linker, while gold NPs coated by the pAb were incubated in the samples. A detection limit ~34 pM was reached in urine diluted with TM buffer, while the detection in real matrices was impeded by matrix effect [96].

Mitchell *et al.* designed a competitive immunobiosensor for testosterone detection first in HEPES (N-2-Hydroxyethylpiperazine-N'-2-Ethanesulfonic Acid) buffer and then in stripped human saliva matrix with

Biacore 2000. A testosterone derivate was immobilized on the CM5 dextran surface by amino-coupling. Primary antibodies were employed for the assay while secondary antibodies (anti-mouse IgG) linked to gold NPs were employed for signal enhancement, increasing 12.5-fold the signal sensitivity of the assay compared with the only primary antibody. Limits of detections (LODs) were 12.8 pM in HEPES and 53.4 pM in matrix, sufficient to detect physiological testosterone in male saliva, ranging from 0.10 to 1.00 nM [97].

In 2010, Frasconi et al. developed an indirect immunoassay for the detection of insulin in human serum samples using Eco Chemie Autolab SPR system and based on surface nanostructuring. GNP was encapsulated in hydroxyl/LC-PDP-functionalized G4-PAMAM dendrimer and immobilized by amino-coupling on a SAM (Self-assembled monolayer)-modified gold surface. Insulin was immobilized on the functionalized surface exploiting again the amino-coupling chemistry, and an indirect assay with anti-insulin antibody was performed in 10-fold diluted sera (Figure 3.6). The original modified surface resulted resistant to unspecific adsorption of proteins with different isoelectric points and molecular weight. Moreover, the electromagnetic coupling between SPs (Surface Plasmons) and LSPs of NPs lowered the DL down to 0.5 pM in diluted matrix. Ten-fold diluted sera from healthy and diabetic patients were analyzed in the 2–43 pM linear concentration range with high reproducibility (CVs ranged between 3.5% and 4.9%) and RIA reference test confirmed the reliability of the obtained results [98].

Besides hormones also peptide protein biomarkers have a relevant interest in molecular diagnostics, since they are indicators of different stages of

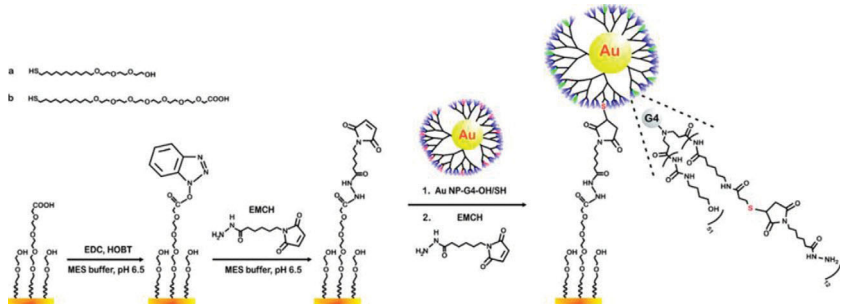

Figure 3.6 Immobilization of hydroxyl/LC-PDP-functionalized G4-PAMAM dendrimer-encapsulated Au NP onto mixed SAMs of alkanethiolates on gold derived from tri(ethylene glycol)-terminated thiol (a) and the hexa(ethylene glycol) carboxylic acid-terminated thiol (b). Reprinted with permission from Frasconi M, Tortolini C, Botre F, Mazzei F (2010) Multifunctional Au Nanoparticle dendrimer-based surface plasmon resonance biosensor and its application for improved insulin detection. *Anal. Chem.* 82: 7335–7342. Copyright (2010) American Chemical Society.

related diseases (e.g., cardiac, inflammatory, and cancer), really helpful to direct the specific molecular therapy and to appraise accordingly the therapeutic response. Also, in this field SPR provides a real-time and label-free platform for daily routine molecular diagnosis [87] and in the past 2 years there has been a really increasing interest in the coupling with NPs enhancing strategies to reach the level of sensitivity required in real matrix.

In 2013, Ri Jang et al. reported a hybrid sandwich assay for the direct ultrasensitive detection of B-type natriuretic peptide (BNP) with a Biacore 3000. A DNA aptamer, covalently immobilized on gold surface, captured the BNP analyte while anti-BNP covalently linked to gold nanocubes specifically recognized the analyte and amplified the signal allowing the attomolar BNP detection in undiluted human serum [99].

More recently (2014), the aptamer technology coupled to NPs-based enhancing strategy was also applied for the detection of CRP in spiked human serum with a SPRi Lab$^+$ (Horiba). CRP is a general inflammatory biomarker related to inflammatory responses in cardiovascular diseases (CVD), neurological disorders, and cancer. The authors developed an aptamer sandwich assay coupling the advantage of aptamer technology with NPs and microwave-assisted surface functionalization. A biotinilated specific aptamer was immobilized on the extravidin-coated chip surface to capture the CRP and with the introduction of specific aptamer-coated quantum dots (QDs), it was possible to enhance sensitivity, improving the selective detection down to 0.2 fM of CRP in spiked human serum [100].

Martinez-Perdiguero et al. developed a sandwich immunoassay for the detection of another anti-inflammatory biomarker, the tumor necrosis factor (TNF-α), a widely studied cytokine activated by macrophages and involved in immune and inflammatory responses. Anti-TNF-α was immobilized via amino-coupling on a MUA (mercaptoundecanoic acid)-coated gold chip of SPR2 (Sierra Sensors GmbH) to capture the analyte. Then, an amplification step was optimized with secondary biotinylated antibodies linked to streptavidin functionalized. The sensitivity was 3.1-fold enhanced, and a detection limit of ~1.0 pM was reached in human serum [101].

Many advances have recently been made for the development of new strategies also for the detection of cancer biomarkers in real matrices.

Uludag and Tothill developed an immunosensor for the detection of total prostate-specific antigen (tPSA), a biomarker for the diagnosis and prognosis of prostate cancer, using a Biacore 3000. PSA capture antibody was covalently immobilized by amino-coupling on the sensor surface, while gold NPs were coated with a secondary PSA antibody. By performing a sandwich assay a detection limit concentrations of 9.0 pM in human serum samples was reached [102].

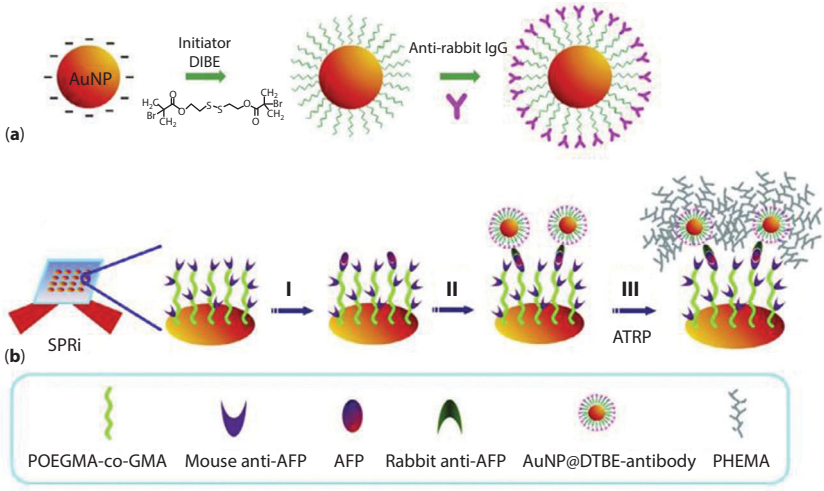

Figure 3.7 (a) Preparation of AuNPs@DTBE–antibody. (b) Dual SPRi signal amplification. Sample was flowed on the SPRi chip surface to directly detect AFP target (step I), followed by AuNPs@DTBE–antibody to form immunocomplexes for the first signal amplification (step II), and on-chip ATRP was triggered to further enhance the signal (step III).

Hu et al. reported the detection in human serum of α-fetoprotein (AFP), a hepatocellular carcinoma biomarker. A sandwich immunoassay was optimized on GWC SPRimager II platform, and a dual signal amplification strategy based on gold NPs and on-chip atom transfer radical polymerization (ATRP) was tuned for the improvement of sensitivity. The scheme of the strategy was reported in the Figure 3.7.

A mouse anti-AFP was immobilized on the gold surface coated by poly[oligo(ethylene glycol) methacrylate-co-glycidyl methacrylate] (POEGMA-co-GMA) to capture the analyte. In parallel, the gold NPs are coated with bis[2-(2 0 -bromoisobutyryloxy)ethyl]disulfide (DTBE) acting as ATRP initiator and linker for the secondary recognition antibody. The nanostructures were added to the preformed immunocomplex for the first signal amplification step. Then 2-hydroxyethyl methacrylate (HEMA, monomer) was secondarily added and polymerized on the sandwich (poly-HEMA) to further amplified the signal down to 14 pM as detection limit in 10% human serum [103].

Gold NPs assumed a key role also in the improvement of sensitivity for gene sensing and in particular for point mutation and SNPs discrimination [89–91]. These mutations have a key role in molecular diagnostics both in pharmacogenomics as well as biomarkers when occur in specific gene coding region related to common diseases.

A method based on sandwich-like assay coupled to NPs was tuned by Yao et al., for the discrimination of SNPs in TP53 gene, the mostly mutated gene in presence of tumors. Gold NPs were covalently linked to thiolated oligonucleotides as signal enhancer for the SNP discrimination down to 1.38 fM target concentration in 15 μL of sample [104].

Another approach, based again on NPs for the high-sensitive detection of SNPs of clinical interest was optimized by Corn group with a SPR imager, GWC technologies. SNPs in BRCA1 gene, associated to breast cancer, were discriminated at picomolar level in unamplified human DNA samples coupling surface enzymatic ligation reactions to signal enhancement by gold NPs. The SPRi DNA microarrays appeared as a very intriguing solution for parallel and multiplexed genotyping of multiple SNPs [50].

Spoto group further enhanced SNP detection sensitivity with the same SPRi instrument down to attomolar concentration and bypassing the PCR step. SNP discrimination of the human β-globin gene, involved in β thalassemia, was performed directly in nonamplified genetic material (extracted from leucocytes). PNA probes were covalently immobilized on the gold surface for the capturing of the gene of interest (with polymorphic site in issue), and streptavidin-coated gold NPs linked to biotinylated DNA probe were subsequently added to the preformed hybrid to amplify the signal down to attomolar gene detection [105]. The scheme of the assay was reported in Figure 3.8.

Although NPs have represented a turning point for ultrasensitive SNPs discrimination with SPR and SPRi, their synthesis is time- and reagent-consuming with relevant implications for cost and speediness of molecular diagnostics assays.

At this purpose, in 2013 our group have tuned a sensitive (140 aM) and label-free DNA-based assay for the detection of unamplified ABCB1 gene fragment (of interest in pharmacogenomic) without the employment of enhancing factor (NPs) but through rational probe selections with OligoWiz 2.0 [3,106] and tuned pre-analytical step (sample pretreatments: fragmentation and denaturation) [107].

In parallel (in the same year), we optimized the assay (secondary probes labeling and length) for the detection of rs1045642 SNP on the ABCB1 (related to susceptibility of many diseases such as renal, colorectal, and breast cancer) in extracted genomic sample enriched by WGA [52].

Really recently, the assay was successfully adapted for the same SNP discrimination in unamplified genomic samples directly extracted from lymphocytes [108], reducing costs push through analytical outputs and lowering analysis costs (features required for a daily routine molecular diagnostics).

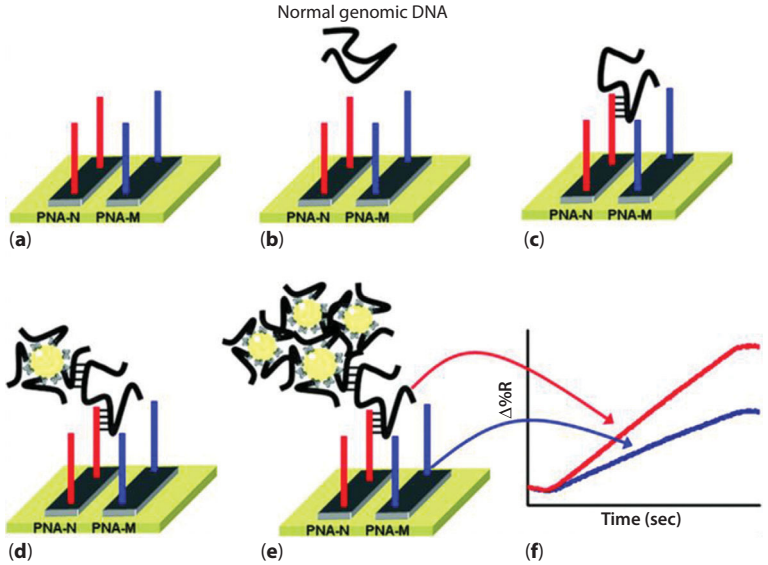

Figure 3.8 Pictorial description of the NP-enhanced SPRI strategy used to detect the normal βN/βN, heterozygous β°39/βN, and homozygous β°39/β°39 genomic DNAs. In order to simplify the pictorial representation, only specifically adsorbed DNA is shown. Nonspecifically adsorbed DNA is also present on the surface and contributes to generate the SPRi-detected signal. PNA-N and PNA-M specifically recognize the normal β-globin and the mutated β°39-globin genomic sequences, respectively. Reprinted (adapted) with permission from D'Agata R, Breveglieri G, Zanoli LM, Borgatti M, Spoto G, Gambari R (2011) Direct detection of point mutations in nonamplified human genomic DNA. *Anal. Chem.* 83: 8711–8717. Copyright (2011) American Chemical Society.

Other nucleotidic analytes of interest for molecular diagnostics studied and detected by SPR- and SPRi-based biosensors are MicroRNAs (miRNAs): about 22 mers relevant nucleic in human blood ranging from high femtomolar to low nanomolar range of concentration. They act as gene regulatory in human regulation of gene expression with a parallel interest as biomarker of serious disease, i.e., cancer, nervous system, liver and heart diseases [95].

An innovative approach for the detection of miRNA, extracted from mouse liver tissue, was reported by Fang et al. LNA microarray was immobilized on the gold chip surface (SPR imager, GWC technologies) for the parallel and multiplexed detection of miR-16, miR-122b, and miR-23b. The SPRi response was enhanced by poly-(A) enzyme chemistry and T30-coated gold NPs signal amplification [109].

3.4.2 Microfluidics and Microsystems

The basic sample handling and processing of commercial SPR and SPRi are often restricted by a basic flow-cell technology with a consequently negative impact on the sensitivity and analytical productivity. In this paragraph, we reported the last trends regarding microfluidics and microsystems technologies to improve the detection of various bioanalyte of wide interest in molecular diagnostics [110].

A three-port microfluidic device combined to a portable SPR signal transducer was reported for the brain natriuretic peptide (BNP) detection, a cardiac hormonal biomarker secreted during cardiac failure. BNP solution from human serum was incubated with acetylcholine esterase-labeled specific antibody and then introduced into the microchannel of the device (Figure 3.9). Only free-BNP conjugate bound to BNP-immobilized surface (by amino-coupling) in the flow channel. Then acetylthiocholine was added as substrate and the thiol compound (thiocholine), generated by the

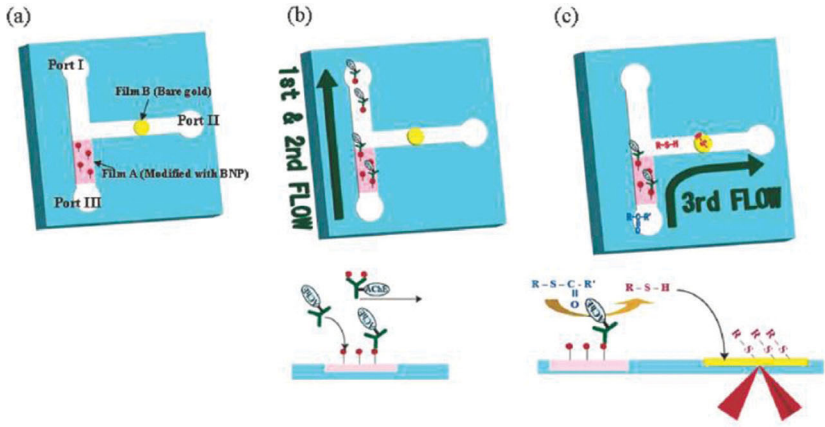

Figure 3.9 Schematic diagram of the procedure for BNP determination in the immunosensor. (a) Preparation of the immunosensor. Film A is modified with BNP for the collection of unreacted anti-BNP–AChE. Film B is a bare gold film for the detection of concentrated thiocholine. (b) Introduction of a mixture solution containing BNP and anti-BNP–AChE from port III to port I. The unreacted anti-BNP–AChE was collected on BNP-modified film A during the first flow. Then, the channel was rinsed with phosphate buffer during the second flow. (c) Acetylthiocholine was introduced from port III to port II. Thiocholine was produced from acetylthiocholine by the collected anti-BNP–AChE on film A, then the thiocholine accumulated on the film B surface located downstream in the microchannel, and was monitored by the SPR angle shift during the third flow. Reprinted (adapted) with permission from Kurita R, Yokota Y, Sato Y, Mizutani F, Niwa O (2006) On-chip enzyme immunoassay of a cardiac marker using a microfluidic device combined with a portable surface plasmon resonance system. *Anal. Chem.* 78: 5525–5531.

enzymatic reaction with the bound conjugate, covalently bound to a thin gold layer located downstream in the microchannel, generating a SPR angle shift monitored as analytical signal. Concentration range of 5 pg/mL–100 ng/mL trace levels (15 fg) were detected in about 30 minutes [111].

A novel microfluidic approach for the detection of biomarkers directly from living cells was described for the first time by Liu *et al.* though the integration of the SPR system with a mini cell culture module applied to PDMS gasket with a gelatin. They tested the microsystem for the VEGF detection, a biomarker abnormally produced from cancer cells in myelodysplastic syndromes examining specifically living SKOV-3 cancer ovarian cells. First the specific anti-VEGF was linked on chip surface via G protein and then the *in vivo* microenvironment of the VEGF signaling pathways was mimicked tuning the cell viability in the PDMS-modified gasket, proving a correlation between carcinoma cell number and analytical signal. The whole procedure represents a starting point for the real-time monitoring of biomarker directly expressed in living cells [112].

More recently (2014), Chuang *et al*. designed a membrane-based sample handling for quantitative interferon-gamma detection (IFN-γ) with a SPR-based aptasensor. A rayon membrane separated the sample chamber, where a specific aptamer was immobilized, from the streptavidin chamber, where streptavidin was stored with the possibility of migration through the membrane pore according to the Darcy law. A bi-functional, hairpin-shaped aptamer acted as bioreceptor, capturing for the IFN-γ, as well as signal amplifier, binding streptavidin after migration from membrane (stopping flow) (Figure 3.10). A detection limit of 10 pM was achieved in only half

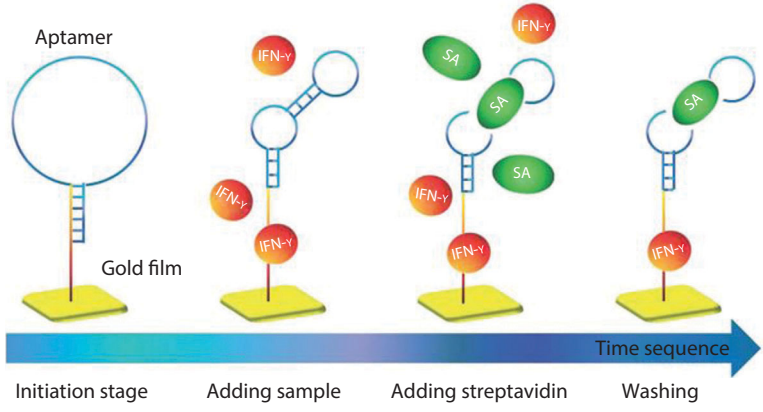

Figure 3.10 Conceptual diagram of the SPR aptasensor operating processes in a membrane-based cartridge.

hour and the device resulted easy to use and cheap compared to the conventional multi-step protocol requiring well-trained clinicians [113].

3.4.3 Hyphenation

The hyphenation of SPR and SPRi with conventional analytical instrumentation has been increasingly implemented in the past decade, especially for a first evaluation of the analytical potential although the application to diagnostics is still at an early stage [92]. In this paragraph, we report just few significant examples.

High-resolution SPR microscopy (SPRM) was used by Wang *et al*. for the label-free and imaging for the mass quantification of H1N1 Influenza viruses particles. Anti-H1N1 antibodies were covalently immobilized by amino-coupling on the sensor surface for the particles virus capturing in PBS (phosphate buffered saline) buffer and a mass detection limit of ~0.2 fg/mm^2 was reached by SPRM measurement, emphasizing the reliability of the method to quantify the mass of single viral particles and to study the binding affinity between antibodies and virus capsid [114].

Remy-Martin *et al*. coupled the SPRi technologies with a MALDI-TOF mass spectrometry (dubbed "SUPRA-MS") for the multiplexed and parallel quantification of bioanalyte (Figure 3.11). In particular, MS (mass spectrometry) analysis could improve the identification and discrimination among eventual several isoforms of the same bioanalyte. In particular, the authors reported a proof-of-concept data validation for the identification and quantification of the LAG3 protein in human plasma, a biomarker of tuberculosis and human breast cancer. Anti-LAG3 and control anti-αRSA (αRSA, rat serum albumin) were covalently immobilized on the gold chip surface of a SPRi-Plex II (Horiba). The method was fast, automated, reliability and specific (100% LAG3 identification with the collateral presence of αRSA) with a detection limit of ~1 μg/mL in human plasma, pointing out also the potential applications in proteomics [115].

3.5 Conclusions

We discussed here recent developments in SPR-based affinity biosensing for applications of interest in molecular diagnostics. In particular, we underlined the importance of key aspects to be considered in the biosensor development for real application to complex matrices, such as human specimens. These days the focus is to push a step forward the technology

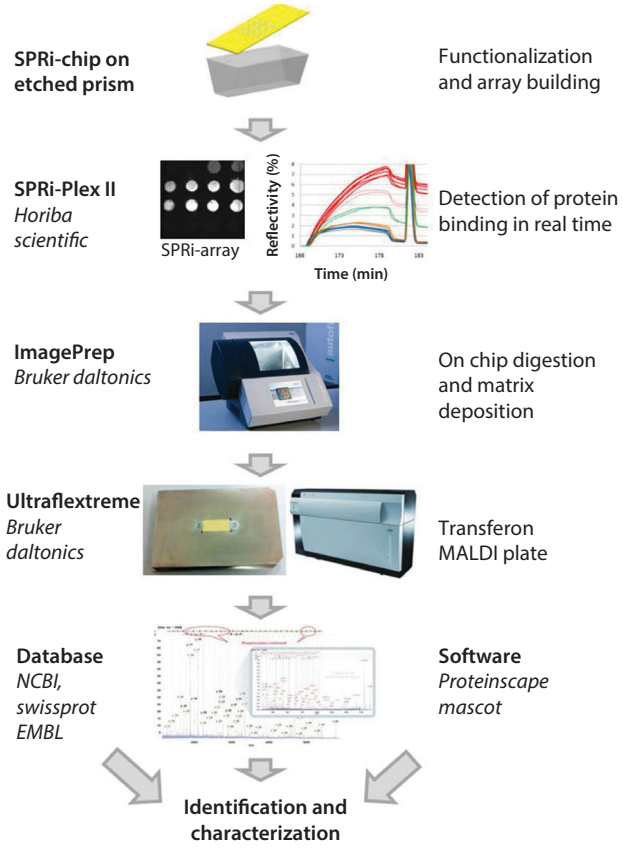

Figure 3.11 Flow chart of the SUPRA-MS technique.

potentialities by rational approaches in the assay, from the rational choice of the bioreceptor, the immobilization strategy (to preserve bioreactivity and, at the same time, preventing unspecific adsorption of matrix components), to tailored sampling and management of SPR results. Finally, attention is also given to strategies for signal amplification, which can be addressed by molecular architectures buildings, eventually coupled to nanostructures. All these aspects contribute to improve the analytical performances of the system, in terms of detection limits and reproducibility. Ultrasensitive detection of DNA sequences bypassing the traditional amplification step by PCR is possible nowadays, eventually for detecting single polymorphisms (SNPs) on genomic DNA from lymphocytes.

Behind these, recent application to affinity biosensing of emerging and relevant molecular clinical markers from real samples is reported as well

as the detection of whole cells. These latter can be addressed for direct detection or for detecting their released factors *in situ*, once the cells are deposited on the chip surface.

These recent advancements, addressing important aspects of clinical diagnostics, will further open this technology to users that may not have access to SPR so far, such as clinical control laboratories.

References

1. S. Scarano, M. Mascini, A. P. F. Turner, and M. Minunni, Surface plasmon resonance imaging for affinity-based biosensors, *Biosens. Bioelectron.*, Vol. 25, p. 957, 2010.
2. F. S. Ong, K. Das, J. Wang, H. Vakil, J. Z. Kuo, W.-L. B. Blackwell, S. W. Lim, M. O. Goodarzi, K. E. Bernstein, J. I. Rotter, and W. W. Grody, Personalized medicine and pharmacogenetic biomarkers: progress in molecular oncology testing, *Expert Rev. Mol. Diagn.*, Vol. 12, p. 593, 2012.
3. M. L. Ermini, S. Scarano, R. Bini, M. Banchelli, D. Berti, M. Mascini, and M. Minunni, A rational approach in probe design for nucleic acid-based biosensing, *Biosens. Bioelectron.*, Vol. 26, p. 4785, 2011.
4. S. Scarano, C. Scuffi, M. Mascini, and M. Minunni, Surface plasmon resonance imaging (SPRi)-based sensing: A new approach in signal sampling and management, *Biosens. Bioelectron.*, Vol. 26, p. 1380, 2010.
5. J. Chen, Y. Chen, J. Xu, Y. Zhang, and T. Liao, Post-experimental denoising and background subtraction of surface plasmon resonance images for better quantification, *Chemom. Intell. Lab. Syst.*, Vol. 114, p. 56, 2012.
6. W. M. Mullett, E. P. Lai, and J. M. Yeung, Surface plasmon resonance-based immunoassays, *Methods*, Vol. 22, p. 77, 2000.
7. Donahue and M. Albitar, in *Recognition Receptors in Biosensors SE* - 5, ed. M. Zourob, Springer, New York, p. 221, 2010.
8. P. B. Luppa, L. J. Sokoll, and D. W. Chan, Immunosensors—principles and applications to clinical chemistry, *Clin. Chim. Acta*, Vol. 314, p 1, 2001.
9. D. Shankaran, K. Gobi, and N. Miura, Recent advancements in surface plasmon resonance immunosensors for detection of small molecules of biomedical, food and environmental interest, *Sens. Actuators B Chem.*, Vol. 121, p. 158, 2007.
10. J. Löfblom, J. Feldwisch, V. Tolmachev, J. Carlsson, S. Ståhl, and F. Y. Frejd, Affibody molecules: engineered proteins for therapeutic, diagnostic and biotechnological applications, *FEBS Lett.*, Vol. 584, p. 2670, 2010.
11. J. Lindgren, P. Segerfeldt, S. B. Sholts, A. Gräslund, A. E. Karlström, and S. K. T. S. Wärmländer, Affibody molecules: engineered proteins for therapeutic, diagnostic and biotechnological applications, *J. Inorg. Biochem.*, Vol. 120, p. 18, 2013.

12. J. Lindgren, A. Wahlström, J. Danielsson, N. Markova, C. Ekblad, A. Gräslund, L. Abrahmsén, A. E. Karlström, and S. K. T. S. Wärmländer, N-terminal engineering of amyloid-β-binding Affibody molecules yields improved chemical synthesis and higher binding affinity, *Protein Sci.*, Vol. 19, p. 2319, 2010.
13. L. Ekerljung, H. Wa, A. Sohrabian, K. Andersson, M. Friedman, F. Y. Frejd, S. Stahl, and L. Gedda, Generation and evaluation of bispecific affibody molecules for simultaneous targeting of EGFR and HER2, *Bioconjugate Chem.*, Vol. 23, p.1802, 2012.
14. R. Zielinski, I. Lyakhov, A. Jacobs, O. Chertov, G. Kramer-Marek, N. Francella, A. Stephen, R. Fisher, R. Blumenthal, and J. Capala, Affitoxin – a novel recombinant, HER2-specific, anti-cancer agent for targeted therapy of HER2-positive tumors, *J. Immunother*, Vol. 32, p. 817, 2009.
15. S. Scarano, A. Vestri, M. L. Ermini, and M. Minunni, SPR detection of human hepcidin-25 : A critical approach by immuno- and biomimetic-based biosensing, *Biosens. Bioelectron.*, Vol. 40, p. 135, 2013.
16. E. Luzi, M. Minunni, S. Tombelli, and M. Mascini, New trends in affinity sensing, *TrAC Trends Anal. Chem.*, Vol. 22, p. 810, 2003.
17. P. Hong, W. Li, J. Li, and B. Hospital, Applications of aptasensors in clinical diagnostics, *Sensors*, Vol. 12, p. 1181, 2012.
18. Aviñó, C. Fàbrega, M. Tintoré and, R. Eritja, Thrombin binding aptamer, more than a simple aptamer: chemically modified derivatives and biomedical applications, *Curr. Pharm. Des.*, Vol. 18, p. 2036, 2012.
19. Y. Bai, F. Feng, L. Zhao, C. Wang, H. Wang, M. Tian, J. Qin, Y. Duan, and X. He, Aptamer/thrombin/aptamer-AuNPs sandwich enhanced surface plasmon resonance sensor for the detection of subnanomolar thrombin, *Biosens. Bioelectron.,* Vol. 47, p. 265, 2013.
20. C. A. Kretz, A. R. Stafford, C. James, J. I. Weitz, and J. C. Fredenburgh, HD1, a thrombin-directed aptamer, binds exosite 1 on prothrombin with high affinity and inhibits its activation by prothrombinase, *J. Biol. Chem.*, Vol. 281, p. 37477, 2006.
21. C. Polonschii, S. David, S. Tombelli, M. Mascini, and M. Gheorghiu, A novel low-cost and easy to develop functionalization platform. Case study: aptamer-based detection of thrombin by surface plasmon resonance, *Talanta*, Vol. 80, p. 2157, 2010.
22. J. Wang, R. Lv, J. Xu, D. Xu, and H. Chen, Characterizing the interaction between aptamers and human IgE by use of surface plasmon resonance, *Anal. Bioanal. Chem.*, Vol. 390, p. 1059, 2008.
23. Bini, S. Centi, S. Tombelli, and M. Minunni, Development of an optical RNA-based aptasensor for C-reactive protein, *Anal. Bioanal. Chem.*, Vol. 390 p. 1077, 2008.
24. H. Chen, Y. Hou, F. Qi, J. Zhang, K. Koh, Z. Shen, and G. Li, Detection of vascular endothelial growth factor based on rolling circle amplification as a means of signal enhancement in surface plasmon resonance, *Biosens. Bioelectron.*, Vol. 61, p. 83, 2014.

25. J.-W. Park, S. Saravan Kallempudi, J. H. Niazi, Y. Gurbuz, B.-S. Youn, and M. B. Gu, Rapid and sensitive detection of Nampt (PBEF/visfatin) in human serum using an ssDNA aptamer-based capacitive biosensor, *Biosens. Bioelectron.*, Vol. 38, p. 233, 2012.
26. Oguro, T. Ohtsu, and Y. Nakamura, An aptamer-based biosensor for mammalian initiation factor eukaryotic initiation factor 4A, *Anal. Biochem.*, Vol. 388, 102, 2009.
27. S. J. Lee, B.-S. Youn, J. W. Park, J. H. Niazi, Y. S. Kim, and M. B. Gu, ssDNA aptamer-based surface plasmon resonance biosensor for the detection of retinol binding protein 4 for the early diagnosis of type 2 diabetes, *Anal. Chem.*, Vol. 80, p. 2867, 2008.
28. T. S. Misono and P. K. R. Kumar, Selection of RNA aptamers against human influenza virus hemagglutinin using surface plasmon resonance, *Anal. Biochem.*, Vol. 342, p. 312, 2005.
29. Q. Wang, J. Huang, X. Yang, K. Wang, L. He, X. Li, and C. Xue, Surface plasmon resonance detection of small molecule using split aptamer fragments, *Sens. Actuators B Chem.*, Vol. 156, p. 893, 2011.
30. M. Zhang, J. Zeng, Y. Wang, and X. Chen, Developments and trends of molecularly imprinted solid-phase microextraction, *J. Chromatogr. Sci.,* Vol. 51, p. 577, 2013.
31. P. Luliński, Molecularly imprinted polymers as the future drug delivery devices, *Acta Pol. Pharm.*, Vol. 70, p. 601, 2013.
32. S. Lépinay, K. Kham, M.-C. Millot, and B. Carbonnier, In-situ polymerized molecularly imprinted polymeric thin films used as sensing layers in surface plasmon resonance sensors: Mini-review focused on 2010–2011, *Chem. Pap.*, Vol. 66, p. 340, 2012.
33. R. Schirhagl, Bioapplications for molecularly imprinted polymers, *Anal. Chem.*, Vol. 86, p. 250, 2014.
34. K. Haupt and K. Mosbach, Molecularly imprinted polymers and their use in biomimetic sensors, *Chem. Rev.*, Vol. 100, p. 2495, 2000.
35. F. Canfarotta, M. J. Whitcombe, and S. a Piletsky, Polymeric nanoparticles for optical sensing, *Biotechnol. Adv.*, Vol. 31, p. 1585, 2013.
36. Poma, A. P. F. Turner, and S. A. Piletsky, Advances in the manufacture of MIP nanoparticles, *Trends Biotechnol.*, Vol. 28, p. 629, 2010.
37. S-W Choi, H-J Chang, N. Lee, J-H Kim, and H-S Chun, Detection of mycoestrogen zearalenone by a molecularly imprinted polypyrrole-based surface plasmon resonance (SPR) sensor, *J. Agric. Food Chem.*, Vol. 57, p. 1113, 2009.
38. Abbas, L. Tian, J. J. Morrissey, E. D. Kharasch, and S. Singamaneni, Hot spot-localized artificial antibodies for label-free plasmonic biosensing, *Adv. Funct. Mater.*, Vol. 23, p. 1789, 2013.
39. S. Piletsky, N. W. Turner, and P. Laitenberger, Molecularly imprinted polymers in clinical diagnostics—future potential and existing problems, *Med. Eng. Phys.*, Vol. 28, p. 971, 2006.

40. O. Y. F. Henry, D. C. Cullen, and S. Piletsky, Optical interrogation of molecularly imprinted polymers and development of MIP sensors: a review, *Anal. Bioanal. Chem.*, Vol. 382, p. 947, 2005.
41. Kugimiya and T. Takeuchi, Surface plasmon resonance sensor using molecularly imprinted polymer for detection of sialic acid, *Biosens. Bioelectron.,* Vol. 16, p. 1059, 2001.
42. E. P. C. Lai, A. Fafara, V. A. VanderNoot, M. Kono, and B. Polsky, Surface plasmon resonance sensors using molecularly imprinted polymers for sorbent assay of theophylline, caffeine, and xanthine, *Can. J. Chem.*, Vol. 76, p. 265, 1998.
43. M. Lotierzo, O. Y. F. Henry, S. Piletsky, I. Tothill, D. Cullen, M. Kania, B. Hock, and A. P. F. Turner, Surface plasmon resonance sensor for lysozyme based on molecularly imprinted thin films, *Biosens. Bioelectron.*, Vol. 20, p. 145, 2004.
44. T. Matsunaga, T. Hishiya, and T. Takeuchi, Surface plasmon resonance sensor for lysozyme based on molecularly imprinted thin films, *Anal. Chim. Acta*, Vol. 591, p. 63, 2007.
45. J. C. C. Yu and E. P. C. Lai, Interaction of ochratoxin A with molecularly imprinted polypyrrole film on surface plasmon resonance sensor, *React. Funct. Polym.*, Vol. 63, p. 171, 2005.
46. Z. Iunu-Iui, C. Hong, and Y. Ruifu, DNA based biosensors, *Biotech. Adv.*, Vol. 15, pp. 43–58, 1997.
47. R. D'Agata and G. Spoto, Surface plasmon resonance imaging for nucleic acid detection, *Anal. Bioanal. Chem.*, Vol. 405, p. 573, 2013
48. R. D'Agata and G. Spoto, Artificial DNA and surface plasmon resonance, *Artif. DNA. PNA XNA*, Vol. 3, p. 45, 2012.
49. U. Bora, A. Sett, and D. Singh, Nucleic acid based biosensors for clinical applications, *Biosens. J.*, Vol. 1, p. 1, 2013.
50. Y. Li, A. W. Wark, H. J. Lee, and R. M. Corn, Single-nucleotide polymorphism genotyping by nanoparticle-enhanced surface plasmon resonance imaging measurements of surface ligation reactions, *Anal. Chem.*, Vol. 78, p. 3158, 2006.
51. M. L. Ermini, S. Mariani, S. Scarano, and M. Minunni, Direct detection of genomic DNA by surface plasmon resonance imaging: an optimized approach, *Biosens. Bioelectron.,* Vol. 40, p. 193, 2013.
52. M. L. Ermini, S. Mariani, S. Scarano, D. Campa, R. Barale, and M. Minunni, Single nucleotide polymorphism detection by optical DNA-based sensing coupled with whole genomic amplification, *Anal. Bioanal. Chem.*, Vol. 405, p. 985, 2013.
53. M. L. Ermini, S. Mariani, S. Scarano, and M. Minunni, Bioanalytical approaches for the detection of single nucleotide polymorphisms by surface plasmon resonance biosensors, *Biosens. Bioelectron.*, Vol. 61C, p. 28, 2014.
54. D. Shi, J. Huang, Z. Chuai, D. Chen, X. Zhu, H. Wang, J. Peng, H. Wu, Q. Huang, and W. Fu, Isothermal and rapid detection of pathogenic

microorganisms using a nano-rolling circle amplification-surface plasmon resonance biosensor, *Biosens. Bioelectron.*, Vol. 62, p. 280, 2014.
55. P. He, W. Qiao, L. Liu, and S. Zhang, Ultrasensitive detection of thrombin using surface plasmon resonance and quartz crystal microbalance sensors by aptamer-based rolling circle amplification and nanoparticle signal enhancement, *Chem. Commun.*, Vol. 50, p. 10718, 2014.
56. Y. Xiang, K. Deng, H. Xia, C. Yao, Q. Chen, L. Zhang, Z. Liu, and W. Fu, Isothermal detection of multiple point mutations by a surface plasmon resonance biosensor with Au nanoparticles enhanced surface-anchored rolling circle amplification, *Biosens. Bioelectron.,* Vol. 49, p. 442, 2013.
57. W. Zhao, M. M. Ali, M. a Brook, and Y. Li, Rolling circle amplification: applications in nanotechnology and biodetection with functional nucleic acids, *Angew. Chem. Int. Ed. Engl.*, Vol. 47, p. 6330, 2008.
58. P. N. Abadian, C. P. Kelley, and E. D. Goluch, Cellular analysis and detection using surface plasmon resonance techniques, *Anal. Chem.*, Vol. 86, p. 2799, 2014.
59. W. Liu, Y. Chen, and M. Yan, Surface plasmon resonance imaging of limited glycoprotein samples, *Analyst*, Vol. 133, p. 1268, 2008.
60. T. Hiragun, Y. Yanase, K. Kose, T. Kawaguchi, K. Uchida, S. Tanaka, and M. Hide, Surface plasmon resonance-biosensor detects the diversity of responses against epidermal growth factor in various carcinoma cell lines, *Biosens. Bioelectron.*, Vol. 32, p. 202, 2012.
61. J. Jose, M. Park, and J.-C. Pyun, *E. coli* outer membrane with autodisplayed Z-domain as a molecular recognition layer of SPR biosensor, *Biosens. Bioelectron.*, Vo. 25, p. 1225, 2010.
62. E.-H. Lee, G. Yoo, J. Jose, M.-J. Kang, S.-M. Song, and J.-C. Pyun, SPR biosensor based on immobilized E.coli cells with autodisplayed Z-domains, *BioChip J.*, Vol. 6, p. 221, 2012.
63. Y. Iribe, H. Shinohara, and M. Suzuki, , Label-free detection of B and T cell responses by using high resolution 2D-SPR imaging sensor, 14th International Conference on Miniaturized Systems for Chemistry and Life Sciences, 3–7 October 2010, Groningen, The Netherlands, p. 1646, 2010.
64. M. Horii, H. Shinohara, Y. Iribe, and M. Suzuki, Living cell-based allergen sensing using a high resolution two-dimensional surface plasmon resonance imager, *Analyst*, Vol. 136, p. 2706, 2011.
65. S. Löfås and A. Mcwhirter, The art of immobilization for SPR sensors, in *Surface Plasmon Resonance Based Sensors SE – 17*, ed. J. Homola, Springer, Berlin, Heidelberg, Vol. 4, p. 117, 2006.
66. D. J. O'Shannessy, M. Brigham-Burke, and K. Peck, Immobilization chemistries suitable for use in the BIAcore surface plasmon resonance detector, *Anal. Biochem.*, Vol. 205, p. 132, 1992.
67. O. Salihoglu, S. Balci, and C. Kocabas, Plasmon-polaritons on graphene-metal surface and their use in biosensors, *Appl. Phys. Lett.*, Vol. 100, p. 213110, 2012.

68. Y. Mao, Y. Bao, W. Wang, Z. Li, F. Li, and L. Niu, Layer-by-layer assembled multilayer of graphene/Prussian blue toward simultaneous electrochemical and SPR detection of H_2O_2, *Talanta*, Vol. 85, p. 2106, 2011.
69. L. Wang, C. Zhu, L. Han, L. Jin, M. Zhou, and S. Dong, Label-free, regenerative and sensitive surface plasmon resonance and electrochemical aptasensors based on graphene, *Chem. Commun. (Camb).*, Vol. 47, p. 7794, 2011.
70. V. V. Singh, G. Gupta, A. Batra, A. K. Nigam, M. Boopathi, P. K. Gutch, B. K. Tripathi, A. Srivastava, M. Samuel, G. S. Agarwal, B. Singh, and R. Vijayaraghavan, Greener electrochemical synthesis of high quality graphene nanosheets directly from pencil and its SPR sensing application, *Adv. Funct. Mater.*, Vol. 22, p. 2352, 2012.
71. S. Szunerits, N. Maalouli, and E. Wijaya, Recent advances in the development of graphene-based surface plasmon resonance (SPR) interfaces, *Anal. Bioanal. Chem.*, Vol. 405, 1435, 2013.
72. E. T. Gedig, Surface chemistry in SPR technology, in *Handbook of Surface Plasmon Resonance*, The Royal Society of Chemistry, p. 173, 2008
73. M. Beseničar, P. Maček, J. H. Lakey, and G. Anderluh, Surface plasmon resonance in protein–membrane interactions, *Chem. Phys. Lipids*, Vol. 141, p. 169, 2006.
74. A.V. Hughes, S.A. Holt, E. Daulton, A. Soliakov, T.R. Charlton, S.J. Roser, J.H. Lakey. High coverage fluid-phase floating lipid bilayers supported by v-thiolipid self-assembled monolayers, *J. R. Soc. Interface*, Vol. 11, p. 20140245, 2014.
75. A. Yildiz, U. H. Yildiz, B. Liedberg, and E.-K. Sinner, Biomimetic membrane platform: Fabrication, characterization and applications, *Colloids Surf. B*, Vol. 103, p. 510, 2013.
76. J. A. Maynard, N. C. Lindquist, J. N. Sutherland, A. Lesuffleur, A. E. Warrington, M. Rodriguez, and S.-H. Oh, Surface plasmon resonance for high-throughput ligand screening of membrane-bound protein, *Biotechnol. J.*, Vol. 4, p. 1542, 2009.
77. H. A. Vincent, J. O. Phillips, C. A. Henderson, A. J. Roberts, C. M. Stone, C. E. Mardle, L. E. Butt, D. M. Gowers, A. R. Pickford, and A. J. Callaghan, An improved method for surface immobilisation of RNA: application to small non-coding RNA – mRNA pairing, *Plos One*, Vol. 8, p. e79142, 2013.
78. G. Bidan, M. Billon, K. Galasso, T. Livache, G. Mathis, A. Roget, L. Torres-Rodriguez, and E. Vieil, Electropolymerization as a versatile route for immobilizing biological species onto surfaces, *Appl. Biochem. Biotechnol.*, Vol. 89, p. 183, 2000.
79. L. Grosjean, B. Cherif, E. Mercey, A. Roget, Y. Levy, P. N. Marche, M.-B. Villiers, and T. Livache, A polypyrrole protein microarray for antibody–antigen interaction studies using a label-free detection process, *Anal. Biochem.*, Vol. 347, p. 193, 2005.
80. M.-B. Villiers, S. Cortès, C. Brakha, P. Marche, A. Roget, and T. Livache, A polypyrrole protein microarray for antibody–antigen interaction studies

using a label-free detection process, IN *Peptide Microarrays SE – 17*, eds. M. Cretich and M. Chiari, Humana Press, Vol. 570, p. 317, 2009.
81. J. Bartoli, A. Roget, and T. Livache, Polypyrrole-oligosaccharide microarray for the measurement of biomolecular interactions by surface plasmon resonance imaging, in *Carbohydrate Microarrays SE – 5*, ed. Y. Chevolot, Humana Press, Vol. 808, pp. 69–86, 2012.
82. E. Maillart, K. Brengel-Pesce, D. Capela, A. Roget, T. Livache, M. Canva, Y. Levy, and T. Soussi, Versatile analysis of multiple macromolecular interactions by SPR imaging: application to p53 and DNA interaction, *Oncogene*, Vol. 23, p. 5543, 2004.
83. Brakha, P. Arvers, F. Villiers, A. Marlu, A. Buhot, T. Livache, R. Calemczuk, J.-P. Zarski, C. Villiers, P. Marche, and M.-B. Villiers, Relationship between humoral response against hepatitis C virus and disease overcome, *Springerplus*, Vol. 3, p. 56, 2014.
84. J. Homola, Surface plasmon resonance sensors for detection of chemical and biological species, *Chemical Reviews*, Vol. 108, p. 462, 2008.
85. G . Spoto and M. Minunni, Surface plasmon resonance imaging: what next? *J. Phys. Chem. Lett.*, Vol. 3, p. 2682, 2012.
86. M. E. Stewart, C. R. Anderton, L. B. Thompson, J. Maria, S. K. Gray, J. A. Rogers, and R. G. Nuzzo, Nanostructured plasmonic sensors, *Chem. Rev.*, Vol. 108, p. 494, 2008.
87. S. Gao and N. Koshizaki, Recent developments and applications of hybrid surface plasmon resonance interfaces in optical sensing, *Anal. Bioanal. Chem.*, Vol. 399, p. 91, 2011.
88. E. E. Bedford, J. Spadavecchia, C. Pradier, and F. X. Gu, Surface plasmon resonance biosensors incorporating gold nanoparticles, *Macromol. Biosci.*, Vol. 12, p. 724, 2012.
89. L. M. Zanoli, R. D'Agata, and G. Spoto, Functionalized gold nanoparticles for ultrasensitive DNA detection, *Anal. Bioanal. Chem.*, Vol. 402, p. 1759, 2012.
90. R. D'Agata R and G. Spoto, Surface plasmon resonance imaging for nucleic acid detection, *Anal. Bioanal. Chem.*, Vol. 405, p. 573, 2013.
91. H. Šípová and J. Homola, Surface plasmon resonance sensing of nucleic acids: a review, *Anal. Chim. Acta*, Vol. 773, p. 9, 2013.
92. A. Abbas, M. J. Linman, and Q. Cheng, New trends in instrumental design for surface plasmon resonance-based biosensors, *Biosens. Bioelectron.*, Vol. 26, p. 1815, 2011.
93. P. V. Baptista, G. Doria, P. Quaresma, M. Cavadas, C. S. Neves, I. Gomes, P. Eaton, E. Pereira, and R. Franco, Nanoparticles in molecular diagnostics, *Prog. Mol. Biol. Transl. Sci.,* Vol. 104, p. 427, 2011.
94. E. Llop, J. Bosch, and J. Segura, Surface plasmon resonance in doping analysis, *Anal. Bioanal. Chem.*, Vol. 401, p 389, 2011.
95. S. Mariani and M. Minunni, Surface plasmon resonance applications in clinical analysis, *Anal. Bioanal. Chem.*, Vol. 406, p. 2303, 2014.

96. X. Jiang, M. Waterland, and A. Partridge, Determination of Estriol 16-glucuronide in human urine with surface plasmon resonance and lateral flow immunoassays, *Anal. Methods*, Vol. 2, p. 368, 2010.
97. J. S. Mitchell and T. E. Lowe, Ultrasensitive detection of testosterone using conjugate linker technology in a nanoparticle-enhanced surface plasmon resonance biosensor, *Biosens. Bioelectron.*, Vol. 24(7), p. 2177, 2009.
98. M. Frasconi, C. Tortolini, F. Botre, and F. Mazzei, Surface plasmon resonance immunosensor for cortisol and cortisone determination, *Anal. Chem.*, Vol. 82, p. 7335, 2010.
99. H. R. Jang, A. W. Wark, S. H. Baek, B. H. Chung, and H. J. Lee, Ultrasensitive and ultrawide range detection of a cardiac biomarker on a surface plasmon resonance platform, *Anal. Chem.*, Vol. 86, p. 814, 2013.
100. S. A. Vance and M. G. Sandros, Zeptomole detection of C-reactive protein in serum by a nanoparticle amplified surface plasmon resonance imaging aptasensor, *Sci. Rep.*, Vol. 4, p. 5129, 2014.
101. J. Martinez-Perdiguero, A. Retolaza, L. Bujanda, and S. Merino, Surface plasmon resonance immunoassay for the detection of the TNFα biomarker in human serum, *Talanta*, Vol. 119, p. 492, 2014.
102. Y. Uludağ and I. E. Tothill, Development of a sensitive detection method of cancer biomarkers in human serum (75%) using a quartz crystal microbalance sensor and nanoparticles amplification system, *Talanta*, Vol. 82, p. 277, 2010.
103. W. Hu, H. Chen, Z. Shi, and L. Yua, Dual signal amplification of surface plasmon resonance imaging for sensitive immunoassay of tumor marker, *Anal. Biochem.*, Vol. 453, p. 16, 2014.
104. X. Yao, X. Li, F. Toledo, C. Zurita-lopez, M. Gutova, J. Momand, and F. Zhou, Sub-attomole oligonucleotide and p53 cDNA determinations via a high-resolution surface plasmon resonance combined with oligonucleotide-capped gold nanoparticle signal amplification, *Anal. Biochem.*, Vol. 354, p. 220, 2006.
105. R. D'Agata, G. Breveglieri, L. M. Zanoli, M. Borgatti, G. Spoto, and R. Gambari, Direct detection of point mutations in nonamplified human genomic DNA, *Anal. Chem.*, Vol. 83, p. 8711, 2011.
106. R. Wernersson, A. S. Juncker, and H. B. Nielsen, Probe selection for DNA microarrays using OligoWiz, *Nat. Protoc.*, Vol. 2, p. 2677, 2007.
107. M. L. Ermini, S. Mariani, S. Scarano, and M. Minunni, Direct detection of genomic DNA by surface plasmon resonance imaging: an optimized approach, *Biosens. Bioelectron.*, Vol. 40, p. 193, 2013.
108. S. Mariani, S. Scarano, M. Carrai, R. Barale, and M. Minunni, Direct optical genotyping of Single Nucleotide Polymorphisms in unamplified human genomic DNA by Surface Plasmon Resonance imaging biosensor: the case of C3435T polymorphism in MDR1 gene, *Anal. Bioanal. Chem.*, Vol. 407(14), p. 4023, 2015.
109. S. Fang, H. J. Lee, A. W. Wark, and R. M. Corn, Attomole microarray detection of microRNAs by nanoparticle-amplified SPR imaging measurements

of surface polyadenylation reactions, *J. Am. Chem. Soc.*, Vol. 128, p. 14044, 2006.

110. L. Malic, T. Veres, and M. Tabrizian, Nanostructured digital microfluidics for enhanced surface plasmon resonance imaging, *Biosens. Bioelectron.*, Vol. 26, p. 2053, 2011.
111. R. Kurita , Y. Yokota, Y. Sato, F. Mizutani, and O. Niwa, On-chip enzyme immunoassay of a cardiac marker using a microfluidic device combined with a portable surface plasmon resonance system, *Anal. Chem.*, Vol. 78, p. 5525, 2006.
112. C. Liu, T. Lei, K. Ino, T. Matsue, and C. Li, Real-time monitoring biomarker expression of carcinoma cells by surface plasmon resonance biosensors, *Chem. Commun.*, Vol. 48, p. 10389, 2012.
113. T.-L. Chuang, C.-C. Chang, Y. Chu-Su, S.-C. Wei, X. Zhao, P.-R. Hsueh, and C.-W. Lin, Disposable surface plasmon resonance aptasensor with membrane-based sample handling design for quantitative interferon-gamma detection, *Lab on Chip*, Vol. 14, p. 2968, 2014.
114. S. Wang, X. Shan, U. Patel, X. Huang, J. Lu, J. Li, and N. Tao, Label-free imaging, detection, and mass measurement of single viruses by surface plasmon resonance, *Proc. Nat. Acad. Soc.*, Vol. 107, p. 16028, 2010.
115. F. Remy-Marti, M. El Osta, G. Lucchi, R. Zeggari, T. Leblois, S. Bellon, P. Ducoroy, and W. Boireau, Surface plasmon resonance imaging in arrays coupled with mass spectrometry (SUPRA–MS): proof of concept of on-chip characterization of a potential breast cancer marker in human plasma, *Anal. Bioanal. Chem.*, Vol. 404, p. 423, 2012.

4

Electropolymerized Materials for Biosensors

Gennady Evtugyn[1], Anna Porfireva[1], and Tibor Hianik*[2]

[1]Department of Analytical Chemistry, Kazan Federal University, Kazan, Russia
[2]Department of Nuclear Physics and Biophysics, Comenius University, Bratislava, Slovakia

Abstract

The review is related to the synthesis and application of electropolymerized materials with their own redox activity in the assembly of biosensors devoted to the detection of biomarkers, proteins, toxins and genotoxic species. Polyaniline, polypyrrole, polythiophene and polyphenazines applied in electrochemical biosensors will be mostly described as well as hybrid polymeric materials with implementation of nanoparticles of metals, their oxides and carbonaceous materials. Besides short description of the mechanism of electropolymerization, main attention will be focused on the role of polymers in the biosensor functioning. The use of polymers as immobilization matrix, their role in the signal generation and protection of biocomponents will be considered with an emphasis to the relationship between the intrinsic properties of the polymers and their applicability in biosensor assembly. Mostly, the biosensors based on the enzymes, antibodies and DNA will be considered.

Keywords: Electropolymerization, biosensor, polyaniline, polypyrrole, polythiophene

4.1 Introduction

There is a growing interest in the development of novel biosensing devices devoted to the detection of various molecules, i.e., disease biomarkers,

**Corresponding author*: Tibor.Hianik@fmph.uniba.sk

Ashutosh Tiwari, Hirak K. Patra and Anthony P.F. Turner (eds.) Advanced Bioelectronic Materials, (89–186)

metabolites, environmental pollutants, pharmaceutical preparations, food additives, etc. Although all of the substances can be reliably detected with conventional analytical techniques, mainly chromatography and spectroscopy, the necessity in consistent preliminary information on the sample content available far from modern equipped laboratories calls for the development of portable devices intended for unqualified users. Biosensor is a portable device providing specific quantitative or semi-quantitative analytical information using a biological recognition element, e.g., enzyme, DNA, or antibodies. It is assumed that the biochemical receptor is in direct spatial contact with a transducer converting biochemical response in electrical or optical signal [1].

The significance of biosensor analysis of many species which have crucial importance for human health, environmental protection and food safety resulted in dramatic enhancement of the biosensor market especially in the area of glucose assay for diabetes patients and some other clinically important compounds like oxalic and uric acid, urea and immunodiagnostics [2]. What important is that biosensors promise significantly decrease of the price of assay and hence are directed to a broad application among population in the framework of personalized medicine concept and point-of-care diagnostic tools. In environmental monitoring, biosensors are mainly intended for the detection of most toxic species, e.g., pesticides and industrial pollutants as well as on the early warning on carcinogenic substances [3].

Starting from the first work on glucose electrode opening the biosensors era [4] electrochemical transducers dominate among other detection principles due to undisputable advantages they possess, i.e., high sensitivity, user friendly design, intuitive operation and results interpretation, automation and miniaturization prospects and compatibility with conventional measurement equipment [5]. Electrochemical biosensors can be used for the analysis of optically non-transparent samples including biological fluids and tissues, they are easily implemented in automation and flow-through system and mostly do not require sophisticated sample treatment. It should be also mentioned that electrochemical sensors are common in medicine and biology (measurements of blood gases, redox potential, electrophysiology, potentiometric detection of K^+/Na^+ ions, etc.) and the principles of electrochemistry are frequently used in biophysics and biochemistry (metabolic paths, photosynthesis, ATP synthesis, etc.) [6]. This makes easier both the development and application of biosensor in appropriate areas of biology and medicine [7].

The determination of the origin and quantity of target species in the presence of many others in ambient conditions is one of the most cited

advantages of biosensors [8]. The selectivity of interaction between the target analyte and biochemical receptor on the biosensor interface is mainly presumed on the nature of biochemical reactants. Meanwhile, the performance of appropriate biosensor highly depends on the way the biochemical receptor is introduced in the biosensor assembly [9]. This is mainly related to fixing the biocomponent of a biosensor on the transducer surface called as immobilization. In addition, the environment most favorable for the biochemical interactions should be provided and the signal corresponded to such interaction generated and recorded. In respect of the selectivity of transduction processes, electrochemical devices are limited by the nature of appropriate redox reactions that take place on the transducer surface. In comparison with optical sensors, electrochemical (mainly voltammetric) sensors offer lower resolution and higher sensitivity toward interfering factors like presence of redox-active species or adsorption of proteins or surfactants. For this reasons, the arrangement of surface layer including besides biochemical components some auxiliary materials intended to suppress any interfering factors is considered as a key step of the biosensor development which often predetermined the final success and applicability of biosensors for real sample assay.

Many modifiers have been reported during the past decades of biosensor development to improve the performance of electrochemical biosensors. From their variety, two main groups deserve special attention. They include (1) polymers which act as carriers of biochemical receptors on the stage of their immobilization and also mechanically protect the biochemical layer from deterioration [10], and (2) redox mediators that decrease the working potential and amplify the current corresponded to the oxidation (rarely reduction) of a target species [11, 12]. The application of the polymers initiated from some relative biochemical techniques like electrophoretic isolation and purification of the proteins or immune blotting in immune and DNA assay. Derivatives of cellulose [13, 14], silk fibroin [15] nylon and polyelectrolytes like Nafion or polystyrene sulfonate [16, 17] are mainly used in biosensor assembly. Depending on the material and its role in biosensor functioning, the polymers can be either attached to the surface (polymeric membranes) or formed directly on site by casting the suspension followed by the solvent evaporation [18]. Both approaches show their drawbacks and advantages. Briefly, the use of commercial membranes assumes periodical regeneration of the surface layer and well conforms to flow-through conditions. The membrane molding on the transducer surface is preferable for miniature devices. It makes it possible to immobilize the biochemical receptors together with polymer deposition in one step by entrapment of the biomolecules in the growing polymer film.

Redox-active species able to reversible electron exchange often called 'redox mediators' decrease the overvoltage of the electrode reaction [19]. The necessity in such additives is due to two reasons most frequently mentioned, i.e., (1) decrease of the working potential and hence of the possible negative effect of other redox-active species present in the sample; and (2) changes in the mechanism of the electrode reaction, e.g., prevention of the deposition of insoluble products (electrode fouling) or provision of reversibility of the electron transfer.

High overvoltage of direct electron transfer from/to biopolymers is explained by the complex structure of most biochemical receptors applied in the biosensor assembly. Both the redox-active site of an oxidoreductase enzyme and nucleotides of a DNA sequence are positioned deeply inside electrochemically inert surrounding and hence cannot be in close direct contact with the electrode. In accordance with Marcus' equation (4.1) [20] the rate constant of the electron transfer k_{et} decreases with increasing real distance of the electron transfer d_0.

$$k_{et} = \exp\left[-\beta\left(d - d_0\right)\right]\exp\left[-\frac{\left(\Delta G^0 + \lambda\right)^2}{4RT\lambda}\right] \tag{4.1}$$

Here, d is Van der Waals' distance; ΔG^0 and λ are Gibbs' and reorganization energies, respectively. Bulky proteins or rigid DNA helixes do not provide the density of the contact points required for remarkable signal, whereas the mediators play role of shuttles that transport electrons from the redox centers and the electrode. Although the contribution of reorganization energy near the electrode interface should be taken into account, the steric hindrance is considered as main reason of low electric signal of proteins and DNA on non-modified electrode.

Various redox mediators have been described for biosensor design during the past decades. They involve oxides and complexes of transient metals, heteroaromatic and polyaromatic structures, carbonaceous materials and nanoparticles of the noble metals. Although shuttle functions are better established with free mediators, they can be also attached to the electrode surface via long flexible linker. This makes it possible to avoid losses in mediators during the biosensor operation in decrease the number of reagents and measurement stages required.

Although the electrochemical biosensors have successfully adopted the protocols of electrode modification previously elaborated for voltammetric sensors, the variety of biochemical receptors and appropriate targets calls for the continuous improvement of modifiers to achieve the sensitivity and

selectivity of bioassay required for their following commercialization and mass production. At present, more sophisticated combinations of several materials are reported to improve the preparation and operation of appropriate biosensors. One of the promising approaches is based on the use of the polymers obtained by electropolymerization directly on the working surface of the transducer and offering both the immobilization and electric wiring the biomolecules [21].

The use of electropolymerized materials was the subject of several excellent reviews published recently with particular emphasis to the immobilization ways [22] or electroconductivity properties [23]. In this review, the literature covering past 10 years is summarized in accordance with the biorecognition element and polymer used in the assembly of the biosensor. It should be mentioned, that some woks are devoted to the use of chemically synthesized polymers which characteristics are similar but not identical to those obtained by electrolysis. This is mainly related to polyaniline (PANI) which chemical oxidation results in higher molecular mass and lesser by products yield in comparison with electrochemical alternative [24]. Nevertheless, main principles of their application in the biosensor assembly remain the same and such references will be also presented in the review. The same refers to conventional polymers containing redox-active groups in the substituents implemented in side-chains of the polymer molecule.

4.2 Electropolymerized Materials Used in Biosensor Assembly

4.2.1 General Characteristic of Electropolymerization Techniques

In all the materials obtained by electropolymerization, the reaction is initiated by oxidation of appropriate monomer to cation radical that is coupled with either another monomer molecule or second radical with subtraction of the hydrogen ion. If the intermediate particle is stable enough, the propagation stage continue to form oligomeric and polymeric products like in ion-radical polymerization of unsaturated compounds initiated by chemical oxidants. Most frequently, the generation of radical particles is required during the whole polymerization period because of the low efficiency of the coupling reaction. The propagation involves the formation of the cation radical of intermediate oligomers. Coupling monomeric unit does not affect dramatically the electrochemical activity of the product so that all

the variety of oligomeric products gives one broaden peak on voltammogram. The electroconductive polymers like PANI, polythiophene derivatives and polypyrrole (PPY) show on voltammogram recorded during the electropolymerization a series of peaks which height progressively increases with the amounts of products deposited on the electrode surface. Redox-active polymers like polyphenothiazines and polyphenazines form two pairs of peaks. One pair corresponds to the monomers present in the solution and the second one to the polymerization products. The pairs differ in the peak potentials. Polymeric products exert higher peak potential difference against that of the monomers due to lower reversibility of the electron exchange. This can be due to blocking of the electron transfer from the transducer followed by the full coverage of the electrode surface and shuttle mechanism of the oxidation–reduction of redox centers within the polymeric film. Due to latter reason, the cyclic voltammogram recorded on the electrode modified with redox active, but non-conductive polymer looks similarly to that of diffusion limited electrode reaction and does not correspond to canonical surface reaction with a bell-shaped peak and sharp decay of the current after reaching its maximal value. Poly(neutral red) is the only exception with the peak potentials equal for monomeric and polymeric form so that changes in the voltammograms do not cover the position and shape of the peaks on the potential axis [25].

As could be already seen from the above description, the redox-active polymers in the assembly of biosensors are mostly classified in accordance with the paths of the electron exchange. In general, three types of the polymers can be mentioned:

- *Electroconductive polymers* that show electronic–ionic conductivity and resistance comparable to that of semiconductors. Such polymers can effectively wire redox centers of biomolecules [26, 27]. PANI, PPY and polythiophene derivatives are mostly used in this group of the polymers together with their derivatives exerting similar electrochemical properties.
- *Electrochemically active polymers* which can mediate electron exchange near their redox peaks' pair but are inactive in the other potential regions [28, 29]. The polymers of this group are quite effective as redox mediators especially due to possibility to establish close contact with biomolecules within the polymerization step. Polycyclic heteroaromatic systems obtained from phenazines, phenoxazines and phenothiazines belong to this group of polymers. Many of them are known under trivial names as dyes or redox indicators (neutral red [30],

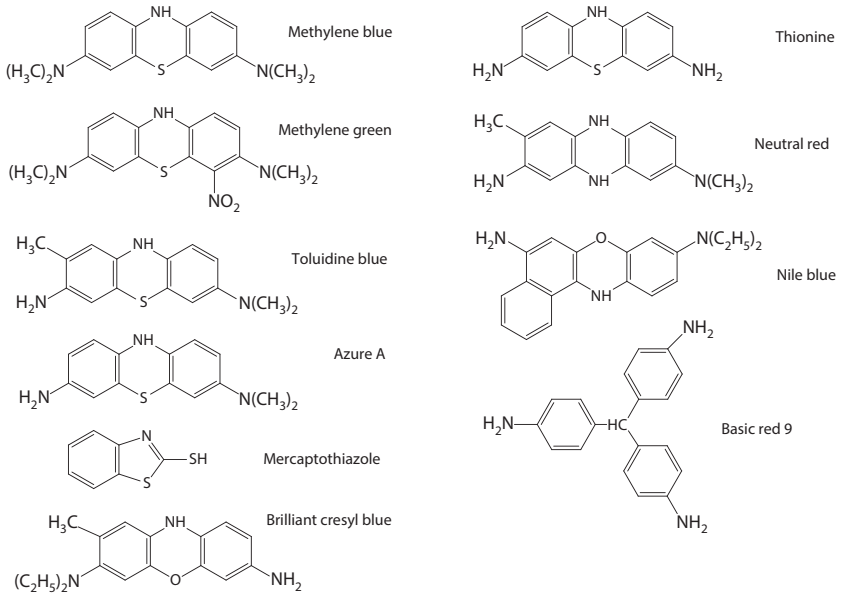

Figure 4.1 Monomers used for the synthesis of redox-active polymers and application in biosensor assembly (reduced forms are presented).

methylene blue [31], etc.). The structures of frequently used monomers of this group are presented in Figure 4.1.

- *Non-conductive polymers with separated redox-active groups*. They differ from the second group mainly by the way of the synthesis. Redox-active units are chemically implemented in the substituents of the main chain in a distance preventing or making ineffective the electron exchange between them. For this reason the polymer works as a micro array of isolated redox centers and the role of the polymer core is limited to establishment of regularity in spatial distribution of such centers and simplicity of transducer modification. Ferrocene-modified polymers for glucose sensors are mostly known representatives of this group [32]. Dendrimers, hyper-branched polymers with a core and repeatedly branched shells, can be also referred to this group [33]. They are commonly used as enzyme carriers and stabilizers. However, dendrimers bearing terminal redox groups facilitate the electron transfer and hence can wire enzyme redox centers. Polyamidoamine (PAMAM) derivatives are mainly used for this purpose.

Chemical synthesis of the redox-active polymers utilizes two strategies, i.e., (1) modification of a polymer via siding functional groups, and (2) polymerization of the monomers already containing redox centers. The second way can be complicated by involvement of redox groups in the initiation and propagation of the reaction so that the modification of already existed polymers is considered more convenient. The possibility of modification directly on the working surface and variety of the products obtained are additional advantages of such an approach.

The details of the chemical synthesis of redox-active polymers are beyond the scope of this review, but they are briefly described in reviews and monographs [18, 34, 35].

The deposition of the electropolymerized film can be performed prior to or together with the biomolecule immobilization. First approach is more flexible because it allows changing the solvent and exclude chemical inactivation of biochemical receptor. The electropolymerization can be performed in polar organic solvent containing monomer(s) and then the electrode is transferred in aqueous solution of a protein/ DNA to finish the assembling of the surface layer. In this case, electropolymerization is performed in potentiostatic mode to increase the mass of the polymer deposited on the surface and control the redox status of the coating.

Second approach assumes the use of water-soluble monomers and involves electropolymerization in aqueous solution compatible with the biopolymers and in conditions mostly comfortable for biomolecules to be implemented/detected. Low solubility of some monomers can be partially compensated for by addition of surfactants or emulsifying agents [36, 37]. However, emulsification and the use of miscellaneous water-organic media decrease the reproducibility of the polymer characteristics and worsen the biosensor performance.

Taking into account biosensor development, multiple scanning of the potential in aqueous monomer solution is preferable. The protocol of such polymerization assumes reversible reduction/oxidation of the redox units in growing polymer film. Being less effective in sense of the current yield than potentiometric mode, multiple scanning exerts other advantages, i.e., continuous information on the polymerization process from the shape and height of the peaks on voltammograms, control of possible formation of by-products, commonly related to oxidative degradation of the functional groups in the side chains of the polymer, and intuitively understandable parameters of optimization. The number of potential scans required for electropolymerization is rather small. The changes of the redox activity of the electrode interface indicating the film deposition started from second cycle. Appropriate changes of the surface morphology indicated by atom

force microscopy (AFM) started from third to fifth cycle. First scans of the potential cannot provide the formation of a high-molecular product and actually oligomers are precipitated on the electrode. The structure and spatial distribution of the polymers were investigated only for PANI and PPY and mainly for chemically synthesized polymers.

Electropolymerization can be easily combined with implementation of other redox mediators which are either pre-deposited onto the surface or implemented into the polymer structure by physical entrapment, simultaneous synthesis or covalent linking. Metal nanoparticles (Au [38, 39] and Pt [40, 41]) and carbon nanotubes (CNTs) [42, 43] are mostly used for such electrode pre-treatment although some other common mediator systems are described [44]. Such protocols are aimed to increase the specific surface of the electrode and hence the amounts of polymers deposited. The additives improve the electron transfer in rather thick films of redox-active polymers and the efficiency of electropolymerization. Increase in the roughness or formation of nanosized domains with regular structure and positioning on the transducer are preferable for the following DNA immobilization.

4.2.2 Instrumentation Tools for Monitoring of the Redox-Active Polymers in the Biosensor Assembly

The characteristics of polymeric coatings on the surface of biosensor transducers are mainly established by electrochemical impedance spectroscopy (EIS) [45], electronic and probe microscopy. Charge transfer resistance and capacitance of the surface layer indicate changes in the charge distribution and permeability of the surface layer for redox probe, e.g., ferricyanide ions or ruthenium complexes. Although conductance measurements require special technique like four-point probe measurements, the redox activity of PANI and PPY correlates with their electroconductivity and allows optimizing measurement conditions in sense of maximal yield of polymerization and efficiency of receptor wiring. Comprehensive EIS consideration makes it possible to characterize non-uniform structure of the polymer including the existence and size distribution of the pores, appearance of the cracks providing direct access of the charge carriers to the electrode, etc. [46, 47]. It should be mentioned that most of the biochemical molecules immobilized with or after electropolymerization significantly increases the irregularity of the surface layer and its thickness due to swelling and excessive hydration caused by counter ions. On the other hand, deposition of DNA and polyelectrolytes suppresses such phenomena and allows using simplified approaches based on Randles equivalent circuit assuming homogeneous structure of the film with near-zero thickness.

Electronic spectroscopy as well as AFM visualizes insoluble products which form on the electrode surface great variety of the shapes, e.g., rods, beads, star-like particles, dendritic structures and nanofibers [48]. Most of the reported results of scanning electron microscopy (SEM), transmission electron microscopy (TEM) and AFM include qualitative description of the surface morphology although the distribution of the clusters by size, height and relative permeability is also available.

Although the images obtained by AFM, SEM and TEM are very convincing and frequently give valuable information about the influence of experimental parameters on the polymerization process, two limitations should be taken into account. First, very small part of the surface is visualized, whereas the whole working surface can contain other inclusions unpredictably affecting the features of the biosensor. Second, the supports used in such investigations are not the same as those in biosensor assembly. Highly ordered pyrographite and mica show a smooth surface which is necessary to check the morphology of newly formed particles, but they differ from glassy carbon and even polished gold commonly used in biosensor and affecting the electropolymerization/polymer casting. Certainly, coverage of the electrode with first quantities of polymer suppresses the influence of the support material, but the morphology of the support determines the specificity of the polymer surface rather significantly.

Spectroscopic studies exploit Fourier transformation–infra red (FTIR), UV–Vis and surface plasmon resonance (SPR) techniques which provide information about the nature of organic components of the surface layer and surface reaction run. Indium-tin oxides (ITO) electrodes and thin transparent golden films on a quartz or glass plates make it possible to simultaneously monitor redox and optical properties of the polymer layers. Thus, for PANI–ClO_4^- films electrochemically deposited onto ITO electrode, the peaks at 793 and 1055 cm^{-1} in FTIR spectra were assigned to stretching and bending vibrations associated with C–N linkage, the strongest band at 1469 cm^{-1} to C–C stretching. The 1545 and 3014 cm^{-1} peaks were ascribed to N–H bending and C–H group, respectively [49]. Similarly, carbodiimide binding of the proteins or DNA oligonucleotides is confirmed by observation of appropriate bands assigned to >C=N– fragments. SPR technique differs from other spectroscopy methods mentioned [50]. In this approach, total reflectance on the laser beam on the interface of two optically transparent media covered with a thin Au film is monitored. The conditions of refraction, specifically, the energy dissipating on the interface as evanescent wave depends on the processes that take place on the Au surface. Although the sensitivity of SPR method is limited by rather large biomolecules, this technique is used for kinetic measurements

of association–dissociation of biomolecular receptors (antigen–antibody and DNA–protein interactions). SPR measurement can be combined with simultaneous electrochemistry so that eletrodeposition of the polymers can be quantified and utilized for the optimization of electrode modification. In a similar manner, surface-enhanced Raman spectroscopy (SERS) utilizes similar optical phenomena on conductive nanoparticles to record Raman spectra of organic molecules, among others those involved in biochemical interactions.

Direct observation of a polymer growth can be performed by quartz crystal microbalance (QCM) and the modification of the method combined with electrochemical measurements (EQCM) [52]. The QCM experiments in liquid phase do not provide exact estimated of a mass deposited on the electrode, changes of the frequency of quartz oscillations are interpreted in terms of efficiency of deposition, both that of the polymer and biological target in biosensor applications [52].

4.2.3 Redox-Active Polymers Applied in Biosensor Assembly

PANI is a linear polymer which is synthesized in strongly acidic conditions necessary to stabilize primary cation radical formed in the initiation step (4.2). The necessity in rather strong oxidants or high anodic voltage often results in formation of quinoid by-products which participate then in the reversible electron exchange and worsen electroconductivity and stability of the polymer. Meanwhile, de-amination does not seriously affect the electrocatalytic features of PANI. The product of primary electron transfer undergoes head-to-tail polymerization. Nitrogen atom directly participates in the polymerization and the PANI redox conversion. The rate of the polymer precipitation increases with the reaction product amount [53].

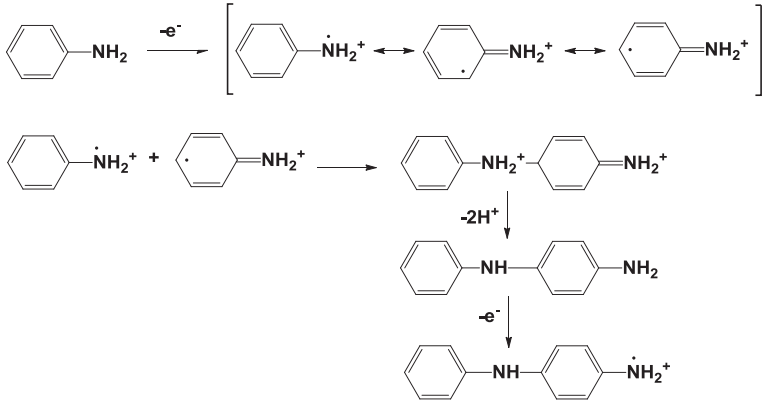

(4.2)

Many characteristics of the PANI depend on the redox equilibria of its reduced and oxidized forms (4.3) which take place depending on the redox potential and pH of the solution [54, 55].

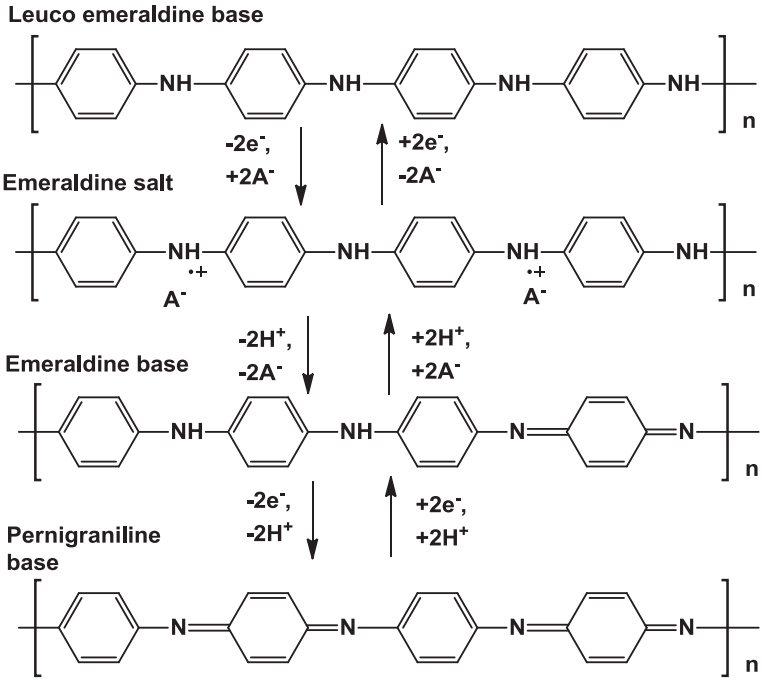

(4.3)

Only a half-oxidized emeraldine salt exerts electroconductivity. In electrosynthesis, the conductivity window, adhesion of the film to the electrode and some other PANI characteristics are regulated by electrolysis regime, temperature and counter ion used. In chemical oxidation, the ratio of monomer/oxidant, temperature and oxidation time are important.

The PANI swells in acidification of the solution or addition of oxidants due to transfer of counter anions bearing hydrate shell. This process is reversible and can change the specific volume of the polymer by 30%. Swelling is one of the reasons to use the potential scanning for PANI electrosynthesis. In periodical changes of the redox-status water and low-molecular components are "squeezed out" from the growing polymer which becomes denser and is better attached to the solid surface. In chemical synthesis, the polymer can be contaminated with the impurities formed from the oxidants. $FeCl_3$, H_2O_2 and $(NH_4)_2S_2O_8$ are used for aniline oxidation [56]. Also, biochemical synthesis with peroxidase/H_2O_2

system [57] and photochemical PANI synthesis [58] are described. The decrease of the temperature down from –30 to –70 °C improves regularity of the PANI structure and minimizes the content of de-amination products.

PANI is insoluble in most organic solvents and requires special treatment like grinding with doping agents (camphorsulfonic acid [59] and some other strong organic acids insoluble in water) and plasticizer (phenol). The formation of thin regular PANI films is one of the most important advantages of electrosynthesis for the biosensor development.

On voltammograms recorded by potential scanning in solution of aniline in a strong acid, three reversible peak pairs are commonly observed. Two of them correspond to redox conversion of leuco-emeraldine/emeraldine salt and emeraldine salt/pernigraniline. In between two peak pairs, reversible peaks of quinoid degradation products often exist. The peaks grow with the number of potential cycling and became broader. If the acidity of the solution is insufficient, the peaks amalgamate with formation of one complex very broaden peak in the middle area of the potentials. Many polyanionic species (Nafion, polystyrene sulfonate, polyacrylic acid, DNA) are used as templates in the PANI synthesis due to their interaction with oxidized (positively charged) from the polymer and hence stabilization of the product [60].

The *o*- or *m*-substituted anilines are able to polymerize similarly to that of unsubstituted aniline. The same mechanism is proposed for polymerization of thionine [61] and some other aminated heterocyclic compounds [28]. Among other cases, the use of sulfonic and carboxylic derivatives is of special interest because of the self-doping effect [62, 63]. Anchoring counter ion covalently attached to the polymeric chain stabilizes the reaction product and improves electrochemical properties of modified electrodes. Insoluble strong organic acids [64] and sulfonated or carboxylated CNTs exert similar influence [65, 66]. For the same reason, PANI can be involved in polyelectrolyte complexes [41, 67, 68, 69].

PPY is formed in the cation radical initiated process similar to that described for PANI (4.4). However, chain propagation does not involve nitrogen atoms which can be modified either in monomer or PPY to improve solubility, hydrophilicity or for covalent attachment of the proteins or DNA molecules. The final product contains rather high (up to 50 mass.%) amount of counter ions located between the planes formed by pyrrole heterocycles. The solubility of PPY in organic solvents is even lower than that of PANI.

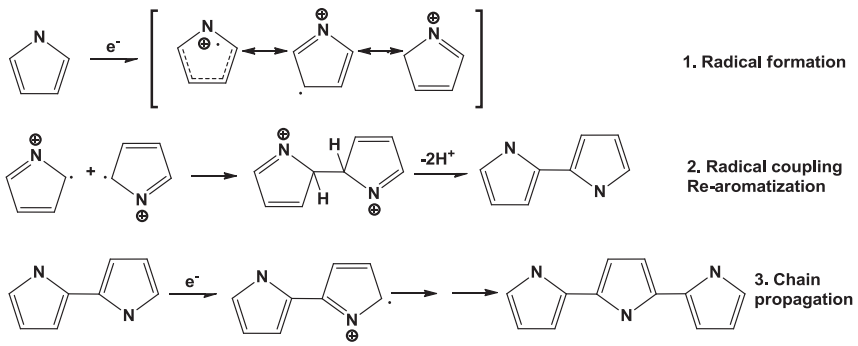

(4.4)

Together with moderate adhesion to electrode materials, this makes chemical synthesis less appropriate for biosensor application in comparison with electrolysis. Also, the PPY redox equilibria are less sensitive than those of PANI toward the pH and doping anion nature. PPY provides only one redox equilibrium and one pair of broaden peaks on cyclic voltammogram.

PPY can form mixed polymeric products which extend the electrocatalytic activity or immobilization abilities of the product. Thus, the copolymers of pyrrole and aniline [70, 71], substituted and unsubstituted pyrroles [72, 73] have been synthesized and used in the DNA and enzyme sensors.

Polythiophenes are synthesized similarly to PPY in accordance with general reaction sequence (4.4) where N atoms are substituted with sulfur. However, the thiophene oligomers are easily oxidized to sulfones (4.5) so that the redox activity and conductivity of the product is limited by the presence of such impurities.

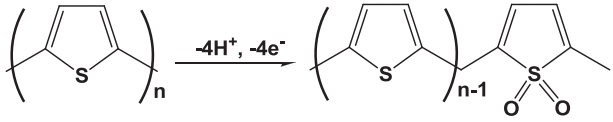

(4.5)

The working potential of electrochemical polymerization can be decreased by the use of thiophene dimers and tetramers instead of the monomer [74]. Presently, substituted polythiophenes are more popular in the biosensor applications due to higher solubility of appropriate monomers in water and organic solvents. Among others, poly(3,4)-ethylenedioxythiophene (PEDOT) and 3-alkylsubstuted polythiophenes are described.

PEDOT has been applied in chemical sensors since early 1990s [75]. The electrosynthesis of PEDOT is performed by cyclic potential scanning in aqueous or organic media in the potential range from about –0.8 to 1.0 V. The initiation step of cation radical formation yields irreversible peak near 0.8–1.0 V which decreases to about full disappearing to tenth cycle. In

parallel, an ill-defined pair of reversible peaks related to redox conversion of PEDOT appears at about –0.5 to –0.3 V. PEDOT in oxidized doped form is much more stable than PPY and PANI and shows high adhesion to the solid support because of the 3,4-dioxyethylene cycle which provides favorite geometry of the polymeric chain and leaves no sites free for carbonyl formation [76]. The electron transduction via PEDOT film is a complex process which probably includes several overlapping redox steps [77] and demonstrates high rate of the transfer of charge carriers and electroconductivity of the final products.

3-Alkyl or alkoxy substituted thiophenes are polymerized preferably in organic solvents, i.e., acetonitrile [78]. They form dense films with regular position of hydrophobic substituents orthogonally to the electrode interface. Such polymers are compatible with other self-assembled monolayers on gold or lipid films. The substituents can be also used for covalent immobilization of biomolecules. Scheme (4.6) shows the attachment of DNA oligonucleotides as an example [79]. Steric access of the bulky reactant can be improved by copolymerization of substituted and un-substituted thiophenes on the same support.

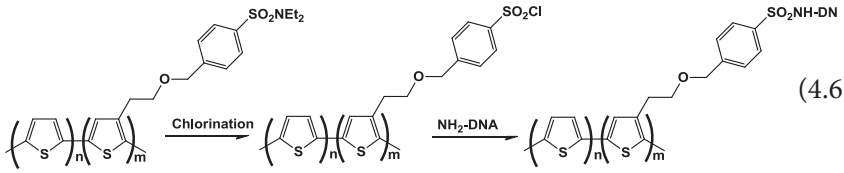

(4.6)

Polyphenoxazines and *polyphenothiazines* can be obtained in neutral and basic aqueous media. The efficiency of electropolymerization and the mass deposited on electrode increase with the pH of reaction mixture. In repeated cycling of the potential, the polymerization results in continuing decrease of the irreversible anodic peak at high potential and increase of the pair of the peaks at lower potentials which formally corresponds to the redox conversion of monomeric form of the phenothiazine [see (4.7) for methylene blue (X = H) and methylene green (X = NO_2) as an example].

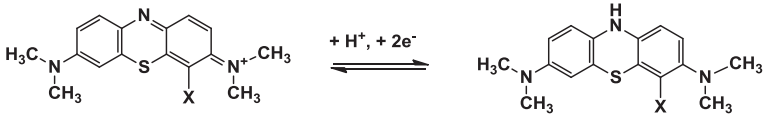

(4.7)

It should be mentioned that contrary to PANI, PPY and their derivatives, no chemical synthesis of polyphenothiazines and polyphenoxazines was described for biosensor development as an alternative to their

electropolymerization. The products of such electropolymerization are mostly undiscovered and their structure is supposed on the base of cyclic voltammetry and spectroelectrochemistry. Thus, polymerization of *methylene blue* results in preferable *N*-demethylation of the initial molecule (*N*-to-ring coupling [80]). Another mechanism assumes ring-to-ring coupling which might involve the following benzidine rearrangement (4.8) [81]. Similar structure of oligomers was confirmed by on-line electrochemistry – electro spray mass spectrometry [82].

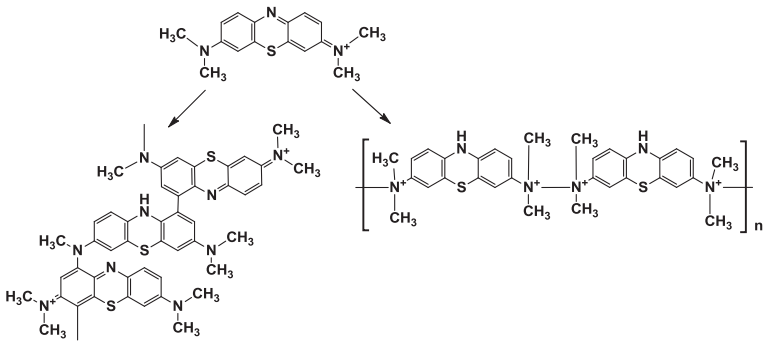

(4.8)

Electrochemical and SPR study of poly(methylene blue) on gold electrode showed the formation of leuco-form of the polymer with reduced electroactivity in concentrated monomer solution [83].

Methylene green shows rather small changes in repeated cycling on glassy carbon electrode if the higher potential does not exceed 0.8 V. The peaks related to the reversible redox reaction (4.7) are drifted to anodic potentials with minor increase of the peak current [84]. Some of explanations suggest reversible sorption of the initial compound on the electrode surface guided by the charge of the molecule [85]. Meanwhile, increase of the higher scanning potential to 1.0–1.2 V makes the voltammogram similar to that observed for methylene blue with a couple of growing reversible peaks related to the polymer and decreasing irreversible anodic peak at high potentials that initiates the polymerization [86].

Neutral red is preferably oxidized in neutral media to form both linear and branched polymers. Cycling the potential increases the primary pair of peaks at –700…–500 mV vs. Ag/AgCl with insignificant changes of the rest of the voltammogram [29]. Changes in the peak currents coincide well with mass of the surface film estimated by EQCM techniques [25]. In some reports, smaller reversible peaks at about 0...200 mV increasing with the number of cycles are mentioned but their relation to the primary polymerization product is not discussed. The *N*-to-ring polymerization products are proposed for the neutral red [see (4.9) for proposed dimer structure].

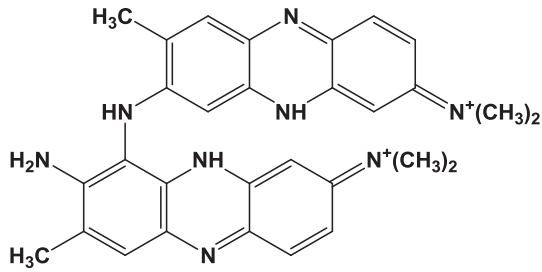

(4.9)

Dendrimers with redox-active functional groups. Among redox-active polymers which are chemically synthesized and do not have analogs obtained by electrosynthesis, dendrimers are of main interest [33]. Dendrimers are composed of three distinct domains, i.e., the core, the Dendron and the terminal functional groups. The space between the branches of a dendrimer molecule forms cavities (Figure 4.2). The properties of the dendrimers are preferably determined by peripheral functional groups, although the internal functionality of the cavities and the core are significant.

Dendrimers are obtained by two approaches. In *divergent approach*, the growth of the dendrimer proceeds from its core to the periphery by consecutive coupling of the monomers to peripheral functional groups. In convergent approach, the growth is initiated by synthesis of dendrons which are then amalgamated by coupling the core fragment. Redox-active dendrimers mainly involve ferrocene units covalently attached to the terminal functional groups of the molecule. They are chemically and electrochemically stable and exert high efficiency of electron transfer. The redox conversion ferrocene–ferrocenium cation is pH independent and can be used for detection of oxidoreductase substrates which reaction is followed by acid release.

The efficiency of the electron transfer depends on the number of shells (dendrimer generation) and ferrocene units and is higher than that of a linear analog [87, 88]. Cobaltocene, an analog of ferrocene, has been

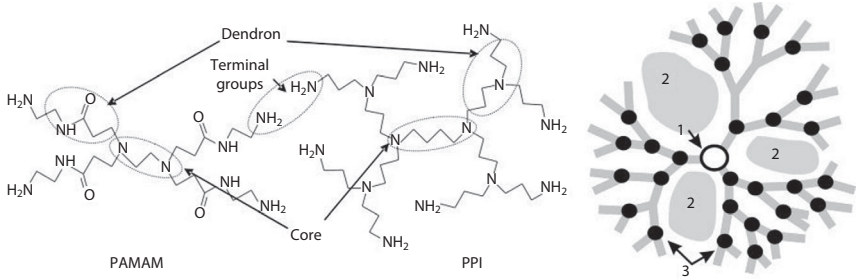

Figure 4.2 The structure and spatial arrangement of dendrimer molecule. PAMAM – poly(amidoamine) and PPI – poly(propylene imine). 1 – core, 2 – internal cavities and 3 – branching points.

successfully introduced in the dendrimers of 1–3 generations to form mono-substituted derivative (4.10) able to reversible electron exchange in aqueous and organic media [89].

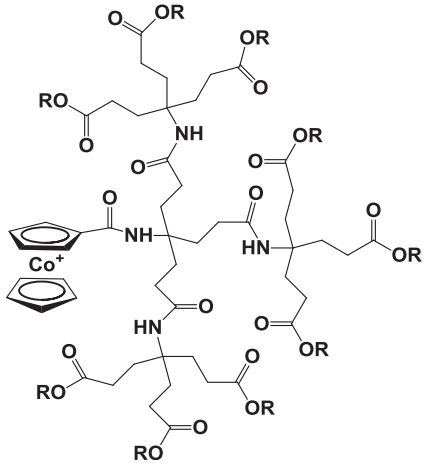

(4.10)

Maximal sensitivity of electrochemical signal detection was achieved for the second generation. The pH dependence of the peak potential and electron transfer rate are due to electrostatic interactions and protonation–deprotonation reactions of the carboxylic groups of dendrimer molecule.

Dendrimers (4.11) with 2, 4, 8, 16, 32 and 64 terminal porphyrine fragments and their complexes with Zn(II) ions were investigated by cyclic voltammetry [90]. The redox potential of porphyrine fragments did not depend on their quantity in the dendrimer molecule.

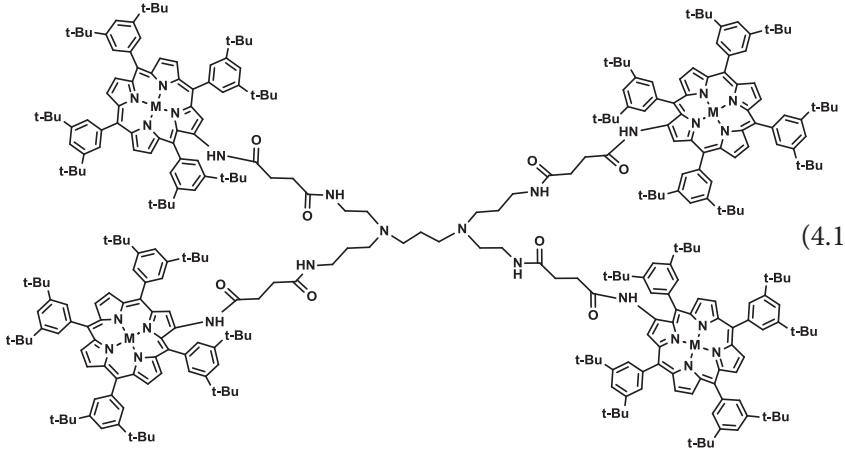

(4.11)

4.3 Enzyme Sensors

4.3.1 PANI-Based Enzyme Sensors

As was mentioned earlier, PANI exerts electrocatalytic and electroconductive properties which make them useful for electric wiring of oxidoreductase enzymes. In addition, PANI-covered electrodes can serve as pH sensors in the assembly of biosensors utilizing hydrolases and oxidoreductases. The analytical characteristics of the PANI based enzyme sensors are summarized in Table 4.1 for the period from 2004 to 2014.

Although the pH sensitivity of the PANI redox potential is observed in rather broad range of the potentials, usually the interval from pH 3.0 to 8.0 is considered as electrochemically reversible with near-Nernstian slope of the calibration graph. In addition, PANI can be used for pH detection in basic media but the mechanism of the reaction differs from that in neutral and acidic conditions. Instead redox conversion, deprotonation takes place so that the number of positive charges on the polymer molecule decreases. The use of PANI-based transducers in basic media is not preferable because of the degradation of the polymer in such conditions. For this reason, the reactions of urea and cholinesterases are conducted in neutral media even though the maximum of the activity of free enzymes is observed at highly basic solutions. The reaction schemes corresponding to the enzymes mentioned are presented in Eqs. (4.12) and (4.13).

(4.12)

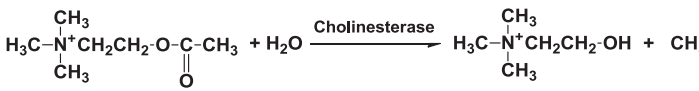

(4.13)

Urea hydrolysis increases the pH of the surface layer and provokes deprotonation of PANI, whereas cholinesterase changes the polymer states in the opposite direction. It is interesting to note that pH shift can be recorded by the appropriate changes in the redox activity of the polymer. Thus, the current recorded at low potential (near 0 V) corresponded to the leuco-emeraldine/emeraldine salt equilibrium and decreases with the PANI deprotonation. Changes in the pH value caused by ammonia released in enzymatic reaction were earlier used for detection of amino acids and amines in enzyme sensors utilizing oxidases of amino acids and aminooxidases. As an example, Scheme (4.14) represents the reactions initiating amperometric response of such sensor based on PANI-modified electrode for the detection of creatinine [124].

Table 4.1 Enzyme sensors based on PANI-covered electrodes (2004–2014).

Enzyme	Analyte	Detection mode	Coating/measurement conditions	Analytical characteristics	Ref.
Hydrolases					
Acetylcholin-esterase	Carbaryl	SWV	Electropolymerized PANI–CNT core–shell composite, pH 7.0, inhibition measurement	LOD 1.4 μM, conc. range 9.9–49.6 μM, HPLC reference in cabbage	[91]
Acetylcholin-esterase	Neurotoxin	DPV	PANI electropolymerized in ionic liquid on silica-modified GCE, pH 7.0	1(R),2*N*-dimethyl-6,7-dihydroxy-1,2,3,4-tetrahydroisoquinoline: Conc. range 0.05–0.15 μM	[92]
Butyrlcholin-esterase	Inhibitors	Pot.	Chemically synthesized PANI–camphorsulfonic acid composite, pH 7.9	LOD 100 nM (trichlorhon), 6 nM (carbofuran), 700 nM (serine), conc. range 0.2–25 (trichlorfon), 0.01–0.2 (carbofuran), 1.0–2.5 (serine) nM	[93]
Urease	Urea	Pot.	PANI chemically synthesized on polyacrylonitrile nanofibers/Pt nanoflowers, pH 6.0	LOD 10 mM, conc. range up to 20 mM	[94]
Urease	Urea	DC	Chemically synthesized PANI on ITO electrode covered with PVA-Ag composite, pH 7.0	Conc. range up to 5 mM	[95]

Urease	Urea	Pot.	Electrochemically synthesized PANI on screen-printed carbon electrode	Conc. range 0.1–100 mM	[96]
Urease	Urea	DC	PANI/PSS hydrogel, pH 7.0.	Conc. range 0.1–100 mM	[97]
Oxidoreductases					
Cellobiose dehydrogenase	Lactose	DC	Electropolymerized PANI on screen-printed carbon electrode, direct electron transfer, pH 5.5	LOD 1 μM, conc. range 1μM–1 μM	[98]
Cholesterol oxidase	Cholesterol	DC	PANI electrochemically deposited on ITO electrode in the presence of Triton-X-100, pH 7.0	LOD 5 mg/L, conc. range 5–400 mg/L	[99]
Cholesterol oxidase	Cholesterol	DC	Micelle polymerization if aniline in the presence of camphorsulfonic acid, deposition on ITO electrode in the presence of ethylene glycol, pH 7.0	LOD 5 mg/L, conc. range 25–500 mg/L	[100]

(*Continued*)

Table 4.1 cont.

Enzyme	Analyte	Detection mode	Coating/measurement conditions	Analytical characteristics	Ref.
Cholesterol oxidase	Cholesterol	DC	Graphene/polyvinylpyrrolidone/PANI nanocomposite on paper based electrode, pH 7.0	LOD 1 μM, conc. range 0.01–10 mM	[101]
Glucose oxidase	Glucose	DC	Enzymatically synthesized PANI encapsulated enzyme, pH 6.0, measurements in the presence of phenazine methylsulfate	20 mM glucose, no interference from ascorbic and uric acids	[56]
Glucose oxidase	Glucose	DC	PANI/polyacrylic acid composite, pH 7.0, cathodic O_2 reduction measurement	LOD 0.06 mM, conc. range up to 20 mM	[103]
Glucose oxidase	Glucose	DPV	Graphene/PANI/nano Au composite on screen-printed electrode	LOD 0.1 mM, conc. range 0.2–11.2 mM, whole blood testing	[104]
Glucose oxidase	Glucose	DC	PANI/PVS electopolymerized on Pt electrode, pH 7.5	LOD 0.1 μM, conc. range 0.1–10 μM	[104]

Glucose oxidase	Glucose	DC	Electropolymerization of N-methylaniline on Pt electrode covered with chitosan, pH 7.4	Conc. range 0.06–1.83 mM	[105]
Hemoglobin	Acrylamide	DPV	PANI/CNTs/Cu nanoparticles, pH 5.5	LOD 0.2 nM, 5 nM–75 mM	[106]
Peroxidase (HRP)/ cholesterol oxidase	Cholesterol	DC	Silica particles modified with PANI and enzymes, direct electron transfer measurements, pH 7.0	Conc. range 1–25 mM	[107]
HRP	H_2O_2	DC	Chemically synthesized PANI, pH 9.0–11.0, direct electron transfer	Not reported	[108]
HRP	H_2O_2	DC	PANI electropolymerized from surfactant solution, pH 7.0	LOD 0.63 μM, conc. range 1.0 μM–2.0 mM	[109]
HRP	H_2O_2	DC	Electropolymerized PANI covered with PSS-PDDA complex and polystyrene particles, pH 6.8	LOD 0.36 μM, conc. range 2.5–190 μM	[110]

(*Continued*)

Table 4.1 cont.

Enzyme	Analyte	Detection mode	Coating/measurement conditions	Analytical characteristics	Ref.
HRP	H_2O_2	DC	Electrosynthesized PANI with/without BSA, pH 6.2	Conc. range 0.01–35.2 mM	[111]
HRP	H_2O_2	DC	Chemically synthesized copolymer of aniline and 3-aminobenzene-sulfonic acid and Au nanoparticles, pH 7.0	LOD .6 μM , conc. range 10–2000 μM	[112]
HRP	Artesunate	DC	Graphene/PANI nano-composite, pH 7.0	LOD 0.012–0.014 ng/mL (human plasma, serum), conc. range 0.05–0.40 ng/ mL (standard solutions)	[113]
Laccase	Guaiacol, total phenolic index	DC	Nano Ni/CNTs/PANI composite electrode-posited on Au elec-trode, pH 5.5	LOD 0.05 μM, conc. range 0.1–10 and 10–500 μM, measurements in fruit juices	[114]
Tyrosinase	Catechol	DC	Electrochemically syn-thesized PANI in ionic liquid, pH 6.0	Conc. range 0.2–80 μM	[115]

Tyrosinase	Benzoic acid	DC	Chemically synthesized PANI, inhibition of catechol oxidation, pH 6.5	LOD 0.7 μM	[116]
Tyrosinase	Benzoic acid	DC	Electrochemically synthesized PANI in ionic liquid, inhibition of catechol oxidation, pH 6.0	LOD 0.3 μM	[117]
Tyrosinase	Catechol	DC	Electrochemically synthesized PANI in ionic liquid, pH 6.5	LOD 0.01 μM, conc. range 1.0–100 μM	[118]
Tyrosinase	Phenolics	DC	Electropolymerized PANI, pH 4.5, 5.5	Conc. range 0.4–6.0 (phenol), 0.2–1.0 (catechol), 2.0–20.0 (l-DOPA) μM	[119]
Tyrosinase	Catechol	DC	PANI electropolymerized in the presence of ionic liquid and carbon nanofiber, pH 7.0	LOD 0.1 (catechol, p-cresol, phenol), 0.5 nM (*m*-cresol), conc. range 0.4 nM–2.1 μM (catechol), 0.4 nM–2.0 μM (*p*-cresol), 0.4 nM–1.9 μM (phenol), 10 nM–6.6 μM (*m*-cresol)	[120]
Sulfite oxidase	Sulfite	DC	PANI electropolymerized on Pt with entrapped enzyme, pH 8.5	LOD 2 μM, conc. range 0.06–5.0 mM	[121]

(*Continued*)

Table 4.1 cont.

Enzyme	Analyte	Detection mode	Coating/measurement conditions	Analytical characteristics	Ref.
Uricase	Uric acid	DC	PANI electropolymerized in the presence of ionic liquid, pH 7.0	Conc. range 1 μM–1 mM	[122]
Uricase	Uric acid	DC	Electropolymerized PANI covered with PAH on Pt electrode, pH 9.0	Conc. range 0.0625–0.75 mM	[123]

Abbreviations: BSA – bovine serum albumin, conc. range – concentration range determined, CNTs – carbon nanotubes, DC – direct current voltammetry (both linear sweep voltammetry and chronoamperometry), HRP – horseradish peroxidase, DPV – differential pulse voltammetry, ITO – indium-tin oxide, LOD – limit of detection, PAH – poly(allylamine hydrochloride), PDDA – poly(diallyldimethylammonium chloride), PSS – polystyrene sulfonate, PVS – polyvinyl styrene, Pot. – direct potentiometry, SWV – square-wave voltammetry

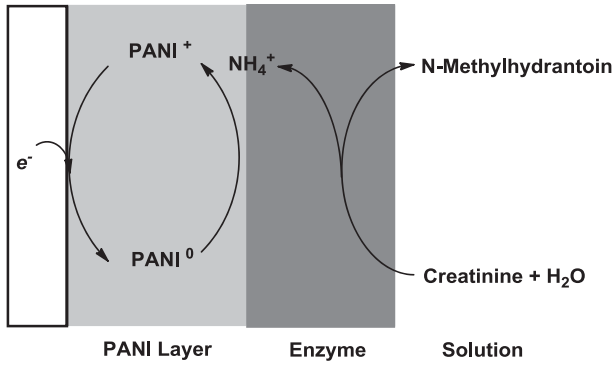

(4.14)

In accordance with common classification of oxidoreductase-based biosensors, appropriate PANI-based representatives can be referred to the *second* (mediated conversion of the substrate/product of enzymatic reaction) and *third* (direct electron transfer from the active site of enzyme) generations [125]. Regarding glucose oxidase, the appropriate reaction paths are presented in Schemes (4.15) and (4.16) and Figure 4.3. Here, FAD/$FADH_2$ is an enzyme cofactor and M_{Ox} and M_{Red} are oxidized and reduced forms of mediator M, respectively. Both bioelectrochemical reduction and oxidation of H_2O_2 can be realized, but first approach seems preferable due to lower effect of possible electrochemically active interferences present in sample. Thus, for biological fluids, this makes it possible to exclude contribution of ascorbic and uric acids present in blood.

Second generation

$$FADH_2 + O_2 \rightarrow FAD + H_2O_2$$
$$FAD + Glucose \rightarrow FADH_2 + Gluconolactone$$
$$H_2O_2 + M_{Red} \rightarrow H_2O + M_{Ox}$$
$$M_{Ox} + e^- \rightarrow M_{Red}$$

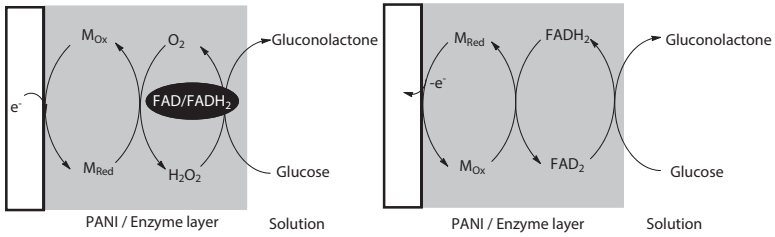

Figure 4.3 Second- and third-generation enzyme sensors based on oxidoreductases.

Third generation

$$FADH_2 + M_{Ox} \rightarrow FAD + M_{Red}$$
$$FAD + Glucose \rightarrow FADH_2 + Gluconolactone$$
$$M_{Ox} + e^- \rightarrow M_{Red}$$

Mediators involved in target process are similar to those used in other oxidoreductase-based biosensors, e.g., transient metal complexes, noble metals and CNTs. In such biosensors, mediators are used to avoid difficulties related to direct oxidation/reduction of H_2O_2 on the electrode. This reaction requires rather high overvoltage and is complicated with instability of the hydrogen peroxide and oxygen dependence of the enzymatic reaction rate.

Canonical third-generation biosensor assumes direct electron transfer between the enzyme cofactor and electrode. However, due to steric reason and specific enzyme structure only few enzymes, e.g., laccase and peroxidase, can be involved in such reaction with current yield convenient for the substrate detection. In PANI-based enzyme sensors, the polymer is used for two purposes, i.e., for a denser physical contact of the enzyme molecule with the electrode and for mediation of the electron transfer. In most cases, the absolute value of such enzyme sensors is lower than that of mediated biosensors belonging to the second generation. However, they exclude oxygen as a natural electron acceptor and hence stabilize the operation of biosensor in real samples. This is especially important for implantable glucose sensors which are intended to use in the conditions of limited oxygen access to the sensor surface.

Regarding assembling PANI-based enzyme sensors, two promising strategies deserve to be mentioned. Besides target species, oxidoreductases can oxidize aniline and hence initiate its polymerization. This makes it possible to amalgamate the stages of PANI synthesis an enzyme immobilization performed in very mild conditions different from those required for electropolymerization. HRP is mainly used in such experiments though glucose oxidase also initiates polymerization. The reaction mixture contains small vesicles with the walls consisted of PANI and the core of hydrated protein. It can be deposited on the surface of transducer and fixed by additional polymeric membrane or cross-linking.

The control of the porosity of PANI layer is another trend of biosensor design. This can be achieved by performing polymerization in the presence of rather high amounts of ionic liquids. Mesoporous layer formed is accessible for low-molecular reactants and shows faster and higher response.

An interesting approach to the PANI synthesis in the assembly of enzyme sensors is presented in Ref. [107]. First, *N*[3-(trimethoxysilyl)

propyl]aniline was synthesized as precursor. Its electrochemical polymerization with simultaneous hydrolysis of silyl fragment resulted in formation of silica particles with covalently attached PANI molecules. The immobilization of HRP and cholesterol oxidase provided electrochemical signal established by direct electron transfer to HRP redox center measured at low potential (–150 mV vs. Ag/AgCl).

Immobilization protocols used for enzyme attachment to the PANI layer do not differ from conventional techniques applied in other enzyme sensors. However, the use of glutaraldehyde and carbodiimides partially suppresses the reversibility of redox conversion and electroconductivity of PANI [126]. Some other aspects of PANI-based enzyme sensors are summarized in reviews [127, 128].

4.3.2 PPY and Polythiophene-Based Enzyme Sensors

General principles of PPY and polythiophene application in the assembly of enzyme sensors are similar to those of PANI. They involve physical entrapment of enzymes and nanosized mediators in the growing polymer film and participation of the polymers in the electron transfer. The application of PPY and polythiophene derivatives for the period from 2004 to 2014 is presented in Table 4.2.

The possibility of simultaneous polymerization and immobilization is limited by insufficient solubility of monomers in water. The use of hydrophilic substituents of thiophene, mainly ethylenedioxythiophene (EDOT) or 3-substituted monomers with carboxylic group can improve situation. Nevertheless, covalent binding to PPY or polythiophene derivatives remains a main way of enzyme sensor development. In a similar manner, mediators can be anchored to polymer substituents. Thus, PPY bearing ferrocene was the first example of enzyme wiring (glucose oxidase, 1988 [166]).

An interesting approach to glucose oxidase immobilization was demonstrated by S. Cosnier's group [138]. The electrode was modified with single-walled CNTs and then pyrrole bearing adamantine was electropolymerized. The enzyme was modified by cyclodextrine moiety which entrapped the adamantane group in the host–guest complex. As a result of spatial separation of enzyme and electrode, the efficiency of bioelectrical wiring was significantly improved. The limiting current was 6.5 times higher than that achieved for covalent immobilization on the same carrier and about 1.5 times higher than that recorded with Au nanoparticles as additional mediator. Affine immobilization via nitrilotriacetic fragment anchoring the glucose oxidase or tyrosinase to PPY chain via Cu^{2+}

Table 4.2 Enzyme sensors based on PPY and thiophene derivatives (2004–2014).

Enzyme	Analyte	Detection mode	Coating/measurement conditions	Analytical characteristics	Ref.
PPY-based enzyme sensors					
Acetylcholin-esterase	Inhibitors	DC	PPY electropolymerized on Au nanoparticles	Methylparathion: LOD 2 ng/mL, conc. range 0.005–0.12 μg/mL	[129]
Acetylcholin-esterase	Inhibitors	DC	PPY/ enzyme composite obtained by electropolymerization in the presence of gelatin followed by cross-linking with glutaraldehyde	LOD 1.1 ppb (paraoxon), 0.12 ppb (carbofuran)	[130]
Fructose dehydro-genase	Fructose	DC	Electropolymerization of pyrrole followed by cross-linking if enzyme or its occlusion in the polymer layer, ferricyanide mediator signal	Conc. range 0.1–0.8 mM	[131]
Glucose oxidase	Glucose	DC	Chemically synthesized PPY-polystyrene sulfonate deposited in polyacrylamide gel on Pt	Conc. range up to 10 mM	[132]
Glucose oxidase	Glucose	DC	Electropolymerized PPY modified with viologen and enzyme, mediator signal	Conc. range up to 20 mM	[133]

Glucose oxidase	Glucose	DC	Pyrrole electropolymerization on Pt electrode covered with poly(hydroxyethylmethacrylate) hydrogel	Conc. range 1–16 mM	[134]
Glucose oxidase	Glucose	DC	Electropolymerization of pyrrole in the presence of CNTs	Conc. range 0.25–4.00 mM	[135]
Glucose oxidase	Glucose	Poten, DC	PPY nanorods electrodeposited on Au disk via anodized alumina template followed by Pt nanoparticles electrodeposition	LOD 5.6 (Poten), 27.7 (DC) μM, conc. range 0.01–1.0 (Poten), 0.1–9 (DC) mM	[136]
Glucose oxidase	Glucose	DC	Electropolymerized PPY covered with Pt nanorods and enzyme implemented in poly(*o*-aminophenol) film	LOD 0.45 μM, conc. range 0.0015–13 mM	[137]
Glucose oxidase	Glucose	DC	Electropolymerized adamantyl-11-pyrrolyl-1-undecyl carboxylic acid amide onto CNTs-modified Pt electrode	Conc. range up to 15 mM	[138]
Glucose oxidase	Glucose	DC	PPY–poly(*N*-methylpyrrole) composite film electropolymerized on Pt electrode	Conc. range 0–50 mM	[139]

(*Continued*)

Table 4.2 cont.

Glucose oxidase	Glucose	DC	Electropolymerization of pyrrole from suspension of CNTs on Au microelectrodes	LOD 50 μM, conc. range 4-100 mM (0.56–12.0 mM in blood sample)	[140]
Glucose oxidase	Glucose	Poten	Core–shell encapsulation of PPY and Fe_3O_4 nanoparticles by enzymatic oxidation	LOD 0.3 μM, conc. range 0.5 μM–34 mM	[141]
Glucose oxidase	Glucose	SPR	Electropolymerization of pyrrole in the presence of enzyme on Au	LOD 0.5 μM, conc. range 1–100 μM	[142]
HRP	Phenol	DC	Electropolymerization of pyrrole on screen-printed electrode modified with Au nanoparticles	Not reported	[143]
l-Lysine oxidase	l-lysine	DC	Over-oxidized PPY on Pt electrode	LOD 4 μM, conc. range 0.02–2 mM	[144]
Tyrosinase	Tyramine	DC	Electropolymerization of pyrrole on Pt followed by enzyme cross-linking	LOD 0.547 μM, conc. range 4–80 μM	[145]
Nitrite reductase	Nitrite	DC	Electropolymerization of pyrrole adsorbed on the glassy carbon electrode together with enzyme	LOD 5.4 μM, conc. range 5.43–43.4 μM	[146]

Purine nucleoside phosphorylase/ xanthine oxidase	Phosphate	DC, Poten	Electropolymerization of pyrrole in the enzymes presence followed by the enzyme cross-linking	LOD 10 (DC), 20 (Poten) μM, conc. range 20–200 μM (Poten) and 0.1–10 μM (DC)	[147]
Sulfite oxidase	SO_2	DC	Electropolymerization of pyrrole in the enzymes presence	LOD 0.9 μM, conc. range 0.9–400 μM, measurements in bear and red wine	[148]
Tyrosinase	Catechol	Poten	Electropolymerization of pyrrole in the presence of enzyme	Conc. range 1–50 μM	[149]
Tyrosinase, glucose oxidase	Catechol, glucose	DC	Electropolymerization of pyrrole–nitrilotriacetic acid derivative on glassy carbon partially blocked with latex particles	LOD 0.38 (catechol) and 19 μM	[150]
Urease	Urea	DC	Copolymer of pyrrole and *N*-3-aminopropylpyrrole electrochemically deposited on ITO glass electrode	Conc. range 0.16–5.02 mM	[151]
Urease	Urea	Pot	PPY-BSA composite electrodeposited on ITO glass electrode	Conc. range 6.6 μM–0.75 mM	[152]

(*Continued*)

Table 4.2 cont.

Uricase	Uric acid	ECL	Electropolymerization of pyrrole in the presence of enzyme on Pt, luminol-H_2O_2 system signal	Conc. range 75 pM–8.3 μM	[153]
Polythiophene-based enzyme sensors					
Acetylcholin-esterase	Inhibitors	DC	Deposition of chemically synthe-sized emulsion of PEDOT/PSS followed by enzyme immobiliza-tion in photocurable PVA-based polymer	LOD 4.0 nM (chloropyrifos-oxon)	[154]
Ascorbate oxidase	Ascorbate	DC	One step electropolymerization of PEDOT-CNTs composite	Not reported	[155]
Ascorbate oxidase	Bilirubin	DC	Electropolymerized complex of ter-thiophene-3-carboxylic acid and Mn(II) covered with polyethylene imine gel containing enzyme	LOD 40 nM, conc. range 0.1–50 μM	[156]
Ascorbate oxidase	Ascorbate	DC	Electrochemical synthesis of PEDOT on CNTs-modified Pt electrode	LOD 0.7 mM, conc. range 1 mM–18 mM	[157]
Glucose oxidase	Glucose	DC	Electropolymerization of EDOT on Au porous electrode, benzoqui-none mediation	Conc. range 0.1–15 mM	[158]

Cholesterol oxidase	Cholesterol	DC	PPY co-immobilized with thiophene, and 3-methylthienyl methacrylate	Conc. range 0.1–12 mM	[159]
Cholesterol oxidase	Cholesterol	DC	Electropolymerization of thiophene and 3-thiopheneacetic acid on Pt electrode	LOD 0.42 mM, conc. range up to 8 mM	[160]
Choline oxidase (ChO), HRP	Choline	DC	Electropolymerization of -5,2:5,2-terthiophene-3-carboxylic acid on screen-printed carbon electrode (H_2O_2 signal)	LOD 0.1 (ChO) and 0.4 (ChO-HRP) μM, conc. range 1.0–80 (ChO) and 1.0–50 μM (ChO-HRP)	[161]
Glutamate oxidase	Glutamate	DC	5,2':5',2"-terthiophene-3-carboxylic acid electropolymerization followed by enzyme cross-linking	LOD 0.1 mM, conc. range 0.2–100 mM, in vivo measurements	[162]
Laccase	Oxygen	DC	Electropolymerized 3-metyhlthiophene containing enzyme, direct electron transfer	Not reported	[163]
Lactate dehydrogenase	Lactate	DC	Electropolymerized 3-methylthiophene on glassy carbon electrode	LOD 0.56 μM, conc. range 1–500 μM	[164]

(*Continued*)

Table 4.2 cont.

Tyrosinase	Phenols, Atrazine, Diuron	DC	Electropolymerization of EDOT on glassy carbon electrode in the presence of enzyme or followed by electrostatic enzyme accumulation	LOD 100 (dopamine), 500 (epinephrine, l-DOPA, 3-chlorophenol), 5 (p-cresol, 4-chlorophenol), 50 (phenol) nM, conc. range up to 25 (catechol, phenol), 200 (dopamine, epinephrine), 10 (l-DOPA, *p*-cresol, 4-chlorophenol), 100 (3-chllorophenol) μM, Inhibitor measurements: LOD 0.5 (atrazine) and 1 (diuron) mg/L	[165]

Abbreviations: ChO – choline oxidase, L-DOPA – L-3,4-dihydroxyphenylalanine and EDOT – 3,4-ethylenedioxythiophene.

ions was realized in [167]. The structure of the complex is represented in Scheme (4.17).

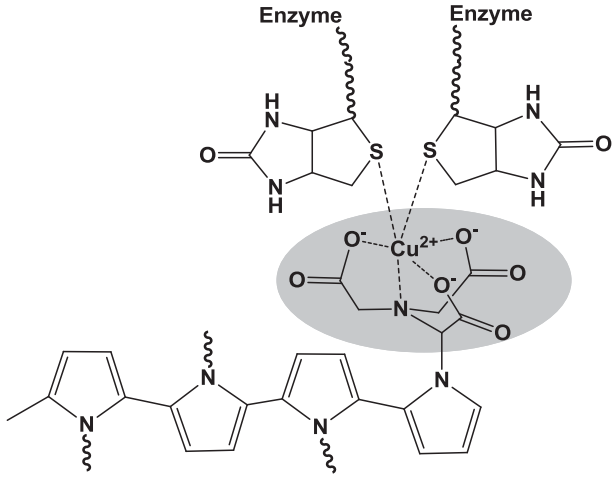

(4.17)

Biotinylated PPY and its ability to bind avidin as a model of affine immobilization of biomolecules was characterized by QCM for various linkers separating the binding site and polymer chain [268].

The thickness of the PPY layer implementing enzyme is another important factor affecting the biosensor performance. Thus, the use of ultra-thin PPY membrane (54 nM) decreased the LOD of sulfite detection down to 0.9 μM against thicker analogs [149].

Thiophene derivatives are less active than pyrrole in reactions of enzyme initiated polymerization and both of them are inferior to PANI. The comparative research of enzyme initiated polymerization showed low electrocatalytic activity of such products due to a lesser permeability of polymeric walls of vesicles formed. Probably for the same reason chemically synthesized polymers have found limited application though polyelectrolyte complexes were used for physical enzyme immobilization due to their hydrophilicity and chemical/electrochemical stability [169]. PEDOT can be rather easily combined with other redox-active polymers which are obtained simultaneously or in consecutive stages of monomer electrolysis. The hybrid products exert improved redox activity and stability against homogeneous coatings of single polymers. Thus, PEDOT/poly(neutral red) coatings were applied for the detection of H_2O_2, a product of many oxidoreductases reaction. The sensor consisted of two polymers deposited on carbon film electrode shoed extended linear range of concentration and lower LOD (30 μM) against an analog consisted of PEDOT stabilized with polystyrene sulfonate and polyvinylpyridine film [170]. 3-Alkylsubstituted

polythiophenes show regular structure and high reproducibility of the surface morphology. However, their application in enzyme sensors does not provide any advantages over PEDOT. Contrary to that, the use of thiophene derivatives with carboxylic groups (polymerized thiophen-2-acetic or propionic acids) simplifies the covalent immobilization of enzyme molecules via carbodiimide binding. The length of alkylene bridge between thiophene ring and carboxylic groups predetermines the accessibility of the enzyme active site toward the substrate molecule. As in the case of affine immobilization via nitrilotriacetic group, high distance improves the detection of moderate concentrations of a substrate and allows increasing the sensitivity (slope of the calibration curve) against similar methods of immobilization in the polymer bode or on its surface. Meanwhile, the changes in LOD are less convincing. This is not very serious for the enzyme sensors intended for medical applications because many of the potential targets (glucose, lactate) are present in the biological fluids in rather high concentrations. On the other hand, the use of short linkers like in thiophene-3-acetic acid improves electric wiring enzyme by electron exchange within the polymer layer.

In many cases, electropolymerization is superposed with partial blocking of the electrode surface or its modification with carbonaceous materials. This approach increases the specific surface concentration of potential binding sites involved in enzyme immobilization and/or electron transduction. The use of hydrophilic non-conductive polymers like polymethacrylates or latex particles improves the compatibility of polymeric layer with biomolecules and increases specific activity of immobilized enzyme. In some cases, plastic arts are used as templates and removed after electropolymerization by dissolution in organic solvent. Together with the use of polycarbonate membranes and oxidized alumina foil this is a main way of templated electrosynthesis resulting in formation of mesoporous films with increased permeability for charge carriers.

In some cases [129, 130, 154], PPY and PEDOT were used in enzyme sensors devoted to the inhibitor detection. Acetylcholinesterase was immobilized in the assembly of polymeric films and the decay of its activity was measured against the pesticide concentration. Indeed, the advantages of redox-active polymers in inhibitor determination are not obvious: in case of irreversible inhibition the decay of enzyme activity expressed mainly by inhibition degree does not depend on the initial signal of the biosensor prior to its contact with the inhibitor. The positive effect of redox-active polymers can be rather referred to better conditions for immobilized enzyme and lower quantities of enzyme used for biosensor preparation.

Specific adsorption of pesticide on polymer layer and higher accessibility of enzyme active site toward inhibitors can increase the sensitivity of their detection, either. The earlier conclusions assume the contact of enzyme with inhibitor performed in the absence of the substrate. In opposite case formally related to kinetics of fully competitive inhibition, positive effect of mediators, including redox-active polymers is in the possibility to decrease the concentration of the substrate used in measurement. This increases the sensitivity of inhibitor detection with no response of the incubation period and initial enzyme activity.

4.3.3 Enzyme Sensors Based on Other Redox-Active Polymers Obtained by Electropolymerization

The use of polyphenothiazines and polyphenoxazines was mainly initiated by searching effective catalysts of NADH oxidation. This process (4.18) performed on naked electrode requires high potentials and results in formation of inactive by-products.

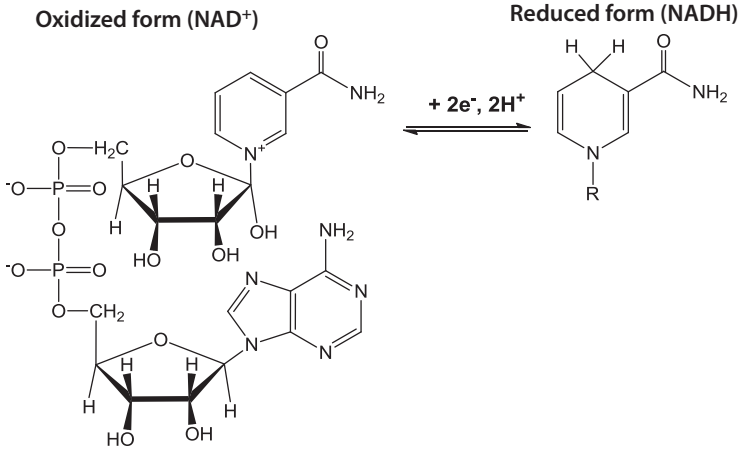

(4.18)

Meanwhile, the reversibility of NADH/NAD$^+$ cycling is one of main requirements for the successive functioning of NAD-dependent oxidoreductases in the assembly of enzyme sensors. The ability of most studied monomeric phenothiazines and phenoxazines to participate in electron transfer from/to NADH/NAD$^+$ was many times confirmed for dissolved and adsorbed on electrode dyes [171–174] as well as for their derivatives covalently attached to various carriers. In this respect, the polymerization of these mediators seems consistent in line of the development of appropriate biosensors. In total, more than 250 enzymes utilize NADH as cofactor

and design of universal platform for the detection of enzyme activity via NADH turnover establishment is one of the reasons explaining interest to new mediators working in this area. Relative activity of various polyphenothiazines and polyphenoxazines was tested before the period of this review using mainly conventional electrochemical tools. Thus, Karyakin *et al.* [28, 80] compared the conditions for electropolymerization and activity in NADH oxidation of methylene blue, methylene green, toluidine blue, brilliant cresyl blue, Meldola's blue, azur A, neutral red and found poly(neutral red) most effective in reversible mediation of target reaction. Later on, the specificity of poly(neutral red) as mediator in the assembly of enzyme sensors and the similarity of cyclic voltammograms recorded during the polymerization of methylene blue, methylene green and neutral red was confirmed by Barsan *et al.* [175].

Other polymers of this group are frequently used for the detection of H_2O_2, another widespread product of enzymatic oxidation of organic substrates. The efficiency of H_2O_2 detection is increased by combination of the oxidoreductase specific for analyte with HRP exerting biocatalytic effect on H_2O_2 electroreduction. It should be mentioned that methylene blue and some other phenothiazines belong to photosensitizers and can be chemically oxidized by dissolved oxygen under UV–Vis irradiation. If not to consider photovoltaic devices, such a property negatively affects possible application of the polymers in biosensors because of reduced lifetime and additional limitations of their use, especially in field. The chemical instability of polyphenothiazines can be to some extent suppressed by copolymerization of EDOT or PPY. The examples of the application of polyphenothiazines and polyphenoxazines in the assembly of enzyme sensors for the period from 2004 to 2014 are presented in Table 4.3.

Of other redox-active polymers, the "upside down" application of electropolymerized material can be mentioned [202]. The detection of urea was performed with potentiometric enzyme sensor in which poly(*o*-phenylene diamine) was immobilized on the urease. This unusual assembly made it possible to significantly decrease losses in potential determining ion (NH_4^+) releasing in enzymatic reaction and transferring from the electrode interface into the bulk solution through the polymer layer with pH-dependent stationary potential. The biosensor developed showed extended linearity of the response at low urea concentration.

Reagentless lactate biosensor based on lactate oxidase immobilized on glassy carbon electrode modified with poly(5-hydroxy-1,4-naphthoquinone-co-5-hydroxy-3-acetic acid-1,4-naphthoquinone), poly(juglone) (4.19), is another example of high efficiency of redox polymers as electron mediators.

Table 4.3 Enzyme sensors based on other electropolymerized redox-active modifiers (2004–2014).

Enzyme	Analyte	Detection mode	Coating/Measurement conditions	Analytical characteristics	Ref.
Polyphenothiazines					
Alcohol oxidase	Ethanol	DC	Electropolymerized thionine with reduced graphene oxide on glassy carbon	Conc. range 0.05–1.0 mM	[176]
Glucose oxidase	Glucose	DC	Poly(methylene blue) doped silica nanoparticles	LOD 3 μM, conc. range 0.01–1.11 mM	[177]
Glucose oxidase	Glucose	DC	Layered coating of enzymatically synthesized poly(toluidine blue) and Prussian Blue on Au electrode	LOD 10 μM, conc. range 0.1–10 mM	[178]
Glucose oxidase, HRP	Glucose	DC	Poly(toluidine blue) electrochemically synthesized on glassy carbon electrode modified with CNTs	Conc. range 0.1–1.2 mM	[179]
HRP	H_2O_2	DC	Poly(toluidine blue) obtained by template electrosynthesis on polycarbonate filter membrane	LOD 1 μM, conc. range 1 μM–28 mM	[180]

(*Continued*)

Table 4.3 cont.

Lactate dehydrogenase Glucose dehydrogenase	Lactate, Glucose	DC	Poly(methylene blue) or poly(methylene green) on toluidine or nile blue derived polymethacrylate polymer	Conc. range up to 80 mM	[181]
Malate dehydrogenase	NADH, Malate	DC	Poly(methylene green) electrodeposited on CNTs-modified "Bucky" paper	Conc. range 0–6 mM (NADH)	[182]
Sorbitol dehydrogenase	Sorbitol	DC	Poly(methylene green) on CNTs	LOD 0.11 mM, conc. range 0.6–2.6 mM	[183]
Tyrosinase	Oestragons	DC	Polythionine electropolymerized on glassy carbon electrode	Conc. range 0.2–0.8 mM (β-oestradiol), 20–60 μM (phenol), up to 0.5 mM (nonylphenol), 0.4 mM (bisphenol A)	[184]
Polyphenazines and polyphenoxazines					
Alcohol dehydrogenase	Ethanol	DC	Poly(nile blue) electropolymerized on glassy carbon electrode	LOD 3.3 μM, conc. range up to 100 μM, measurements in red wine	[185]
Alcohol dehydrogenase	Ethanol	DC	Poly(brilliant cresyl blue) electropolymerized on glassy carbon electrode modified with CNTs	LOD 0.1 mM, conc. range 0.4–2.4 mM	[186]

Alcohol dehydrogenase	Ethanol	DC	Poly(nile blue) electropolymerized on glassy carbon electrode	LOD 0.05 mM, conc. range 0.1–3.0 mM	[187]
Cholesterol oxidase	Cholesterol	DC	10,13-bis(2,3-dihydrothieno[3,4-b][1,4] dioxin-5-yl)dibenzo[a,c] phenazine electropolymerized on graphite electrode followed by enzyme and sepiolite deposition	LOD 0.36 μM, conc. range up to 40 μM	[188]
Cholesterol oxidase	Cholesterol	DC	Poly(neutral red) electropolymerized on carbon film electrode	LOD 1.9 μM	[189]
Glucose oxidase	Glucose	DC	Poly(nile blue) electropolymerized on glassy carbon electrode	LOD 5 μM, conc. range 0.1–8.5 mM	[190]
Glucose oxidase, pyruvate oxidase	Glucose, pyruvate	DC	Poly(neutral red) electropolymerized on carbon film electrode	LOD 35 (glucose), 34 (pyruvate) μM, conc. range up to 1.8 (glucose), 0.6 (pyruvate) mM, measurements in wine (glucose), onion and garlic (pyruvate)	[191]
Glucose oxidase	Glucose	DC	Poly(neutral red) electropolymerized on glassy carbon electrode	Conc. range up to 12 mM	[192]

(*Continued*)

Table 4.3 cont.

Glucose oxidase	Heavy metals	DC	Poly(neutral red) electropolymerized on glassy carbon, inhibition measurement	LOD 1 (Cd), 6 (Cu), 3 (Pb), 9 (Zn) µg/L, conc. range 4–16 (Cd), 33–580 (Cu), 83–460 (Pb), 410–2500 (Zn) µg/L	[193]
HRP	H2O2	DC	Electropolymerization of neutral red in the presence of Pt nanoparticles on glassy carbon electrode modified with CNTs	LOD 1.1 µM, conc. range 3.6 µM–4.3 mM	[194]
HRP	Chromium ions	DC	Poly(neutral red) electropolymerized on carbon film electrode, inhibition measurement in H_2O_2 presence	I_{50} = 3.8 µM (Cr(III)) and 3.9 µM (Cr(VI))	[195]
Other polymers					
Glucose oxidase	Glucose	DC	Layered poly(*o*-phenylene diamine)/enzyme/Prussian blue composite obtained by electrosynthesis on Au electrode, H_2O_2 signal	LOD 8 µM, conc. range 0.05–10 mM	[196]
Glucose oxidase	Glucose	DC	Electropolymerization of 5-hydroxytyramine on glassy carbon electrode	LOD 0.1 mM, conc. range up to 5 mM	[197]

Glucose oxidase, catalase	Glucose	DC	Electropolymerization of neutral red or brilliant cresyl blue on CNTs-modified glassy carbon electrodes	LOD 11 µM, conc. range up to 1.1 mM	[198]
Glucose oxidase	H_2O_2, Glucose	DC	Poly(brilliant cresyl blue) on glassy carbon electrode	Not reported	[199]
Laccase	Oxygen	DC	Poly(o-aminophenol), direct electron transfer on glassy carbon electrode	Not reported	[200]
Lactate oxidase	Lactate	DC	Poly(5-hydroxy-1,4-naphthoquinone-co-5-hydroxy-3-acetic acid-1,4-naphthoquinone) electropolymerized on Pt	Conc. range up to 8 mM, direct measurements in yogurt	[201]
Urease	Urea	Pot	Poly(*o*-phenylene diamine) electropolymerized onto urease layer on glassy carbon	Conc. range 10 µM–1 mM	[202]
Uricase	Uric acid	DC	Poly(3-amino-5-mercapto-1,2,4-triazole) on glassy carbon electrode	LOD 0.52 nM, conc. range 40 nM–0.1 mM	[203]

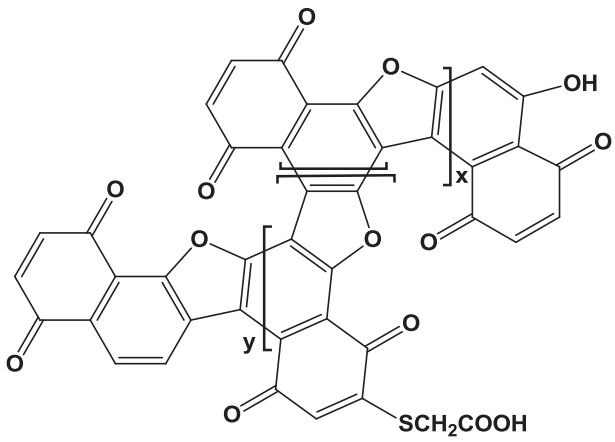

(4.19)

Contrary to lactate dehydrogenase, lactate oxidase contains FAD as cofactor which is involved in reactions (4.20) and (4.21) for anaerobic and aerobic regimes of functioning.

Anaerobic regime:

$$\begin{aligned} &FAD + S \rightleftharpoons FAD\text{-}S \\ &FAD\text{-}S \rightarrow FADH_2 + P \\ &FADH_2 + M_{Ox} \rightarrow FAD + M_{Red} \end{aligned} \tag{4.20}$$

Aerobic regime:

$$\begin{aligned} &FAD + S \rightleftharpoons FAD\text{-}S \\ &FAD\text{-}S \rightarrow FADH_2 + P \\ &FADH_2 + O_2 \rightarrow FAD + H_2O_2 \\ &FADH_2 + M_{Ox} \rightarrow FAD + M_{Red} \end{aligned} \tag{4.21}$$

In the presence of oxygen mediated oxidation of $FADH_2$ competes with electron transfer on dissolved oxygen. The comparison of spectrophotometric and electrochemical determination of the rate of enzymatic reaction showed that a part of enzyme is better recycled by quinone, whereas another fraction reacts predominantly with oxygen. Kinetics analysis estimates that about 4% of immobilized lactate oxidase participates in mediated electron transfer. Generally, the necessity of deoxygenation for the exploration of mediated biosensor behavior is a weak point of such systems and low effect of natural electron acceptor in conditions similar to those of real sample analysis promises commercialization of such lactate sensor.

4.3.4 Enzyme Sensors Based on Other Polymers Bearing Redox Groups

As was already mentioned, the use of ferrocene derived polymers with no original redox activity was suggested for simpler manufacture of the surface layer and more regular structure of the surface layer. Most of the interest to this topic was exerted about 20–25 years ago [204]. Now only few works have been published in the past decade. Thus, polyvinylferrocene was applied for glucose monitoring in the assembly of enzyme sensor [205]. The surface concentration of ferrocene units was determined form the charge passed the electrode [1 nanomol on bare glassy carbon and up to 15 nanomol/cm^2 on the electrode preliminary modified with multi-walled CNTs (MWCNTs)]. The calibration curve exhibited the linear range up to 8 mM (LOD 41 μM). The usability of the glucose sensor was tested by measurements in horse blood.

Similar approach was suggested in [206] where glucose oxidase was co-immobilized by carbodiimide binding with ferrocene on carboxylated polyvinylalcohol in PVC matrix. The biosensor was tested in fruit juices and sport drinks.

Os bipyridine complex was synthesized and introduced in the methacrylate polymers and copolymers containing allylmethacrylate, polyethylene glycolmethacrylate, butylacrylate methacrylic acid, or dimethylaminoethylmethacrylate [207]. Mediation of glucose oxidation was tested in the presence of glucose oxidase or FAD-dependent glucose dehydrogenase. Both enzymes showed remarkable wiring with Os complex able to reversible electron exchange with the electrode and cofactor. The surface coverage calculated for such sensors was found to be higher than that of ferrocene (1.3×10^{-8}/cm^2). The biosensor showed quite stable reproducible response to glucose with linear range of concentration up to 5 mM.

PAMAM with covalently attached ferrocene units was used in the assembly of reagent-less enzyme sensor for glucose [208]. Terminal aminogroups of PAMAM were modified with ferrocene aldehyde and then the product was introduced in cystamine monolayer on Au electrode. Glucose oxidase was first oxidized by periodate and then included in the surface layer (Fig. 4.4) The surface concentration of ferrocene participating in the electron exchange was estimated by cyclic voltammetry (2.5×10^{-9} mol/cm^2, or 32% of the total number of ferrocene units). The biosensor makes it possible to detect 0.1–15.8 μM of glucose (LOD 0.05 μM).

Opposite sequence of reactant addition was realized in [209]. Au electrode was first covered with thiolated ferrocene derivative and then PAMAM and glucose oxidase were simultaneously deposited. Similar protocol with asymmetrical dendrimer bearing single ferrocene units was

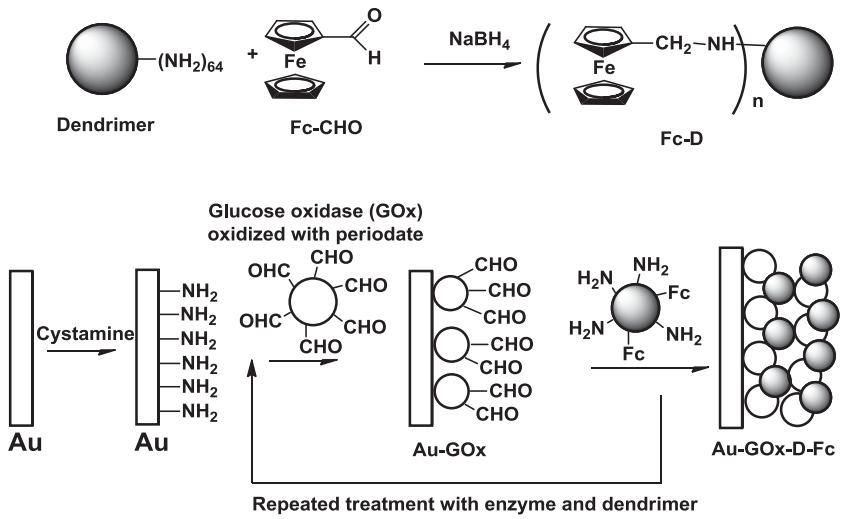

Figure 4.4 Assembling of the surface layer based on repeated treatment with ferrocene–dendrimer conjugate and glucose oxidase oxidized with periodate.

described in [210]. The glucose biosensor show linear response within 1–22 mM and rather low working potential (+0.25 V).

Direct electron transfer from glucose oxidase was realized with glassy carbon electrode modified with dendrite poly[*meso*-tetrakis(2-thienyl) porphirynate] Co(II) and single-walled CNTs [211]. The immobilized glucose oxidase showed reversible fast electron exchange (rate constant 1.01 s^{-1}) and low working potential (–0.2 V). Uric and ascorbic acids did not interfere with glucose detection (conc. range 0.02–10 mM and LOD 4 μM).

Simultaneous immobilization of glucose oxidase and HRP has been used for glucose detection with the sensor based on 1–3 generations PPI with methylferrocene units (4.22) [212]

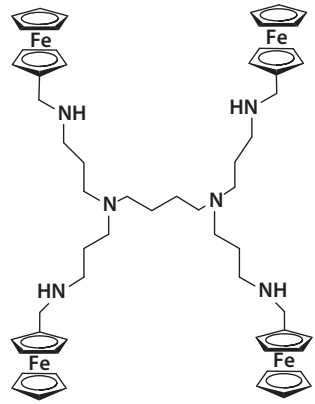

(4.22)

Maximal response was detected with 1.8×10^{-9} mol ferrocene/cm^2. The LOD increased from 12.8 μM for first generation to 22.1 μM for third generation of dendrimer. This was explained by steric limitation of the electron exchange and lower efficiency of mediated electron transfer.

Mixed ferrocene-cobaltocene-modified poly(ethylene imine–tetramine) dendrimer (1–4 generations) was applied for electrostatic immobilization of glucose oxidase and enzyme wiring for glucose detection [213]. The sensitivity (slope of calibration curve) increased from the first to fourth generation and the biosensor performance was tested both in aerobic and anaerobic conditions. The surface coverage estimated by cyclic voltammetry was about 10^{-10} mol ferrocene/cm^2.

4.4 Immunosensors Based on Redox-Active Polymers

Immunosensors belong to affinity biosensors in which the reactants, i.e., antibody (Ab) and antigen (Ag) participate in reversible reaction (4.23) which equilibrium is shifted toward the Ag–Ab complex. Contrary to enzymes, the maximal signal of such biosensors corresponds to the equilibrium and does not assume any chemical changes in the nature of immunoreagents.

$$Ag + Ab \underset{}{\overset{K_a}{\rightleftharpoons}} Ag - Ab \tag{4.23}$$

The equilibrium constant called also as affinity constant varies for immunochemical assay from 10^2 to 10^{15} M^{-1}, so that the reverse reaction can be not taken into account accept special treatment of immunosensor required for its repeated use. Ab is a Y-shaped protein consisted of two long (heavy) and two short (light) chains symmetrically combined via disulfide bridges of cystine residues (Figure 4.5).

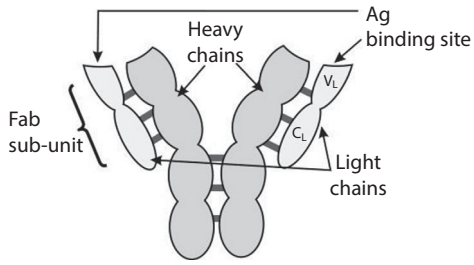

Figure 4.5 Outline presentation of Ab structure. V_L and C_L are variable and constant domains, respectively (shown for light chain only).

The efficiency and variety of Ag binding is achieved due to variable parts of the chains which form binding sites of the structure mimicking the properties of the analyte molecule. Very high specificity of immunochemical reactions as well as universal principles of Ab selection make immunochemistry approaches popular in biomedical assays and other areas requiring a sensitive and specific detection of biologically active compounds.

Although most of the commercial applications of immunoassay work with so-called polyclonal Abs isolated from the serum of immunized animals, a significant part of research has concern with development and application of novel immunorecognition elements. In addition to monoclonal Abs produced by genetic engineering approaches based on hybridoma cells, reduced replicas of traditional Abs are of special attention.

Thus, Fab subunits combine the domains of heavy and light chains participating in recognition of Ag. The Fab fragments can be isolated after treating the Ab molecules with papain. They can be used instead of the full molecules to recognize the same analytes with lesser non-specific binding of interferences and higher stability in immunotests and immunosensors. The Ab molecules can be also split into two identical parts consisting of one heavy and one light chain each. The reduced Ab receptors are easily immobilized on Au electrode or Au nanoparticles by spontaneous Au–S bonding [214]. Recently, another type of Ab has found application in immunoassay. Nanobodies are single-domain Ab fragments consisting of the variable part of the heavy chain only [215]. The nanobodies are the smallest Ab fragments with the molar mass ranging from 12 to 14 kDa which are encoded by a single gene easily implemented in bacteria and yeast cells.

The detection of Ag–Ab interactions depends on the nature of Ag molecules. For high-molecular compounds, competitive and sandwich assay modes are mainly applied. In *competitive assay* sample containing target Ag molecules is mixed with the solution of the same Ag molecules bearing a label. After that, immunosensor with Abs immobilized on the electrode is treated with the mixture and surface concentration of the label determined by its redox signal. Both labeled and non-labeled Ag molecules compete for the same binding site of Ab molecules so that the higher the label signal the lesser the content of non-bonded Ag in the sample tested.

In *sandwich assay*, two types of Abs are required, i.e., capturing and signaling (secondary) Ab. First, immunosensor is incubated in the sample tested. Then the product of Ag–Ab interaction accumulated on the surface is treated with secondary Ab bearing label. The signal of label is increased with the concentration of analyte in the sample.

If the analyte is a small low-molecular compound (hapten), *indirect competitive assay* is used. In this method, the transducer is modified with analyte molecules commonly bonded to high-molecular carrier like BSA (so-called conjugate). The sample is first mixed with solution of specific Abs taken in excess against Ag to be tested. The unreacted Ab molecules then react with Ag conjugate on the sensor surface. After that, secondary Abs are used to detect the analyte by the label signal. As in direct competitive assay, the signal of such immunosensor decreases with increased analyte concentration.

All the measurement protocols mentioned earlier were adapted from conventional immunoassay techniques. Among Ag–Ab affinity, the sensitivity of detection depends on the non-specific adsorption of immunoreactants on the transducer and cross-reactivity of capturing and signaling Abs. To some extent, the undesired interactions can be suppressed by careful washing of immunosensor between the reagent addition and blocking the naked electrode surface with inert proteins. For the same reason, the decrease in the stages of immunoassay is desirable to shorten general measurement time and the intermediate washing steps.

From all the reasons, competitive immunoassay is simpler and more convenient for automation and flow-through (flow injection) analysis, whereas sandwich assay is more sensitive and labor and time consuming.

In addition to traditional methods, immunosensor format makes possible direct measurement of Ab–Ag formation on the electrode surface by recording the permeability of the surface layer toward small charged molecules called as redox probes. Thus, EIS measurement with ferricyanide ions $[Fe(CN)_6]^{3-/4-}$ indicates the inclusion of bulky non-conductive Ag molecules by increase of the charge transfer resistance. In DC mode, similar information can be obtained from consideration of cyclic voltammograms of the same anions. Immunoreaction decreases the peak currents and the reversibility of the electrode reaction (difference of the peak potentials and forma redox potential). The sensitivity can be additionally enhanced by the use of secondary Abs or nanoparticles as Ab labels. Ii could be expected that own redox activity of the polymers also alters with the Ag capture. However, this signal is less sensitive and presently is not used for immunosensing. More often, the electron transduction is applied for increasing sensitivity of label detection, e.g., oxidoreductases applied in so-called immunoenzyme assay variants. The examples of electrochemical immunosensors based on redox polymers are summarized in Table 4.4 (2004–2014).

As could be seen from the Table 4.4, HRP/hydroquinone (HQ) [216, 228, 235, 241, 242] and alkaline phosphatase/1-naphtyl phosphate [232]

Table 4.4 Immunosensors based on redox-active polymers (2004–2014).

Polymer	Immunoreagent/ analyte	Signal/measurement conditions	Analytical characteristics	Ref.
PANI/Fe_3O_4	Benzo[a]pyrene Ab/ benzo[a]pyrene	Sandwich assay with secondary Ab labeled with carbon nanospheres bearing HRP, benzoquinone signal	LOD 4 pM, conc. rage 8 pM–2 nM	[216]
PANI	Ab/*Escherichia coli* O157:H7	Direct EIS measurements (charge transfer resistance changes)	Conc. range 10^2–10^7 CFU (coli forming units)/mL	[217]
PANI	Cortisol Ab/cortisol	Chemically synthesized Au nanoparticles covered with PANI and deposited on AU electrode, direct EIS measurements (charge transfer resistance changes)	Conc. range 1 pM–100 nM	[218]
PANI	β-Estradiol-BSA conjugate/β-estradiol	Indirect competitive assay, secondary Ab conjugated with graphene oxide and HRP	LOD 0.02 ng/mL, conc. range 0.04–7.00 ng/mL	[219]

PANI	Ab/carcinoembryonic Ag, α-fetoprotein	PANI deposited on cellulose fibers of paper working electrode of microfluidic device, sandwich assay with secondary antibodies labeled with graphene–methylene blue (ferrocene carboxylic acid) composite	LOD 0.5 (carcinoembryonic Ag) and 0.8 (α-fetoprotein) pg/mL, conc. range 4 orders of magnitude	[220]
Copolymer of aniline and 2-aminobenzylamine	Anti-human Ad5 capsid protein/ adenovirus	Direct EIS measurements (charge transfer resistance changes)	LOD 10^3 virus particles/mL, conc. range up to 10^{12} virus particles/mL	[221]
Poly(*o*-phenylene diamine)	Ag/Japanese B encephalitis vaccine	Prussian blue as mediator, $Fe^{2+/3+}$ as probe	LOD 6×10^{-9} lg pfu/mL, conc. range 1.1×10^{-8}–1.9×10^{-6} lg pfu/mL	[222]
Poly(*o*-phenylene diamine)	Anti-prolactin-HRP conjugate/prolactin	Sandwich assay with secondary Ab-HRP conjugate on Au nanoparticles covered with poly(*o*-phenylene diamine)	LOD 0.1 ng/mL, conc. range 05–180 ng/mL	[223]

(*Continued*)

Table 4.4 cont.

Poly(anthranilic acid)	Anti-cancer antigen CA 125/CA 125	Sandwich assay, secondary Ab labeled with Au nanoparticles, EIS measurements (charge transfer resistance changes)	LOD 2.0 u/mL, conc. range 5.0–25.0 U/mL	[224]
Poly(anthranilic acid)	Tumor necrosis factor α (TNFα) or TNFα Ab/TNFα	Direct EIS measurements (charge transfer resistance changes) or sandwich assay (DPV), secondary Ab labeled with HRP	LOD 5.0 pg/mL (EIS), 3.2 pg/mL (sandwich assay, DPV)	[225]
Polythionine	Aflatoxin-BSA-HRP conjugate on nano Au/Aflatoxin B1	Indirect competitive assay with anti-aflatoxin Ab, HRP signal (DPV)	LOD 0.07 ng/mL, conc. range 0.6–2.4 ng/mL	[226]
PPY	Bovine leukemia virus protein/Ab	Sandwich assay, EIS measurement with secondary HRP-labeled Abs	Not reported	[227]
PPY	Ovalbumin-ofloxacin conjugate/ofloxacin	Sandwich assay with secondary Ab conjugated with Au nanoparticles and HRP, benzoquinone signal	LOD 0.03 ng/mL, conc. range 0.08–410 ng/mL	[228]

PPY	Prostate-specific antigen (PSA) Ab/PSA	Electropolymerization of pyrrole on Au nanoarray with doping by ant-PSA Ab, DPV signal of redox probe ($[Fe(CN)_6]^{3-/4-}$) and EIS measurements	LOD 0.3 fg/mL, conc. range 10 fg/mL–10 ng/mL, human serum and urine spiked samples testing	[229]
Poly(pyrrolepropylic acid)	Anti-mouse IgG/IgG	Sandwich assay with alkaline phosphatase as label, amperometric *p*-aminophenol signal	LOD 20 pg/mL, conc. range 5 orders of magnitude	[230]
Poly(pyrrolepropyonic acid)	Hepatitis surface antigen Ab/hepatitis surface antigen	Sandwich assay with secondary Ab labeled with alkaline phosphatase, p-aminophenol signal	LOD 0.01 ng/mL, conc. range 5 orders of magnitude	[231]
Poly(pyrrolepropyonic acid)	Insulin-like growth factor 1 (IGF1) Ab/IGF1	Direct EIS measurements and sandwich assay with secondary Ab conjugated with HRP, catechol signal	LOD 0.25 pg/mL, conc. range 0.5–1000 pg/mL, spiked human serum testing	[232]
Poly(pyrrolepropyonic acid)	Prolactin hormone conjugate/prolactin hormone	Indirect competitive assay, secondary Ab immobilized on CNTs bearing alkaline phosphatase, 1-naphtol DPV signal	LOD 3 pg/mL, conc. range 0.01–10^4 ng/mL	[233]

(*Continued*)

Table 4.4 cont.

Copolymer of pyrrole and *N*- hydroxyphthalimide pyrrole	Fab fragment hyst-ScAc/BSA conjugate	EIS measurements on polarized electrode covered with PPY copolymer after Ab immobilization via Cu^{2+}/NTA association and Ag binding	LOD 21.4 pg/mL, conc. range 0.1 ng–10 mg/mL depending on the potential of electrode polarization	[234]
Copolymer of pyrrole-benzophenone and tris(bipyridine pyrrole) ruthenium (II) monomers	T7 bacteriophage/ West Nile virus	Sandwich assay with HRP label, covalently attached benzoquinone signal, amperometric measurement	Ab titer from 1:1 to $1:10^6$	[235]
Copolymer of pyrrole and pyrrole bearing pyrrole bearing N-hydroxyphthalimidyl ester group	Biotinylated single-chain variable fragment Sc-Fv/Ag	Sandwich assay, primary Ab is immobilized via avidin–streptavidin binding, DPV signal of own PPY activity	Conc. range 1–100 pg/mL	[236]
Polymerized 5,2': 5', 2'-terthiophene-3'-carboxylic acid	Monoclonal Ab/ osteoproteogerin	Competitive immunoassay with HRP as label, immobilization on Au nanoparticles implemented in polymer, H_2O_2 reduction signal	LOD 2 pg/mL, conc. range 2.5–25 pg/mL	[237]

Polymerized 5,2';5',2''-terthiophene-3-carboxylic acid	Ab/thrombin	Sandwich assay with thrombin captured by aptamer and signaling Ab labeled with ferrocene, polymer layer contains Au nanoparticles	LOD 5 ng/L, conc. range 5–2000 ng/L	[238]
Polytyrosine	PSA Ab/Ag	Competitive immunoassay on electrode covered with CNTs and polymer, DPV detection of polytyrosine	LOD 1 nM, conc. range up to 10 nM	[239]
Polydopamine	α-Fetoprotein Ab/α-fetoprotein	Polydopamine loaded on Au graphene in the presence of thionine, direct DPV signal	LOD 0.03 ng/mL, conc. range 0.1–150.0 ng/ mL	[240]
Polydopamine	3-Brombiphenyl conjugate/3-brom-biphenyl	Indirect competitive assay with secondary Ab on carbon hollow nanochains bearing HRP, benzoquinone signal	LOD 0.5 pM, conc. range 1 pM–2 nM	[241]

(*Continued*)

Table 4.4 cont.

Polydopamine	3-Brombiphenyl Ag/3-brombiphenyl	Sandwich assay, polydopamine immobilized together with Prussian Blue on ITO glass, secondary Ab labeled with HRP on reduced graphene nanoflakes, benzoquinone signal	LOD 2.25 pM, conc. range 5 pM–2 nM	[242]

or *p*-aminophenylphosphate [230, 231] pairs are mainly used as labels in immunosensors with to respect of the polymer carrier. The reactions generating voltammetric signal are presented in Schemes (4.24) and (4.25).

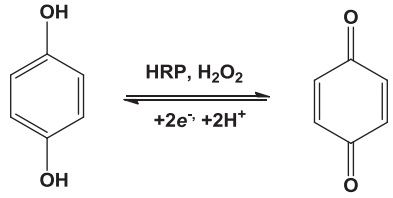

(4.24)

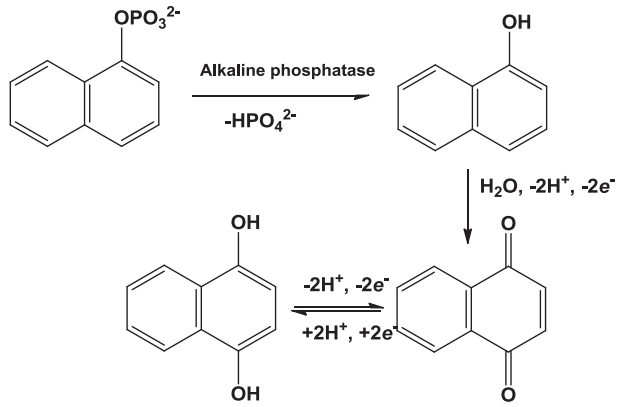

(4.25)

Figutre 4.6 shows a typical competitive assay scheme realized with Abs toward osteoproteogerin immobilized on poly(thiophene-3-carboxylic acid) synthesized from terthiohene derivative [237]. The polymer was preliminary reached with Au nanoparticles to accelerate direct electron transfer to HRP used as Ag label.

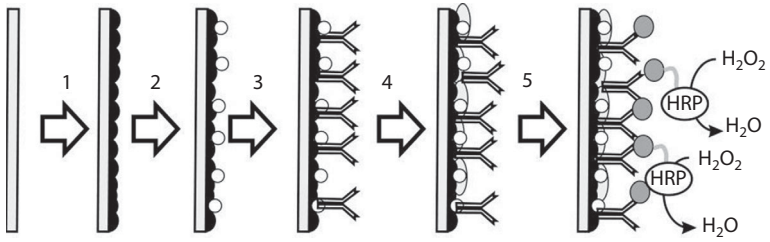

Figure 4.6 Competitive assay of osteoproteogerin with electrochemical immunosensor. 1 – poly(thiophene-3-carboxylic acid) modification, 2 – Au nanoparticles electrodeposition, 3 – specific Ab immobilization by carbodiimide binding to –COOH groups of the polymer, 4 – blocking free electrode surface with casein and 5 – binding free and HRP-labeled analyte molecules followed by direct electron transfer recording.

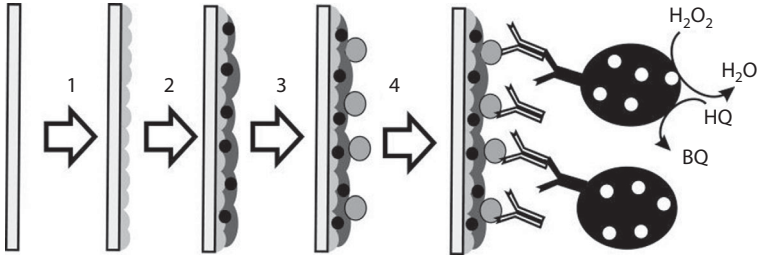

Figure 4.7 Sandwich assay of benz[a]pyrene with electrochemical immunosensor. 1 – ITO glass electrode covered with Nafion, 2 – PANI/Fe_3O_4 suspension deposition, 3 – benz[a]pyrene loading and 4 – incubation with anti-benz[a]pyrene Ab and secondary Ab attached to carbon nanospheres together with HRP.

The use of secondary Abs can be amplified by nanoparticles providing multiple binding of auxiliary reagents. Thus, PANI-based immunosensor has been developed for benz[a]pyrene detection [216]. The ITO glass electrode was first covered with negatively charged Nafion for electrostatic attraction of positively charged PANI obtained by persulfate oxidation in the presence of ferrite nanoparticles. After that, target Ag–Ab interaction was amplified by the use of carbon nanospheres obtained by pyrolysis of glucose solution. The nanoparticles were modified by carbodiimide binding with secondary Abs conjugates with HRP. Thus, a single target interaction resulted in attachment of multiple label molecules (HRP) to the biosensor interface. The surface activity of HRP was finally recorded by HQ oxidation product, benzoquinone (BQ) (Figure 4.7).

A similar magnification of the signal was attained using carbon hollow nanochains (polytyramine polymer as immobilization matrix [241]), CNTs (alkaline phosphatase label [232]) and graphene oxide (polythionine [240]). In the latter case, redox-active polydopamine polymer was applied for the modification of the label. For this purpose, graphene suspension was mixed with dopamine, thionine and $HAuCl_4$ solution. The redox reaction resulted in chemical reduction of Au(III) ions to form nanoparticles and consecutive oxidation of dopamine to polymeric product deposited together with metal and thionine molecules on the graphene nanoflakes. Glassy carbon electrode was treated with the modified graphene flakes, Ab and BSA to block unoccupied place of the electrode. The reaction with Ag (α-fetoprotein) resulted in remarkable changes of both EIS parameters and the thionine DPV signal. In a similar manner, reduced graphene oxide was applied for amplification of HRP signal with HQ as organic substrate [242].

Dendrimers bearing redox-active groups offer broad opportunities for immunosensor development due to combination of hydrophilic moieties

for Ab immobilization in close contact with redox centers and of simple one-step assembling of the surface layer.

Thus, sandwich assay was utilized for the detection of anti-biotin Abs as model target on the base of glassy carbon covered with PAMAM–ferrocene conjugate and secondary antibodies bearing alkaline phosphatase [243]. The LOD of 0.1 mg/mL was achieved by recording the mediated oxidation of *p*-aminophenol, a product of substrate hydrolysis.

Immunosensor based on ITO glass electrode with physically adsorbed PAMAM (4 generations) modified with terminal ferrocene units [244]. Anti-mouse IgG Abs were immobilized by avidin–streptavidin binding. Sandwich assay with alkaline phosphatase as label makes it possible to detect 10 pg/mL of the analyte. The addition of hydrazine amplifying the signal due to recovery of *p*-aminophenol decreased the LOD to 100 fg/mL.

4.5 DNA Sensors Based on Redox-Active Polymers

4.5.1 PANI-Based DNA Sensors and Aptasensors

First and foremost, DNA sensors have been developed for the detection of complementary sequences of oligonucleotides. This was achieved by involvement of target oligonucleotides in the hybridization reaction with complementary sequence introduced in the biosensor assembly and called as DNA probe. The hybridization detection is demanded in medical diagnostics of pathological microorganisms and viruses but also found growing application in food chemistry [detection of the tissues of genetically modified organisms (GMO) in the foodstuffs] and environmental monitoring (bacterial contamination).

Three strategies are mainly applied for detection of a hybridization event:

- Determination of the changes in the redox signal related to the electrochemically active labels incorporated in the DNA probe or to the redox indicators specifically interacted with hybridization product;
- Monitoring of the changes in the electrochemical characteristics of the polymeric support resulted from its interaction with DNA probe and/or target oligonucleotide;
- Recording changes in the electrode characteristics due to different permeability of the surface layer caused by hybridization.

Not all of them are realized in appropriate DNA sensors involving PANI. Meanwhile, the mechanism of the signal generation in PANI-based DNA sensors is commonly suggested but rarely proved with appropriate techniques. It should be also mentioned that most of the articles do not contain conventional analytical characteristics of the hybridization detection. Mostly, the possibility to detect a certain complementary sequence is stated and the possibility to differentiate the behavior of fully not fully complementary sequences is explored as selectivity criterion.

Aligned PANI nanofibers were synthesized on glassy carbon modified with oxidized graphene [245]. The electrosynthesis was performed in three steps, i.e., galvanostatic initiation at high current density and then at twice decreased current, in aniline–HCl solution. The immobilization of the 24-mer DNA probe was performed by carbodiimide binding. The hybridization of complementary DNA target increased the peak current measured by DPV and referred to the graphene redox activity. The PANI exerted synergetic effect on the graphene signal. The DNA sensor described distinguished complementary and three-mismatch oligonucleotides. The target DNA sequence was determined in the range from 2.12×10^{-6} to 2.12×10^{-12} M (LOD 3.25×10^{-13} M).

ITO coated glass electrode with PANI potentiostatically polymerized from HCl containing 1% chitosan was described in [246]. The 42-mer DNA sequence was immobilized onto the polymer by electrostatic accumulation. The formation of double-stranded (ds-) DNA helix decreased the permeability of ferricyanide as redox probe and hence decreased the peak current. Concentration range from 0.1 to 25 fM (LOD 0.05 fM) was achieved. The DNA sensor was proposed for early breast cancer diagnostics.

Highly sensitive detection of pathogen of *Mycobacterium tuberculosis* was described with DNA sensor and diffusionally free methylene blue as redox label [247]. Aminated DNA probe was immobilized onto electropolymerized PANI layer by cross-linking with glutaraldehyde. The cathodic peak current of methylene blue reduction decreased in the presence of target oligonucleotide due to involvement of the redox probe in the ds-DNA formed on the electrode. The DNA sensor made it possible to determine from 2.5×10^{-18} to 15×10^{-18} M of target oligonucleotide. The sensitivity toward biological target was then increased by displacement of DNA probe with appropriate protein nucleic acid (PNA, the lowest quantification level of 0.125×10^{-18} M).

Nanowires of PANI synthesized in potentiostatic electrolysis were used for carbodiimide binding of aminated oligonucleotides and the following hybridization detection [248]. The electrode was consecutively incubated in the sample and methylene blue solution and then transferred in

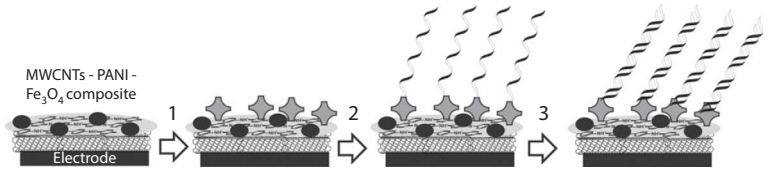

Figure 4.8 Outline presentation of the DNA sensor assembling based on PANI/Fe_3O_8 composite. 1 – Avidin deposition, 2 – biotinylated DNA probe binding and 3 – hybridization event.

the buffer with no free methylene blue. The decrease of the peak current related to redox probe depended on the analyte concentration in the range from 0.225 nM to 2.25 pM (LOD 1.0 pM).

ITO glass electrodes were covered with potentiometrically deposited PANI and then DNA oligonucleotide related *Neisseria gonorrhoeae* by avidin–biotin binding [249]. The intrinsic redox activity of the PANI–DNA adduct was characterized by the current plateau at 200–400 mV. Both the plateau current and guanine oxidation signal recorded at 0.85 V decreased in hybridization event. The range of the concentrations determined with DNA sensor was 1×10^{-6}–1×10^{-16} M (logarithmic scale) and the LOD was 0.5×10^{-16} M.

The same target oligonucleotides were detected by ITO glass electrode covered with MWCNTs, Fe_3O_4 nanoparticles and PANI electropolymerized in galvanostatic mode [250]. The principle scheme of the biolayer preparation and signal measurement is presented in Figure 4.8.

The hybridization event was detected by changes in the methylene blue current (LOD 1×10^{-19} M). The use of glutaraldehyde instead of avidin–biotin binding increased the LOD to 1×10^{-17} M [251].

A highly sensitive method for the detection of hybridization event was proposed in Ref. [252]. Glassy carbon electrode was first coated by electropolymerized polytyramine film. Then it was coated with chemically synthesized mesoporous zirconia particles covered with PANI. The immobilization of DNA probe related to gene of phosphinothricin acetyltransferase, one of the screening detection genes of the transgenic plants, was immobilized by the affinity of DNA to ZrO_2. The integrity of the surface layer was checked by cyclic voltammetry, whereas hybridization was detected by EIS. The charge transfer resistance increased with the analyte concentration within 1.0×10^{-13}–1.0×10^{-6} M (LOD 2.68×10^{-14} M).

Another target of GMO screening, a fragment of CAMV35S gene, was detected with electrochemical immunosensor based on glassy carbon modified with electrochemically reduced graphene coupled with chemically synthesized PANI and $[Ru(NH_3)_6]^{3+}$ ions as intercalators [253]. The

intercalator current measured in DPV mode decreased with the analyte concentration in the range from 1×10^{-13} to 1×10^{-7} M (LOD 3.2×10^{-14} M).

Detection principle relative to competitive assay was realized in [254]. Glassy carbon electrode was consecutively covered with electropolymerized PANI, Au nanoparticles and 17-mer target DNA sequence. The hybridization was detected by involvement of biotinylated target sequence detected by alkaline phosphatase–streptavidin conjugate. Presence of Au nanoparticles is of crucial importance for the sensitive detection. In PANI–Ab layer the sensitivity of detection was about 10 times lower and did not allow distinguishing complementary and non-complementary sequences. The LOD corresponded to 10% shift of the signal was found to be 10 nM.

Enzymatic polymerization resulted in formation of amyloid-like nanofibers of PANI self-assembled on the surface of protein molecules on glassy carbon electrode [255]. The surface of the nanotubes was modified with hairpin-loop DNA probe. Treatment with target DNA related to hepatitis B virus gene resulted in formation of partially hybridized product. In the second step, signaling DNA probe labeled with HRP was used. As a result, enzyme was fixed near the PANI surface and produced the current of direct electron transfer measured in DC mode. The DNA sensor makes it possible to detect 2.0–800.0 fM (LOD 1.0 fM) of biological target. The scheme of DNA sensor assembling and operation is presented in Figure 4.9.

The *aptasensors* include aptamers, synthetic oligonucleotides synthesized by combinatorial chemistry approach, and specifically bind various biomolecules [256]. Being sensitive as conventional Abs, aptamers are more stable and easier modified for implementation in the biosensor assembly. Aptamers find increasing application in detection of biopolymers and low-molecular compounds able to selective DNA binding [257]. Single wires of PANI have been grown in the microchannel obtained by e-beam lithography between two Au electrodes separated with a 5 μm gape [258]. The

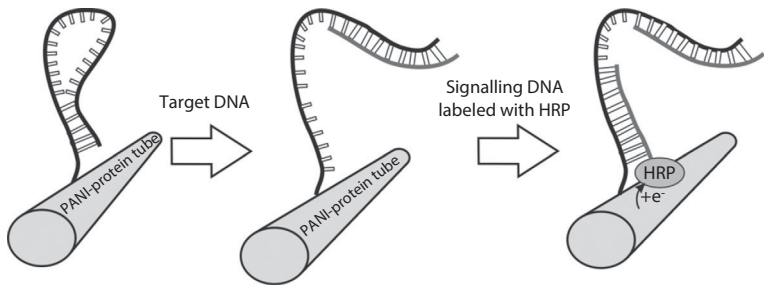

Figure 4.9 Hairpin-loop DNA probe-based biosensor for detection of hepatitis B virus gene.

interaction of DNA aptamers with immunoglobulin IgI resulted in changes of the PANI conductivity. The aptasensor makes it possible to detect 1.0 pg/mL–22.0 ng/mL (LOD 0.56 pg mL^{-1}, or 2.8 fM) of target Ab.

4.5.2 PPY-Based DNA Sensors

Substituted PPY films were first applied for positioning of DNA probes on the solid support required for DNA chip development. It was an alternative to covalent modification on activated nylon beds [259] which offered better opportunities for automation of the chip manufacture. For targeted immobilization, carboxylic, amide or ester groups were introduced in 3-position of pyrrole ring. To get access of bulky DNA oligonucleotides, the substituted monomers were "diluted" with unsubstituted pyrrole on the electropolymerization step [see (4.26) as an example].

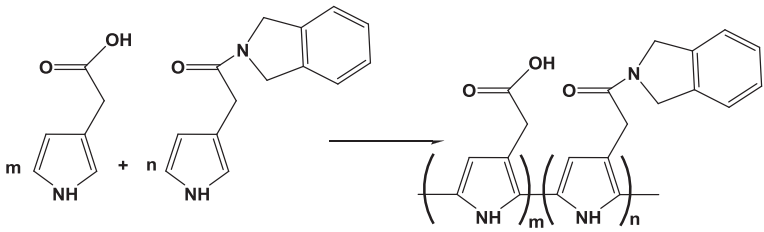

(4.26)

The DNA probe can be then immobilized via terminal amino groups [260]. The reaction was confirmed with IR spectroscopy by disappeared vibration frequencies at 1650 cm^{-1} associated to the pyrrolidinone moiety of the leaving group as well as by new appeared bands at 695 cm^{-1} and about 790–820 cm^{-1} related to the phosphorylamide and oligonucleotide groups, respectively. The hybridization of the DNA probe with complementary DNA sequence suppressed the redox peak of PPY probably due to charge influence exerted on the electron transfer in the polymer film.

Terminal covalent immobilization of DNA probes can be also achieved by N-substituted pyrrole monomers bearing terminal carboxylic groups via carbodiimide binding. [261]. The polymerization product exhibited nearly reversible behavior with standard potential of 0.58 V and surface coverage of 3.5×10^{-7} mol cm^{-2}. The DNA sensor was applied for detection of gene specific to West Nile virus in competitive assay mode. After the incubation in the sample tested the DNA sensor was treated with biotinylated complementary DNA sequence and then glucose oxidase was attached via biotin–avidin–biotin linking. The signal of H_2O_2 oxidation was measured at 0.6 V vs. Ag/AgCl (Figure 4.10). The range of the DNA target sequence determination was from 10^{-10} to 10^{-15} g/mL.

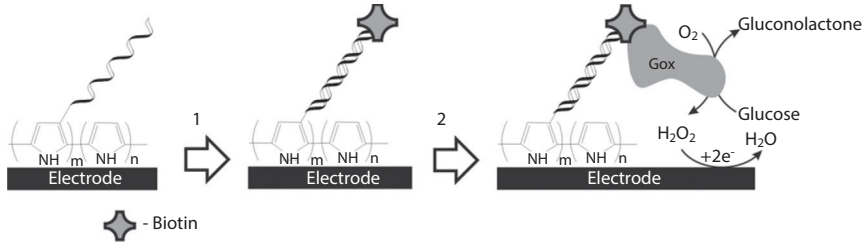

Figure 4.10 PPY-based DNA sensor for the detection of gene related to West Nile virus.

Copolymer of 4-(3-pyrrolyl)butanoic acid and unsubstituted pyrrole was applied for immobilization of DNA probe specific for *Salmonella* virulence *invA* gene [262]. The hybridization resulted in charge transfer resistance increase and suppression of the PPY redox peak recorded in DC mode.

In Ref. [263], DNA probe specific for West Nile virus was attached to the PPY film by intercalation. The acridone derivative that anchored the DNA probe was covalently immobilized to PPY bearing succinimide groups. Labeling the hybridization product with glucose oxidase made it possible to reach 1 pg/mL detection limit.

Impedimetric DNA sensor with PPY–CNTs composite with aminated DNA probe covalently attached to terminal carboxylic groups of the carrier was successfully applied for detection of 1.0×10^{-11}–1.0×10^{-7} M of target DNA (LOD 5.0×10^{-12} M) [264]. Contrary to many other reports, the decrease of the charge transfer resistance due to hybridization was observed due to own electric conductivity of the DNA helix⁻.

Avidin-biotin binding is one of the most effective immobilization ways for targeted binding the DNA oligonucleotides [265, 266]. Some of the monomers used for this purpose are shown in the following (4.27). The DNA grafting can be performed prior to or after electropolymerization. Such hybrid films are suitable not only for voltammetric but also photovoltaic [267], SPR, or fluorescence signal measurements [268].

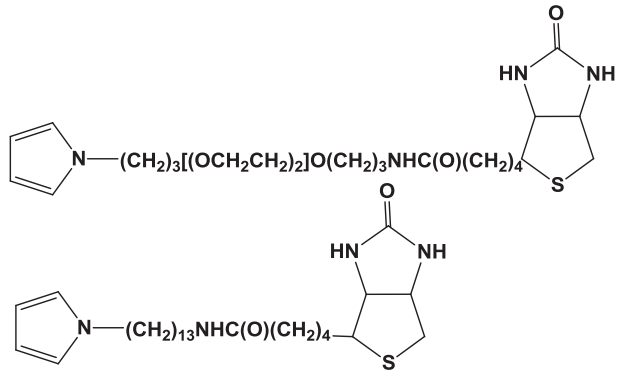

(4.27)

The poly(pyrrole-nitrilotriacetic acid) film provides another example of affine immobilization realized via metal chelation with biotin or histidine tags as ligands. Thus, biotinylated 48-mer DNA target specific for HIV was immobilized by incubation of the electrode covered with such PPY film preliminary soaked in $CuCl_2$ [269]. The hybridization was indicated by increase in the resistance of the charge transfer measured in the presence of neutral redox probe, HQ, at 0.4 V.

Carbon paste electrode with CNTs added to the electrode material was used for electropolymerization of pyrrole in the presence of 32-mer DNA probe [270]. The hybridization was monitored by the oxidation current of intercalator ethidium bromide in the range from 1.0×10^{-10} to 1.0×10^{-8} M (LOD 8.5×10^{-11} M). Five-point mismatch sequence can be distinguished from fully complementary oligonucleotide at the lowest level of quantification.

Bilayer DNA microsensor was developed by combination of PPY and polymer of 2,5-bis(2-thienyl)-N-(3-phosphorylpropyl)pyrrole which were obtained in two separate steps of electrolysis onto the Pt microelectrode [271]. The electrolysis was performed from acetonitrile in potentiostatic regime with control of the charge passed to reach reproducible conductive films. The DNA probes were linked to the polymer by a bidentate complex between Mg^{2+} and alkyl phosphonate group of the polymer. The hybridization increases electrostatic barrier onto the layer which prevents chloride anion exchange. As a results, the charge passed decreased with the analyte concentration varied from 10^{-16} to 10^{-6} M. This protocol was used for sensitive determination of 244-mer DNA sequence related to HIV (LOD 1.82×10^{-21} M [272]).

DNA sensor based on interdigitated Au electrodes covered with PPY-DNA film was developed for detection of herpes simplex virus [273]. The immobilization was performed by entrapment of the DNA probe in the growing PPY layer obtained by cycling voltammetry. The PPY redox peak was suppressed by hybridization product within 4-22 nM of the target DNA (LOD 2 nM).

Ferrocene functionalized PPY was synthesized on Au electrode by polymerization 1-(phthalimidylbutanoate)-1'-(*N*-(3-butylpyrrole)butanamide)ferrocene and pyrrole performed in acetonitrile [274]. The 25-mer DNA probe was then covalently attached to the film via terminal amino group by substitution of phthalimide fragment. The redox signal of ferrocene decreased with the analyte concentration. As was shown by SEM for macro- and microelectrodes, reducing size of the electrode allowed nucleation and increased growth rate of the polymer film during the polymerization. This increased the sensitivity and selectivity of hybridization detection.

Among diseases and pathologies, DNA hybridization was applied for GMO monitoring by detection of some biomarkers like subunit 35S of ribosomal RNA of Cauliflower mosaic virus (promoter) and nopaline synthase (NOS) gene from *Agrobacterium tumefaciens*. For this purpose, DNA sensor with PPY doped with CNTs was described [275]. Herbicide-resistance soybean (Monsanto, Inc.) was chosen as a model. The DNA probes specific for 35S promoter and NOS gene were introduced in growing PPY film deposited on pre-oxidized CNTs on the Au planar interdigitated microelectrodes. The hybridization was monitored by QCM and EIS. The increase of the charge transfer resistance made it possible to detect 25–292 pM of 35S sequence.

The idea of DNA entrapment in the growing polymer film was combined with the molecular imprinting concept [276]. Pyrrole was immobilized on pencil graphite electrode by cyclic voltammetry and potential pulse technique. After that, the DNA molecules entrapped were removed by hydrolysis. The AFM study showed remarkable changes in the surface morphology of the electrodes covered with modified PPY prior to and after DNA removal and that of conventional PPY film. The biosensor preserved the ability to selective adsorb DNA from solution and detect the amounts of analyte by DPV signal measured in the region of nucleotide oxidation.

A hybrid PANI–PPY polymer was chemical synthesized and then casted on Au electrode followed by gold nanoparticles deposition [277]. Thiolated DNA probe was then immobilized on Au surface by self-assembling. Comparative research showed that the presence of polymers increases the sensitivity of hybridization detection by 2.5 times against similar electrode covered with Au nanoparticles only. The dynamic detection range observed for complementary target was from 1×10^{-6} to 1×10^{-13} M (LOD 1.0×10^{-13} M).

Among DNA sensors, two assemblies of aptasensors based on PPY films have been described. The first one is based on affine immobilization via chelation realized by electropolymerization of pyrrole–nitrilotriacetic acid followed by Cu^{2+} treatment and incubation in aptamers against thrombin [278]. Charge transfer resistance increased in the range of the analyte concentration from 4.7×10^{-12} to 5.0×10^{-10} M. No significant influence of BSA and lysozyme was found. In second example, human cellular prions were determined with aptasensor based on PPY–PAMAM (4 generations) composite and ferrocenyl group as redox marker. The aptamers were immobilized via avidin–biotin binding and ferrocene groups positioned between polymer and aptamer layers. Specific changes in the redox activity were because of the lower diffusion of ions in the surface layer caused by implementation of bulky protein molecules. The detection limit of 0.8 pM and the direct testing of blood plasma were achieved.

An electrochemical aptasensor based on PPY modified with redox dendrimers, able to detect human cellular prions (PrP^C) with high sensitivity has been recently reported [279]. In this work the gold surface was modified by conductive PPY film coupled to PAMAM dendrimers of fourth generation and ferrocenyl group as redox marker.The DNA aptamers were immobilized on the surface via biotin/streptavidin chemistry. Electrochemical signal was detected by ferrocenyl group incorporated between dendrimers and aptamers layers. The association of redox dendrimers with conducting PPY leads to high sensitivity of PrP^C determination with detection limit of 0.8 pM, which is three orders of magnitude lower, compared to flat ferrocene-functionalized PPY [280]. Detection of PrP^C in spiked blood plasma has been achieved and demonstrated a recovery up to 90%. Similar detection limit (0.5 pM) and a wide linear range of detection from 1 pM to 10 μM has been demonstrated for PrP^C sensitive aptasensor based on MWCNTs modified with PAMAM dendrimers of fourth generation [281]. Electrochemical signal was detected by a ferrocenyl redox marker incorporated between the dendrimers and aptamers interlayer.

4.5.3 Thiophene Derivatives in the DNA Sensors

The assembling and operating of the DNA sensors including polythiophene derivatives does not differ significantly from those already described in previous sections. Polythiophene moiety like PPY shows one broaden reversible peak on voltammogram which changes with the DNA-specific interactions, namely, hybridization. All the changes observed can be related to either electron exchange suppression or counter ion transfer. The use of substituted polythiophenes enhances the performance of DNA sensors due to increased capacity of the polymer film towards anionic biomolecules or improved procedure of polymerization. Steric limitations of the DNA hybridization can be partially avoided by using copolymers with unsubstituted thiophene or those with rather small substituent. In some cases, di- and terthiophenes are applied instead of thiophene itself on the step of electropolymerization to exclude over-oxidation of thiophene fragment to sulfone.

Thus, cyclopentadithiophene was electropolymerized with 4-cyclopenta[1,2-b;3,4-b']dithiophene-4-ylidenemethyl-N,N-diethylbenzene sulfonamide from acetonitrile solution by potential cycling between –0.75 and 0.40 V vs. SCE [282]. After that, 42-mer DNA oligonucleotide was covalently attached to terminal groups of copolymer. The 675-mer target was hybridized and changes in the polythiophene redox peaks,

permeability of the surface film and mass increase were recorded by DC voltammetry, EIS and QCM, respectively.

The terthiophene functionalized with alkylenecarboxylic fragment (4.28) was synthesized polymerized on Pt electrode by potential cycling [283]. The 18-mer DNA oligonucleotide bearing amino group was then grafted to the polymer by carbodiimide binding. The hybridization with the complementary target increased the charge transfer resistance measured in the presence of $[Fe(CN)_6]^{3-/4-}$.

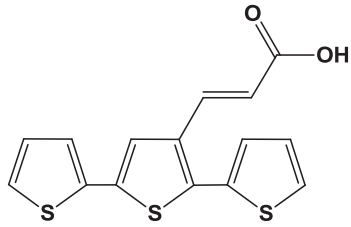

(4.28)

The DNA chip on 2×3 cm glass plate with Pt pads was prepared by the electropolymerization of 3-carboxylic derivative of thiophene and aminated DNA probe [284]. All the reactions including the hybridization detection were performed in acetonitrile. The formation of ds-DNA onto the electrode surface suppressed own polythiophene redox activity.

Polythiophene layer with covalently attached methylene blue was synthesized in accordance with (4.29).

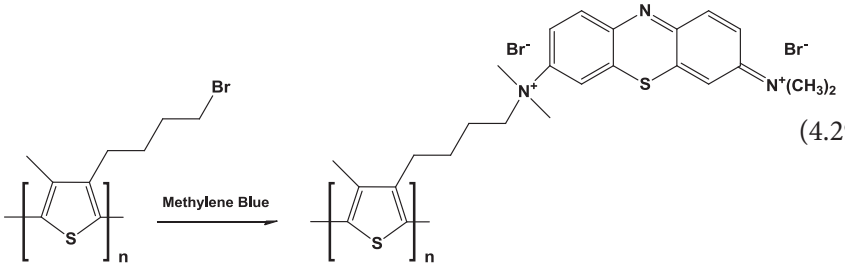

(4.29)

Methylene blue changes its redox activity in hybridization event depending on the analyte concentration [285]. In low-concentration region, the signal increases due to electrostatic interactions of positively charged redox probe with negatively charged DNA target. At higher concentrations, intercalation of methylene blue decreases the current of its oxidation/reduction on cyclic voltammogram.

PEDOT-ds-DNA film was obtained by cycling the potential and physical adsorption of DNA followed by drying the surface [286]. After that, the modified electrode was immersed in the solution of Nile blue for 10 min. Phenazine dye intercalated the DNA helix but retained its electrochemical

and electrocatalytic activity. This was shown on the example of H_2O_2 detection. The reversible peak of nile blue at –0.37 V regularly changed with the analyte concentration between 6 μM and 0.2 mM (LOD 0.1 μM).

Some analogs of EDOT (4.30) were tested in electropolymerization and label-free hybridization detection [287]. The DNA probe related to Cauliflower mosaic virus, GMO biomarker, was casted on the electrode. The hybridization resulted in suppression of own polythiophene activity, whereas fully non-complementary sequences do not interfere with oxidation current recorded at 0.9–1.2 V.

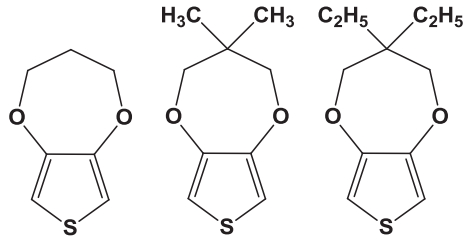

(4.30)

4.5.4 DNA Sensors Based on Polyphenazines and Other Redox-Active Polymers

As was mentioned before, thionine is electropolymerized similarly to aniline with formation of the product exerting the pH-dependent redox activity and electron mediation. However, contrary to PANI the polythionine retains its redox activity in neutral media. This offers good opportunities for the application of this material in the DNA sensor assembly. The electropolymerization of thionine is performed in the pH range from 6 to 8 [288]. The position of redox peaks corresponding to the polymer conversion shift with the pH value to higher cathodic potentials.

The 40-mer DNA probe was covalently attached to the polymer via terminal phosphate group. The hybridization was monitoring by intrinsic redox activity of polythionine measured by DPV. A clear decrease in the reversible peak current was observed in hybridization due to suppression of the rearrangement of the polymer chains required for electron transfer. The LOD of 1.0×10^{-10} M was reported for complementary target.

Polythionine amplifies the signals of guanine and adenine oxidation [289]. For this purpose, CNTs/Au nanoparticles suspension was first casted on glassy carbon electrode from DMF. After that, thionine was electropolymerized from aqueous solution. The oxidation of nucleotides can be performed in DPV mode either individually or simultaneously by their oxidation peaks recorded at 0.6 and 0.9 V. The analytical applications of the method involve the detection of individual nucleotides (LOD about 1 nM)

and estimation of their ratio for ds-DNA samples after their digestion with concentrated HCl.

Among phenothiazines, methylene blue and methylene green have found predominant attention in the DNA sensor development due to high electrochemical activity and intercalator properties. Electropolymerized methylene blue and methylene green were used for the detection of specific anti-DNA antibodies [290]. Contrary to PANI, the antibody binding to DNA in phenothiazine matrix is not complicated by the pH sensitivity of the redox activity. This simplifies measurement and increases the sensitivity toward the analyte molecules. The same protocol was used for the detection of thrombin with aptamer introduced in the biosensor assembly instead of ds-DNA. In both cases, the electropolymerization was performed by potential cycling and the stationary potential or charge transfer resistance were measured prior to and after the contact of the DNA sensor with an analyte solution. For thrombin, the LOD of 1 nM was obtained. The aptasensors based on polymeric phenothiazines show high sensitivity and are less affected by serum proteins than other electrochemical DNA sensors especially based on gold electrodes. This was confirmed by comparative investigation of the response toward serum albumin and direct measurements in spiked serum samples.

The impedimetric aptasensors have been developed for the detection of thrombin. The aptamer was immobilized onto the poly(methylene blue) layer by avidin-biotin binding [291]. Electropolymerization was performed on the glassy carbon electrode covered with MWCNTs. The interaction of the aptamer with thrombin resulted in an increase of the charge transfer resistance and decrease of the capacity of the surface layer. Aptasensors developed determine thrombin in the concentration range 1 nM–1 μM with the LOD of 0.7 nM (monitoring resistance changes) and 0.5 nM (capacitance changes).

Poly(neutral red) was employed as a metric for immobilization of Au nanoparticles with the thiolated 26-mer DNA probes attached. The hybridization event was recorded by the changes in the reduction peak at –0.078 V which decreased with the concentration of complementary sequence. The LOD of 4×10^{-12} M was obtained. It should be noted that the peak used for hybridization indication is not referred to polymeric dye in accordance with other works [38, 292]. Probably, some other products of oligomerization and/or oxidative destruction of the monomer can be responsible for such a response.

Eriochorome Black T (4.31) was electropolymerized on glassy carbon electrode and used for both electron transduction and covalent immobilization of DNA probe via sulfanilamide bond [293].

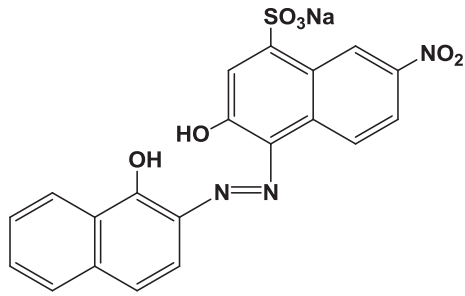

(4.31)

The 18-mer DNA oligonucleotide related to Cauliflower mosaic virus gene was detected by changes in redox activity of diffusionally free methylene blue added to the solution after hybridization. The concentration range from 5.0 fM to 5.0 pM (LOD 0.11 fM) was attained.

The use of dendrimers in DNA sensor assembly is described in several works. Thus, metallodendrimer with Co salicylaldimine was used for hybridization detection by decrease of the Co signal in SWV mode and charge transfer increase in EIS measurement [294]. Besides cobalt, hydrazine covalently attached to PAMAM (4 generations) can be oxidized for the same purpose [295]. Ferrocene-modified PAMAM was applied for detection of PNA–DNA interactions on Au electrode covered with self-assembled monolayer of 6-mercapto-1-hexanol [296]. High sensitivity was reached with impedimetric sensors. DNA sensors with PPI dendrimer (1–3 generations) modified with Ni complex (4.32) exerted reversible redox behavior with charge transfer resistance decreased with hybridization event.

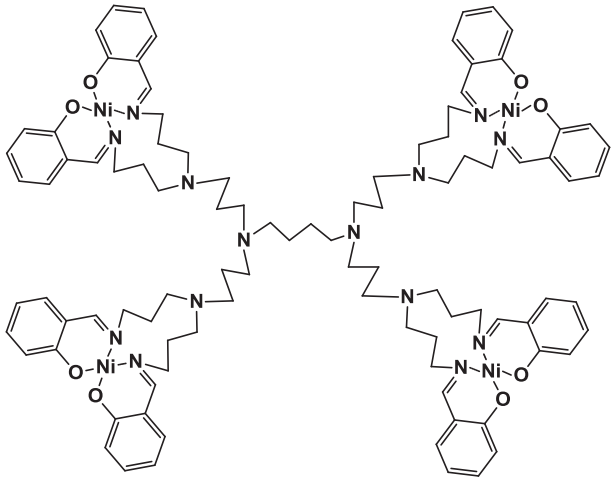

(4.32)

4.6 Conclusion

Summarizing the results obtained in the review area, three approaches to the use of redox-active polymeric materials in the biosensors can be specified:

- redox-active polymers as a tool for the biomolecule immobilization and their wiring;
- polymeric mediators for the enzyme/DNA wiring;
- new ways for the signal generation based on own electrochemical activity.

Electrosynthesis provides simple and cost-effective route to the direct control of the polymer growth and variation of the content of the biorecognition layer. The impact of electropolymerizations is pronounced for microsensors and planar electrodes (electrode arrays). For this reason, the use of PPY for the biochip development was described even earlier than that for macro systems including enzyme sensors. Chemical synthesis has found some applications for the monomers insoluble in water to avoid the contact of biomolecules with aggressive media (strong acids, organic solvents, high voltage). This is especially true for PANI which performance is preferable in acidic media. Meanwhile, the use of pulse technique and modification of monomers with hydrophilic substituents extends the opportunities of electrosynthesis.

The application of redox-active polymers as mediators is mostly based on the experience of successful use of the structurally relative low-molecular compounds in the assembly of enzyme and DNA sensors. The use of phenothiazine dyes, especially methylene blue, is one of the most evident examples. This dye has found broad application as one of the best electrochemically active intercalators and mediators for NADH and H_2O_2 oxidation in the appropriate biosensors. Neutral red is one of the best mediators for NADH oxidation. Even in the case when the redox-active substituents do not interact with each other, polymeric support be it PPY, polythiophene or polyvinyl alcohol, simplifies the implementation of mediators in biosensor assembly and improves operational and analytical characteristics over those of diffusionally free mediators due to higher regularity and reproducibility of the surface layer.

The composites of redox-active polymers with metal nanoparticles and CNTs additionally improve the electric wiring of the proteins/oligonucleotides with the electrodes and hence reversibility of redox reactions affected by biorecognition events. In some cases, it is rather difficult to distinguish the real function of nanoparticles

which can either promote the electron transduction or act as biomolecule support with increased density of the binding site against unmodified analogs.

PPY and polythiophene derivative and to a lesser extent PANI make it possible to rely on their own redox activity as detection signal. Even though the sensitivity of such sensors can be below that observed with mediated systems, this is compensated for by simpler one-step assembling and short response.

Regarding immunosensors, the progress in their development is still the subject of immunochemistry and is related to new immunoreagents discovered and applied in appropriate biosensors. The mechanism of detection of Ag–Ab interaction either involves the detection of electrochemically active labels like enzymes, ferrocene or metal nanoparticles or changes in accessibility of the electrode for redox markers like ferricyanide ions or HQ. The functions of redox-active polymers are mainly related to immobilization and spatial orientation of Abs on the electrode surface.

The following progress in the development of the redox-active materials for biosensors can be related to the molecular imprinting techniques which improve the performance of electrochemical sensors by mimicking multipoint interactions on the electrode surface. There are only few examples of such approach regarding biosensors. In addition to the biorecognition, molecular imprinting can improve the positioning of DNA probe or proteins on the carrier without additional efforts [297, 298].

Acknowledgments

GE announces financial support of RFBR (grant 14-03-00409) and the support by Russian Government Program of Competitive Growth of Kazan Federal University. AP announces fellowship of the Russian President Program for young scientists (SP-1337.2012.4). TH is grateful to Slovak Research and Development Agency (Project No. APVV-14-0267) and to Slovak Science Grant Agency (Project No. VEGA 1/0152/15) for financial support.

References

1. D.R. Thevenot, K. Toth, R.A. Durst, and G.S. Wilson, Electrochemical biosensors: Recommended definitions and classification (Technical Report), *Pure Appl. Chem.* Vol. 71, p. 2333, 1999.
2. S. Andreescu and O.A. Sadik, Trends and challenges in biochemical sensors for clinical and environmental monitoring, *Pure Appl. Chem.* Vol. 76, p. 861, 2004.

3. S. Rodriguez-Mozaz, M.J.L. de Alda, M.-P. Marco, and D. Barcelo, Biosensors for environmental monitoring: A global perspective, *Talanta* Vol. 65, p. 291, 2005.
4. L.C. Clark, Jr. and C. Lyons, Electrode systems for continuous monitoring in cardiovascular surgery, *Ann. N.Y. Acad. Sci*. Vol. 148, p. 133, 1962.
5. D.W. Kimmel, G. Le Blanc, M.E. Meschievitz, and D.E. Cliffel, Electrochemical sensors and biosensors, *Anal. Chem*. Vol. 84, p. 685, 2012.
6. K.L. Adams, M. Puchades, and A.G. Ewing, In vitro electrochemistry of biological systems, *Annu. Rev. Anal. Chem*. Vol. 1, p. 329, 2008.
7. N.J. Ronkainen, H.B. Halsall, and W.R. Heineman, Electrochemical biosensors, *Chem. Soc. Rev*. Vol. 39, p. 1747, 2010.
8. P.T. Kissinger, Biosensors – a perspective, *Biosens. Bioelectron*. Vol. 20, p. 2512, 2005.
9. J.E. Pearson, A. Gill, and P. Vadgama, Analytical aspects of biosensors, *Ann. Clin. Biochem*. Vol. 37, p. 119, 2000.
10. J.M. Goddard and J.H. Hotchkiss, Polymer surface modification for the attachment of bioactive compounds, *Prog. Polym. Sci*. Vol. 32, p. 698, 2007.
11. M. Moyo, J.O. Okonkwo, and N.M. Agyei, Recent advances in polymeric materials used as electron mediators and immobilizing matrices in developing enzyme electrodes, *Sensors* Vol. 12, p. 923, 2012.
12. K.S. Ryder, D.G. Morris, and J.M. Cooper, Role of conducting polymeric interfaces in promoting biological electron transfer, *Biosens. Biolelectron*. Vol. 12, p. 721, 1997.
13. R. Villalonga, A. Fujii, H. Shinohara, S. Tachibana, and Y. Asano, Covalent immobilization of phenylalanine dehydrogenase on cellulose membrane for biosensor construction, *Sens. Actuat. B* Vol. 129, p. 195, 2008.
14. B. Krajewska, Application of chitin- and chitosan-based materials for enzyme immobilizations: a review, *Enzyme Microb. Technol*. Vol. 35, p. 126, 2004.
15. Y. Liu, H. Liu, J. Qian, J. Deng, and T. Yu, Entrapment of both glucose oxidase and peroxidase in regenerated silk fibroin membrane, *Fresenius J. Anal. Chem*. Vol. 355, p. 78, 1996.
16. V.T. Dimakis, V.G. Gavalas, and N.A. Chaniotakis, Polyelectrolyte-stabilized biosensors based on macroporous carbon electrode, *Anal. Chim. Acta* Vol. 467, p. 217, 2002.
17. N.A. Chaniotakis, Enzyme stabilization strategies based on electrolytes and polyelectrolytes for biosensor applications, *Anal. Bioanal. Chem*. Vol. 378, p. 89, 2004.
18. B. Adhikari and S. Majumdar, Polymers in sensor applications, *Prog. Polym. Sci*. Vol. 29, p. 699, 2004.
19. A. Chaubey and B.D. Malhotra, Mediated biosensors, *Biosens. Bioelectron*. Vol. 17, p. 441, 2002.
20. R.A. Marcus and N. Sutin, Electron transfers in chemistry and biology, *Biochem. Biophys. Acta* Vol. 811, p. 265, 1985.

21. S. Cosnier and M. Holzinger, Electrosynthesized polymers for biosensing, *Chem. Soc. Rev.* Vol. 40, p. 2146, 2011.
22. S. Cosnier, Recent advances in biological sensors based on electrogenerated polymers: A review, *Anal. Lett.* Vol. 40, p. 1260, 2007.
23. H. Peng, L. Zhang, C. Soeller, and J. Travas-Sejdic, Conducting polymers for electrochemical DNA sensing, *Biomaterials* Vol. 30, p. 2132, 2009.
24. A.A. Karyakin, M. Vuki, L.V. Lukachova, E.E. Karyakina, A.V. Orlov, G.P. Karpachova, and J. Wang, Processible polyaniline as an advanced potentiometric pH transducer. Application to biosensors, *Anal. Chem.* Vol. 71, p. 2534, 1999.
25. M.M. Barsan, E.M. Pinto, and C.M.A. Brett, Electrosynthesis and electrochemical characterisation of phenazine polymers for application in biosensors, *Electrochim. Acta* Vol. 53, p. 3973, 2008.
26. J.-C. Vidal, E. Garcia-Ruiz, and J.-R. Castillo, Recent advances in electropolymerized conducting polymers in amperometric biosensors, *Microchim. Acta*. Vol. 143, p. 93, 2003.
27. T.A. Skotheim, *Handbook of Conductive Polymers*. Second Edition. Boca Raton, CRC Press, 1997.
28. A.A. Karyakin, E.E. Karyakina, and H.-L. Schmidt, Electropolymerized azines: A new group of electroactive polymers, *Electroanalysis*, Vol. 11, p. 149, 1999.
29. R. Pauliukaite, M.E. Ghica, M.M. Barsan, and C.M.A. Brett, Phenazines and polyphenazines in electrochemical sensors and biosensors, *Anal. Lett.* Vol. 43, p. 1588, 2010.
30. S.-M. Chen and K.-C. Lin, The electrocatalytic properties of polymerized neutral red film modified electrodes, *J. Electroanal. Chem.* Vol. 511, p. 101, 2001.
31. F.S. Damos, R.C.S. Luz, and L.T. Kubota, Study of poly(methylene blue) ultrathin films and its properties by electrochemical surface plasmon resonance, *J. Electroanal. Chem.* Vol. 581, p. 231, 2005.
32. B. Šljukić, C.E. Banks, C. Salter, A. Crossley, and R.G. Compton, Electrochemically polymerised composites of multi-walled carbon nanotubes and poly(vinylferrocene) and their use as modified electrodes: Application to glucose sensing, *Analyst*. Vol. 131, p. 670, 2006.
33. J. Satija, V.V.R. Sai, and S. Mukherji, Dendrimers in biosensors: Concept and applications, *J. Mater. Chem.* Vol. 21, p. 14367, 2011.
34. A. Pron, P. Gawrys, M. Zagorska, D. Djurado, and R. Demadrille, Electroactive materials for organic electronics: preparation strategies, structural aspects and characterization techniques, *Chem. Soc. Rev.* Vol. 39, p. 2577, 2010.
35. G.G. Wallace, P.R. Teasdale, G.M. Spinks, L.A.P. Kane-Maguire, *Conductive Electroactive Polymers: Intelligent Polymer Systems*. Third Edition. Boca Raton, CRC Press, 2008.
36. N. Sakmeche, E.A. Bazzaoui, M. Fall, S. Aeiyach, M. Jouini, J.C. Lacroix, J.J. Aaron, and P.C. Lacaze, Application of sodium dodecylsulfate (SDS) micellar

solution as an organized medium for electropolymerization of thiophene derivatives in water, *Synth. Metals*. Vol. 84, p. 191, 1997.
37. B. Dong, S. Zhang, L. Zheng, and J. Xu, Ionic liquid microemulsions: A new medium for electropolymerization, *J. Electroanal. Chem.* Vol. 619–620, p. 193, 2008.
38. H.-B. Noh, P. Kumar, T.K. Biswas, D.-S. Kim, and Y.-B. Shim, Improved performance of an amperometric biosensor with polydiaminonaphthalene on electrochemically deposited Au nanoparticles, *Electroanalysis*. Vol. 22, p. 632, 2010.
39. Y.-C. Li and K.-H. Yang, Catalytic electroxidation pathway for electropolymerization of polypyrrole in solutions containing gold nanoparticles, *Electrochim. Acta*. Vol. 25, p. 5376, 2007.
40. F. Shang, J.D. Glennon, and J.H.T. Luong, Glucose oxidase entrapment in an electropolymerized poly(tyramine) film with sulfobutylether-β-cyclodextrin on platinum nanoparticle modified boron-doped diamond electrode, *J. Phys. Chem. C*. Vol. 112, p. 20258, 2008.
41. V.N. Andreev, Electrocatalytic oxidation of formic acid on a glassy-carbon–Nafion–polyaniline-palladium nanoparticle electrode: effect of the polymer matrix state, *Russ. J. Electrochem.* Vol. 42, p. 193, 2006.
42. M. Chen, J.-Q. Xu, S.-N. Ding, D. Shan, H.-G. Xue, S. Cosnier, and M. Holzinger, Poly(brilliant Cresyl blue) electrogenerated on single-walled carbon nanotubes modified electrode and its application in mediated biosensing system, *Sens. Actuat. B* Vol. 152, p. 14, 2011.
43. D. Wei, C. Kvarnström, T. Lindfors, and A. Ivaska, Electrochemical functionalization of single walled carbon nanotubes with polyaniline in ionic liquids, *Electrochem. Commun.* Vol. 9, p. 206, 2007.
44. L.V. Lukachova, E.A. Kotel'nikova, D. D'Ottavi, E.A. Shkerin, E. E. Karyakina, D. Moscone, G. Palleschi, A. Curulli, and A. A. Karyakin, Electrosynthesis of poly-o-diaminobenzene on the Prussian Blue modified electrodes for improvement of hydrogen peroxide transducer characteristics, *Bioelectrochemistry* Vol. 55, p. 145, 2002.
45. G. Inzelt and G.G. Lang, "Electrochemical impedance spectroscopy (EIS) for polymer characterization", in: S. Cosnier and A. Karyakin, eds., *Electropolymerization: Concept, Materials and Applications*, Wiley-VCH Verlag, pp. 51–76, 2010.
46. V.V. Malev and V.V. Kondratiev, Charge transfer processes in conducting polymer films, *Russ. Chem. Rev.* Vol. 75, p. 147, 2006.
47. A.S. Sarac, M. Ates, and B. Killic, Electrochemical impedance spectroscopic study of polyaniline on platinum, glassy carbon and carbon fiber microelectrodes, *Int. J. Electrochem. Sci.* Vol. 3, p. 777, 2008.
48. L. Liang, J. Liu, C.F. Windisch, Jr., G.J. Exarhos, and Y. Lin, Direct assembly of large arrays of oriented conducting polymer nanowires, *Angew.Chem. Int. Ed.* Vol. 41, p. 3665, 2002.

49. P.R. Solanki, N. Prabhakar, M.K. Pandey, and B.D. Malhotra, Nucleic acid sensor for insecticide detection, *J. Mol. Recognit.* Vol. 21, p. 217, 2008.
50. E. Muñoz, A. Colina, A. Heras, V. Ruiz, S. Palmero, and J. Lopez-Palacios, Electropolymerization and characterization of polyaniline films using a spectroelectrochemical flow cell, *Anal. Chim. Acta* Vol. 573-574, p. 20, 2006.
51. K. A. Marx, Quartz crystal microbalance: A useful tool for studying thin polymer films and complex biomolecular systems at the solution-surface interface, *Biomacromolecules* Vol. 4, p. 1099, 2003.
52. S. Suematsu, Y. Oura, H. Tsujimoto, H. Kanno, and K. Naoi, Conducting polymer films of cross-linked structure and their QCM analysis, *Electrochim. Acta* Vol. 45, p. 3813, 2000.
53. G. Zotti, S. Cattarin, and N .Comisso, Cyclic potential sweep electropolymerization of aniline: The role of anions in the polymerization mechanism, *J. Electroanal. Chem.* Vol. 239, p. 387, 1988.
54. T. Lindfors, S. Ervelä, and A. Ivaska, Cyclic potential sweep electropolymerization of aniline: The role of anions in the polymerization mechanism, *J. Electroanal. Chem.* Vol. 560, p. 69, 2003.
55. R. Prakash, Electrochemistry of polyaniline: study of the pH effect and electrochromism, *J. Appl. Polym. Sci.* Vol. 83, p. 378, 2002.
56. A. Eftekhari, *Nanostructured Materials in Electrochemistry*, Weinheim, Wiley-VCH Verlag, 2008.
57. A. Kausaite-Minkstimiene, V. Mazeiko, A. Ramanaviciene, and A. Ramanavicius, Evaluation of amperometric glucose biosensors based on glucose oxidase encapsulated within enzymatically synthesized polyaniline and polypyrrole, *Sens. Actuat. B* Vol. 158, p. 278, 2011.
58. S. Bhadra, D. Khastgir, N.K. Singh, and J.H. Lee, Progress in preparation, processing and applications of polyaniline, *Prog. Polym. Sci.* Vol. 34, p. 783, 2009.
59. L. Zhang and S. Dong, The electrocatalytic oxidation of ascorbic acid on polyaniline film synthesized in the presence of camphorsulfonic acid, *J. Electroanal. Chem.* Vol. 568, p. 189, 2004.
60. I.Yu. Sapurina and M.A. Shishov "Oxidative polymerization of aniline: molecular synthesis of polyaniline and the formation of supramolecular structures", in: A.D.S. Gomes, ed., *New Polymers for Special Applications*, InTech, pp. 251–312, 2012.
61. Q. Gao, X. Cui, F. Yang, Y. Ma, and X. Yang, Preparation of poly(thionine) modified screen-printed carbon electrode and its application to determine NADH in flow injection analysis system, *Biosens. Bioelectron.* Vol. 19, p. 277, 2003.
62. A.A. Karyakin, I.A. Maltsev, and L.V. Lukachova, The influence of defects in polyaniline structure on its electroactivity: optimization of 'self-doped' polyaniline synthesis, *J. Electroanal. Chem.* Vol. 402, p. 217, 1996.

63. C.M.A. Brett and C. Thiemann, Conducting polymers from aminobenzoic acids and aminobenzenesulphonic acids: influence of pH on electrochemical behavior, *J. Electroanal. Chem.* Vol. 538–539, p. 215, 2002.
64. L. Zhang and S. Dong, The electrocatalytic oxidation of ascorbic acid on polyaniline film synthesized in the presence of camphorsulfonic acid, *J. Electroanal. Chem.* Vol. 568, p. 189, 2004.
65. H. Zhou, Y. Lin, P. Yu, L. Su, and L. Mao, Doping polyaniline with pristine carbon nanotubes into electroactive nanocomposite in neutral and alkaline media, *Electrochem. Commun.* Vol. 11, p. 965, 2009.
66. Z. Wei, M. Wan, T. Lin, and L. Dai, Polyaniline nanotubes doped with sulfonated carbon nanotubes made via a self-assembly process, *Adv. Mater.* Vol. 15, p. 136, 2003.
67. Y.-H. Chen, J.-Y. Wu, and Y.-C. Chung, Preparation of polyaniline-modified electrodes containing sulfonated polyelectrolytes using layer-by-layer techniques, *Biosens. Bioelectron.* Vol. 22, p. 489, 2006.
68. X. Luo, G.D. Vidal, A.J. Killard, A. Morrin, and M.R. Smyth, Synthesis of polyelectrolyte complexes of polyaniline and sulfonated polystyrene by palm tree peroxidase, *Electroanalysis* Vol. 19, p. 876, 2007.
69. X. Wang, T. Yang, X. Li, and K. Jiao, Three-step electrodeposition synthesis of self-doped polyaniline nanofiber-supported flower-like Au microspheres for high-performance biosensing of DNA hybridization recognition, *Biosens. Bioelectron.* Vol. 26, p. 2953, 2011.
70. B. Sar and M. Talu, Electrochemical copolymerization of pyrrole and aniline, *Synth. Metals* Vol. 94, p. 221, 1998.
71. R. Rajagopalan and J.O. Iroh, A one-step electrochemical synthesis of polyaniline–polypyrrole composite coatings on carbon fibers, *Electrochim. Acta* Vol. 47, p. 1847, 2002.
72. Y.H. Park, S.J. Kim, and J.Y. Lee, Preparation and characterization of electroconductive polypyrrole copolymer Langmuir–Blodgett films, *Thin Solid Films* Vol. 425, p. 233, 2003.
73. J.-W. Lee, F. Serna, and C.E. Schmidt, Carboxy-endcapped conductive polypyrrole: Biomimetic conducting polymer for cell scaffolds and electrodes, *Langmuir* Vol. 22, p. 9816, 2006.
74. Y. Wei, C.C. Chan, J. Tran, G.W. Jang, and K.F. Hsueh, Electrochemical polymerization of thiophenes in the presence of bithiophene or terthiophene: kinetics and mechanism of the polymerization, *Chem. Mat.* Vol. 3, p. 888, 1991.
75. J. Roncali, Conjugated poly(thiophenes): synthesis, functionalization, and applications, *Chem. Rev.* Vol. 92, p. 711, 1992.
76. H. Yamato, O. Ohwa, and W. Wernet, Stability of polypyrrole and poly(3,4-ethylenedioxythiophene) for biosensor application, *J. Electroanal. Chem.* Vol. 397, p. 163, 1995.

77. X. Chen and O. Inganas, Three-step redox in polythiophenes: Evidence from electrochemistry at an ultramicroelectrode, *J. Phys. Chem.* Vol. 100, p. 15202, 1996.
78. D. Bouchta, N. Izaoumen, H. Zejli, M. El Kaoutit, and K.R. Temsamani, A novel electrochemical synthesis of poly-3-methylthiophene-γ-cyclodextrin film: Application for the analysis of chlorpromazine and some neurotransmitters, *Biosens. Bioelectron.* Vol. 20, p. 2228, 2005.
79. C. Gautier, C. Cougnon, J.-F. Pilard, N. Casse, B. Chénais, and M. Laulier, Detection and modelling of DNA hybridization by EIS measurements: Mention of a polythiophene matrix suitable for electrochemically controlled gene delivery, *Biosens. Bioelectron.* Vol. 22, p. 2025, 2007.
80. A.A. Karyakin, E.E. Karyakina, W. Schuhmann, and H.-L. Schmidt, Electropolymerized azines. P.II. In a search of the best electrocatalyst of NADH oxidation, *Electroanalysis* Vol. 11, p. 553, 1999.
81. J. Liu and S. Mu, The electrochemical polymerization of methylene blue and properties of polymethylene blue, *Synth. Metals* Vol. 107, p. 159, 1999.
82. V. Kertesz and G.J. Van Berkel, Electropolymerization of Methylene blue investigated using on-line electrochemistry/electrospray mass spectrometry, *Electroanalysis* Vol. 13, p. 1425, 2001.
83. F.S. Damos, R.C.S. Luz, and L.T. Kubota, Study of poly(methylene blue) ultrathin films and its properties by electrochemical surface plasmon resonance, *J. Electroanal. Chem.* Vol. 581, p. 231, 2005.
84. D. Zhou, H. Fang, H. Chen, H. Ju, and Y. Wang, The electrochemical polymerization of methylene green and its electrocatalysis for the oxidation of NADH, *Anal. Chim. Acta* Vol. 329, p. 41, 1996.
85. R.P. Akkermans, S.L. Roberts, F. Marken, B.A. Coles, S.J. Wilkins, J.A. Cooper, K.E. Woodhouse, and R.G. Compton, Methylene green voltammetry in aqueous solution: Studies using thermal, microwave, laser, or ultrasonic activation at platinum electrodes, *J. Phys. Chem. B* Vol. 103, p. 9987, 1999.
86. Y.V. Ulyanova, A.E. Blackwell, and S.D. Minteer, Poly(methylene green) employed as molecularly imprinted polymer matrix for electrochemical sensing, *Analyst* Vol. 131, p. 257, 2006.
87. A. Wang, C. Ornelas, D. Astruc, and P. Hapiot, Electronic communication between immobilized ferrocenyl-terminated dendrimers, *J. Am. Chem. Soc.* Vol. 131, 6652, 2009.
88. J. Huo, L. Wang, H. Yu, L. Deng, J. Ding, Q. Tan, Q. Liu, A. Xiao, and G. Ren, Hyperbranched ferrocenyl polymer film with high charge transport efficiency, *J. Phys. Chem. B* Vol. 112, p. 11490, 2008.
89. D. Sobransingh and A. Kaifer, New dendrimers containing a single cobaltocenium unit covalently attached to the apical position of Newkome dendrons: Electrochemistry and guest binding interactions with cucurbit[7]uril, Electrochemical studies of porphyrin-appended dendrimers, *Langmuir* Vol. 22, p. 10540, 2006.

90. C.F. Hogan, A.R. Harris, A.M. Bond, J. Slyc, and M.J. Crossley, Electrochemical studies of porphyrin-appended dendrimers, *Phys. Chem. Chem. Phys.* Vol. 8, p. 2058, 2006.
91. I. Cesarino, F.C. Moraes, M.R.V. Lanza, and S.A.S. Machado, Electrochemical detection of carbamate pesticides in fruit and vegetables with a biosensor based on acetylcholinesterase immobilised on a composite of polyaniline–carbon nanotubes, *Food Chem.* Vol. 135, p. 873, 2012.
92. Y. Teng, Y. Fu, L. Xu, B. Lin, Z. Wang, Z. Xu, L. Jin, and W. Zhang, Three-dimensional ordered macroporous (3DOM) composite for electrochemical study on acetylcholinesterase inhibition induced by endogenous neurotoxin, *J. Phys. Chem. B* Vol. 116, p. 11180, 2012.
93. M. Snejdarkova, L. Svobodova, G. Evtugyn, H. Budnikov, A. Karyakin, D.P. Nikolelis, and T. Hianik, Acetylcholinesterase sensors based on gold electrodes modified with dendrimer and polyaniline: A comparative research, *Anal. Chim. Acta* Vol. 514, p. 79, 2004.
94. W. Ji, L. Su, and Y. Lei, Pt nanoflower/polyaniline composite nanofibers based urea biosensor, *Biosens. Bioelectron.* Vol. 30, p. 158, 2011.
95. F.N. Crespilho, R.M. Iost, S.A. Travain, O.N. Oliveira Jr., and V. Zucolotto, Enzyme immobilization on Ag nanoparticles/polyaniline nanocomposites, *Biosens. Bioelectron.* Vol. 24, p. 3073, 2009.
96. B. Lakard, D. Magnin, O. Deschaume, G. Vanlancker, K. Glinel, S. Demoustier-Champagne, B. Nysten, P. Bertrand, S. Yunus, and A.M. Jonas, Optimization of the structural parameters of new potentiometric pH and urea sensors based on polyaniline and a polysaccharide coupling layer, *Sens. Actuat. B* Vol. 166–167, p. 794, 2012.
97. A. Słoniewska and B. Pałys, Supramolecular polyaniline hydrogel as a support for urease, *Electrochim. Acta* Vol. 126, p. 90, 2014.
98. S.A. Trashin, D. Haltrich, R. Ludwig, L. Gorton, and A.A. Karyakin, Improvement of direct bioelectrocatalysis by cellobiose dehydrogenase on screen printed graphite electrodes using polyaniline modification, *Bioelectrochemistry* Vol. 76, p. 87, 2009.
99. R. Khan, P.R. Solanki, A. Kaushik, S.P. Singh, S. Ahmad, and B.D. Malhotra, Cholesterol biosensor based on electrochemically prepared polyaniline conducting polymer film in presence of a nonionic surfactant, *J. Polym. Res.* Vol. 16, p. 363, 2009.
100. C. Dhand, M. Das, G. Sumana, A.K. Srivastava, M.K. Pandey, C.G. Kim, M. Datta, and B.D. Malhotra, Preparation, characterization and application of polyaniline nanospheres to biosensing, *Nanoscale* Vol. 2, p. 747, 2010.
101. N. Ruecha, R. Rangkupan, N. Rodthongkum, and O. Chailapakul, Novel paper-based cholesterol biosensor using graphene/polyvinylpyrrolidone/polyaniline nanocomposite, *Biosens. Bioelectron.* Vol. 52, p. 13, 2014.
102. T. Homma, D. Sumita, M. Kondo, T. Kuwahara, and M. Shimomura, Amperometric glucose sensing with polyaniline/poly(acrylic acid) composite film bearing covalently-immobilized glucose oxidase: A novel method

combining enzymatic glucose oxidation and cathodic O_2 reduction, *J. Electroanal. Chem.* Vol. 712, p. 119, 2014.
103. F.-Y. Kong, S.-X. Gu, W.-W. Li, T.-T. Chen, Q. Xu, and W. Wang, A paper disk equipped with graphene/polyaniline/Au nanoparticles/glucose oxidase biocomposite modified screen-printed electrode: Toward whole blood glucose determination, *Biosens. Bioelectron.* Vol. 56, p. 77, 2014.
104. F. Arslan, S. Ustabaş, and H. Arslan, An amperometric biosensor for glucose determination prepared from glucose oxidase immobilized in polyaniline-polyvinylsulfonate film, *Sensors* Vol. 11, p. 8152, 2011.
105. A. G. Yavuz, A. Uygun, and V. R. Bhethanabotl, Preparation of substituted polyaniline/chitosan composites by in situ electropolymerization and their application to glucose sensing, *Carbohydr. Polym.* Vol. 81, p. 712, 2010.
106. B. Batra, S. Lata, M. Sharma, and C.S. Pundir, An acrylamide biosensor based on immobilization of hemoglobin onto multiwalled carbon nanotube/copper nanoparticles / polyaniline hybrid film, *Anal. Biochem.* Vol. 433, p. 210, 2013.
107. K.M. Manesh, P. Santhosh, A.I. Gopalan, and K.-P. Lee, Silica-polyaniline based bienzyme cholesterol biosensor: Fabrication and characterization, *Electroanalysis* Vol. 22, 2467, 2010.
108. K.F. Fernandes, C.S. Lima, F.M. Lopes, and C.H. Collins, Properties of horseradish peroxidase immobilised onto polyaniline, *Proc. Biochem.* Vol. 39, p. 957, 2004.
109. Q. Xu, J.-J. Zhu, and X.-Y. Hu, Ordered mesoporous polyaniline film as a new matrix for enzyme immobilization and biosensor construction, *Anal. Chim. Acta* Vol. 597, p. 151, 2007.
110. X. Luo, G.D. Vidal, A.J. Killard, A. Morrin, and M.R. Smyth, Nanocauliflowers: a nanostructured polyaniline-modified screen-printed electrode with a self-assembled polystyrene template and its application in an amperometric enzyme biosensor, *Electroanalysis* Vol. 19, p. 876, 2007.
111. C.-C. Chen and Y. Gu, Enhancing the sensitivity and stability of HRP/PANI/Pt electrode by implanted bovine serum albumin, *Biosens. Bioelectron.* Vol. 23, p. 765, 2008.
112. X. Chen, Z. Chen, J. Zhu, C. Xu, W. Yan, and C. Yao, A novel H_2O_2 amperometric biosensor based on gold nanoparticles/self-doped polyaniline nanofibers, *Bioelectrochemistry* Vol. 82, p. 87, 2011.
113. K. Radhapyari, P. Kotoky, M.R. Das, and R. Khan, Graphene–polyaniline nanocomposite based biosensor for detection of antimalarial drug artesunate in pharmaceutical formulation and biological fluids, *Talanta* Vol. 111, p. 47, 2013.
114. S. Chawla, R. Rawal, S. Sharma, and C.S. Pundir, An amperometric biosensor based on laccase immobilized onto nickel nanoparticles/carboxylated multiwalled carbon nanotubes/polyaniline modified gold electrode for determination of phenolic content in fruit juices, *Biochem. Eng. J.* Vol. 68, p. 76, 2012.

115. P. Wang, M. Liu, and J. Kan, Amperometric phenol biosensor based on polyaniline, *Sens. Actuat. B* Vol. 140, p. 577, 2009.
116. D. Shan, Q. Shi, D. Zhu, and H. Xue, Inhibitive detection of benzoic acid using a novel phenols biosensor based on polyaniline–polyacrylonitrile composite matrix, *Talanta* Vol. 72, p. 1767, 2007.
117. S. Li, Y. Tan, P. Wang, and J. Kan, Inhibition of benzoic acid on the polyaniline–polyphenol oxidase biosensor, *Sens. Actuat. B* Vol. 144, p. 18, 2010.
118. H. Chen, S. Li, S. Wang, Y. Tan, and J. Kan, A new catechol biosensor immobilized polyphenol oxidase by combining electropolymerization and crosslinking process, *Inter. J. Polym. Mater. Polym. Biomater.* Vol. 62, p. 620, 2013.
119. S. Timur, N. Pazarlıoglu, R. Pilloton, and A. Telefoncu, Thick film sensors based on laccases from different sources immobilized in polyaniline matrix, *Sens. Actuat. B* Vol. 97, p. 132, 2004.
120. J. Zhang, J. Lei, Y. Liu, J. Zhao, and H. Ju, Highly sensitive amperometric biosensors for phenols based on polyaniline–ionic liquid–carbon nanofiber composite, *Biosens. Bioelectron*. Vol. 24, p. 1858, 2009.
121. B. Bahmani, F. Moztarzadeh, M. Rabiee, and M. Tahriri, Development of an electrochemical sulfite biosensor by immobilization of sulfite oxidase on conducting polyaniline film, *Synth. Metals* Vol. 160, p. 2653, 2010.
122. Y. Jiang, A. Wang, and J. Kan, Selective uricase biosensor based on polyaniline synthesized in ionic liquid, *Sens. Actuat. B* Vol. 124, p. 529, 2007.
123. N. Wathoni, A. N. Hasanah, D. Gozali, Y. Wahyuni, and L. L. Fauziah, Determination of uric acid level by polyaniline and poly (allylamine) based biosensor, *J. Adv. Pharm. Technol. Res.* Vol. 5, p. 13, 2014.
124. Y.-T. Shih and H.-J. Huang, A creatinine deiminase modified polyaniline electrode for creatinine analysis, *Anal. Chim. Acta* Vol. 392, p. 143, 1999.
125. G. Evtugyn, *Biosensors: Essentials*, Heidelberg, Springer, 2014.
126. J.V. de Melo, M.E. Bello, W.M. de Azevedo, J.M. de Souza, and F.B. Diniz, The effect of glutaraldehyde on the electrochemical behavior of polyaniline, *Electrochim. Acta* Vol. 44, p. 2405, 1999.
127. C. Dhand, M. Das, M. Datta, and B.D. Malhotra, Recent advances in polyaniline based biosensors, *Biosens. Bioelectron*. Vol. 26, p. 2811, 2011.
128. D. Wei and A. Ivaska, Electrochemical biosensors based on polyaniline, *Chem. Anal. (Warsaw)* Vol. 51, p. 839, 2006.
129. J. Gong, L. Wang, and L. Zhang, Electrochemical biosensing of methyl parathion pesticide based on acetylcholinesterase immobilized onto Au–polypyrrole interlaced network-like nanocomposite, *Biosens. Bioelectron*. Vol. 24, p. 2285, 2009.
130. R.R. Dutta and P. Puzari, Amperometric biosensing of organophosphate and organocarbamate pesticides utilizing polypyrrole entrapped acetylcholinesterase electrode, *Biosens. Bioelectron.* Vol. 52, p. 166, 2014.
131. C.A.B. Garcia, G. de Oliveira Neto, and L. T. Kubota, New fructose biosensors utilizing a polypyrrole film and d-fructose 5-dehydrogenase immobilized by different processes, *Anal. Chim. Acta* Vol. 374, p. 201, 1998.

132. J.R. Retama, E.L. Cabarcos, D. Mecerreyes, and B. Lopez-Ruiza, Design of an amperometric biosensor using polypyrrole-microgel composites containing glucose oxidase, *Biosens. Bioelectron*. Vol. 20, p. 1111, 2004.
133. X. Liu, K.G. Neoh, L. Cen, and E.T. Kang, Enzymatic activity of glucose oxidase covalently wired via viologen to electrically conductive polypyrrole films, *Biosens. Bioelectron.* Vol. 19, p. 823, 2004.
134. C. N. Kotanen, C. Tlili, and A. Guiseppi-Elie, Bioactive electroconductive hydrogels: the effects of electropolymerization charge density on the storage stability of an enzyme-based biosensor, *Appl. Biochem. Biotechnol*. Vol. 166, p. 878, 2012.
135. Y.-C. Tsai, S.-C. Li, and S.-W. Liao, Electrodeposition of polypyrrole–multiwalled carbon nanotube–glucose oxidase nanobiocomposite film for the detection of glucose, *Biosens. Bioelectron*. Vol. 22, p. 495, 2006.
136. G. Xu, S.B. Adeloju, Y. Wu, and X. Zhang, Modification of polypyrrole nanowires array with platinum nanoparticles and glucose oxidase for fabrication of a novel glucose biosensor, *Anal. Chim. Acta* Vol. 755, p. 100, 2012.
137. J. Li and X. Lin, Glucose biosensor based on immobilization of glucose oxidase in poly(o-aminophenol) film on polypyrrole-Pt nanocomposite modified glassy carbon electrode, *Biosens. Bioelectron*. Vol. 22, p. 2898, 2007.
138. M. Holzinger, L. Bouffier, R. Villalonga, and S. Cosnier, Adamantane/β-cyclodextrin affinity biosensors based on single-walled carbon nanotubes, *Biosens. Bioelectron.* Vol. 24, p. 1128, 2009.
139. S.B. Kadam, K. Datta, P. Ghosh, and M.D. Shirsat, Poly(pyrrole)-poly(N-methylpyrrole) composite matrix for amperometric biosensor design, *Intern. J. Polym. Mater.* Vol. 60, p. 233, 2011.
140. F. Valentini, L.G. Fernández, E. Tamburri, and G. Palleschi, Single walled carbon nanotubes/ polypyrrole–GO_x composite films to modify gold microelectrodes for glucose biosensors: Study of the extended linearity, *Biosens. Bioelectron*. Vol. 43, p. 75, 2013.
141. Z. Yang, C. Zhang, J. Zhang, and W. Bai, Potentiometric glucose biosensor based on core–shell Fe_3O_4-enzyme–polypyrrole nanoparticles, *Biosens. Bioelectron*. Vol. 51, p. 268, 2014.
142. L. Tian, J. Qiu, Y.-C. Zhou, and S.-G. Sun, Application of polypyrrole/GOx film to glucose biosensor based on electrochemical-surface plasmon resonance technique, *Microchim. Acta* Vol. 169, p. 269, 2010.
143. R. Kumpangpet, B. Jongsomjit, C. Thanachayanont, and S. Prichanont, Solid oxide fuel cell technology, *Eng. J.* Vol. 16, p. 45, 2012.
144. A. Guerrieri, R. Ciriello, and T.R.I. Cataldi, Novel amperometric biosensor based on a co-crosslinked l-lysine-α-oxidase/overoxidized polypyrrole bilayer for the highly selective determination of l-lysine, *Anal. Chim. Acta* Vol. 795, p. 52, 2013.
145. I.M. Apetrei and C. Apetrei, Amperometric biosensor based on polypyrrole and tyrosinase for the detection of tyramine in food samples, *Sens. Actuat. B* Vol. 178, p. 40, 2013.

146. S. Da Silva, S. Cosnier, M. G. Almeida, and J. J. G. Moura, An efficient poly(pyrrole–viologen)-nitrite reductase biosensor for the mediated detection of nitrite, *Electrochem. Commun*. Vol. 6, p. 404, 2004.
147. A.T. Lawal and S.B. Adeloju, Polypyrrole based amperometric and potentiometric phosphate biosensors: A comparative study B, *Biosens. Bioelectron*. Vol. 40, p. 377, 2013.
148. Q. Ameer and S.B. Adeloju, Galvanostatic entrapment of sulfite oxidase into ultrathin polypyrrole films for improved amperometric biosensing of sulfite, *Electroanalysis* Vol. 20, p. 2549, 2008.
149. Q. Ameer and S.B. Adeloju, Development of a potentiometric catechol biosensor by entrapment of tyrosinase within polypyrrole film, *Sens. Actuat. B* Vol. 140, p. 5, 2009.
150. A. Cernat, A.L. Goff, M. Holzinger, R. Sandulescu, and S. Cosnier, Micro- to nanostructured poly(pyrrole-nitrilotriacetic acid) films via nanosphere templates: applications to 3D enzyme attachment by affinity interactions, *Anal. Bioanal. Chem.* Vol. 406, p. 1141, 2014.
151. Rajesh, V. Bisht, W. Takashima, and K. Kaneto, An amperometric urea biosensor based on covalent immobilization of urease onto an electrochemically prepared copolymer poly (N-3-aminopropyl pyrrole-co-pyrrole) film, *Biomaterials* Vol. 26, p. 3683, 2005.
152. T. Ahuja, I.A. Mir, and D. Kumar, Potentiometric urea biosensor based on BSA embedded surface modified polypyrrole film, *Sens. Actuat. B* Vol. 134, p. 140, 2008.
153. H. Chu, X. Wei, M. Wu, J. Yan, and Y. Tu, An electrochemiluminescent biosensor based on polypyrrole immobilized uricase for ultrasensitive uric acid detection, *Sens. Actuat. B* Vol. 163, p. 247, 2012.
154. G. Istamboulie, T. Sikora, E. Jubete, E. Ochoteco, J.-L. Marty, and T. Noguer, Screen-printed poly(3,4-ethylenedioxythiophene) (PEDOT): A new electrochemical mediator for acetylcholinesterase-based biosensors, *Talanta* Vol. 82, p. 957, 2010.
155. M. Liu, Y. Wen, D. Li, H. He, J. Xu, C. Liu, R. Yue, B. Lu, and G. Liu, Electrochemical immobilization of ascorbate oxidase in poly(3,4-ethylenedioxythiophene)/multiwalled carbon nanotubes composite films, *J. Appl. Polym. Sci.* Vol. 122, p. 1142, 2011.
156. Md.A. Rahman, K.-S. Lee, D.-S. Park, M.-S. Won, and Y.-B. Shim, An amperometric bilirubin biosensor based on a conductive poly-terthiophene–Mn(II) complex, *Biosens. Bioelectron*. Vol. 23, p. 857, 2008.
157. M. Liu, Y. Wen, D. Li, R. Yue, J. Xu, and H. He, A stable sandwich-type amperometric biosensor based on poly(3,4-ethylenedioxythiophene)-single walled carbon nanotubes/ascorbate oxidase/nafion films for detection of L-ascorbic acid, *Sens. Actuat. B* Vol. 159, p. 277, 2011.
158. X. Xiao, M. Wang, H. Li, and P. Si, One-step fabrication of bio-functionalized nanoporous gold/poly(3,4-ethylenedioxythiophene) hybrid electrodes for amperometric glucose sensing, *Talanta* Vol. 116, p. 1054, 2013.

159. H.B. Yildiz, D.O. Demirkol, S. Sayin, M. Yilmaz, O. Koysuren, and M. Kamaci, New amperometric cholesterol biosensors using poly(ethyleneoxide) conducting polymers, *J. Macromol. Sci. A* Vol. 50, p. 1075, 2013.
160. P.-C. Nien, P.-Y. Chen, and K.-C. Ho, Fabricating an amperometric cholesterol biosensor by a covalent linkage between poly(3-thiopheneacetic acid) and cholesterol oxidase, *Sensors* Vol. 9, p. 1794, 2009.
161. Md.A. Rahman, D.-S. Park, and Y.-B. Shim, A performance comparison of choline biosensors: anodic or cathodic detections of H_2O_2 generated by enzyme immobilized on a conducting polymer, *Biosens. Bioelectron*. Vol. 19, p. 1565, 2004.
162. . Md.A. Rahman, N.-H. Kwon, M.-S. Won, E.S. Choe, and Y.-B. Shim, Functionalized conducting polymer as an enzyme-immobilizing substrate: An amperometric glutamate microbiosensor for in vivo measurements, *Anal. Chem.* Vol. 77, p. 4854, 2005.
163. T. Kuwahara, T. Asano, M. Kondo, and M. Shimomura, Bioelectrocatalytic O_2 reduction with a laccase-bearing poly(3-methylthiophene) film based on direct electron transfer from the polymer to laccase, *Bioelectrochemistry* Vol. 91, p. 28, 2013.
164. L. Agüí, M. Eguílaz, C. Peña-Farfal, P. Yáñez-Sedeño, and J.M. Pingarrón, Lactate dehydrogenase biosensor based on an hybrid carbon nanotube-conducting polymer modified electrode, *Electroanalysis* Vol. 21, p. 386, 2009.
165. C. Védrine, S. Fabiano, and C. Tran-Minh, Amperometric tyrosinase based biosensor using an electrogenerated polythiophene film as an entrapment support, *Talanta* Vol. 59, p. 535, 2003.
166. N. C. Foulds and C. R. Lowe, Immobilization of glucose oxidase in ferrocene-modified pyrrole polymers, *Anal. Chem.* Vol. 60, p. 2473, 1988.
167. J. Baur, M. Holzinger, C. Gondran, and S. Cosnier, Immobilization of biotinylated biomolecules onto electropolymerized poly(pyrrole-nitrilotriacetic acid)-Cu^{2+} film, *Electrochem. Commun*. Vol. 12, p. 1287, 2010.
168. L.-M.T. Rodrigez, M. Billon, A. Roget, and G. Bidan, Electrosynthesis of a biotinylated polypyrrole film and study of the avidin recognition by QCM, *J. Electroanal. Chem*. Vol. 523, p. 70, 2002.
169. P. Asberg and O. Inganäs, Hydrogels of a conducting conjugated polymer as 3-D enzyme electrode, *Biosens. Bioelectron*. Vol. 19, p. 199, 2003.
170. A.R. Gonçalves, M.E. Ghica, and C.M.A. Brett, Preparation and characterisation of poly(3,4-ethylenedioxythiophene) and poly(3,4-ethylenedioxythiophene)/poly(neutral red) modified carbon film electrodes, and application as sensors for hydrogen peroxide, *Electrochim. Acta* Vol. 56, p. 3685, 2011.
171. D. Dicu, L. Muresan, I.C. Popescu, C. Cristea, I.A. Silberg, and P. Brouant, Modified electrodes with new phenothiazine derivatives for electrocatyltic oxidation of NADH, *Electrochim. Acta* Vol. 45, p. 3951, 2000.
172. B. Prieto-Simón, J. Macanás, M. Muñoz, and E. Fàbregas, Evaluation of different mediator-modified screen-printed electrodes used in a flow system as amperometric sensors for NADH, *Talanta* Vol. 71, p. 2102, 2007.

173. C.A. Borgo, A.M. Lazarin, and Y. Gushikem, Methylene blue–zirconium phosphate-cellulose acetate hybrid membrane film attached to a platinum electrode and its application in electrocatalytic oxidation of NADH, *Sens. Actuat. B* Vol. 87, p. 498, 2002.
174. C.M. Maroneze, L.T. Arenas, R.C.S. Luz, E.V. Benvenutti, R. Landers, and Y. Gushikem, Meldola blue immobilized on a new $SiO_2/_{TiO2}$/graphite composite for electrocatalytic oxidation of NADH, *Electrochim. Acta* Vol. 53, p. 4167, 2008.
175. M.M. Barsan, E.M. Pinto, and C.M.A. Brett, Electrosynthesis and electrochemical characterisation of phenazine polymers for application in biosensors, *Electrochim. Acta* Vol. 53, 3973, 2008.
176. Z. Li, Y. Huang, L. Chen, X. Qin, Z. Huang, Y. Zhou, Y. Meng, J. Li, S. Huang, Y. Liu, W. Wang, Q. Xie, and S. Yao, Amperometric biosensor for NADH and ethanol based on electroreduced graphene oxide-polythionine nanocomposite film, *Sens. Actuat. B* Vol. 181, p. 280, 2013.
177. X. Xiao, B. Zhou, L. Zhu, L. Xu, L. Tan, H. Tang, Y. Zhang, Q. Xie, and S. Yao, An reagentless glucose biosensor based on direct electrochemistry of glucose oxidase immobilized on poly(methylene blue) doped silica nanocomposites, *Sens. Actuat. B* Vol. 165, p. 126, 2012.
178. D. Zhang, K. Zhang, Y.L. Yao, X.H. Xia, and H.Y. Chen, Multilayer assembly of Prussian blue nanoclusters and enzyme-immobilized poly(toluidine blue) films and its application in glucose biosensor construction, *Langmuir* Vol. 20, p. 7303, 2004.
179. W. Wang, F. Wang, Y. Yao, S. Hu, and K.-K. Shiu, Amperometric bienzyme glucose biosensor based on carbon nanotube modified electrode with electropolymerized poly(toluidine blue O) film, *Electrochim. Acta* Vol. 55, p. 7055, 2009.
180. L.-M. Lu, S.-P. Wang, F.-L. Qu, X.-B. Zhang, S. Huan, G.-L. Shen, and R.-Q. Yu, Synthesis and characterization of poly(toluidine blue) nanowires and their application in amperometric biosensors, *Electroanalysis* Vol. 21, p. 1152, 2009.
181. E. Al-Jawadi, S. Pöller, R. Haddad, and W. Schuhmann, NADH oxidation using modified electrodes based on lactate and glucose dehydrogenase entrapped between an electrocatalyst film and redox catalyst-modified polymers, *Microchim. Acta* Vol. 177, p. 405, 2012.
182. C.W.N. Villarrubia, R.A. Rincón, V.K. Radhakrishnan, V. Davis, and P. Atanassov, Methylene green electrodeposited on SWNTs-based "bucky" papers for NADH and l-malate oxidation, *ACS Appl. Mater. Interfaces* Vol. 3, p. 2402, 2011.
183. Z. Wang, M. Etienne, V. Urbanova, G.-W. Kohring, and A. Walcarius, Reagentless d-sorbitol biosensor based on d-sorbitol dehydrogenase immobilized in a sol-gel carbon nanotubes-poly(methylene green) composite, *Anal. Bioanal. Chem.* Vol. 405, p. 3899, 2013.

184. E. Dempsey, D. Diamond, and A. Collier, Development of a biosensor for endocrine disrupting compounds based on tyrosinase entrapped within a poly(thionine) film, *Biosens. Bioelectron*. Vol. 20, p. 367, 2004.
185. M.E. Ghica, R. Pauliukaite, N. Marchand, E. Devic, and C.M.A. Brett, An improved biosensor for acetaldehyde determination using a bienzymatic strategy at poly(neutral red) modified carbon film electrodes, *Anal. Chim. Acta* Vol. 591, p. 80, 2007.
186. D.-W. Yang and H.-H. Liu, Poly(brilliant Cresyl blue)-carbonnanotube modified electrodes for determination of NADH and fabrication of ethanol dehydrogenase-based biosensor, *Biosens. Bioelectron*. Vol. 25, p. 733, 2009.
187. P. Du, S. Liu, P. Wu, and C. Cai, Single-walled carbon nanotubes functionalized with poly(nile blue A) and their application to dehydrogenase-based biosensors, *Electrochim. Acta* Vol. 53, p. 1811, 2007.
188. S. Soylemez, F. E. Kanik, S. Tarkuc, Y. A. Udum, and L. Toppare, A sepiolite modified conducting polymer based biosensor, *Colloids Surf. B* Vol. 111, p. 549, 2013.
189. A. C. Torres, M. E. Ghica, and C. M. A. Brett, Poly(neutral red)/cholesterol oxidase modified carbon film electrode for cholesterol biosensing, *Electroanalysis* Vol. 24, p. 1547, 2012.
190. P. Du, P. Wu, and C. Cai, A glucose biosensor based on electrocatalytic oxidation of NADPH at single-walled carbon nanotubes functionalized with poly(nile blue A), *J. Electroanal. Chem*. Vol. 624, p. 21, 2008.
191. M. E. Ghica and C. M. A. Brett, Development of novel glucose and pyruvate biosensors at poly(neutral red) modified carbon film electrodes. Application to natural samples, *Electroanalysis* Vol. 18, p. 748, 2006.
192. R. Pauliukaite, M. E. Ghica, M. Barsan, and C. M. A. Brett, Characterisation of poly(neutral red) modified carbon film electrodes; application as a redox mediator for biosensors, *J. Solid State Electrochem.* Vol. 11, p. 899, 2007.
193. M. E. Ghica and C. M. A. Brett, Glucose oxidase inhibition in poly(neutral red) mediated enzyme biosensors for heavy metal determination, *Microchim. Acta* Vol. 163, p. 185, 2008.
194. Y. Zhang, R. Yuan, Y. Chai, Y. Xiang, C. Hong, and X. Ran, An amperometric hydrogen peroxide biosensor based on the immobilization of HRP on multiwalled carbon nanotubes/electro-copolymerized nano-Pt-poly(neutral red) composite membrane, *Biochem. Eng. J.* Vol. 51, p. 102, 2010.
195. A. Attar, M. E. Ghica, A. Amine, and C. M.A. Brett, Poly(neutral red) based hydrogen peroxide biosensor for chromium determination by inhibition measurements, *J. Hazardous Mater.* Vol. 279, p. 348, 2014.
196. C. Deng, M. Li, Q. Xie, M. Liu, Y. Tan, X. Xu, and S. Yao, New glucose biosensor based on a poly(o-phenylendiamine)/glucose oxidase-glutaraldehyde/Prussian blue/Au electrode with QCM monitoring of various electrode-surface modifications, *Anal. Chim. Acta* Vol. 557, p. 85, 2006.

197. S. Yabukia and F. Mizutani, Preparation of amperometric glucose sensor based on electrochemically polymerized films of indole derivatives, *Sens. Actuat. B* Vol. 108, p. 651, 2005.
198. M.E. Ghica and C.M.A. Brett, The influence of carbon nanotubes and polyazine redox mediators on the performance of amperometric enzyme biosensors, *Microchim. Acta* Vol. 170, p. 257, 2010.
199. M. E. Ghica and C.M.A. Brett, Poly(brilliant Cresyl blue) modified glassy carbon electrodes: Electrosynthesis, characterisation and application in biosensors, *J. Electroanal. Chem.* Vol. 629, p. 35, 2009.
200. B. Pałys, M. Marzec, and J. Rogalski, Poly-o-aminophenol as a laccase mediator and influence of the enzyme on the polymer electrodeposition, *Bioelectrochemistry* Vol. 80, p. 43, 2010.
201. J. Haccoun, B. Piro, V. Noël, and M.C. Pham, The development of a reagentless lactate biosensor based on a novel conducting polymer, *Bioelectrochemistry* Vol. 68, p. 218, 2006.
202. D. Chirizzi and C. Malitesta, Potentiometric urea biosensor based on urease immobilized by an electrosynthesized poly(o-phenylenediamine) film with buffering capability, *Sens. Actuat. B* Vol. 157, p. 211, 2011.
203. X. Xiao, B. Zhou, L. Zhu, L. Xu, L. Tan, H. Tang, Y. Zhang, Q. Xie, and S. Yao, An reagentless glucose biosensor based on direct electrochemistry of glucose oxidase immobilized on poly(methylene blue) doped silica nanocomposites, *Sens. Actuat. B* Vol. 165, p. 126, 2012.
204. M. F. Dautartas, E. F. Bowde and J. F. Evans, Chemical and mechanical properties of redox polymer-modified electrodes: Part II. Redox thermodynamics of plasma-polymerized vinylferrocene electrodes, *J. Electroanal. Chem*. Vol. 219, p. 71, 1987.
205. B. Šljukić, C.E. Banks, C. Salter, A. Crossley, and R.G. Compton, Electrochemically polymerised composites of multi-walled carbon nanotubes and poly(vinylferrocene) and their use as modified electrodes: Application to glucose sensing, *Analyst* Vol. 131, p. 670, 2006.
206. C.X. Li, Y.L. Zeng, and C.R. Tang, Glucose biosensor based on carbon/PVC-COOH/ferrocene composite with covalently immobilized enzyme, *Chinese Chem. Lett*. Vol. 16, p. 1357, 2005.
207. P.Ó. Conghaile, S. Pöller, D.M. Aodha, W. Schuhmann, and D. Leech, Coupling osmium complexes to epoxy-functionalised polymers to provide mediated enzyme electrodes for glucose oxidation, *Biosens. Bioelectron.* Vol. 43, p. 30, 2013.
208. C.H. Yoon, M.-Y. Hong, and H.-S. Kim, Functionalization of a poly(amidoamine) dendrimer with ferrocenyls and its application to the construction of a reagentless enzyme electrode, *Anal. Chem*. Vol. 72, p. 4420, 2000.
209. M. Karadag, C. Geyik, D.O. Demirkol, F.N. Ertas, and S. Timur, Modified gold surfaces by 6-(ferrocenyl)hexanethiol/dendrimer/gold nanoparticles as

a platform for the mediated biosensing applications, *Mater. Sci. Eng. C* Vol. 33, p. 634, 2013.
210. M. Şenel, C. Nergiz, and E. Çevik, Novel reagentless glucose biosensor based on ferrocene cored asymmetric PAMAM dendrimers, *Sens. Actuat. B* Vol. 176, p. 299, 2013.
211. W. Chen, Y. Ding, J. Akhigbe, C. Brückner, C. Li, and Y. Lei, Enhanced electrochemical oxygen reduction-based glucose sensing using glucose oxidase on nanodendritic poly[meso-tetrakis(2-thienyl)porphyrinato]cobalt(II)-SWNTs composite electrodes, *Biosens. Bioelectron*. Vol. 26, p. 504, 2010.
212. M. Frasconi, D. Deriu, A. Dannibale, and F. Mazzei, Nanostructured materials based on the integration of ferrocenyl-tethered dendrimer and redox proteins on self-assembled monolayers: an efficient biosensor interface, *Nanotechnology* Vol. 20, p. 505501, 2009.
213. B. Alonso, P.G. Armada, J. Losada, I. Cuadrado, B. González, and C.M. Casado, Amperometric enzyme electrodes for aerobic and anaerobic glucose monitoring prepared by glucose oxidase immobilized in mixed ferrocene–cobaltocenium dendrimers, *Biosens. Bioelectron*. Vol. 19, p. 1617, 2004.
214. N. Backmann, C. Zahnd, F. Huber, A. Bietsch, A. Plückthun, H.-P.Lang, H.-J. Güntherodt, M. Hegner, and C. Gerber, A label-free immunosensor array using single-chain antibody fragments, *PNAS* Vol. 102, p. 14587, 2005.
215. S. Muyldermans, T.N. Baral, V.Cortez Retamozzo, P.De Baetselier, E. De Genst, J. Kinne, H. Leonhardt, S. Magez, V.K. Nguyen, H. Revets, U. Rothbauer, B. Stijlemans, S. Tillib, U. Wernery, L. Wyns, Gh. Hassanzadeh-Ghassabeh, and D. Saerens, Camelid immunoglobulins and nanobody technology, *Veter. Immun. Immunopath*. Vol. 128, p. 178, 2009.
216. M. Lin, Y. Liu, Z. Sun, S. Zhang, Z. Yang, and C. Ni, Electrochemical immunoassay of benzo[a]pyrene based on dual amplification strategy of electron-accelerated Fe_3O_4/polyaniline platform and multi-enzyme-functionalized carbon sphere label, *Anal. Chim. Acta* Vol. 722, p. 100, 2012.
217. A.D. Chowdhury, A. De, C.R. Chaudhuri, K. Bandyopadhyay, and P. Sen, Label free polyaniline based impedimetric biosensor for detection of *E. coli* O157:H7 Bacteria, *Sens. Actuat. B* Vol. 171-172, p. 916, 2012.
218. S.K. Arya, A. Dey, and S. Bhansali, Polyaniline protected gold nanoparticles based mediator and label free electrochemical cortisol biosensor, *Biosens. Bioelectron*. Vol. 28, p. 166, 2011.
219. J. Li, S. Liu, J. Yu, W. Lian, M. Cui, W. Xu, and J. Huang, Electrochemical immunosensor based on graphene–polyaniline composites and carboxylated graphene oxide for estradiol detection, *Sens. Actuat. B* Vol. 188, p. 99, 2013.
220. L. Li, W. Li, H. Yang, C. Ma, J. Yu, M. Yan, and X. Song, Sensitive origami dual-analyte electrochemical immunodevice based on polyaniline/Au-paper electrode and multi-labeled 3D graphene sheets, *Electrochim. Acta* Vol. 120, p. 102, 2014.

221. R.L. Caygill, C.S. Hodges, J.L. Holmes, S.P.J. Higson, G.E. Blair, and P.A. Millner, Novel impedimetric immunosensor for the detection and quantitation of Adenovirus using reduced antibody fragments immobilized onto a conducting copolymer surface, *Biosens. Bioelectron*. Vol. 32, p. 104, 2012.
222. R. Yuan, L. Zhang, Q. Li, Y. Chai, and S. Cao, A label-free amperometric immunosenor based on multi-layer assembly of polymerized o-phenylenediamine and gold nanoparticles for determination of Japanese B encephalitis vaccine, *Anal. Chim. Acta* Vol. 531, p. 1, 2005.
223. H. Chen, Y. Cui, B. Zhang, B. Liu, G. Chen, and D. Tang, Poly(o-phenylenediamine)-carried nanogold particles as signal tags for sensitive electrochemical immunoassay of prolactin, *Anal. Chim. Acta* Vol. 728, p. 18, 2012.
224. Z. Taleat, A. Ravalli, M. Mazloum-Ardakani, and G. Marrazza, CA 125 immunosensor based on poly-anthranilic acid modified screen-printed electrodes, *Electroanalysis* Vol. 25, p. 269, 2013.
225. M. Mazloum-Ardakani, L. Hosseinzadeh, and Z. Taleat, Two kinds of electrochemical immunoassays for the tumor necrosis factor α in human serum using screen-printed graphite electrodes modified with poly(anthranilic acid), *Microchim. Acta* Vol. 181, p. 917, 2014.
226. J.H.O. Owino, O.A. Arotiba, N. Hendricks, E.A. Songa, N. Jahed, T.T. Waryo, R.F. Ngece, P.G .L. Baker, and E.I. Iwuoha, Electrochemical immunosensor based on polythionine/gold nanoparticles for the determination of aflatoxin B1, *Sensors* Vol. 8, p. 8262, 2008.
227. A. Ramanavicius, A. Finkelsteinas, H. Cesiulis, and A. Ramanaviciene, Electrochemical impedance spectroscopy of polypyrrole based electrochemical immunosensor, *Bioelectrochemistry* Vol. 79, p. 11, 2010.
228. S. Zang, Y. Liu, M. Lin, J. Kang, Y. Sun, and H. Lei, A dual amplified electrochemical immunosensor for ofloxacin: Polypyrrole film-Au nanocluster as the matrix and multi-enzyme-antibody functionalized gold nanorod as the label, *Electrochim. Acta* Vol. 90, p. 246, 2013.
229. J.-M. Moon,Y.H. Kim, and Y. Cho, A nanowire-based label-free immunosensor: Direct incorporation of a PSA antibody in electropolymerized polypyrrole, *Biosens. Bioelectron*. Vol. 57, p. 157, 2014.
230. H. Dong, C.M. Li, W. Chen, Q. Zhou, Z.X. Zeng, and J.H.T. Luong, Sensitive amperometric immunosensing using polypyrrolepropylic acid films for biomolecule immobilization, *Anal. Chem*. Vol. 78, p. 7424, 2006.
231. Y. Hu, Z. Zhao, and Q. Wan, Facile preparation of carbon nanotube-conducting polymer network for sensitive electrochemical immunoassay of Hepatitis B surface antigen in serum, *Bioelectrochemistry* Vol. 81, p. 59, 2011.
232. V. Serafín, L. Agüí, P. Yáñez-Sedeño, and J.M. Pingarrón, Electrochemical immunosensor for the determination of insulin-like growth factor-1 using electrodes modified with carbon nanotubes–poly(pyrrole propionic acid) hybrids, *Biosens. Bioelectron*. Vol. 52, p. 98, 2014.

233. V. Serafín, L. Agüí, P. Yáñez-Sedeño, and J.M. Pingarrón, Termination of prolactin hormone in serum and urine using an electrochemical immunosensor based on poly(pyrrolepropionic acid)/carbon nanotubes hybrid modified electrodes, *Sens. Actuat. B* Vol. 195, p. 494, 2014.
234. I. Hafaid, S. Chebil, H. Korri-Youssoufi, F. Bessueille, A. Errachid, Z. Sassi, Z. Ali, A. Abdelghani, and N. Jaffrezic-Renault, Effect of electrical conditions on an impedimetric immunosensor based on a modified conducting polypyrrole, *Sens. Actuat. B* Vol. 144, p. 323, 2010.
235. R.E. Ionescu, S. Cosnier, G. Herzog, K. Gorgy, B. Leshem, S. Herrmann, and R.S. Marks, Amperometric immunosensor for the detection of anti-West Nile virus IgG using a photoactive copolymer, *Enzyme Microb.Technol.* Vol. 40, p. 403, 2007.
236. H.Q.A. Lê, H. Sauriat-Dorizon, and H. Korri-Youssoufi, Investigation of SPR and electrochemical detection of antigen with polypyrrole functionalized by biotinylated single-chain antibody: A review, *Anal. Chim. Acta* Vol. 674, p. 1, 2010.
237. K. Singh, Md.A. Rahman, J.I. Son, K.C. Kim, and Y.-B. Shim, An amperometric immunosensor for osteoproteogerin based on gold nanoparticles deposited conducting polymer, *Biosens. Bioelectron*. Vol. 23, p. 1595, 2008.
238. Md. A. Rahman, J.I. Son, M.-S. Won, and Y.-B. Shim, Gold nanoparticles doped conducting polymer nanorod electrodes: ferrocene catalyzed aptamer-based thrombin immunosensor, *Anal. Chem*. Vol. 81, p. 6604, 2009.
239. Y. Gao and R. Cranston, Polytyrosine as an electroactive label for signal amplification in electrochemical immunosensors, *Anal. Chim. Acta* Vol. 659, p. 109, 2010.
240. H.-P. Peng, Y. Hu, A.-L. Liu, W. Chen, X.-H. Lin, and X.-B. Yu, Label-free electrochemical immunosensor based on multi-functional gold nanoparticles–polydopamine–thionine–graphene oxide nanocomposites film for determination of alpha-fetoprotein, *J. Electroanal. Chem*. Vol. 712, p. 89, 2014.
241. M. Lin, Y. Liu, X. Chen, S. Fei, C. Ni, Y. Fang, C. Liu, and Q. Cai, Poly(dopamine) coated gold nanocluster functionalized electrochemical immunosensor for brominated flame retardants using multienzyme-labeling carbon hollow nanochains as signal amplifiers, *Biosens. Bioelectron*. Vol. 45, p. 82, 2013.
242. Z. Sun, Z. Luo, C. Gan, S. Fei, Y. Liu, and H. Lei, Electrochemical immunosensor based on hydrophilic polydopamine-coated prussian blue-mesoporous carbon for the rapid screening of 3-bromobiphenyl, *Biosens. Bioelectron*. Vol. 59, p. 99, 2014.
243. S.J. Kwon, E. Kim, H. Yang, and J. Kwak, An electrochemical immunosensor using ferrocenyl-tethered dendrimer, *Analyst* Vol. 131, p. 402, 2006.
244. D.-M. Kim, H.-B. Noh, D.S. Park, S.H. Ryu, J.S. Koo, and Y.-B. Shim, Immunosensors for detection of Annexin II and MUC5AC for early diagnosis of lung cancer, *Biosens. Bioelectron*. Vol. 25, p. 456, 2009.

245. J. Wu, Y. Zou, X. Li, H. Liu, G .Shen, R. Yu, Y .Bo, H. Yang, Y. Hu, T. Yao, and S. Huang, A novel electrochemical DNA biosensor based on graphene and polyaniline nanowires, *Electrochim. Acta* Vol. 56, p. 2676, 2011.
246. A. Tiwari and S. Gong, Electrochemical detection of a breast cancer susceptible gene using cDNA immobilized chitosan-co-polyaniline electrode, *Talanta* Vol. 77, p. 1217, 2009.
247. N. Prabhakar, K. Arora, H. Singh, and B.D. Malhotra, Polyaniline based nucleic acid sensor, *J. Phys. Chem. B* Vol. 112, p. 4808, 2008.
248. N. Zhu, Z. Chang, P. He, and Y. Fang, Electrochemically fabricated polyaniline nanowire-modified electrode for voltammetric detection of DNA hybridization, *Electrochim. Acta* Vol. 51, p. 3758, 2006.
249. R. Singh, R. Prasad, G. Sumana, K. Arora, S. Sood, R.K. Gupta, and B.D. Malhotra, STD sensor based on nucleic acid functionalized nanostructured polyaniline, *Biosens. Bioelectron*. Vol. 24, p. 2232, 2009.
250. R. Singh, R. Verma, G. Sumana, A.K. Srivastava, S. Sood, R.K. Gupta, and B.D. Malhotra, Nanobiocomposite platform based on polyaniline-iron oxide-carbon nanotubes for bacterial detection, *Bioelectrochemistry* Vol. 86, p. 30, 2012.
251. R. Singh,C. Dhand,G. Sumana, R. Prasad, S. Sood, R.K. Gupta, and B.D. Malhotra, Polyaniline/carbon nanotubes platform for sexually transmitted disease detection, *J. Mol. Recognit.* Vol. 23, p. 472, 2010.
252. J. Yang, X. Wang, and H. Shi, An electrochemical DNA biosensor for highly sensitive detection of phosphinothricin acetyltransferase gene sequence based on polyaniline-(mesoporous nanozirconia)/poly-tyrosine film, *Sens. Actuat. B* Vol. 162, p. 178, 2012.
253. M. Du, T. Yang, X. Li, and K. Jiao, Fabrication of DNA/graphene/polyaniline nanocomplex for label-free voltammetric detection of DNA hybridization, *Talanta* Vol. 88, p. 439, 2012.
254. R.-S. Saberi, S. Shahrokhian, and G. Marrazza, Amplified electrochemical DNA sensor based on polyaniline film and gold nanoparticles, *Electroanalysis* Vol. 25, p. 1373, 2013.
255. Y. Hao, B. Zhou, F. Wang, J. Li, L. Deng, and Y.-N. Liu, Construction of highly ordered polyaniline nanowires and their applications in DNA sensing, *Biosens. Bioelectron*. Vol. 52, p. 422, 2014.
256. T. Šmuc, I.-Y. Ahn, and H. Ulrich, Nucleic acid aptamers as high affinity ligands in biotechnology and biosensorics, *J. Pharm. Biomed. Anal.* Vol. 81-82, p. 210, 2013.
257. T. Hianik and J. Wang, Electrochemical aptasensors – recent achievements and perspectives, *Electroanalysis* Vol. 21, p. 1223, 2009.
258. X. Luo, I. Lee, J. Huang, M. Yun, and X.T. Cui, Ultrasensitive protein detection using an aptamer-functionalized single polyaniline nanowire, *Chem. Commun.* Vol. 47, p. 6368, 2011.

259. J. Van Ness, S. Kalbfleisch, C.R. Petrie, M.W. Reed, J.C. Tabone, and N.M.J. Vermeulen, A versatile solid support system for oligodeoxynucleotide probe-based hybridization assays, *Nucleic Acids Res.* Vol. 19, p. 3345, 1991.
260. F. Garnier, H. Korri-Yousouffi, P. Srivastava, B. Mandrand, and T. Delair, Toward intelligent polymers: DNA sensors based on oligonucleotide-functionalized polypyrroles, *Synth. Metals.* Vol. 100, p. 89, 1999.
261. R.E. Ionescu, S. Herrmann, S. Cosnier, and R.S. Marks, A polypyrrole cDNA electrode for the amperometric detection of the West Nile Virus, *Electrochem. Commun*. Vol. 8, p. 1741, 2006.
262. J. Travas-Sejdic, H. Peng, P.A. Kilmartin, M.B. Cannell, G.A. Bowmaker, R.P. Cooney, and C. Soeller, DNA sensor based on functionalized polypyrrole, *Synth. Metals* Vol. 152, p. 37, 2005.
263. S. Cosnier, R.E. Ionescu, S. Herrmann, L. Bouffier, M. Demeunynck, and R.S. Marks, Electroenzymatic polypyrrole-intercalator sensor for the determination of west Nile virus cDNA, *Anal. Chem.* Vol. 78, p. 7054, 2006.
264. Y. Xu, X. Ye, L. Yang, P. He, and Y. Fang, Impedance DNA biosensor using electropolymerized polypyrrole/multiwalled carbon nanotubes modified electrode, *Electroanalysis* Vol. 18, p. 1471, 2006.
265. L.M. Torrez-Rodriguez, M. Billon, A. Roget, and G. Bidan, A polypyrrole-biotin based biosensor: elaboration and characterization, *Synth. Metals* Vol. 102, p. 1328, 1999.
266. A. Dupont-Filliard, M. Billon, T. Livache, and S. Guillerez, Biotin/avidin system for the generation of fully renewable DNA sensor based on biotinylated polypyrrole film, *Anal. Chim. Acta* Vol. 515, p. 271, 2004.
267. N. Lasalle, E. Vieil, J.P. Correia, and L.M. Abrantes, Study of DNA hybridization on polypyrrole grafted with oligonucleotides by photocurrent spectroscopy, *Biosens. Bioelectron*. Vol. 16, p. 295, 2001.
268. T. Livache, P. Guedon, G. Brakha, A. Roget, Y. Levi, and G. Bidan, Polypyrrole electrospotting for the construction of oligonucleotide arrays compatible with a surface plasmon resonance hybridization detection, *Synth. Metals* Vol. 121, p. 1443, 2001.
269. J. Baur, M. Holzinger, C. Gondran, and S. Cosnier, Immobilization of biotinylated biomolecules onto electropolymerized poly(pyrrole-nitrilotriacetic acid)-Cu^{2+} film, *Electrochem. Commun*. Vol. 12, p. 1287, 2010.
270. H. Qi, X. Li, P. Chen, and C. Zhang, Electrochemical detection of DNA hybridization based on polypyrrole/ss-DNA/multi-wall carbon nanotubes paste electrode, *Talanta* Vol. 72, p. 1030, 2007.
271. C.S. Riccardi, H. Yamanaka, M. Josowicz, J. Kowalik, B. Mizaikoff, and C. Kranz, Label-free DNA detection based on modified conducting polypyrrole films at microelectrodes, *Anal. Chem*. Vol. 78, p. 1139, 2006.
272. C.S. Riccardi, C. Kranz, J. Kowalik, H. Yamanaka, B. Mizaikoff, and M. Josowicz, Label-free DNA detection of hepatitis C virus based on modified conducting polypyrrole films at microelectrodes and atomic force microscopy tip-integrated electrodes, *Anal. Chem*. Vol. 80, p. 237, 2008.

273. P. D. Tam, M.A. Tuan, T.Q. Huy, A.-T. Le, and N.V. Hieu, Facile preparation of a DNA sensor for rapid herpes virus detection, *Mater. Sci. Eng. C* Vol. 30, 1145, 2010.
274. H.Q.A. Lê, S. Chebil, B. Makrouf, H. Sauriat-Dorizon, B. Mandrand, and H. Korri-Youssoufi, Effect of the size of electrode on electrochemical properties of ferrocene-functionalized polypyrrole towards DNA sensing, *Talanta* Vol. 81, p. 1250, 2010.
275. T.T.N. Lien, T.D. Lam, V.T.H. An, T.V. Hoang, D.T. Quang, D.Q. Khieu, T. Tsukahara, Y.H. Lee, and J.S. Kim, Multi-wall carbon nanotubes (MWCNTs)-doped polypyrrole DNA biosensor for label-free detection of genetically modified organisms by QCM and EIS, *Talanta* Vol. 80, p. 1164, 2010.
276. V. Ratautaite, S.N. Topkay, L. Mikoliunaite, M. Ozsoz, Y. Oztekin, A. Ramanaviciene, and A. Ramanavicius, Molecularly imprinted polypyrrole for DNA determination, *Electroanalysis* Vol. 25, p. 1169, 2013.
277. J. Wilson, S. Radhakrishnan, C. Sumathi, and V. Dharuman, Polypyrrole-polyaniline-Au (PPy-PANi-Au) nano composite films for label-free electrochemical DNA sensing, *Sens. Actuat. B* Vol. 171–172, p. 216, 2012.
278. H. Xu, K. Gorgy, C. Gondran, A. Le Goff, N. Spinelli, C. Lopez, E. Defrancq, and S. Cosnier, Label-free impedimetric thrombin sensor based on poly(pyrrole-nitrilotriacetic acid)-aptamer film, *Biosens. Bioelectron*. Vol. 41, p. 90, 2013.
279. A. Miodek, G. Castillo, T. Hianik, and H. Korri-Youssoufi, Electrochemical aptasensor of cellular prion protein based on modified polypyrrole with redox dendrimers, *Biosens. Bioelectron*. Vol. 56, p. 104, 2014.
280. A. Miodek, A. Poturnayova, M. Snejdarkova, T. Hianik, and H. Korri-Youssoufi, Binding kinetics of human cellular prion detection by DNA aptamers immobilized on a conducting polypyrrole, *Anal. Bioanal. Chem.* Vol. 405, p. 2505, 2013.
281. A. Miodek, G. Castillo, T. Hianik, and H. Korri-Youssoufi, Electrochemical aptasensor of human cellular prion based on multiwalled Ccarbon nanotubes modified with dendrimers: A platform for connecting redox markers and aptamers, *Anal. Chem.* Vol. 85, p. 7704, 2014.
282. C. Cougnon, C. Gautier, J.-F. Pilard, N. Casse, and B. Chénais, Redox and ion-exchange properties in surface-tethered DNA-conducting polymers, *Biosens. Bioelectron*. Vol. 23, p. 1171, 2008.
283. H. Peng, L. Zhang, J. Spires, C. Soeller, and J. Travas-Sejdic, Synthesis of a functionalized polythiophene as an active substrate for a label-free electrochemical genosensor, *Polymer* Vol. 48, p. 3413, 2007.
284. S.K. Kang, J.-H. Kim, J. An, E.K. Lee, J. Cha, G. Lim, Y.S. Park, and D.J. Chung, Synthesis of polythiophene derivatives and their application for electrochemical DNA sensor, *Polymer J.* Vol. 36 p. 937, 2004.
285. M. Liu, C. Luo, and H. Peng, Electrochemical DNA sensor based on methylene blue functionalized polythiophene as a hybridization indicator, *Talanta* Vol. 88, p. 216, 2012.

286. Z.-W. Chen, A. Balamurugan, and S.-M. Chen, Detection of DNA by using bio-conducting polymer–Nile blue composite electrode; Nile blue as an indicator, *Bioelectrochemistry* Vol. 75, p. 13, 2009.
287. C. Dulgerbaki, A.U. Oksuz, and S. Ahmad, Electrochemically determined biosensing ability of DNA probed by using poly(propylenedioxythiophene), *Electrochim. Acta* Vol. 122, p. 87, 2014.
288. Y. Xu, Y. Jiang, L. Yang, P.-G. He, and Y.-Z .Fang, Direct electrochemical detection of oligonucleotide hybridization on poly(thionine) film, *Chin. J. Chem*. Vol. 23, p. 1665, 2005.
289. H. Liu, G. Wang, D. Chen, W. Zhang, C. Li, and B. Fang, Fabrication of polythionine/NPAu/MWNTs modified electrode for simultaneous determination of adenine and guanine in DNA, *Sens. Actuat. B* Vol. 128, p. 414, 2008.
290. G.A. Evtugyn, A.V. Porfireva, T. Hianik, M.S. Cheburova, and H.C. Budnikov, Potentiometric DNA sensor based on electropolymerized phenothiazines for protein detection, *Electroanalysis* Vol. 20, p. 1300, 2008.
291. A.V. Porfireva, G.A. Evtugyn, A.N. Ivanov, and T. Hianik, Impedimetric aptasensors based on carbon nanotubes – poly(methylene blue) composite, *Electroanalysis* Vol. 22, p. 2187, 2010.
292. R. Pauliukaite and C.M.A. Brett, Poly(neutral red): electrosynthesis, characterization, and application as a redox mediator, *Electroanalysis* Vol. 20, p. 1275, 2008.
293. L. Wang, X. Liao, Y. Ding, F. Gao, and Q. Wang, DNA biosensor based on a glassy carbon electrode modified with electropolymerized Eriochrome Black T, *Microchim. Acta* Vol. 181, p. 155, 2014.
294. M. Humenik, C. Pöhlmann, Y. Wang, and M. Sprinzl, Enhancement of electrochemical signal on gold electrodes by polyvalent esterase-dendrimer clusters, *Bioconjugate Chem.* Vol. 19, p. 2456, 2008.
295. J. Martinovic, J. Wyk, S. Mapolie, N. Jahed, P. Baker, and E. Iwuoha, Electrochemical and spectroscopic properties of dendritic cobalto-salicylaldiimine DNA biosensor, *Electrochim. Acta* Vol. 55, p. 4296, 2010.
296. N. Zhu, Y. Gu, Z. Chang, P. He, and Y. Fang, PAMAM dendrimers-based DNA biosensors for electrochemical detection of DNA hybridization, *Electroanalysis* Vol. 18, p. 2107, 2006.
297. G. Evtugyn, A. Porfireva, A. Ivanov, O. Konovalova, and T. Hianik, Molecularly imprinted polymerized Methylene green as a platform for electrochemical sensing of aptamer–thrombin interactions, *Electroanalysis* Vol. 21, p. 1272, 2009.
298. E. Stern, S. Jay, J. Bertram, B. Boese, I. Kretzschmar, D. Turner-Evans, C. Dietz, D.A. LaVan, T. Malinski, T. Fahmy, and M.A. Reed, Electropolymerization on microelectrodes: Functionalization technique for selective protein and DNA conjugation, *Anal. Chem.* Vol. 78, p. 6340, 2006.

Part 2

ADVANCED NANOSTRUCTURES IN BIOSENSING

5

Graphene-Based Electrochemical Platform for Biosensor Applications

Norazriena Yusoff*[1], Alagarsamy Pandikumar*[1], Huang Nay Ming*[1], and Lim Hong Ngee*[2,3]

[1]*Low Dimensional Materials Research Centre, Department of Physics, Faculty of Science, University of Malaya, Kuala Lumpur, Malaysia*
[2]*Department of Chemistry, Faculty of Science, Universiti Putra Malaysia, UPM Serdang, Selangor, Malaysia*
[3]*Functional Device Laboratory, Institute of Advanced Technology, Universiti Putra Malaysia, UPM Serdang, Selangor, Malaysia*

Abstract

Graphene, which is a single layer of carbon atoms organized in a closely packed honeycomb two-dimensional lattice, has attracted great attention since its discovery in 2004 because of its unique nanostructure and extraordinary physicochemical properties, such as high surface area, excellent conductivity, high mechanical strength, and ease of functionalization and mass production. Incorporation of metal and metal oxide into the graphene sheets significantly improves the aforesaid properties. This chapter selectively compiles the recent advances in graphene-based nanocomposite for electrochemical biosensors toward detection of biologically important molecules, such as glucose, nicotinamide adenine dinucleotide (NADH), nitric oxide (NO), and hydrogen peroxide (H_2O_2).

Keywords: Graphene, nanocomposites, electrochemical sensors, biosensors, biomolecules

5.1 Introduction

Biomolecules can be defined as an organic compound composed of two or more atoms bonded together that occurred naturally in living organisms.

**Corresponding authors*: norazrienasraf@gmail.com, pandikumarinbox@gmail.com, huangnayming@um.edu.my, janet_limhn@yahoo.com

Ashutosh Tiwari, Hirak K. Patra and Anthony P.F. Turner (eds.) Advanced Bioelectronic Materials, (189–214)

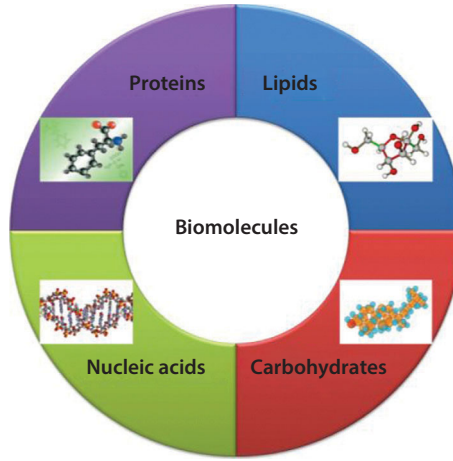

Figure 5.1 Four major classes of biomolecules.

Most of the biomolecules are made up from basic element of atom such as oxygen, hydrogen, carbon, and nitrogen that acts as chemical building blocks of living organisms. These fundamental elements can be combined in different ways which next determine the types of organic compound formed. Basically, biomolecules can be divided into four major classes that are proteins, nucleic acids, carbohydrates, and lipids (Figure 5.1). The most abundant molecules in the living organism are called protein. It composed of subunits called amino acids which formed from the element of carbon, hydrogen, nitrogen, and oxygen. These amino acids attached to each other in long chain to create unique three-dimensional structures which have its own function in the body. In general, proteins contribute to the structural and support for cells, defense the body from germs, and viruses and also involved in the transporting the chemical reaction happens in the cells. Hormones, antibodies, and enzymes are some of the examples of proteins. Other than protein, carbohydrate also has a significant impact in biological system because it is the key intermediates of metabolism which not only provide energy to the body but also help to transport and store the energy. Some examples of carbohydrate are glucose, sucrose, maltose, starch, and cellulose.

Major sources of energy for most cells of the body including brain are come from glucose which also known as blood sugar because it is a free sugar that circulates in blood. This energy is important and it helps the cells to execute nerve cell conduction, muscle cell contraction, and the production of chemical substances. Even though glucose is important biomolecule in human body, the level of glucose must be controlled because higher than

normal glucose levels may cause diabetes and lower than normal glucose levels may cause hypoglycemia and other effects. Other biomolecules that is important in living organism is nitric oxide (NO) which is a hydrophobic, highly labile-free radical that is naturally produced within the body. It plays a vital role in a wide range of biological and cellular functions. NO is used for communication between cells and is involved in the regulation of blood pressure, the immune response, platelet aggregation and clotting, neurotransmission, and possibly respiration [1, 2]. Abnormal NO production and bioavailability may cause several diseases such as obesity, diabetes (both types I and II), atherosclerosis, hypertension, and heart failure [3, 4]. Thus, the development of a sensor for the precise and selective measurement of NO at the low-level characteristic of living systems can make a great contribution to disease diagnosis.

Hydrogen peroxide (H_2O_2) and nicotinamide adenine dinucleotide (NADH) are other examples of biomolecules that bring beneficial to human body. Both biomolecules are by-product in a variety of enzymatic reactions. H_2O_2 which produced by a sub-class of white blood cells called neutrophils acts as a first line of defense against toxins, parasites, bacteria, viruses, and yeast. H_2O_2 also plays a role in the regulation of renal function and as an antibacterial agent in the urine [5]. In addition, high concentrations of H_2O_2 generated in blood plasma could give a negative effect on human health, and it also constitutes a pathogenic factor in vascular organ damage attendant upon systemic hypertension [6]. On the other hand, NADH is a natural chemical produced in the body and involved in the chemical process such as energy generation. NADH is a kind of coenzyme which enhances or is necessary for the action of all enzymes in the body. Besides that, it also helps to protect the liver from alcohol damage, enhances a person's memory and immune system. NADH also frequently used to treating high blood pressure and high cholesterol. NADH levels are crucial to monitored because it acts as a sensor that regulates the activity of certain genes and enzymatic reaction; therefore, the abnormal level of NADH may give a sign of failure certain activity to occurred and have numerous detrimental effects to the human body.

As mentioned, biomolecules are essential for life because it plays an important role in almost every aspect of organism, including as a source of energy and energy storage. Every living organism only required a certain level of biomolecules contents to ensure that every parts of the living system would operate at their optimum level. Therefore, the content of biomolecules in the living organism especially in human body should be monitored because it would bring an adverse effect on the body's systems such as metabolic disorder, thus cause of many diseases. Even though there

are many techniques reported can be used to detect biomolecules such as chemiluminescence [7], paramagnetic resonance spectrometry [8], paramagnetic resonance imaging spectrophotometry [9], and bioassay [10], all these methods required high cost, difficult to operate, and have low sensitivity. Strong demand to create a sensing technique which provides a rapid response and sensitivity, ease of use, and low cost led to the discovery of an electrochemical technique for the detection of biomolecules. One of the advantages of electrochemical sensors is that it has an excellent repeatability and accuracy as well as a wide linear response range with low detection limits and real time measurements. Therefore, a number of recent reports specifically used by electrochemical technique for biomolecules sensing.

Owing to the intense research activity in this field, a few types of material based on graphene have discovered and they showed a great performance as a biosensor such as functionalized graphene, graphene/metal oxide, graphene/metal composites, and graphene/polymer composites. These materials show an improvement in the sensitivity, selectivity, and accuracy of the biosensor which is the vital criteria for sensor to meet the future needs. In this chapter, an overview of graphene-based materials as a biosensor is provided where we are focusing on four biomolecules that are glucose, NO, NADH, and H_2O_2. The selection of graphene as the main material in the biosensor application is driven by its unique properties which will be discussed in the following section.

5.2 Graphene

In 1859, Brodie [11] had unintentionally discovered a method to prepare a material so-called graphitic acid. It is called so because it is insoluble in acids and saline solution but dispersed well in pure water and alkalines. His method is based on the ideas of graphite undergo an oxidation process by treating it with a strong acidic mixture containing potassium chlorate and fuming nitric acid. At first, Brodie had done several experiments toward graphite as he was keen to study the structure of graphite. From the first attempt of oxidizing the graphite, he found that (i) the final substance form as a peculiar compound of carbon with its weight larger than that graphite and (ii) the final substance changed to light yellow color substance composed of transparent plates after fourth or fifth times of treatments. Following experiments had changed his initial interest from study the structure to molecular formula of graphite and its discrete molecular weight. His investigation has revealed that (i) the obtained product consists of mainly carbon, hydrogen and oxygen with a net molecular formula

of $C_{2.19}H_{0.80}O_{1.00}$, (ii) the atomic weight of graphite is 33, and (iii) carbon in the form of graphite functions as a distinct element where it forms a distinctive system of combination [11]. Brodie finally named this substance as graphon, and thus becomes the starting point that led to the current research of graphene.

Over the past decades, an atom-thick layer of crystalline carbon arranges in a honeycomb lattice known as graphene has attracted enormous interest due to its remarkable physical and electrical properties that hold great promise for future applications. In the year of 2010, Geim and Novoselov, physicists from the University of Manchester had won the Nobel Prize in Physics for groundbreaking experiments in discovering the two-dimensional (2-D) material named graphene [12]. Based on this experiment, graphite flakes used as the starting materials for producing few layer graphene before peel off to isolating the graphene layers from bulk graphite using scotch tape. This process is called micromechanical cleavage method which is one of the earlier methods that able to produce graphene with millimeter in size. Graphene has known as a member of the carbon family that composed of sp^2-bonded carbon atoms arranged in a 2-D honeycomb lattice. This honeycomb structure has a d-spacing of about 0.34 nm, making it the thinnest material in the world so far. Graphene consists of one layer of carbon atom that can be wrapped up into zero-dimensional buckyballs, rolled into one-dimensional nanotube or stacked into three-dimensional graphite (Figure 5.2). Besides that, graphene exhibits a semimetal behavior proven by the existence of a small overlap between valence and conduction bands in graphene.

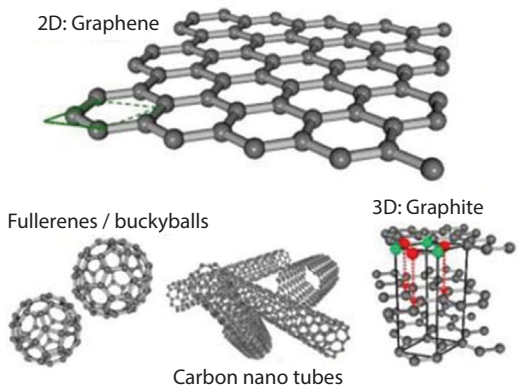

Figure 5.2 The form of graphene: zero-dimensional buckyballs, one-dimensional nanotube, and three-dimensional stacked graphite (http://evworld.com/article.cfm?storyid=1950).

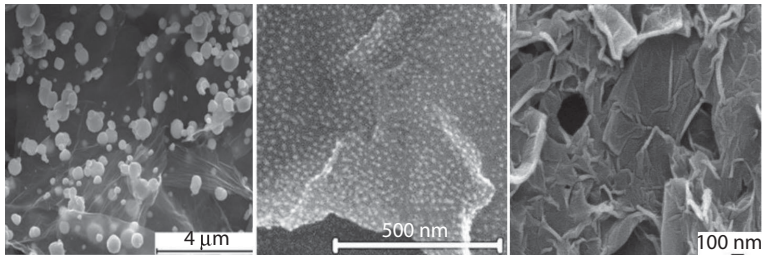

Figure 5.3 SEM images of (a) graphene/CuO nanocomposite [19], (b) graphene/Ag nanocomposite [20], and (c) graphene/PANI composite [21].

Since this discovery, the journey of graphene has begins. At first, researchers are interested in finding the best method for the synthesis of single-layer graphene and till date several methods had been reported to prepare graphene such as chemical vapor deposition (CVD) [13], rapid thermal reduction [14], and others. After that, this graphene sheets is hybridized with other polymers [15], metal [16], and metal oxide [17] as they believed that by anchoring these materials on the graphene sheet can enhance its properties as an interesting material to be applied in a wide field of application (Figure 5.3). Unfortunately, graphene has the hydrophobic properties toward water and other organic and inorganic solvents which limit its application. Graphene sheets tend to form irreversible agglomerates and even restocked to form graphite via van der Waal's interaction. This issue drives the researchers to manipulate graphene properties by introducing new functional groups on the surface of graphene sheets. Functionalized graphene with hydrophilic groups was then used to prepare nanocomposites with other materials [18].

However, graphene produced by typical physical and chemical routes including micromechanical cleavage, reduction of exfoliated graphene oxide [22], and solvothermal synthesis [23] are generally micrometer-sized graphene sheets, which limits their direct application in nanodevices. To facilitate the application of graphene in nanodevices and effectively tune the band-gap of graphene, a promising approach is to convert the 2-D graphene sheets into zero-dimensional graphene quantum dots (GQDs). Theoretical and experimental studies have shown that GQDs possess strong quantum confinement and edge effects when their sizes are down to 100 nm (Figure 5.4). If their sizes are reduced to 10 nm, comparable with the widths of semiconducting graphene nanoribbons, the two effects will become more pronounced and hence induce novel physical properties. Other than that, GQDs have generated enormous excitement because of their superiority in chemical inertness, biocompatibility, and low toxicity.

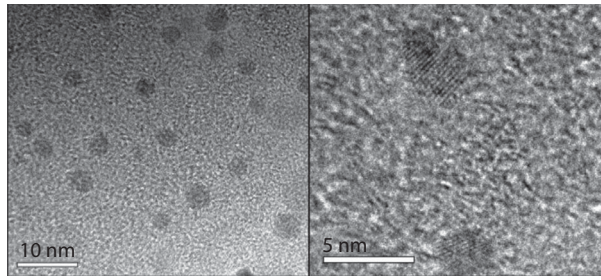

Figure 5.4 High-resolution transmission elecrtron microscopy (HRTEM) images of GQDs [24].

Besides GQDs consisting of a single atomic layer of nano-sized graphite have the excellent performances of graphene, such as high surface area, large diameter, and better surface grafting using π–π conjugation and surface groups.

5.3 Synthetic Methods for Graphene

Recently, there are many experimental methods that had been reported to fabricate single-layer graphene sheet. Each of these methods is evaluated based on the different requirements needed by the researcher. The most important aspect emphasized by the researchers is the quality in term of the purity of the graphene which defined by the numbers of defects and degree of oxidation of graphene. Lack in the number of intrinsic defects and higher in the degree of oxidation will lead to the outstanding properties of graphene. The aspect of the number and size of the layers obtained which each of the methods that have been reported is intended to produce multi- or single layer of graphene with different size of surface area. Besides that, the amount of graphene that can be produced is another crucial aspect that needs to be take note as most of the methods demonstrated have a low productivity, which makes it unsuitable for large-scale use. Other than that, the complexity also plays an important role in the choosing the best method for production of graphene as method that possess complicated designed machines will wasted researcher time and cost. Complicated method with lack of controllability also will lead to the less reproducible results that can achieved so the ability to control is another aspect that cause the difference exist between each method.

In general, the production of graphene can be approached in two ways named top-down and bottom-up approach (Figure 5.5). For top-down approach, the process involves breaking down the macroscopic structures which are the graphite into microscopic structural material that is

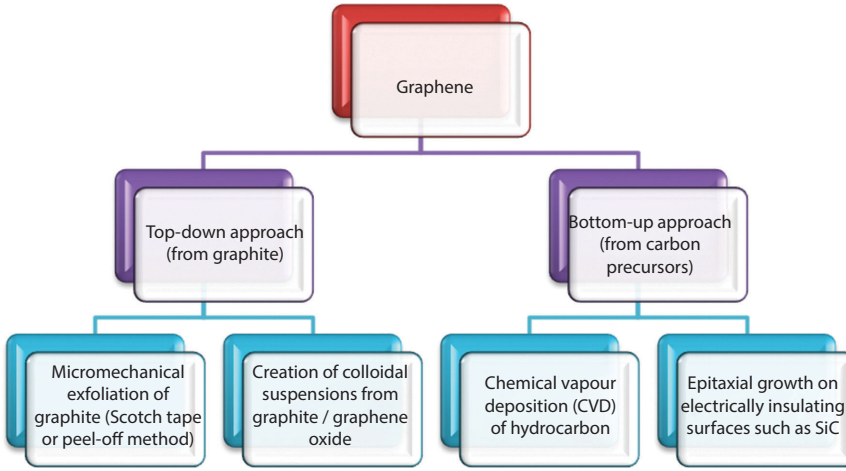

Figure 5.5 Various synthetic methods for graphene.

the single-layer graphene. There are two types of method that used in the top-down approaches that are micromechanical exfoliation of graphite (which also known as the scotch tape or peel off method) and also including the ultrasonication method. Wang *et al.* reported a way to synthesize a stable high-concentration suspensions of non-oxidized few layers of graphene with micrometer long edges by tip ultrasonication where graphite flakes are directly exfoliate in ionic liquids, such as 1-butyl-3-methyl-imidazolium bis(trifluoro-methane-sulfonyl)imide([Bmim]-[Tf2N]) [25]. Another type is the creation of colloidal suspensions from graphite oxide or GO. In order to form graphene, these GOs will undergo reduction through chemically or thermally, and currently by microwave assisted [26].

Another approach is the bottom-up approach where graphene is obtained from a carbon material as the precursor which can be grown directly on the substrate surface. The bottom-up approach is divided into two parts that are by CVD of hydrocarbon and by epitaxial growth on electrically insulating surfaces such as silicon carbide (SiC). The CVD process involved the exposure of a substrate to a gaseous compound where then decomposes on the surface in order to grow a thin film, whereas the by-products was evaporated (Figure 5.6). This can be achieved either by heating the sample with a filament or with plasma. Wang and co-workers had successfully synthesized a large scale of substrate free graphene *via* the CVD of methane over cobalt supported on magnesium oxides at 1000 °C in a gas flow of argon [27]. They found the presence of localized sp^3 defects within the sp^2 carbon network and small sp^2 domains in the few-layered graphene particles obtained from this method. Meanwhile, Sprinkle *et al.*

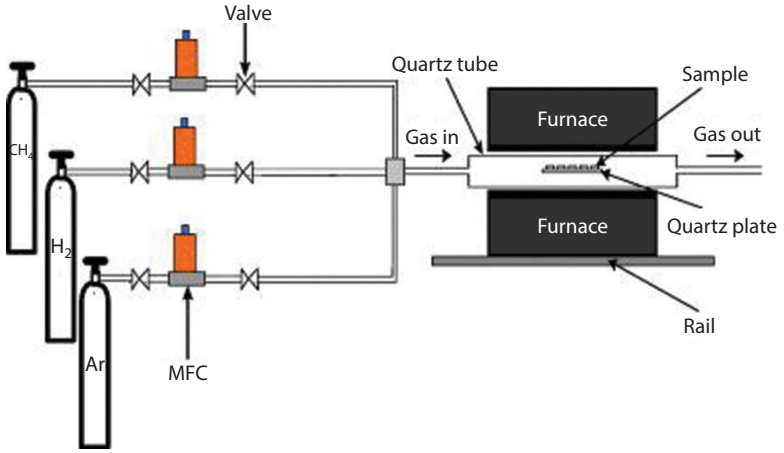

Figure 5.6 Schematic of the CVD setup for the fabrication of graphene films [29].

had demonstrated a way to produce the graphene nanoribbons with self-organized growth on a template SiC substrate using scalable photolithography and microelectronics processing [28].

5.4 Properties of Graphene

Recently, graphene has attracted much attention due to its unique properties, which make it as an outstanding material that having a profound impact in many areas of science and technology. It is well known that graphene is built up from the sp^2-bonded carbon atoms that arranged in the 2-D honeycomb crystal lattices. The carbon atoms bonded in sp^2 bonding will bind to three neighbors (Figure 5.7), which also known as trigonal hybridization forming planar structures of graphene. Each carbon atom in the lattice has a π orbital that contributes to a delocalized network of electrons.

The C–C covalent bond is one of the strongest bond in nature and well known of its basic constitution of the graphite lattice. Graphene has an excellent mechanical property with a high Young's modulus of almost 1 TPa [30] due to the atoms that have covalently locked in place by the C–C bond. Besides that, it also possesses a high mobility of charge carriers of up to 20,000 $m^2 V^{-1} s^{-1}$ at room temperature [31] due to its extensive 2-D π–π conjugation net and also has a high specific surface area of up to 2600 $m^2 g^{-1}$ [32]. Moreover, graphene possess extraordinary properties including the electronic properties and electron transport capabilities, and excellent

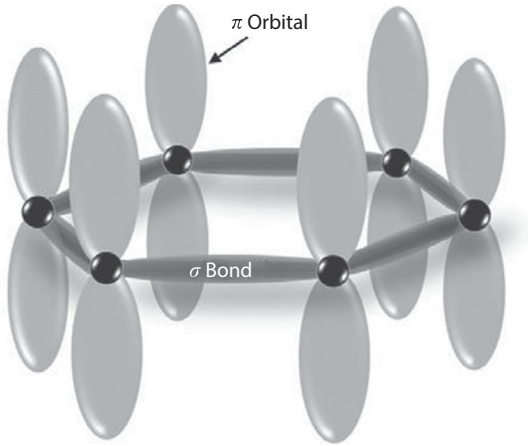

Figure 5.7 The sp^2-hybridized orbitals between the carbon atoms and the π bonds.

Table 5.1 The summary of the properties of graphene.

Property	**Value**	**Ref.**
Structural		
Surface area	1256 m^2/g	[33]
Crystal structure	2-D hexagonal	[34]
Electrical		
Electron mobility	> 200,000 $cm^2\ V^{-1}\ s^{-1}$	[35]
Electrical conductivity	in the order of 10^2 S/cm (R_s < 1 kΩ/square)	[36]
Optical		
Optical transmittance	80% in 400–1800 nm wavelength range	[36]
Band-gap	0–250 meV (tunable)	[37]
Mechanical		
Young's modulus	1.1 TPa	[30]
Fracture strength	10 GPa	[38]

thermal and electrical conductivity as a consequence of its structure. Some of the extraordinary properties of graphene are summarized in Table 5.1. These fascinating properties render graphene as a promising candidate for application in electronic devices such as transistor [39] and solar cell [40]. Moreover, it is ensured that graphene is an ideal 2-D catalyst support to anchor metal and semiconductor catalyst nanoparticles, offering versatile selective catalytic or sensing performances.

5.5 Multi-functional Applications of Graphene

Due to the remarkable physicochemical properties, graphene offers great potential in various fields of applications ever since its discovery in 2004. These unique physicochemical properties suggest it has great potential for providing new approaches and critical improvements and it showed multi-functional applications (Figure 5.8). For example, the high surface area of electrically conductive graphene sheets can give rise to high densities of attached analyte molecules. This in turn can facilitate high sensitivity and device miniaturization in biosensor application. Kang and co-workers have found that graphene-modified glassy carbon electrodes (GCEs) showed an excellent electrocatalytic activity toward the reduction and oxidation of paracetamol. This modified electrode also shows high sensitivity and selectivity for detecting paracetamol in commercial tablets and plasma samples [41].

Besides that, graphene also shows a great performance as a catalyst support due to its high surface area that helps to enhance the adsorption and desorption of reactants. Zhao et al. have successfully fabricate graphene/TiO_2 composites with a high-performance visible-light photocatalyst, thus shows a great potential in the application of photocatalytic degradation

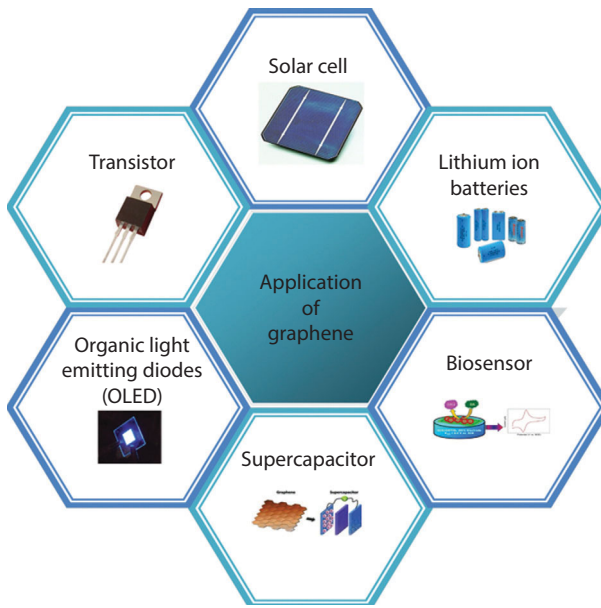

Figure 5.8 Multi-functional application of graphene.

of organic compounds [42]. Moreover, the high speed at which electrons in graphene move and facile electron transfer opens up opportunities for built-up higher-frequency transistors [43], solar cell [44], and many more. Other than that, graphene could also be used to make lithium-ion battery that are rechargeable faster than before due to the presence of defects in the graphene sheet that provide pathways for the lithium ions to attach to the anode substrate [45].

5.6 Electrochemical Sensor

In medical, biological, and biotechnological, the quantitative measurement of biomolecules is of utmost importance because it helps to detecting the abnormal level of biomolecules contents, hence could prevent and diagnosis the disease in the initial stage. In the past decades, several sensing techniques and devices that directly connect to a biological environment for detecting biomolecules have been developed such as laser-induced native fluorescence and high-performance liquid chromatography-mass spectrometry. Basically, the idea of biosensor is to convert the biological information to a processed electronic signal through complex circuit. Therefore, most of biosensors require a high cost and larger in size which is not convenient to handle. Besides that, it also has a low sensitivity toward specific biomolecules. Hence, electrochemical sensor has been actively introduced in the biosensor due to its low cost and exhibits higher level of sensitivity and selectivity.

An electrochemical biosensor is a device that has been used to measure the concentration of biomolecule due to the direct transforms of electrochemical information produced by biochemical mechanism into an analytically useful signal. Electrochemical biosensor has a series of advantages such as high sensitivity and selectivity toward electroactive species, fast and accurate response, and most importantly it is portable and inexpensive compared to other existing biosensor. Besides that, it also offers advantages of wide linear response range and good stability and reproducibility. There are two basic components of an electrochemical sensor which work together as a working or sensing electrode that are a chemical recognition system and physicochemical transducer. Other than working electrode, reference and counter electrodes are also required in this sensor where next enclosed in the sensor housing in contact with a liquid electrolyte and biomolecules.

In order to acts as biosensor, the recognition layers will interaction with the target biomolecules and the physicochemical transducer will translates the bio-recognition event into a useful electrical signal which can be

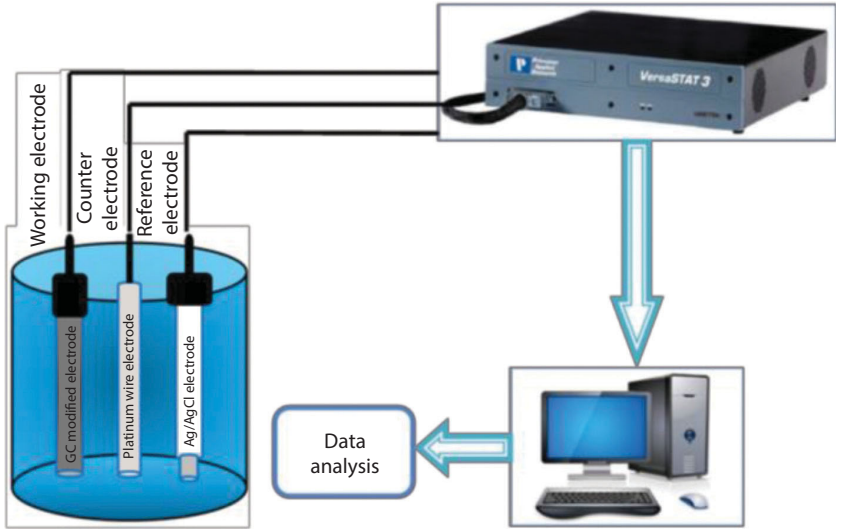

Figure 5.9 Operation design for electrochemical sensor.

detected by electrical instrumentation. Amperometry, cyclic voltammetry, and potentiometry are some of the examples of electrical signal resulted from the transduction of biological signal. The surface architectures which link the sensing element with the biological samples play an important role in determining the performance of electrochemical sensor. The sensitivity of the sensor will be affected based on the surface modification techniques, electrochemical transduction mechanisms, and the choice of the recognition receptor molecules. The general electrochemical biomolecule sensor setup is shown in Figure 5.9.

5.7 Graphene as Promising Materials for Electrochemical Biosensors

5.7.1 Graphene-Based Modified Electrode for Glucose Sensors

Glucose is a simple sugar that most commonly found in human body especially in blood, which play a vital role as an energy source in metabolism. It can be produced by proteins, fats, and carbohydrates. Glucose provides energy to all cells in the body through the bloodstream; hence, it is known as blood glucose. Blood glucose levels need to be controlled because high concentration of glucose in the blood causes multiple health problems associated with diabetes such as cardiovascular diseases. Thus, researchers have taken great effort to develop a sensor to measure the glucose content

in body with graphene-based materials, with high sensitivity, reliable, rapid, and low-cost fabrication.

The electrochemical method is most commonly used technique for glucose measurements. Researchers have proven that graphene-based materials are promising for glucose sensors that can be modified with GCE. Metal oxides such as copper oxide (CuO), zinc oxide (ZnO), and iron oxide (Fe_2O_3) have widely been used to anchoring on the graphene sheets, aiming to find novel properties in the composites and their uses in glucose sensors. Hsu *et al.* has constructed a glucose biosensors based on CuO/graphene nanocomposite [46]. The CuO/graphene nanocomposite was synthesized using simple heating and annealing techniques, and the powder of this nanocomposite was dissolved in the solution of ethanol–water and used for electrode fabrication with bare GCE. The CuO/graphene/GCE shows a great sensor performance against glucose lower detection limit of 1 μM with the aid of chronoamperometry. Lu *et al.* have developed a graphene/palladium nanoparticles (PdNPs) modified electrode for the electrochemical glucose biosensor [47]. It is believed that the well-distributed PdNPs on the surface of graphene helps to increase the electrocatalytic activity due to the increase of active sites for the catalytic redox reaction thus increase the sensitivity of glucose sensor. Graphene–polymer composites and functionalized graphene are common materials used in glucose biosensor and give a good sensing response. Yang *et al*. had synthesized nanocomposites of chitosan/reduced graphene oxide/nickel nanoparticles (CS-RGO–NiNPs) onto a screen-printed electrode (SPE) [48]. This CS-RGO–NiNPs composite facilitated electron transfers and possesses high electrocatalytic activity for glucose sensing which led to the outstanding performance for enzymeless glucose sensing in alkaline media. The schematic diagram of the electrodeposition processes of CS-RGO–NiNPs on SPE surface and the glucose detecting mechanism is shown in Figure 5.10. Meanwhile, Kwak and co-workers have used other than modified electrode to detect glucose, where they fabricate graphene-based field-effect transistor (FET) sensor using CVD method for the detection of glucose [49]. This sensor could detect glucose levels in the range of 3.3–10.9 μM. This could be another promising technique to construct glucose sensor with wide detection range and low detection limit. Table 5.2 displays the performance of glucose sensor from different modified electrodes reported in literature.

5.7.2 Graphene-Based Modified Electrode for NADH Sensors

NADH and its oxidized form NAD^+ are an important coenzyme involved in metabolic processes and enzymatic reactions. Besides that, researchers

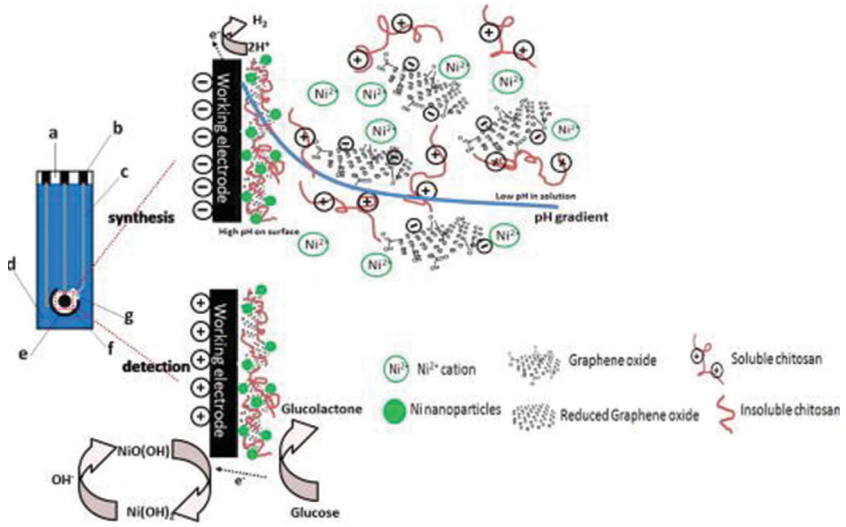

Figure 5.10 The schematic diagram of the electrodeposition processes of CS-RGO–NiNPs on SPE surface and glucose detection mechanism [48].

have intensively studying the electrochemical oxidation NADH due to the potential application in NAD^+/NADH-dependent dehydrogenase-based biosensors [62]. Guo *et al.* have fabricated a NADH biosensor based on graphene sheets-modified electrode which has been synthesized using Staudenmaier method before being reduced by hydrazine solution [63]. The graphene-modified electrode performed a response time less than 10 sec based on the current–time response curves. This result indicates a fast process and well catalytic oxidation of NADH by graphene-modified electrode. In another case, a novel electrode system, based on graphene nanosheets-modified glassy carbon electrode (GNS/GC), has been proposed as an electrochemical sensing platform for NADH as reported by Keeley *et al.* [64]. In this study, graphene has been produced from liquid-phase exfoliation process. The detection limit for NADH at the GNS/GC electrode was calculated to be 1.4 μM with a sensitivity of 22.3 mAM^{-1}.

Moreover, the incorporation of metal nanoparticles into graphene materials can further benefit NADH electrochemical biosensors. Li and co-workers report that the graphene hybrid with Au NRs has showed an excellent performance toward NADH oxidation, with a LOD of 6 μM [65]. Besides that, the GN–AuNRs-modified electrode also exhibited high selectivity toward NADH with the interference of UA, AA, and Glu. On the other hands, graphene–polymer composites also have shown a great potential in NADH sensing application. Li *et al.* reported the preparation

Table 5.2 Comparison of the sensing characteristics of glucose sensors with graphene-based modified electrodes reported in the literature.

Electrode	Detection limit	Sensitivity	Linear range	Ref.
Cu2O/G/GC	3.3 μM	0.285 μA cm^{-2} $μM^{-1}$	0.3–3.3 μM	[50]
CuO/G/SPC	34.3 nM	2367 μA cm^{-2} $μM^{-1}$	0.122 μM–0.5 μM	[51]
GOD/Co3O4/G/GC	0.05 μM	13.52 μA cm^{-2} $μM^{-1}$	0.5–16.5 μM	[52]
NiO/G/GC	1 μM	1571 μA cm^{-2} $μM^{-1}$	5 μM–2.8 μM	[53]
GOD/rGO-Au/GC	10 μM	0.835 μA $μM^{-1}$	1–8 μM	[54]
Cu NPs/G/GC	0.5 μM	–	0.5 μM–4.5 μM	[55]
Pd NPs/G/Nf/GC	1 μM	–	10 μM–5 μM	[47]
PdCu/G/GC	20 μM	48 μA mg^{-1} $μM^{-1}$	1–18 μM	[56]
GOD/CS/G/GC	0.02 μM	37.93 μA cm^{-2} $μM^{-1}$	0.08–12 μM	[57]
GOD/AuNPs/PPy/rGO/CS	–	123.8 μA cm^{-2} $μM^{-1}$	0.2–1.2 μM	[58]
GOD/PBBIns/G/Au	–	143.5 μA cm^{-2} $μM^{-1}$	10 μM–10 μM	[59]
GOD/IL-RGO/S-RGO/Nf/GC	3.33 μM	–	10–500 μM	[60]
GOD/PDDA-G/GC	8 μM	154.9 μA cm^{-2} $μM^{-1}$	0.02–1.8 μM	[61]

Abbreviation: GC: glassy carbon; SPC: screen-printed carbon; GOD: glucose oxidase; Nf: nafion; PBBIns: nanostructured poly(*N*-butyl benzimidazole); CS: chitosan; $\{IL\text{-}RGO/S\text{-}RGO\}_n$: layer-by-layer self-assembling of amine-terminated ionic liquid-sulfonic acid-functionalized graphene; PDDA: poly(diallyldimethylammonium chloride).

of a NADH sensor based on electrochemically reduced graphene oxide/polythionine (ERGO/PTH) deposited on GCE [66]. The synergistic catalytic effect of graphene and PTH polymer is believed helps to improve the electrocatalytic characteristic toward the oxidation of NADH, thus enhanced the sensitivity. Table 5.3 displays the comparison of the sensing characteristics of NADH sensors with other modified electrodes reported in the literature.

5.7.3 Graphene-Based Modified Electrode for NO Sensors

NO is known to be one of the important biological messenger and signaling functions in human body. Monitoring the level of NO concentration

Table 5.3 Comparison of the sensing characteristics of NADH sensors with graphene-based modified electrodes reported in the literature.

Electrode	Detection limit (μM)	Sensitivity	Linear range	Ref.
G/GC	20	12.6 μA μM^{-1}	0.05–1.4 μM	[63]
GNS/GC	1.4	22.3 μA M^{-1}	–	[64]
rGO/GC	0.6	–	0–500 μM	[67]
AuNPs/G/GC	6	10.27 μA cm^{-2} μM^{-1}	20–160 μM	[65]
ERGO/PTH/GC	0.1	143 μA cm^{-2} μM^{-1}	0.01–3.9 μM	[66]

Abbreviation: ADH: alcohol dehydrogenase; AuNPs: gold nanorods; GNS: graphene nanosheets; G: graphene; ERGO: electrochemically reduced graphene oxide; PTH: polythionine.

in the body is crucial for disease diagnosis and early prevention from malfunction of our body system. Graphene-based is reported to be an excellent electrode material for electrochemical NO sensors due to their principally advantageous properties including wide potential windows, fairly inert electrochemistry, and excellent electrocatalytic activities. Using an electrochemical deposition technique, Wang and co-workers have fabricated a reduced graphene-modified GC electrode for NO detection [68]. Based on the amperometric results, the modified electrode exhibited a wider linear range (from 0.72 to 78.4 μM), a lower limit of detection (0.2 μM), and a higher sensitivity (299.1 μA μM^{-1}). Highly conductive pathways for electron conduction provided by graphene have improved the electrode performance in detecting NO.

Graphene/metal composite materials are also widely used in the fabrication of NO sensor especially graphene/gold nanoparticles nanocomposite. Ting *et al.* fabricated a NO sensor using a modified GCE where they depositing AuNPs on ERGO through electrochemical deposition technique [69]. The result shows that this modified GCE exhibit LOD calculated as 133 nM due to the presence of AuNPs that act as an efficient electrocatalysts toward the oxidation of NO. Other than that, Jayabal et al. has successfully incorporating Au NRs with rGO which embedded in an amine-functionalized silicate sol–gel matrix [70]. This composite is used to modify the GCE for the detection of NO. Based on the experiment, they found that the modified electrode has higher selectivity toward NO and the detection did not interfered by the presence of common interferences such as glucose, urea,

Table 5.4 Comparison of the sensing characteristics of NO sensors with graphene-based modified electrodes reported in the literature.

Electrode	Detection limit	Sensitivity	Linear range	Ref.
ERG/GC	0.2 μM	299.1 μA μM^{-1}	0.72–78.4 μM	[68]
AuNPs/ERGO/GC	133 nM	5.38 μA cm^{-2} μM^{-1}	–	[69]
RGO/Au-TPDTNRs/GC	6.5 nM	–	10–140 nM	[70]

Abbreviation**:** ERG: electrochemically reduced graphene; ERGO: electrochemically reduced graphene oxide; AuNPs: gold nanoparticles; RGO/Au-TPDT NRs: reduced graphene oxide/gold nanorods embedded in amine-functionalized silicate sol–gel matrix.

oxalate, and NaCl. Besides that, this modified electrode also exhibited low detection limit (6.5 nM) with a linear range from 10 to 140 nM. The summary of NO sensing properties of other modified electrode is shown in Table 5.4.

5.7.4 Graphene-Based Modified Electrode for H_2O_2

A most important biomolecule hydrogen peroxide (H_2O_2) has been shown to be involved in regulation of renal function and as an antibacterial agent in the urine. It also acts as a sensor that warns the cell in the levels are too high as a sign of less white blood level in the body. Therefore, the creation of a device that can detect the concentration of H_2O_2 is very important. A variety of graphene-based materials such as graphene–metal composite, graphene–metal oxide composite, graphene–polymer composite, and functionalized graphene have shown a great ability as an electrochemical biosensor for H_2O_2 sensing. The hybridization of graphene with metal or metal oxide nanoparticles will induce the synergic effect which leads to the improvement in conductivity, strengthen the stability and enhanced catalytic activity of the new nanocomposite material.

Gao *et al*. have reported a H_2O_2 sensor of $Ni(OH)_2$/ERGO/MWCNT nanocomposites fabricated via convenient electrodeposition of $Ni(OH)_2$ nanoparticles on ERGO/MWCNT film-modified GCE [71]. This $Ni(OH)_2$/ERGO/MWCNT-modified electrode exhibits excellent sensing behavior toward H_2O_2 with low detection limit of 4 μM and high sensitivity of 711 μA μM^{-1} cm^{-2}. In addition, Fang et al. developed the Fe_3O_4/self-reduced graphene/GC-modified electrode for sensitive non-enzymatic detection of H_2O_2 [72]. The interference from glutathione (GSH), Glu, AA, l-Cys, and UA were also been studied using amperometric technique. The result showed that the $Ni(OH)_2$/ERGO/MWCNT-modified electrode

has a high selective detection toward H_2O_2 as no interference occurred upon adding mentioned materials with low limit of detection of 0.17 μM (S/N = 3).

Meanwhile, due to the excellent properties owned by cadmium sulfide (CdS) nanoparticles such as good biocompatible, conductive materials and could provide larger surface area and sufficient amount of binding points for biomolecules immobilization, Xiaoqiang and co-workers have constructed an enzyme-free biosensor for H_2O_2 based on CdS/rGO nanocomposites [73]. The amperometric response of CdS/rGO/GC-modified electrode shows an increment upon addition of H_2O_2 and exhibits a limit of detection of 1.67 μM (S/N = 3) and a sensitivity of 95 μA cm^{-2} μM^{-1}. The incorporation of polymers like polypyrrole, polyaniline, chitosan, and nafion into graphene materials can further benefit electrochemical biosensors. For example, ErhanZor et al. have used the enzymatic polymerization technique to entrapped nano-PPy into rGO using glucose oxidase in aqueous solution to construct a nano-PPy/rGO-modified GCE (GOD/nPPy/rGO/GCE) for H_2O_2 sensing [74]. The amperometric results shows that the modified electrode exhibits very fast amperometric response behavior toward H_2O_2 with low LOD of 34 nM due to the excellent conductivity of nano-PPy that acts as a mediator enhancing the electron transfer rate, thus increasing the electrochemical properties of GOD/nPPy/rGO/GC-modified electrode. Electrochemical H_2O_2 biosensors based on functionalized graphene are also extensively studied. Fengna Xi *et al.* have successfully fabricated graphene electrode functionalized with thionine molecules using *in situ* polymerized poly-dopamine as the linker [75]. Thionine is used to functionalized graphene because it could offers fast electron transfer rate, excellent reversibility and helps to mediate H_2O_2 reduction, thus demonstrates outstanding performance for non-enzymatic electrochemical sensing of H_2O_2. The comparison of the sensing characteristics of H_2O_2 sensors with graphene-based modified electrodes reported in the literature is presented in Table 5.5.

5.8 Conclusion and Future Outlooks

In this chapter, the importance of biomolecules such as, glucose, NADH, NO, and H_2O_2 and their role in the body functions were described first. Also the preparation, properties, and their multi-functional application of graphene were briefly described. The level of these biomolecules (glucose, NADH, NO, and H_2O_2) inside the body is very essential and the impact of these biomolecules concentration under exceeds and lower concentration

Table 5.5 Comparison of the sensing characteristics of H_2O_2 sensors with graphene-based electrodes reported in the literature.

Electrode	Detection limit	Sensitivity	Linear range	Ref.
Cu2O/GNs/GC	20.8 μM	0.285 mA cm^{-2} μM^{-1}	0.3–7.8 μM	[50]
Co3O4/G/GC	0.06 μM	1.14 μA cm^{-2} μM^{-1}	0.2–211.5 μM	[52]
Fe3O4/rGO/GC	0.17 μM	387.6 μA cm^{-2} μM^{-1}	0.001–20 μM	[72]
CeO2/rGO/GC	30.40 nM	1.978×10^{-4} μA μM^{-1}	60.7 nM–3.0 μM	[76]
Ag NPs/rGO/GC	3.6 μM	–	0.1–100 μM	[77]
Ag NPs/rGO/GC	0.01 μM	255 μA cm^{-2} μM^{-1}	0.05–5 μM	[78]
CdS/rGO/GC	1.67 μM	95 μA cm^{-2} μM^{-1}	5 μM–15 μM	[73]
CuS/rGO/GC	10 μM	–	1 μM–1 μM	[79]
nPPy/rGO/GC	34 nM	–	0.1–4.0 μM	[74]
PoPD/rGO/GC	0.84 μM	16.2 μA cm^{-2} M^{-1}	2.5–25 μM	[80]
IL-RGO/S-RGO	0.21 μM	0.1364 μA μM^{-1}	0.1–3.4 μM	[60]
PDDA-G/GC	10 μM	–	0.04–9.42 μM	[61]
pDA/TH/G	80 nM	169.7 μA μM^{-1}	0.4–660 μM	[75]

Abbreviation**:** nPPy: nano-polypyrrole; CdS: cadmium sulfide; TH: thionine; pDA: polydopamine; PoPD: poly(o-phenylenediamine).

also explained. Hence, sensing of these biomolecules, such as glucose, NADH, NO, and H_2O_2, is very essential and the sensing strategy with graphene and its composites-based modified electrodes are promising and it contributes more in this concern. However, the NADH and NO sensors based on graphene and their composites-modified electrode is very few and it opens up a new possibility to explore with these kinds of modified electrodes in near future.

References

1. D.S. Bredt, S.H. Snyder, Nitric oxide: a novel neuronal messenger, *Neuron*, 8 pp. 3–11, 1992.
2. A.L. Burnett, Nitric oxide in the penis: physiology and pathology, *The Journal of Urology*, 157, pp. 320–324, 1997.
3. A. Petros, D. Bennett, P. Vallance, Effect of nitric oxide synthase inhibitors on hypotension in patients with septic shock, *The Lancet*, 338, 1557–1558, 1991.

4. C. Napoli, L.J. Ignarro, Nitric oxide and atherosclerosis, *Nitric Oxide*, 5, pp. 88–97, 2001.
5. B. Halliwell, M.V. Clement, L.H. Long, Hydrogen peroxide in the human body, *FEBS Letters*, 486, pp. 10–13, 2000.
6. F. Lacy, D.T. O'Connor, G.W. Schmid-Schönbein, Plasma hydrogen peroxide production in hypertensives and normotensive subjects at genetic risk of hypertension, *Journal of Hypertension*, 16, pp. 291–303, 1998.
7. J.S. Beckman, K.A. Congert, Direct measurement of dilute nitric oxide in solution with an ozone chemiluminescent detector, *Methods*, 7, pp. 35–39, 1995.
8. Å. Wennmalm, B. Lanne, A.-S. Petersson, Detection of endothelial-derived relaxing factor in human plasma in the basal state and following ischemia using electron paramagnetic resonance spectrometry, *Analytical Biochemistry*, 187, pp. 359–363, 1990.
9. P. Kuppusamy, P. Wang, A. Samouilov, J.L. Zweier, Spatial mapping of nitric oxide generation in the ischemic heart using electron paramagnetic resonance imaging, *Magnetic Resonance in Medicine*, 36, pp. 212–218, 1996.
10. J.L. Wallace, R.C. Woodman, Detection of nitric oxide by bioassay, *Methods*, 7, pp. 55–58, 1995.
11. B.C. Brodie, On the atomic weight of graphite, *Philosophical Transactions of the Royal Society of London*, 149, pp. 249–259, 1859.
12. A.K. Geim, K.S. Novoselov, The rise of graphene, *Nature Materials*, 6, pp. 183–191, 2007.
13. C. Bautista, D. Mendoza, Multilayer graphene synthesized by CVD using liquid hexane as the carbon precursor, *World Journal of Condensed Matter Physics*, 1, pp. 157–160, 2011.
14. W. Chen, L. Yan, P.R. Bangal, Preparation of graphene by the rapid and mild thermal reduction of graphene oxide induced by microwaves, *Carbon*, 48, pp. 1146–1152, 2010.
15. G. Carotenuto, L. Nicolais, Graphene–Polymer Composites, *Wiley Encyclopedia of Composites*; L. Nicolais, A. Borzacchiello, Eds., Wiley: New York, 5 pp. 1232–1236, 2012.
16. C. Xu, X. Wang, J. Zhu, Graphene−metal particle nanocomposites, *The Journal of Physical Chemistry C*, 112, pp. 19841–19845, 2008.
17. Y. Zou, Y. Wang, NiO nanosheets grown on graphene nanosheets as superior anode materials for Li-ion batteries, *Nanoscale*, 3, pp. 2615–2620, 2011.
18. G. Psarras, I. Tantis, D. Tasis, Functionalized graphene–poly (vinyl alcohol) nanocomposites: physical and dielectric properties, *eXPRESS Polymer Letters*, 6, pp. 283–292, 2012.
19. N. Yusoff, N. Huang, M. Muhamad, S. Kumar, H. Lim, I. Harrison, Hydrothermal synthesis of CuO/functionalized graphene nanocomposites for dye degradation, *Materials Letters*, 93, pp. 393–396, 2013.
20. M. Zainy, N.M. Huang, S. Vijay Kumar, H.N. Lim, C.H. Chia, I. Harrison, Simple and scalable preparation of reduced graphene oxide–silver

nanocomposites via rapid thermal treatment, *Materials Letters*, 89, pp. 180–183, 2012.
21. Y. Li, H. Peng, G. Li, K. Chen, Synthesis and electrochemical performance of sandwich-like polyaniline/graphene composite nanosheets, *European Polymer Journal*, 48, pp. 1406–1412, 2012.
22. S. Pei, H.-M. Cheng, The reduction of graphene oxide, *Carbon*, 50, pp. 3210–3228, 2012.
23. M. Choucair, P. Thordarson, J.A. Stride, Gram-scale production of graphene based on solvothermal synthesis and sonication, *Nature Nanotechnology*, 4, pp. 30–33, 2008.
24. S. Benítez-Martínez, M. Valcárcel, Graphene quantum dots as sensor for phenols in olive oil, *Sensors and Actuators B: Chemical*, 197, pp. 350–357, 2014.
25. X. Wang, P.F. Fulvio, G.A. Baker, G.M. Veith, R.R. Unocic, S.M. Mahurin, M. Chi, S. Dai, Direct exfoliation of natural graphite into micrometre size few layers graphene sheets using ionic liquids, *Chemical Communications*, 46, pp. 4487–4489, 2010.
26. Y. Zhu, S. Murali, M.D. Stoller, A. Velamakanni, R.D. Piner, R.S. Ruoff, Microwave assisted exfoliation and reduction of graphite oxide for ultracapacitors, *Carbon*, 48, pp. 2118–2122, 2010.
27. X. Wang, H. You, F. Liu, M. Li, L. Wan, S. Li, Q. Li, Y. Xu, R. Tian, Z. Yu, Large-scale synthesis of few-layered graphene using CVD, *Chemical Vapor Deposition*, 15, pp. 53–56, 2009.
28. M. Sprinkle, M. Ruan, Y. Hu, J. Hankinson, M. Rubio-Roy, B. Zhang, X. Wu, C. Berger, W. De Heer, Scalable templated growth of graphene nanoribbons on SiC, *Nature Nanotechnology*, 5, pp. 727–731, 2010.
29. H.B. Nguyen, T.T.T. Ngo, N.T. Nguyen, T.T.H. Dang, P.Q. Do, X.N. Nguyen, X.P. Nguyen, H.K. Phan, N.M. Phan, Graphene patterned polyaniline-based biosensor for glucose detection, *Advances in Natural Sciences: Nanoscience and Nanotechnology*, 3, 025011, 2012.
30. J.-W. Jiang, J.-S. Wang, B. Li, Young's modulus of graphene: a molecular dynamics study, *Physical Review B*, 80, 113405, 2009.
31. S.V. Morozov, K.S. Novoselov, M.I. Katsnelson, F. Schedin, D.C. Elias, J.A. Jaszczak, A.K. Geim, Giant intrinsic carrier mobilities in graphene and its bilayer, *Physical Review Letters*, 100, 016602, 2008.
32. Y.S. Yun, Y.H. Bae, D.H. Kim, J.Y. Lee, I.-J. Chin, H.-J. Jin, Reinforcing effects of adding alkylated graphene oxide to polypropylene, *Carbon*, 49, pp. 3553–3559, 2011.
33. M. Wang, Q. Liu, H. Sun, E.A. Stach, J. Xie, Preparation of high surface area nano-structured graphene composites, *ECS Transactions*, 41, pp. 95–105, 2012.
34. M.I. Katsnelson, Graphene: carbon in two dimensions, *Materials Today*, 10, pp. 20–27, 2007.

35. K.I. Bolotin, K.J. Sikes, Z. Jiang, M. Klima, G. Fudenberg, J. Hone, P. Kim, H.L. Stormer, Ultrahigh electron mobility in suspended graphene, *Solid State Communications*, 146, pp. 351–355, 2008.
36. H.A. Becerril, J. Mao, Z. Liu, R.M. Stoltenberg, Z. Bao, Y. Chen, Evaluation of solution-processed reduced graphene oxide films as transparent conductors, *ACS Nano*, 2, pp. 463–470, 2008.
37. Y. Zhang, T.T. Tang, C. Girit, Z. Hao, M.C. Martin, A. Zettl, M.F. Crommie, Y.R. Shen, F. Wang, Direct observation of a widely tunable bandgap in bilayer graphene, *Nature*, 459, pp. 820–823, 2009.
38. Y. Liu, B. Xie, Z. Zhang, Q. Zheng, Z. Xu, Mechanical properties of graphene papers, *Journal of the Mechanics and Physics of Solids*, 60, pp. 591–605, 2012.
39. L. Britnell, R.V. Gorbachev, R. Jalil, B.D. Belle, F. Schedin, A. Mishchenko, T. Georgiou, M.I. Katsnelson, L. Eaves, S.V. Morozov, N.M.R. Peres, J. Leist, A.K. Geim, K.S. Novoselov, L.A. Ponomarenko, Field-effect tunneling transistor based on vertical graphene heterostructures, *Science*, 335, pp. 947–950, 2012.
40. X. Wang, L. Zhi, K. Mullen, Transparent, conductive graphene electrodes for dye-sensitized solar cells, *Nano Letters*, 8, pp. 323–327, 2007.
41. X. Kang, J. Wang, H. Wu, J. Liu, I.A. Aksay, Y. Lin, A graphene-based electrochemical sensor for sensitive detection of paracetamol, *Talanta*, 81, pp. 754–759, 2010.
42. D. Zhao, G. Sheng, C. Chen, X. Wang, Enhanced photocatalytic degradation of methylene blue under visible irradiation on graphene@ TiO_2 dyade structure, *Applied Catalysis B: Environmental*, 111, pp. 303–308, 2012.
43. F. Schwierz, Graphene transistors, *Nature Nanotechnology*, 5, pp. 487–496, 2010.
44. H. Kim, S.-H. Bae, T.-H. Han, K.-G. Lim, J.-H. Ahn, T.-W. Lee, Organic solar cells using CVD-grown graphene electrodes, *Nanotechnology*, 25, pp. 014–012, 2014.
45. X. Li, Y. Hu, J. Liu, A. Lushington, R. Li, X. Sun, Structurally tailored graphene nanosheets as lithium ion battery anodes: an insight to yield exceptionally high lithium storage performance, *Nanoscale*, 5, pp. 12607–12615, 2013.
46. Y.-W. Hsu, T.-K. Hsu, C.-L. Sun, Y.-T. Nien, N.-W. Pu, M.-D. Ger, Synthesis of CuO/graphene nanocomposites for nonenzymatic electrochemical glucose biosensor applications, *Electrochimica Acta*, 82, pp. 152–157, 2012.
47. L.-M. Lu, H.-B. Li, F. Qu, X.-B. Zhang, G.-L. Shen, R.-Q. Yu, In situ synthesis of palladium nanoparticle–graphene nanohybrids and their application in nonenzymatic glucose biosensors, *Biosensors and Bioelectronics*, 26, pp. 3500–3504, 2011.
48. J. Yang, J.-H. Yu, J. Rudi Strickler, W.-J. Chang, S. Gunasekaran, Nickel nanoparticle–chitosan-reduced graphene oxide-modified screen-printed electrodes for enzyme-free glucose sensing in portable microfluidic devices, *Biosensors and Bioelectronics*, 47, pp. 530–538, 2013.

49. Y.H. Kwak, D.S. Choi, Y.N. Kim, H. Kim, D.H. Yoon, S.-S. Ahn, J.-W. Yang, W.S. Yang, S. Seo, Flexible glucose sensor using CVD-grown graphene-based field effect transistor, *Biosensors and Bioelectronics*, 37, pp. 82–87, 2012.
50. M. Liu, R. Liu, W. Chen, Graphene wrapped Cu_2O nanocubes: non-enzymatic electrochemical sensors for the detection of glucose and hydrogen peroxide with enhanced stability, *Biosensors and Bioelectronics*, 45, pp. 206–212, 2013.
51. C.-L. Sun, W.-L. Cheng, T.-K. Hsu, C.-W. Chang, J.-L. Chang, J.-M. Zen, Ultrasensitive and highly stable nonenzymatic glucose sensor by a CuO/graphene-modified screen-printed carbon electrode integrated with flow-injection analysis, *Electrochemistry Communications*, 30, pp. 91–94, 2013.
52. C. Karuppiah, S. Palanisamy, S.-M. Chen, V. Veeramani, P. Periakaruppan, A novel enzymatic glucose biosensor and sensitive non-enzymatic hydrogen peroxide sensor based on graphene and cobalt oxide nanoparticles composite modified glassy carbon electrode, *Sensors and Actuators B: Chemical*, 196, pp. 450–456, 2014.
53. S.-J. Li, N. Xia, X.-L. Lv, M.-M. Zhao, B.-Q. Yuan, H. Pang, A facile one-step electrochemical synthesis of graphene/NiO nanocomposites as efficient electrocatalyst for glucose and methanol, *Sensors and Actuators B: Chemical*, 190, pp. 809–817, 2014.
54. M.A. Tabrizi, J.N. Varkani, Green synthesis of reduced graphene oxide decorated with gold nanoparticles and its glucose sensing application, *Sensors and Actuators B: Chemical*, 202, pp. 475–482, 2014.
55. J. Luo, S. Jiang, H. Zhang, J. Jiang, X. Liu, A novel non-enzymatic glucose sensor based on Cu nanoparticle modified graphene sheets electrode, *Analytica Chimica Acta*, 709, pp. 47–53, 2012.
56. M. Yuan, A. Liu, M. Zhao, W. Dong, T. Zhao, J. Wang, W. Tang, Bimetallic PdCu nanoparticle decorated three-dimensional graphene hydrogel for non-enzymatic amperometric glucose sensor, *Sensors and Actuators B: Chemical*, 190, pp. 707–714, 2014.
57. X. Kang, J. Wang, H. Wu, I.A. Aksay, J. Liu, Y. Lin, Glucose oxidase–graphene–chitosan modified electrode for direct electrochemistry and glucose sensing, *Biosensors and Bioelectronics*, 25, pp. 901–905, 2009.
58. K. Xue, S. Zhou, H. Shi, X. Feng, H. Xin, W. Song, A novel amperometric glucose biosensor based on ternary gold nanoparticles/polypyrrole/reduced graphene oxide nanocomposite, *Sensors and Actuators B: Chemical*, 203, pp. 412–416, 2014.
59. H.-C. Chen, R.-Y. Tsai, Y.-H. Chen, R.-S. Lee, M.-Y. Hua, A colloidal suspension of nanostructured poly (N-butyl benzimidazole)-graphene sheets with high oxidase yield for analytical glucose and choline detections, *Analytica Chimica Acta*, 792, pp. 101–109, 2013.
60. H. Gu, Y. Yu, X. Liu, B. Ni, T. Zhou, G. Shi, Layer-by-layer self-assembly of functionalized graphene nanoplates for glucose sensing in vivo integrated with on-line microdialysis system, *Biosensors and Bioelectronics*, 32, pp. 118–126, 2012.

61. L. Jia, J. Liu, H. Wang, Preparation of poly(diallyldimethylammonium chloride)-functionalized graphene and its applications for H_2O_2 and glucose sensing, *Electrochimica Acta*, 111, pp. 411–418, 2013.
62. A. Radoi, D. Compagnone, Recent advances in NADH electrochemical sensing design, *Bioelectrochemistry*, 76, pp. 126–134, 2009.
63. K. Guo, K. Qian, S. Zhang, J. Kong, C. Yu, B. Liu, Bio-electrocatalysis of NADH and ethanol based on graphene sheets modified electrodes, *Talanta*, 85, pp. 1174–1179, 2011.
64. G.P. Keeley, A. O'Neill, M. Holzinger, S. Cosnier, J.N. Coleman, G.S. Duesberg, DMF-exfoliated graphene for electrochemical NADH detection, *Physical Chemistry Chemical Physics*, 13, pp. 7747–7750, 2011.
65. L. Li, H. Lu, L. Deng, A sensitive NADH and ethanol biosensor based on graphene–Au nanorods nanocomposites, *Talanta*, 113, pp. 1–6, 2013.
66. Z. Li, Y. Huang, L. Chen, X. Qin, Z. Huang, Y. Zhou, Y. Meng, J. Li, S. Huang, Y. Liu, Amperometric biosensor for NADH and ethanol based on electroreduced graphene oxide–polythionine nanocomposite film, *Sensors and Actuators B: Chemical*, 181, pp. 280–287, 2013.
67. M.A. Tabrizi, Z. Zand, A facile one-step method for the synthesis of reduced graphene oxide nanocomposites by NADH as reducing agent and its application in NADH aensing, *Electroanalysis*, 26, pp. 171–177, 2014.
68. Y.-L. Wang, G.-C. Zhao, Electrochemical sensing of nitric oxide on electrochemically reduced graphene-modified electrode, *International Journal of Electrochemistry*, pp. 1–6, 2011.
69. S.L. Ting, C.X. Guo, K.C. Leong, D.-H. Kim, C.M. Li, P. Chen, Gold nanoparticles decorated reduced graphene oxide for detecting the presence and cellular release of nitric oxide, *Electrochimica Acta*, 111, pp. 441–446, 2013.
70. S. Jayabal, P. Viswanathan, R. Ramaraj, Reduced graphene oxide–gold nanorod composite material stabilized in silicate sol–gel matrix for nitric oxide sensor, *RSC Advances*, 4, pp. 33541–33548, 2014.
71. W. Gao, W.W. Tjiu, J. Wei, T. Liu, Highly sensitive nonenzymatic glucose and H_2O_2 sensor based on $Ni(OH)_2$/electroreduced graphene oxide–multiwalled carbon nanotube film modified glass carbon electrode, *Talanta*, 120, pp. 484–490, 2014.
72. H. Fang, Y. Pan, W. Shan, M. Guo, Z. Nie, Y. Huang, S. Yao, Enhanced nonenzymatic sensing of hydrogen peroxide released from living cells based on Fe_3O_4/self-reduced graphene nanocomposites, *Analytical Methods*, 6, pp. 6073–6081, 2014.
73. X. An, X. Yu, C.Y. Jimmy, G. Zhang, CdS nanorods/reduced graphene oxide nanocomposites for photocatalysis and electrochemical sensing, *Journal of Materials Chemistry A*, 1, pp. 5158–5164, 2013.
74. E. Zor, M.E. Saglam, I. Akin, A.O. Saf, H. Bingol, M. Ersoz, Green synthesis of reduced graphene oxide/nanopolypyrrole composite: characterization and H_2O_2 determination in urine, *RSC Advances*, 4, pp. 12457–12466, 2014.

75. F. Xi, D. Zhao, X. Wang, P. Chen, Non-enzymatic detection of hydrogen peroxide using a functionalized three-dimensional graphene electrode, *Electrochemistry Communications*, 26, pp. 81–84, 2013.
76. K.J. Shailendra, C. Naveen Kumar, R. Pavul Raj, S.J. Niki, S. Mohan, Synthesis of 3D porous CeO_2/reduced graphene oxide xerogel composite and low level detection of H_2O_2, *Electrochimica Acta*, 120, pp. 308–313, 2013.
77. Q. Li, X. Qin, Y. Luo, W. Lu, G. Chang, A.M. Asiri, A.O. Al-Youbi, X. Sun, One-pot synthesis of Ag nanoparticles/reduced graphene oxide nanocomposites and their application for nonenzymatic H_2O_2 detection, *Electrochimica Acta*, 83, pp. 283–287, 2012.
78. M.Y. Wang, T. Shen, M. Wang, D. Zhang, J. Chen, One-pot green synthesis of Ag nanoparticles-decorated reduced graphene oxide for efficient nonenzymatic H_2O_2 biosensor, *Materials Letters*, 107, pp. 311–314, 2013.
79. Y.J. Yang, W. Li, X. Wu, Copper sulfide| reduced graphene oxide nanocomposite for detection of hydrazine and hydrogen peroxide at low potential in neutral medium, *Electrochimica Acta*, 123, pp. 260–267, 2014.
80. V.H. Nguyen, T.H. Tran, J.-J. Shim, Glassy carbon electrode modified with a graphene oxide/poly(o-phenylenediamine) composite for the chemical detection of hydrogen peroxide, *Materials Science and Engineering: C*, 44, pp. 144–150, 2014.

6

Fluorescent Carbon Dots for Bioimaging

Suresh Kumar Kailasa[1], Vaibhavkumar N. Mehta[1], Nazim Hasan[2], and Hui-Fen Wu*[2,3,4]

[1]*Department of Applied Chemistry, S. V. National Institute of Technology, Surat, India*
[2]*Department of Chemistry, National Sun Yat-Sen University, Kaohsiung, Taiwan*
[3]*Center for Nanoscience and Nanotechnology, National Sun Yat-Sen University, Kaohsiung, Taiwan*
[4]*Doctoral Degree Program in Marine Biotechnology, National Sun Yat-Sen University, Kaohsiung, Taiwan*

Abstract

In recent years carbon dots (CDs) have emerged as a new class of carbon nanostructures with sizes <10 nm, due to their physico-chemical, biocompatible and strong tunable photoluminescence. We highlight here the importance, especially with the aim of cell labeling, by using CDs as probes. We then briefly present the state-of-the-art and the progress of bioimaging. We present many recent examples using CDs as cell labels for imaging of various cells.

Keywords: Carbon dots, biomolecules, cells, fluorescence microscopy and spectrometry

6.1 Introduction

Recently, carbon nanoparticles (C-NPs) and carbon dots (CDs) have been widely used as fluorescent probes for biosensing and imaging [1-3]. The CDs were first produced *via* laser ablation of a carbon target in the presence of water vapor with argon as carrier gas [4]. The bright and multicolor fluorescent emissions (at various excitation wavelengths from UV to near IR) were observed in both single-walled and multiple-walled carbon

**Corresponding author*: hwu@faculty.nsysu.edu.tw

Ashutosh Tiwari, Hirak K. Patra and Anthony P.F. Turner (eds.) Advanced Bioelectronic Materials, (215–228)

nanotubes, which is due to the passivation of surface defects with the chemical functionalization on the surfaces of carbon nanotubes [5-7]. The CDs are composed of carbon, oxygen, nitrogen, hydrogen and some doped elements. In CDs, the high amount of carbon–carbon bonding predominantly in graphene-type sp^2 hybridization, but reveal a relatively high amount of the diamond-type sp^3 hybridization (or disorder) of carbon atoms in conjugated systems [8]. Moreover, the CDs can be viewed as a highly defected composition of coexisting aromatic and aliphatic regions just like graphene, graphene oxide and diamond that are assembled in proportions and with variations of surface groups that depend on the precursors [9]. The bright fluorescence is mainly due to radiative recombination of CDs surface-confined electrons and holes. In recent years, CDs have been exploited as alternatives to conventional QDs and already show encouraging performance in biosensing and bioimaging due to their excellent photostability, favorable biocompatibility, low toxicity, outstanding water solubility, high sensitivity and excellent selectivity to target analytes, tunable fluorescence emission and excitation, high quantum yield and large Stokes shifts. Since its preparation in 2006, research groups worldwide have developed "bottom-up" dehydration and "top-down" cutting routes for preparation of CDs using various materials as precursors [10]. Furthermore, various methods have been developed to prepare CDs, including laser ablation, arc-discharge, pyrolysis, oxidation, electrochemical exfoliation, hydrothermal treatments, plasma treatment and microwave/ultrasonic passivation electrochemical oxidation.

In recent years, numerous CDs-based analytical technologies have been developed to detect various trace target analytes and to visualize biomolecules in various cells, tissues, and living organisms due to their low photobleaching, biocompatibility, and good stability [11]. Therefore, in this book chapter the existing uses of CDs in fluorescence imaging of cells and tissues are highlighted, and issues and prospects in such applications discussed.

6.2 CDs as Fluorescent Probes for Imaging of Biomolecules and Cells

Imaging of biomolecules and cells, both *in vitro* and *in vivo*, has long relied on fluorescence microscopy (imaging) and is currently attracting increasing attention as a powerful bioanalytical tool for proteomic and genomic studies [12]. Substantial progress in the ability to prepare water soluble biocompatible nanomaterials using green synthetic approaches and understanding

of their outstanding and size dependent optical, physico-chemical features have stimulated their use in imaging [13-14]. In recent years, CDs have begun to be applied as fluorescent imaging probes for imaging of a wide variety of molecules (metal ions, organic species, biomolecules and cells) *in vitro* and *in vivo*. Since, CDs have attractive features (biocompatibility, excellent chemical and colloidal stability, facile low-cost synthesis, scalability and multicolor emission) that make them efficient candidates in cell microscopy to visualize cells with long fluorescence lifetimes (nanoseconds). Due to their advantages such as visible excitation and emission wavelengths, their fluorescence brightness at the individual dot level, their high photostability, CDs have been used as fluorescent probes for imaging of cells *in vitro* and *in vivo*. Sun *et al*. first reported the use of PEGylated CDs as probes for imaging of *Escherichia coli* and studied the internalization of oligomeric aminopolymer-functionalized CDs in Caco-2 cells [4]. Later on, the same group developed CDs-based microscopic method for multiphoton bioimaging of live cells [15]. Yang and co-workers explored the use of fluorescent CDs as fluorescent and biocompatible probes for imaging of cells in mice [16]. Srivastava's group described the use of iron oxide-doped CDs for multi-modality bioimaging [17]. Similarly, Hsu *et al.* prepared highly stable CDs in ionic-strength media (e.g. 500 μM NaCl) and used as probes for imaging of MCF-10A, MCF-7 and MDA-MB-231 cells [18]. Authors found that the prepared CDs are mostly localized in the cell membranes and cytoplasms, with evidence of excitation-wavelength cell images. Callan's group prepared CDs using citrate as precursor and functionalized with octadecene and 1-hexadecylamine [19]. Authors used CDs as bioimaging probes for CHO cells and the results revealed that fluorescence was observed within the cells and emission intensity profiles were predominantly localized at the periphery of the cells, rather than in their central region. The pH sensitivity of fluorescence response of different carbon nanomaterials has been reported in different studies and is due to the presence of different ionizable groups on their surface [20]. Wang and co-workers utilized a cationic branched polyelectrolyte of large molecular weight, i.e., polyethylenimine (PEI) of 25,000 Da as both a carbon source and passivating agent to prepare photoluminescent CDs in one step [21]. The prepared CDs have shown a distinct pH-sensitive response and served as a proton sensor in monitoring cell metabolization process with proton release. As a result, the CDs were effectively penetrate the cell membrane and provided HeLa cell images with good resolution.

Monodisperse highly fluorescent CDs have been synthesized at gram scale with a high yield (41.8%) by carbonization of sucrose with oil acid in one step [22]. Authors demonstrated their potential applications in

bioimaging of 16HBE cells. Cellular uptake of the CDs can be observed at excitation wavelength 488 nm laser. The photoluminescent spots were observed only in the cytoplasmic area of the cell, whereas PL intensity of nucleus at the central region is very weak, indicating that the CDs easily penetrated into the cell but did not enter the nuclei, which avoids genetic disruption. Wu *et al.* developed CDs-based FRET with organic dye-based ratiometric sensor for sensing and imaging of H_2S in biological fluids and in living cells [23]. Strongly green fluorescent graphene CDs were prepared in one-step solvothermal method using graphene oxide as precursor [24]. It was noticed that the bright green area was observed inside the cells, which confirms that the translocation of carbon nanomaterials through cell's membrane. Hahn's team demonstrated the application of polyethylene glycol (PEG) diamine-capped CDs for real time bioimaging of target specific delivery of hyaluronic acid (HA) derivatives [25]. Authors carried out *in vitro* bioimaging of target specific intracellular delivery of the HA–CDs conjugates by HA receptor-mediated endocytosis. It was noticed that the cellular uptake of HA–CDs conjugates was drastically reduced due to the competitive binding of HA to the receptors (Figure 6.1a). Similarly, the cellular uptake of CDs after conjugation to HA was significantly reduced in HEK293 cells without HA receptors (Figure 6.1b). This approach can be useful for the treatment of liver diseases and for various bioimaging applications. Jana's group developed a chemical method for synthesis of highly fluorescent CDs and used as cell imaging probes [26]. To prove the functionalized CDs as fluorescent probes, authors investigated their applications in cell imaging (Figure 6.2). The functionalized CDs were successfully increased cell labeling and uptake. Tan's group prepared multicolor CDs by chemical nitric acid oxidation using the reproducible plant soot as raw material [27]. Authors investigated their potential applications for imaging of Chinese Hamster Ovary (CHO) cells and guppy fish imaging and showed enhanced luminescence as compared with its control with a signal-to-noise (S/N) ratio. The same group prepared high PL CDs using commercial Nescafe instant coffee as carbon source [28]. To explore their potential use in cell imaging, authors performed *in vitro* cellular uptake experiment of CDs in human hepatocellular carcinoma cells (Figure 6.3a). As a result, the hepatocellular carcinoma cells incubated with CDs become bright as compared with the control cells without adding the CDs. In order to investigate its practical application, CDs applied as probes to observe PL of CDs-food mixture (Figure 6.3b). These results demonstrated that the guppy fish fed with CDs-food mixture clearly showed the enhanced PL, which was much higher than that of the control fish (Figure 6.3c). Authors

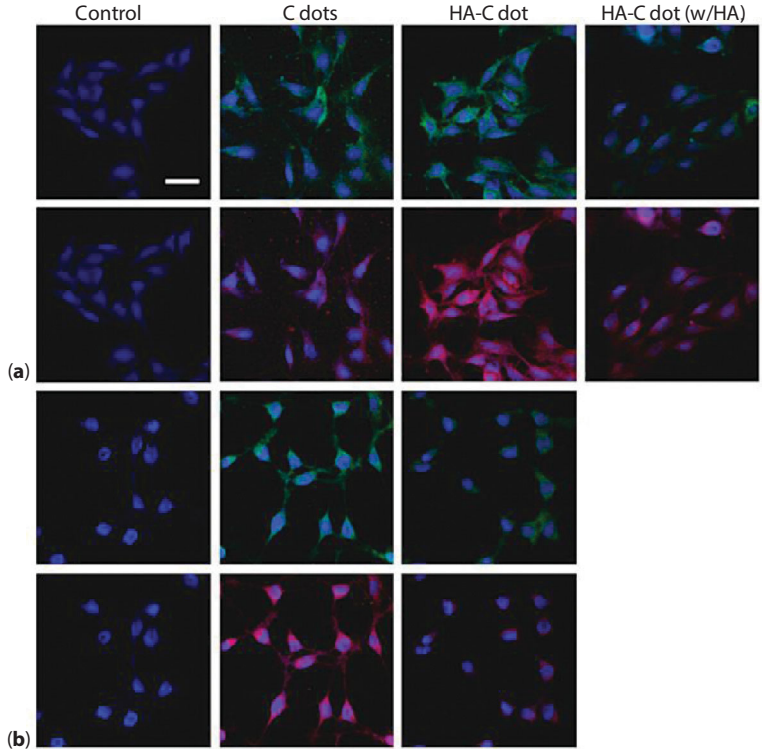

Figure 6.1 Confocal laser scanning microscopic images of (a) B16F1 and (b) HEK293 cells after incubation at 37°C for 24 h with CDs and HA–CDs conjugates in the absence and presence of 100-fold molar excess HA. Scale bar indicates 30 μm. (Copyright permission from Ref. 25)

found that the CDs showed low biotoxicity, which confirms that CDs are good candidates for *in vivo* small animal imaging.

An innovative and green strategy has been developed for preparation of CDs with good quantum yield (QY) using honey as a raw material [29]. The prepared CDs were used as fluorescent probes for detection of Fe^{3+} ion based on the quenching of their fluorescence. Eventually, the CDs were applied as probes for cell imaging and coding of HEp-2 and Hela cells. Recently, our group also described a green synthetic approach for preparation of CDs using *Saccharum officinarum* juice as precursor [30]. The CDs are well dispersed in water with an average size of ~3 nm and used as fluorescent probes for cellular imaging of bacteria (*Escherichia coli*) and yeast (*Saccharomyces cerevisiae*). Kim *et al.* investigated that CDs as a promising fluorescent nanomaterial to monitor the association/dissociation of polymeric carrier/plasmid DNA (pDNA) complex during

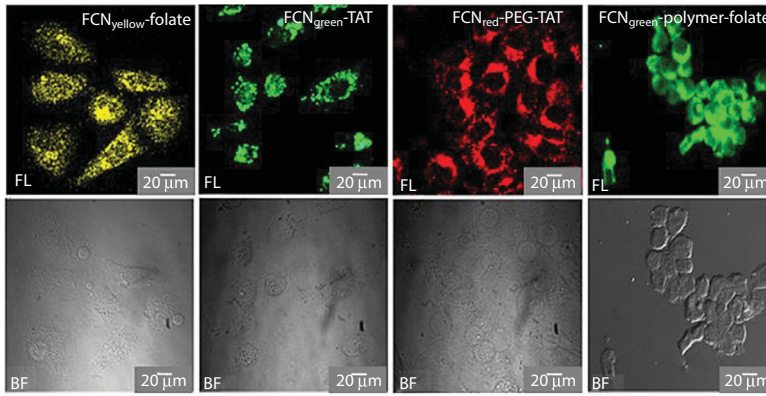

Figure 6.2 CDs as fluorescent cell label. CDs are incubated with HeLa cells for 3–6 hours and labeled cells are imaged under fluorescence microscope. Cells are imaged under bright field (BF) and fluorescence (FL) mode with confocal or Apotome microscope. Details of functional CDs are described in text and supporting information. (Copyright permission from Ref.26)

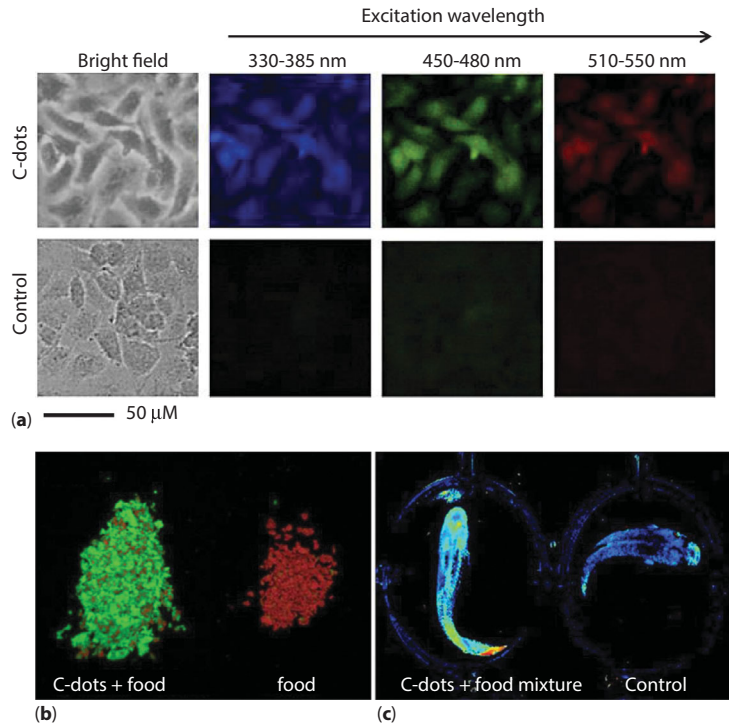

Figure 6.3 Bright field and fluorescence microscope images of human hepatocellular carcinoma cells incubated with CDs from the Nescafe® Original instant coffee for 24h. Exposure time was 400 ms. Unmixed fluorescence images of fish food (a) and fish treated with CDs-food mixture (b) and its control. (Copyright permission from Ref.28)

transfection [31]. The developed probe acted as a highly efficient hybrid transfecting agent with high cell viability and significantly improved gene delivery. Liu and co-workers functionalized CDs with PEI by the pyrolysis of glycerol and branched PEI25k mixture [32]. Authors observed that the CDs-PEIs were effectively internalized into cells displayed tunable fluorescent emission under varying excitation wavelength, which suggests that the CDs-PEIs acted as probe for gene delivery and bioimaging (COS-7 and HepG2 cells). Recently, Pascu's and Marken's groups prepared a novel two-photon-fluorescent N,O-heteroatom-rich carbon nanomaterial using poly(4-vinylpyridine) (P4VP) as a precursor [33]. It was noticed that the CDs-P4VP have retained their intrinsic fluorescence in a cellular environment and exhibit an average excited-state lifetime of 2.0 ± 0.9 ns in the cell. Moreover, the CDs-P4VP dots enter HeLa cells and do not cause significant damage to outer cell membranes, which confirms that CDs-P4VP is biocompatible in nature. Yan *et al.* prepared two kinds of CDs using citric acid-ethylenediamine (CDs-1) and citric acid-N-(b-aminoethyl)-g-aminopropyl methyldimethoxysilane (CDs-2) as precursors [34]. Two new fluorescent sensors were used for sensing of Hg^{2+} ion and monitoring of Hg^{2+} ion NIH-3T3 cells. As a result, the bright fluorescence was observed from within the cell and CDs can be observed mainly in the cell membrane and the cytoplasmic area. The PL of CDs was very weak in the cell nucleus. Wei and co-workers prepared highly PL CDs with a quantum yield (PLQY) of 7.7% using cornflour as a raw material [35]. The bright luminescence CDs were observed in S180 sarcoma cells at different excitations, which indicate that the CDs can be considered to be safe for *in vitro* and *in vivo* applications. The same group prepared water dispersible CDs with tunable PL using nanodiamond as a carbon source *via* one-pot hydrothermal oxidation [36]. The prepared CDs showed good biocompatibility with NIH-3T3 and A549 cells. It was observed that the morphology of CDs-conjugated cells is just like normal cell and the CDs could uptake by cells and accumulated in cells, indicating that the CDs could translocate into cells and locate at cytoplasm. Similarly, Li's and Feng's group synthesized strong fluorescent CDs by the hydrothermal refluxing method using lactose as a carbon source and tris(hydroxymethyl) aminomethane (i.e. Tris) as a surface passivation reagent [37]. The CDs were successfully acted as a probe for labeling of cytoplasm without causing any damage to cell nucleus, which confirms that the CDs easily penetrated into the cell but did not enter the nucleus. Their methylthiazolyldiphenyl-tetrazolium bromide (MTT) assay suggested that the CDs did not cause significant cytotoxicity to the HeLa cells. Zhang *et al.* described a method for preparation of two types of CDs with excitation-independent blue emission and excitation-dependent full-color emissions *via* a mild one-pot process

from chloroform and diethylamine [38]. The prepared CDs exhibited highly stable crystalline structures with tunable surface functionalities and observed the continuously adjustable full color emissions, which is due to the surface functional groups (C=O and C=N) on the surfaces of CDs that can efficiently introduce new energy levels for electron transitions in CDs. The high-resolution confocal images were obtained and the CDs were not evenly distributed throughout the whole cell, which confirms that their high biocompatible nature with cells. Blue and green fluorescent CDs (<10 nm) with high fluorescence quantum yield were prepared using vitamin B_1 as a carbon source and used as probes for labeling of cells [39]. The cell labeling was performed by incubating the CDs solution with different cell lines and imaged under a fluorescence microscope. Authors demonstrated that the CDs acted as excellent imaging probes and labels for different cells and CDs were enter into the cell *via* nonspecific uptake. They illustrated the tentative reason for labeling and uptake of CDs is due to the vitamin B_1-like surface structure, which can induce transporter-mediated cell uptake, similar to cellular uptake of vitamin B_1. Their CDs-based MTT assay demonstrated that the cell viability is >95% at a concentration of 1 mg/mL, which shows that the vitamin-derived CDs exhibited insignificant cytotoxicity and can be used as a highly efficient fluorescent cell label.

In recent years, CDs-based research has opened new opportunities for imaging living cells and *in vivo* animal models with excellent sensitivity and spatial resolution. Imaging of cells using CDs as probes is one of the hottest areas in the imaging field. There have been a number of studies illustrated the use of CDs as probes for monitoring of the cellular uptake [1,8,10,11,12]. For examples, the fluorescence detection of CDs with surface-passivation by 4,7,10-trioxa-1,13-tridecanediamine (TTDDA) in COS-7 cells and the cell membrane and cytoplasm exhibited bright fluorescence [40]. Similarly, Wang *et al.* incubated silica-encapsulated CDs with BGC823 cells and studied their fluorescence ability in the cytoplasmic area, which confirms that the CDs can be penetrated into the cells but not into the nuclei [41]. Liu's group prepared strong photoluminescent CDs by one-step microwave assisted pyrolysis using glycerol in the presence of TTDDA as a carbon source [42]. The CDs were incubated with HepG-2 cells and investigated multicolor fluorescence emissions of CDs under different excitation conditions under a laser scanning confocal microscope. As a result, the CDs taken up by HepG-2 cells exhibited bright blue, green, and red emission colors at 405 nm, 488 nm, and 543 nm excitations, respectively. Zhu and co-workers described the application of CDs for imaging of MG-63 cells [24]. The bright fluorescence emissions

from the cytoplasm were observed at excitation wavelengths 405 and 488 nm. Yang *et al.* prepared CDs by hydrothermal carbonization of chitosan and used as probes for imaging of A549 cells [43]. Authors observed that the CDs exhibited bright fluorescence spots only in the cell membrane and cytoplasmic area, with much weaker signals in the cell nucleus region. Jaiswal's team prepared CDs from the microwave-mediated caramelization of PEG oligomers to label cells under UV excitation [44]. Lai *et al.* studied the potential use of PEG functionalized CDs as probes for the delivery of the anti-cancer drug doxorubicin (DOX) [45]. Authors observed that the DOX loaded on CDs exhibited more toxicity to HeLa cells than free DOX, and the fluorescence imaging results suggested that the release of DOX from the carrier CDs occurred inside the cells. In order to enhance CDs utility to wide range of cells, several researches have been devoted their work on the development of CDs as probes for imaging of different cell lines [46-47], including Caco-2 cells [4], MG-63 cells [24], murine P19 progenitor cells [48], and pig kidney cell line (LLC-PK1 cells) [49]. These results suggested that CDs were acted as efficient eco-friendly probes to enter into the cells to their localization in the cytoplasm.

To alter their physico-chemical properties, surface modification is necessary for their biological applications. For example, Han's group modified the surfaces of CDs with PEI and used as probes for the fluorescence labeling of HeLa cells [50]. The CDs conjugated with the CEA8 antibody could label HeLa cells and the labeling was visualized by the green fluorescence contour of the cell shape. Authors observed that the CDs did not observe without CEA8 antibody under UV excitation, which reveals that functionalization of CDs play key role for labeling of HeLa cells. Similarly, Lee *et al.* prepared CDs with the maleimide-terminated TTA1 aptamer (targeting tenascin C proteins (Tnc) proteins) for the fluorescence imaging of cancer cells [51]. Since Tnc proteins are highly expressed in HeLa cells and C6 cells, but rarely expressed in CHO cells, the TTA1–CDs were found to be significantly selective to HeLa cells and C6 cells, with only minor up-taking by CHO cells. Ding's group prepared luminescent CDs from single-walled carbon nanotubes and then CDs were passivated with TTDDA [52]. Authors investigated their cytotoxicity by MTT assay method, and the results revealed that CDs exhibited very low cytotoxicity and the cell viability was over 90% when the concentration of CDs is below 500 mg mL^{-1}. These results suggested that the CDs showed good biocompatibility with biological cells. However, there were a couple of reports on the internalization of CDs in the cell nucleus. Based on the above results, the CDs exhibited multicolor emission and taken up by the cells for their localization in the cytoplasm without damaging the morphology of nucleus.

6.3 Conclusions and Perspectives

Since their discovery in 2006, a great deal of progress has been made on the CDs in the ten years, and a wide variety of green chemistry reagents has been used in various synthetic routes for the preparation of highly water dispersible multicolor emitting CDs and their applications in multidisciplinary research area. As a result, CDs have significant potential to serve as nontoxic replacements to traditional heavy-metal based QDs. Even though the CDs have exhibited unique optical and physico-chemical properties, unfortunately their uses in biomedical research areas are still infancy. Aiming at expanding CDs functionality even further, the synthesis of CDs with bright fluorescence emissions emphasized in the red/near- IR spectral regions, thus more effective in tissue penetration, is desired. Therefore, more studies can be explored on the surface functionalization in CDs for controlled coupling with bioactive species to enable specific targeting in cellular and *in vivo* imaging and related biomedical applications in near future.

References

1. P. G. Luo, S. Sahu, S. T. Yang, S. K. Sonkar, J. Wang, H. Wang, G. E. LeCroy, L. Cao, and Y. P. Sun, Carbon "quantum" dots for optical bioimaging, *J. Mater. Chem. B*, Vol. 37, p. 2116, 2013.
2. K. Scida, P. W. Stege, G. Haby, G. A. Messina, and C. D. García, Recent applications of carbon-based nanomaterials in analytical chemistry: Critical review, *Anal. Chim. Acta*, Vol. 691, p. 6, 2011.
3. D. Jariwala, V. K. Sangwan, L. J. Lauhon, T. J. Marks, and M. C. Hersam, Carbon nanomaterials for electronics, optoelectronics, photovoltaics, and sensing, *Chem. Soc. Rev.*, Vol. 42, p. 2824, 2013.
4. Y. P. Sun, B. Zhou, Y. Lin, W. Wang, K. A. S. Fernando, P. Pathak, M. J. Meziani, B. A. Harruff, X. Wang, H. Wang, P. G. Luo, H. Yang, M. E. Kose, B. Chen, L. M. Veca, and S. Y. Xie, Quantum-sized carbon dots for bright and colorful photoluminescence, *J. Am. Chem. Soc.*, Vol. 128, p. 7756, 2006.
5. J. E. Riggs, Z. Guo, D. L. Carroll, and Y.-P. Sun, Strong luminescence of solubilized carbon nanotubes, *J. Am. Chem. Soc.*, Vol. 122, p. 5879, 2000.
6. Y. P. Sun, K. Fu, Y. Lin, and W. Huang, Functionalized carbon nanotubes: Properties and applications, *Acc. Chem. Res.*, Vol. 35, p. 1096, 2002.
7. Y. Lin, B. Zhou, R. B. Martin, K. B. Henbest, B. A. Harruff, J. E. Riggs, Z. X. Guo, L. F. Allard, and Y. P. Sun, Visible luminescence of carbon nanotubes and dependence on functionalization, *J. Phys. Chem. B*, Vol. 109, p. 14779, 2005.

8. W. Wei, C. Lu, and L. W. Guang, Biological applications of carbon dots, *Sci. China Chem.*, Vol. 57, p. 522, 2014.
9. A. P. Demchenko, and M. O. Dekaliuk, Novel fluorescent carbonic nanomaterials for sensing and imaging, *Method. Appl. Fluoresc.*, Vol. 1, p. 042001, 2013.
10. P. G. Luo, F. Yang, S. T. Yang, S. K. Sonkar, L. Yang, J. J. Broglie, Y. Liu, and Y. P. Sun, Carbon-based quantum dots for fluorescence imaging of cells and tissues, *RSC Adv.*, Vol. 4, p. 10791, 2014.
11. C. Ding, A. Zhu, and Y. Tian, Functional surface engineering of C-dots for fluorescent biosensing and *in vivo* bioimaging. *Acc. Chem. Res.*, Vol. 47, p. 20, 2014.
12. A. M. C. Garcia, E. S. González, M. T. F. Argüelles, R. Pereiro, J. M. C. Fernández, and A. S. Medel, Nanoparticles as fluorescent labels for optical imaging and sensing in genomics and proteomics, *Anal. Bioanal. Chem.*, Vol. 399, p. 29, 2011.
13. Y. Song, S. Zhu, and B. Yang, Bioimaging based on fluorescent carbon dots, *RSC Adv.*, Vol. 4, p. 27184, 2014.
14. Y. Wang, and A. Hu, Carbon quantum dots: synthesis, properties and applications, *J. Mater. Chem. C*, Vol. 2, p. 6921, 2014.
15. L. Cao, X. Wang, M. Meziani, F. Lu, H. Wang, P. G. Luo, Y. Lin, B. A. Harruff, L. M. Veca, D. Murray, S. Y. Xie, and Y. P. Sun, Carbon dots for multiphoton bioimaging, *J. Am. Chem. Soc.*, Vol. 129, p. 11318, 2007.
16. S. T. Yang, X. Wang, H. Wang, F. Lu, P. G. Luo, L. Cao, M. J. Meziani, J. H. Liu, Y. Liu, M. Chen, Y. Huang and, Y. P. Sun, Carbon dots as nontoxic and high-performance fluorescence imaging agents, *J. Phys. Chem. C*, Vol. 113, p. 18110, 2009.
17. S. Srivastava, R. Awasthi, D. Tripathi, M. K. Rai, V. Agarwal, V. Agrawal, N. S. Gajbhiye, and R. K. Gupta, Magnetic-nanoparticle-doped carbogenic nanocomposite: an effective magnetic resonance/fluorescence multimodal imaging probe, *Small*, Vol. 8, p. 1099, 2012.
18. P. C. Hsu, P. C. Chen, C. M. Ou, H. Y. Chang, and H. T. Chang, Extremely high inhibition activity of photoluminescent carbon nanodots toward cancer cells, *J. Mater. Chem. B*, Vol. 1, p. 1774, 2013.
19. C. Fowley, B. McCaughan, A. Devlin, I. Yildiz, F. M. Raymo, and J. F. Callan, Bifunctional fluorescent carbon nanodots: green synthesis *via* soy milk and application as metal-free electrocatalysts for oxygen reduction, *Chem. Commun.*, Vol. 48, p. 9361, 2012.
20. F. Lin, W. N. He, and X. Q. Guo, Fluorescent carbon dots as a pH Sensor *Adv. Mater. Res.*, Vol. 415, p. 1319, 2012.
21. L. Shen, L. Zhang, M. Chen, X. Chen, and J. Wang, The production of pH-sensitive photoluminescent carbon nanoparticles by the carbonization of polyethylenimine and their use for bioimaging, *Carbon*, Vol. 55, p. 343, 2013.
22. B. Chen, F. Li, S. Li, W. Weng, H. Guo, T. Guo, X. Zhang, Y. Chen, T. Huang, X. Hong, S. You, Y. Lin, K. Zeng, and S. Chen, Large scale synthesis of

photoluminescent carbon nanodots and their application for bioimaging, *Nanoscale*, Vol. 5, p. 1967, 2013.
23. C. Yu, X. Li, F. Zeng, F. Zheng, and S. Wu, Carbon-dot-based ratiometric fluorescent sensor for detecting hydrogen sulfide in aqueous media and inside live cells, *Chem. Commun.*, Vol. 49, p. 403, 2013.
24. S. Zhu, J. Zhang, C. Qiao, S. Tang, Y. Li, W. Yuan, B. Li, L. Tian, F. Liu, R. Hu, H. Gao, H. Wei, H. Zhang, H. Sun, and B. Yang, Strongly green-photoluminescent graphene quantum dots for bioimaging applications, *Chem. Commun.*, Vol. 47, p. 6858, 2011.
25. E. J. Goh, K. S. Kim, Y. R. Kim, H. S. Jung, S. Beack, W. H. Kong, G. Scarcelli, S. H. Yun, and S. K. Hahn, Bioimaging of hyaluronic acid derivatives using nanosized carbon dots, *Biomacromolecules*, Vol. 13, p. 2554, 2012.
26. S. K. Bhunia, A. Saha, A. R. Maity, S. C. Ray, and N. R. Jana, Carbon nanoparticle-based fluorescent bioimaging probes, *Sci. Rep.*, Vol. 3, p. 1473, 2013.
27. M. Tan, L. Zhang, R. Tang, X. Song, Y. Li, H. Wu, Y. Wang, G. Lv, W. Liu, and X. Ma, Enhanced photoluminescence and characterization of multicolor carbon dots using plant soot as a carbon source, *Talanta*, Vol. 115, p. 950, 2013.
28. C. Jiang, H. Wu, X. Song, X. Ma, J. Wang, and M. Tan, Presence of photoluminescent carbon dots in Nescafe® original instant coffee: Applications to bioimaging, *Talanta*, Vol. 127, p. 68, 2014.
29. X. Yang, Y. Zhuo, S. Zhu, Y. Luo, Y. Feng, and Y. Dou, Novel and green synthesis of high-fluorescent carbon dots originated from honey for sensing and imaging, *Biosens Bioelectron.*, Vol. 60, p. 292, 2014.
30. V. N. Mehta, S. Jha, and S. K. Kailasa, One-pot green synthesis of carbon dots by using *Saccharum officinarum* juice for fluorescent imaging of bacteria (*Escherichia coli*) and yeast (*Saccharomyces cerevisiae*) cells, *Mater. Sci. Eng., C*, Vol. 38, p. 20, 2014.
31. J. Kim, J. Park, H. Kim, K. Singha, and W. J. Kim, Transfection and intracellular trafficking properties of carbon dot-gold nanoparticle molecular assembly conjugated with PEI-pDNA, *Biomaterials*, Vol. 34, p. 7168, 2013.
32. C. Liu, P. Zhang, X. Zhai, F. Tian, W. Li, J. Yang, Y. Li, H. Wang, W. Wang, W. Liu, Nano-carrier for gene delivery and bioimaging based on carbon dots with PEI-passivation enhanced fluorescence. *Biomaterials*, Vol. 33, p. 3604, 2012.
33. K. Lawrence, F. Xia, R. L. Arrowsmith, H. Ge, G. W. Nelson, J. S. Foord, M. F. Sotelo, N. D. M. Evans, J. M. Mitchels, S. E. Flower, S. W. Botchway, D. Wolverson, G. N. Aliev, T. D. James, S. I. Pascu, and F. Marken, Hydrothermal conversion of one-photon-fluorescent poly(4-vinylpyridine) into two-photon-fluorescent carbon nanodots, *Langmuir*, Vol. 30, p. 11746, 2014.
34. F. Yan, Y. Zou, M. Wang, X. Mu, N. Yang, and L. Chen, Highly photoluminescent carbon dots-based fluorescent chemosensors for sensitive and selective detection of mercury ions and application of imaging in living cells, *Sens. Actuators, B*, Vol. 192, p. 488, 2014.
35. J. Wei, X. Zhang, Y. Sheng, J. Shen, P. Huang, S. Guo, J. Pan, and B. Feng, Dual functional carbon dots derived from cornflour *via* a simple one-pot hydrothermal route, *Mater. Lett.*, Vol. 123, p. 107, 2014.

36. X. Zhang, S. Wang, C. Zhu, M. Liu, Y. Ji, L. Feng, L. Tao, and Y. Wei, Carbon-dots derived from nanodiamond: Photoluminescence tunable nanoparticles for cell imaging, *J. Colloid Interface Sci.*, Vol. 397, p. 39, 2013.
37. Y. Y. Zhang, M. Wu, Y. Q. Wang, X. W. He, W. Y. Li, and X. Z. Feng, A new hydrothermal refluxing route to strong fluorescent carbon dots and its application as fluorescent imaging agent, *Talanta*, Vol. 117, p. 196, 2013.
38. H. Nie, M. Li, Q. Li, S. Liang, Y. Tan, L. Sheng, W. Shi, and S. X. Zhang, Carbon dots with continuously tunable full-color emission and their application in ratiometric pH sensing, *Chem. Mater.*, Vol. 26, p. 3104, 2014.
39. S. K. Bhunia, N. Pradhan, and N. R. Jana, Vitamin B_1 derived blue and green fluorescent carbon nanoparticles for cell-imaging application, *ACS Appl. Mater. Interfaces*, Vol. 6, p. 7672, 2014.
40. Z. A. Qiao, Y. Wang, Y. Gao, H. Li, T. Dai, Y. Liu, and Q. Huo, Commercially activated carbon as the source for producing multicolor photoluminescent carbon dots by chemical oxidation, *Chem. Commun.*, Vol. 46, p. 8812, 2010.
41. F. Wang, Z. Xie, H. Zhang, C. Y. Liu, and Y. G. Zhang, Highly luminescent organosilane-functionalized carbon dots, *Adv. Funct. Mater.*, Vol. 21, p. 1027, 2011.
42. C. Liu, P. Zhang, F. Tian, W. Li, F. Li, and W. Liu, One-step synthesis of surface passivated carbon nanodots by microwave assisted pyrolysis for enhanced multicolor photoluminescence and bioimaging, *J. Mater. Chem.*, Vol. 21, p. 13163, 2011.
43. Y. Yang, J. Cui, M. Zheng, C. Hu, S. Tan, Y. Xiao, Q. Yang, and Y. Liu, One-step synthesis of amino-functionalized fluorescent carbon nanoparticles by hydrothermal carbonization of chitosan, *Chem. Commun.*, Vol. 48, p. 380, 2012.
44. A. Jaiswal, S. S. Ghosh, and A. Chattopadhyay, One step synthesis of C-dots by microwave mediated caramelization of poly(ethylene glycol), *Chem. Commun.*, Vol. 48, p. 407, 2012.
45. C. W. Lai, Y. H. Hsiao, Y. K. Peng, and P. T. Chou, Facile synthesis of highly emissive carbon dots from pyrolysis of glycerol; gram scale production of carbon dots/mSiO_2 for cell imaging and drug release, *J. Mater. Chem.*, Vol. 22, p. 14403, 2012.
46. J. Wei, J. Shen, X. Zhang, S. Guo, J. Pan, X. Hou, H. Zhang, L. Wang, and B. X. Feng, Simple one-step synthesis of water-soluble fluorescent carbon dots derived from paper ash, *RSC Adv.*, Vol. 3, p. 13119, 2013.
47. Y. Xu, M. Wu, Y. Liu, X. Z. Feng, X. B. Yin, X. W. He, and Y. K. Zhang, Nitrogen-doped carbon dots: A facile and general preparation method, photoluminescence investigation, and imaging applications, *Chem. Eur. J.*, Vol. 19, p. 2276, 2013.
48. R. Liu, D. Wu, S. Liu, K. Koynov, W. Knoll, and Q. Li, An aqueous route to multicolor photoluminescent carbon dots using silica spheres as carriers, *Angew. Chem. Int. Ed.*, Vol. 48, p. 4598, 2009.
49. P. C. Hsu, Z. Y. Shih, C. H. Lee, and H. T. Chang, Synthesis and analytical applications of photoluminescent carbon nanodots, *Green Chem.*, Vol. 14, p. 917, 2012.

50. B. Han, W. Wang, H. Wu, F. Fang, N. Wang, X. Zhang, and S. Xu, Polyethyleneimine modified fluorescent carbon dots and their application in cell labeling, *Colloids Surf., B*, Vol. 100, p. 209, 2012.
51. C. H. Lee, R. Rajendran, M. S. Jeong, H. Y. Ko, J. Y. Joo, S. Cho, Y. W. Chang, and S. Kim, Bioimaging of targeting cancers using aptamer-conjugated carbon nanodots, *Chem. Commun.*, Vol. 49, p. 6543, 2013.
52. H. Ding, L. W. Cheng, Y. Y. Ma, J. L. Kong, and H. M. Xiong, Luminescent carbon quantum dots and their application in cell imaging, *New J. Chem.*, Vol. 37, p. 2515, 2013.

7

Enzyme Sensors Based on Nanostructured Materials

Nada F. Atta*, Shimaa M. Ali, and Ahmed Galal

Department of Chemistry, Faculty of Science, Cairo University, Giza, Egypt

Abstract

Carbon nanotubes, magnetic nanoparticles, and quantum dots have many distinct properties that may be exploited to develop next the generation of sensors. They play an important role in the detection of DNA, RNA, proteins, glucose, pesticides, and other small molecules from clinical samples, food industrial samples, as well as environmental monitoring. This chapter is targeting people in engineering fields, who build biosensors/biosystems, and researchers in molecular biology who use these technologies.

Keywords: Carbon nanotubes, magnetic nanoparticles, quantum dots, enzyme sensors

7.1 Biosensors and Nanotechnology

Many interests have been directed to the biosensing of drugs and biological molecules [1–3]. The nanotechnology of sol–gel based on molecular recognition [4,5] and nanoparticles (NPs) play a very important role in scientific researches [6–10]. Due to extremely small size of nanomaterials, they are more readily taken up by the human body. Nanomaterials are able to cross biological membranes and access cells, tissues, and organs that larger-sized particles normally cannot. NPs are stable, solid colloidal particles and range in size from 10 to 1,000 nm. Drugs can be absorbed onto the particle surface, entrapped inside the particle, or dissolved within the particle matrix. NPs have benefits because of its size. Because of their size,

**Corresponding author*: nada_fah1@yahoo.com

Ashutosh Tiwari, Hirak K. Patra and Anthony P.F. Turner (eds.) Advanced Bioelectronic Materials, (229–276)

they can easily enter small places. NPs have attracted the attention of scientists because of their multifunctional character. NPs have large surface area to volume ratio that helps in diffusion also leading to special properties such as increased heat and chemical resistance.

The development of active nanostructures, capable of performing a function or executing a specific task, is currently a major focus of research efforts in bio-/nanotechnology. One already highly successful nanodevice paradigm is the nanosensor: a designed nanostructure, which can provide information about its local environment through its response. Nanomaterials are exquisitely sensitive chemical and biological sensors. Each sensor should be sensitive for one chemical or biological component of a substance. Thus, by having sensor arrays it is possible to tell the composition of an unknown substance. The application area will be wide, encompassing food industry, detection of pollution, medical sector, brewery, etc. A nanobiosensor also referred to a nanosensor, is a biosensor with dimensions on the nanometer scale (1 nm = 10^{-9} m). So, nanosensors are any biological, chemical, or physical sensory points used to convey information about NPs to the macroscopic world. Though humans have not yet been able to synthesize nanosensors, predictions for their use mainly include various medicinal purposes and as gateways to building other nanoproducts, such as computer chips that work at the nanoscale and nanorobots. Presently, there are several ways proposed to make nanosensors, including top-down lithography, bottom-up assembly, and molecular self-assembly. As will follow, various kinds of nanomaterials have been being actively investigated for their applications in biosensors, such as carbon nanotubes (CNTs), magnetic NPs (MNPs), and quantum dots (QDs) which have been applied for the detection of DNA, RNA, proteins, glucose, pesticides, and other small molecules from clinical samples, food industrial samples, as well as environmental monitoring.

7.2 Biosensors Based on Carbon Nanotubes (CNTs)

Since their discovery in 1991 [11], CNTs have generated great interest in future applications based on their field emission and electronic transport properties, their high mechanical strength and their chemical properties. There is increasing potential for CNTs to be used as field emission devices, nanoscale transistors, tips for scanning microscopy, or components for composite materials. CNTs are one of the most commonly used building blocks of nanotechnology. With 100 times the tensile strength of steel, thermal conductivity better than all but the purest diamond, and electrical conductivity similar to copper, but with the ability to carry much

higher currents, they are very interesting. CNTs include both single-walled and multi-walled structures (Figure 7.1). Single-walled CNTs (SWCNTs) (Figure 7.1A) comprise of a cylindrical graphite sheet of nanoscale diameter capped by hemispherical ends. The closure of the cylinder is result of pentagon inclusion in the hexagonal carbon network of the nanotube walls during the growth process. SWCNTs have diameters typically 1 nm with the smallest diameter reported to date of 0.4 nm. This corresponds to the theoretically predicted lower limit for stable SWCNT formation based on consideration of the stress energy built into the cylindrical structure of the SWCNT. The multi-walled CNTs (MWCNTs) (Figure 7.1B) comprise several to tens of incommensurate concentric cylinders of these graphitic shells with a layer spacing of 0.3–0.4 nm. MWCNTs tend to have diameters in the range 2–100 nm. The MWCNT can be considered as a mesoscale graphite system, whereas the SWCNT is truly a single large molecule.

CNTs can have metallic or semiconducting properties. Because of the small diameter of CNTs, CNTs combine in a unique way high electrical conductivity, high chemical stability and extremely high mechanical strength. These special properties of both SWCNTs and MWCNTs have attracted the interest of many researchers in the field of electrochemical sensors. CNTs can be either used as single probes after formation in situ or even individually attached onto a proper transducing surface after synthesis. Both SWCNTs and MWCNTs can be used to modify several electrode surfaces in either vertically oriented "nanotube forests" or even a non-oriented way. They can be also used in sensors after mixing them with a polymer matrix to form CNT composites.

The remarkable physical properties of CNTs create a host of application possibilities. Some of these are derived as an extension of traditional carbon, carbon fiber or bead applications, but many are new possibilities, based on the novel electronic and mechanical behavior of CNTs. The

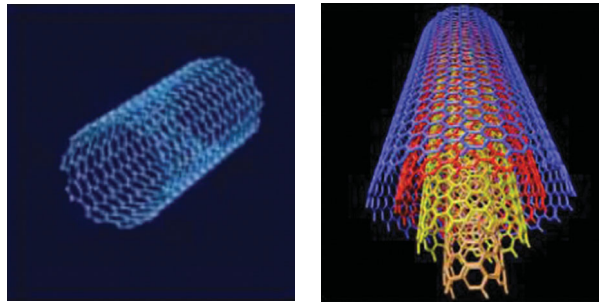

Figure 7.1 Schematics of an individual (A) SWCNT and (B) MWCNT [12].

excitement in this field arises from the versatility of CNT material and the possibility of predicting novel properties and applications. There are various advantages that CNTs bring to electrochemical-sensor design. Perhaps the most attractive feature of the CNT enzyme-based biosensor found to date is improved operational stability. Nevertheless, to assess the feasibility and the advantages of using CNTs in designing sensors, there needs to be thorough examination and resolution of issues, such as how CNTs are produced and dispersed, surface chemistry and morphology, effective surface area, and presence of metal impurities. Works reported to date have tried to provide evidence of the electrochemical activity of CNT-based electrochemical sensors, including potential shifts compared to the corresponding non-modified sensors. The majority of the authors agree that the presence of oxidants, such as strong acids, can open the ends of CNTs or introduce defects in their sidewalls [13,14]. Acid treatment (purification and/or casting) also introduces oxygen-containing surface groups (e.g., carboxyl or quinone), which are believed to improve the electrocatalytic properties of CNTs. The extent to which different factors affect the electrochemical behavior depends on the mechanisms of the particular redox systems. Contrary to this widespread opinion, Musameh et al. [15] demonstrated that introducing oxygen functionalities at the end of the caps or the walls does not enhance the electrocatalytic ability of CNTs. Oxidation phenomena of CNTs need to be examined carefully in the future. The open ends of CNTs have been linked to edge planes of highly oriented pyrolytic graphite (HOPG) with the nanotube walls suggested to have properties similar to those of basal planes of HOPG electrodes [16,17]. Compton recently demonstrated evidence that electrocatalytic properties of MWCNTs originate from their ends [18,19]. He showed that MWCNTs have an electrocatalytic effect similar to edge planes of HOPG and carbon powder, while fullerene (fullerene "ball-like" molecule does not contain any "open edges")-modified electrodes showed behavior similar to basal plane HOPG electrodes. This discovery is consistent with Wang's explanation of the electrocatalytical effect of CNTs and his description of the electrochemical activation of MWCNTs [14]. He compared two different types of MWCNT:

1. One produced by the arc method, which creates CNTs with closed (fullerene-like) ends.
2. The other produced by the chemical vapor deposition (CVD) method, which creates MWCNTs with open ends [14,20].

The open-ended, CVD-produced MWCNTs showed higher electrocatalytic activity than the end-capped, arc-produced MWCNTs. Anodic

pretreatment of the arc produced MWCNTs resulted in dramatic improvement in their electrochemical activity, while anodic pretreatment of CVD-produced MWCNTs did not show any significant difference. The authors suggested that anodization of arc produced CNTs produces stress on the CNTs and this effectively breaks their end caps. The exploitation of CNTs in the design of electrochemical sensors is still in its infancy. Future efforts should aim at better understanding the structural electrochemical reactivity of CNT-modified electrodes and the factors that govern the electron transfer kinetics of these attractive devices, so as to avoid precipitate conclusions in attributing electrocatalytic properties to nanotubes without conducting the appropriate control experiments. It was shown that, in some cases, the electrocatalytic effect of carbon powder is similar to that of CNTs [18,19], while, in other cases, there is a huge difference between carbon powder and CNTs [21,22]. Interesting information on electrochemical properties of CNTs can be also obtained from studies (i.e., impedance spectroscopy [23]) for other applications. The research in the applications of CNTs to sensors can also take advantage of a variety of CNT applications in materials science. Other configurations of CNTs can be foreseen in future applications of electrochemical sensors. For example, small-diameter zigzag SWCNTs, produced by cross linking of side walls of short CNTs, should show novel physical, chemical, and electronic properties [24]. DNA-directed self-assembly of CNTs [25] can also bring new possibilities for CNT configurations to sensor applications. The combination of the electronic properties and the dimensions of CNTs make them ideal building blocks for molecular electronics. The reported technology based on the use of a DNA-scaffold molecule, which provides the address for precise localization of a semiconducting SWCNT [26] as well as the template for the extended metallic wires contacting it, may open new possibilities for designing individual CNT sensors. The possibility of producing an SWCNT nanoelectrode may also open the way to electrochemical studies of single redox molecules [27].

As will follow, CNTs have been demonstrated as biosensors for glucose, cholesterol, tyrosinase, urease, acetylcholinesterase (AChE), horseradish peroxidase (HRP), and DNA detection, and their performance has been found to be much superior to those of other carbon electrodes in terms of reaction rate, reversibility, and detection limit.

7.2.1 Glucose Biosensors

The bioelectrochemical characteristics of a novel MWCNT-based biosensor for glucose detection are studied and compared with those of glassy

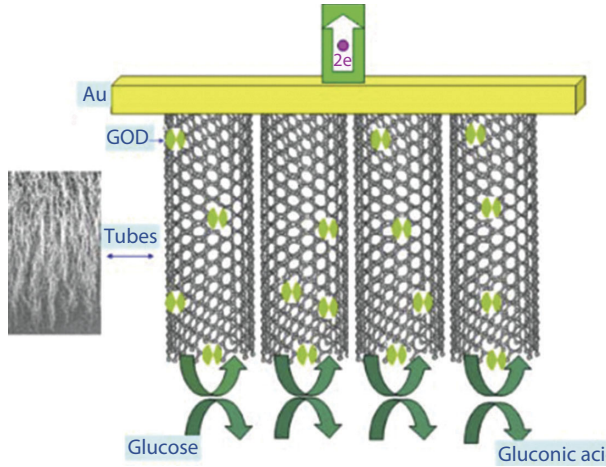

Figure 7.2 Schematic illustration of the MWCNT-based biosensor for glucose detection [28].

carbon (GC)-based biosensor [28]. The MWCNT-based biosensor exhibits a strong glucose response at applied potentials of 0.65 and 0.45 V versus Ag/AgCl, respectively, while GC-based biosensor shows a weak glucose response at 0.65 V and no response at 0.45 V. Besides, the MWCNT-based biosensor shows a high stability of 86.7% of the initial activity to glucose after 4-month storage, much higher than 37.2%, the corresponding value for a GC-based biosensor.

An amperometric glucose biosensor was formed by cross-linking glucose oxidase (GOx) on nanocomposite material prepared by entrapping silica gel (SG) and MWCNT in polyacrylonitrile (PAN) film [29]. SG/MWCNT/PAN/GOD has linear range for the detection of glucose from 5 μM to 2 μM (a correlation coefficient of 0.999) with 16 s response time. The sensitivity of the biosensor was found to be 16.5 μA/μM. Moreover, its experimental detection limit is 1 μM [signal-to-noise (S/N) ratio= 3] and the apparent Michaelis–Menten constant was calculated to be 13.9 μM. The designed biosensor is stable in the period of 30 days and retains 70% of its activity. This is due to the appropriate compound of the nanocomposite matrix for GOx immobilization. SG provides higher specific surface for immobilization and enhanced hydrophilic properties of matrix. The high sensitivity of the biosensor implies that MWCNT can provide superior conductivity for electron transfer. Thus, the biosensor performance was effectively improved. All the results show that SG/MWCNT/PAN/GOx can provide a promising material for the biosensor designs and other biological applications.

A glucose biosensor has been fabricated by immobilizing GOx into a sol–gel composite at the surface of a basal plane pyrolytic graphite (bppg) electrode modified with MWCNT [38]. First, the bppg electrode is subjected to abrasive immobilization of CNTs by gently rubbing the electrode surface on a filter paper supporting the CNTs. Second, the electrode surface is covered with a thin film of a sol–gel composite containing encapsulated GOx. The CNTs offer excellent electrocatalytic activity toward reduction and oxidation of hydrogen peroxide liberated in the enzymatic reaction between GOx and glucose, enabling sensitive determination of glucose. The amperometric detection of glucose is carried out at 0.3 V (vs saturated calomel electrode)

Table 7.1 Performances of SG/MWCNT/PAN/GOx biosensor compared to the previously reported biosensors [29].

References	Km (μM)	Detection limit (μM)	Sensitivity (μA/μM)	Configuration of biosensor
[29]	13.9	1	16.52	SG /MWCNT/PAN/ GOx
[30]	–	50	0.196	Silica sol–gel/GOx/ CNTs
[31]	22	–	0.6	Sol–gel/GOx/copolymer of poly(vinyl alcohol) with 4-vinylpyridine
[32]	20.3	10	–	SG/GOx
[33]	14.4	1	4.20 mA/ Mcm^{-2}	PAN/GOx
[34]	7.3	0.5	6.82 mA/ Mcm^{-2}	poly(acrylonitrile-co-acrylic acid) (PANAA)/GOx
[35]	18	1	16 mA/ Mcm^{-2}	Polyaniline (PANI)/ poly(AN-co-AA)/ GOx
[36]	10.12	1	3.7048	polymethylmethacrylate (PMMA)–MWCNT(PDDA)/ GOx–nanofibrous electrode (NFE)
[37]	8.9	250 nM	50.2 mA/ Mcm^{-2}	PDDA/GOx/ZnO/ MWCNTs

in 0.05 M phosphate buffer solution (pH 7.4) with linear response range of 0.2–20 μM glucose, sensitivity of 196 nA/μM, and detection limit of 50 μM (S/N = 3). The response time of the electrode is <5s when it is stored dried at 4 °C, the sensor showed almost no change in the analytical performance after operation for 3 weeks. This CNT sol–gel biocomposite GOx sensor showed excellent properties for the sensitive determination of glucose with good reproducibility, remarkable stability, and rapid response and in comparison to bulk-modified composite biosensors the amounts of enzyme and CNT needed for electrode fabrication are dramatically decreased.

The GOx is entrapped in the composite of CNTs/chitosan (CS) and direct electron transfer reaction between GOx and electrode takes place [39]. The electron transfer rate of GOx is greatly enhanced to 7.73 s^{-1} in the system, which is more than one-fold higher than that of flavin adenine dinucleotide adsorbed on the CNTs (3.1 s^{-1}). This may be results from the conformational change of GOx in the microenvironment enabling the accessibility of active site for GOx to the electrode. Additionally, the bioactivity of GOx modified in the composite on electrode surface is kept. So, as-prepared electrode can be used as a glucose biosensor exhibiting higher sensitivity (0.52 μA.μM^{-1}) and better stability. The facile procedure of immobilizing GOx will promote the developments of electrochemical research for protein, biosensors and other bioelectrochemical devices.

By combining the advantageous features of CNTs and Au–Pt bimetallic NPs, a novel glucose biosensor has been constructed by integrating CNTs

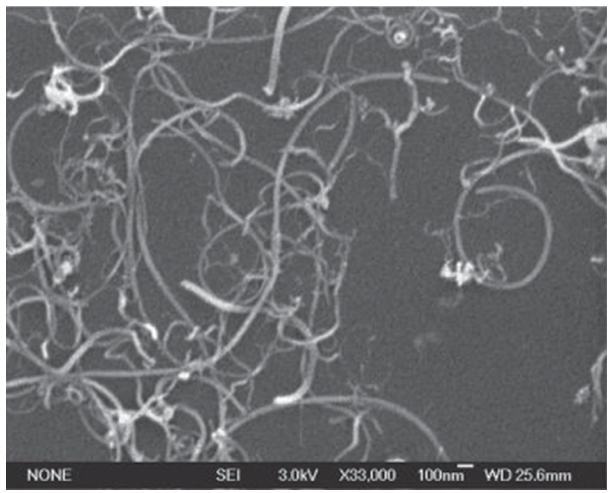

Figure 7.3 Scanning electron microscopy (SEM) image of CNTs used to fabricate CNT-modified bppg electrode; magnification 33,000 [38].

with Au–Pt alloy NPs [40]. A novel glucose biosensor was constructed, based on the immobilization of GOx with cross-linking in the matrix of biopolymer CS on a glassy carbon electrode (GCE), which was modified with gold–platinum alloy NPs (Au–PtNPs) by electrodeposition on MWCNT in CS film (CNTs/CS). Primary study indicated that Au–PtNPs/CNTs had a better synergistic electrocatalytic effect on the reduction of hydrogen peroxide than did AuNPs/CNTs or PtNPs/CNTs at a low applied potential window. With GOx as a model enzyme, a new glucose biosensor was fabricated. The biosensor exhibited excellent performances for glucose at a low applied potential (0.1 V) with a high sensitivity (8.53 $\mu A.\mu M^{-1}$), a low detection limit (0.2 μM), a wide linear range (0.001–7.0 μM), a fast response time (<5 s), and good reproducibility, stability, and selectivity. In addition, the biosensor was applied in the determination of glucose in human blood and urine samples.

7.2.2 Cholesterol Biosensors

A CNT-modified biosensor for monitoring total cholesterol in blood was studied by Li *et al.* [41]. This sensor consists of a carbon working electrode and a reference electrode screen-printed on a polycarbonate substrate. Cholesterol esterase, cholesterol oxidase, peroxidase, and potassium ferrocyanide were immobilized on the screen-printed carbon electrodes (SPCEs). MWCNTs were added to prompt electron transfer. Experimental results show that the CNT-modified biosensor offers a reliable calibration profile and stable electrochemical properties. The modification of the CNTs promoted the electron transfer so as to improve the sensitivity of the cholesterol sensor. Within the total cholesterol range of 100–400 mg/dl,

Table 7.2 Determination of glucose in human blood and urine samples [40].

Determination of glucose in human blood and urine samples						
Sample	**Hospital (mM)**	**Biosensor (mM)**	**Relative error (%)**	**RSD (%)**	**Added (mM)**	**Recovery (%)**
Blood	3.40	3.78	11.1	3.21	0.4	98.5
	7.08	7.02	–0.9	3.45	0.4	97.6
	6.24	6.28	0.7	2.81	0.4	103.3
Urine	7.83	7.76	–0.9	3.12	0.4	98.8
	3.87	3.80	–1.9	3.57	0.4	96.8

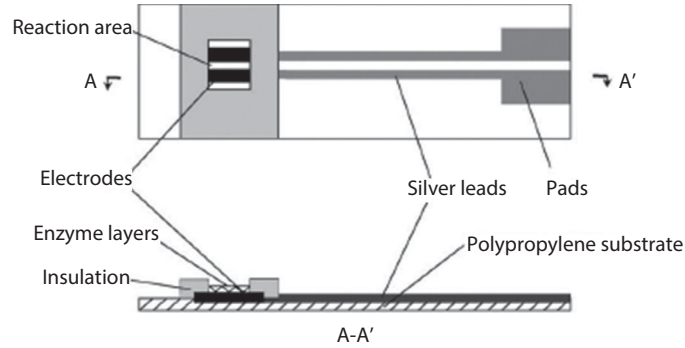

Figure 7.4 The structure of the cholesterol biosensor [41].

the testing results have shown a fairly good correlation with clinical laboratory method while only 2 μL blood sample was required for a test. The screen-printing method provides a way for rapid, economic and reproducible manufacture of sensor electrode. The sensor developed did therefore provide a promising economic and easy method for monitoring the total cholesterol in blood.

Nanocomposite film composed of PANI and MWCNTs, prepared electrophoretically onto indium tin oxide (ITO)-coated glass plate, was used for covalent immobilization of cholesterol oxidase (ChOx) via N-ethyl-N0-(3-dimethylaminopropyl) carbodiimide (EDC) and N-hydroxysuccinimide (NHS) chemistry [42]. Results of linear sweep voltammetric measurements reveal that ChOx/PANI–MWCNT/ITO bioelectrode can detect cholesterol in the range of 1.29–12.93 μM with high sensitivity of 6800 $nA.\mu M^{-1}$ and a fast response time of 10 s. Photometric studies for ChOx/PANI–MWCNT/ITO bioelectrode indicate that it is thermally stable up to 45 °C and has a shelf life of approximately 12 weeks when stored at 45 °C. The results of these studies have implications for the application of this interesting matrix (PANI–MWCNT) toward the development of other biosensors.

A highly sensitive and fast-response biosensor was successfully fabricated [49]. Platinum NPs were electrochemically deposited in MWCNT–CS matrix by a cyclic voltammetry (CV) method. A Pt(IV) complex was reduced to Pt on the surface of MWCNTs. The doped Pt NPs demonstrate the abilities to electrocatalyze the oxidation of hydrogen peroxide and substantially raise the response current. The results indicated that the Pt NPs exhibited efficiently electrocatalytic activity. The influence of enzyme loading within the MWCNT–CS–Pt–ChOx nanobiocomposite was explored

Table 7.3 Characteristics of electrophoretically deposited PANI–MWCNT-based ChOx/PANI–MWCNT/ITO bioelectrode along with those reported in the literature [42].

Reference	Shelf life	Sensitivity	Transducer used	Linearity (μM)	Method of immobilization	Sensing element	Immobilization matrix
[43]	–	0.559 $\mu A.cm^{-2}$ μM^{-1}	Amperometric	0.5–6	Physical entrapment	ChOx	MWCNT
[44]	11 weeks	7.76×10^{-5} Abs. mg.dl	Spectrophotometric	0.6–10.3	Covalent	ChOx	PANI
[45]	15 days	-	Spectrophotometric	1.3–5.2	Covalent	ChOx	Fe_3O_4 NPs
[46]	10 days	69 $nA.\mu M^{-1}$	Square wave voltammetric	1–6	Biotin–Avidin	ChOx/ChEt	Thiotic acid/ gold
[47]	–	0.13 $\mu A.\mu M^{-1}$	Amperometric	0–2.1	Physical adsorption	ChOx	Gold electrode
[48]	2 months	0.0059 $\mu A.mg^{-1}.dl$	Amperometric	2.5–10.3	Physical adsorption	ChOx, ChEt, HRP, $K_4Fe(CN)_6$	MWCNT/SPCE
[42]	12 weeks	6800 $nA.\mu M^{-1}$	Amperometric and spectroscopic	1.2–12.9	Covalent	ChOx	PANI–MWCNT

to optimize the electroanalytical performance of the cholesterol biosensor. The optimized cholesterol biosensor shows a sensitivity of 0.044 $A.M^{-1}.cm^{-2}$ and a response time of about 8 s. No response currents were observed at the MWCNT–CS–Pt–ChOx nanobiocomposite-modified electrode after the additions of 100 μM glucose and 1 μM ascorbic acid to 100 μM cholesterol in 0.1 M phosphate buffer solution (pH 7) in the interference study. The prepared cholesterol biosensor retained 60% of initial activity after 7 days when stored in 0.1 M phosphate buffer solution at 4°C. A novel amperometric biosensor was fabricated based on the immobilization of ChOx into a cross-linked matrix of CS (Chi)–room-temperature ionic liquid (IL) (1-butyl-3-methylimidazolium tetrafluoroborate) [50]. Initially, the surface of bare electrode (ITO-coated glass) was modified with the electrodeposition of Au particles onto thiol (–SH) functionalized MWCNTs. The biosensor electrode is designated as MWCNT(SH)–Au/Chi–IL/ChOx. SEM image of MWCNT(SH)–Au/Chi–IL/ChOx reveals that Chi–IL exists as the interconnected wires covering the Au particles on the surface of MWCNT(SH)–Au. The presence of Au particles in the matrix of CNTs provides an environment for the enhanced electrocatalytic activities. The MWCNT(SH)–Au/Chi–IL/ChOx biosensor exhibited a linear response to cholesterol in the concentration range of 0.5–5 μM with a correlation coefficient of 0.998, good sensitivity (200 $\mu A.M^{-1}$), a low response time (~7 s), repeatability (R.S.D value of 1.9%) and long-term stability (20 days with a decrease of 5% response). The synergistic influence of MWCNT(SH), Au particles, Chi, and IL contributes to the excellent performance for the biosensor.

7.2.3 Tyrosinase Biosensors

Amperometric biosensors for the determination of phenolic compounds (phenol, *o*-cresol, *p*-cresol, *m*-cresol, catechol, dopamine, and epinephrine) have been constructed by Yu-Chen Tsai [51]. It comprises a MWCNTs conduit, a Nafion backbone, and a tyrosinase function. The modification of GCE is made by a simple solution-evaporation method. The resulting MWCNT-nafiontyrosinase (MWCNT-nafion-Tyr) nanobiocomposite film-modified electrode is inexpensive, reliable, and easy to use. The homogeneity of the MWCNT-nafion-Tyr nanobiocomposite films was characterized by atomic force microscopy (AFM). The measurement of phenolic compounds is based on the signal produced by the electrochemical reduction of *o*-quinones, the product of the enzymatic reaction. Optimization studies were performed in stirred solution and the magnitude of response currents were found to be dependent on applied potential and enzyme loading. The

Table 7.4 Performance of the biosensors based on MWCNT-nafion-Tyr nano-biocomposite film-modified GCE to various phenolic compounds [51].

Response time (s)	K_{mapp} (μM)	Detection limit (μM)	r	Sensitivity (μA.μM^{-1})	Linear range (μM)	Substrate
< 8	52	0.13	0.998	303	1–19	Phenol
< 20	16	0.28	0.997	135	1–13	*m*-Cresol
< 20	13	0.34	0.997	59	1–11	*p*-Cresol
–	–	–	–	–	–	*o*-Cresol
< 8	26	0.22	0.997	346	1–23	Catechol
< 20	60	0.52	0.998	12	5–23	Dopamine
–	–	–	–	–	–	Epinephrine

optimized biosensor for phenol determination displayed a sensitivity of 303 μA.μM^{-1} and a response time of less than 8 s.

A flow injection catechol biosensor based on tyrosinase entrapped in CNT-modified polypyrrole (PPy) biocomposite film on a GC surface has been developed [52]. Amperometric response was measured as a function of concentration of catechol, at a fixed bias voltage of –50 mV at a flow rate of 1 mL/min. The proposed biosensor exhibited impressive analytical performance such as a linear range between 3 and 50 μM, a short response time (10 s), a detection limit of 0.671 μM, and an excellent operational (with a relative standard deviation of 0.54%) and long-term stability (85% remained after 10th week). CNT was shown to enhance the electron transfer between the electrode and enzyme and capable to carry higher bioactivity owing to its intensified surface area.

An amperometric bisphenol A (BPA) biosensor was fabricated by immobilizing tyrosinase on MWCNTs-cobalt phthalocyanine (CoPc)-silk fibroin (SF) composite-modified GCE [53]. In MWCNTs-CoPc-SF composite film, SF provided a biocompatible microenvironment for the tyrosinase to retain its bioactivity, MWCNTs possessed excellent inherent conductivity to enhance the electron transfer rate and CoPc showed good electrocatalytic activity to electro-oxidation of BPA. The cyclic voltammogram of BPA at this biosensor exhibited a well defined anodic peak at 0.625 V. Compared with bare GCE, the oxidation signal of BPA significantly increased; therefore, this oxidation signal was used to determine BPA. Under optimum conditions, the oxidation current was proportional to BPA concentration in the range from 5.0×10^{-8} to 3.0×10^{-6} M with correlation coefficient of 0.9979 and detection limit of 3.0×10^{-8} M (S/N = 3).

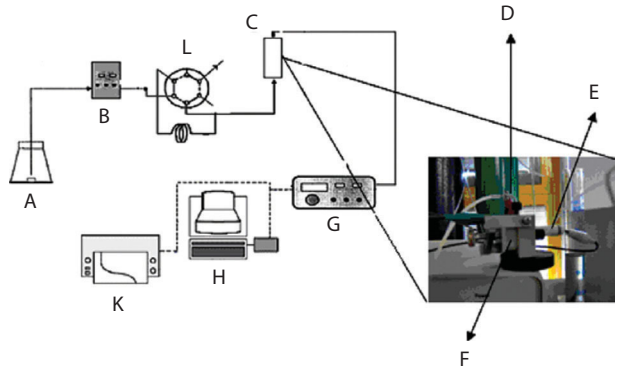

Figure 7.5 Schematic diagram of the flow injection biosensor: running solution (A), High-performance liquid chromatography (HPLC) pump (B), injection valve (L), flow cell (C), Pt counter electrode (D), Ag/AgCl reference electrode (E), GC working electrode (F), potentiostat (G), computer (H), and data recorder (K) [52].

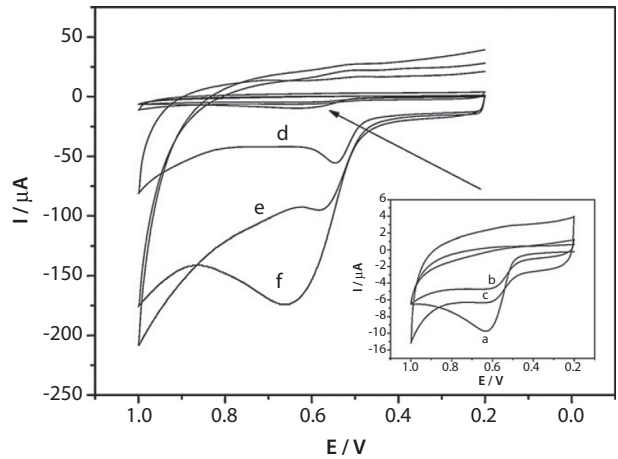

Figure 7.6 Cyclic voltammograms of 2.5 µM BPA at GCE (a), Tyr/GCE (b), Tyr-SF/GCE (c), MWCNTs-CoPc/GCE (d), Tyr-MWCNTs-CoPc/GCE (e), and Tyr-SF-MWCNTs-CoPc/GCE (f) in 0.1 M PBS (pH 7.4). Scan rate: 100 mV.s^{-1} [53].

The proposed method was successfully applied to determine BPA in plastic products and the recovery was in the range from 95.36% to 104.39%.

Tyrosinase (TYR, EC 1.14.18.1) was physically adsorbed onto a carbon felt (CF) together with acridine orange (AO) [54]. Co-adsorption of AO was essential to prevent the denaturation of the TYR at the CF surface. The resulting TYR and AO-coadsorbed CF (TYR/AOCF) was successfully utilized as a detection unit of novel and highly sensitive amperometric flow-biosensor for toxic chlorophenol compounds. Standard solutions of

phenolic compounds (200 μL) were injected, and the cathodic peak currents due to the reduction current of *o*-quinones produced by the TYR-catalyzed oxidation (phenolase activity) were detected at the applied potential of –50 mV versus Ag/AgCl. In this reaction, the electrochemically generated catechol compounds from *o*-quinones are re-oxidized repeatedly by catecholase activity of the TYR, leading to a sufficient amplified signal. The TYR/AO-CF exhibited much higher selectivity toward *p*-chlorophenol as compared with other chlorophenol compounds. When 0.1 mol/L phosphate buffer (pH 7.0) was used as a carrier at flow rate of 3.0 mL/min, cathodic peaks for *p*-chlorophenol was linear in the concentration range between 0.1 and 10 μmol/L (sensitivity: 1.41 (mA·L)/mmol) with sampling rate (30 samples/h), and the detection limit of *p*-chlorophenol was found to be 2.13×10^{-8} mol/L (S/N = 3. The ratio of signal and noise is 3). The TYR/AO-CF kept more than 80% of original activity after the storage in 0.1 mol/L phosphate buffer (pH 7.0) containing 0.2 mmol/L AO at 4 °C.

7.2.4 Urease Biosensors

A novel potentiometric urea biosensor has been fabricated with urease (Urs) immobilized MWCNTs embedded in silica matrix deposited on the surface of ITO-coated glass plate [55]. The enzyme Urs was covalently linked with the exposed free –COOH groups of functionalized MWCNTs (F-MWCNTs), which are subsequently incorporated within the silica matrix by sol–gel method. The synergistic effect of silica matrix, F-MWCNTs and biocompatibility of Urs/MWCNTs/SiO2 made the biosensor to have the excellent electro catalytic activity and high stability. The resulting biosensor exhibits a good response performance to urea detection with a wide linear range from 2.18×10^{-5} to 1.07×10^{-3} M urea. The biosensor shows a short response time of 10–25 s and a high sensitivity of 23 mV/decade/cm^2.

The pH-sensitive property of the SWCNT-modified electrode based on the electroactive group on the SWCNT was explored by differential pulse voltammetry (DPV) technique [56]. In pH range 1–13 investigated in Britton–Robinson (B–R) buffer, the anodic peak shifted negatively along with the increase of pH exhibiting a reversible Nernstian response. Experiments were carried out to investigate the response of the SWCNT-modified electrode to analytes associated with pH change. The response behavior of the modified electrode to ammonia was studied as an example. The potential response could reach equilibrium within 5 min. The modified electrode had good operational stability. Voltammetric urease and AChE biosensors were constructed by immobilizing the enzymes with

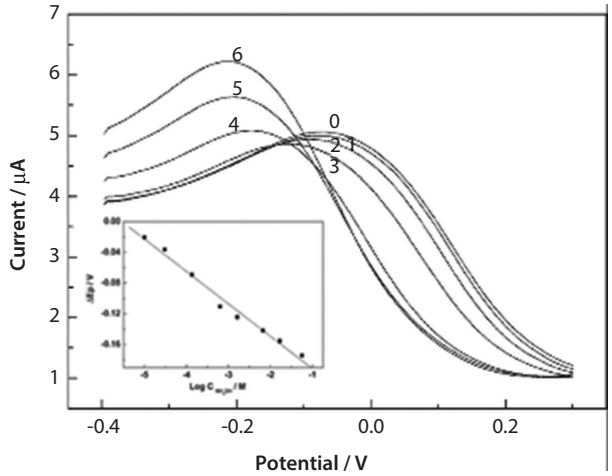

Figure 7.7 The DPV of the SWCNT-modified electrode in 0.1 M NaCl at different concentrations of ammonia (0) 0, (1) 1.00×10^{-5}, (2) 3.00×10^{-5}, (3) 1.30×10^{-4}, (4) 6.30×10^{-4}, (5) 1.63×10^{-3}, and (6) 6.63×10^{-3} M. The inset is The SWCNT-peak-potential shift as a function of the logarithm of ammonia concentration [56].

sol–gel hybrid material. The maximum potential shift could reach 0.130 and 0.220 V for urea and acetylthiocholine (ATCl), respectively. The methods for preparing sensor and biosensor were simple and reproducible and the range of analytes could be extended to substrates of other hydrolyases and esterases. This broadened the biosensor application of CNT in electrochemical area.

7.2.5 Acetylcholinesterase Biosensors

A highly sensitive amperometric biosensor for organophosphates (OPs) pesticides based on immobilization of AChE on MWCNTs-β-cyclodextrin (β-CD) composite-modified GCE was reported by Dan Du et al. [57]. Due to the good dispersibility and porous structures of MWCNTs-β-CD composite, the resulting surface provided a favorable microenvironment for AChE biosensor fabrication and maintained the bioactivity of AChE for screening of OPs exposure. MWCNTs promoted electron transfer reactions at a lower potential and catalyzed the electro-oxidation of thiocholine, thus increasing detection sensitivity. Based on the inhibition of OPs on the AChE activity, using dimethoate as a model compound, the inhibition of dimethoate was proportional to its concentration ranging from 0.01 to 2.44 and 2.44 to 10.00 μM, with a detection limit was 2 nM (S/N = 3). The developed biosensor exhibited good reproducibility and acceptable

stability, thus providing a new promising tool for analysis of enzyme inhibitors. A simple method to immobilize AChE on PPy and PANI copolymer doped with MWCNTs was also proposed [58]. The synthesized PAn-PPy-MWCNTs copolymer presented a porous and homogeneous morphology which provided an ideal size to entrap enzyme molecules. Due to the biocompatible microenvironment provided by the copolymer network, the obtained composite was devised for AChE attachment, resulting in a stable AChE biosensor for screening of OPs exposure. MWCNTs promoted electron transfer reactions at a lower potential and catalyzed the electro-oxidation of thiocholine, thus increasing detection sensitivity. Based on the inhibition of OPs on the AChE activity, using malathion as a model compound, the inhibition of malathion was proportional to its concentration ranging from 0.01 to 0.5 and from 1 to 25 μg/mL, with a detection limit of 1.0 ng/mL. The developed biosensor exhibited good reproducibility and acceptable stability, thus providing a new promising tool for analysis of enzyme inhibitors. In addition, immobilization of AChE on MWCNTs–CS (MC) composite was proposed and thus a sensitive, fast, and stable amperometric sensor for quantitative determination of organophosphorous insecticide was developed [59]. AFM showed that this matrix possessed homogeneously netlike structure, which prevented enzyme from leaving out of the electrode. MWCNTs promoted electron transfer reactions at a lower potential and catalyzed the electro-oxidation of thiocholine, thus increasing detection sensitivity. Under optimal conditions, the inhibition of triazophos was proportional to its concentration in two ranges, from 0.03 to 7.8 and 7.8 to 32 μM with a detection limit of 0.01 μM. A 95% reactivation of the inhibited AChE could be regenerated for using pralidoxime iodide within 8 min. The constructed biosensor processing prominent characteristics and performance such as good precision and reproducibility, acceptable stability and accuracy, fast response and low detection limit has potential application in the characterization of enzyme inhibitors and detection of toxic compounds against to enzyme.

A facile, one-step synthesis of nanocomposites using MWCNT coating gold NPs (GNPs) (MWCNTs-Au) was presented by Dan Du et al. [60]. SEM and UV–vis spectroscopy confirmed that more than 97% of GNPs have been loaded on the surface of CNTs without congregation. The formed MWCNTs-Au nanocomposites offered an extremely hydrophilic surface for biomolecule adhesion, leading to a stable AChE biosensor. Due to the excellent conductivity of the nanocomposites, the immobilized AChE showed favorable affinity to ATCl and could catalyze the hydrolysis of ATCl with a K^{m}_{app} value of 268 μM to form thiocholine, which was then oxidized to produce a detectable and fast response. Based on the inhibition

of OPs on the enzymatic activity of AChE, the magnitude of peak current from thiocholine on the biosensor is a simple and effective way to biomonitoring of OPs exposure. Using malathion as a model compound, the inhibition of malathion was proportional to its concentration ranging from 1.0 to 1000 ng.mL^{-1} and 2 to 15 μg.mL^{-1}, with a detection limit 0.6 ng.mL^{-1}. The developed biosensor exhibited good reproducibility and acceptable stability, thus providing a new promising tool for analysis of enzyme inhibitors.

7.2.6 Horseradish Peroxidase Biosensors

An amperometric biosensor based on HRP and CNT/PPy nanobiocomposite film on a gold surface has been developed [61]. The HRP was incorporated into the CNT/PPy nanocomposite matrix in one-step electropolymerization process without the aid of cross-linking agent. Amperometric response was measured as a function of concentration of phenol derivatives, at a fixed bias voltage of −50 mV. The linear range, sensitivity and detection limit of the biosensor were investigated for eighteen phenol derivatives. The sensitivity in the linear range increased in this order: 4-methoxyphenol > 2-aminophenol > guaiacol =*m*-cresol > 2-chlorophenol = 4-chlorophenol = hydroquinone = pyrocatechol > 2,6-dimethoxyphenol > 3-chlorophenol > *p*-cresol > *p*-benzoquinone = 4-acetamidophenol > catechol > phenol = pyrogallol = 2,4-dimethylphenol. CNTs were shown to enhance the electron transfer as a mediator and capable to carry higher bioactivity owing to its intensified surface area. The biosensor exhibited low detection limits with a short response time (2 s) for the tested phenolics compared to the reported working electrodes. It retained 70% of its initial activity after using for 700 measurements in 1 month.

The application of the composites of MWCNTs and core–shell organosilica at CS cross-linked nanospheres as an immobilization matrix for the construction of an amperometric hydrogen peroxide (H_2O_2) biosensor was described by Ruo Yuan et al. [62]. MWCNTs and positively charged organosilica at CS nanospheres were dispersed in acetic acid solution (0.6 wt%) to achieve organosilica at CS/MWCNTs composites, which were cast onto a glass carbon electrode (GCE) surface directly. And then, HRP, as a model enzyme, was immobilized onto it through electrostatic interaction between oppositely charged organosilica at CS nanospheres and HRP. The direct electron transfer of HRP was achieved at HRP/organosilica at CS/MWCNTs/GCE, which exhibited excellent electrocatalytic activity for the reduction of H_2O_2. The catalysis currents increased linearly to H_2O_2

Table 7.5 Calibration plot parameters and analytical characteristics for various phenolic compounds at CNT/PPy/HRP nanobio-composite film electrode [61].

RSD%	Response time (s)	Level of detection (LOD) (μM)	Linear range (μM)	Sensitivity (nA/μM)	*r*	Compound
2.89	2	3.52	16-44	1	0.99	Phenol
4.43	2	0.027	0.02-0.16	3	0.99	*p*-Benzoquinone
6.5	2	6.42	16-240	8	0.99	Hydroquinone
1.8	2	0.29	1.6-9.2	7	0.99	2,6-Dimethoxyphenol
1.7	2	0.26	1.6-8	8	0.99	2-Chlorophenol
1.1	2	0.2	1.6-12.8	6	0.99	3-Chlorophenol
1.87	2	0.3	1.6-14.4	8	0.99	4-Chlorophenol
5.4	2	1.53	8-60.8	40	0.99	2-Aminophenol
2.8	2	1.06	1.6-81.6	50	0.99	4-Methoxyphenol
6.7	2	6.27	1.6-446.4	8	0.99	Pyrocatechol
1.92	2	0.3	1.6-9.6	9	0.98	Guaiacol
2.84	2	1.5	8-20.8	9	0.99	*m*-Cresol
No response						*o*-Cresol
2.5	2	24	128-832	5	0.98	*p*-Cresol
3.8	2	0.93	1.6-8	2	0.98	Catechol
2.57	2	1.11	1.6-16	3	0.99	4-Acetamidophenol
1.2	2	1.24	1.6-22.4	1	0.98	Pyrogallol
2.2	2	27.9	64-240	1	0.98	2,4-Dimethylphenol

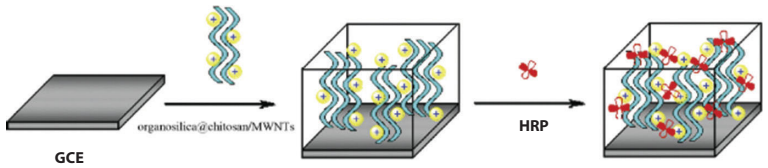

Figure 7.8 Illustration of the preparation process of the biosensor [62].

concentration in a wide range of 7.0×10^{-7} to 2.8×10^{-3} M, with a sensitivity of 49.8 $\mu A.\mu M^{-1}.cm^{-2}$ and with a detection limit of 2.5×10^{-7} M at 3σ. A Michaelis–Menten constant K^{M}_{app} value was estimated to be 0.32 μM, indicating a high catalytic activity of HRP. Moreover, the proposed biosensor displayed a rapid response to H_2O_2 and possessed good stability and reproducibility. When used to detect H_2O_2 concentration in disinfector samples and sterilized milks, respectively, it showed satisfactory results.

A novel amperometric biosensor for the analytical determination of hydrogen peroxide was developed [63]. The fabrication of the biosensor was based on the co-immobilization of HRP, methylene green (MG) and MWCNTs within ormosils; 3-aminopropyltrimethoxysilane (APTMOS), 2-(3,4-epoxycyclohexyl)ethyltrimethoxysilane (ETMOS) and phenyltrimethoxysilane (PHTMOS). APTMOS determined the hydrophilicity/hydrophobicity of the ormosils and PHTMOS and ETMOS increased the physical and mechanical strength of the ormosil matrix. CV and amperometric measurements demonstrated the MG co-immobilized with HRP in this way, displayed good stability and could efficiently shuttle electrons between immobilized enzyme and electrode, and MWCNTs facilitated the electrocatalytic reduction of H_2O_2 at reduced over potential. The Michaelis constant of the immobilized HRP was 1.8 μM, indicating a high affinity of the HRP to H_2O_2 without loss of enzymatic activity in ormosil matrix. The prepared biosensor had a fast response of H_2O_2, less than 10 s, and excellent linear range of concentration from 5×10^{-7} to 2×10^{-5} M with the detection limit of 0.5 μM (S/N = 3) under the optimum conditions. The enzyme electrode retained about 90% of its initial activity after 30 days of storage in a dry state at 4 °C. The preparation of the developed biosensor was convenient and showed high sensitivity with good stability.

7.2.7 DNA Biosensors

A Mn(II) complex, MnL (L = sodium (E)-3-((1-carboxyethylimino) methyl)-4-hydroxybenzenesulfonate), was synthesized and characterized using elemental analysis and IR spectroscopy. CV and fluorescence spectroscopy were used to investigate the interaction between MnL and salmon

Table 7.6 Comparison of the efficiency of MWCNTs/MG/HRP-modified electrode used in determination of H_2O_2 [63].

RT (s)	LCR (μM)	LOD (μM)	Electrolyte	Method	Electrode
<30	4×10^{-6} to 2×10^{-3}	1	pH 7 PBS	CV	MWCNT/MB/HRP/GCE
–	2×10^{-5} to 5×10^{-4}	25	pH 7 PBS	CV	MWCNT/PS/HRP/SPE
20	2×10^{-5} to 4.5×10^{-3}	5	pH 6.8 PBS	CV, FIA	MWCNT/FMC-BSA/HRP/GCE
15	7×10^{-6} to 7.8×10^{-3}	2	pH 6 PBS	CV	PDDA-Au/DNA-Ag/HRP
20	5×10^{-7} to 1.6×10^{-3}	0.1	pH 7 PBS	CV	SG/MG/nafion/HRP/GCE
–	9.9×10^{-6} to 6.49×10^{-4}	3	pH 7 PBS	CV	MB/HRP/GA/GPE
–	45×10^{-6} to 6×10^{-3}	10	pH 7 PBS	CV	Ag-nano/PVA/Pt
<20	1×10^{-5} to 1.2×10^{-3}	4	pH 7 PBS	CV	Gelatine/MB/HRP/GCE
<20	2.5×10^{-6} to 1×10^{-4}	2.07	pH 7 PBS	CV	NMB/HRP/GCE
40	2.5×10^{-6} to 2.4×10^{-4}	0.5	pH 7 PBS	CV	MG/HRP/zeolite/GCE
<10	5×10^{-7} to 2×10^{-5}	0.5	pH 7.2 PBS	CV	MWCNT/MG/HRP/GCE
–	1×10^{-7} to 2×10^{-4}	–	pH 7.4 PBS	CV	PEGDGE/SBP/GCE

sperm DNA. It was revealed that MnL presented high electrochemical activity on GCE, and it could be intercalated into the double helices of double-stranded DNA (dsDNA). Using MnL as the hybridization indicator, a novel and sensitive electrochemical DNA biosensor based on MWCNTs functionalized with carboxyl groups (MWCNTs–COOH, on which DNA probes were covalently immobilized) was prepared [64]. The target single-stranded DNA (ssDNA) could be quantified ranging from 6.7×10^{-10} to 8.4×10^{-9} M with good linearity ($r = 0.9922$). A detection limit of 1.4×10^{-10} M (3σ, $n = 9$) was achieved.

The manganese complex of rutin(R) $C_{54}H_{58}MnO_{32}$ (abbreviated by MnR2) was synthesized and characterized by elemental analysis and IR spectroscopy. CV and fluorescence spectroscopy were used to investigate the interaction of MnR2 with salmon sperm DNA. It was revealed that MnR2 presented an excellent electrochemical activity on GCE and could intercalate into the double helix of dsDNA. A novel and sensitive

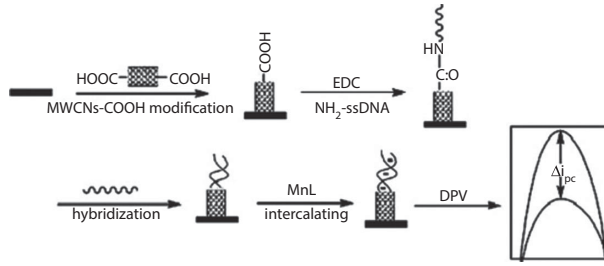

Figure 7.9 Procedure for the preparation of MWCNT-modified GCE and immobilization and detection of DNA [64].

electrochemical DNA biosensor based on MWCNTs functionalized with a carboxylic acid group (MWCNTs–COOH) for covalent DNA immobilization and enhanced hybridization detection was described [65]. The MWCNTs–COOH-modified GCE was fabricated and oligonucleotides with the 5'-amino group were covalently bonded to the carboxyl group of CNTs. Compared with DNA sensors with oligonucleotides directly incorporated on GCEs, this CNT-based assay with its large surface area and good charge-transport characteristics dramatically increased DNA attachment quantity and complementary ssDNA detection sensitivity. The target ssDNA could be quantified ranged from 1.60×10^{-9} M to 4.80×10^{-8} M with good linearity (r = 0.9898) and a detection limit of 3.81×10^{-11} M (3σ, n = 7) was achieved by the constructed electrochemical DNA biosensor. A novel and sensitive electrochemical DNA biosensor has been developed for the detection of DNA hybridization [66]. The biosensor was proposed by using copper(II) complex of Luteolin $C_{30}H_{18}CuO_{12}$ (CuL2) as an electroactive indicator based on silver NPs and MWCNTs (Ag/MWCNTs)-modified GCE. In this method, the 4-aminobenzoic acid (4-ABA) and Ag NPs were covalently grafted on MWCNTs to form Ag/4-ABA/MWCNTs. The proposed method dramatically increased DNA attachment quantity and complementary ssDNA detection sensitivity for its large surface area and good charge transport characteristics. DNA hybridization detection was performed using CuL2 as an electroactive indicator. CV and fluorescence spectroscopy were used to investigate the interaction between CuL2 and ds-oligonucleotides (dsDNA). It was revealed that CuL2 presented high electrochemical activity on GCE, and it could be intercalated into the double helices of dsDNA. The target ssDNA of the human hepatitis B virus (HBV) was quantified in a linear range from 3.23×10^{-12} to 5.31×10^{-9} M (r = 0.9983). A detection limit of 6.46×10^{-13} M (3σ, n = 11) was achieved.

The fabrication of a sensitive electrochemical DNA biosensor for the detection of sequence-specific target DNA was reported by Y. Zhang *et al.*

[67]. Zinc oxide nanowires (ZnONWs) were first immobilized on the surface of a GCE. MWCNTs with carboxyl groups were then dropped onto the surface of the ZnONWs. GNPs (AuNPs) were subsequently introduced to the surface of the MWCNTs/ZnONWs by electrochemical deposition. A ssDNA probe with a thiol group at the end (HS–ssDNA) was covalently immobilized on the surface of the AuNPs by forming an Au–S bond. DPV was used to monitor DNA hybridization by measuring the electrochemical signals of $[Ru(NH_3)_6]^{3+}$ bounding to dsDNA. The incorporation of ZnONWs and MWCNTs in this sensor design significantly enhances the sensitivity and the selectivity. This DNA biosensor can detect the target DNA quantitatively in the range of 1.0×10^{-13} to 1.0×10^{-7} M, with a detection limit of 3.5×10^{-14} M (S/N = 3). In addition, the DNA biosensor exhibits excellent selectivity, even for single-mismatched DNA detection.

MWCNTs–CONH–(CH2)2–SH was synthesized via carboxylation, and investigated a thickness-tunable multilayer films DNA biosensor built by layer-by-layer (LbL) covalent attachment of GNPs and MWCNTs on an Au electrode [68]. The hybridization events were monitored through measurement the signal of intercalated doxorubicin by DPV, and the oxidation peak currents show a good linear relationship with the logarithm of the

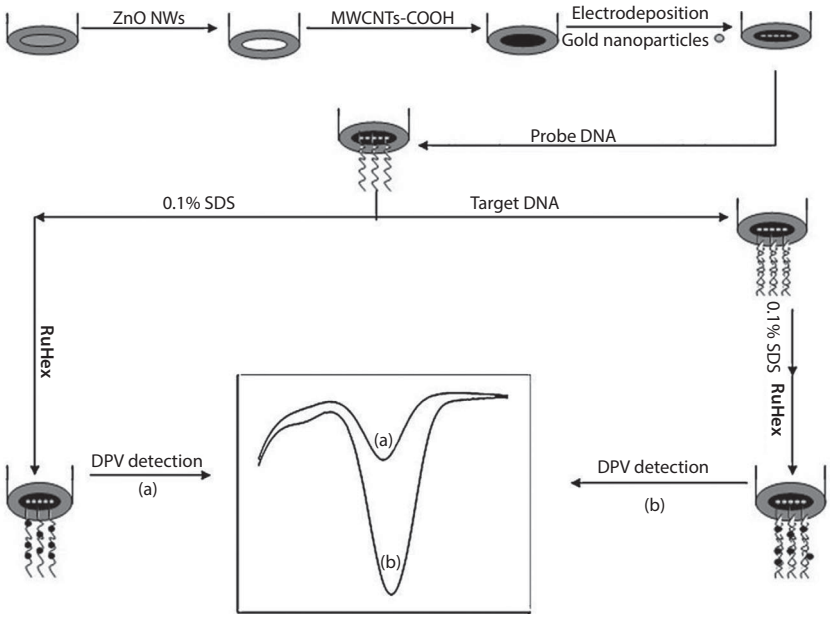

Figure 7.10 Schematic representation of the immobilization and hybridization detection of probe DNA [67].

concentration of target DNA from 5.0×10^{-10} to 1.0×10^{-11} M with a detection limit of 6.2 pM. The improved DNA biosensor has a good stability and reproducibility

7.3 Biosensors Based on Magnetic Nanoparticles

Magnetic biomaterials can be used to separate and concentrate biological molecules. They have been successfully used in clinical diagnostics. The immobilization of GOx or other enzymes on magnetic particles could potentially lead to unique properties, since nano-sized magnetic bioconjugated materials have unique properties such as large surface area, high bioactivity, and excellent stability. In addition, it provides magnetic control of the bioelectrocatalytic process for the detection of analytes. Comparing with the magnetic polymer microspheres, magnetic inorganic NPs are more suitable for the fabrication of sensitive electrochemical biosensors owing to its electro-conductivity, biocompatibility and easiness of synthesis. The MNPs-based electrochemical sensors provide a sensitive tool for the rapid detection of analytes. Magnetic biosensors have been used to detect extremely low concentrations of biomolecules in very small volumes of samples within just a few minutes. A glucose biosensor was prepared with Fe_3O_4 NPs containing Prussian blue (PB) and GOx attracted to the surface of solid paraffin carbon paste electrode (CPE) by magnetic force [69]. The prepared Fe_3O_4/PB composite NPs were about 50 nm in diameter and the GOx was covalently conjugated to the amine-modified NPs. Because of the high reactivity of hydrogen peroxide with PB contained in the glucose biosensor, the hydrogen peroxide formed during the enzymatic reaction with glucose was measured by the current generated to determine the glucose concentration. The biosensor showed high sensitivity, selectivity, stability, and short response time. It exhibited a linear response to glucose over the range from 5.0×10^{-7} to 8.0×10^{-5} M with a detection limit of 1.0×10^{-7} M. The apparent Michaelis–Menten constant K_m was found to be 1.44×10^{-5} M. Reductive substances in biological samples did not interfere with the detection of glucose. The biosensor was also used to determine the glucose concentration in human blood samples.

Magnetic Fe_3O_4 NPs were prepared by co-precipitation method and a disposable glucose biosensor was fabricated by drop coating of ferricyanide (Ferri)-nano-Fe_3O_4 mixture onto the surface of SPCEs, and then by layering on GOx [70]. The glucose biosensors exhibit a relatively fast response (<15 s) and high sensitivity (ca. 1.74 $mA.\mu M^{-1}$) with a wide linear range up to 33.3 μM (600 $mg.dL^{-1}$) of glucose.

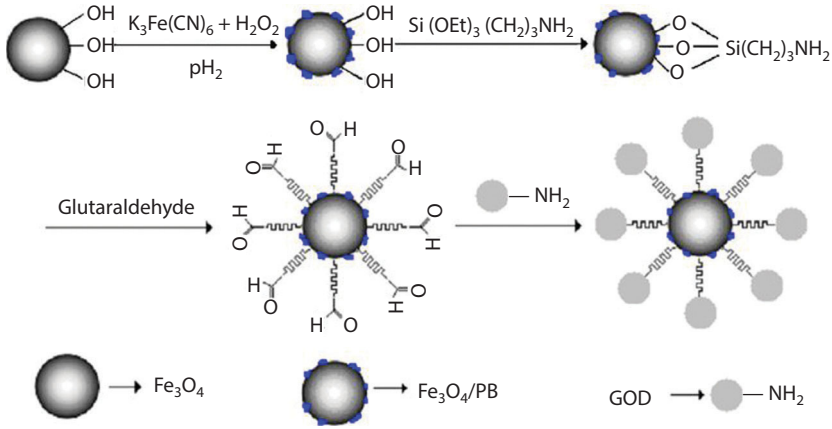

Figure 7.11 Synthesis of Fe_3O_4/PB and covalent conjugation of GOx to Fe_3O_4/PB NPs [69].

Table 7.7 Determination of glucose in blood samples [69].

Samples	Added (10^{-5} M)	Found (10^{-5} M) ($n = 5$)	R.S.D. (%)	Recoveries (%)
a	0.0 2.0 3.0	1.16 3.24 4.11	1.9 1.6 1.8	– 104 98.3
b	0.0 2.0 3.0	1.25 3.28 4.19	2.1 1.4 0.8	– 101.5 98

An electrochemiluminescence (ECL) glucose biosensor based on Fe_3O_4 NPs was presented by LI Jian-Ping et al. [71]. GOx was covalently cross-linked to the surface of synthesized magnetic Fe_3O_4 NPs. The composite particles of Fe_3O_4/GOx were adhered onto solid paraffin CPE surface by magnetic force to act as a working electrode. Hydrogen peroxide was produced by enzymatic reaction of GOx, and ECL could be obtained by the reaction between luminol and hydrogen peroxide; then, a novel ECL glucose biosensor was fabricated. There was a linear relationship between ECL intensity and glucose concentration in the range of $1x10^{-5}$–$1x10^{-2}$ M with a regression equation of $I = 65.4374\ C + 23.9017$ ($r = 0.9987$), and the detection limit was 1 μM. The ECL biosensor has shown short response time and high stability, and the electrode surface was easily renewable. The proposed biosensor has been applied for the determination of glucose in plasma samples.

Table 7.8 Determination of glucose in human serum and recovery test results [71].

Sample	Glucose found (μM)	RSD (%, *n* =5)	Reference values (μM)	Glucose added (μM)	Total found (μM)	Recovery (%)
1	5.78	3.41	5.73	0.5	6.30	104.0
2	4.26	3.10	4.35	1.0	5.22	96.2
3	6.00	2.53	5.92	1.5	7.46	97.1
4	7.80	3.34	7.78	2.0	9.84	102.0
5	8.87	2.76	8.95	3.0	11.72	95.2

A sensitive and selective amperometric glucose biosensor was obtained by using the electrodeposition of Pt NPs on iron oxide-MWCNTs/CS (Fe_yO_x-MWCNTs/CS) magnetic composite-modified GCE followed by the adsorption of GOx at the surface of the electrode [72]. The proposed biosensor exhibit excellent electrocatalytic activity and good response performance to glucose. Under the optimal conditions, a linear dependence of the catalytic current upon glucose concentration was obtained in the range of 6.0×10^{-6} to 6.2×10^{-3} M with a detection limit of 2.0×10^{-6} M, and a response time of less than 8 s. The apparent Michaelis–Menten constant (K^M_{app}) was evaluated to be 9.0 μM. Furthermore, the sensitivity for the determination of glucose at the GOx/Pt/Fe_yO_x-MWCNTs/CS magnetic composite-modified GCE is better than at common GOx/Pt/MWCNTs/CS and GOx/Pt-Fe_yO_x/CS composite-modified electrodes. The proposed biosensor has good anti-interferent ability and long-term storage stability after coating with Nafion, and it can be used for the determination of glucose in synthetic serum.

Ferrites are a group of important magnetic materials for technological application and fundamental studies. Nickel ferrite ($NiFe_2O_4$) with an inverse spinel structure shows ferrimagnetism that originates from magnetic moment of anti-parallel spins between Fe^{3+} ions at tetrahedral sites and Ni^{2+} ions at octahedral sites. The quantitative cytotoxicity test verified that both uncoated and CHIT-coated $NiFe_2O_4$ NPs had noncytotoxicity [73]. Thus, combining the advantageous features of MNPs ($NiFe_2O_4$NPs) and biopolymer (CHIT), a new CHIT/$NiFe_2O_4$/GOx nanocomposite was constructed on GCE [74]. The GCE modified with the CHIT/$NiFe_2O_4$NPs/GOx showed excellent electrocatalytical response to the oxidation of glucose when ferrocene carboxylic acid was used as an artificial redox mediator. The biosensor was applied to detect glucose with a linear range of 1×10^{-4} to 2.0×10^{-2} mol.L^{-1}. The biosensor exhibited excellent performance for glucose at applied potential of 0.6 V with a fast response time (<4 s).

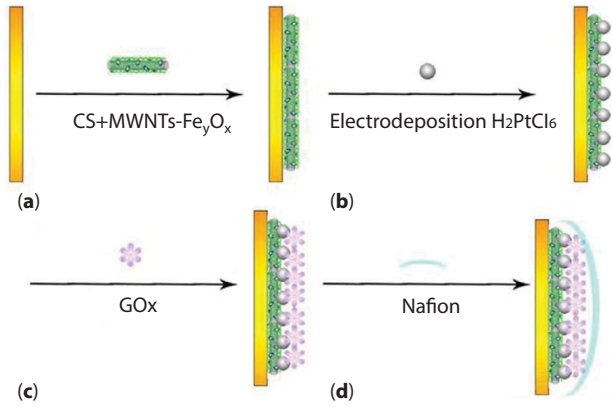

Figure 7.12 The stepwise fabrication processes of the modified electrode [72].

A phenol biosensor was developed based on the immobilization of tyrosinase on the surface of modified magnetic $MgFe_2O_4$ NPs [75]. The tyrosinase was first covalently immobilized to core-shell ($MgFe_2O_4$–SiO_2) MNPs, which were modified with amino group on its surface. The resulting magnetic bio-NPs were attached to the surface of CPE with the help of a permanent magnet. The immobilization matrix provided a good microenvironment for the retaining of the bioactivity of tyrosinase. Phenol was determined by the direct reduction of biocatalytically generated quinone species at −150mV versus SCE. The resulting phenol biosensor could reach 95% of steady-state current within 20 s and exhibited a high sensitivity of 54.2 μA/μM, which resulted from the high tyrosinase loading of the immobilization matrix. The linear range for phenol determination was from 1×10^{-6} to 2.5×10^{-4} M with a detection limit of 6.0×10^{-7} M obtained at a S/N ratio of 3. Also, a hydroquinone biosensor was developed and used to determine hydroquinone concentration in compost extracts based on the immobilization of laccase on the surface of modified magnetic core–shell (Fe_3O_4–SiO_2) NPs [76]. Laccase was covalently immobilized on the MNPs by glutaraldehyde, which was modified with amino groups on its surface. The obtained magnetic bio-NPs were attached to the surface of CPE with the aid of a permanent magnet to determine hydroquinone. A good microenvironment for retaining the bioactivity of laccase was provided by the immobilization matrix. The linear range for hydroquinone determination was 1×10^{-7} to 1.375×10^{-4} M, with a detection limit of 1.5×10^{-8} M. The current reached 95% of the steady-state current within about 60 s. Hydroquinone concentration in compost extracts was determined by laccase biosensor and HPLC, the results of the two methods were approximately the same.

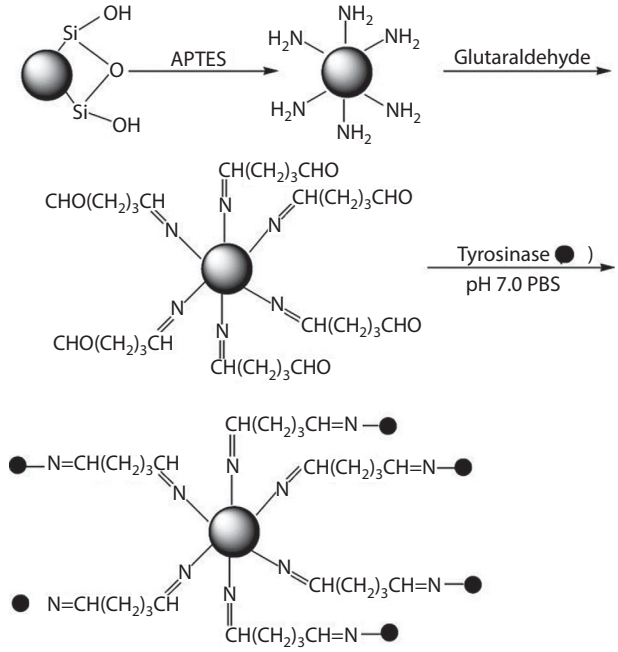

Figure 7.13 Schematic diagram for preparation of magnetic bio-NPs [75].

A novel tyrosinase biosensor based on Fe_3O_4 NPs–CS nanocomposite has been developed for the detection of phenolic compounds [77]. The large surface area of Fe_3O_4 NPs and the porous morphology of CS led to a high loading of enzyme and the entrapped enzyme could retain its bioactivity. The prepared biosensor was used to determine phenolic compounds by amperometric detection of the biocatalytically liberated quinone at −0.2 V versus saturated calomel electrode (SCE). The biosensor was applied to detect catechol with a linear range of 8.3×10^{-8} to 7.0×10^{-5} mol.L^{-1}, and the detection limit of 2.5×10^{-8} mol.L^{-1}. The tyrosinase biosensor exhibits good repeatability and stability. Such new tyrosinase biosensor shows great promise for rapid, simple, and cost-effective analysis of phenolic contaminants in environmental samples. The proposed strategy can be extended for the development of other enzyme-based biosensors.

A tyrosinase (Tyr) biosensor was developed based on Fe_3O_4 MNPs-coated CNTs nanocomposite and further applied to detect the concentration of coliforms with flow injection assay (FIA) system [78]. Coliforms which are found in large numbers among the intestinal of humans and other warm-blooded animals spread abroad in natural environment. The presence of coliforms, more specifically *Escherichia coli* (*E. coli*), is

Table 7.9 The response characteristics of the biosensor to various phenolic compounds [77].

Phenolic	Linear range (mol L^{-1})	Correlation coefficient	Detection limit (mol L^{-1})	Sensitivity (A(mol L^{-1}) $^{-1}$)	Relative standard deviation ($n = 5$), %	K_M^{App} (μmol L^{-1})	I_{max} (μA)
Catechol	8.3×10^{-5} to 7.0×10^{-5}	0.999	2.5×10^{-5}	0.514	4.5	96.9	83.6
p-Cresol	8.3×10^{-5} to 7.8×10^{-5}	0.999	2.5×10^{-5}	0.360	3.2	130.0	73.4
Phenol	8.3×10^{-5} to 7.3×10^{-5}	0.999	2.5×10^{-5}	0.225	5.0	159.5	53.9

routinely used as an indicator to monitor potential enteric pathogen contamination of waters. They may cause illness ranging from mild watery diarrhea to life-threatening conditions, such as hemolytic uremic syndrome and hemorrhagic colitis. Negatively charged MNPs were absorbed onto the surface of CNTs which were wrapped with cationic polyelectrolyte poly(dimethyldiallylammonium chloride) (PDDA). The Fe_3O_4 MNPs-coated CNTs nanocomposite was modified on the surface of the GCE, and Tyr was loaded on the modified electrode by glutaraldehyde. The immobilization matrix provided a good microenvironment for retaining the bioactivity of Tyr, and CNTs incorporated into the nanocomposite led to the improved electrochemical detection of phenol. The Tyr biosensor showed broad linear response of 1.0×10^{-8} to 3.9×10^{-5} M, low detection limit of 5.0×10^{-9} M and high sensitivity of 516 mA/M for the determination of phenol. Moreover, the biosensor integrated with a FIA system was used to monitor coliforms. The detection principle was based on determination of phenol which was produced by enzymatic reaction in the *E. coli* solution. Under the optimal conditions, the current responses obtained in the FIA system were proportional to the concentration of bacteria ranging from 20 to 1×10^5 cfu/mL with detection limit of 10 cfu/mL and the overall assay time of about 4 h. The developed biosensor with the FIA system was well suited for quick and automatic clinical diagnostics and water quality analysis.

As a specific nanomaterial, MNPs have gained increasing interest for their novel properties recently, and been widely studied and applied in various fields including enzyme immobilization. However, pure MNPs themselves may not be very useful in practical applications because they are more likely to aggregate for their large ratio of surface area to volume and strong magnetic dipole–dipole attractions between particles compared with other NPs, and have limited functional groups for selective binding. Therefore, one of the main problems in the application of superpara MNPs is the surface modification with various useful materials, which can make them to achieve desirable surface functionalities and be tailored to specific applications. Polymers magnetic microsphere is one kind of useful magnetic carriers which was synthesized by coating a layer of polymers film onto the MNPs. It has been successfully applied in enzyme immobilization because of its abundant functional groups and superparamagnetic character, which can make it as useful support for the immobilization of enzymes and separate from the reaction medium by using a magnetic field. A novel magnetic CS microsphere (MCMS) was prepared using carbon-coated iron MNPs and CS [79]. Hemoglobin (Hb) was successfully immobilized on the surface of MCMS-modified GCE with the cross-linking of glutaraldehyde,

and the immobilized Hb displayed an excellent electrocatalytic property to the reduction of H_2O_2 in the presence of the mediator of methylene blue (MB). This biosensor had a fast response of H_2O_2 less than 10 s and excellent linear relationships were obtained in the concentration range of 0.069–0.29 μM and 0.29–3.0 μM with the detection limit of 0.021 μM (S/N = 3) under the optimum conditions. Moreover, the selectivity, stability, and reproducibility of this biosensor were evaluated with satisfactory results.

In recent years, conducting polymers combined with metallic NPs have been paid more attention due to their potential applications in microelectronics, microsystems, optical sensors and photoelectronic chemistry. An assembly of MNPs were immobilized on PPy films under appropriate magnetic field in order to control their organization on the PPy film and finally to improve the sensitivity of the system in potential sensing applications [80]. By using streptavidin-labeled magnetic particles, it was possible to functionalize the NPs assembly with biotin-Fab fragment K47 antibody. The designed biosensor had been successfully applied in rapid, simple, and accurate measurements of atrazine concentrations, with a significantly low detection limit of 5 ng/ml.

Magnetic polymer nanostructures are a new class of multifunctional nanomaterials that are recently being explored in biosensor devices. The novel application of electrically active magnetic (EAM) NPs as

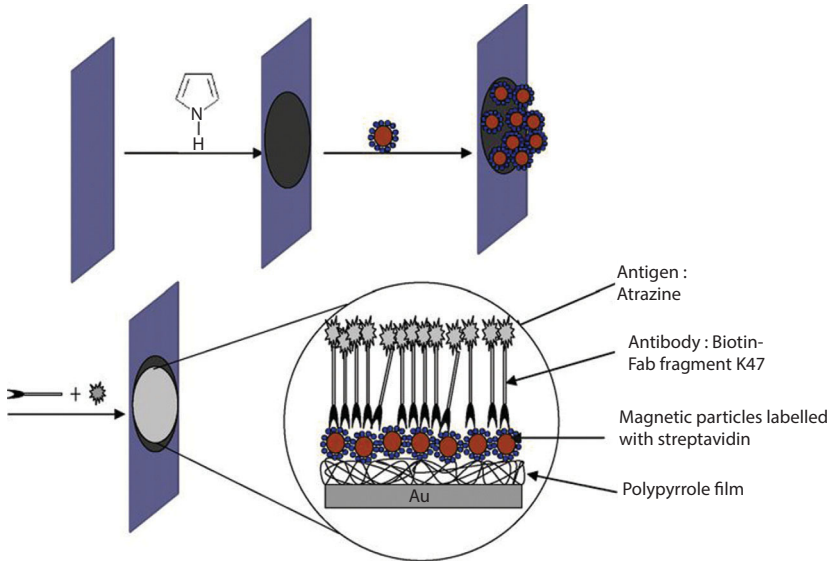

Figure 7.14 A schematic diagram of the immunosensor showing the stepwise immunosensor fabrication process [80].

concentrator of DNA targets as well as electrochemical transducers for detection of the *Bacillus anthracis* protective antigen A (pag A) gene was reported by C. Alocilja *et al.* [81]. The EAM NPs are synthesized by chemical polymerization and have dimensions of 80–100 nm. The biosensor detection encompasses two sets of DNA probes that are specific to the target gene: the detector probe labeled with the EAM NPs and the biotinylated capture probe. The DNA targets are double hybridized to the detector and the capture probes and concentrated from nonspecific DNA fragments by applying a magnetic field. Subsequently, the DNA sandwiched targets (EAM-detector probe–DNA target–capture probe-biotin) are captured on streptavidin-modified SPCEs through the biotinylated capture probes. Detection is achieved electrochemically by measuring the oxidation–reduction signal of the EAM NPs. Preliminary results indicate that the biosensor is able to detect the redox signal of the EAM NPs at DNA concentrations as low as 0.01 ng/μL.

7.4 Biosensors Based on Quantum Dots

Semiconductor QDs, also called semiconductor nanocrystals, are generally composed of atoms from groups II and VI or III and V of the periodic table. The nanoscaled size of QDs leads to the quantum-confinement effect, which results in interesting optical and electronic properties, such as high quantum yield, high molar extinction coefficients, broad absorption with narrow and symmetric photoluminescence (PL) spectra, large effective Stokes shifts, high resistance and exceptional resistance to photo- and chemical degradation. In 1998, the first milestone application of QDs as luminescence labels in biological detection was reported by Bruchez et al. [82], and then the biological applications of QD attracted intense attention. Recently, many uses of QDs in biology have existed, such as cellular labeling, in vivo tissue imaging, QD assay labeling. Its ability to promote the direct electron transfer between the biomolecules and electrode surfaces was also explored. Because of their unique chemical, physical and electronic properties, QDs and CNTs are now extremely attractive and important nanomaterials in bioanalytical applications. CdTe QDs with the size of about 3 nm were prepared and a novel electrochemical biosensing platform of glucose based on CdTe/CNTs electrode was presented by J. Li [83]. This CdTe/CNTs electrode was prepared by first mixing CdTe QDs, CNTs, nafion, and GOx in appropriate amounts and then modifying this mixture on the GCE. Transmission electron microscopy (TEM) was used to observe the dispersion of CdTe QDs on CNTs and CV was used to investigate the

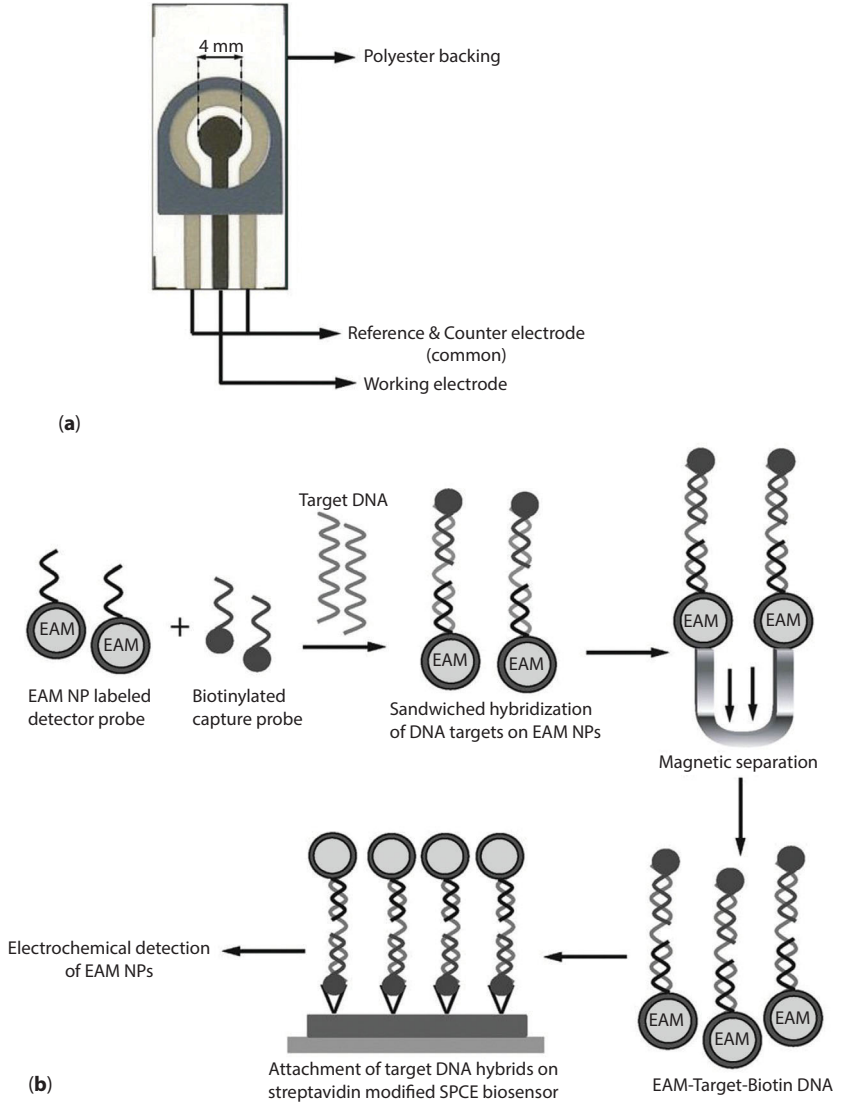

Figure 7.15 Schematic illustration of (a) screen-printed three-electrode sensor and (b) EAM-based electrochemical DNA biosensor detection principle [81].

electrochemical behavior of the CdTe/CNTs electrode. A pair of well-defined quasi-reversible redox peaks of GOx was obtained at the CdTe/CNTs-based enzyme electrode by direct electron transfer between the protein and the electrode. The immobilized GOx could retain bioactivity and catalyze the reduction of dissolved oxygen. Due to the synergy between the

CdTe QDs and CNTs, this novel biosensing platform based on QDs/CNTs electrode responded even more sensitively than that based on GCE modified by CdTe QDs or CNTs alone. The inexpensive, reliable and sensitive sensing platform based on QDs/CNTs electrode provides wide potential applications in clinical, environmental, and food analysis.

A reagentless amperometric uric acid biosensor based on zinc sulfide (ZnS) QDs was developed [84]. It could detect uric acid without the presence of an electron mediator. The carboxyl group functionalized ZnS QDs were synthesized, and they were soluble biocompatible and conductive. ZnS QDs conjugates could provide increased enzyme binding sites, which may result in higher enzyme loading. Thus, the proposed uricase/ZnS QDs/l-cys biosensor exhibited higher amperometric response compared to the one without QDs (uricase/l-cys biosensor). In addition, there was little ascorbic acid interference. It showed a linear dependence on the uric acid concentration ranging from 5.0×10^{-6} to 2.0×10^{-3} mol.L^{-1} with a detection limit of 2.0×10^{-6} mol.L^{-1} at 3 σ.

HRP and lipophilic QDs were incorporated onto the surface of GCEs in various ways [85]. It was found that HRP transfers electron directly onto the GCE only when the electrode was modified with QDs through vapor deposition. The response currents were linearly correlated with scan rate, indicating that the reaction is a surface controlled process. The average coverage of HRP on the electrode surface can be calculated as 2.29×10^{-11} mol.cm^{-2}, and the heterogeneous electron transfer rate constant k was 5.80 ± 0.70 s^{-1}. Absorption spectra and Fourier transform infrared spectra showed that the conformation of HRP immobilized on the electrode has no obvious change. Further studies indicated that immobilized HRP

Table 7.10 Determination of uric acid level in blood samples [84].

Sample number	Determined by spectrophotometry (×10−3 mol L−1)	Measured by biosensor (×10−3 mol L−1)	R.S.D. (n=34) (%)
1[a]	0.50	0.52	1.3
2[a]	0.48	0.49	1.8
3[a]	0.68	0.65	4.4
4	0.35	0.36	3.5
5	0.28	0.26	3.0

[a]The hyper- or hypo-level of uric acid in blood samples, the normal uric acid level in blood is between 0.15 and 0.4 mmol.L^{-1}.

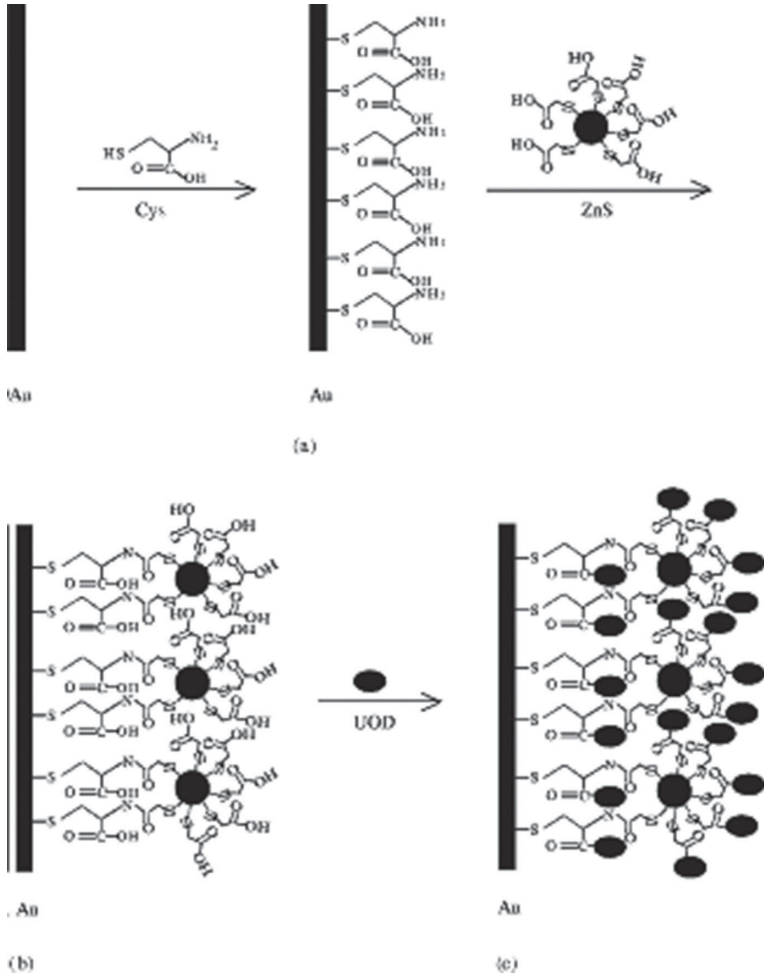

Figure 7.16 Schematic representation of the steps to develop a uricase/ZnS QDs/l-cysteamine sensor [84].

retains excellent catalytic activity to H_2O_2. The apparent Michaelis–Menten constant was calculated as 0.152 μM. It was also found that the modified electrode could be used as a sensor for H_2O_2, and the linear range of detection was 5.0×10^{-6} to 1.0×10^{-4} M, with a detection limit of 2.84×10^{-7} M. The sensor exhibited reproducibility, stability.

A simple method for immobilization of AChE on cysteamine self-assembled monolayers-modified gold electrode coupled with CdTe QDs was proposed [86] and thus a sensitive, fast and stable amperometric biosensor for quantitative determination of carbaryl was developed. The NPs

of CdTe QDs led to an increased effective surface area for immobilization of enzyme and their electrocatalytic activity promoted electron transfer reactions and catalyzed the electro-oxidation of thiocholine, thus amplifying the detection sensitivity. Due to the notable decrease in voltammetric signal of the immobilized AChE, a simple method for determination of carbaryl was established. The inhibition of carbaryl was proportional to its concentration in two ranges, from 1 to 50 and 50 to 500 ng.mL^{-1}, with a detection limit of 0.6 ng.mL^{-1}. The constructed biosensor which processes prominent characteristics and performance, such as good precision and reproducibility, acceptable stability and accuracy, fast response and low detection limit, has potential application in the characterization of enzyme inhibitors and detection of toxic compounds against to enzyme. The optical transducer of CdTe semiconductor QDs has been integrated with AChE enzyme by the LbL assembly technique, resulting in a highly sensitive biosensor for detection of organophosphorus pesticides (OPs) in vegetables and fruits based on enzyme inhibition mechanism [87]. The detection limits of the proposed biosensors are as low as 1.05×10^{-11} M for paraoxon and 4.47×10^{-12} M for parathion, which are significantly better than those of the conventional GC/MS methods or amperometric biosensors (0.5 nM). These biosensors are used for quick determination of low concentrations of OPs in real vegetable and fruit samples and exhibit satisfactory reproducibility and accuracy. Moreover, the stock stability of the biosensors is very good due to the stabilizing environment for the enzyme in the nanostructures made by LbL technique. Many advantages provided by these biosensors, like fluorescent change recognized by naked eyes and mass production with low cost, will facilitate future development of rapid and high-throughput screening of OPs.

A novel AChE biosensor was constructed by modifying GCE with CdTe QDs and excellent conductive GNPs though CS microspheres to immobilize AChE [88]. Since GNPs have shown widespread use particularly for constructing electrochemical biosensors through their high electron transfer ability, the combined AChE exhibited high affinity to its substrate and thus a sensitive, fast and cheap method for determination of monocrotophos. The combination of CdTe QDs and GNPs promoted electron transfer and catalyzed the electro-oxidation of thiocholine, thus amplifying the detection sensitivity. This novel biosensing platform based on CdTe QDs-GNPs composite responded even more sensitively than that on CdTe QDs or GNPs alone because of the presence of synergistic effects in CdTe-GNPs film. The inhibition of monocrotophos was proportional to its concentration in two ranges, from 1 to 1000 ng.mL^{-1} and 2 to 15 μg.mL^{-1}, with a detection limit of 0.3 ng.mL^{-1}. The proposed biosensor showed good precision and reproducibility, acceptable stability and accuracy in garlic samples analysis.

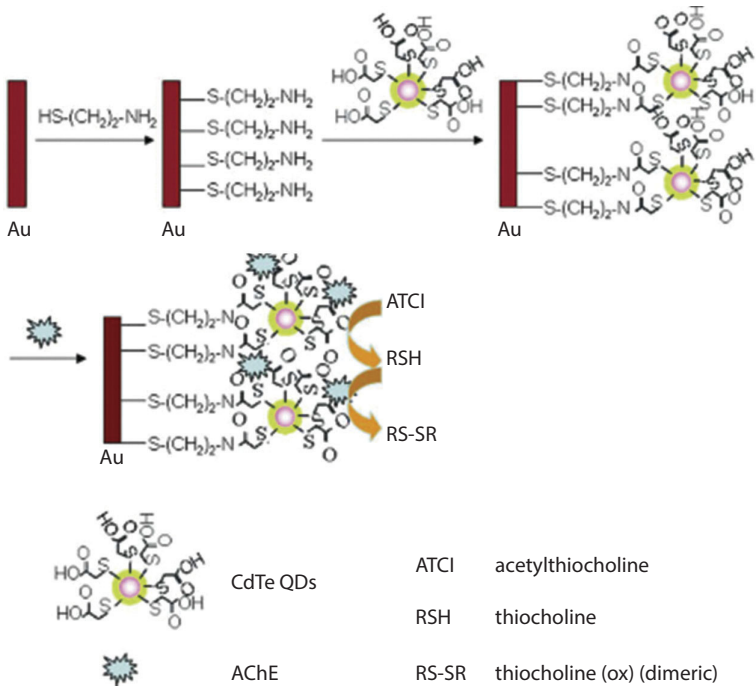

Figure 7.17 Schematic illustration of amperometric AChE biosensor for sensitive determination of carbaryl based on the immobilization of AChE to cysteamine self-assembled monolayer and CdTe QDs composite interface [86].

Ultra-sensitive DNA detection was achieved using a new biosensing platform based on QDs and total internal reflection fluorescence, which featured an exceptional detection limit of 3.2 a mol of bound target DNA [89]. The reusable sensor surface was produced by covalently immobilizing streptavidin onto a self-assembled alkanethiol monolayer of fiber optic probe through a heterobifunctional reagent. Streptavidin served as a versatile binding element for biotinylated ssDNA. The ssDNA coated fiber probe was evaluated as a nucleic acid biosensor through a DNA–DNA hybridization assay for a 30-mer ssDNA, which were the segments of the uidA gene of *E. coli* and labeled by QDs using avidin–biotin interaction. Several negative control tests revealed the absence of significant nonspecific binding. It also showed that bound target DNA could easily be eluted from the sensor surface using SDS solution (pH 1.9) without any significant loss of performance after more than 30 assay cycles. A quantitative measurement of DNA binding kinetics was achieved with high accuracy, indicating an association rate of 1.38×10^{6} $M^{-1}.s^{-1}$ and a dissociation rate of 4.67×10^{-3} s^{-1}. The proposed biosensing platform provides a simple, cheap, fast, and robust solution for many potential applications including clinical diagnosis, pathology, and genetics.

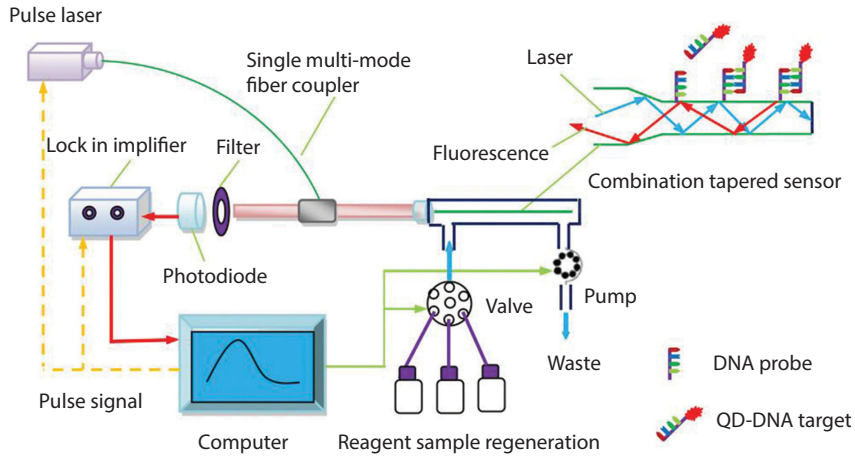

Figure 7.18 (a) Schematic diagram of the structure of evanescent wave DNA biosensor and (b) schematic diagram of combination-tapered fiber sensor and mechanical schematic of DNA detection [89].

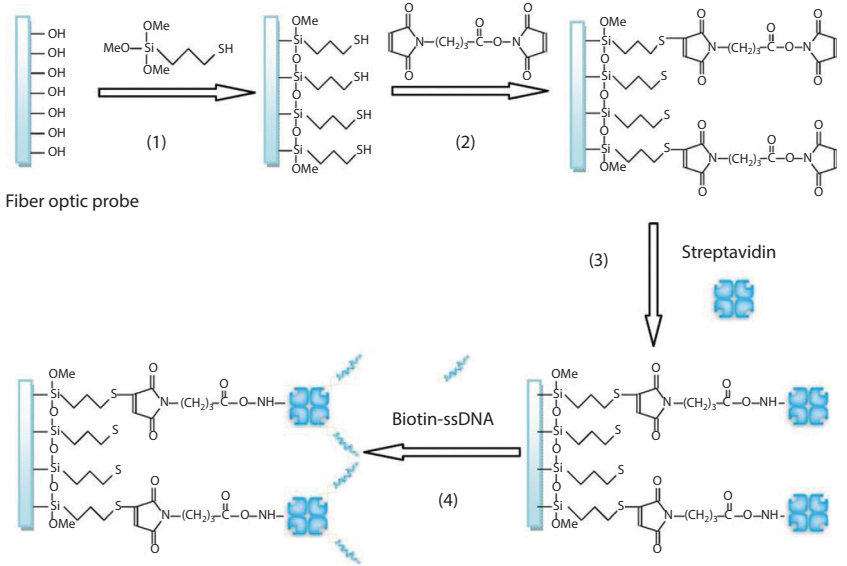

Figure 7.19 Schematic of optical fiber sensor modification. Firstly, the hydroxyl groups on the probe surface were covalently attached with MTS molecules (step 1). Secondly, the thiol group of silane reacted with the maleimide function of the bifunctional cross-linker GMBS (step 2). Thirdly, the ester moiety of the GMBS allowed the covalent linking of the streptavidin through an amino group (step 3). Finally, biotinylated ssDNA probes were attached to the immobilized streptavidin (step 4) [89].

Two new classes of QD-mediated biosensing methods have been developed to detect specific DNA sequences in a separation-free format. Both methods use two target-specific oligonucleotide probes to recognize a specific target [90]. The first method is based on cross-linking of two QDs with distinct emission wavelengths caused by probe-target hybridization. The second method uses QDs as both fluorescent tags and nanoscaffolds that capture multiple fluorescently labeled hybridization products, resulting in amplified target signals. The presence of targets is determined according to spatiotemporal coincidence of two different wavelength fluorescent signals emitted from the QD/DNA/probe complexes. With a single wavelength excitation, dual wavelength emission confocal spectroscopic system, the fluorescent signals can be measured with single-dot/molecule sensitivity. Compared with other NP-based, separation-free assays, this method shows advantages in simplicity, testing speed, and multiplexed applications.

7.5 Conclusion

Nanotechnology has been widely and successively applied in the field of sensing of drugs and biological molecules. Several kinds of nanosensors were used such as the following:

1. CNTs which offer high mechanical strength, thermal conductivity better than all but the purest diamond, and

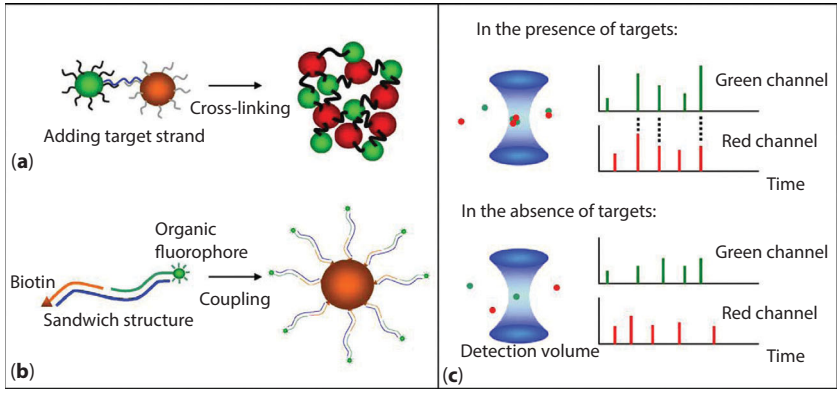

Figure 7.20 Schematic concept of two QD-mediated biosensing methods. (A) A cross-linking system using two QDs with distinct emission wavelengths. (B) Organic fluorophore-labeled sandwich structures coupled to a QD. (C) Coincidence detection: The coincident signals (marked with dash lines) are detected in the presence but not the absence of specific targets [90].

electrical conductivity similar to copper and unique chemical properties.
2. MNPs which have unique properties such as large surface area, high bioactivity, and excellent stability. In addition, it provides magnetic control of the bioelectrocatalytic process for the detection of analytes. Comparing with the magnetic polymer microspheres, magnetic inorganic NPs are more suitable for the fabrication of sensitive electrochemical biosensors owing to its electro-conductivity, biocompatibility and easiness of synthesis.
3. QDs which have interesting optical and electronic properties, such as high quantum yield, high molar extinction coefficients, broad absorption with narrow and symmetric PL spectra, large effective Stokes shifts, high resistance and exceptional resistance to photo- and chemical degradation.

The biomaterials to be sensed include a large variety of materials such as the following:

1. Glucose and cholesterol which are largely attributed to the human health and the food industry.
2. Phenolic compounds whose identification and quantification are very important for environment monitoring.
3. Some carbamate and OP pesticides which affect food, water and environment, and leads to a severe threat to human health.
4. H_2O_2 whose quantification is justified by the industrial, chemical and biomedical applications of this oxidant compound. In addition, H_2O_2 constitutes a relevant biochemical mediator in many cellular processes, as well as a by-product of several oxidases with analytical applications.
5. DNA and nucleic acids sequences detection which are directed to gene analysis, clinical disease diagnosis, or even forensic applications.

References

1. N.F. Atta, A. Galal, R.A. Ahmed, Direct and simple electrochemical determination of morphine at PEDOT modified Pt electrode. *Electroanalysis*, Vol. 23, pp. 1–10, 2011.

2. N.F. Atta, A. Galal, R.A. Ahmed, Poly(3,4-ethylene-dioxythiophene) electrode for the selective determination of dopamine in presence of sodium dodecyl sulfate. *Bioelectrochemistry*, Vol. 80, pp. 132–141, 2011.
3. N.F. Atta, A. Galal, F.M. Abu-Attia, S.M. Azab, Carbon paste gold nanopatricles sensor for the selective determination of dopamine in buffered solutions. *J. Electrochem. Soc.*, Vol. 157, pp.F116–F123, 2010.
4. N.F. Atta, A.M. Abdel-Mageed, Smart electrochemical sensor for some neurotransmitters using imprinted sol-gel films. *Talanta*, Vol. 80, pp. 511–518, 2009.
5. N. Iqbal, A. Lieberzeit, "Artificial Receptors for Mass-Sensitive Sensors: Taegeting Analytes from Surfaces, Nanoparticles, and Bioanalytes by Molecular Imprinting," Chapter 9, pp. 192–235, in "*Molecularly Imprinted Sensors: Overview and Applications*." L. SongJun, Y. Ge, A.P. Sergy, J. Lunec, Editors, Elsevier, 2012.
6. N.F. Atta, M.F. El-Kady, Poly(3-methylthiophene)/palladium sub-micro-modified sensor electrode. Part II: Voltammetric and EIS studies, and analysis of catecholamine neurotransmitters, ascorbic acid and acetaminophen. *Talanta*, Vol. 79, pp. 639–647, 2009.
7. N.F. Atta, M.F. El-Kady, Novel poly(3-methylthiophene)/Pd nanoparticles sensor: Synthesis, characterization and its application to the simultaneous analysis of dopamine and ascorbic acid in biological fluid. *Sens. Actuat. B Chem.*, Vol. 145, pp. 299–310, 2010.
8. N.F. Atta, A. Galal, M.F. El-Kady, Palladium nanoclusters-coated poly(furan) as a novel sensor for catecholamine neurotransmitters and paracetamol. *Sens. Actuat. B Chem.*, Vol. 141, pp. 566–574, 2009.
9. N.F. Atta, A. Galal, M.F. El-Kady, Simultaneous determination of catecholamines, uric acid and ascorbic acid at physiological levels using poly(N-methylpyrrole)/Pd-nanoclusters sensor. *Anal. Biochem.*, Vol. 400, pp. 78–88, 2010.
10. N.F. Atta, A. Galal, F.M. Abu-Attia, S.M. Azab, Characterization and electrochemical investigations of micellar/drug interactions. *Electrochim. Acta*, Vol. 56, pp. 2510–2517, 2011.
11. S. Iijima, Helical microtubules of graphitic carbon. *Nature (London)* 354, pp. 56–58, 1991.
12. A. Merkoçi, M. Pumera, X. Llopis, B. Perez, M. Valle, S. Alegret, New materials for electrochemical sensing. VI. Carbon nanotubes. *Trend. Anal. Chem.,* Vol. 24, pp. 826–838, 2005.
13. T.M. Day, N. Wilson, J.V.J. Macpherson, Electrochemical and conductivity measurements of single-wall carbon nanotube network electrodes. *J. Am. Chem. Soc.,* Vol. 126, pp. 16724–16725, 2004.
14. Rao C.N.; Satishkumar B.C.; Govindaraj A.; Nath M. Nanotubes. *Chem. Phys. Chem.,* Vol. 2, pp. 78–105, 2001.
15. M. Musameh, N.S. Lawrence, J. Wang, Electrochemical activation of carbon nanotubes. *Electrochem. Commun.,* Vol. 7, pp. 14–18, 2005.

16. J.J. Gooding, R. Wibowo, J. Liu, W. Yang, D. Losic, S. Orbons, F.J. Mearns, J.G. Shapter, D.B. Hibbert, Protein electrochemistry using aligned carbon nanotube arrays. *J. Am. Chem. Soc.,* Vol. 125, pp. 9006–9007, 2003.
17. J.M. Nugent, K.S.V. Santhanam, A. Rubio, P.M. Ajayan, Fast electron transfer kinetics on multi-walled carbon nanotube microbundle electrodes. *Nano. Lett.,* Vol. 1, pp. 87–91, 2001.
18. M. Zhang, A. Smith, W. Gorski, Coimmobilization of dehydrogenase and their cofactors in electrochemical biosensors. *Anal. Chem.,* Vol. 76, pp. 5045–5050, 2004.
19. R.R. Moore, C.E. Banks, R.G. Compton, Basal plane pyrolitic graphite electrodes; comparison of carbon nanotubes and graphite powder as electrocatalysis. *Anal. Chem.,* Vol. 76, pp. 2677–2682, 2004.
20. M. Musameh, J. Wang, A. Merkoc, Y. Lin, Low-potential stable NADH detection at carbon-nanotube-modified glassy carbon electrodes. *Electrochem. Commun.*, Vol. 4, pp. 743–746, 2004.
21. F. Valentini, A. Amine, S. Orlanducci, M.L. Terranova, G. Palleschi, Nanotube purification: Preparation and characterization of carbon paste electrodes. *Anal. Chem.,* Vol. 75, pp. 5413–5421, 2003.
22. J.Wang, M. Musameh, Carbon nanotube/Teflon composite electrochemical sensors and biosensors. *Anal. Chem.,* Vol. 75, pp. 2075–2079, 2003.
23. Z. Yang, H. Wu, The electrochemical impedance measurements of carbon nanotubes. *Chem. Phys. Lett.,* Vol. 343, pp. 235–240, 2001.
24. H. Cheng, G.P. Pez, A.C. Cooper, Spontaneous cross linking of small-diameter single-walled carbon nanotubes. *Nano Lett.,* Vol. 3, pp. 585–587, 2003.
25. S. Li, P. He, J. Dong, Z. Guo, L. Dai, DNA-direct self-assembling of carbon nanotubes. *J. Am. Chem. Soc.,* Vol. 127, pp. 14–15, 2005.
26. K. Keren, R.S. Berman, E. Buchstab, U. Sivan, E. Braun, DNA-templated carbon nanotube field-effect transistor. *Science (Washington, DC),* Vol. 302, pp. 1380–1382, 2003.
27. R.H. Baughman, A. Anvar, A. Zakhidov, W.A. Heer, Carbon nanotubes – The route toward applications. *Science (Washington, DC),* Vol. 297, pp. 787–792, 2002.
28. S.G. Wang, O. Zhang, R. Wang, S.F. Yoona, A novel multi-walled carbon nanotube-based biosensor for glucose detection. *Biochem. Biophy. Res. Comm.,* Vol. 311, pp. 572–576, 2003.
29. R. Nenkova, D. Ivanova, J. Vladimirova, T. Godjevargova, New amperometric glucose biosensor based on cross-linking of glucose oxidase on silica gel/multiwalled carbon nanotubes/polyacrylonitrile nanocomposite film. *Sens. Actuat. B,* Vol. 148, pp. 59–65, 2010.
30. A.Salimi, R.G. Compton, R. Hallaj, Glucose biosensor prepared by glucose oxidase encapsulated sol-gel and carbon-nanotube-modified basal plane pyrolytic graphite electrode. *Anal. Biochem.*, Vol. 333, 49–56, 2004.

31. B. Wang, B. Li, Q. Deng, S. Dong, Amperometric glucose biosensor based on sol-gel organic inorganic hybrid material. *Anal. Chem*., Vol. 70, pp. 3170–3174, 1998.
32. W. Jia, K. Wang, Z. Zhu, H. Song, X. Xia, One-step immobilization of glucose oxidase in a silica matrix on a Pt electrode by an electrochemically induced sol–gel process. *Langmuir*, Vol. 23, pp. 11896–11900, 2007.
33. H. Zheng, H. Xue, Y. Zhang, Z. Shen, A glucose biosensor based on microporous polyacrylonitrile synthesized by single rare-earth catalyst. *Biosens. Bioelectron*., Vol. 17, pp. 541–545, 2002.
34. D. Shan, Y. He, S. Wang, H. Xue, H. Zheng, A porous poly(acrylonitrile-co-acrylic acid) film-based glucose biosensor constructed by electrochemical entrapment. *Anal. Biochem*., Vol. 356, pp. 215–221, 2006.
35. D. Shan, S. Wang, Y. He, H. Xue, Amperometric glucose biosensor based on in situ electropolymerized polyaniline/poly(acrylonitrile-*co*-acrylic acid) composite film. *Mater. Sci. Eng. C,* Vol. 28, pp. 213–217, 2008.
36. K. Manesh, H. Kim, P. Santhosh, A. Gopalan, K.P. Lee, A novel glucose biosensor based on immobilization of glucose oxidase into multi-wall carbon nanotubes-polyelectrolyte-loaded electro-spun nanofibrous membrane. *Biosens. Bioelectron*., Vol. 23, pp. 771–779, 2008.
37. Y.T. Wang, L. Yu, Z.Q. Zhu, J. Zhang, J.Z. Zhu, C. Fan, Improved enzyme immobilization for enhanced bio electro catalytic activity of glucose sensor. *Sens. Actuat. B*, Vol. 136, pp. 332–337, 2009.
38. A. Salimi, R.G. Compton, R. Hallaj, Glucose biosensor prepared by glucose oxidase encapsulated sol-gel and carbon-nanotube-modified basal plane pyrolytic graphite electrode. *Anal. Biochem*., Vol. 333, pp. 49–56, 2004.
39. Y. Liu, M. Wang, F. Zhao, Z. Xu, S. Dong, The direct electron transfer of glucose oxidase and glucose biosensor based on carbon nanotubes/chitosan matrix. *Biosens. Bioelectron*., Vol. 21, pp. 984–988, 2005.
40. X. Kang, Z. Mai, X. Zou, P. Cai, J. Mo, A novel glucose biosensor based on immobilization of glucose oxidase in chitosan on a glassy carbon electrode modified with gold-platinum alloy nanoparticles/multiwall carbon nanotubes. *Anal. Biochem*., Vol. 369, pp. 71–79, 2007.
41. G. Lia, J.M. Liaoa, G.Q. Hua, N.Z. Maa, P.J. Wub, Study of carbon nanotube modified biosensor for monitoring total cholesterol in blood. *Biosens. Bioelectron*., Vol. 20, pp. 2140–2144, 2005.
42. C. Dhand, S.K. Arya, M. Datta, B.D. Malhotra, Polyaniline–carbon nanotube composite film for cholesterol biosensor. *Anal. Biochem*., Vol. 383, pp. 194–199, 2008.
43. M. Guo, J. Chen, J. Li, L. Nie, S. Yao, Carbon nanotubes-based amperometric cholesterol biosensor fabricated through layer-by-layer technique. *Electroanalysis*, Vol. 16, pp. 1992–1998, 2004.
44. C. Dhand, S.P. Singh, S.K. Arya, M. Datta, B.D. Malhotra, Cholesterol biosensor based on electrophoretically deposited conducting polymer film derived

from nano-structured polyaniline colloidal suspension. *Anal. Chim. Acta*, Vol. 602, pp. 244–251, 2007.
45. G.K. Kouassi, J. Irudayaraj, G.J. McCarty, Examination of Cholesterol oxidase attachment to magnetic nanoparticles. *Nanobiotechnology*, Vol. 3, pp. 1–8, 2005.
46. S. Aravamudhan, A. Kumar, S. Mohapatra, S. Bhansali, Sensitive estimation of total cholesterol in blood using Au nanowires based microfluidic platform. *Biosens. Bioelectron*., Vol. 22, pp. 2289–2294, 2007.
47. A. Parra, E. Casero, F. Pariente, L. Vazquez, E. Lorenzo, Cholesterol oxidase modified gold electrodes as bioanalytical devices. *Sens. Actuat. B,* Vol. 124, pp. 30–37, 2007.
48. G. Li, J.M. Liao, G.Q. Hu, N.Z. Ma, P.J. Wu, Study of carbon nanotube modified biosensor for monitoring total cholesterol. *Biosens. Bioelectron.,* Vol. 20, pp. 2140–2144, 2005.
49. Y. Tsai, S. Chen, C. Lee, Amperometric cholesterol biosensors based on carbon nanotube-chitosan-platinum-cholesterol oxidase nanobiocomposite. *Sens. Actuat. B,* Vol. 135, 96–101, 2008.
50. A.I. Gopalana, K.P. Leea, D. Ragupathya, Development of a stable cholesterol biosensor based on multi-walled carbon nanotubes-gold nanoparticles composite covered with a layer of chitosan-room-temperature ionic liquid network. *Biosens. Bioelectron*., Vol. 24, pp. 2211–2217, 2009.
51. Y. Tsai, C. Chiu, Amperometric biosensors based on multiwalled carbon nanotube-Nafion-tyrosinase nanobiocomposites for the determination of phenolic compounds. *Sens. Actuat. B,* Vol. 125, pp. 10–16, 2007.
52. S.K. Ozoner, M. Yalvac, E. Erhan, Flow injection determination of catechol based on polypyrrole-carbon nanotube-tyrosinase biocomposite detector. *Cur. Appl. Phys*., Vol. 10, pp. 323–328, 2010.
53. H. Yina, Y. Zhoua, J. Xua, S. Aia, L. Cuia, L. Zhub, nanotubes-cobalt phthalocyanine-silk fibroin film and its application to determine bisphenol A. *Anal. Chim. Acta*, Vol. 659, pp. 144–150, 2010.
54. Y. Wang, H. Yasushi, Highly sensitive biosensor for toxic phenol compounds using tyrosinase and acridine orange-adsorbed carbon felt. *J. Environ. Sci.* Suppl., pp. S100–S104, 2009.
55. T. Ahuja, D. Kumar, N. Singh, A.M.R. Biradar, Potentiometric urea biosensor based on multi-walled carbon nanotubes (MWCNTs)/silica composite material. *Mater. Sci. Eng. C,* Vol. 31, pp. 90–94, 2011.
56. Z. Xu, X. Chen, X. Qu, J. Jia, S. Dong, Single-wall carbon nanotube-based sensor and biosensor. *Biosens. Bioelectron*., Vol. 20, pp. 579–584, 2004.
57. D. Dua, M. Wanga, J. Caib, A. hang, Sensitive acetylcholinesterase biosensor based on assembly of β-cyclodextrins onto multiwall carbon nanotubes for detection of organophosphates pesticide. *Sens. Actuat. B*, Vol. 146, pp. 337–341, 2010.
58. D. Dua, X. Yea, J. Caib, J. Liua, A. Zhang, Acetylcholinesterase biosensor design based on carbon nanotube-encapsulated polypyrrole and polyaniline

copolymer for amperometric detection of organophosphates. *Biosens. Bioelectron*., Vol. 25, pp. 2503–2508, 2010.
59. D. Du, X. Huang, J. Cai, A. Zhang, Amperometric detection of triazophos pesticide using acetylcholinesterase biosensor based on multiwall carbon nanotube-chitosan matrix. *Sens. Actuat. B*, Vol. 127, pp. 531–535, 2007.
60. D. Du, M. Wang, J. Cai, Y. Qin, A. Zhang, A novel biosensor based on photoelectro-synergistic catalysis for flow-injection analysis system/amperometric detection of organophosphorous pesticides. *Sens. Actuat. B*, Vol. 143, pp. 524–529, 2010.
61. S. Korkut, B. Keskinler, E. Erhan, An amperometric biosensor based on multiwalled carbon nanotube-poly(pyrrole)-horseradish peroxidase nano-biocomposite film for determination of phenol derivatives. *Talanta*, Vol. 76, pp. 1147–1152, 2008.
62. S. Chen, R. Yuan, Y. Chai, B. Yin, W. Li, L. Min, Amperometric hydrogen peroxide biosensor based on the immobilization of horseradish peroxidase on core–shell organosilica@chitosan nanospheres and multiwall carbon nanotubes composite. *Electrochim. Acta,* Vol. 54, pp. 3039–3046, 2009.
63. A.K. Upadhyay, T. Ting, S. Chen, Amperometric biosensor for hydrogen peroxide based on coimmobilized horseradish peroxidase and methylene green in ormosils matrix with multiwalled carbon nanotubes. *Talanta*, Vol. 79, pp. 38–45, 2009.
64. S. Niu, M. Zhao, R. Ren, S. Zhang, Carbon nanotube-enhanced DNA biosensor for DNA hybridization detection using manganese(II)–Schiff base complex as hybridization indicator. *J. Inorg. Biochem*., Vol. 103, pp. 43–49, 2009.
65. S. Niu, M. Zhao, L. Hu, S. Zhang, Carbon nanotube-enhanced DNA biosensor for DNA hybridization detection using rutin-Mn as electrochemical indicator. *Sens. Actuat. B,* Vol. 135, pp. 200–205, 2008.
66. S. Niu, B. Han, W. Cao, S. Zhang, Sensitive DNA biosensor improved by Luteolin copper(II) as indicator based on silver nanoparticles and carbon nanotubes modified electrode. *Anal. Chim. Acta*, Vol. 651, pp. 42–47, 2009.
67. J. Wanga, S. Li, Y. Zhang, A sensitive DNA biosensor fabricated from gold nanoparticles, carbon nanotubes, and zinc oxide nanowires on a glassy carbon electrode. *Electrochim. Acta*, Vol. 55, pp. 4436–4440, 2010.
68. Y. Zhang, H. Ma, K. Zhang, S. Zhang, J. Wang, An improved DNA biosensor built by layer-by-layer covalent attachment of multi-walled carbon nanotubes and gold nanoparticles. *Electrochim. Acta*, Vol. 54, pp. 2385–2391, 2009.
69. J. Li, X. Wei, Y. Yuan, Synthesis of magnetic nanoparticles composed by Prussian blue and glucose oxidase for preparing highly sensitive and selective glucose biosensor. *Sens. Actuat. B,* Vol. 139, pp. 400–406, 2009.
70. B.-W. Lu, W.C. Chen, A disposable glucose biosensor based on drop-coating of screen-printed carbon electrodes with magnetic nanoparticles. *J. Mag. Mag. Mater.,* Vol. 304, e400–e402, 2006.

71. X. Zhi-Gang, L. Jian-Ping, T. Li, C. Zhi-Qiang, A novel electro-chemiluminescence biosensor based on glucose oxidase immobilized on magnetic nanoparticles. *Chin. J. Anal. Chem*., Vol. 38, pp. 800–804, 2010.
72. J. Li, R. Yuan, Y. Chai, X. Che, Fabrication of a novel glucose biosensor based on Pt nanoparticles-decorated iron oxide-multiwall carbon nanotubes magnetic composite. *J. Mol. Catal. B Enz.,* Vol. 66, pp. 8–14, 2010.
73. S. Baea, S.W. Lee, Applications of $NiFe_2O_4$ nanoparticles for a hyperthermia agent in biomedicine. *Appl. Phys. Lett.,* Vol. 89, pp. 252–503, 2006.
74. L. Luo, Q. Li, Y. Xu, Y. Ding, X. Wang, D. Deng, Y. Xu, Amperometric glucose biosensor based on $NiFe_2O_4$ nanoparticles and chitosan. *Sens. Actuat. B,* Vol. 145, pp. 293–298, 2010.
75. Z. Liu, Y. Liu, H. Yang, Y. Yang, G. Shen, R. Yu, A phenol biosensor based on immobilizing tyrosinase to modified core-shell magnetic nanoparticles supported at a carbon paste electrode. *Anal. Chim. Acta*, Vol. 533, 3–9, 2005.
76. Y. Zhang, G. Zeng, L. Tang, D. Huang, X. Jiang, Y. Chen, A hydroquinone biosensor using modified core-shell magnetic nanoparticles supported on carbon paste electrode. *Biosens. Bioelectron*., Vol. 22, pp. 2121–2126, 2007.
77. S. Wang, Y. Tan, D. Zhao, G. Liu, Amperometric tyrosinase biosensor based on Fe_3O_4 nanoparticles–chitosan nanocomposite. *Biosens. Bioelectron*., Vol. 23, pp. 1781–1787, 2008.
78. Y. Cheng, Y. Liu, J. Huang, K. Li, Y. Xian, W. Zhang, L. Jin, Amperometric tyrosinase biosensor based on Fe_3O_4 nanoparticles-coated carbon nanotubes nanocomposite for rapid detection of coliforms. *Electrochim. Acta*, Vol. 54, pp. 2588–2594, 2009.
79. G. Lai, H. Zhang, D. Hana, A novel hydrogen peroxide biosensor based on hemoglobin immobilized on magnetic chitosan microspheres modified electrode. *Sens. Actuat. B*, Vol. 129, pp. 497–503, 2008.
80. H.B. Fredj, S. Helali, C. Esseghaier, L. Vonna, L. Vidal, A. Abdelghani, Labeled magnetic nanoparticles assembly on polypyrrole film for biosensor applications. *Talanta*, Vol. 75, pp. 740–747, 2008.
81. S. Pal, E.C. Alocilja, Electrically active magnetic nanoparticles as novel concentrator and electrochemical redox transducer in Bacillus anthracisDNA detection. *Biosens. Bioelectron*., Vol. 26, pp. 1624–1630, 2010.
82. M. Bruchez, J.M. Moronne, P. Gin, Semiconductor nanocrystals as fluorescent biological labels. *Science*, Vol. 281, pp. 2013–2016, 1998.
83. Q. Liu, X. Lu, J. Li, X. Yao, J. Li, Direct electrochemistry of glucose oxidase and electrochemical biosensing of glucose on quantum dots/carbon nanotubes electrodes. *Biosens. Bioelectron*., Vol. 22, pp. 3203–3209, 2007.
84. F. Zhang, C. Li, X. Li, X. Wang, Q, Wan, Y. Xian, L. Jin, K. Yamamotob, ZnS quantum dots derived a reagentless uric acid biosensor. *Talanta*, Vol. 68, pp. 1353–1358, 2006.
85. Z. Wang, Q. Xu, H. Wang, Q. Yang, J. Yu, Y. Zhao, Hydrogen peroxide biosensor based on direct electron transfer of horseradish peroxidase with vapor deposited quantum dots. *Sens. Actuat. B*, Vol. 138, pp. 278–282, 2009.

86. D. Dua, W. Chen, J. Cai, J. Zhang, F. Qu, H. Li, Development of Acetylcholinesterase biosensor based on CdTe quantum dots modified cysteamine self-assembled monolayers. *J. Electroanal. Chem*., Vol. 623, pp. 81–85, 2008.
87. Z. Zheng, Y. Zhou, X. Li, S. Liu, Z. Tang, Highly-sensitive organo-phosphorous pesticide biosensors based on nanostructured films of acetyl-cholinesterase and CdTe quantum dots. *Biosens. Bioelectron*., Vol. 26, pp. 3081–3085, 2011.
88. D. Du, S. Chen, D. Song, H. Li, X. Chen, Development of acetyl-cholinesterase biosensor based on CdTe quantum dots/gold nanoparticles modified chitosan microspheres. *Biosens. Bioelectron*., Vol. 24, pp. 475–479, 2008.
89. F. Long, S. Wu, M. He, T. Tong, H. Shi, Ultrasensitive quantum dots-based DNA detection and hybridization kinetics analysis with evanescent wave biosensing platform. *Biosens. Bioelectron*., Vol. 26, pp. 2390–2395, 2011.
90. H. Yeh, Y. Ho, T. Wang, Quantum dot–mediated biosensing assays for specific nucleic acid detection. *Nanomed. Nanotech. Biol. Med*., Vol. 1, pp. 115–121, 2005.

8

Biosensor Based on Chitosan Nanocomposite

Baoqiang Li*[1], Yinfeng Cheng[1], Feng Xu[2,3], Lei Wang[1], Daqing Wei[1], Dechang Jia[1], Yujie Feng[1], and Yu Zhou[1]

** [1]Institute for Advanced Ceramics; State Key Laboratory of Urban Water Resource and Environment, Harbin Institute of Technology, Harbin, PR China*
[2]MOE Key Laboratory of Biomedical Information Engineering, School of Life Science and Technology, Xi'an Jiaotong University, Xi'an, PR China
[3]Bioinspired Engineering and Biomechanics Center (BEBC), Xi'an Jiaotong University, Xi'an, PR China

Abstract

A biosensor is characterized as sensitive, cost-effective, and easy-to-use detection electrode, which can respond to the target object (e.g., biomolecular species and toxic candidates) in clinical diagnosis, environmental pollutants analysis, and pharmaceutical screening and transform the target concentration to more easily detectable electrical or optical signals. Due to the pH-sensitive solubility, film-forming ability, and excellent biocompatibility, chitosan is unique and low-cost polysaccharide biomaterial with plenty of amino groups that can immobilize the biomolecules via physical and chemical interactions. However, the poor conductivity of chitosan is the main limitation for the immobilization of recognizing agents on electrode in the construction of biosensor. This chapter presents versatile chitosan nanocomposite including nanoparticles (e.g., nano gold, silver, zinc oxide, carbon dot); nanotube and nanosheet have been incorporated into the chitosan to improve the conductivity of chitosan and the immobilization efficiency of bioreceptor. This chapter has also summarized the progress on high-sensitive, reliable, selective, and low-cost biosensor based on chitosan nanomaterials. The biodegradable, implantable, wearable, wireless biosensor with aims of healthcare services, food safety, and environment protection would converge

**Corresponding author*: libq@hit.edu.cn

Ashutosh Tiwari, Hirak K. Patra and Anthony P.F. Turner (eds.) Advanced Bioelectronic Materials, (277–308)

on the bionanomaterials for immobilization of the specific and sensitive detection probes, electronic engineering for minimization and MEMS or microfluidic devices, computer science for smart portable and cloud platform.

***Keywords*:** Biosensor, chitosan, carbon nanoparticles, immobilization of bioreceptor

8.1 Introduction

Biosensor composing of transducer and sensitive bioactive molecules can quickly analyze specific targets qualitatively or quantitatively (e.g., biomolecular species and toxic candidates) for clinical diagnosis, environmental pollutants analysis, and pharmaceutical screening, which transforms the target concentration to more easily detectable electrical or optical signals. Compared with the traditional analytic techniques (e.g., chromatography, atomic absorption spectroscopy, enzyme-linked immunosorbent assay), biosensor has the advantage of high sensitivity, short analysis time and low cost [1]. Hence, the interest in biosensor has increased over the past recent years [2]. However, challenges remain for the application of biosensors, such as effective immobilization of sensitive materials and the regeneration of the biosensor [3]. Due to the size effect and surface effect, nanomaterials are magic substances for improving the performance and capabilities of biosensor [4]. Chitosan is a biocompatible, biodegradable, and non-toxic natural polysaccharides derived from an abundant renewable resource. Biosensors based on chitosan nanomaterials have attracted the great interest to successfully solve the problem of biosensor above-mentioned [5–8]. Based on the pH-responsive solubility, reaction activity, and chemical cross-linking contributed by of amino groups, the chitosan nanocomposite was introduced for biosensor through blending, *in situ* hybridization, and chemical grafting. We highlight the incorporation of versatile nanomaterials on biosensor, including carbon nanomaterials, metal and metal oxide nanoparticles (NPs), quantum dots (QDs), and ionic liquid (ILs) for purpose of improving the conductivity of chitosan film and effective immobilization of bioreceptors, enhancing the sensitivity adaptability and selectivity DNA biosensor, enzyme biosensor, and immunosensor. Finally, emerging biosensors and the perspective of biosensor are highlighted.

8.2 Chitosan and Chitosan Nanomaterials

NPs integrated with specific probes can realize the monitoring and detecting in real time and provide the signals related with specific targets [9].

NPs allow for the noninvasive interactions bimolecular of cells, various nanomaterials have been reported, such as carbon nanomaterials, metal and metal oxide nanomaterials, semiconductor nanomaterials, and polymeric nanomaterials [10–13].

Among the natural biomedical polymers, chitosan is well-documented candidate in biomedicine because of the following advantages [7]. Chitosan is a low-cost biomaterial derived from abundant exoskeletons of crustaceans and has plenty of amine groups and hydroxyl groups, which allows chitosan dissolving in acidic solution and provides reactive sites for chelation interaction, chemical modification, and linkage of biomolecules or NPs [14]. Thus, chitosan and its derivatives have been widely used as scaffold in tissue engineering, carrier in drug delivery system and immobilization and linkage of bioactive substance for biosensor [15].

8.2.1 Physical and Chemical Properties of Chitosan

Linear chitosan chains contain the randomly distributed acetyl glucosamine and glucosamine units as shown in Figure 8.1. Chitosan is achieved by removing acetyl groups of chitin and when the degree of deacetylation

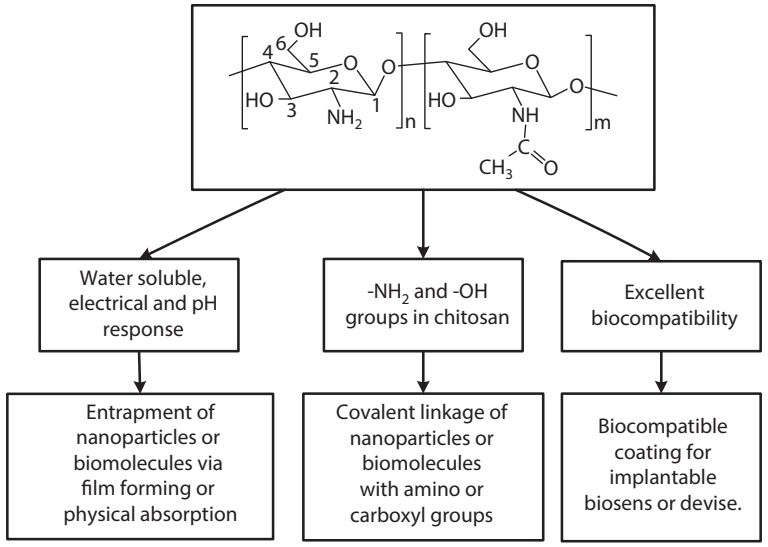

Figure 8.1 Schematic structure of chitosan and its favorable as biomaterials in biosensor. Chitosan is a natural-derived and biocompatible biomedical polymer with amino and hydroxyl groups. Amino groups in chitosan endow chitosan with pH-responsive solubility, immobilization of NPs and biomolecules via physical entrapment, chemical cross-linking or covalent linkage. The biocompatibility of chitosan allows increasing the biocompatibility of implanted biosensor.

is larger than 65 mol% [16]. Deacetylation releases free amine groups (–NH_2) and endows chitosan with polycationic feature. Chitosan has a pKa value of about 6.0~6.7 [17]. The molecular weight and solubility of chitosan strongly depend on the degree of deacetylation. Chitosan is a unique weak basic polysaccharide with amino groups [18]. Firstly, chitosan is soluble in acidic solutions when pH is below 6.5 due to the protonation of the amino groups. Thus, the solubility and positively charge density of chitosan depend on the pH, and it can absorb anions or neutral molecules by electrostatic attraction [19, 20]. The ionic conductivities of dry chitosan membrane range from 10^{-10} to 10^{-9} S cm^{-1}; however, in swollen state, the intrinsic ionic conductivity of chitosan reaches as high as 10^{-4} S cm^{-1} [21]. The entire conduction of swelling chitosan occurs when the water was incorporated into the membrane. Besides, chitosan has good film-forming ability, it can form homogeneous film after the solvent evaporated [22]. Due to these especial properties, chitosan has been extensively used for entrapment of NPs or biomolecules in the application of biomedicine and biosensor [23]. Moreover, chitosan also exhibits other special physical properties, such as viscosity, mucoadhesivity, polyoxysalt formation, polyelectrolyte behavior, and optical property [24].

In the scheme of chitosan, the hydroxy group on the C2 of the cellulose is replaced by the amino group. Thus, chitosan have both amino group and hydroxyl groups in glucosidic residue [25]. The presence of amino group enables chitosan to synthesize nanocomposites and immobilize biomolecules for biosensors via covalent bonds or hydrogen bond between amino group and carboxyl group with many biomolecules (antibodies, enzymes, amino acids, and nucleic acids) or functionalized NPs [26]. The amino groups in chitosan bind with metal ions to form chitosan/metal ions complex via chelation effect to synthesize many chitosan nanomaterials [27–30]. Although the activity of hydroxyl groups in chitosan is weaker than the amino group, they can be activated with some active agents (e.g., carbodiimide) to form covalent bonds with amino groups in biomolecules [31], which provides another method for the covalent immobilization of biomolecules.

8.2.2 Biocompatibility of Chitosan

Chitosan exhibits excellent biocompatibility and has been approved by FDA, and is generally recognized as safe natural biomedical polymers and clinical application in hemostatic dressing [32]. *In vivo*, chitosan is primarily modulated by lysozyme action during normal metabolism with degradation products of glycosides, which are nontoxic, nonimunogenic, and

noncarcinogenic [33]. The rate of the degradation is strongly dependent on the molecular weight and degree of deacetylation [34]. The acute toxicity of chitosan is oral LD_{50} was 16 g/kg in mice [35]. Thus chitosan is candidate in tissue engineering and orthopedic implants or drug delivery [36–39].

8.2.3 Chitosan Nanomaterials

The poor conductivity of chitosan hinders the direct electron transfer between molecules and biosensing platform [40], limiting its applications of chitosan in biosensing. To address this, chitosan has been combined with various nanomaterials for better electrochemical biosensing, such as carbon nanomaterials [carbon nanotubes (CNTs), graphene, and carbon dots (CDs)] [41–43], redox mediators [44], metal NPs [45], QDs [46], and ionic liquid [47] for electrochemical biosensing platforms. The nanomaterials exhibit many novel characteristics (e.g., good conductivity, large specific surface, excellent catalytic activity) [48–51]. Chitosan in combination with nanomaterials is a good candidate for biosensors [52]. Chitosan-based nanocomposites had been prepared by blending, *in situ* hybridization and chemical grafting.

8.2.3.1 Blending

Under the condition of thermodynamic equilibrium, blending at least two materials in the amorphous state which may exist as a single phase, the obtained blend will be homogenous on a microscopic scale [53–55].

The poor conductivity of chitosan limits the wide applications in biosensor. An effective approach for improving the conductivity of chitosan is to prepare chitosan nanocomposite by blending some good conductivity nanocomposite, such as carbon nanomaterials, metal or metal oxide NPs, and the procedure of the blending method was shown in Figure 8.2A. Jeyapragasam T *et al.* prepared a Fe_3O_4–chitosan nanocomposite by blending and the porous morphology of Fe_3O_4–chitosan nanocomposite was shown in Figure 8.3A [56]. Fe_3O_4–chitosan nanocomposite was favor for the effective immobilization of the acetylcholinesterase enzyme on electrode. Magnetic chitosan nanocomposite was used for the construction of a sensitive square wave voltammetric biosensor to detect carbofuran. CNT–chitosan nanocomposite was obtained by blending CNT with the solution of chitosan under ultrasonic and the morphology of the CNT–chitosan nanocomposite was shown in Figure 8.3B [57], in which chitosan was coated on the CNTs. Due to the good electrocatalysis and conductivity, CNT–chitosan nanocomposite modified glass carbon electrode (GCE)

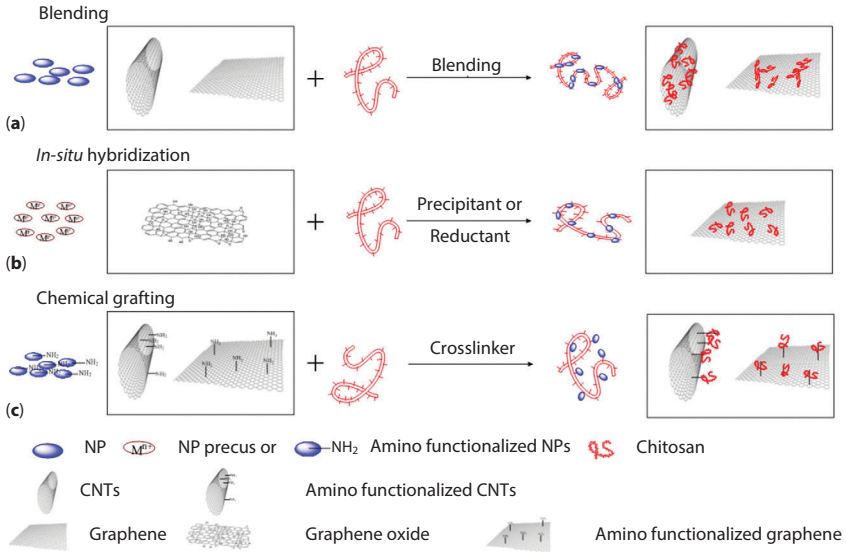

Figure 8.2 Schematic presentation of the three strategies for chitosan nanocomposite including blending usually accompanying with aggregation of NPs (a), *in situ* hybridization for homogenous chitosan nanocomposite (b), and chemical grafting for form covalent bonds between chitosan and nanomaterials (c).

was used for the detection of H_2O_2. Figure 8.3C shows the TEM image of GR–CS nanocomposite, clearly clarifying the crumpled and wrinkled flake structure [58]. The electrochemical study of the GR–CS nanocomposite proved the unique two-dimensional nanostructure of graphene could benefit to the conductivity of the nanocomposite. The chitosan/graphene films modified GCE was applied to detect the concentration of rutin. Blending is the simplest strategy for chitosan nanomaterials by mechanically mixing; however, the aggregation of NPs is still challenge, which is shown in Figure .3A–C.

8.2.3.2 In Situ *Hybridization*

To address the aggregation of NPs in chitosan nanomaterials, the *in situ* hybridization strategy is proposed as shown in Figure 8.2B. The precursor solution of metal or metal oxide or graphene oxide is added into chitosan solution, then the precipitant or reductant is dropped slowly in the previously chitosan solution to synthesize chitosan-based nanocomposites. Chitosan hydrogel acts as a chemical reactor and provides a hydrogel environment for precursor of reductant or precipitant solution. The graphene, metal, or metal oxide NPs are *in situ* synthesized in the chitosan

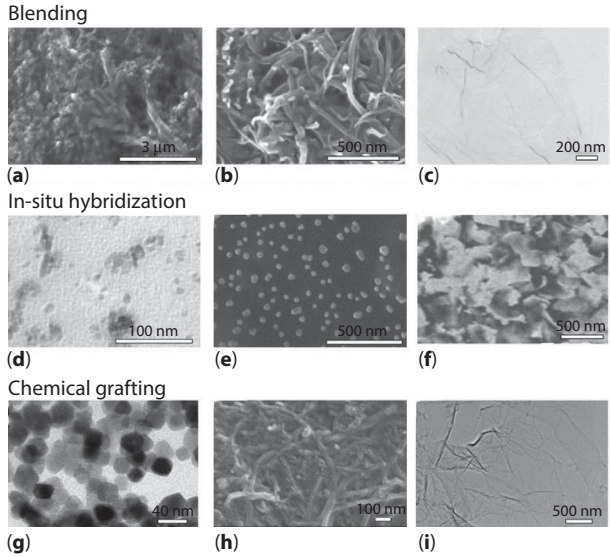

Figure 8.3 Morphologies of chitosan nanocomposite via different strategies, such as blending (A~C), *in situ* hybridization (D~F), and chemical grafting (G~I). Fe_3O_4–chitosan nanocomposite (scanning electron microscopy (SEM) image) (A) Reproduced with permission from T. Jeyapragasam and R. Saraswathi, *Sensors and Actuators B: Chemical*, 2014, **191**, 681. ©2014, Elsevier [56]; CNTs–chitosan nanocomposite (SEM image) (B) Reproduced with permission from Y.-T. Shieh, Y.-C. Tsai and Y.-K. Twu, *International Journal of Electrochemical Science*, 2013, **8**, 831. © 2013, [57]; graphene–chitosan (GR–CS) nanocomposite (scanning electron microscopy (SEM) image) (C) Reproduced with permission from J. An, Y.-Y. Bi, C.-X. Yang, F.-D. Hu and C.-M. Wang, *Journal of Pharmaceutical Analysis*, 2013, **3**, 102. © 2013, Elsevier [58]; Fe_3O_4–chitosan nanocomposite (TEM image) (D) Reproduced with permission from Y. Wang, B. Li, Y. Zhou, D. Jia and Y. Song, *Polymers for Advanced Technologies*, 2011, **22**, 1681. ©2011, John Wiley & Sons, Ltd. [59]; Fe_3O_4–chitosan nanocomposite (SEM image) (E) Reproduced with permission from L. D. Tran, B. H. Nguyen, N. Van Hieu, H. V. Tran, H. L. Nguyen and P. X. Nguyen, *Materials Science and Engineering C*, 2011, **31**, 477. © 2011, Elsevier [62]; GR–CS nanocomposite (F) Reproduced with permission from D. Han, T. Han, C. Shan, A. Ivaska and L. Niu, *Electroanal*, 2010, **22**, 2001. © 2010, WILEY-VCH Verlag GmbH & Co. KGaA, Weinheim [64]; Fe_3O_4–chitosan nanocomposite (TEM image) (G) Reproduced with permission from X. Liu, Q. Hu, Z. Fang, X. Zhang and B. Zhang, *Langmuir: The ACS Journal of Surfaces and Colloids*, 2008, **25**, 3. © 2009, American Chemical Society [65]; CNTs–chitosan nanocomposite (SEM image) (H) Reproduced with permission from D. Wan, S. Yuan, G. Li, K. Neoh and E. Kang, *ACS Applied Materials & Interfaces*, 2010, **2**, 3083. © 2010, American Chemical Society [66]; GR–CS nanocomposite (TEM image) (I), Reproduced with permission from Q. Zeng, J.-S. Cheng, X.-F. Liu, H.-T. Bai and J.-H. Jiang, *Biosensors and Bioelectronics*, 2011, **26**, 3456. © 2011, Elsevier [67].

framework via reduction or precipitation reaction. Due to chemical reduction or co-precipitation, the distribution of nanocomposites in chitosan is well homogeneous than blending. Wang Y *et al*. had synthesized chitosan-modified magnetite NPs by *in situ* hybridization [59–61]. Chitosan hydrogel was formed by glutaraldehyde or alkali treatment of chitosan solution. Then, chitosan hydrogel was impregnated by the $FeCl_3$ and $FeCl_2$ solution to achieve chitosan–iron ions complex which acts as the precursor of magnetite. Finally, the complex was soaked in the NaOH solution and degradation by lysozyme, chitosan/magnetite nanocomposite was achieved. The morphologies of the magnetite NPs modified by chitosan were shown in Figure 8.3D. The magnetic NPs with a diameter of 10 nm were uniformly dispersed in the chitosan. Tran L *et al.* prepared Fe_3O_4–chitosan nanocomposite by *in situ* hybridization [62]. The chitosan solution containing $FeCl_2$ and $FeCl_3$ with 1:2 (molar ratio) was dropped slowly into NaOH 30 wt.% solution to achieve Fe_3O_4–chitosan nanocomposite. As shown in Figure 8.3E, the Fe_3O_4 NPs were well dispersed in the chitosan matrix. The cyclic voltammograms of chitosan and Fe_3O_4–chitosan screen-printed electrodes (SPE) were used to evaluate the advantages of nanocomposite. This nanocomposite exhibited excellent electroactivity and conductivity. The resulted nanocomposites were applied for the construction of a DNA biosensor based on SPE for the electrochemical detection of short HIV sequences. The silver–chitosan nanocomposite was synthesized by considering chitosan acting as stabilizer and reductant for silver NPs [63]. The silver nitrate solution was dropped into a chitosan suspension to formation of Ag/chitosan colloids confirmed by coloration of the solution. GR–CS nanocomposite also can be prepared by *in situ* hybridization strategy. Chitosan-functionalized graphene was synthesized by blending in combination with *in situ* chemical reduction [64]. In their research, hydrazine and ammonia were used to reduce the mixture of chitosan and graphene oxide for the preparation of GR–CS nanocomposite. The morphology of the composite in Figure 8.3F shows that chitosan molecules are tightly attached onto the surface of the graphene nanosheets. The GR–CS-modified GCE with good catalytic activity was applied to detect the ascorbic acid, dopamine, and uric acid simultaneously.

In the case of *in situ* hybridization, the NPs were synthesized from ionic or soluble precursor in the chitosan hydrogel which guaranteed the well dispersion of NPs in the chitosan matrix. The synthesis of NPs or reduction process is simple and low cost similar to the blending. However, the *in situ* hybridization is only useful for the synthesis of graphene, metal, or metal oxide NPs–chitosan composites. During the synthesis of chitosan/metal oxide NPs including Fe_3O_4–chitosan nanocomposite, the alkali treatment limits the uptake of cell and drug during synthesis steps.

8.2.3.3 *Chemical Grafting*

The NPs were either entrapped by blending or *in situ* synthesized in chitosan by *in situ* hybridization; however, no covalent bonds between NPs and chitosan were formed. Thus, the stability of the chitosan nanocomposite is not maintained during service. To form covalent bonds between chitosan and NPs, surface modified NPs by grafting several functional groups was chemical grafted on chitosan chains as shown in Figure 8.2C. The Fe_3O_4–chitosan nanocomposite with high adsorption capacity was obtained adding amine-functionalized Fe_3O_4 NPs in chitosan solution and using glutaraldehyde as a coupling agent [65]. The TEM image of Fe_3O_4–chitosan nanocomposite was shown in Figure 8.3G. This nanocomposite provides a very efficient, fast, and convenient way to remove the heavy-metal ions in the pollution water. CNT–chitosan nanocomposite was constructed by carboxyl-functionalized CNTs (CNTs-COOH) in concentrated nitric/sulfuric acid and subsequent acryl chloride-functionalized CNTs (CNTs-COCl) in thionyl chloride solution [66], respectively. Then, the CNTs-COCl and chitosan were added to anhydrous DMF to achieve homogeneous and long-term stable CNT-chitosan nanocomposite. As shown in Figure 8.3H, the CNTs were uniformly dispersed in the chitosan, which enhanced the conductivity of chitosan. Meanwhile, chitosan improved the biocompatibility of CNTs. This composite was used for immobilization of glucose oxidase (GOD) to construct a glucose biosensor. Graphene was covalently linked with chitosan with purpose of improving the biocompatibility and hydrophilicity. Chitosan–graphene nanocomposites for glucose biosensor was synthesized by chemical grafting [67], in which chitosan was covalent bonded on the surface of graphene with flake-like wrinkled shapes (Figure 8.3I).

The new formed covalent bonds between chitosan and nanomaterials are favorable to maintain the stable conductivity of chitosan nanocomposite and immobilization efficiency of bioreceptor. However, the complex steps, long period of time and high cost for chitosan nanocomposite are main drawbacks of chemical grafting.

8.3 Application of Chitosan Nanocomposite in Biosensor

8.3.1 Biosensor Configurations and Bioreceptor Immobilization

Biosensor can proportionally respond the concentration of target analyte and transform the response to fathomable signals, such as optical,

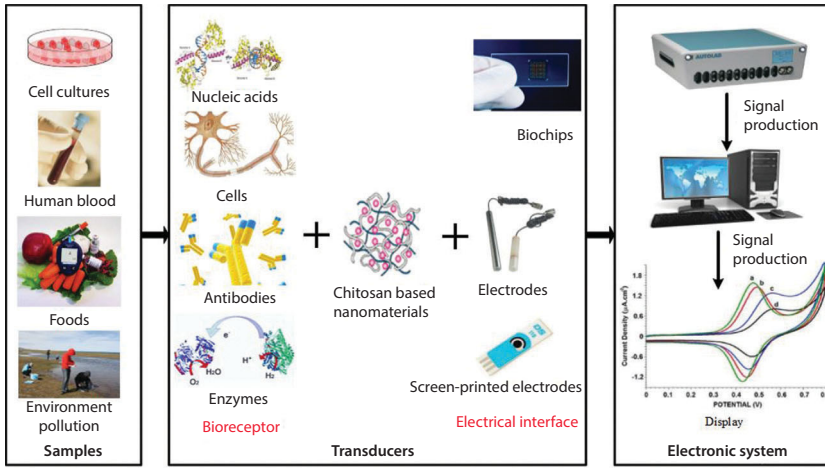

Figure 8.4 The elements of biosensor and chitosan nanomaterials used in the construction of biosensor.

electrochemical, or thermal signals [68]. Thus, according to the types of fathomable signals, biosensors are classified into optical, electrochemical, and thermal biosensors [69]. The biosensors mainly refer to electrochemical biosensors. As shown in Figure 8.4, biosensor has been widely used in the analysis of cell culture, human blood, food, and environment pollution samples. Electrochemical biosensors are composed of two main parts: transducers (bioreceptor immobilized on electrical interface) and electronic system [70]. Bioreceptor usually includes nucleic acids, cells, antibodies, and enzymes, while electrical includes biochips, electrodes, and SPE. Based on the different bioreceptors, biosensors can be categorized as DNA sensors, whole-cell sensors, immunosensors, and enzymatic sensors [71]. Electronic system consists of an electrochemical workstation for signal producing and a computer for signal processing and displaying. Compared with the traditional analytical methods, the biosensors have many advantages, such as the quickly response, potential miniaturization, portability, and low cost.

The efficient immobilization of bioreceptor on the electrical interface is still a challenge in biosensor research [72]. Bioreceptor immobilization provides a favorable environment for the maximum activity of the biological system [73]. Thus, the way of the bioreceptor immobilized is the main influence factor for the selectivity, sensitivity, and stability of the biosensor [74]. Therefore, finding more effective methods for the immobilization of bioreceptor is the valid way to improve the properties of biosensors. Chitosan nanomaterials have many advantages, such as good

biocompatibility, conductivity, large surface, and film-forming ability. Moreover, the amino groups and the positive charges of chitosan are key features for the immobilization of bioreceptor based on covalent linkage and physical absorption.

8.3.2 Biosensor Based on Chitosan Nanocomposite

The chitosan nanomaterials used in the construction of biosensor mainly include carbon nanomaterials–chitosan nanocomposite, metal and metal oxide–chitosan nanocomposite, QDs–chitosan nanocomposite, and ionic liquid–chitosan composite. The role of chitosan nanomaterials in the fabrication of biosensor usually refers to the immobilization of bioreceptor and biological labeling.

8.3.2.1 Biosensors Based on Carbon Nanomaterials–Chitosan Nanocomposite

The carbon nanomaterials normally consist of CNTs, graphene, and CDs. CNTs are one-dimensional nanomaterials, graphene is two-dimensional nanomaterial, and CDs are zero-dimensional nanomaterials [75]. Compared with carbon nanomaterials, carbon nanomaterials–chitosan nanocomposite introduced the functional groups and charges of chitosan to the nanocomposite. Thus, it is suitable for the construction of biosensors.

Usually, there are only few carboxyl groups on the surface of CNTs. However, these carboxyl groups are not enough for the immobilization of biomolecules. And, the film forming of CNTs on the electrodes is also very hard. The appearance of CNTs–chitosan nanocomposite successfully solved this problem. Zhang M *et al*. developed an ultrasensitive ECL immunosensor for prostate protein antigen (PSA) detection [76]. CNTs–chitosan nanocomposite was prepared by blending method. Then, AuNPs are adsorbed on the surface of this nanocomposite to form CNTs-CHIT/AuNPs nanocomposite. As shown in Figure 8.5A, chitosan nanocomposite was used for modifying SPCEs to immobilize antibodies of PSA. The analytical properties of the immunosensor were greatly improved by the dual-amplification techniques. The CNTs–CHIT/AuNPs can absorb more antibodies than naked CNTs. The second anti-PSA was labeled by PtAg@CDs which significantly improve the ECL intensity (up to six times) than the naked CDs-labeled anti-PSA. The detection range and detection limit of the concentration of PSA are for from 1 pg mL^{-1} to 50 ng mL^{-1} and 0.6 pg mL^{-1}, respectively. This PSA-specific ECL immunosensor with high sensitivity provided a diagnosis tool for tumor marker detection.

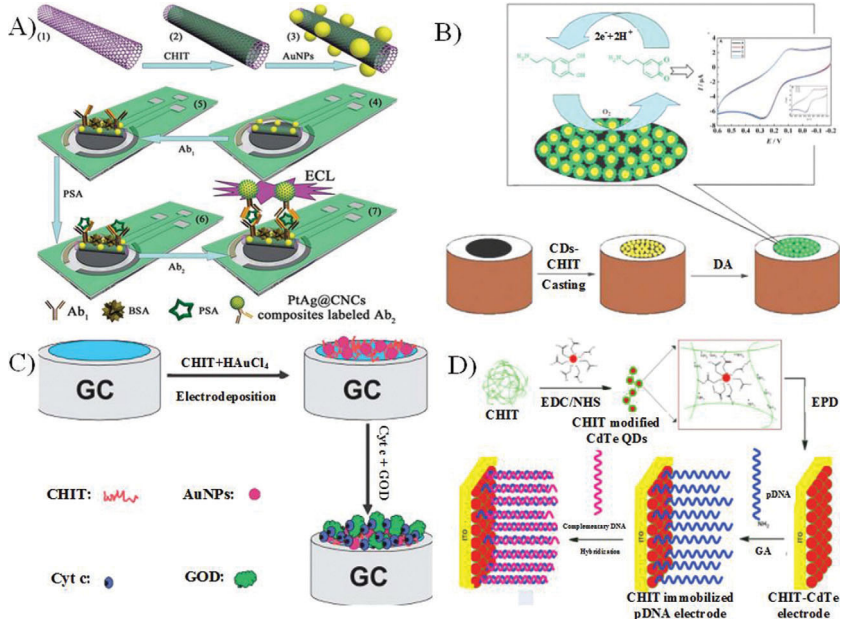

Figure 8.5 Biosensors based on chitosan nanocomposite. Sandwiched electrochemiluminescence (ECL) immunosensor with chitosan (CHIT)-functionalized CNTs modified screen-printed carbon electrode (SPCE) for the immobilization of prostate-specific antigen (PSA) antibodies for detecting PSA antigens (A) Reproduced with permission from M. Zhang, W. Dai, M. Yan, S. Ge, J. Yu, X. Song and W. Xu, *The Analyst*, 2012, **137**, 2112. ©2012, Royal Society of Chemistry [76]; A dopamine biosensor with the electrocatalysis of CDs-CHIT modified electrode (B) Reproduced with permission from Q. Huang, S. Hu, H. Zhang, J. Chen, Y. He, F. Li, W. Weng, J. Ni, X. Bao and Y. Lin, *The Analyst*, 2013, **138**, 5417. ©2013, Royal Society of Chemistry [91]; A glucose biosensor based on cytochrome c (cyt c) and GOD co-entrapped in CHIT–Au NPs modified electrode (C) Reproduced with permission from Y. Song, H. Liu, Y. Wang and L. Wang, *Analytical Methods*, 2013, **5**, 4165. ©2013, Royal Society of Chemistry [97]; A DNA biosensor for the detection of leukemia with probe DNA covalent bonded on CHIT encapsulated QDs platform (D) Reproduced with permission from A. Sharma, C. M. Pandey, G. Sumana, U. Soni, S. Sapra, A. Srivastava, T. Chatterjee and B. D. Malhotra, *Biosensors and Bioelectronics*, 2012, **38**, 107. © 2013, Elsevier [107].

The electrochemical DNA sensor based on DNA hybridization was a simple and effective method for detecting short DNA sequences. Wang *et al.* prepared a new DNA sensor based on CNTs–CHIT composite modified GCE with the capture probe DNA [77]. The chitosan nanocomposite in the biosensor could not only anchor capture DNA on the surface of GCE effectively, but also make the electron transfer easier for the electroactive molecules. The polypyridyl copper complex embedded in the nanocomposite was used as indicator which can distinguish double-stranded

DNA (dsDNA) from single-stranded DNA (ssDNA) in blood. The indicator could effectively identify the complementary DNA, three-base mismatched DNA and non-complementary DNA. In another research, the immobilization of probe DNA on the modified electrode was realized through covalent reaction between DNA and CNTs–chitosan nanocomposite with glutaraldehyde as an arm linker [78]. CNTs endow chitosan nanocomposite with high specific surface area and improve the electron conductivity of chitosan nanocomposite; meanwhile, chitosan is favorable to covalently immobilize the probe ssDNA through glutaraldehyde. Compared with other DNA sensors, this sensor obtained obvious advantages on the hybridization rate and efficiency. The cross-linking spacer of glutaraldehyde not only improved the freedom degree of ssDNA but also increased its space density on the electrode surface. Besides, CNTs–chitosan nanocomposite was also used in the fabrication of enzymatic sensors and nonenzymatic sensors [79–82].

Individual graphene sheets have extraordinary electronic transport properties [83]. But for reduced graphene, there was no functional group in its structure. Thus, it was not suitable for the application in biosensors. One possible route to harnessing this defect for application would be to incorporate graphene sheets in a composite material. Chitosan is the favorable candidate for the massive functional groups in its structure. Wen W *et al*. prepared a gas biosensor based on GR–CS nanocomposite with immobilization of hemoglobin (Hb) for detection of nitric oxide [84]. GR–CS nanocomposite with porous structure was synthesized to achieve the rough surface with high specific area. The pores of the rough GR–CS provided a favorable platform for the immobilization of the Hb. The Hb bioactivity was effectively maintained owing to the 3D interconnect pore structure of GR–CS. Thus, the sensitivity of electrochemical biosensor was greatly improved. A direct electrochemistry biosensor which was used for detecting hydrogen peroxide was proposed [85]. In the process of the construction of this biosensor, the Hb was grafted on the GR–CS, which created a beneficial microenvironment for retaining the bioactivity of the immobilized biomolecules. Additional, the carbon lattice in the two-dimensional GR–CS was composed of many sp^2-conjugated bonds.

The GR–CS can form on the electrode by direct electrodeposition. This method highly simplified the process for the fabrication of biosensors. GR–AuNPs–CS nanocomposite was obtained through electrochemical reduction of a solution containing graphene oxide, $HAuCl_4$ and chitosan by a cyclic voltammetry procedure between –1.6 and 0.6 V [86]. The incorporation of graphene and AuNPs in GR–CS enhances electrical conductivity and chitosan has good film-forming ability and water permeability. Owing

to combining the benefits of graphene, AuNPs and chitosan, the prepared sensor exhibited excellent response to Pb^{2+}. Under the optimum conditions, this sensor has a wide liner range from 0.5 to 100 μg L^{-1} and a detection limit of 0.1 ng L^{-1} in the detection of Pb^{2+}. This sensor was successfully applied in the detection of Pb^{2+} in the polluted water for environmental monitoring. Moreover, GR–CS has also been applied in DNA sensor and immunosensor [87]. To design the microstructure of GR–CS-modified electrode, He *et al.* prepared a GR–CS with multi-scale porous structure by ice segregation induced self-assembly technique [88]. Layered pores with size of 40~50 μm were formed by ice template, while micropores with size of 200~500 nm were formed by vacuum stripping. GR–CS with dual-mode porous structure could be used to immobilize biomolecules for the construction of biosensors.

As a class of zero-dimensional carbon nanomaterials, CDs have recently received considerable attention for their excellent water solubility, biocompatibility, and good photo stability [89]. These advantageous characteristics make CDs especially useful for fluorescent biosensing or imaging [90]. Compared with other electrode-modified materials, the exploration of CDs as electrochemical sensors also has high selectivity and sensitivity. Huang *et al.* designed a new quantitative method for quick, simple, and sensitive determination of dopamine with chitosan–CDs nanocomposite-based biosensor [91]. The process for the construction of the biosensor was shown in Figure 8.5B. CDs with carboxyl and hydroxyl groups were synthesized by microwaves. The hybrid film of CDs and chitosan could significantly enhance the electrochemical redox response of dopamine. Therefore, compare with bare GCE, the prepared biosensor showed better electrochemical response toward the detection of dopamine. A wide liner relationship between the oxidation peak current of dopamine was obtained.

8.3.2.2 Biosensors Based on Metal and Metal Oxide–Chitosan Nanocomposite

Metal and metal oxide nanomaterials were considered to have many advantages, such as superior conductivity, excellent catalytic activity, and good biocompatibility [92]. They can combine with biomolecules by physical adsorption or weak chemical bonds. The resulted composites were not stable for the binding force was too weak. It is the main limitation for the application of metal and metal oxide nanomaterials in biosensors. While the synthesis of metal and metal oxide–chitosan nanocomposite successfully solved this problem.

Gold NPs (AuNPs) are the most stable metal NPs with feasible linkage of biological molecules, such as antibodies, enzymes, and nucleic acids [93–95]. Moreover, AuNPs have obvious electrocatalytic activity for many electrochemical reactions [96]. Based on the above reasons, AuNPs have been widely used in the fabrication of biosensors. In the year 2013, Song *et al*. designed a glucose biosensor by co-entrapping cyt c and GOD on AuNPs–chitosan nanocomposite [97]. As shown in Figure 8.5C, the gold NPs–chitosan nanocomposite was constructed on glassy carbon electrode by one-step electrodeposition, which provided a rough surface for the immobilization of GOD. The surrounding cyt c around GOD offered a biocompatible microenvironment which could keep the biological activity of GOD successfully. Simultaneously, this nanostructure is better for the realization of the direct electron transfer of GOD. Due to above advantages, the biosensor exhibited superior sensitivity, detection limit and linear range in the detection of glucose. Compared with the naked AuNPs and iron NPs (FeNPs), gold-coated iron NPs (Au@FeNPs) have super paramagnetic property and good stability, for gold coating hinders the oxide of iron. Rooma D *et al*. designed the electrochemical biosensor based on CS-Au@FeNPs for detecting xanthine in fish meat. The CS-Au@FeNPs-modified pencil graphite electrode (PGE) was prepared by direct electrodeposition with a solution containing CS-Au@FeNPs and electrolyte. The applied potential was between –0.37 and 0.6 V with a scan rate of 50 mV/s. Then, xanthine oxidase was immobilized on the CS-Au@FeNPs-modified PGE by covalent grafting with glutaraldehyde as a cross-linker. Here, Au@FeNPs were used as electron transfer mediator which enhanced the direct electrons transport between electrode and xanthine oxidase. Applying in detection of xanthine in fish meat, this biosensor exhibited a quickly response time of 3 s, and had a wide liner range from 0.1 to 300 μmol L^{-1} and a low detection limit of 0.1μmol L^{-1}. Due to these advantages, the prepared biosensor was becoming a powerful tool for food monitoring [98].

Biosensors based on gold NPs–chitosan nanocomposite have to be integrated with specific ligand molecule in order to gain molecular recognition ability. However, ligand molecules, including enzymes, antibodies, and nucleic acids, are expensive and vulnerable to the change of outside environment. In the meantime, anchoring procedure of the ligand molecules to surface of the nanocomposites may hinder the bioactivity of these molecules. In order to overcome the disadvantages, Liu *et al*. developed a new colloid-type sensor by using naked Au nanorods (AuNRs) deposited on the surface of a colloidal chitosan carrier [99]. In their research, the stabilization of the bare-surfaced AuNRs in the presence of positively charged chitosan NPs colloids was achieved. The author found the reason

was the electrostatic attraction which ensures the stability for the resulting AuNR–chitosan colloids nanosuspension. The bare-surfaced AuNRs can generate a response of the analyte molecule by providing a pronounced spectral shift of the SPR spectrum. Tuning the solution pH, the resulting colloidal nanoprobe was able to detect human serum albumin with high specificity and sensitivity.

However, from the view of optical sensing, compared with Au NPs, the silver particles (AgNPs) are more desirable [100]. Besides, the shape of the NP also determines the sensitivity [101]. NPs with sharp shapes showed higher sensitivity refractive index than spherical NPs. Song and co-workers reports the preparation of triangular AgNPs–chitosan nanocomposite and its application in a surface plasmon resonance (SPR) biosensor [102]. This AgNPs–chitosan nanocomposite was prepared by blending the 3-mercaptopropinic acid-modified triangular AgNPs with chitosan and glutaraldehyde which was used as a chemical cross-linking agent. This composite was casted on Au film for modifying this platform for the biosensor. The chitosan cross-linked by glutaraldehyde ensures the antibodies can be effectively immobilized on the sensing platform via covalent bonds. The high-sensitive response of triangular AgNPs in the nanocomposite for the changes of the refractive index leads to the excellent performance of this biosensor in the detection of bovine IgG.

Due to its advantage of improving the transport of electrons between biomolecules and the electrode, metal oxides NPs were good candidates for the immobilization of bioreceptors in the construction of biosensors. Among all kinds of the metal oxide NPs, Fe_3O_4 NPs were considered as one of the most interesting materials due to its excellent biocompatibility and super paramagnetic behavior. Singh *et al*. constructed an electrochemical DNA biosensor based on Fe_3O_4–chitosan nanocomposite for detection of *Neisseria gonorrhoeae* which was the pathogen of a sexually transmitted disease [103]. In their research, the Fe_3O_4/chitosan nanostructure composite was formed onto ITO substrate by electrochemical approach. The biotinylated probe DNA was immobilized on chitosan–Fe_3O_4 nanocomposite-modified ITO electrode with avidin as a cross-linking agent. The detection of *N. gonorrhoeae* was realized by the change of electrochemical signals which generates from the discriminating the mismatches between the DNA probe and the targets with methylene blue as a redox indicator.

Zinc oxidation NPs (ZONPs), which possess a variety of fascinating properties, such as superior specific surface area, high catalytic efficiency, strong adsorption ability, and chemical stability, are considered as potential candidates for biosensing. An amperometric biosensor based on ZONPs–chitosan nanocomposite film for the detecting triglyceride was constructed

by Narang J [104]. The ZONPs–chitosan nanocomposite was formed by simply dispersing ZnO NPs into transparent chitosan solution. The nanocomposite was casted on the surface of a Pt electrode to provide a platform for the immobilization of three kinds of biomolecules (lipase, glycerol kinase, and glycerol-3-phosphate oxidase). The above biomolecules was covalently immobilized onto the chitosan–ZnO nanocomposite film with glutaraldehyde as a linker. The application of ZONPs–chitosan nanocomposite for the preparation of an amperometric biosensor has improved its performance in the detection of triglyceride in the terms of short response time, high sensitivity, and stability compared to earlier biosensors.

8.3.2.3 Biosensors Based on Quantum Dots–Chitosan Nanocomposite

QDs show the interesting application due to their optical properties, high catalytic efficiency, strong adsorption ability, and high surface activity [105]. Chitosan, as a natural cationic polysaccharide with abundant amino groups, offers ample binding sites for QDs and biomolecules [106]. Thus, surface functionalization of QDs with chitosan has been widely used in biosensors. To high efficiency link DNA probe with QDs via chitosan, Sharmav A *et al*. reported the DNA sensor based on chitosan encapsulated QDs for leukemia detection [107]. As shown in Figure 8.5D, chitosan was covalently conjugated with thioglycolic acid-modified CdTe QDs through amino-carboxyl reaction in presence of N-ethyl-N-(3-dimethylaminopropyl carbodiimide) (EDC). Then, the film of chitosan encapsulated CdTe QDs nanocomposite was coated on ITO electrode by electrophoretic deposition. Glutaraldehyde allows amine-terminated DNA covalently immobilization onto decoration electrode with chitosan–CdTe nanocomposite. The nanostructure composite-modified electrode exhibited wide liner range, high sensitivity, and stability in the detection of leukemia. A high ECL intensity biosensor based on CdSe QDs–graphene oxide–chitosan nanocomposite was developed by Wang T. *et al*. [108]. The porous structure of graphene oxide–chitosan composite provided not only abundant binging sites for the loading of CdSe QDs, but also large interface for electrochemical reactions on electrode. Especially, the amine groups of chitosan decreased the excitation energy of the ECL reaction which could enhance the ECL of CdSe QDs.

8.3.2.4 Biosensors Based on Ionic Liquid–Chitosan Nanocomposite

Ionic liquid (IL), a liquid electrolyte at temperature below 100 °C, consists of organic cations and various anions, such as imidazolium or pyridinium.

The features of IL favorable to the electrochemical biosensor include intrinsically high ionic conductivities, high electrochemical stability, and wide electrochemical windows. Ruan *et al*. designed a biosensor based on graphene–IL–chitosan nanocomposite with immobilization of myoglobin molecules for detection of trichloroacetic acid exhibited satisfying properties via direct electrochemistry and electrocatalysis [109]. The chitosan nanocomposite provides a gentle microenvironment for the direct electron transfer of myoglobin on the graphene–IL–chitosan-modified electrode. IL–chitosan was used to modify GCE, and gold–platinum alloy NPs were subsequently deposited on modified electrode by electrodeposition [110]. Finally, cholesterol oxidase was immobilized on the modified electrode. The fabricated biosensor was used to detect cholesterol in biochemical analysis.

Different kinds of chitosan nanocomposite constructed different types of biosensors. The bioreceptors were immobilized on the sensing platforms by different ways (physical adsorption, film forming, covalent linkage, or electrodeposition). The summary of the analytical performance of the biosensors based on chitosan nanocomposite above-mentioned was listed in Table 8.1.

8.4 Emerging Biosensor and Future Perspectives

The integration of biomaterials, information technology, and biosensor interfaces have led to the vision of implantable biosensor for monitoring personal health information and detecting the contaminant in food and environment. Based on biocompatible and biodegradable properties of chitosan, development of detection and signal communication, emerging biosensors, such as implanted biodegradable biosensor, wireless biosensor and wearable biosensor, have been developed to monitor the biomarker related with disease and personal health information. Schwerdt H *et al*. designed a fully passive microsystem that can wirelessly records and transmits neuropotentials exclusively [111]. As shown in Figure 8.6A, this microsystem is implanted in human brain and it works by means of electromagnetic backscattering techniques, affording substantially simpler circuitry and potentially safer and more reliable approach for implantable wireless neurorecording. Tolosa V *et al*. reported an implantable multi-electrode array microprobe for rapid glutamate detection [112]. The scheme of this device was shown in Figure 8.6B. For this biosensor, it used an iridium oxide reference electrode as an alternative to the common Ag/AgCl. Schazmann B *et al*. developed a wearable sodium sensor belt for real-time monitoring

Table 8.1 A summary of analytical performance of biosensors based on chitosan nanocomposite.

Chitosan nanocomposite	Type of biosensor	Immobilization of bioreceptor	Analyte	Linear range	Detection limit	Reference
CNTs–chitosan	Immunosensor	Physical adsorption	PSA antigen	1 pg mL^{-1}~50 ng mL^{-1}	0.6 pg mL^{-1}	[76]
CNTs–chitosan	DNA sensor	Covalent linkage	Cauliflower mosaic virus 35S DNA	1.0×10^{-13}~5.0×10^{-10} mol L^{-1}	8.5×10^{-14} mol L^{-1}	[77]
Graphene–chitosan	Enzyme biosensor	Film forming	Hydrogen peroxide	6.5×10^{-6}~2.3×10^{-4} mol L^{-1}	5.1×10^{-7} mol L^{-1}	[85]
Graphene–chitosan	Non-enzyme biosensor	Electrodeposition	Pb^{2+}	0.5~100 μg L^{-1}	0.1ng L^{-1}	[86]
CDs–chitosan	Non-enzyme biosensor	–	Dopamine	1.0×10^{-7}~3.0×10^{-5} mol L^{-1}	1.12×10^{-8} mol L^{-1}	[91]
Au@FeNPs–chitosan	Enzyme biosensor	Covalent linkage	Xanthine	0.1 ~300 μmol L^{-1}	0.1μmol L^{-1}	[98]
Silver nanoplates–chitosan	Immunosensor	Covalent linkage	Bovine IgG	7.5×10^{-8}~4.0×10^{-4} g mL^{-1}	7.5×10^{-8} g mL^{-1}	[102]
Fe_3O_4–chitosan	DNA sensor	Electrodeposition	*N. gonorrhoeae*	1.0×10^{-16}~1.0×10^{-6} mol L^{-1}	1.0×10^{-15} mol L^{-1}	[103]
ZnO–chitosan	Enzyme biosensor	Covalent linkage	Triglyceride	50–650 mg dL^{-1}	20 mg dL^{-1}	[104]
CdTe QDs–chitosan	DNA sensor	Covalent linkage	Leukemia	1.0×10^{-11}~1.0×10^{-6} mol L^{-1}	2.56×10^{-12} mol L^{-1}	[107]
Graphene–IL–chitosan	Enzyme biosensor	Film forming	Trichloroacetic acid	2.0×10^{-3}~1.0×10^{-2} mol L^{-1}	5.8×10^{-4} mol L^{-1}	[109]
IL–chitosan	Enzyme biosensor	Covalent linkage	Cholesterol	5.0×10^{-5}~6.2×10^{-3} mol L^{-1}	1.0×10^{-5} mol L^{-1}	[110]

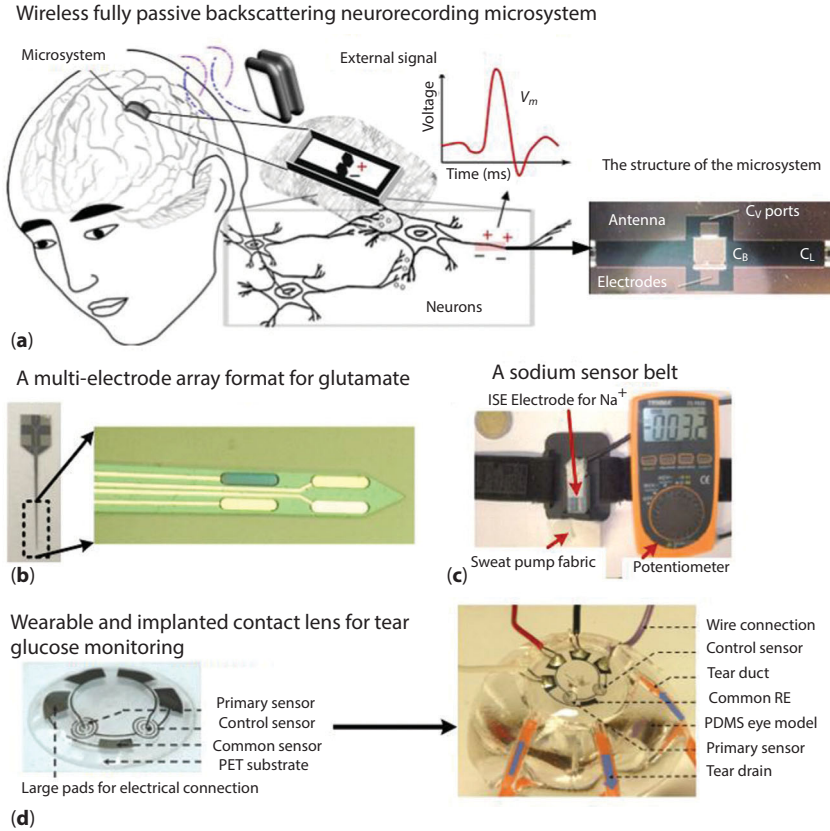

Figure 8.6 Emerging biosensors involved inter disciplinary, such as wireless fully passive backscattering neurorecording microsystem which was implanted in human head tissue in electronic engineering (A) Reproduced with permission from H. N. Schwerdt, F. A. Miranda and J. Chae, *IEEE Transactions on Microwave Theory and Techniques*, 2013, **61**, 2070. © 2013, IEEE [111]; implantable micromachined multi-electrode array microprobe with four platinum electrode sites at the tip for utilization as a complete electrochemical biosensor for rapid glutamate detection (B) Reproduced with permission from V. M. Tolosa, K. M. Wassum, N. T. Maidment and H. G. Monbouquette, *Biosensors and Bioelectronics*, 2013, **42**, 256. © 2013, Elsevier [112]; and fully biodegradable conduct polymers in material science; wearable sodium sensor belt consists of a sodium selective ion selective electrode integrated into a platform (C) Reproduced with permission from B. Schazmann, D. Morris, C. Slater, S. Beirne, C. Fay, R. Reuveny, N. Moyna and D. Diamond, *Analytical Methods*, 2010, **2**, 342. © 2010, Royal Society of Chemistry [113]; the molded contact lens and its initial system test setup with a polydimethylsiloxane (PDMS) eye model (D) Reproduced with permission from H. Yao, Y. Liao, A. R. Lingley, A. Afanasiev, I. Lähdesmäki, B. P. Otis and B. A. Parviz, *Journal of Micromechanics and Microengineering*, 2012, **22**, 075007. © 2012, IPO Science [114].

sodium concentrations of sweat [113], in which a sodium ion-selective electrode was installed into a platform. This platform could be interfaced with the human body in sports (Figure 8.6C). Implanted biosensor can be chronically implanted while wirelessly transmitting and processing massive amounts of data are necessary. As shown in Figure 8.6D, Yao H *et al.* reported the smart contact lens integrated with an electrochemical for non-invasively glucose sensor, in which activated and deactivated GODs were immobilized on transparent polyethylene terephthalate (PET) [114]. To real-time detect glucose concentration of tear wirelessly, sensor read-out circuit, antenna and telecommunication circuit were also integrated into contact lens. The detection of glucose concentrations with a range of 0~2 μM covers normal tear (0.1~0.6 μM). Google also developed smart contact lens in form of thin, flexible polymer to crack the mystery of tear glucose and measure it with greater accuracy. To design the patterned microstructure for construction of wearable biosensors, natural silk was used as template to flexible PDMS conducting membrane with high specific area and replicated silk-patterned microstructure [115]. The flexible PDMS with silk-like structure can be integrated with the uniform free-standing ultrathin film of single-walled CNTs to fabricate pressure sensors (e-skins). The application of e-skin in the detection of feather-light pressures presented superior sensitivity (1.80 kPa^{-1}), very low detectable pressure limit (0.6 Pa), fast response time (<10 ms), and high stability (>67500 cycles). A wearable ultrathin membrane device, consisting of TiO_2 nanomembrane, Au NPs and mesoporous silica NPs, could diagnose and treat some diseases caused by movement disorders. With the integration of some electronic components and drugs in this membrane, this wearable integrated system realized the diagnosis of diseases and then controlled the delivery of drugs on the basis of the diagnosis results [116].

Advancements in the fields of sensing chemistry, signal transduction mechanism, sensor fabrication technology, and data management will boost the development of biodegradable, implantable, wearable, wireless biosensor focusing on simultaneous detection of multiple species, minimization of devise and integration of different functional units. First, biosensors capable of analyzing multiple components simultaneously can represent an interesting tool in biomedicine and environmental monitoring. Biosensor based on large-scale biosensor array with detection areas of different species will help to reveal the potential relationships of multiple components related with biofunctions, to shorten testing time and reduce sample volume. Second, miniaturization of analytical systems will handle low-volume samples, reduce reagent consumption, and increase sample throughput. The use of a miniaturized flow cell and a microsensor will be

the key to realize this purpose. Moreover, the intelligence and integration degree of the biosensor will be improved continuously. The future biosensor will convergence nanobiomaterials with immobilized biomolecular, implanted biosensor with controlled biodegradation, wireless transition and diagnosis on portable devices, and collecting and processing the data automatically. The appearance of MEMS and microfluidic chip makes biosensor embedded into a microsystem with collecting, sampling, detecting, and processing units. Biosensor based on low-cost chitosan nanocomposite and automated manufacturing technologies will accelerate the popularity of affordable and reliable biosensor for healthcare, food safety, and environment protection.

Acknowledgments

Authors thank the financial support from National Science Foundation of China (51372051, 51321061, 11372243), National Basic Science Research Program (2012CB339300), State Key Laboratory of Urban Water Resource and Environment of Harbin Institute of Technology (2013TS09), Innovation Talents of Harbin Science and Engineering (2013RFLXJ023), and Fundamental Research Funds for Central Universities (HIT. IBRSEM.201302). F. Xu was financially supported by the Major International Joint Research Program of China (11120101002) and the Key (Key grant) Project of Chinese Ministry of Education (313045).

References

1. Y. Pang, G.-M. Zeng, L. Tang, Y. Zhang, Z. Li and L.-J. Chen, Laccase biosensor using magnetic multiwalled carbon nanotubes and chitosan/silica hybrid membrane modified magnetic carbon paste electrode. *Journal of Central South University of Technology*, 18, 1849–1856, 2011.
2. X. Feng, Y. Liu, Q. Kong, J. Ye, X. Chen, J. Hu and Z. Chen, Direct electrochemistry of myoglobin immobilized on chitosan-wrapped rod-constructed ZnO microspheres and its application to hydrogen peroxide biosensing. *Journal of Solid State Electrochemistry*, 14, 923–930, 2010.
3. F. N. Crespilho, M. E. Ghica, C. Gouveia-Caridade, O. N. Oliveira Jr and C. Brett, Enzyme immobilisation on electroactive nanostructured membranes (ENM): Optimised architectures for biosensing. *Talanta*, 76, 922–928, 2008.
4. G. Liu, M. N. Paddon-Row and J. Justin Gooding, A molecular wire modified glassy carbon electrode for achieving direct electron transfer to native glucose oxidase. *Electrochemistry Communications*, 9, 2218–2223, 2007.

5. K. Madhumathi, P. S. Kumar, S. Abhilash, V. Sreeja, H. Tamura, K. Manzoor, S. Nair and R. Jayakumar, Development of novel chitin/nanosilver composite scaffolds for wound dressing applications. *Journal of Materials Science: Materials in Medicine*, 21, 807–813, 2010.
6. K. Madhumathi, N. Binulal, H. Nagahama, H. Tamura, K. Shalumon, N. Selvamurugan, S. Nair and R. Jayakumar, Preparation and characterization of novelchitin–hydroxyapatite composite membranes for tissue engineering applications. *International Journal of Biological Macromolecules*, 44, 1–5, 2009.
7. G. Singh Dhillon, S. Kaur, S. Jyoti Sarma, S. Kaur Brar, M. Verma and R. Yadagiri Surampalli, Recent development in applications of important biopolymer chitosan in biomedicine, pharmaceuticals and personal care products. *Current Tissue Engineering*, 2, 20–40, 2013.
8. A. Tiwari and S. Gong, Electrochemical study of chitosan-SiO2-MWNT composite electrodes for the fabrication of cholesterol biosensors. *Electroanalysis*, 20, 2119–2126, 2008.
9. S. Rudershausen, C. Grüttner, M. Frank, J. Teller and F. Westphal, Multifunctional superparamagnetic nanoparticles for life science applications. *European Cells and Materials*, 3, 81–83, 2002.
10. J. K. Oh and J. M. Park, Iron oxide-based superparamagnetic polymeric nanomaterials: design, preparation, and biomedical application. *Progress in Polymer Science*, 36, 168–189, 2011.
11. J. M. Spruell and C. J. Hawker, Triggered structural and property changes in polymeric nanomaterials. *Chemical Science*, 2, 18–26, 2011.
12. C. S. Kumar, *Nanomaterials for Cancer Therapy*, Weinheim, Germany: Wiley-VCH, 2006.
13. C. S. Kumar, *Nanomaterials for Cancer Diagnosis*, Weinheim, Germany: Wiley-VCH, 2007.
14. F. Qian, F. Cui, J. Ding, C. Tang and C. Yin, Chitosan graft copolymer nanoparticles for oral protein drug delivery: preparation and characterization. *Biomacromolecules*, 7, 2722–2727, 2006.
15. I. Aranaz, R. Harris and A. Heras, Chitosan amphiphilic derivatives. Chemistry and applications. *Current Organic Chemistry*, 14, 308, 2010.
16. M. Rinaudo, Chitin and chitosan: properties and applications. *Progress in Polymer Science*, 31, 603–632, 2006.
17. D. R. Bhumkar and V. B. Pokharkar, Studies on effect of pH on cross-linking of chitosan with sodium tripolyphosphate: a technical note. *Aaps Pharmscitech*, 7, E138–E143, 2006.
18. P. K. Dutta, J. Dutta and V. Tripathi, Chitin and chitosan: Chemistry, properties and applications. *Journal of Scientific and Industrial Research*, 63, 20–31, 2004.
19. Y. Lin, Q. Chen and H. Luo, Preparation and characterization of (2-carboxybenzyl) chitosan as a potential pH-sensitive hydrogel for drug delivery. *Carbohydrate Research*, 342, 87–95, 2007.

20. L. Ilium, Chitosan and its use as a pharmaceutical excipient. *Pharmaceutical Research*, 15, 1326–1331, 1998.
21. Y. Wan, K. A. Creber, B. Peppley and V. T. Bui, Ionic conductivity of chitosan membranes. *Polymer*, 44, 1057–1065, 2003.
22. Y. Xu, K. M. Kim, M. A. Hanna and D. Nag, Chitosan–starch composite film: preparation and characterization. Industrial Crops and Products. *Industrial Crops and Products*, 21, 185–192, 2005.
23. A. Sugunan, C. Thanachayanont, J. Dutta and J. Hilborn, Heavy-metal ion sensors using chitosan-capped gold nanoparticles. *Science and Technology of Advanced Materials*, 6, 335–340, 2005.
24. S. K. Shukla, A. K. Mishra, O. A. Arotiba and B. B. Mamba, Chitosan-based nanomaterials: a state-of-the-art review. *International Journal of Biological Macromolecules*, 59, 46–58, 2013.
25. P. Agrawal, G. J. Strijkers and K. Nicolay, Chitosan-based systems for molecular imaging. *Advanced Drug Delivery Reviews*, 62, 42–58, 2010.
26. H. Yi, L.-Q. Wu, W. E. Bentley, R. Ghodssi, G. W. Rubloff, J. N. Culver and G. F. Payne, Biofabrication with chitosan. *Biomacromolecules*, 6, 2881–2894, 2005.
27. Y. L. Wang, B. Q. Li, Y. Zhou, D. C. Jia and Y. Song, CS-Fe(II,III) complex as precursor for magnetite nanocrystal. *Polymers for Advanced Technologies*, 22, 1681–1684, 2011.
28. A. Corma and H. Garcia, Supported gold nanoparticles as catalysts for organic reactions. *Chemical Society Reviews*, 37, 2096–2126, 2008.
29. Y. Wang, B. Li, Y. Zhou, Z. Han, Y. Feng and D. Wei, A facile concentric-layered magnetic chitosan hydrogel with magnetic field remote stimulated drug release. *Journal of Controlled Release*, 172, e90, 2013.
30. Y. L. Wang, B. Q. Li, Y. Zhou and D. C. Jia, *In situ* mineralization of magnetite nanoparticles in chitosan hydrogel. *Nanoscale Research Letters*, 4, 1041–1046, 2009.
31. S.-H. Chiou and W.-T. Wu, Immobilization of Candida rugosalipase on chitosan with activation of the hydroxyl groups. *Biomaterials*, 25, 197–204, 2004.
32. K. Y. Lee, W. S. Ha and W. H. Park, Blood compatibility and biodegradability of partially N-acylated chitosan derivatives. *Biomaterials*, 16, 1211–1216, 1995.
33. F.-L. Mi, Y.-C. Tan, H.-F. Liang and H.-W. Sung, *In vivo* biocompatibility and degradability of a novel injectable-chitosan-based implant. *Biomaterials*, 23, 181–191, 2002.
34. D. Pantaleone, M. Yalpani and M. Scollar, Unusual susceptibility of chitosan to enzymic hydrolysis. *Carbohydrate Research*, 237, 325–332, 1992.
35. M. Dash, F. Chiellini, R. Ottenbrite and E. Chiellini, Chitosan—a versatile semi-synthetic polymer in biomedical applications. *Progress in Polymer Science*, 36, 981–1014, 2011.
36. P. J. VandeVord, H. W. Matthew, S. P. DeSilva, L. Mayton, B. Wu and P. H. Wooley, Evaluation of the biocompatibility of a chitosan scaffold in mice. *Journal of Biomedical Materials Research*, 59, 585–590, 2002.

37. X.-G. Chen, C.-S. Liu, C.-G. Liu, X.-H. Meng, C. M. Lee and H.-J. Park, Preparation and biocompatibility of chitosan microcarriers as biomaterial. *Biochemical Engineering Journal*, 27, 269–274, 2006.
38. Y. Liu, X. Qu, H. Guo, H. Chen, B. Liu and S. Dong, Facile preparation of amperometric laccase biosensor with multifunction based on the matrix of carbon nanotubes–chitosan composite. *Biosensors and Bioelectronics*, 21, 2195–2201, 2006.
39. N. Bhattarai, J. Gunn and M. Zhang, Chitosan-based hydrogels for controlled, localized drug delivery. Advanced drug delivery reviews. *Advanced Drug Delivery Reviews*, 62, 83–99, 2010.
40. X. Lu, J. Hu, X. Yao, Z. Wang and J. Li, Composite system based on chitosan and room-temperature ionic liquid: direct electrochemistry and electrocatalysis of hemoglobin. *Biomacromolecules*, 7, 975–980, 2006.
41. M. Zhang, A. Smith and W. Gorski,Carbon nanotube-chitosan system for electrochemical sensing based on dehydrogenase enzymes. *Analytical Chemistry*, 76, 5045–5050, 2004.
42. P. Deng, Z. Xu and Y. Kuang, Electrochemical determination of bisphenol A in plastic bottled drinking water and canned beverages using a molecularly imprinted chitosan–graphene composite film modified electrode. *Food Chemistry*, 157, 490–497, 2014.
43. Q. Huang, H. Zhang, S. Hu, F. Li, W. Weng, J. Chen, Q. Wang, Y. He, W. Zhang and X. Bao, A sensitive and reliable dopamine biosensor was developed based on the Au@ carbon dots–chitosan composite film. *Biosensors and Bioelectronics*, 52, 277–280, 2014.
44. T. Gu, J. Wang, H. Xia, S. Wang and X. Yu, Direct electrochemistry and electrocatalysis of horseradish peroxidase immobilized in a DNA/chitosan-Fe_3O_4 magnetic nanoparticle bio-complex film. *Materials*, 7, 1069–1083, 2014.
45. B. Wang, X. Ji, H. Zhao, N. Wang, X. Li, R. Ni and Y. Liu, An amperometric β-glucan biosensor based on the immobilization of bi-enzyme on Prussian blue–chitosan and gold nanoparticles–chitosan nanocomposite films. *Biosensors and Bioelectronics*, 55, 113–119, 2014.
46. Q. Ma, Z.-H. Lin, N. Yang, Y. Li and X.-G. Su, A novel carboxymethyl chitosan–quantum dot-based intracellular probe for Zn^{2+}ion sensing in prostate cancer cells. *Acta Biomaterialia*, 10, 868–874, 2014.
47. B. Kavosi, A. Salimi, R. Hallaj and K. Amani, A highly sensitive prostate-specific antigen immunosensor based on gold nanoparticles/PAMAM dendrimer loaded on MWCNTS/chitosan/ionic liquid nanocomposite. *Biosensors and Bioelectronics*, 52, 20–28, 2014.
48. S. Cuenot, C. Frétigny, S. Demoustier-Champagne and B. Nysten, Surface tension effect on the mechanical properties of nanomaterials measured by atomic force microscopy. *Physical Review B*, 69, 165410, 2004.
49. A. Stroyuk, A. Kryukov, S. Y. Kuchmii and V. Pokhodenko, Quantum size effects in semiconductor photocatalysis. *Theoretical and Experimental Chemistry*, 41, 207–228, 2005.

50. E. L. Tae, K. E. Lee, J. S. Jeong and K. B. Yoon, Synthesis of diamond-shape titanate molecular sheets with different sizes and realization of quantum confinement effect during dimensionality reduction from two to zero. *Journal of the American Chemical Society*, 130, 6534–6543, 2008.
51. R. Wang, C. Liu, H. Zhang, C. Chen, L. Guo, H. Xu and S. Yang, Porous nanotubes of Co_3O_4: synthesis, characterization, and magnetic properties. *Applied Physics Letters*, 85, 2080–2082, 2004.
52. L. Zhang, G. Han, Y. Liu, J. Tang and W. Tang, Immobilizing haemoglobin on gold/graphene–chitosan nanocomposite as efficient hydrogen peroxide biosensor. *Sensors and Actuators B: Chemical*, 197, 164–171, 2014.
53. L. Averous, N. Fauconnier, L. Moro and C. Fringant, Blends of thermoplastic starch and polyesteramide: processing and properties. *Journal of Applied Polymer Science*, 76, 1117–1128, 2000.
54. N. Grizzuti, G. Buonocore and G. Iorio, Viscous behavior and mixing rules for an immiscible model polymer blend. *Journal of Rheology (1978-Present)*, 44, 149–164, 2000.
55. C. L. Tucker III and P. Moldenaers, Microstructural evolution in polymer blends. *Annual Review of Fluid Mechanics*, 34, 177–210, 2002.
56. T. Jeyapragasam and R. Saraswathi, Electrochemical biosensing of carbofuran based on acetylcholinesterase immobilized onto iron oxide–chitosan nanocomposite. *Sensors and Actuators B: Chemical*, 191, 681–687, 2014.
57. Y.-T. Shieh, Y.-C. Tsai and Y.-K. Twu, Electrocatalytic behavior and H_2O_2 detection of carbon nanotube/chitosan nanocomposites prepared via different acidic aqueous solutions. *International Journal of Electrochemical Science*, 8, 831–845, 2013.
58. J. An, Y.-Y. Bi, C.-X. Yang, F.-D. Hu and C.-M. Wang, Electrochemical study and application on rutin at chitosan/graphene films modified glassy carbon electrode. *Journal of Pharmaceutical Analysis*, 3, 102–108, 2013.
59. Y. Wang, B. Li, Y. Zhou, D. Jia and Y. Song, CS-Fe (II, III) complex as precursor for magnetite nanocrystal. *Polymers for Advanced Technologies*, 22, 1681–1684, 2011.
60. Y. Wang, B. Li, F. Xu, D. Jia, Y. Feng and Y. Zhou, *In vitro* cell uptake of biocompatible magnetite/chitosan nanoparticles with high magnetization: a single-step synthesis approach for in-situ-modified magnetite by amino groups of chitosan. *Journal of Biomaterials Science, Polymer Edition*, 23, 843–860, 2012.
61. B. Li, D. Jia, Y. Zhou, Q. Hu and W. Cai, In situ hybridization to chitosan/magnetite nanocomposite induced by the magnetic field. *Journal of Magnetism and Magnetic Materials*, 306, 223–227, 2006.
62. L. D. Tran, B. H. Nguyen, N. Van Hieu, H. V. Tran, H. L. Nguyen and P. X. Nguyen, Electrochemical detection of short HIV sequences on chitosan/Fe_3O_4nanoparticle based screen printed electrodes. *Materials Science and Engineering: C*, 31, 477–485, 2011.
63. Y. K. Twu, Y. W. Chen and C. M. Shih, Preparation of silver nanoparticles using chitosan suspensions. *Powder Technology*, 185, 251–257, 2008.

64. D. Han, T. Han, C. Shan, A. Ivaska and L. Niu, Simultaneous determination of ascorbic acid, dopamine and uric acid with chitosan-graphene modified electrode. *Electroanalysis*, 22, 2001–2008, 2010.
65. X. Liu, Q. Hu, Z. Fang, X. Zhang and B. Zhang, Magnetic chitosan nanocomposites: a useful recyclable tool for heavy metal ion removal. *Langmuir: The ACS Journal of Surfaces and Colloids*, 25, 3–8, 2008.
66. D. Wan, S. Yuan, G. Li, K. Neoh and E. Kang, Glucose biosensor from covalent immobilization of chitosan-coupled carbon nanotubes on polyaniline-modified gold electrode. *ACS Applied Materials & Interfaces*, 2, 3083–3091, 2010.
67. Q. Zeng, J.-S. Cheng, X.-F. Liu, H.-T. Bai and J.-H. Jiang, Palladium nanoparticle/chitosan-grafted graphene nanocomposites for construction of a glucose biosensor. *Biosensors and Bioelectronics*, 26, 3456–3463, 2011.
68. R. Singhal, W. Takashima, K. Kaneto, S. Samanta, S. Annapoorni and B. Malhotra, Langmuir–Blodgett films of poly (3-dodecyl thiophene) for application to glucose biosensor. *Sensors and Actuators B: Chemical*, 86, 42–48, 2002.
69. P. Arora, A. Sindhu, N. Dilbaghi and A. Chaudhury, Biosensors as innovative tools for the detection of food borne pathogens. *Biosensors and Bioelectronics*, 28, 1–12, 2011.
70. J.-M. Kauffmann, Biosensors: unique tools in the pharmaceutical era. *Arhiv za farmaciju*, 52, 121–127, 2002.
71. S. Rodriguez-Mozaz, M.-P. Marco, M. de Alda and D. Barceló, Biosensors for environmental applications: future development trends. *Pure and Applied Chemistry*, 76, 723–752, 2004.
72. A. P. Turner, Current trends in biosensor research and development. *Sensors and Actuators*, 17, 433–450, 1989.
73. A. Salimi, E. Sharifi, A. Noorbakhsh and S. Soltanian, Direct electrochemistry and electrocatalytic activity of catalase immobilized onto electrodeposited nano-scale islands of nickel oxide. *Biophysical Chemistry*, 125, 540–548, 2007.
74. B. Pejcic, R. De Marco and G. Parkinson, The role of biosensors in the detection of emerging infectious diseases. *The Analyst*, 131, 1079–1090, 2006.
75. W. Yang, K. R. Ratinac, S. P. Ringer, P. Thordarson, J. J. Gooding and F. Braet, Carbon nanomaterials in biosensors: should you use nanotubes or graphene? *Angewandte Chemie International Edition*, 49, 2114–2138, 2010.
76. M. Zhang, W. Dai, M. Yan, S. Ge, J. Yu, X. Song and W. Xu, Ultrasensitive electrochemiluminescence immunosensor using PtAg@ carbon nanocrystals composites as labels and carbon nanotubes-chitosan/gold nanoparticles as enhancer. *The Analyst*, 137, 2112–2118, 2012.
77. Q. Wang, J. Shi, J. Ni, F. Gao, F. Gao, W. Weng and K. Jiao, DNA hybridization biosensor using chitosan-carbon nanotubes composite film as an immobilization platform and [Cu (bpy)$(MBZ)_2$(H2O)](bpy= 2, 2′-bipyridine, MBZ=p-methylbenzoate) as a novel redox indicator. *Electrochimica Acta*, 56, 3829–3834, 2011.

78. Q. Wang, B. Zhang, X. Lin and W. Weng, Hybridization biosensor based on the covalent immobilization of probe DNA on chitosan–mutiwalled carbon nanotubes nanocomposite by using glutaraldehyde as an arm linker. *Sensors and Actuators B: Chemical*, 156, 599–605, 2011.
79. Y. Tan, W. Deng, B. Ge, Q. Xie, J. Huang and S. Yao, Biofuel cell and phenolic biosensor based on acid-resistant laccase–glutaraldehyde functionalized chitosan–multiwalled carbon nanotubes nanocomposite film. *Biosensors and Bioelectronics*, 24, 2225–2231, 2009.
80. X. Che, R. Yuan, Y. Chai, J. Li, Z. Song, W. Li and X. Zhong, A glucose biosensor based on chitosan–Prussian blue–multiwall carbon nanotubes–hollow PtCo nanochains formed by one-step electrodeposition. *Colloids and Surfaces B: Biointerfaces*, 84, 454–461, 2011.
81. M. Diaconu, S. C. Litescu and G. L. Radu, Bienzymatic sensor based on the use of redox enzymes and chitosan–MWCNT nanocomposite. *Microchimica Acta*, 172, 177–184, 2011.
82. A. Fatoni, A. Numnuam, P. Kanatharana, W. Limbut, C. Thammakhet and P. Thavarungkul, A highly stable oxygen-independent glucose biosensor based on a chitosan-albumin cryogel incorporated with carbon nanotubes and ferrocene. *Sensors and Actuators B: Chemical*, 185, 725–734, 2013.
83. S. Stankovich, D. A. Dikin, G. H. Dommett, K. M. Kohlhaas, E. J. Zimney, E. A. Stach, R. D. Piner, S. T. Nguyen and R. S. Ruoff, Graphene-based composite materials. *Nature*, 442, 282–286, 2006.
84. W. Wen, W. Chen, Q.-Q. Ren, X.-Y. Hu, H.-Y. Xiong, X.-H. Zhang, S.-F. Wang and Y.-D. Zhao, A highly sensitive nitric oxide biosensor based on hemoglobin–chitosan/graphene–hexadecyltrimethylammonium bromide nanomatrix. *Sensors and Actuators B: Chemical*, 166, 444–450, 2012.
85. H. Xu, H. Dai and G. Chen, Direct electrochemistry and electrocatalysis of hemoglobin protein entrapped in graphene and chitosan composite film. *Talanta*, 81, 334–338, 2010.
86. Z. Lu, S. Yang, Q. Yang, S. Luo, C. Liu and Y. Tang, A glassy carbon electrode modified with graphene, gold nanoparticles and chitosan for ultrasensitive determination of lead (II). *Microchimica Acta*, 180, 555–562, 2013.
87. A. Singh, G. Sinsinbar, M. Choudhary, V. Kumar, R. Pasricha, H. Verma, S. P. Singh and K. Arora,Graphene oxide-chitosan nanocomposite based electrochemical DNA biosensor for detection of typhoid. *Sensors and Actuators B: Chemical*, 185, 675–684, 2013.
88. Z. He, J. Liu, Y. Qiao, C. M. Li and T. T. Y. Tan, Architecture engineering of hierarchically porous chitosan/vacuum-stripped graphene scaffold as bioanode for high performance microbial fuel cell. *Nano Letters*, 12, 4738–4741, 2012.
89. S. Zhu, Q. Meng, L. Wang, J. Zhang, Y. Song, H. Jin, K. Zhang, H. Sun, H. Wang and B. Yang, Highly photoluminescent carbon dots for multicolor patterning, sensors, and bioimaging. *Angewandte Chemie*, 125, 4045–4049, 2013.

90. P. G. Luo, S. Sahu, S.-T. Yang, S. K. Sonkar, J. Wang, H. Wang, G. E. LeCroy, L. Cao and Y.-P. Sun, Carbon "quantum" dots for optical bioimaging. *Journal of Materials Chemistry B*, 1, 2116–2127, 2013.
91. Q. Huang, S. Hu, H. Zhang, J. Chen, Y. He, F. Li, W. Weng, J. Ni, X. Bao and Y. Lin, Carbon dots and chitosan composite film based biosensor for the sensitive and selective determination of dopamine. *The Analyst*, 138, 5417–5423, 2013.
92. X. Shi, W. Gu, B. Li, N. Chen, K. Zhao and Y. Xian, Enzymatic biosensors based on the use of metal oxide nanoparticles. *Microchimica Acta*, 181, 1–22, 2014.
93. M.-C. Daniel and D. Astruc, Gold nanoparticles: assembly, supramolecular chemistry, quantum-size-related properties, and applications toward biology, catalysis, and nanotechnology. *Chemical Reviews*, 104, 293–346, 2004.
94. I. H. El-Sayed, X. Huang and M. A. El-Sayed, Surface plasmon resonance scattering and absorption of anti-EGFR antibody conjugated gold nanoparticles in cancer diagnostics: applications in oral cancer. *Nano Letters*, 5, 829–834, 2005.
95. J. A. Copland, M. Eghtedari, V. L. Popov, N. Kotov, N. Mamedova, M. Motamedi and A. A. Oraevsky, Bioconjugated gold nanoparticles as a molecular based contrast agent: implications for imaging of deep tumors using optoacoustic tomography. *Molecular Imaging & Biology*, 6, 341–349, 2004.
96. M. Haruta, Size-and support-dependency in the catalysis of gold. *Catalysis Today*, 36, 153–166, 1997.
97. Y. Song, H. Liu, Y. Wang and L. Wang, A glucose biosensor based on cytochrome c and glucose oxidase co-entrapped in chitosan–gold nanoparticles modified electrode. *Analytical Methods*, 5, 4165–4171, 2013.
98. R. Devi, S. Yadav, R. Nehra, S. Yadav and C. Pundir, Electrochemical biosensor based on gold coated iron nanoparticles/chitosan composite bound xanthine oxidase for detection of xanthine in fish meat. *Journal of Food Engineering*, 115, 207–214, 2013.
99. R.-D. Jean, W.-D. Cheng, M.-H. Hsiao, F.-H. Chou, J.-S. Bow and D.-M. Liu, Highly electrostatically-induced detection selectivity and sensitivity for a colloidal biosensor made of chitosan nanoparticle decorated with a few bare-surfaced gold nanorods. *Biosensors and Bioelectronics*, 52, 111–117, 2014.
100. J. Hu, Z. Wang and J. Li, Gold nanoparticles with special shapes: controlled synthesis, surface-enhanced Raman scattering, and the application in biodetection. *Sensors*, 7, 3299–3311, 2007.
101. M. Pelton, J. E. Sader, J. Burgin, M. Liu, P. Guyot-Sionnest and D. Gosztola, Damping of acoustic vibrations in gold nanoparticles. *Nature Nanotechnology*, 4, 492–495, 2009.
102. J. Zhang, Y. Sun, H. Zhang, B. Xu, H. Zhang and D. Song, Preparation and application of triangular silver nanoplates/chitosan composite in surface Plasmon resonance biosensing. *Analytica Chimica Acta*, 769, 114–120, 2013.
103. R. Singh, R. Verma, A. Kaushik, G. Sumana, S. Sood, R. K. Gupta and B. Malhotra, Chitosan–iron oxide nano-composite platform for mismatch-discriminating DNA hybridization for Neisseria gonorrhoeae detection causing

sexually transmitted disease. *Biosensors and Bioelectronics*, 26, 2967–2974, 2011.
104. J. Narang and C. Pundir,Construction of a triglyceride amperometric biosensor based on chitosan–ZnO nanocomposite film. *International Journal of Biological Macromolecules*, 49, 707–715, 2011.
105. U. Soni and S. Sapra, The importance of surface in core–shell semiconductor nanocrystals. *The Journal of Physical Chemistry C*, 114, 22514–22518, 2010.
106. A. Boccaccini, S. Keim, R. Ma, Y. Li and I. Zhitomirsky, Electrophoretic deposition of biomaterials. *Journal of the Royal Society Interface*, 7, S581–S613, 2010.
107. A. Sharma, C. M. Pandey, G. Sumana, U. Soni, S. Sapra, A. Srivastava, T. Chatterjee and B. D. Malhotra, Chitosan encapsulated quantum dots platform for leukemia detection. *Biosensors and Bioelectronics*, 38, 107–113, 2012.
108. T. Wang, S. Zhang, C. Mao, J. Song, H. Niu, B. Jin and Y. Tian, Enhanced electrochemiluminescence of CdSe quantum dots composited with graphene oxide and chitosan for sensitive sensor. *Biosensors and Bioelectronics*, 31, 369–375, 2012.
109. C. Ruan, T. Li, Q. Niu, M. Lu, J. Lou, W. Gao and W. Sun, Electrochemical myoglobin biosensor based on graphene–ionic liquid–chitosan bionanocomposites: direct electrochemistry and electrocatalysis. *Electrochimica Acta*, 64, 183–189, 2012.
110. A. Safavi and F. Farjami, Electrodeposition of gold–platinum alloy nanoparticles on ionic liquid–chitosan composite film and its application in fabricating an amperometric cholesterol biosensor. *Biosensors and Bioelectronics*, 26, 2547–2552, 2011.
111. H. N. Schwerdt, F. A. Miranda and J. Chae, Analysis of electromagnetic fields induced in operation of a wireless fully passive backscattering neurorecording microsystem in emulated human head tissue. *IEEE Transactions on Microwave Theory and Techniques*, 61, 2170–2176, 2013.
112. V. M. Tolosa, K. M. Wassum, N. T. Maidment and H. G. Monbouquette, Electrochemically deposited iridium oxide reference electrode integrated with an electroenzymatic glutamate sensor on a multi-electrode arraymicroprobe. *Biosensors and Bioelectronics*, 42, 256–260, 2013.
113. B. Schazmann, D. Morris, C. Slater, S. Beirne, C. Fay, R. Reuveny, N. Moyna and D. Diamond, A wearable electrochemical sensor for the real-time measurement of sweat sodium concentration. *Analytical Methods*, 2, 342–348, 2010.
114. H. Yao, Y. Liao, A. R. Lingley, A. Afanasiev, I. Lähdesmäki, B. P. Otis and B. A. Parviz, A contact lens with integrated telecommunication circuit and sensors for wireless and continuous tear glucose monitoring. *Journal of Micromechanics and Microengineering*, 22, 075007, 2012.

115. X. Wang, Y. Gu, Z. Xiong, Z. Cui and T. Zhang, Electronic skin: silk-molded flexible, ultrasensitive, and highly stable electronic skin for monitoring human physiological signals. *Advanced Materials*, 26, 1309–1309, 2014.
116. D. Son, J. Lee, S. Qiao, R. Ghaffari, J. Kim, J. E. Lee, C. Song, S. J. Kim, D. J. Lee and S. W. Jun, Multifunctional wearable devices for diagnosis and therapy of movement disorders. *Nature Nanotechnology*, 9, 397–404, 2014.

Part 3

SYSTEMATIC BIOELECTRONIC STRATEGIES

9

Bilayer Lipid Membrane Constructs: A Strategic Technology Evaluation Approach

Christina G. Siontorou*

Department of Industrial Management and Technology, University of Piraeus, Piraeus, Greece

Abstract

Lipid membranes are two-dimensional fluid nano-constructs in which preferably two monolayers are held together by non-covalent hydrophobic interactions of amphipathic molecules. Biological moieties (enzymes, ion carriers, receptors, DNA, etc.) are incorporated into the membranes to add functionality. Unlike other biosensor formats, lipid membrane platforms do not hold a straightforward function within the detection system, but, depending on carefully tuned physical chemistry, assume a multifaceted role balancing (a) superior physisorptive capabilities for embedding, immobilising, controlling and optimising bioelement function; (b) rapid signal transduction (milliseconds speed) and in-built amplification properties for translating the biochemical information to an electric signal; (c) high resolution capacity for enabling the identification and quantitation of similar targets within one assay format; (d) multi-sensing potential at hosting different biochemical systems within one probe and (e) the best-fitting modelling of natural membrane systems for in-depth studies or drug permeability testing.

This review presents a critical overview of the membrane technology, putting emphasis on design, construction, modularisation, functionalisation and manipulation for niche applicability. A strategic technology evaluation, based on the analytic hierarchy process (AHP) framework, is also presented, considering two future trajectories: the technology path and the science path.

***Keywords*:** Graphene electrodes, electroanalysis, toxicants, health and environmental monitoring

**Corresponding author*: csiontor@unipi.gr

Ashutosh Tiwari, Hirak K. Patra and Anthony P.F. Turner (eds.) Advanced Bioelectronic Materials, (311–354)

9.1 The Lipid Bilayer Concept and the Membrane Platform

Lipid bilayers are two-dimensional fluid nano-constructs in which two monolayers of amphiphilic molecules are held together by non-covalent hydrophobic interactions. The reconstituted bilayer appearing in the 1960s [1], evolved from the principles of colloid and interfacial chemistry, as demonstrated in Hooke's soap bubble (1672) [2], Langmuir's film balance (1917) [3] and Langmuir–Blodgett (LB) monolayers (1934) [4], received much attention on the promise of simulating the cell membrane with a view to exploring and exploiting its multifaceted and dynamic nature (Figure 9.1). Fitted early to the emerging biosensor trajectory, in concept and context [5], the advantages of the bilayer platform, as postulated in the majority of the 1990s papers, were strategically focused towards biomimicking for trace detection, investing on (i) the natural operational environment provided for membrane-bound proteinaceous moieties, (ii) the non-denaturing conditions used for their coupling to the transducer and (iii) their thermodynamically driven (but largely rampant) well-defined molecular orientation.

The artificial bilayer lipid membrane (BLM), assembled mostly on electrochemical transducers, has been invariably adapted to reproduce the molecular mechanisms of natural membrane function, such as ion sensing, material transport, electric excitability, gated channels, antigen–antibody binding, phase shifting and conformational re-arrangements (Fig. 9.2). An advantageous feature of the BLM platform lies in its versatile applicability that enables easy device tailoring to operate different biochemical schemes within one transducer set-up. Employing one type of transducer, a researcher can construct as many detectors as the number of biological elements (bioelements) that can be immobilised or attached on the lipid bilayer. For example, the same electrochemical BLM system can be:

- Adopted '*as is*', in the analysis of mixtures of lipophilic herbicides, the discrimination of which, at high resolution, is provided by the slight differences in their partition coefficients (panel (e) in Fig. 9.2) [52].
- Loaded with hydrolytic enzymes to detect the corresponding substrates via the pH shifting resulted from the catalytic reaction (panel (b) in Fig. 9.2) [53].
- Modified with antibody to detect the corresponding antigen by monitoring the electrostatic alterations that accompany complementation (panel (a) in Fig. 9.2) [54]; similar bioaffinity mechanisms can be employed to monitor other

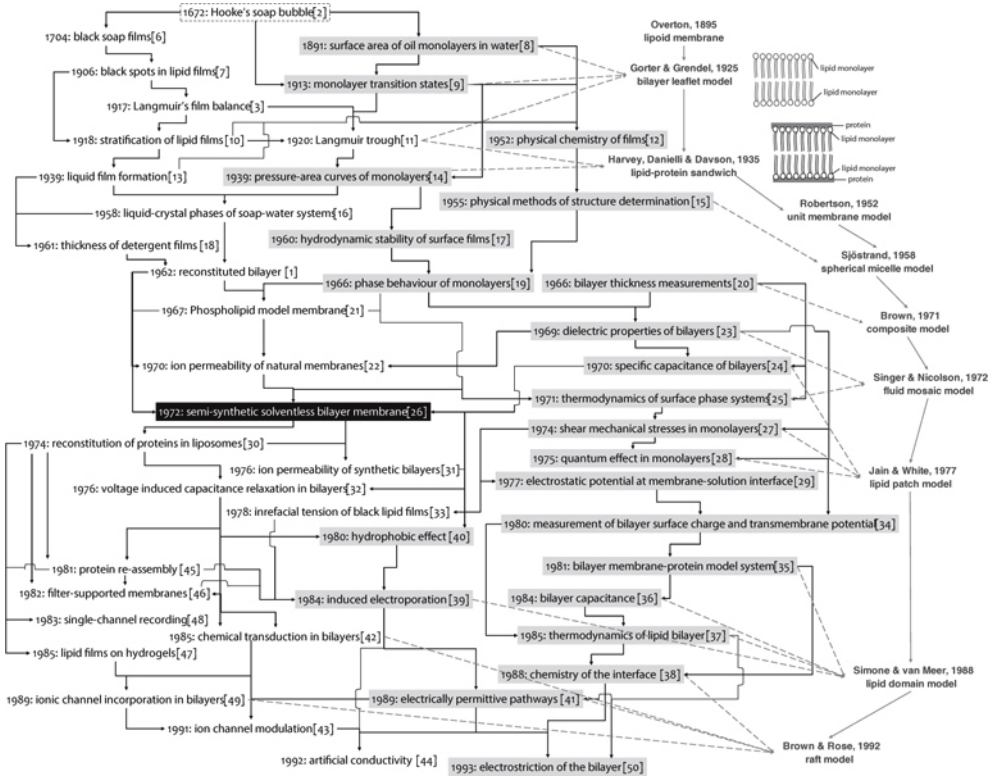

Figure 9.1 The science path from Hooke's soap bubble (dashed box) to model membranes (black box), composed using the PFNETs (pathfinder networks) program developed by Ref. [51]. The map reveals two interrelated trajectories: lipid self-assembly (left nodes), that later supported bilayer construction approaches, and the physical chemistry of lipid films (shaded right nodes), that later supported research on bilayer stability. The arrows show the connection between the nodes, i.e., they indicate the flow of information. The knowledge provided by the model membrane path, supported (dashed arrows) the parallel attempts on the membrane model (far right panel in bold), i.e., the elucidation of the structure of natural membranes. Bracketed numbers refer to published papers that presented the necessary theoretical background, tools and mechanisms (see References for details).

complexation reactions, e.g., of haemoglobin with carbon dioxide [55] or methaemoglobic with cyanides [56].
- Modified with DNA to detect and differentiate hydrophilic pesticides (panel (d) in Fig. 9.2) [57].
- Incorporated with the membrane spanning gramicidin to detect ammonium ions (panel (c), case (i) in Figure 9.2) [58].

These examples indicate briefly the multiple roles that the bilayer platform plays throughout one detection process, i.e., that of (a) the bioelement, (b) the support to other bioelements, (c) the (bio)chemical transducer and (d) the signal amplifier. Although sensor's sensitivity and selectivity towards a given analyte are endowed by the biological moiety (dependent on its affinity for the target), speed of response and reversibility rest on the lipid film. In any solid-state sensor, analyte molecules have to diffuse into and react with the bioelement component while any products of the reaction must diffuse out [59]. It, therefore, follows that the thinner the sensing layer is, the less time this will take and thereby, speed of response and sensor reversibility may well be improved; ultra-thin films make the use of even highly expensive bioelements (e.g., engineered receptors or DNA) economically possible [60].

From an analytical point of view, BLMs are the basic platforms for ion-channel recordings, since ion-channel moieties function only within a fluid lipid bilayer. The on/off gating of ion permeation through a single channel provides a novel tool for designing molecular sensing interfaces for ions. Other electrical signals, such as transmembrane potential, conductance and impedance are also analytically relevant for sensing ion species.

The impact of membrane science and technology upon many areas of biosensor and relevant research (such as material sciences, biochemistry, biophysics and engineering) is well acknowledged. The potential for technological applications, based heavily on the relevancy to natural processes, interests mostly the healthcare/life sciences industry and the energy/environment sector [5], whereas (bio)electronics and manufacturing can be benefited by analogous concepts; e.g., liquid crystals platforms resemble the physical chemistry of lipid molecules but at a robustness that can withstand industrial manufacturing and harsh operational conditions [62].

Although there is no sharp distinction between them, membrane science is concerned with understanding some phenomena, such as surface tension/properties, quantum effects or molecular assembly, and their influence on the properties of the platform, whereas membrane technology aims to exploit these effects to create structures, devices and systems with novel and significantly improved performance and functions due to their

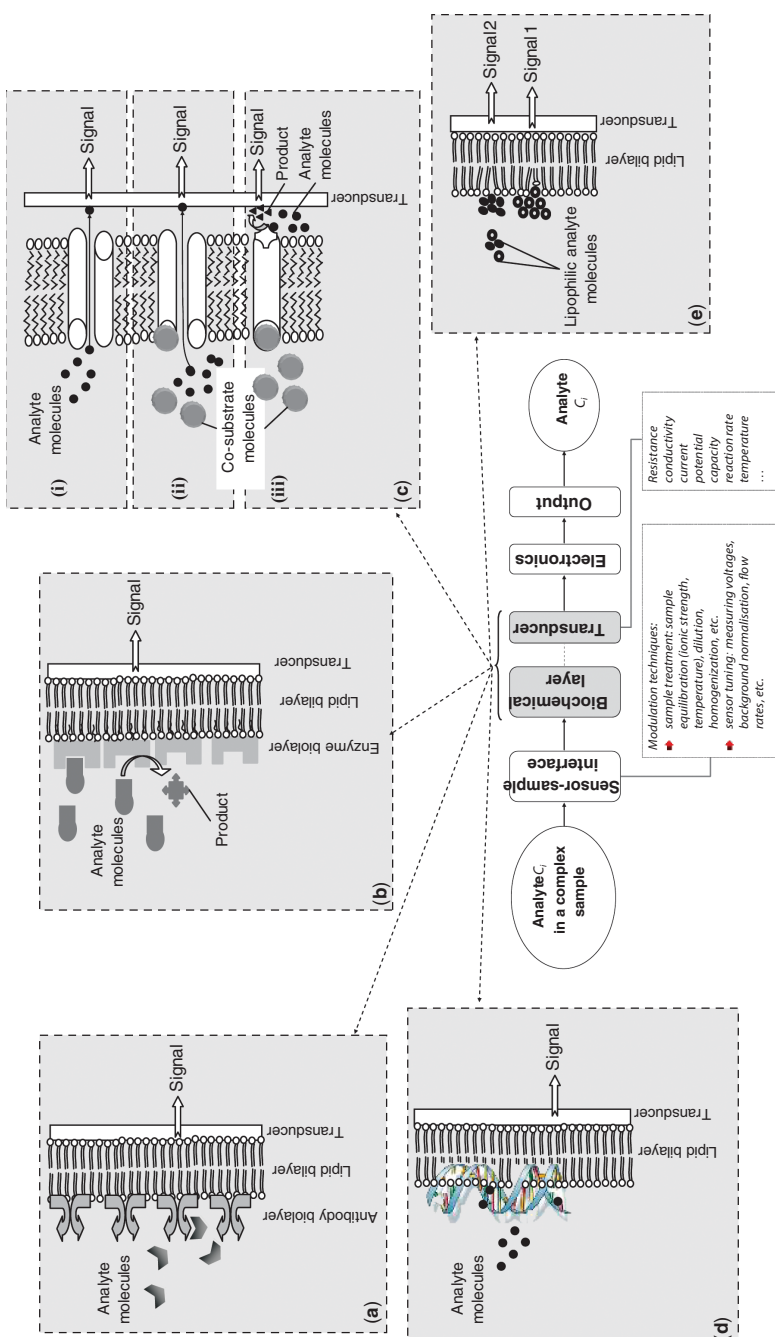

Figure 9.2 Example of an electrochemical membrane-based biosensor platform (central panel) and the flow of information leading from a complex sample to an output signal that provides qualitative and quantitative data concerning the target analyte. Boxed shaded panels (a)–(e)

(see next page)

Figure 9.2 cont.
demonstrate different principles of biosensing via structured lipid bilayer interfaces. (a) Bioaffinity sensors: the analyte (e.g., antigen) is recognised by the complementary biological layer (e.g., antibody); complementation induces structural changes to the immobilised unit that trigger transient modifications to the packing of lipids, expressed as a transient modification of the transmembrane current. (b) Biocatalytic sensors: the analyte is converted by the membrane-immobilised enzymes; the reaction induces electrochemical changes to the bilayer–solution interface (Debye's length) resulting in modifications of surface charge or dipolar potential of the membrane, expressed as a transient modification of the transmembrane current. (c) Transmembrane sensors: transport or channel proteins (i), or receptor proteins (ii and iii), are incorporated into the lipid bilayer; these moieties (i) transfer the analyte through the membrane, thereby increasing permanently the transmembrane current, (ii) bind the analyte and open a channel for another species, resulting in transient current modifications, or (iii) activate a separate enzymatic cascade that is readily detected by the underlying transducer. (d) DNA sensors: double-stranded (ds) DNA attached on the lipid bilayer undergoes unzipping at the presence of DNA adducts, manifested as permanent modifications of the transmembrane current. (e) Adsorption sensors: mixtures of similar lipophilic compounds are adsorbed onto the bilayer surface inducing lipid packing modifications that result in transmembrane current alterations; using a slight difference at the partition coefficients of the mixture components, a series of discrete signals can be produced, each one indicating, with adequate resolution, each analyte species present in the mixture.

nano-size. At times, the science part, rationally, preceded the technology part, even with very short lag times, but usually technology preceded scientific explanation, especially for signal generation. Much of the pioneering and fundamental research had a strong Edisonian character: through trial and error, the many possibilities of the BLM-based biosensors have been disclosed, establishing a curiosity-driven, mostly opportunistic, era.

Indisputably, the work produced is novel, advanced, promising and well promoted through dedicated and specialised groups. Before the nanotechnology tools become available, researchers could use a bunch of macroparameters to manipulate lipid films at angstrom (Å) dimensions. Despite, however, the commercialisation of other biosensor formats, in some cases successful (e.g., glucose meters), the transfer of the bilayer concept to marketed devices still remains a distant prospect. The general notion that the inherent membrane fragility is the most critical obstacle to commercialisation is not entirely true [5, 61], yet it guided research towards more rugged systems. The misalignment of academy and industry may, also, critically involve science policies and research strategies. The structure of the scientific network, especially in Europe, is such that knowledge production remains the scope of research. Within that framework research on membrane platforms is very attractive: after more than 50 years of study, the bilayer concept has still some aspects to clarify, while, compared to other bio-research areas, lipid membrane technology requires fewer resources to provide fast a significant academic output with a high scientific value [63]. Nonetheless, a market view requires engineering strategies and interdisciplinary collaborations, quite common in the general biosensor domain but quite limited in the membrane sector [64]. At a glance, research over the lipid membrane platform structures a flourishing knowledge sector with an intense push basis, represented by the continuous knowledge dissemination through publications, but an internal (i.e., purely academic) pull-basis, where research targets are set by the involved researchers with minimal to none industry involvement.

In cases as such, the framing of the technological sector and the assessment of the technology opportunities cannot be placed along future market targets to evaluate the university–industry transfer mechanisms [63], but, inevitably, has to consider the self-regulating role of the research network that progresses the sector along certain dominant dimensions established *ad hoc* [5]. This analysis will highlight the sector's technological competences, but, more importantly, it will provide a measure of its absorptive and transformative capacity; while the former indicates the capability to recognise, value and assimilate exogenous technological change within its scope of research [65], the latter indicates its capacity

to constantly redefine the research objectives based on the endogenously produced knowledge [66].

This review presents a critical outline of the membrane technology, putting emphasis on design and construction approaches, state-of-the-art modularisation, functionalisation and niche applicability (proven or feasible). Technology evaluation is based on the analytic hierarchy process (AHP) framework, considering two future trajectories: the technology path and the science path.

9.2 Strategic Technology Evaluation: The Approach

The AHP is a comprehensive framework for commercial technology evaluation through three steps: technology characterisation, hierarchical modelling and technology evaluation (Figure 9.3). The technology is evaluated against pre-set objectives by establishing a hierarchy of criteria and factors affecting these criteria over a range of technology alternatives. In order to adapt the model to academic output with an established commercialisation potential, technology alternatives may be replaced by the internal technology barriers, i.e., drawbacks, disadvantages or knowledge gaps [5]; by addressing these drawbacks, the sector can satisfy the pre-set objectives and formulate efficient strategies for more realistic market targets.

When considering the lipid bilayer sector, one should be quite careful in setting the objectives. When researchers focus on knowledge production, 'technological competitiveness' and not 'marketability' is the primary objective. Looking for criteria and factors, academic research places the emphasis on novelty, performance, reliability and the economic aspect driving the technological competitiveness. In academic endeavours, 'economics' refer to the cost of intra-university research, limited by the established infrastructure and institution policies and evaluated by the added (scientific) value created for knowledge improvement [67]. Lacking an external (i.e., industrial) assessment for this added value, the articulation of the last level on technology barriers should be based on self-referencing: how the involved researchers define (directly or indirectly) and manage (experimentally or theoretically) the weaknesses of their research object. Allowing for a long time span, in order to normalise the input from past university traditions (methods, experiences and way of thinking) and reveal the sector's own 'scientific culture', the examination of the body of publications, especially on how work is interrelated in space and time within and between research groups, would provide the paths that aggregate research efforts. These paths structure the dominant dimensions of the

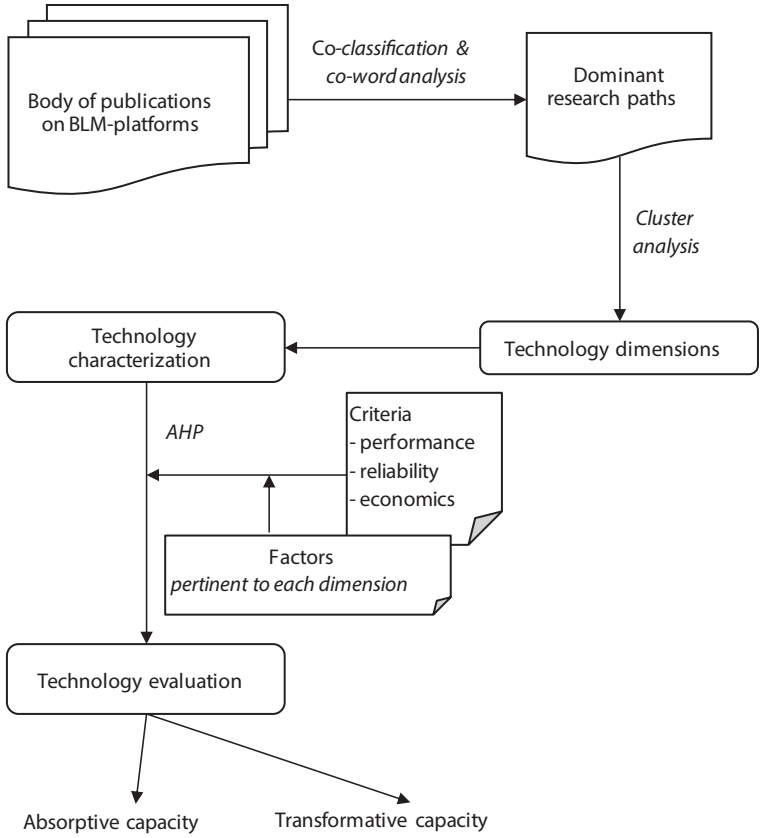

Figure 9.3 Overview of the methodological framework within which the BLM constructs are reviewed and evaluated.

technology that could be evaluated in terms of their feasibility to achieve technological competitiveness.

9.3 The Dimensions of the Membrane-Based Technology

Currently, 12.4% of the global biosensor research output reports on membrane platforms spanning a wide range of topics. Considering the 1980–2013 period, co-classification and co-word analysis of 5081 publications in the Thomson Reuters Web of Science database produced cognitive maps of the membrane-based biosensor domain and its aligning fields (see Ref.

[61] for a comprehensive description of the procedure); the taxonomic criterion was the focus of each research project, substantiated by the content of the resultant publication. Three research paths dominate, namely: modelling, fabrication and chemoreception (Figure 9.4). The development rate of these paths varies with time, depending on the impact of exogenous inputs to research tendencies. The modelling path, accounting for the 22.26% of the body of publications, provides the methods and tools for the estimation of the bilayer properties and for the elucidation of the underlying mechanisms of signal generation. The fabrication path, covering the 35.52% of the bilayer research, hosts all projects on bilayer assembly, proposing methods, techniques, tools and set-ups; a proof of the bilayer structure is always provided, either electrochemical or biochemical, along with a verification of its function, usually demonstrated as a small chemoreception event. Research along the chemoreception path, demonstrated at the 22.38% of the published papers, utilises existing assembly techniques to produce and validate a complete detection method.

During the 1980s, the very sound physicochemical background and the simple lipid paint technique provided the necessary proof of principle to support exploratory studies and feed the artificial chemoreception potential. This first period demonstrated feasibilities, mostly for biomedical applications, used physisorption to incorporate proteinaceous moieties, mostly enzymes and antibodies, and developed bilayer specifications, mostly on electrochemical parameters. A combination of the enormous technology potential and the limited number of researchers involved, pulled more players into the sector [63], evident by a sharp 55% increase in the 1990 publications and a steadily increasing trend thereafter (Fig. 9.4). Each new addition in the membrane biosensor network contributed new knowledge, experience and infrastructure that was rapidly absorbed within the sector and transformed into the next period's scopes.

The inherent fragility of the bilayer necessitated a shift towards fabrication that during the next decade developed many methods, techniques and set-ups, linking lipid composition and assembly to stability. The more stable the constructs, the broader the applicability, dragging along the chemoreception path. The number of bioelement classes expanded greatly (nucleic acids, DNA, receptors, aptamers, haptens, multi-arrays, etc.), whereas the range of chemical transducers broadened to include optical, acoustical, piezoelectric and conductimetric systems. Towards late 1990s, device engineering remained at bench scale whereas a trade-off started to emerge: the more stable the lipid membrane, the more rugged, controllable

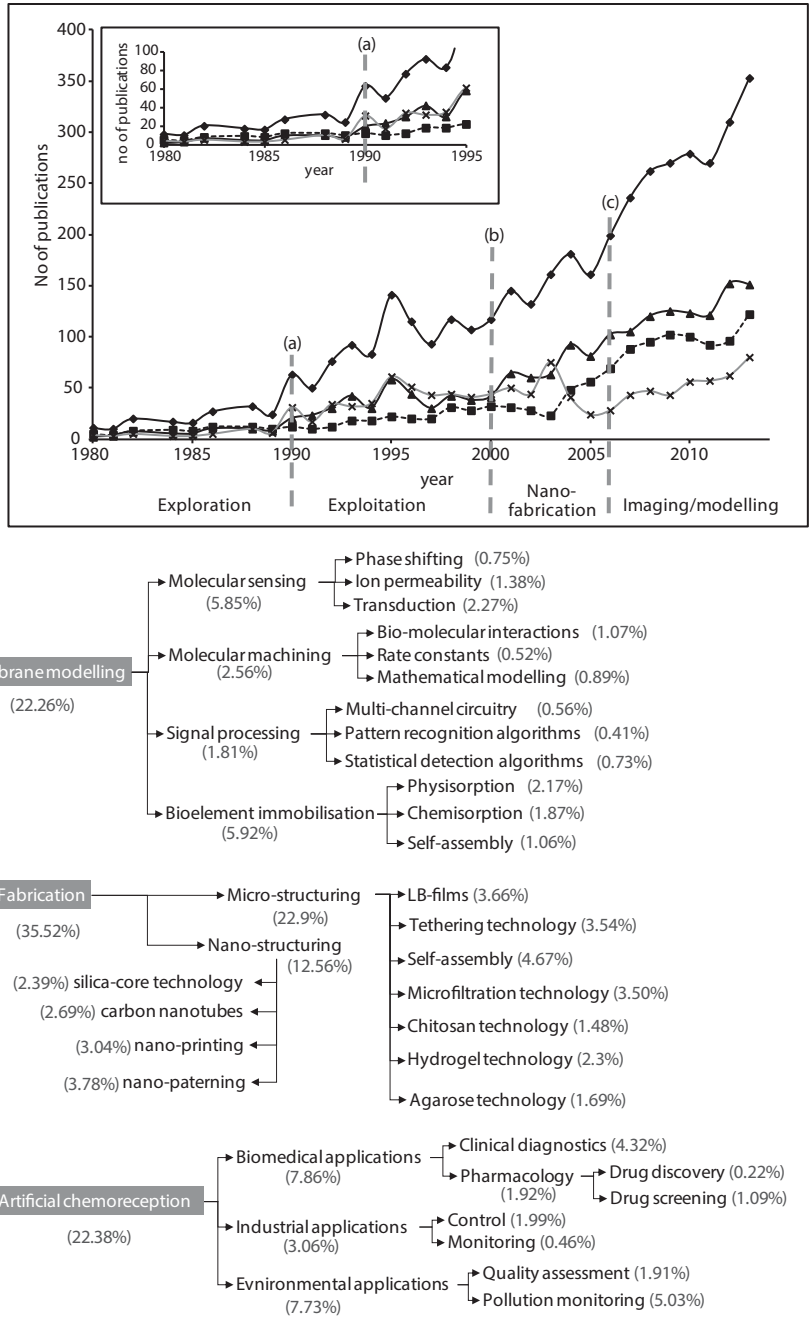

Figure 9.4 Main research trends in BLM platforms (top diagram), resulting from the higher taxonomic values (shown as percentages in the bottom schematic) of the context and content of the published works. The cumulative trend (♦) includes research on membrane modelling (■), fabrication (▲) and artificial chemoreception (×). Three shifts in the rate of publications are apparent, (a) (b) and (c), separating four phases: the early exploration phase (inset), the subsequent exploitation phase, the nanofabrication phase and the ongoing modelling and imaging phase. Each phase apprehended available (at the time) technologies, presenting drawbacks that pushed the path(s) forward.

and reproducible the construction process but the less dynamic the bilayer and the less relevant to natural membranes.

At the advent of nanotechnology, new tools and sizes became available to support construction, shifting considerably fabrication towards different engineering concepts. The next generation membrane constructs introduced the sector to the nano-era and its trajectories. The mid-decade rise in publications is due to a remarkable comeback of old concepts: the revisiting of the physiochemical background with advanced imaging techniques, and the revival of the 'model membranes to assess membrane models' objective, with special emphasis put on membrane energetics and permeation of pharmaceuticals.

9.4 Technology Dimension 1: Fabrication

In the simplest experimental set-up, a BLM is formed by spreading lipids onto a small aperture in a hydrophobic partition interposed between two aqueous solutions; changes in the membrane properties, such as electrical potential, capacitance and current, can be monitored by reference electrodes placed on either side of the membrane. A wide range of materials has been used, employing a variety of techniques for guiding thin film formation (Figure 9.5) in order to satisfy certain parameters of the membrane platforms that will not only expand the range of feasible applications, but will, also, support industrial engineering (Table 9.1). Following the shifts in the bilayer trend (Figure 9.4), initial efforts involved the construction of freely suspended films, the fragility of which triggered research towards supported platforms, the rigidity of which, aided, recently, by micro- and nano-tools, prompted research over the decoupling of the biomimetic membranes from the supporting surfaces. From the academic point of view, the easiest platforms require existing laboratory instrumentation and home-made devices to apply simple procedures utilising self-assembly, still amenable to limited control over both, the process and the properties of the produced membranes; better manageability requires expertise and expensive set-ups to support complicated protocols. Industry wise, only a few attempts have been made to standardise procedures and deduce models to work on scalability.

9.4.1 Suspended Lipid Platforms

The original painting method [1], made use of several driving forces to guide lipid self-assembly towards thick (ca. 50 μm) bilayers that were

dubbed 'black' as they appeared dark under reflected light; a droplet of lipid solution in alkane solvent is released around the rim of a small (few hundreds μm in diameter) aperture (panel (a) in Fig. 9.5). A lipid monolayer forms spontaneously between the organic and aqueous phases on either side of the lipid/solvent droplet; the film is initially thick but thins spontaneously to the bilayer state in three stages [68]. In the first stage, the major driving force is the Plateau–Gibbs border suction, which arises from the curvature of the annulus. The curvature is necessary to satisfy simultaneously the contact angles the border must make with the aperture and the film, directly related to interfacial tension. The existence of the curved interface brings about a hydrostatic pressure difference across the film which causes the film to shrink (thin). During the second phase, as the film approaches thickness of a few hundred Å, van der Waals' attraction between the aqueous phases separated by the thin film leads to the final thinning to the bilayer thickness. When the opposing surfaces of the thick film meet, there is a tendency for the opposed acyl chains on the lipid to interdigitate and to exclude the solvent molecules trapped in the film. However, the tendency to 'demix' lowers the entropy of the bilayer and consequently raises the free energy of the system, giving rise to the third phase governed by an opposing force called 'steric repulsive force'. The chemical potentials of the solvent and the lipid in the bilayer must be equal to those of the annulus when the film reaches its local equilibrium. Because the annulus is much more massive than the bilayer, the solvent in the bilayer tends to come into equilibrium with the annulus.

Owing to the low success probability of membrane formation and the presence of the residual solvent that could denature proteins, the method was modified to produce 'solvent-less' membranes [26, 44]: a lipid monolayer, spread on the air/water interface, is folded over an aperture (panel (b) in Fig. 9.5); lowering the electrolyte level at one chamber below the aperture, 'paints' the aperture with a monolayer, which zips up to a bilayer when the solution level is restored. The process can be aided by volatile hydrocarbons that are allowed to evaporate before the bilayer is formed.

The deposition of monolayers with the 'tip-dip method' [69–71], produces solvent-free bilayers with very short lifetimes. The tip of a glass capillary (ca. 1 μm) is dipped in electrolyte solution prior to the spreading of lipids at the air/water interface (panel (c) in Fig. 9.5). When the glass capillary is risen, a lipid monolayer is deposited (transferred) on its tip as it passes through the lipid layer; the second monolayer is attached as the capillary is dipped again.

Suspended BLMs are prone to structural failure and collapse in response to even weak mechanical or electrical shock. This is a direct result of the

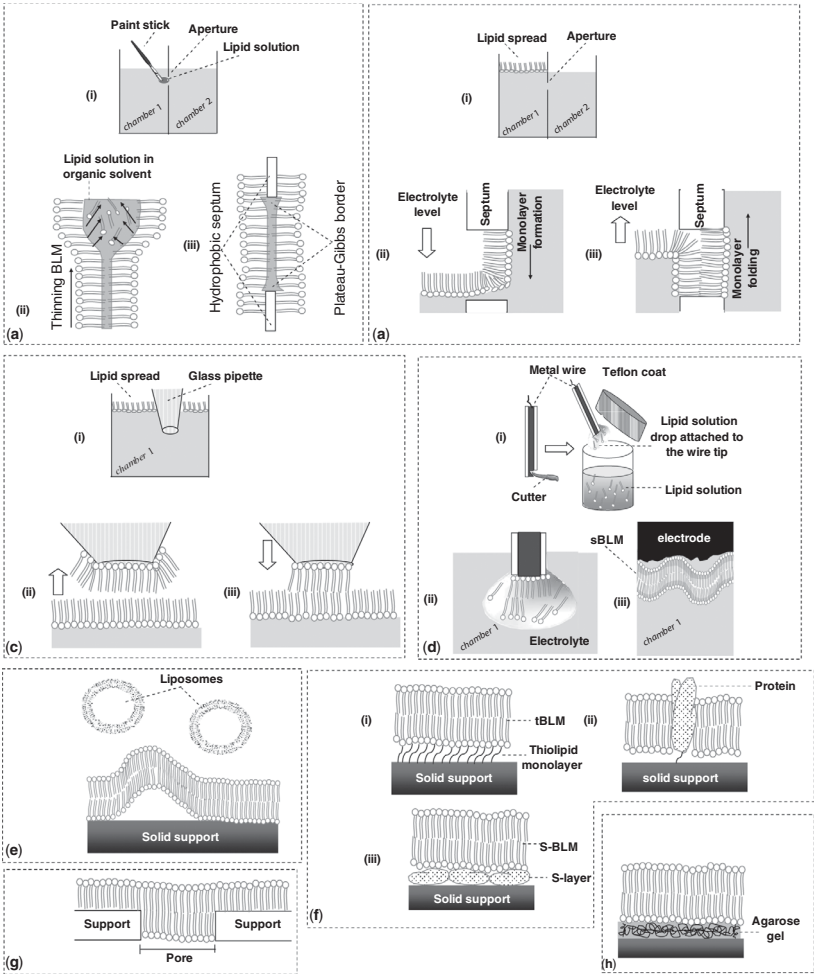

Figure 9.5 Schematic of membrane fabrication techniques. (a) Lipid painting: (i) two electrolyte chambers are separated by a hydrophobic septum punched to produce an aperture; a small stick is used to paint the aperture with lipid solution in organic solvent. (ii) The solvent diffuses towards the outer rim of the aperture supporting the membrane; the membrane starts to thin until the two monolayers at the lipid–electrolyte interfaces approach to finally form a bilayer. (iii) The solvent is being incorporated into the bilayer (black lipid membrane), forming an annulus at the edge of the aperture (Plateau–Gibbs border). (b) Monolayer folding: (i) A lipid monolayer is being spread onto electrolyte surface, allowing organic solvent to be evaporated. (ii) Upon lowering the level of the electrolyte below the aperture, the first monolayer is formed at the aperture. (iii) Rising the electrolyte level over the aperture brings the hydrophobic tails of the two monolayers into contact, forming a solvent-less lipid bilayer. (c) Tip-dip: (i) The tip of a glass pipette is immersed in electrolyte, and lipids are spread on the surface. (ii) When the pipette is raised, a lipid monolayer is attached on its tip. (iii) Upon re-immersion, a second monolayer is attracted to produce solvent-free bilayers. (d) Self-assembly on metal support: (i) An electrode is tipped and immersed in lipid solution; when risen, it carries along a small drop of lipid solution. (ii) Upon its immersion in electrolyte, a lipid monolayer is anchored onto the tip. (iii) After a while, a second monolayer is attached forming a supported bilayer [S-layer-stabilised BLM (S-BLM]. (e) Vesicle fusion: Lipid vesicles are injected onto a solid support surface; upon contacting the support, they spontaneous rupture and form a lipid bilayer. (f) Tethering: (i) A tethered BLM (tBLM) consisting of a thiolipid monolayer with a lipid monolayer on top. (ii) A protein-tBLM. (iii) An S-layer supports a lipid bilayer on top (S-BLM). (g) Supporting on porous materials: The total lipid membrane area would approximately span the aperture, yet only those areas in the pores would provide for conduction. (h) Gel-cushioning provides mechanical support and an electrolyte reservoir for the salt-bridged BLMs (sb-BLMs).

Table 9.1 Membrane platform parameters related to fabrication processes.

Parameter	Requirements	Current status
Operational stability	Stable and functional for at least one day for screening applications, or longer for monitoring applications; tolerance to mild drying conditions, e.g., air exposure, during sample mounting, might be, also, required.	Demonstrated in several supported formats [55–58, 74–121]; pilot implementation to validate operability under real (working) conditions has not been reported.
Shelf stability	Capability of storage for at least one month, in a state that can be easily regenerated or reconstituted.	Shown in polymerised films [155–158]; further studies on film ageing are required.
Straightforward fabrication process	Standardised, step-by-step controlled and validated; capability to be performed by non-experts, after some training.	Demonstrated in patterning [139–153]; however, the procedures are expensive and complicated.
Effective fabrication process	Membrane formed as specified in more than 90% of the attempts; high reproducibility of properties is required.	Demonstrated in simple self-assembly processes but at low reproducibility [55, 56, 58, 74–85]; micro- and nano-patterning show better results [122–160].
Easy and effective modulation	Depends on the intended use; e.g., for ion channel recording, gigaOhm resistance, ultra-thin films and multi-arrays are required; for pollution monitoring, more robust platforms are required to withstand extreme conditions and/or abrupt variations.	Demonstrated in many advanced formats: micro-patterning allows for high customisation [122–160], whereas robustness, mostly mechanical, has been achieved with supported membranes [55–58, 74–121]; lipid–protein interactions and transmembrane conductivity needs further verification.
Cost	At bench scale, experimentation should be feasible using common laboratory instrumentation, available and low-cost commercial units and home-assembled devices. At industrial scale, modification of existing processes and operations should suffice.	Most platforms can be easily adapted to existing academic infrastructure. Miniaturisation, achieved with recent technology, has been thought of as a suitable framework for the transfer to industry; yet industrial engineering has not been investigated.
Scalability	For scaling up to pilot or industrial production, modelling of the fabrication process and easy to control parameters is required.	There are some attempts on process modelling [e.g., [161]) but, in general, scalability of production has not been investigated.

molecular thickness of the bilayer structure. Lipid membranes can undergo two basic kinds of instability: (a) rupture, leading to formation of pores or/and fragmentation of the membrane and (b) buckling, resulting in bending or folding of the membranes [72, 73]. The rupture is usually due to growth of local disturbances of the membrane thickness (surface waves, holes and cracks, etc.); buckling can be induced by decreasing the membrane tension (e.g., by applying a compressing force to the membrane edges), as well as, by different effects due to membrane asymmetry. In literature, the term 'stable' is generally used to denote a membrane that does not change significantly some characteristic properties (structure, packing, etc.) during the action of external constraints or internal transformations within a certain characteristic time, e.g., the time of the experiment. Although these definitions are reasonable and clear for basic experiments, they do not provide rigorous criteria for membrane instability and, further, they cannot clarify the fundamental difference between an 'unstable membrane state' and a 'stable one that continuously is changing state'.

The general conditions for stability of a system, particularly a membranous one, are given by the thermodynamics: the membrane is stable when its free energy has a minimum value in the space of the independent thermodynamic variables [73]. This means that any infinitesimal change of the independent parameters (pressure, temperature, electrical potential, surface tension, etc.) should lead to an increase of the free energy of the system. However, in many cases, as during protein function or flip-flop, the membrane can be unstable with respect to some of the thermodynamic parameters, but the rate of change of the membrane state is so small that during the characteristic time-scale of the experiment, this membrane behaves as stable; that is the case of 'meta-stable' membranes.

Notwithstanding, membrane instability can be brought about by a variety of reasons [4], including osmotic pressure difference, hydrodynamic instability or dielectric breakdown that will alter the surface tension of the lipid film leading initially to molecular re-arrangement and finally to membrane discontinuity. While the former does not alter substantially the functionality of the membrane, the latter is irreversible and results in terminal rupture [72, 73]. The organisation of the lipid films into the bilayer structure during membrane formation plays an important role in the film tolerance towards rupture, as the viscoelasticity properties of the films are built-in and defined during the process of bilayer assembly [73]. Hence, at a phenomenological level, membrane stability is defined by (i) septum properties that provide the edge mechanical support and govern the solvent–film equilibrium at the annulus [5] and (ii) the geometry of the lipid film, determined by the membrane diameter to thickness ratio (d/t),

defined by the aperture thickness to diameter ratio (t_a/d_a) [54]. Ideal (theoretical) stability is achieved at small and thick apertures: considering a 50 Å bilayer thickness, a small diameter aperture favours substantially the film geometry whereas the thickness of the platform helps maintaining a bulky annulus, i.e., stability requires a high t_a/d_a at a low d/t. On the other hand, extremely small aperture diameter values will prohibit ion flow through the bilayer, whereas extremely thick platforms tend to favour multilayer structures.

9.4.2 Supported Lipid Platforms

Supported lipid bilayers (sBLMs) exhibit higher mechanical stability than the suspended films. The construction methods developed range from simple self-assembly procedures to cumbersome, yet amenable to control, protocols. A variety of supports have been validated, including metals, porous materials, gels, glass, mica and silicon [55, 56, 58, 74–85]. Perhaps the easiest way to prepare a metal-supported bilayer is to dip a freshly tipped Teflon-coated metal wire (e.g., Pt, Ag, Cu, Ni, stainless steel or other alloys) into a lipid solution and carefully transfer the wire (along with the attached lipid solution drop) into an aqueous solution [74, 75] (panel (d) in Fig. 9.5); depending on the diameter of the wire and the lipid composition, within 5–20 min a lipid bilayer is self-assembled onto the wire tip [55, 56, 58, 81–83]. Self-assembly might possibly proceed in two steps: the first monolayer is anchored onto the support during immersion in the electrolyte solution, probably by colloidal interactions with an estimated separation of about 10 Å [86], whereas the second is slowly self-assembled on top of it; it follows that lipid movements within the anchored monolayer are restricted, whereas the outer layer is more 'fluid'. The presence of a water layer trapped between the lipid monolayer and the surface ensures lateral mobility of lipid molecules in the bilayer (fluidity), which is an important property of the biological membrane [77]. This technique yields extremely stable platforms and has been used for the development of a variety of probes [55, 56, 58, 81–83] or interdigitated electrodes [87, 88]; however, the metallic substrate precludes the ion translocation across the lipid bilayer and, thus, the use of transmembrane proteins, while compatible transduction set-ups are limited to two or three electrode systems, allowing for voltammetric or amperometric devices. Nonetheless, there are various optical and electrochemical analytical techniques that can detect interfacial events with an extremely high sensitivity, such as surface plasmon resonance (SPR) and quartz crystal microbalance with dissipation monitoring (QCM-D) [89, 90].

More options are available from the LB technology that allows building up lamellar lipid stacking by transferring a monomolecular film formed at the air/water interface onto any solid support. When all parameters are optimised, this technique corresponds to one of the most promising for preparing thin films of amphiphilic molecules [91–96], as it enables (i) accurate control of the thickness and the molecular organisation, (ii) homogeneous deposition of the monolayer over large areas compared to the dimension of the molecules, (iii) transfer of monolayers on almost any kind of solid substrate and (iv) formation of hybrid bilayer structures with varying layer compositions. However, surface analysis revealed several defects in LB films [97–99], such as disclinations, inhomogeneous crystalline domains, pinholes, collapsed domains, vacancies, trans-bilayers and lateral heterogeneities. These defects can prevent applicability in molecular electronic devices which have specific functions at the molecular level.

Vesicle spreading (fusion) is a less instrument-demanding technique, where the lipid bilayer is formed on solid supports by rupturing unilamella vesicles on the supports. In this technique, small, large, or giant unilamella vesicles are injected onto a solid support (panel (e) in Fig. 9.5); the vesicles rupture spontaneously due to the oppositely charged lipids and the support surface to form the bilayer [77, 84, 85]. Bioelements can be incorporated into the sBLM during vesicle generation, i.e., prior to bilayer formation, or adsorbed onto the prepared bilayer membrane. The major drawbacks of liposomal deposition include excessive vesicles that need to be rinsed off and susceptibility to membrane defects [100]. Moreover, both the process of membrane deposition and the physical properties of the membrane strongly depend on ionic interactions between lipids and the support [101].

The applicability of sBLMs is restricted by their close surface proximity, which is an obstacle to incorporating large membrane-spanning proteins under non-denaturing conditions. Besides, the higher, sometimes tenfold, background ion currents of the sBLMs compared to those of the suspended bilayers, hinder the recordings of channel activities. These drawbacks have been overcome by tethering lipid bilayers to solid surfaces via a spacer unit [102] (panel (f) in Fig. 9.5). The commonly used tethering layers are thiolipids [103] and silanelipids [104] containing spacers of gold and silicon oxide, respectively. The advantages of the tethered lipid bilayer (tBLM) platform are (a) the ionic reservoir underneath the membrane and (b) the avoidance of direct contact of embedded proteins with the support surface. The main disadvantages refer to device engineering and functionality: as the tethering part requires a certain amount of space inaccessible to the bioelement, water or ions, precarious *in situ* insulation

or compartmentalisation should take place; in addition, the tethering molecules apply diffusional constraints to the membrane lipids restricting free movement and conformational transitions of both, the membrane and the bioelement. It follows that single-channel recordings with tethered membranes are still no easy matter [105], so changes in impedance are often preferable as analytical signals that reflect channel activities; alternatively, single-channel activities can be observed by increasing the electrical resistance of tBLMs linked to a gold surface [106]. Even better, a proteinaceous surface (S-) layer lattice can be used as a stabilising and tethering structure [107]; this biomimetic approach adopts the supramolecular building principle of most archaeal cell envelopes, composed of a plasma membrane and a closely associated S-layer lattice. Membranes (S-BLMs) can be stabilised either by an S-layer lattice attached in series or can be generated on S-layer lattices. Model membrane proteins and, also, membrane-active peptides can be incorporated into these composite structures and their biological function could be demonstrated on the single functional unit level.

Suspension and support can be simultaneously achieved in mixed lipid bilayers formed on porous substrates, where part of the membrane is sustained in the pores and the rest is supported on the non-porous part of the substrate (panel (g) in Fig. 9.5). The total lipid membrane area would approximately span the aperture, yet only those areas in the pores would provide for conduction [52–54, 57]. The lipid configuration, thus, resembles a network of micro-films that cover the whole available space increasing manifold protein loading and expanding applicability to multi-array formats. A variety of micro- and ultra-filtration membranes [46, 52–54, 57, 108, 109] and porous alumina [110, 111] have been used as porous supports. Polycarbonate filters [54, 106, 109] have been frequently used since they are characterised by a highly uniform series of holes separated by smooth, non-porous polymer; it is known that membrane formation is optimised by the relative smoothness and circular regularity of the support aperture [46]. However, the appearance of multiple pores too close to each other may comprise up to 30% of the filter area [54] leading to irregularly shaped apertures unfavourable for bilayer formation. In addition, some pores may not span the filter, manifested as wells of undetermined depth in the filter [54]; lipid solution trapped in these wells will be electrically inactive and will provide a sink for the lipid-soluble membrane stimulants added to the surrounding solution. Cellulose ester, polytetrafluoropolyethylene (PTFE) and glass microfiber (GF) filters have pores which are irregular in shape and vary greatly in size [54]. Various studies have shown that thick materials with dense and small-sized pores are more successful in

enhancing membrane stability without compromising functionality, since they provide for high aperture (pore) thickness to diameter (t_a/d_a) ratios at low membrane thickness to diameter (d/t) ratios [46, 54, 112, 113]. These advances promise both, robust and packageable sensors with a greater variety of membrane receptors and ion channels and/or transporters as functional components. They, also, fulfil the miniaturisation requirement while allowing for easier control of low leakage current and parasitic capacitance that permits chip integration. Solution exchange, a prerequisite for physiology experiments [105], has been only achieved with lipid bilayers supported on porous membranes.

Hydrogels (e.g., agarose or chitosan) have often been used as supports for lipid bilayers [114–116] (panel (h) in Fig. 9.5). Polymer interlayers have a great potential for effectively decoupling lipid membranes from supports such as glass, gold, indium tin oxide or silicon devices [77]. Therefore, numerous efforts have been made to prepare suitable polymer cushions, physisorbed or chemically coupled to an underlying support and physisorbed or chemically coupled to the lipid membrane on top. At the simplest set-up, lipid solutions are deposited on top of precast gels to form solvent-containing salt-bridged bilayers (sb-BLMs). Polyethyleneimine (PEI) was used as an interlayer between a solid support and an amphiphile membrane [117]. Additionally, the polysaccharides dextran, cellulose [118, 119] and polyacrylamide [47] were applied to prepare polymer-supported mono-layer lipid membrane and BLM.

Lipid membranes that are either completely or partially chemically coupled to the polymer cushion are regarded to be advantageous to membrane stability, while increasing the accessibility of the bilayers to the bulk aqueous environment. Sandwiching a lipid bilayer between two gels gives a membrane-limited stability in air [120]. Still, several issues should be addressed and further improvements would be necessary for this technique to scale up: (a) cushioning increases the synthetic expense and considerably reduce fluidity [114] and protein coverage [116]; (b) cracking and shrinkage of the gel matrix due to aging can lead to serious problems with sensor responses [121]; (c) controlling or modifying *in situ* the membrane/substrate spacing by varying the thickness of the interlayer polymer cushion is extremely difficult [114]; thus, sb-BLMs cannot be used in surface sensitive transducers, such as those using evanescent fields; (d) the electrical analysis of single membrane channels requires a large ionic reservoir necessitating a polymer cushion of sufficient thickness [105]; and the use of polymers, which are soluble under particular conditions and otherwise form a water-insoluble gel, is a way to avoid this problem [116].

9.4.3 Micro- and Nano-Fabricated Lipid Platforms

Advances in lithography have enabled microfabricated devices to be coupled with lipid bilayers. Two approaches have been extensively studied: (i) preparation of lipid bilayers in micro-apertures [122–124] and (ii) automatic formation of lipid bilayers in microfluidic devices [125–127]. The machining of apertures at μm dimensions limits bilayer undulations and satisfies the geometry ratios for membrane stability [105]. Most of the apertures fabricated are vertically orientated (instead of laterally) resulting in formation of lipid bilayers in a horizontal plane. Although silicon, due to its well-established methods in microfabrication, is often used as a material to fabricate the apertures [122, 125], various hydrophobic materials, such as parylene sheet [128], polymethylmethacrylate [129], Teflon [113] and Delrin [130] might prove more suitable to create a stable bilayer. Decreasing the size of the aperture, decreases electrical noise, as well [113]; however, apertures less than 40 μm allow external noise to become dominant.

Various techniques have been demonstrated to form suspended lipid bilayers on micro-apertures. Lipid painting is applied when the apertures are accessible from the outside [122], but reproducibility and success rates are low. Stretching [131] or air exposure [129] may be used to speed up the thinning process. The former technique slightly stretches out the lipid bulk by lifting one chamber, whereas the latter exposes repeatedly the lipid bulk to air by removing and adding electrolyte into the chamber. When the apertures are inaccessible, vesicle spreading may be used, provided that the diameter of the vesicles is larger than the aperture to prevent their slipping through the aperture.

Automatic formation of solvent-containing lipid bilayers in microfluidic devices was proposed by (i) solvent extraction through the walls of microfluidic channels [126], (ii) assembling two lipid monolayers at the interface between organic and aqueous phases [132] and (iii) flowing lipid solution and aqueous buffer alternately into a microfluidic channel [125, 127]. Simultaneous parallel recordings of alamethicin and gramicidin have been demonstrated [128], showing promise for multi-channel monitoring.

Droplet interface bilayer is a microfluidics technique where a lipid bilayer is created by contacting two aqueous droplets respectively bounded by a lipid monolayer in a lipids/solvent mixture [133–138]: two independent aqueous droplets are being deposited into a lipid–solvent mixture (lipid-out); alternatively, aqueous droplets containing lipid vesicles are being deposited into an organic solvent solution (lipid-in). In both approaches, the lipid monolayers spontaneously surround the aqueous surfaces orienting lipid polar heads to the aqueous surface and the lipid tails to the organic

solvent solution. A lipid bilayer can then be formed by bringing the two monolayer droplets into contact by (i) dropping them directly next to each other [133], (ii) manipulating the electrodes that are attached to the droplets [135] or (iii) using electrowetting on dielectric (EWOD) method [136].

Microfabrication offers, also, many tools to engineer customised lipid surfaces. Patterning may proceed mainly via three approaches: (a) spatial control of the deposition or the removal of lipid membranes involve the use of mechanical scratching [139], microcontact printing [140, 141], microfluidics [142–144], micropipettes [145], scanning probe microscope tips [146], inkjet printer [147] and air bubble collapse [148]; (b) deposition of lipid membranes on pre-patterned substrates, i.e., surfaces with lipid diffusion barriers that force the separation of membranes into distinct areas, yields microarrays that permit high-throughput screening for drugs and proteins [149, 150]; (c) photolithographic modification of lipid bilayers includes decomposition of lipid membranes by deep UV light and UV polymerisation of lipid bilayers [151]. Ease of fabrication, pattern size, stability and adsorptivity varies greatly among these approaches, yet they enabled studies in the electrophysiology field, as immunological synapse formation [152] and signal transduction in cells [153].

Extension of these methods into the nano-scale has allowed capture of both microdomains and cytoskeletal barriers (154). While these methods offer a high degree of control over the barrier and substrate layout, they are expensive to use over large areas. Polymerisation of lipidic molecules in lyotropic, self-assembled aggregations (lamellar, cubic, inverted hexagonal, etc.) presents a more suitable alternative. Stabilisation of lipid vesicles by polymerisation of lipids has been studied in conjunction with the potential application for encapsulation of medicinal materials (drug delivery). Lipid molecules carrying various moieties (e.g., dienoyl, sorbyl, diacetylene) were synthesised and polymerised *in situ* within the bilayers. Upon polymerisation, the solubility of the bilayers in organic solvents or detergent solutions decreases [155, 156], along with the lateral diffusion constant and the permeation coefficient [157], thus permitting imaging interrogation. The area fraction of polymeric bilayers can be regulated easily by changing the UV irradiation dose, allowing the engineering of customised composites with different bilayers occupying nano-sized domains [154]. The resulting structures tend to be less well defined than those of other fabricated systems, but are highly effective in capturing the targeting and segregation of specific classes of biomolecules into the gel phase domains, which are relatively immobile [158].

Carbon nanotube membranes offer better defined and manageable structures. Transport through these membranes is primarily based on

ionic diffusion near bulk expectation, although gas flow and fluid flow can be achieved; due to specular reflection, and nearly ideal slip–boundary interface, respectively, transport can be modulated at the pore entrance using steric hindrance, electrostatic forces or biochemical state [159, 160]. These nano-structures are mechanically far more robust than other platforms, allowing for large-scale chemical separations, drug delivery, sensing or energy generation.

9.5 Technology Dimension 2: Membrane Modelling

A major challenge in membrane-based biosensing is the identification of the mechanisms by which the biochemical event is converted into a signal. Most studies support the hypothesis that changes in the physical properties of the bilayer can have significant effects on signalling dynamics. It has been recognised that mechanical and/or electrical perturbations of the lipid bilayer may lead to changes in static and dynamic properties of the membrane, such as membrane thickness [162], polarity [163, 164], surface charge density [165, 166], structural order [165–167] and fluidity [44, 166]. According to the Gouy–Chapman–Stern model, the total electrical potential of a bilayer [168, 169] is made up of the transmembrane potential ($\Delta\Psi$), due to gradients in ion concentrations across the membrane, the surface potential due to lipids with charged head groups (Ψ), and the dipole potential (Ψ_D), which arises due to the alignment of dipolar lipid head groups and water dipoles in the interface region between the hydrophobic membrane interior and the aqueous phase (Fig. 9.6). Typical value for $\Delta\Psi$ across the membrane of a resting cell is around 70 mV, corresponding to the electric field strength of ca. 10^7 V/m inside the 50 Å thick membrane. In contrast, the dipole potential Ψ_D changes sharply across the head group area resulting in much stronger electric fields, on the order of 10^9 V/m. It is well established that the total transmembrane potential can modulate and even control functioning of various membrane proteins such as voltage gated ion channels [122, 163], enzymes [53, 170, 171], ligand gated channels [105, 113, 128, 129, 156], ion transporters [58, 78, 105, 120, 163] and, recently, gating charge effects [172]. Application of external potential $\Delta\Psi$ in these systems governs, affects or triggers functional conformational transitions [173]; the stronger the electric field of the dipolar potential Ψ_D, the stronger the influence on the conformational dynamics of membrane proteins.

The transmembrane potential ($\Delta\Psi$) can be measured and controlled using electrodes [174]. A lipid bilayer membrane can be thought of as a biological

parallel plate capacitor, and this similarity has led to the extensive use of capacitance measurements to assess the area, thickness, and surface potential of cell membranes [161, 163, 174–177]. Notwithstanding, the Gouy–Chapman–Stern theory neglects interfacial molecular structure, hydration and inter-ionic correlation effects, i.e., ion distribution in the diffused layer is assumed to be governed solely by coulombic forces between the ions and the interface; when membrane electrostatics is a cofactor in intermolecular interactions, the lipid bilayer interface should be dealt with carefully [178]. The interface is a conglomerate of lipid head groups, bounded ions and organised water molecules not easily described with macroscopic theories. Even the interface of one-component lipid bilayer is a region with complex structure where many important physicochemical properties change dramatically. For example, when water concentration decreases, dielectric permittivity decreases dramatically [163], and dipole potential affects electrostatic potential at the immediate vicinity of the membrane or within the interface. The presence of dipoles on the interface leads to qualitatively new effects. An electrically neutral surface induces an electrostatic field if the dipoles density is not zero [179]. Charged lipid membranes usually have a charge density less than zero and a dipole density more than zero. If the thickness of the interface is small compared to the Debye length, the effective surface charge is determined only by the net charge density, whereas the potential is reduced to the classical Gouy–Chapman–Stern approximation. On the other hand, if the dipole density is sufficiently large, the effective surface charge depends on the thickness of the interface, as well as, the Debye length of the solution [163].

Simulations with molecular dynamics modelling techniques [173] aided substantially the elucidation of surface phenomena. Three approaches have been suggested, namely: atomistic, coarse-grained and water-free models. The most detailed modelling is presented in the atomistic approach, which, further to molecular structure, it can, also, describe intra- and inter-molecular interactions, such as chemical bonds, electrostatic, and van der Waals' forces [180–184]. Direct comparison with experiments, e.g., Nuclear magnetic resonance (NMR) [185], has shown the effectiveness and accuracy of such models. Some atomistic attempts to model supported platforms have been reported [180, 182, 184].

Coarse models use large sites with large interaction distances that usually result in overestimations. Most approaches make use of the Martini model developed over several years [186–188]; the model is considered more suitable for simulating supported platforms and uses one interaction site to represent four heavy atoms on average. Water-free models have limited applicability in hydrophilic–hydrophobic interactions that

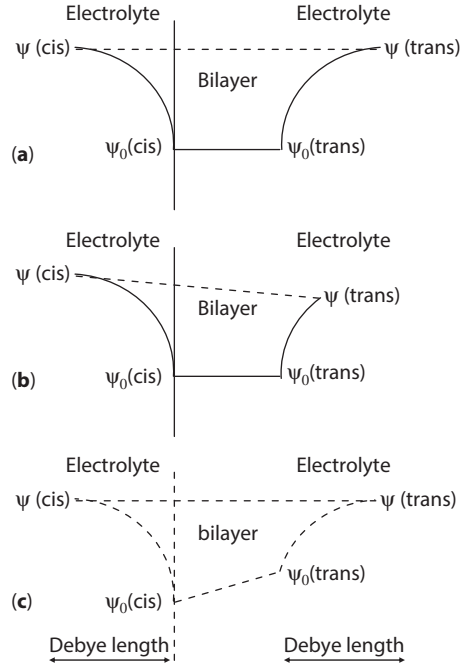

Figure 9.6 The effect of surface potential on the transmembrane potential, based on the Gouy–Chapman–Stern theory: Consider a hypothetical electrostatic potential profile across a bilayer separating two electrolyte solutions; (a) in symmetric systems, the surface potentials $[\Psi_0(\text{cis})-\Psi(\text{cis})]$ and $[\Psi_0(\text{trans})-\Psi(\text{trans})]$ at the bilayer–solution interfaces are equal so that the bilayer potential difference $[\Psi_0(\text{cis})-\Psi_0(\text{trans})]$ equals the applied potential difference in the bulk electrolyte solution $[\Psi(\text{cis})-\Psi(\text{trans})]$; (b) under open-circuit conditions, a change in surface potential on the (cis) side of the bilayer causes a change in the potential difference between the bulk solutions; (c) under voltage-clamp conditions, a change in surface potential on the (cis) side of the membrane shifts the bilayer potential difference although the bulk potential remains unchanged.

make the self-assembly process feasible; to compensate, these effects are implicitly represented in the lipid potentials [189]. Some models include, also, planarity potentials [187] that segregate tail particles and polar head particles to different sides of an imaginary plane, or by using modified cohesive forces among tail particles in order to keep the system planar [190].

Computer simulations, in principle, can calculate any physical parameters based on the configurations generated by a Monte Carlo or molecular dynamics algorithm. Although modelling of suspended bilayers is straightforward, since most of these parameters can be experimentally verified, supported platforms pose several issues that need to be resolved. For

example, the area per molecule can be, also, determined experimentally for the suspended systems [191]. For the supported formats, however, the simulations have to be performed with fixed area per molecule and fixed normal pressure which is set to ambient pressure; in effect, simulations use pressure–area isotherms under constant area but varying numbers of particles or fixed number of particles and varying area [192]. Another example is seen in the thickness the bilayer, calculated from the density profile: in the case of suspended bilayers, simulations have been proven accurate; in supported membranes, the asymmetry has to be considered and, in addition, the shape of the underlying density profile has to be characterised in detail [193].

9.6 Technology Dimension 3: Artificial Chemoreception

Lipid bilayer constructs present a highly ordered structural organisation at ultra-thin dimensions that are well fitted to micro- and nano-sensors or biochips. The functionalisation of lipid bilayer platforms can be achieved by the association of biological species presenting specific recognition properties, such as enzymes, antibodies, receptors or specific ligands, in order to develop ordered bioelement–lipid molecular assemblies, actually, forming supramolecular arrangements. In general, two approaches may be used, each presenting its own advantages and disadvantages, depending on the fabrication process, the biochemical system and the transduction system: liposome fusion and direct deposition. In the former approach [77, 84, 85, 100, 101, 105, 129], bioelements, especially proteinaceous ones, are reconstituted into lipid vesicles, which are fused with a lipid bilayer by creating a salt gradient across the membrane. The salt gradient promotes the fusion of the liposomes at the surface of the bilayer because an efflux of water from the low-salt (trans) side through the bilayer into the vesicle induces swelling and stressing of the liposome at the bilayer surface [194]. The procedure is more applicable to suspended bilayers separating two aqueous chambers with adjustable compositions. Liposome suspension is introduced into the (cis) chamber with a higher salt concentration; owing to the asymmetric salt gradient, a membrane potential is established driving the immobilisation process. Liposome fusion leads to spontaneous bioelement incorporation, though the probability of fusion is still a matter of great interest [105].

Direct deposition of bioelements has been reported in various versions, for both, suspended and supported platforms [44, 52–58, 69–71, 81–83, 91–96, 156, 166, 171]; in effect, the bioelement is allowed to physically

adsorb onto or absorb into the membrane prior to or after the formation of the bilayer. Adsorbing the bioelement onto pre-formed bilayers [52–58, 81–83] lies on the possibility of associating the bioelement with a hydrophilic lipid surface or a hydrophobic lipid surface; nevertheless, the interactions involved in this type of association are often too weak to prevent the release of protein molecules, which remains a major drawback, especially for flow-through set-ups [53, 54, 57], leading mostly to poor reproducibility of responses [59]. Gel-cushioned [114–120] or polymerised formats [155–157] may present better results as regards longevity but do not solve the problem entirely. In order to minimise desorption, some authors have suggested to covalently immobilise the bioelement on the film surfaces by means of cross-linking agents [195–197], the avidin–streptavidin system [198, 199], organic and inorganic nanoparticles [200] and cell attachment-promoting agents [201]. The fact remains, however, that covalent attachment to the lipid structure may induce changes to the protein conformation which may cause a loss of its biological activity.

More controllable procedures are available with LB technology. The bioelement may be adsorbed onto the interfacial film before transfer of the mixed proteo-lipidic monolayer and then super-imposed by the second monolayer. This method is particularly suited to extrinsic peripheral proteins capable of associating with biological membranes or to anchoring proteins inserting themselves into one leaflet of a bilayer [105]. The presence, however, of the bioelement in the interfacial film may affect its transferability properties [96]; for example, the surface pressure required for the transfer procedure may not be suitable for the bioelement association, leading to its disorption at high surface pressure, or the bioelement may hinder the adhesion of the monolayer on the substrate. Another alternative called 'inclusion process' allows the sandwiching of the bioelement in a hydrophobic or a hydrophilic environment while keeping the homogeneity of the supporting layers [96]. The lipid composition of the protective leaflet can be easily modified, reproducing, to some extent the membrane asymmetry which can favour the physical retention of the bioelement and preserve its biological activity.

9.7 Technology Evaluation

The development of the artificial lipid bilayer has made it possible to study directly electrical properties and transport phenomena and harness these phenomena for designing sensors for a variety of analytes and measuring apparatuses for channel activities and drug parameters. The lipid bilayer is

a dynamic system that changes in response to external stimuli and should be considered in molecular and electronic terms: it is capable of supporting ion and/or electron transport while it gathers information, processes them and delivers a response based on that information. Undoubtedly, the body of knowledge produced over the years on model membranes is significant, while the impact on electrophysiology is vast. The sector was fast to absorb new technological trends, successfully embedded in highly sophisticated tools for manipulating and monitoring membrane systems. Yet several issues remain unresolved: stability, engineering and cost. While stability requires intensification of the science path, device engineering and cost reduction reside on the technology path.

Biomimicking rests on fluidity which is fully demonstrated in fragile platforms. Fabrication is revealed as a critical parameter in membrane performance and applicability since any desired property has to be built-in the bilayer during the self-assembly process. Supported platforms are usually more robust than suspended bilayers due to the strong interactions they have with their support. Lipid composition, bioelement immobilisation and membrane curvature can be controlled allowing for easy patterning. Conversely, the support restricts fluidity and forces high packing densities usually unfit for biological systems. The hydration layer between the bilayer and its support may be insufficient to accommodate large bioelements or retain their functionality; this may lead to the displacement or deformation of the bioelements, potentially leading to their adsorption onto the support or even their denaturation. Tethering or cushioning the membrane may reduce this problem to various extents, but the underlying support will always have some influence on the structural and functional properties of the lipid bilayer; further, the fabrication process may lead to relatively poor membrane integrity due to the presence of defects in the bilayer. Pore-suspending membranes may eliminate the effect of the support, preserving, at the same time, the advantages of the supported formats. Micro- and nano-fabrication, if microscopically accessible, seem as an appropriate advancement for the production of nature-relevant platforms with defined composition, structures and built-in properties.

Device engineering for industrial production is a field of study largely unexplored. Essential improvement on the academy-to-industry transfer chain necessitates (i) optimisation of the technological routes of fabrication and validation of procedures; (ii) optimisation of methods for bioelement deposition allowing for post-deposition treatment to control orientation and maximum loading; (iii) control of film thickness, size, shape, and porosity; and (iv) modelling of the processes to allow for easy parameter control and scalability. Reaching the market might, also, require

'stability' to assume a co-notation other than reproducibility. A commercial device should be characterised by adequate longevity, during both, storage and operation, maintenance protocols and fault diagnostics. The shelf- or operational life of the membrane-based biosensor is restricted by the lifetime of the immobilised bioelement; unless synthetic moieties are engineered, commercialisation may only become feasible for ready-to-use diagnostic kits.

The issue of cost should be carefully revised. Despite the 'low-cost' tag linked to almost all membrane-based biosensors published, the actual cost-per-data point remains high, even for academic set-ups unless a basic high-cost infrastructure is available. Even when the fabrication process becomes cost-effective, e.g., employing economies of scale, and the data provided by the sensor is of high quality, the recordings of picoampere currents in field applications is only feasible with expensive instrumentation. Sufficient cost-reductions can be achieved by multi-array formats and high-throughput bilayer platforms. To that end, patterned platforms seem to have a higher probability to reach the market.

Notwithstanding, the design of membrane platforms should fit the intended use bearing in mind that an inherent drawback of the lipid bilayer technique lies in the fact that the system *in vitro* could never represent the real physiological condition. Nature relies on complex hierarchical structures that are optimised *in vivo* (via gene activation, transcriptional control and hormonal function) to achieve the mechanical and physicochemical performance that each subsystem requires for optimising the whole super-structure. Seen in isolation, the change of each subsystem function is triggered by electrical current, ionic strength, phase transitions, channel switching, temperature fluctuations, concentration and potential gradients, that can be easily simulated; the simulation, however, of the underlying entropy may be neither accurate nor easy: diffusion has to be replaced by bulk flow, viscosity by inertia, energy fluctuations by thermal adaptations, membrane-protein dynamic assembly by immobilisation, and environmentally controlled protein–analyte binding and dissociation mechanisms by pushing the sample towards the bilayer.

9.8 Concluding Remarks

For several years, self-assembly of lipid molecules received more and more attention because of their ability to spontaneously organise into nanostructures mimicking the living cell membranes. As attested by the number of papers quoted in this chapter, BLMs containing biological recognition

systems are suitable for designing highly sensitive biosensors, ion-channel recorders and drug-screening devices for minute investigations of biological processes at the molecular level. Although the physical and temporal instability of the bilayers remains an obstacle to their full exploitation, improvements demonstrated in micro- and nano-fabricated platforms are expected to expand applicability in academic research and improve the commercialisation prospects. Especially, the fields of membrane modelling and drug screening that have been recently set off are very intriguing. What remains to be seen is an engineering view within the scope of the BLM research.

Abbreviations

Å:	Angstrom
AHP:	Analytic hierarchy process
BLM:	(artificial) Bilayer lipid membrane
DNA:	Deoxyribonucleic acid
dsDNA:	Double-stranded deoxyribonucleic acid
EWOD:	Electrowetting on dielectric method
GF:	Glass microfiber
LB:	Langmuir–Blodgett
NMR:	Nuclear magnetic resonance
PEI:	Polyethyleneimine
PTFE:	Polytetrafluoropolyethylene
QCM-D:	Quartz crystal microbalance with dissipation monitoring
sBLM:	Supported bilayer lipid membrane
S-BLM:	S-layer-stabilised bilayer lipid membrane
sb-BLM:	Salt-bridged bilayer lipid membrane
SPR:	Surface plasmon resonance
tBLM:	Tethered bilayer lipid membrane
UV:	Ultraviolet

References

1. P. Mueller, D.O. Rudin, H.T. Tien and W.C. Wescott, Reconstitution of cell membrane structure *in vitro* and its transformation into an excitable system, *Nature*, 194, 979, 1962.
2. R. Hooke, Royal society meeting, in *The History of the Royal Society of London*, Ed., T. Birch, A. Miller, Johnson Reprint Corp., London, 3, p. 1757, 1672.

3. I. Langmuir, The constitution and fundamental properties of solids and liquids. II. Liquids, *Journal of the American Chemical Society*, 39, 1848, 1917.
4. K.B. Blodgett, Monomolecular films of fatty acids on glass, *Journal of the American Chemical Society*, 56, 495, 1934.
5. C.G. Siontorou and F.A. Batzias, A methodological combined framework for roadmapping biosensor research: a fault tree analysis approach within a strategic technology evaluation frame, *Critical Reviews in Biotechnology,* 34, 31, 2014.
6. I. Newton, *Optics*, Dover, New York, USA, p. 215 (1704 reprinted), 1952.
7. E.S. Johonnot, LXVIII. The black spot in thin liquid films, *The London, Edinburgh, and Dublin Philosophical Magazine and Journal of Science*, 11, 746, 1906.
8. A. Pockels, Surface tension, *Nature,* 43, 437, 1891.
9. H. Devaux, Oil films on water and on mercury, *Annual report of the Board of Regents of the Smithsonian Institution,* p. 261, 1913.
10. J. Perrin, The stratification of liquid films, *Annals of Physics*, 10, 160, 1918.
11. I. Langmuir, The mechanism of the surface phenomena of flotation, *Transactions of the Faraday Society*, 15, 62, 1920.
12. W.D. Harkins, *The Physical Chemistry of Surface Films*, Reinhold, New York, USA, 1952.
13. W.H. Bragg, Liquid films, *Proceedings of the Royal Institution of Great Britain*, 30, 687, 1939.
14. G.C. Nutting and W.D. Harkins, Pressure-area relations of fatty acid and alcohol monolayers, *Journal of the American Chemical Society*, 61, 1180, 1939.
15. E.A. Braude, F.C. Nachod and W.D. Phillips, *Determination of Organic Structures by Physical Methods*, Academic Press, New York, USA, 1955.
16. V. Lutzzati, H. Mustacchi and A. Skoulios, The structure of the liquid-crystal phases of some soap + water systems, *Discussions of the Faraday Society*, 25, 43, 1958.
17. J.W. Miles, The hydrodynamic stability of a thin film of liquid in uniform shearing motion, *Journal of Fluid Mechanics*, 8, 593, 1960.
18. J.M. Corkill, J.F. Goodmanan, D.R. Haisman and S.P. Harrold, The thickness and composition of thin detergent films, *Transactions of the Faraday Society*, 57, 821, 1961.
19. G.L. Gaines, *Insoluble Monolayers at Liquid Gas Interfaces*, Interscience Publishers, New York, USA, p. 184, 1966.
20. D. Branton, Fracture faces of frozen membranes, *Proceedings of the National Academy of Sciences USA*, 55, 1048, 1966.
21. D. Papahadjopoulos and N. Miller, Phospholipid model membranes. I. Structural characteristics of hydrated liquid crystals, *Biochimica et Biophysica Acta–Biomembranes*, 135, 624, 1967.
22. J. Gutknecht and D.C. Tosteson, Ionic permeability of thin lipid membranes. Effects of n-alkyl alcohols, polyvalent cations, and a secondary amine, *The Journal of General Physiology*, 55, 359, 1970.

23. S. Ohki, Properties of lipid bilayer membranes: determination of membrane thickness, *Journal of Theoretical Biology*, 23, 158, 1969.
24. S.H. White, A study of lipid bilayer membrane stability using precise measurements of specific capacitance, *Biophysical Journal*, 10, 1127, 1970.
25. J.C. Eriksson, Thermodynamics of surface-phase systems. VI. On the rigorous thermodynamics of insoluble surface films, *Journal of Colloid and Interface Science*, 37, 659, 1971.
26. M. Montal and P. Mueller, Formation of bimolecular membranes from lipid monolayers and a study of their electrical properties, *Proceedings of the National Academy of Sciences USA,* 69, 3561, 1972.
27. M. Edidin, Rotational and translational diffusion in membranes, *Annual Review of Biophysics and Bioengineering,* 3, 179, 1974.
28. R.J. Dam, K.F. Kongslie and O.H. Griffith, Photoelectron quantum yields and photoelectron microscopy of chlorophyll and chlorophyllin, *Photochemistry and Photobiology*, 22, 265, 1975.
29. S. McLaughlin, Electrostatic potentials at membrane-solution interfaces, in *Current Topics in Membranes and Transport*, Eds, F. Bronner and A. Kleinzeller, Academic Press, New York, USA, 9, p. 71, 1977.
30. D. Oesterhelt and W. Stoeckenius, Isolation of the cell membrane of *Halobacterium halobium* and its fractionation into red and purple membrane, *Methods in Enzymology*, 31, 667, 1974.
31. D. Marsh, A. Watts and P.F. Knowles, Cooperativity of the phase transition in single- and multibilayer lipid vesicles, *Biochimica et Biophysica Acta (BBA) – Biomembranes*, 465, 500, 1977.
32. R. Benz and K. Janko, Voltage-induced capacitance relaxation of lipid bilayer membranes Effects of membrane composition, *Biochimica et Biophysica Acta – Biomembranes*, 455, 721, 1976.
33. Y. Suezaki, Statistical mechanical analysis of interfacial tension of black lipid membrane, *Journal of Theoretical Biology*, 71, 279, 1978.
34. V.V. Cherny, V.S. Sokolov and I.G. Abidor, Determination of surface charge of bilayer lipid membranes, *Bioelectrochemistry and Bioenergetics*, 7, 413, 1980.
35. I.G. Kharitonenkov, S. ElKaradahgi, D.J. Bucher, J.A. Zakomirdin, and V.A. Tverdislov, Interaction of influenza virus proteins with planar lipid bilayers: a model for virion assembly, *Biochemical and Biophysical Research Communications*, 102, 308, 1981.
36. J.C. Weaver, K.T. Powell, R.A. Mintzer, H. Ling and S.R. Sloan, The electrical capacitance of bilayer membranes. The contribution of transient aqueous pores, *Bioelectrochemistry and Bioenergetics,* 12, 393, 1984.
37. H.T. Tien, Planar bilayer lipid membranes, *Progress in Surface Science*, 19, 169, 1985.
38. H.J.R Leidheiser and P.D. Deck, Chemistry of metal-polymer interfacial region, *Science,* 241, 1176, 1988.

39. C. Vigo, S.H. Grossman and W. Drost-Hansen, Interaction of dolichol and dolichyl phosphate with phospholipid bilayers, *Biochimica et Biophysica Acta – Biomembranes*, 774, 221, 1984.
40. C. Tanford, *The Hydrophobic Effect: Formation of Micelles and Biological Membranes*, 2nd ed., Wiley, New York, USA, 1980.
41. P.C. Jordan, J.A. McCammon, R.J. Bacquet and P. Tran, How electrolyte shielding influences the electrical potential in transmembrane ion channels, *Biophysical Journal*, 55, 1041, 1989.
42. U.J. Krull and M. Thompson, The lipid membrane as selective transducer, *IEEE Transactions on Electron Devices*, ED-32, 1180, 1985.
43. D.A. Stenger, DA Cribbs and T.L. Fare, Modulation of a gated ion channel admittance in lipid bilayer membranes, *Biosensors and Bioelectronics*, 6, 425, 1991.
44. D.P. Nikolelis and U.J. Krull, Establishment and control of artificial ion-conductive zones for lipid membrane biosensor development, *Analytica Chimica Acta*, 257, 239, 1992.
45. M. Montal, A. Darszon, and H. Schindler, Functional reassembly of membrane proteins in planar lipid bilayers, *Quarterly Reviews of Biophysics*, 14, 1, 1981.
46. M. Thompson, R. Bruce Lennox and R.A. McClelland, Structure and electrochemical properties of microfiltration filter-lipid membrane systems, *Analytical Chemistry*, 54, 76, 1982.
47. A. Arya, U.J. Krull, M. Thompson and H.E. Wong, Langmuir–Blodgett deposition of lipid films on hydrogel as a basis for biosensor development, *Analytica Chimica Acta*, 173, 331, 1985.
48. B.A. Suarez-Isla, K. Wan, J. Lindstrom and M. Montal, Single channel reporting from purified acetylcholine receptor reconstituted in bilayers at the tip of patch pipettes, *Biochemistry*, 22, 2319, 1983.
49. F. Gomezlagunas, A. Pena, A. Lievano and A. Darszon, Incorporation of ionic channels from yeast plasma membranes into black lipid membranes, *Biophysical Journal*, 56, 115, 1989.
50. T. Hianik, J. Dlugopolsky and M. Gyepessova, Electrostriction of lipid bilayers on a solid support. Influence of hydrocarbon solvent and d.c. voltage, *Bioelectrochemistry and Bioenergetics*, 31, 99, 1993.
51. H.D. White, Pathfinder networks and author cocitation analysis: a remapping of paradigmatic information scientists, *Journal of the American Society for Information Science and Technology*, 54, 423, 2003.
52. D.P. Nikolelis and C.G. Siontorou, Flow injection monitoring and analysis of mixtures of simazine, atrazine, and propazine using filter-supported bilayer lipid membranes (BLMs), *Electroanalysis,* 8, 907, 1996.
53. D.P. Nikolelis and C.G. Siontorou, Bilayer lipid membranes for flow injection monitoring of acetylcholine, urea, and penicillin, *Analytical Chemistry,* 67, 936, 1995.

54. D.P. Nikolelis, C.G. Siontorou, V.G. Andreou, K.G. Viras and U.J. Krull, Bilayer lipid membranes as electrochemical detectors for flow injection immunoanalysis, *Electroanalysis,* 7, 1082, 1995.
55. D.P. Nikolelis and C.G. Siontorou, Hemoglobin modified bilayer lipid membranes (BLMs) biosensor for carbon dioxide detection, *Bioelectrochemistry and Bioenergetics,* 42, 71, 1997.
56. C.G. Siontorou and D.P. Nikolelis, Cyanide ion minisensor based on methemoglobin incorporated in metal supported self-assembled bilayer lipid membranes and modified with platelet-activating factor, *Analytica Chimica Acta,* 355, 227, 1997.
57. C.G. Siontorou, D.P. Nikolelis and U.J. Krull, Flow injection monitoring and analysis of mixtures of hydrazine compounds using filter-supported bilayer lipid membranes with incorporated DNA, *Analytical Chemistry*, 72, 180, 2000.
58. D.P. Nikolelis, C.G. Siontorou, U.J. Krull and P.L. Katrivanos, Ammonium ion minisensors from self-assembled bilayer lipid membranes using gramicidin as an ionophore. modulation of ammonium selectivity by platelet-activating factor, *Analytical Chemistry*, 68, 1735, 1996.
59. F.A. Batzias and C.G. Siontorou, Investigating the causes of biosensor SNR decrease by means of fault tree analysis, *IEEE Transactions on Instrumentation and Measurement*, 54, 1395, 2005.
60. F. Davis and S.P.J. Higson, Structured thin films as functional components within biosensors, *Biosensors and Bioelectronics*, 21, 1, 2008.
61. F.A. Batzias and C.G. Siontorou, Creating a specific domain ontology for supporting R&D in the science-based sector – the case of biosensors, *Expert Systems with Applications,* 39, 9994, 2012.
62. P.-Y. Chen, J. McKittrick and M.A. Meyers, Biological materials: functional adaptations and bioinspired designs, *Progress in Materials Science*, 57, 1492, 2012.
63. C.G. Siontorou and F.A. Batzias, Innovation in biotechnology: moving from academic research to product development-the case of biosensors, *Critical Reviews in Biotechnology,* 30, 79, 2010.
64. S.M. Breznitz, R.P. O'Shea and T.J. Allen, University commercialization strategies in the development of regional bioclusters, *Journal of Product Innovation Management,* 25,129, 2008.
65. W.M. Cohen and D.A. Levinthal, Absorptive capacity: a new perspective on learning and innovation, *Administrative Science Quarterly*, 35, 128, 1990.
66. R. Garud and P.R. Nayyar, Transformative capacity: continual structuring by intertemporal technology transfer, *Strategic Management Journal*, 27, 365, 1994.
67. L.L. Glenna, R. Welsh, D. Ervin, W.B. Lacy and D. Biscotti, Commercial science, scientists' values, and university biotechnology research agendas, *Research Policy*, 40, 957, 2011.

68. S.H. White, Analysis of the torus surrounding planar lipid bilayer membranes, *Biophysical Journal*, 12, 432, 1972.
69. R. Coronado and R. Lattore, Phospholipid bilayers made from monolayers on patch-clamp pipettes, *Biophysical Journal*, 43, 231, 1983.
70. H. Sato, H. Hakamada, Y. Yamazaki, M. Uto, M. Sugawara and Y. Umezawa, Ionophore incorporated bilayer lipid membranes that selectively respond to metal ions and induce membrane permeability changes, *Biosensors & Bioelectronics,* 13, 1035, 1998.
71. Y. Matsuno, C. Osono, A. Hirano and M. Sugawara, Single-channel recordings of gramicidin at agarose-supported bilayer lipid membranes formed by the tip-dip and painting methods, *Analytical Sciences*, 20, 1217, 2004.
72. D.S. Dimitrov, Dynamic interactions between approaching surfaces of biological interest, *Progress in Surface Science*, 14, 295, 1983.
73. D.S. Dimitrov and R.K. Jain, Membrane stability, *Biochimica et Biophysica Acta*, 779, 437, 1984.
74. H.T. Tien and Z. Salamon, Formation of self-assembled lipid bilayers on solid substrates, *Bioelectrochemistry and Bioenergetics*, 22, 211, 1989.
75. H.T. Tien, Self-assembled lipid bilayers for biosensors and molecular electronic devices, *Advanced Materials,* 2, 316, 1990.
76. M. Uto. M. Araki, T. Taniguchi, S. Hoshi and S. Inoue, Stability of an agar-supported bilayer lipid membrane and its application to a chemical sensor, *Analytical Sciences*, 10, 943, 1994.
77. E. Sackmann, Supported membranes: scientific and practical applications, *Science,* 271, 43, 1996.
78. C. Steinem, A. Janshoff, W.P. Ulrich, M. Sieber and H.J. Galla, Impedance analysis of supported lipid bilayer membranes: a scrutiny of different preparation techniques, *Biochimica et Biophysica Acta,* 1279, 169, 1996.
79. H.-P. Yuan, A. Ottova-Leitmannova and H.T. Tien, An agarose-stabilized BLM: a new method for forming bilayer lipid membranes, *Material Science and Engineering C*, 4, 35, 1996.
80. X.-D. Lu, A.L Ottova and H.T. Tien, Biophysical aspects of agar-gel supported bilayer lipid membranes: a new method for forming and studying planar bilayer lipid membranes, *Bioelectrochemistry and Bioenergetics*, 39, 285, 1996.
81. C.G. Siontorou, A.M.O. Brett and D.P. Nikolelis, Evaluation of a glassy carbon electrode modified by a bilayer lipid membrane with incorporated DNA, *Talanta*, 43, 1137, 1996.
82. C.G. Siontorou, D.P. Nikolelis, U.J. Krull and K.L. Chiang, A triazine herbicide minisensor based on surface-stabilized bilayer lipid membranes, *Analytical Chemistry*, 69, 3109, 1997.
83. C.G. Siontorou, D.P. Nikolelis, A. Miernik and U.J. Krull, Rapid methods for detection of Aflatoxin M1 based on electrochemical transduction by self-assembled metal-supported bilayer lipid membranes (s-BLMs) and on

interferences with transduction of DNA hybridization, *Electrochimica Acta*, 43, 3611, 1998.
84. O. Purrucker, H. Hillebrandt, K. Adlkofer and M. Tanaka, Deposition of highly resistive lipid bilayer on silicon-silicon dioxide electrode and incorporation of gramicidin studied by ac impedance spectroscopy, *Electrochimica Acta,* 47, 791, 2001.
85. E.T. Castellana and P.S. Cremer, Solid supported lipid bilayers: from biophysical studies to sensor design, *Surface Science Reports,* 61, 429, 2006.
86. B.W. Koenig, S. Krueger, W.J. Orts, C.F. Majkrzak, N.F. Berk, J.V. Silverton, and K. Gawrisch, Neutron reflectivity and atomic force microscopy studies of a lipid bilayer in water adsorbed to the surface of a silicon single crystal, *Langmuir,* 12, 1343, 1996.
87. J. Sabo, A. Ottova, G. Laputkova, M. Legin, L. Vojeikova and H.T. Tien, A combined AC–DC method for investigation supported lipid membranes, *Thin Solid Films,* 306, 112, 1997.
88. A. Ottova, V. Tvarozek, J. Racek, J. Sabo, W. Ziegler, T. Hianik and H.T. Tien, Self-assembled BLMs: biomembrane models and biosensor applications, *Supramolecular Science*, 4, 101, 1997.
89. R. Richter, A. Mukhopadhyay and A. Brisson, Pathways of lipid vesicle deposition on solid surfaces: a combined QCM-D and AFM study, *Biophysical Journal*, 85, 3035, 2003.
90. K. Tawa and K. Morigaki, Substrate-supported phospholipid membranes studied by surface plasmon resonance and surface plasmon fluorescence spectroscopy, *Biophysical Journal*, 89, 2750, 2005.
91. P. Bassereau and F. Pincet, Quantitative analysis of holes in supported bilayers providing the adsorption energy of surfactants on solid substrate, *Langmuir,* 13, 7003, 1997.
92. T. Charitat, E. Bellet-Amalric, G. Fragneto and F. Graner, Adsorbed and free lipid bilayers at the solid-liquid interface, *European Physical Journal B,* 8, 583, 1999.
93. G. Fragneto, T. Charitat, F. Graner, K. Mecke, L. Perino-Gallice and E. Bellet-Amalric, A fluid floating bilayer, *Europhysics Letters*, 53, 100, 2001.
94. P. Desmeules, M. Grandbois, V.A. Bondarenko, A. Yamazaki and C. Salesse, Measurement of membrane binding between recoverin, a calcium-myristoyl switch protein, and lipid bilayers by AFM-based force spectroscopy, *Biophysical Journal*, 82, 3343, 2002.
95. T.F. Schmidt, L. Caseli, T. Viitala and O.N. Oliveira Jr., Enhanced activity of horseradish peroxidase in Langmuir–Blodgett films of phospholipids, *Biochimica et Biophysica Acta – Biomembranes*, 1778, 2291, 2008.
96. T. Jiao, B.D. Leca-Bouvier, P. Boullanger, L.J. Blum and A.P. Girard-Egrot, A chemiluminescent Langmuir-Blodgett membrane as the sensing layer for the reagentless monitoring of an immobilized enzyme activity, *Colloids and Surfaces A: Physicochemical and Engineering Aspects*, 354, 284, 2010.

97. H.A. Rinia, R.A. Demel, P.J.M. van der Eerden Jan and B. de Kruijff, Blistering of Langmuir-Blodgett bilayers containing anionic phospholipids as observed by atomic force microscopy, *Biophysical Journal*, 77, 1683, 1999.
98. J.K. Basu and M.K. Sanyal, Ordering and growth of Langmuir–Blodgett films: X-ray scattering studies, *Physics Reports,* 363, 1, 2002.
99. M.E. Díaz, R.L. Cerro, F.J. Montes and M.A. Galán, Hydrogenation of phenol in aqueous phase with palladium on activated carbon catalysts, *Chemical Engineering Journal*, 131, 65, 2007.
100. R.P. Richter, R. Berat and A.R. Brisson, Formation of solid-supported lipid bilayers: an integrated view, *Langmuir,* 22, 3497, 2006.
101. R.P. Richter and A.R. Brisson, Following the formation of supported lipid bilayers on mica: a study combining AFM, QCM-D, and ellipsometry, *Biophysical Journal*, 88, 3422, 2005.
102. B.A. Cornell, V.L.B. Braach-Maksvytis, L.G. King, P.D.J. Osman, B. Raguse, L. Wieczorek and R.J. Pace, A biosensor that uses ion-channel switches, *Nature,* 387, 580, 1997.
103. S. Terrettaz, M. Mayer and H. Vogel, Highly electrically insulating tethered lipid bilayers for probing the function of ion channel proteins, *Langmuir,* 19, 5567, 2003.
104. V. Atanasov, N. Knorr, R.S. Duran, S. Ingebrandt, A. Offenhäusser, W. Knoll and I. Köper, Membrane on a chip: a functional tethered lipid bilayer membrane on silicon oxide surfaces, *Biophysical Journal*, 89, 1780, 2005.
105. P. Kongsuphol, K.B. Fang and Z. Ding, Lipid bilayer technologies in ion channel recordings and their potential in drug screening assay, *Sensors and Actuators B*, 185, 530, 2013.
106. M. Andersson, H.M. Keizer, C. Zhu, D. Fine, A. Dodabalapur and R.S. Duran, Detection of single ion channel activity on a chip using tethered bilayer membranes, *Langmuir,* 23, 2924, 2007.
107. B. Schuster, D. Pum and U.B. Sleytr, S-layer stabilized lipid membranes, *Biointerphases,* 3, FA3, 2008.
108. G. Favero, L. Campanella, A. D'Annibale, R. Santucci and T. Ferri, Mixed hybrid bilayer lipid membrane incorporating valinomycin: improvements in preparation and functioning, *Microchemical Journal*, 74, 141, 2003.
109. T. Phung, Y. Zhang, J. Dunlop and J. Dalziel, Porous materials to support bilayer lipid membranes for ion channel biosensors, *Biosensors and Bioelectronics*, 26, 3127, 2011.
110. W. Römer and C. Steinem, Impedance analysis and single-channel recordings on nano-black lipid membranes based on porous alumina, *Biophysical Journal*, 86, 955, 2004.
111. E.K. Schmitt, M. Vrouenraets and C. Steinem, Channel activity of OmpF monitored in nano-BLMs, *Biophysical Journal*, 91, 2163, 2005.
112. J.C. Weaver and Y. Chizmadzhev, Theory of electroporation: a review, *Bioelectrochemistry and Bioenergetics*, 41, 135, 1996.

113. M. Mayer, J.K. Kriebel, M.T. Tosteson and G.M. Whitesides, Microfabricated Teflon membranes for low-noise recordings of ion channels in planar lipid bilayers, *Biophysical Journal*, 85, 2684, 2003.
114. T. Baumgart and A. Offenhäusser, Polysaccharide-supported planar bilayer lipid model membranes, *Langmuir,* 19, 1730, 2003.
115. J.A. Beddow, I.R. Peterson, J. Heptinstall and D.J. Walton, Reconstitution of nicotinic acetylcholine receptors into gel-protected lipid membranes, *Analytical Chemistry*, 76, 2261, 2004.
116. Y. Zhang, Y. Chen and G. Jin, Chitosan cushioned phospholipid membrane and its application in imaging ellipsometry based-biosensor, *Applied Surface Science,* 257, 9407, 2011.
117. J.Y. Wong, J. Majewski, M. Seitz, C.K. Park, J.N. Israelachvili and G.S. Smith, Polymer-cushioned bilayers. II. An investigation of interaction forces and fusion using the surface forces apparatus, *Biophysical Journal*, 77, 1445, 1999.
118. H. Hillebrandt, G. Wiegand, M. Tanaka and E. Sackmann, High electric resistance polymer/lipid composite films on indium-tin-oxide (ITO) electrodes, *Langmuir,* 15, 8451, 1999.
119. G. Wiegand, T. Jaworek, G. Wegner and E. Sackmann, Heterogeneous surfaces of structured hairy-rod polymer films: preparation and methods of functionalization, *Langmuir,* 13, 3563, 1997.
120. J.W. Shim and L.Q. Gu, Stochastic sensing on a modular chip containing a single-ion channel, *Analytical Chemistry*, 79, 2207, 2007.
121. X. Tana, M. Lia, P. Caia, L. Luoa and X. Zou, An amperometric cholesterol biosensor based on multiwalled carbon nanotubes and organically modified sol-gel/chitosan hybrid composite, *Analytical Biochemistry,* 337, 111, 2005.
122. R. Pantoja, D. Sigg, R. Blunck, F. Benzanilla and J.R. Heath, Bilayer reconstitution of voltage-dependent ion channels using a microfabricated silicon chip, *Biophysical Journal*, 81, 2389, 2001.
123. S.J. Wilk, L. Petrossian, M. Goryll, T.J. Thornton, S.M. Goodnick, J.M. Tang and R.S. Eisenberg, Integrated electrodes on a silicon based ion channel measurement platform, *Biosensors and Bioelectronics*, 23, 183, 2007.
124. N. Fertig, Ch. Meyer, R.H. Blick, Ch. Trautmann and J.C. Behrends, Microstructured glass chip for ion-channel electrophysiology, *Physical Review E, Statistical Physics, Plasmas, Fluids, and Related Interdisciplinary Topics*, 64, 040901R, 2001.
125. H. Suzuki, K.V. Tabata, H. Noji and S. Takeuchi, Highly reproducible method of planar lipid bilayer reconstitution in polymethyl methacrylate microfluidic chip, *Langmuir,* 22, 1937, 2006.
126. N. Malmstadt, M.A. Nash, R.F. Purnell and J.J. Schmidt, Automated formation of lipid-bilayer membranes in a microfluidic device, *Nano Letters*, 6, 1961, 2006.
127. H. Suzuki, K.V. Tabata, H. Noji and S. Takeuchi, Electrophysiological recordings of single ion channels in planar lipid bilayers using a polymethyl methacrylate microfluidic chip, *Biosensors and Bioelectronics*, 22, 1111, 2007.

128. B. Le Pioufle, H.K. Suzuki, V. Tabata, H. Noji and S. Takeuchi, Lipid bilayer microarray for parallel recording of transmembrane ion currents, *Analytical Chemistry,* 80, 328, 2008.
129. M. Zagnoni, M.E. Sandison and H. Morgan, Microfluidic array platform for simultaneous lipid bilayer membrane formation, *Biosensors and Bioelectronics,* 24, 1235, 2009.
130. A.M. El-Arabi, C.S. Salazar and J.J. Schmidt, Ion channel drug potency assay with an artificial bilayer chip, *Lab on a Chip,* 12, 2409, 2012.
131. T. Ide and T. Ichikawa, A novel method for artificial lipid-bilayer formation, *Biosensors and Bioelectronics,* 21, 672, 2005.
132. C. Schmidt, M. Mayer and H. Vogel, A chip-based biosensor for the functional analysis of single ion channels, *Angewandte Chemie International Edition in English*, 39, 3137, 2000.
133. K. Funakoshi, H. Suzuki and S. Takeuchi, Lipid bilayer formation by contacting monolayers in a microfluidic device for membrane protein analysis, *Analytical Chemistry,* 78, 8169, 2006.
134. A.J. Heron, J.R. Thompson, A.E. Mason and M.I. Wallace, Direct detection of membrane channels from gels using water-in-oil droplet bilayers, *Journal of the American Chemical Society,* 129, 16042, 2007.
135. W.L. Hwang, M. Chen, M.A. Holden and H. Bayley, Asymmetric droplet interface bilayers, *Journal of the American Chemical Society,* 130, 5878, 2008.
136. J.L. Poulos, S.A. Portonovo, H. Bang and J.J. Schmidt, Automatable lipid bilayer formation and ion channel measurement using sessile droplets, *Journal of Physics: Condensed Matter,* 22, 454105, 2010.
137. L.C. Gross, A.J. Heron, S.C. Baca and M.I. Wallace, Determining membrane capacitance by dynamic control of droplet interface bilayer area, *Langmuir*, 27, 14335, 2011.
138. S.-H. Jung, S. Choi, Y.-R. Kim and T. Jeon, Storable droplet interface lipid bilayers for cell-free ion channel studies, *Bioprocess and Biosystems Engineering,* 35, 241, 2012.
139. J.T. Groves, S.G. Boxer and H.M. McConnell, Electric field-induced reorganization of two-component supported bilayer membranes, *Proceedings of the National Academy of Sciences USA*, 94, 13390, 1997.
140. J.S. Hovis and S.G. Boxer, Patterning barriers to lateral diffusion in supported lipid bilayer membranes by blotting and stamping, *Langmuir,* 16, 894, 2000.
141. S. Majd and M. Mayer, Hydrogel stamping of arrays of supported lipid bilayers with various lipid compositions for the screening of drug-membrane and protein-membrane interactions, *Angewandte Chemie International Edition in English,* 44, 6697, 2005.
142. L. Kam and S.G. Boxer, Formation of supported lipid bilayer composition arrays by controlled mixing and surface capture, *Journal of the American Chemical Society*, 122, 12901, 2000.
143. S. Künneke and A. Janshoff, Visualization of molecular recognition events on microstructured lipid-membrane compartments by *in situ* scanning force

microscopy, *Angewandte Chemie International Edition in English,* 41, 314, 2002.
144. T. Yang, S. Jung, H. Mao and P.S. Cremer, Fabrication of phospholipid bilayer-coated microchannels for on-chip immunoassays, *Analytical Chemistry*, 73, 165, 2001.
145. P.S. Cremer and T. Yang, Developing biosensors from supported phospholipid bilayer, *Journal of the American Chemical Society*, 121, 8130, 1999.
146. S. Lenhert, P. Sun, Y. Wang, H. Fuchs and C.A. Mirkin, Massively parallel dip-pen nanolithography of heterogeneous supported phospholipid multilayer patterns, *Small,* 3, 71, 2007.
147. Y. Fang, A.G. Frutos and J. Lahiri, Membrane protein microarrays, *Journal of the American Chemical Society*, 124, 2394, 2002.
148. M.D. Mager and N.A. Melosh, Lipid bilayer deposition and patterning via air bubble collapse, *Langmuir,* 23, 9369, 2007.
149. A.T.A. Jenkins, N. Boden, R.J. Bushby, S.D. Evans, P.F. Knowles, R.E. Miles, S.D. Ogier, H. Schönherr and G.J. Vancso, Microcontact printing of lipophilic self-assembled monolayers for the attachment of biomimetic lipid bilayers to surfaces, *Journal of the American Chemical Society*, 121, 5274, 1999.
150. L.A. Kung, L. Kam, J.S. Hovis and S.G. Boxer, Patterning hybrid surfaces of proteins and supported lipid bilayers, *Langmuir,* 16, 6773, 2000.
151. C.K. Yee, M.L. Amweg and A.N. Parikh, Membrane photolithography: direct micropatterning and manipulation of fluid phospholipid membranes in the aqueous phase using deep-UV light, *Advanced Materials*, 16, 1184, 2004.
152. K.D. Mossman, G. Campi, J.T. Groves and M.L. Dustin, Altered TCR signaling from geometrically repatterned immunological synapses, *Science,* 310, 1191, 2005.
153. M. Wu, D. Holowka, H.G. Craighead and B. Baird, Visualization of plasma membrane compartmentalization with patterned lipid bilayers, *Proceedings of the National Academy of Sciences USA*, 101, 13798, 2004.
154. L.C. Kam, Capturing the nanoscale complexity of cellular membranes in supported lipid bilayers, *Journal of Structural Biology,* 168, 3, 2009.
155. T.M. Sisson, H.G. Lamparski, S. Köchens, A. Elayadi and D.F. O'Brien, Two-dimensional polymerization of lipid bilayers: effect of lipid lateral diffusion on the rate and degree of polymerization, *Macromolecules,* 29, 8321, 1996.
156. D.P. Nikolelis, M.G. Simantiraki, C.G. Siontorou and K. Toth, Flow injection analysis of carbofuran in foods using air stable lipid film based acetylcholinesterase biosensor, *Analytica Chimica Acta*, 537, 169, 2005.
157. S. Kölchens, H. Lamparski and D.F. O'Brien, Gelation of two-dimensional assemblies, *Macromolecules,* 26, 398, 1993.
158. M.C. Giocondi, F. Besson, P. Dosset, P.E. Milhiet and C. Le Grimellec, Remodeling of ordered membrane domains by GPI-anchored intestinal alkaline phosphatase, *Langmuir*, 23, 9358, 2007.
159. J.-S. Ye, H.-F. Cui, Y. Wen, W.D. Zhang, A. Ottova, H.T. Tien, G.Q. Xu and F.-S. Sheu, Self-assembly of bilayer lipid membrane at multiwalled carbon

nanotubes towards the development of photo-switched functional devices, *Electrochemistry Communications,* 7, 81, 2005.
160. B. Hinds, Dramatic transport properties of carbon nanotube membranes for a robust protein channel mimetic platform, *Current Opinion in Solid State and Materials Science,* 16, 1, 2012.
161. W. Hoiles, V. Krishnamurthy and B. Cornell, Mathematical models for sensing devices constructed out of artificial cell membranes, *Nanoscale Systems MMTA*, 1, 143, 2012.
162. B. Martinac and O.P. Hamill, Gramicidin A channels switch between stretch activation and stretch inactivation depending on bilayer thickness, *Proceedings of the National Academy of Sciences USA*, A. 99, 4308, 2002.
163. M. Thompson and U.J. Krull, Lipid membrane dipole perturbation and chemoreception as models for selective chemical sensing, *Analytica Chimica Acta*, 147, 1, 1983.
164. Y.L. Zhang, J.A. Frangos and M. Chachisvilis, Laurdan fluorescence senses mechanical strain in the lipid bilayer membrane, *Biochemical and Biophysical Research Communications,* 347, 838, 2006.
165. U.J. Krull, M. Thompson and H.E. Wong, Chemical modification of the bilayer lipid membrane biosensor dipolar potential, *Bioelectrochemistry and Bioenergetics*, 15, 371, 1986.
166. D.P. Nikolelis, J.D. Brennan, R.S. Brown and U.J. Krull, Control of ion transport across bilayer lipid membranes by adjustment of surface charge associated with phase domain structures, *Analytica Chimica Acta*, 257, 49, 1992.
167. P.D. Blood, G.S. Ayton and G.A. Voth, Probing the molecular-scale lipid bilayer response to shear flow using nonequilibrium molecular dynamics, *Journal of Physical Chemistry B*, 109, 18673, 2005.
168. K. Gawrisch, D. Ruston, J. Zimmerberg, V.A. Parsegian, R.P. Rand and N. Fuller, Membrane dipole potentials, hydration forces, and the ordering of water at membrane surfaces, *Biophysical Journal*, 61, 1213, 1992.
169. R.J. Clarke, The dipole potential of phospholipid membranes and methods for its detection, *Advances in Colloid and Interface Science*, 89, 263, 2001.
170. A. Devadoss A, M.S. Palencsár, D. Jiang, M.L. Honkonen and J.D. Burgess, Enzyme modification of platinum microelectrodes for detection of cholesterol in vesicle lipid bilayer membranes, *Analytical Chemistry*, 77, 7393, 2005.
171. D.P. Nikolelis, G. Raftopoulou, G.-P. Nikoleli and M. Simantiraki, Stabilized lipid membrane based biosensors with incorporated enzyme for repetitive uses, *Electroanalysis*, 18, 2497, 2006.
172. Y. Ben Chaim, B. Chanda, N. Dascal, F. Bezanilla, I. Parnas and H. Parnas, Movement of "gating charge" is coupled to ligand binding in a G-protein coupled receptor, *Nature,* 444, 106, 2006.
173. D.T. Warshaviak, M.J. Muellner and M. Chachisvilis, Effect of membrane tension on the electric field and dipole potential of lipid bilayer membrane, *Biochimica et Biophysica Acta,* 1808, 2608, 2011.

174. P. Kramar, D. Miklavčič, M. Kotulska and A. Maček Lebar, Voltage- and current-clamp methods for determination of planar lipid bilayer properties, *Advances in Planar Lipid Bilayers and Liposomes*, 11, 29, 2010.
175. T. Starke-Peterkovic, N. Turner, M.F. Vitha, M.P. Waller, D.E. Hibbs and R.J. Clarke, Cholesterol effect on the dipole potential of lipid membranes, *Biophysical Journal,* 90, 4060, 2006.
176. K.B. Oldham, A Gouy-Chapman-Stern model of the double layer at a (metal)/(ionic liquid) interface, *Journal of Electroanalytical Chemistry,* 613, 131, 2008.
177. D.H. Mengistu, E.E. Kooijman and S. May, Ionization properties of mixed lipid membranes: a Gouy–Chapman model of the electrostatic–hydrogen bond switch, *Biochimica et Biophysica Acta,* 1808, 1985, 2011.
178. M. Langner and K. Kubica, The electrostatics of lipid surfaces, *Chemistry and Physics of Lipids*, 101, 3, 1999.
179. M. Belaya, V. Levadny and D.A. Pink, Electric double layer near soft permeable interfaces. I Local electrostatics, *Langmuir,* 10, 2010, 1994.
180. D.R. Heine, A.R. Rammohan and J. Balakrishnan, Atomistic simulations of the interaction between lipid bilayers and substrates, *Molecular Simulation*, 33, 391, 2007.
181. A. Dickey and R. Faller, Examining the contributions of lipid shape and headgroup charge on bilayer behavior, *Biophysical Journal*, 95, 2636, 2008.
182. M. Roark and S.E. Feller, Structure and dynamics of a fluid phase bilayer on a solid support as observed by a molecular dynamics computer simulation, *Langmuir,* 24, 12469, 2008.
183. M.J. Skaug, M.L. Longo and R. Faller, Computational studies of Texas Red–1, 2-dihexadecanoyl-sn-glycero-3-phosphoethanolamine. Model building and applications, *The Journal of Physical Chemistry B*, 113, 8758, 2009.
184. C.M. Hartshorn, C.M. Jewett and J.A. Brozik, Molecular effects of a nanocrystalline quartz support upon planar lipid bilayers, *Langmuir,* 26, 2609, 2010.
185. S.E. Feller, C.A. Brown, D.T. Nizza and K. Gawrisch, NOESY cross-relaxation rates and ethanol distribution across membranes, *Biophysical Journal*, 82, 1396, 2002.
186. S.J. Marrink, A.H. de Vries and A. Mark, Coarse grained model for semiquantitative lipid simulations, *Journal of Physical Chemistry B*, 108, 750, 2004.
187. O. Lenz and F. Schmid, A simple computer model for liquid lipid bilayers, *Journal of Molecular Liquids*, 117, 147, 2005.
188. L. Monticelli, S. Kandasamy, X. Periole, R. Larson, D. Tieleman and S. Marrink, The MARTINI coarse-grained force field: extension to proteins, *Journal of Chemical Theory and Computation*, 4, 819, 2008.
189. G. Brannigan, L. Lin and F.L.H. Brown, A consistent model for thermal fluctuations and protein-induced deformations in lipid bilayers, *European Biophysics Journal*, 35, 104, 2006.

190. I.R. Cooke, K. Kremer and M. Deserno, Tunable generic model for fluid bilayer membranes, *Physical Review E*, 72, 011506, 1, 2005.
191. J.F. Nagle and S. Tristram-Nagle, Structure of lipid bilayers, *Biochimica et Biophysica Acta – Biomembranes*, 1469, 159, 2000.
192. C. Xing and R. Faller, What is the difference between a free and a supported lipid bilayer? Insights from molecular modeling on different scales, *Advances in Planar Lipid Bilayers and Liposomes,* 11, 127, 2010.
193. J.A. Killian, Hydrophobic mismatch between proteins and lipids in membranes, *Biochimica et Biophysica Acta – Biomembranes,* 1376, 401, 1998.
194. D.J. Woodbury and K. Rognlien, The t-SNARE syntaxin is sufficient for spontaneous fusion of synaptic vesicles to planar membranes, *Cell Biology International*, 24, 809, 2000.
195. W. Göpel and P. Heiduschka, Interface analysis in biosensor design, *Biosensors and Bioelectronics*, 10, 853, 1995.
196. T. Hianik, M. Šnejdárková, V.I. Passechnik M. Rehák and M. Babincova, Immobilization of enzymes on lipid bilayers on a metal-support allows study of the biophysical mechanisms of enzymatic-reactions, *Bioelectrochemistry and Bioenergetics*, 41, 221, 1996.
197. H. Chen, Y. Zheng, J.-H. Jiang, H.-L. Wu, G.-L. Shen and R.-Q. Yu, An ultrasensitive chemiluminescence biosensor for cholera toxin based on ganglioside-functionalized supported lipid membrane and liposome, *Biosensors and Bioelectronics*, 24, 684, 2008.
198. A. Lundquist, S.B. Hansen, H. Nordström, U.H. Danielson and K. Edwards, Biotinylated lipid bilayer disks as model membranes for biosensor analyses, *Analytical Biochemistry*, 405, 153, 2010.
199. I. Vikholm-Lundin, S. Auer, M. Paakkunainen, J.A.E. Määttä, T. Munter, J. Leppiniemi, V.P. Hytönen and K. Tappura, Cysteine-tagged chimeric avidin forms high binding capacity layers directly on Gold, *Sensors and Actuators B: Chemical*, 171–172, 440, 2012.
200. E.P. Cipolatti, M.J.A. Silva, M. Klein, V. Feddern, M.M.C. Feltes, J.V. Oliveira, J.L. Ninow and D. de Oliveira, Immobilization of *Candida antarctica* lipase B on PEGylated poly(urea-urethane) nanoparticles by step mini emulsion polymerization, *Journal of Molecular Catalysis B: Enzymatic,* 99, 56, 2014.
201. X. Zhu, Z. Wang, A. Zhao, N. Huang, H. Chen, S. Zhou and X. Xied, Cell adhesion on supported lipid bilayers functionalized with RGD peptides monitored by using a quartz crystal microbalance with dissipation, *Colloids and Surfaces B: Biointerfaces*, 116, 459, 2014.

10

Recent Advances of Biosensors in Food Detection Including Genetically Modified Organisms in Food

T. Varzakas[1], Georgia-Paraskevi Nikoleli[2], and Dimitrios P. Nikolelis[3]

[1]TEI Peloponnese, Department of Food Technology, Kalamata, Greece
[2]Laboratory of Inorganic & Analytical Chemistry, School of Chemical Engineering, Dept 1, Chemical Sciences, National Technical University of Athens, Athens, Greece
[3]Laboratory of Environmental Chemistry, Department of Chemistry, University of Athens, Panepistimiopolis-Kouponia, Athens, Greece

Abstract

Biosensors are analytical devices with a sensing biological material including microorganisms, antibodies, enzymes, cell receptors, tissues, derived biomaterials, and, finally a transducing microsystem. The transducer is the main component in a biosensor that converts biological signal into a measurable electrical signal. The transducer component is comprised of electrochemical, optical, thermometric, magnetic, or piezoelectric material. The biosensors have got major importance in medical diagnosis, environmental monitoring, genetics, and food industry and defense applications due to their simplicity, high sensitivity, and practical usability for real sample analysis and on-spot analysis.

Different categories of biosensors have been described such as electrochemical biosensors and more specifically nitrite electrochemical biosensing based on coupled graphene and gold nanoparticles, optical biosensors using monoclonal antibodies or plasmonic biosensors for ochratoxin detection, biosensors for pesticide residue detection, surface plasmon resonance detectors, electronic tongues, DNA biosensors for detection of genetically modified organisms (GMOs) in food and feed, multichannel biosensors for detection of natural and artificial sweeteners, biosensor strains for toxoflavin detection, xanthine biosensors, nanostructured voltammetric biosensors, amperometric glucose biosensor based on layer-by-layer

**Corresponding author*: tvarzakas@teikal.gr

Ashutosh Tiwari, Hirak K. Patra and Anthony P.F. Turner (eds.) Advanced Bioelectronic Materials, (355–388)

films of microperoxidase-11 and liposome-encapsulated glucose oxidase, aptamer-based magnetic separation system as a sample preparation method for subsequent identification and quantification of the contaminant bacteria by real-time PCR, lateral flow biosensor for DNA extraction-free detection of *Salmonella* based on aptamer-mediated strand displacement amplification and finally surface acoustic wave (SAW) biosensors for odor detection in the food industry.

***Keywords*:** Biosensors, food detection, genetically modified organisms

10.1 Electrochemical Biosensors

Graphene (GA), a two-dimensional single-atom-thick conjugated carbon network, has attracted tremendous attention recently (Allen *et al*., 2010), because of its extraordinary properties, such as excellent electronic conductivity, large specific surface area, strong mechanical strength, and enhanced electrocatalytic activity.

Many nanomaterials such as Au (Goncalves *et al*., 2009), Pt (Guo *et al*., 2010), Pd (Sundaram *et al*., 2008), TiO_2 (Williams *et al*., 2008), tin oxide (Paek *et al*., 2009), latex (Liu *et al*., 2010), and carbon nanotube (CNT) (Tung *et al*., 2009) were used to fabricate functional grapheme nanocomposites. Among them, gold nanoparticles (AuNPs) with unique properties provide suitable microenvironments for immobilization of biomacromolecules (Shan *et al*., 2010) and allow for direct electron transfer between redox-active proteins and bulk electrode materials (Pingarrón *et al*., 2008).

Biofunctionalized GA–AuNP hybrids were prepared by Jiang *et al*. (2014) using a facile approach of *in situ* growth, with homogeneous distribution of AuNPs on the grapheme nanosheets. Hemoglobin (Hb) was immobilized on the GA–AuNP composites to fabricate biosensors for determination of nitrite (NO_2^-). A pair of well-defined redox peaks was observed for Hb immobilized on the GA–AuNP hybrids with a formal potential ($E^{0\prime}$) of –0.314 V in 0.1 M phosphate-buffered saline (0.15 M NaCl, pH 7.0). The novel biosensors exhibited many advantages, such as wide linear response range (from 0.05 to 1000 μM, R^2=0.997), low detection limit [0.01 μM, a signal-to-noise (S/N) ratio of 3], high sensitivity (0.15 μA μM^{-1} cm^{-2}), and excellent selectivity. These constructed biosensors were further used for determination of nitrite in pickled radish. The results obtained were in good agreement with those using spectrophotometry based on the National Food Safety Standard (GB5009.33-2010), which indicates that these novel and sensitive biosensors have promising application for determination of nitrite in food.

Antiochia and Gorton (2014) described the development and performance of the first fructose biosensor based on a commercial screen-printed GA electrode (SPGE).

Screen-printed electrodes (SPEs) offer a number of advantages versus conventional electrodes as they are suitable for working with microvolumes and for decentralized assays and allow the development of mass produced portable, accurate, and reproducible sensors (Biscay *et al*., 2012). The electrode was modified with an osmium polymer, which allowed the efficient wiring of the enzyme fructose dehydrogenase (FDH). The immobilization of both osmium polymer and FDH was realized in an easy way. Aliquots of 10 μL Os polymer and 10 μL FDH were thoroughly mixed with poly (ethylene glycol) (400) diglycidyl ether (PEDGE) and deposited on the electrode surface and left there to dry overnight. The biosensor exhibits a detection limit of 0.8 μM, a linear range between 0.1 and 8 mM, high sensitivity to fructose (2.15 μA cm^{-2}/μM), good reproducibility (RSD = 1.9%), fast response time (3 s), and a stability of 2 months when stored in the freezer. The proposed fructose biosensor was tested in real food samples and validated with a commercial spectrophotometric enzymatic kit. No significant interference was observed with the proposed biosensor.

The self-assembly of layered molybdenum disulfide–GA (MoS_2–Gr) and horseradish peroxidase (HRP) by electrostatic attraction into a novel hybrid nanomaterial (HRP–MoS_2–Gr) is reported by Song *et al*. (2014). The properties of the MoS_2–Gr were characterized by X-ray diffraction (XRD), high-resolution transmission electron microscopy (TEM), electrochemical impedance spectroscopy (EIS), and cyclic voltammetry (CV). UV–vis and Fourier transform infrared spectroscopy (FT-IR) indicate that the native structure of the HRP is maintained after the assembly, implying good biocompatibility of MoS_2–Gr nanocomposite. Furthermore, the HRP–MoS2–Gr composite is utilized as a biosensor, which displays electrocatalytic activity to hydrogen peroxide (H_2O_2) with high sensitivity (679.7 μA μM^{-1} cm^{-2}), wide linear range (0.2 μM–1.103 μM), low detection limit (0.049 μM), and fast amperometric response. In addition, the biosensor also exhibits strong anti-interference ability, satisfactory stability, and reproducibility. These desirable electrochemical properties are attributed to the good biocompatibility and electron transport efficiency of the MoS_2–Gr composite, as well as the high loading of HRP. Therefore, this biosensor is potentially suitable for H_2O_2 analysis in environmental, pharmaceutical, food, or industrial applications.

There is an increasing need to develop biosensors for the detection of harmful pesticide residues in food and water. Zhang *et al*. (2014) reported on a versatile strategy to synthesize functionalized GA oxide

(GO) nanomaterials with abundant affinity groups that can capture histidine (His)-tagged acetylcholinesterase (AChE) for the fabrication of paraoxon biosensors. Initially, exfoliated GO was functionalized by a diazonium reaction to introduce abundant carboxyl groups. Then, N_a,N_a-bis (carboxymethyl)-L-lysine hydrate (NTA-NH_2) and Ni^{2+} were anchored onto the GO-based materials step by step. AChE was immobilized on the functionalized GO (FGO) through the specific binding between Ni-NTA and His-tag. A low anodic oxidation potential was observed due to an enhanced electrocatalytic activity and a large surface area brought about by the use of FGO. Furthermore, a sensitivity of 2.23 mA mM^{-1} to the acetylthiocholine chloride (ATChCl) substrate was found for our composite covered electrodes. The electrodes also showed a wide linear response range from 10 to 1 mM ($R^2 = 0.996$), with an estimated detection limit of 3 mM based on an S/N = 3. The stable chelation between Ni-NTA and His-tagged AChE endowed our electrodes with great short-term and long-term stability. In addition, a linear correlation was found between paraoxon concentration and the inhibition response of the electrodes to paraoxon, with a detection limit of 6.5×10^{-10} M. This versatile strategy provides a platform to fabricate GO-based nanomaterials for biosensor applications.

The immobilization of AChE within GA-based nanomaterials introduced tremendous momentum to pesticide biosensor fabrication. A nanocomposite of chemically reduced GO and AuNPs with the assistance of poly(diallyldimethylam-monium chloride) (PDDA) for dispersion was synthesized for the immobilization of AChE by electrostatic interaction and ultrasensitive detection of paraoxon (Wang *et al*., 2011a). In another report on organo-phosphate pesticide detection, TiO_2 and GA hybrids were developed for AChE immobilization by adsorption (Wang *et al*., 2011b). Similarly, AChE was immobilized by adsorption within the hybrid of ionic liquid and GA (Li and Han, 2012). The immobilization method using specific binding was also developed for AChE in a GO/gold composite system, exhibiting great potential for specific binding immobilization in terms of repeatability and stability of biosensors (Liu *et al*., 2011).

AChE biosensor was developed through silica sol–gel (SiSG) immobilization of AChE on the carbon paste electrode (CPE) and used as working electrode. AChE catalyses the cleavage of ATChCl (or substrate) to thiocholine, which was oxidized to give a disulphide compound by dimerization at 0.60 V versus saturated calomel electrode. All the experiments were carried out in 0.1 M phosphate buffer solution (PBS) at pH 7.0 and 0.1 M KCl solution at room temperature. The limit of detection (LOD) and limit of quantification values were found to be 0.058, 0.044 and 0.194, 0.147 ppm for Malathion and Acephate, respectively. The response of the

biosensor showed a good linearity range with an incubation time of 4 min for Malathion and Acephate, respectively. This biosensor was used for the direct determination of pesticides without any pretreatment and it requires less time for analysis (Raghu *et al*., 2014).

Two electrochemical biosensors for the detection of bacteria *Aeromonas hydrophila* are presented by Ligaj *et al*. (2014). *A. hydrophila* is a food-borne human pathogen of emerging importance, very often isolated from a variety of food products. Pathogenicity of *A. hydrophila* is associated with the presence of aerolysin gene (aerA); therefore, specific and effective tool for its detection is a DNA probe complementary to this gene. Such DNA probe at the sequence 5_GTCAAGACGGTGGTGGGCTG was designed and used as a sensing element in the presented biosensors. The detection layer of biosensor I was a gold electrode covered with self-assembled monolayer (SAM) consisting of mercaptohexanol and thiolated DNA probe. The detection layer of biosensor II was a CPE modified with multiwalled CNTs (MWCNTs) containing covalently immobilized DNA probe. The composition of biosensors detection layers, a way of probe immobilization as well as all parameters influencing hybridization event including preparation of target DNA samples, contamination of non-complementary DNA were carefully investigated. Several electroactive hybridization indicators were examined with both detection layers and two of them were selected for the final determinations: Hoechst 33258 (biosensor I) and daunomycin (biosensor II). Upon hybridization of DNA probes immobilized in the detection layers of biosensors with the target DNA isolated from *A. hydrophila* peak currents were found to increase by 75–135% with the use of biosensor I and 34–92% with biosensor II. Both biosensors were used successfully for the detection of pathogenic strains of *A. hydrophila* in food samples (fishes and vegetables), and it was established that the optimal DNA concentration in analyzed samples for the effective analysis was 2.0 μg cm^{-3} (biosensor I) and 0.8 μg cm^{-3} (biosensor II). All results obtained with both biosensors were correlated with results made by polymerase chain reaction (PCR).

The importance of the so-called reactive nitrogen and oxygen species (RNOS) in biology and food technology has been widely recognized. However, when these species are in excess, the steady state maintained by physiological processes is disturbed. At this point, the nitro-oxidative metabolic stress develops and its action *in vivo* over time leads to nitro-oxidative reactions in food and in living organisms, but also results in chronic degenerative diseases. Analytical methods enabling the assessment of the total antioxidant activity of a biological sample or a plant extract is therefore largely sought after. The ability of biosensors for rapid and real-time analysis that decreases the assay time and the possibility of automated and

multi-analyte analysis at low cost has also allowed the quantitative and qualitative detection of RNOS. Among these RNOS, peroxynitrite ($ONOO^-$) is a well-known inflammatory mediator during a number of physiological and pathological processes. Consequently, many efforts are under way to detect peroxynitrite in the biomedical field. This urgent demand makes the development of $ONOO^-$ specific probes of great interest. Not only they can be useful for the detection of disease states, but they will also allow for a screening-type analysis of potential signal transduction pathways in the cells. Peteu *et al*. (2014) critically discuss the very latest advancements and the challenges in the field of peroxynitrite biosensors and probes for *in vivo* and *in vitro* studies. Also, the main trends will be extracted, in order to chart the future directions and hence create an instrumental outlook.

The first examples of peroxynitrite-sensitive electrochemical sensors are based on the reduction of peroxynitrite with polymeric films of manganese (II) tetraaminophthalocyanine [Mn(TAPc)] (Xue *et al*., 2000; Sandoval Cortes *et al*., 2007) or manganese porphyrin [Mn(III)-[2,2] paracyclophenylporphyrin] (Kubant *et al*., 2006).

The detection of contaminated food in every stage of processing required new technology for fast identification and isolation of toxicity in food. Since effect of food contaminant are severe to human health, the need of pioneer technologies also increasing over last few decades.

In the study reported by Kumar *et al*. (2014), malonaldehyde (MDA) was prepared by hydrolysis of 1,1,3,3-tetramethoxypropane in HCl media and used in the electrochemical studies. The electrochemical sensor was fabricated with modified glassy carbon electrode with polyaniline. These sensors were used for detection of sodium salt of MDA and observed that a high sensitivity in the concentration range 1×10^{-1} M and 1×10^{-2} M. Tafel plots show the variation of over potential from –1.73 to –3.74 V up to 10^{-5} mol/L indicating the lower LOD of the system.

Differential pulse adsorptive stripping voltammogram of glassy carbon electrode was used as working electrode for detecting various concentrations of pure sodium salts of MDA.

10.2 DNA Biosensors for Detection of GMOs Nanotechnology

Recently, marine environmental pollution has become more and more serious due to oil spills or the collapse of nuclear power plant resulting in a massive release of hazardous materials to the ocean as was the case in Fukushima Daiichi. These harmful radioactive materials are associated

with the random mutation of genes leading to deformity of individuals. So far, there has been no effective system for monitoring this marine pollution. Therefore, rapid detection of DNA mutations has become increasingly important in a variety of fields including medical diagnostics and food safety. Herein, Zhou *et al.* (2014) reported a rapid, sensitive, qualitative, and quantitative approach for DNA detection based on the magnetophoretic assay. The Au–magnetic microparticles (MMPs) nanocomplex was used to generate a color signal and uncombined AuNPs contributed an optical signal that could be directly quantified by UV–Vis absorption spectroscopy of the supernatant after the sample was placed in a magnetic field for 2 min. The linear relationship between signal intensity and the target DNA concentrations (0.1 nM–1.0 μM) was investigated and a limit of quantitation of 0.1 nM was achieved using this method.

Numerous platforms based upon nanomaterials have recently been developed for the detection of DNA sequences with regard to increased sensitivity and selectivity (Zhang *et al.*, 2007; Liu *et al.*, 2002; Zhou *et al.*, 2012; An *et al.*, 2011; Zhou *et al.*, 2013a; Zhou *et al.*, 2013b; Meng *et al.*, 2009). A simple, sensitive, inexpensive, and quantitative approach for DNA detection has also been reported based on the optical properties of AuNPs and Fe_3O_4@AuNPs (Zhou *et al.*, 2012).

Great progress has been achieved in the past few years in the development of DNA sensors allowing for a simple, fast, and reliable DNA testing (Sassolas *et al.*, 2008). DNA biosensors are the leading edge technology that focuses on simple, rapid, and inexpensive way of testing and represents an interesting alternative in detection of genetically modified organisms (GMOs) (Nica *et al.*, 2004). The raw materials and the processed foods with GMOs contain an additional trait encoded by inserted gene (DNA), which produces additional protein. Therefore, the presence of introduced DNA could be traced by its capture by a specific oligonucleotide probe (recognition layer) that is attached to the surface of the sensor.

Biosensors for GMO detection are categorized into optical, piezoelectric, and electrochemical systems.

Surface plasmon resonance (SPR) is a powerful optical technique that can detect various biomolecular interactions happening at the interface of a thin gold-coated prism in contact with the analyte solution that flows through. The principle of this instrument lies on determining the refractive index changes occurring at the interface between materials with different refraction indices such as a surface of the prism covered with thin metal layer (Arugula *et al.*, 2014).

Mariotti *et al.* (2002) first reported their application of a SPR-based biosensor for screening analyses of GMOs. Target sequences P35S and T-NOS

that many GMOs have in common were detected. Synthesized 25-mer oligonucleotides were first immobilized onto 11-mercaptoundecanol and a carboxylated dextran modified gold sensor chip. Hybridization at sensor surface between 25-mer P35S and T-NOS (concentration ranging from 0.001 to 2.5 μM) and their fully complementary oligonucleotide probes were monitored.

Feriotto *et al.* also demonstrated the feasibility of SPR-based biospecific interaction analysis (BIA) for detection of soybean lectin and Roundup Ready gene sequences. Different formats using Lectin or Roundup Ready oligonucleotide or PCR generated probes for detection against target single-stranded PCR products were all demonstrated to be useful. Lectin and Roundup Ready oligonucleotide probes with suitable length (13- and 15-mer) showed more efficient hybridization with 21-mer target DNAs monitored with SPR response (Feriotto *et al.*, 2002). Moreover, PCR-generated probes were found to have better sensing performance than oligonucleotide probe upon hybridization with its complementary single-stranded PCR products in terms of (final RU–initial RU) values, and this method was far more efficient in detecting and quantifying GMOs (Feriotto *et al.*, 2012).

Spadavecchia *et al.* (2005) studied hybridization processes of multiple oligonucleotides with complementary oligonucleotides (probe) immobilized on novel photolithographic patterned gold substrates with SPR-based imaging equipment. Thiolated oligonucleotides probes (HS-ssDNA) were self-assembled onto gold trap by dropping method and morphology of the surface of substrate were observed with Atomic Force Microscopy (AFM) technique. A SPR imaging apparatus was used to observe the hybridization between probes and complementary strand in real time. The proposed SPR biosensor with suitable generated samples and probe immobilization showed potential in detection of various GMOs (Spadavecchia *et al.*, 2005).

Optical thin-film biosensor chips were developed to detect unique transgenes in genetically modified (GM) crops and SNP markers in model plant genomes (Bai *et al.*, 2007). Later, this work was extended for detecting six GM maize lines (Bt11, Bt176, GA21, MON810, NK603, and T25). Hydrazine-derivatized chip surface of the biosensor was covalently attached with arrays of aldehyde-labeled probes to hybridize with biotinylated PCR amplicons. Later, the system was subjected to brief incubation with an antibiotin IgG HRP conjugate and a precipitable HRP substrate. This assay is extremely robust, exhibits high sensitivity (numbers) and specificity, and could be extended to detect virtually all GMOs on the chip (Bai *et al.*, 2010). The proposed sensor method consists of immobilization of biotin probe using streptavidin-coated magnetic beads (MBs) upon a platinum working electrode by activating the magnetic field. Later, the

GMO target DNA was hybridized with the immobilized biotin probe and ruthenium(II) tris-bipyridal tris-(2,2'-bipyridyl) ruthenium (TBR) probe to form a sandwich complex. Hybrid with TBR reacts with tripropylamine TPA to emit light for ECL detection. The results indicate the sensor sensitivity was 5 nmol/L of CaMV35S DNA. The calibration curve was stable and linear from 5 nmol/L to 5 μmol/L. The distinct difference between the non GM tobacco and GM tobacco Equivalent chain length (ECL) values were obtained which enables this sensor to be a simple, inexpensive, safe, sensitive, and reliable tool (Zhu *et al*., 2010).

To quantitatively trace the GM products, a chemiluminometric immunosensor array for the detection of recombinant marker proteins expressed in GMOs, i.e., 5-enolpyruvylshikimate-3-phosphate synthase (EPSPS), neomycin phosphotransferase II (NPT II), and phosphinothricin acethyltransferase (PAT), was constructed. Specific to each marker proteins respective monoclonal and polyclonal antibodies were raised and characterized. The raised antibodies were then immobilized on predetermined regions of a glass slide for the sandwich-type immunoassays to be carried out. At the bottom of the glass slides, photodiodes were located in an aligned arrangement to the immobilized antibody sites such that the light signals resulting from the immunoassays could be detected *in situ*. The sensor array developed was able to detect 1% GMO marked with EPSPS, which was the minimum content over the total content, and 3% GMOs labeled with NPT II or PAT under optimal conditions (Jang *et al*., 2011).

Novel methods were developed using surface-enhanced Raman spectroscopy (SERS) which is a flexible tool for biological analysis due to its excellent properties for detecting wide varieties of target biomolecules including nucleic acids. SERS is powerful phenomenon involving interaction of light, molecules, and metal nanostructures to enhance Raman signals that can resolve the structures down to the single molecule level.

Recently, a novel method for detection of target 35S DNA was developed by combining magnetic separation (MS) and SERS. First, the target specific oligonucleotide probe was immobilized onto gold-coated magnetic nanospheres to form oligonucleotide-coated nanoparticles (NPs). Later, 5,5′-dithiobis (2-nitrobenzoic acid) (DTNB) was deposited on the nanorods to form a SAM followed by immobilization of the second oligonucleotide probe on the activated nanorod surfaces to form sandwich layers. Target probes were then allowed to hybridize with the NPs. The system was fully optimized and the SERS analysis was done using 35S sequence of Bt-176 maize sample. The results showed working range of concentration from 25 and 100 nM with a detection limit of 11 nM. The total assay time was less than 40 min (Guven *et al*., 2012).

Recent advancements have been made in SERS, surface-enhanced infrared spectroscopy (SEIRA), and surface plasmon-enhanced fluorescence (PEF) spectroscopy (Hoppener and Novotny, 2012; Lal *et al*., 2008; Sharma *et al*., 2012; Dostalek and Knoll, 2008; Lacowicz *et al*., 2008) over the past years. This progress was accompanied with the implementation of plasmonics to a range of analytical technologies for the detection of chemical and biological species that are relevant to important areas of medical diagnostics, food control, and security (Giljohann and Mirkin, 2009; Lazcka *et al*., 2007).

Surfaces of metallic films and metallic NPs can strongly confine electromagnetic field through its coupling to propagating or localized surface plasmons. This interaction is associated with large enhancement of the field intensity and local optical density of states which provides means to increase excitation rate, raise quantum yield, and control far field angular distribution of fluorescence light emitted by organic dyes and quantum dots (QDs). Such emitters are commonly used as labels in assays for detection of chemical and biological species. Their interaction with surface plasmons allows amplifying fluorescence signal (brightness) that accompanies molecular binding events by several orders of magnitude. In conjunction with interfacial architectures for the specific capture of target analyte on a metallic surface, PEF that is also referred to as metal-enhanced fluorescence (MEF) represents an attractive method for shortening detection times and increasing sensitivity of various fluorescence-based analytical technologies.

Review by Bauch *et al*. (2013) provides an introduction to fundamentals of PEF, illustrates current developments in design of metallic nanostructures for efficient fluorescence signal amplification that utilizes propagating and localized surface plasmons, and summarizes current implementations to biosensors for detection of trace amounts of biomarkers, toxins, and pathogens that are relevant to medical diagnostics and food control. In this work, electrochemical DNA biosensor was designed for routine screening of genetically GMOs. The idea was to construct a biosensor based on simple and satisfactory reliable solutions based on a 21-mer single-stranded oligonucleotide (ssDNA probe) specific to either 35S promoter or NOS terminator directly, without amplification of analyzed DNA fragments with PCR. The gold surface electrode was modified with a cysteamine SAM which allowed its amino group to covalently attach to the 5′-phosphate end of ssDNA probe with the use of activating reagents water soluble 1-ethyl-3(3′- dimethylaminopropyl)-carbodiimide (EDC) and N-hydroxy-sulfosuccinimide (NHS) (Tichoniuk *et al*., 2008).

Four modified gene sequences from maize and GM maize were detected by multiplexed labeling with osmium tetroxide bipyridine ([OsO4(bipy)]).

Multiplexed labeling was performed by mixing the four target strands with the respective oligonucleotides 80% homologous to the central target recognition sequences to avoid the latter from binding of [OsO4(bipy)]. As a positive control, two probes SSIIb and ivrp were used to detect the starch synthase gene IIb and invertase gene of natural maize. Two other probes, CRY that detect the existence of the cry-Ia/b transgene within the sample and the probe 810 that detects the existence of the transgene at the MON 810 in the GM maize genome were also used. The idea is to (a) detect the presence of maize (SSIIb and ivrp), (b) detect the presence of a specific transgene cry-Ia/b (CRY), and (c) detect the presence of the specific event Mon 810 (Duwensee *et al*., 2009).

Maize lineCBH351 (trade name StarLink*) contains a modified cry9c gene (confers resistance to feeding damage of lepidopteran insects) from *Bacillus thuringiensis* subsp. and the bar gene (resistance against the herbicide phosphinotricin) from *Streptomyces hygroscopicus*. The expression for both the genes are activated by the 35S promoter, and termination of transcription for the cry9c and the bar gene are regulated by the NOS adenylation signal and the 35S terminator, respectively.

Ahmed *et al*. (2009) reported an efficient, accurate, and inexpensive rapid detection system which employs loop-mediated isothermal amplification (LAMP) with higher efficiency than PCR for the detection of maize CBH 351 variety (StarLink*). The amplification samples were anchored with a redox-active molecule Hoechst 33258 [H33258, 20-(4-hydroxyphenyl)-5-(4-methyl-1-piperazinyl)-2,50-bi(1H-benzimidazole)] and analyzed by a DNA stick (DS) which is integrated with a disposable electrochemical printed (DEP) chip using Linear sweep voltammetry (LSV).

In another embodiment, MWCNTs-doped polypyrrole (PPy)-based CaMV35S DNA hybridization was studied by QCM and EIS. The MWCNTs-PPy-DNA system showed "signal on" behavior when the concentration of complementary target DNA was increased, with a corresponding decrease in the faradic charge transfer resistance (Rct). The sensor with MWCNTs-PPy films obtained a LOD as low as 4 pM as indicated by QCM data. In principle, this system can be suitable not only for DNA but also for protein biosensor construction (Truong *et al*., 2010).

It is imperative to select the right immobilization method and suitable matrix type for DNA probe immobilization to produce a high-performance GM DNA biosensor. This is because the method and immobilization matrix used may affect the nature of the immobilized DNA probes. An effective DNA probe immobilization and a compatible matrix with DNA probe would render an improved performance of the biosensor. On the other hand, the use of larger surface area materials allows more DNA

probes to be immobilized on the matrix to promote better sensitivity of biosensors.

Nanomaterials such as NPs and microspheres with three-dimensional structure have a wider surface area as the immobilization site of DNA probe (Mercoci, 2010) than one-dimensional structure membrane.

A regenerable electrochemical DNA biosensor based on a new type of acrylic microspheres and AuNPs composite coated onto a SPE has been successfully developed by Ulianas *et al*. (2014) for specific determination of the 35 S promoter from cauliflower mosaic virus (CaMV 35S) gene in soybean. DNA probe was immobilized onto acrylic microspheres via covalent bonding. The presence of modified gene in soybean can be detected via hybridization of CaMV 35S gene-modified DNA with immobilized DNA probe, which was monitored by differential pulse voltammetry of anthraquinone-2-sulfonic acid monohydrate sodium salt (AQMS) as redox indicator during hybridization event. The peak current signal of AQMS was linearly related to the target CaMV 35S gene concentration over the range of 2×10^{-15} to 2×10^{-9}M ($R^2 = 0.982$) with a very low concentration detect limit (7.79×10^{-16} M). The recovery test showed satisfactory results of 94.6 ± 5.1–105.4 ± 4.9% (n = 5) when the biosensor was used for the determination of GM DNA sequences extracted from GM soybean samples. The DNA biosensor showed good reproducibility [relative standard deviation (RSD) below 5.0%, n = 5] and regenerability (RSD below 5.0%, n = 7). The biosensor response was stable up to 45 days of storage period at 4°C. The main advantages of this biosensor design are very low detection limit and capability of reusing the biosensor for at least seven times after regeneration with mild sodium hydroxide.

Easy, sensitive, rapid, and low cost ochratoxin biosensors are strongly demanded in food analysis since ochratoxin A (OTA) is a widely diffused food contaminant, highly detrimental for human health. Todescato *et al*. (2014) described a novel plasmonic-based optical biosensor prototype for OTA. They exploited the MEF phenomenon due to the silver film over nanosphere plasmonic substrate. Since OTA could be present in different food commodities, sensor performances have been tested on three different matrices (dried milk, juices, and wheat mix). Firstly, a common OTA extraction solvent and a labeling and detection protocol were defined for the analyzed matrices. Then, the efficiency of the Ag-film over nanosphere (FON) surfaces in signal amplification for the detection of low OTA concentrations was defined. Using samples spiked with OTA-AF647 or with unlabeled OTA they were able to detect the mycotoxin at concentrations

lower than EU specifications of 0.5 μg/kg in wheat, milk and apple juice. The test performances are comparable to those of ELISA kits but the platform presented here, once optimized, present some perspective advantages, such as: low cost and time consuming, versatility of the protocol for the investigation of different matrices, employment also in non-qualified laboratories, small dimensions that allow its integration in a compact device for OTA on-site detection.

A novel electrochemical aptasensor based on glassy carbon electrode modified with electropolymerized Neutral red and polycarboxylated macrocyclic ligand bearing redox probe was recently appeared in the literature (Gennady Evtugyn *et al.*) for sensitive detection of aflatoxin B1 (AFB1). DNA aptamer specific for AFB1 with aminated C_{12} linker was covalently attached to terminal carboxylate groups of the carrier. The interaction with an analyte resulted in implementation of electrochemically inactive AFB1 in the sensing layer. As a result, the cathodic peak current of the probe measured by linear voltammetry decreased and the electron transfer resistance measured by EIS increased with the concentration of the analyte within 0.1–100 nM. The LOD was found to be 0.1 nM for voltammetric detection and 0.05 nM for EIS detection for 30 min incubation. The aptasensor makes it possible to detect AFB1 in peanuts, cashew nuts, white wine and soy sauce with 85–100% recovery.

QDs could also be used to detect DNA sequences instead of fluorophores. A QD is a semiconductor particle (e.g., ZnS, CdSe, and CdS) that can be used as a fluorophore (Bruchez *et al*., 1998; Medintz *et al*., 2005; Somers *et al*., 2007). They are candidates for replacing conventional fluorescent markers such as rhodamine in biodetection assays and are more photostable and sensitive than an organic fluorophore.

QDs can be used for *in situ* hybridization and immunolabeling in plants. Nanoarrays containing multiple features, such as a range of different proteins or small-molecule ligands, are difficult to fabricate. Atomic force microscopy-based nanografting of DNA nanopatches allows nonspecific binding of nanografted DNA to proteins and antibodies. Therefore, nanografted patches of ssDNA within a monolayer of protein-repellent ethylene glycol-terminated alkylthiols were generated on a flat gold substrate.

Subsequently, proteins covalently modified with cDNA sequences were immobilized onto the nanopatch by means of DNA-directed immobilization, thus producing detector for protein interaction studies. Interactions between the proteins and antibodies were assessed between nanografted patches by using atomic force microscopy. These nanografted patches are

suitable for application in biosensing and fabrication of multifeature nanoprotein array (Bano *et al*., 2009).

The emergence of nanotechnology developments using nanodevices/nanomaterials opens up potential novel applications in agriculture and food sector. Smart delivery systems, biosensors, and nanoarrays are being designed to solve the problems faced in agriculture sector. Similarly, food sector is also benefited through the use of smart biosensors, packaging materials, and nanonutraceuticals. Despite the great potential of nanotechnology in agri-food sector, people are ambiguous about use in food applications because of suspected potential health risks and environmental concerns. NPs, due to their unique characteristics, including small size, shape, high surface area, charge, chemical properties, solubility, and degree of agglomeration can cross cell boundaries or pass directly from the lungs into the blood stream and ultimately reach to all of the organs in the body. This is the reason why they may pose higher risk than the same mass and material of larger particles. Kumari and Yadav (2014) made an attempt to give an overview of nanotechnology developments in agri-food sector, risks associated with nanomaterials and toxicity regulations for policy framework.

The use of nanotechnology in the food industry is in its infancy but has the capability to introduce changes at all levels of food production, including nano-based food materials, active packaging, new delivery mechanisms for nutrients and agrochemicals, biosensors for food safety and many other potential applications (Chen and Yada, 2011; Cushen *et al*., 2012; Magnuson *et al*., 2011).

Nanotechnology offers many potential advantages in the processing and manufacture of foods: enhanced bioavailability, color, and flavor; novel food textures; new delivery mechanisms; and access to biosensors to enhance food safety. In fact, many of the foods we have been consuming for centuries already contain nanostructures, leading many to assume that they are safe (Raynes *et al*., 2014). The extent to which novel nanostructures may afford new risks has not been adequately resolved, however, leading to concern within some consumer groups. They used proteins as a case study to explore the current understanding of nanostructures in foods and the extent to which novel nanostructures may introduce new properties. It is well recognized that some protein nanostructures are toxic and are associated with disease, so there is legitimate concern as to whether such species should be deliberately introduced into our foods. This review highlights current literature on protein nanostructures in food and possible risks associated with their use. They aim to provide a balanced assessment to inform future decision-making regarding the utilization of nanostructures in food.

Patulin is a toxic secondary metabolite of a number of fungal species belonging to the genera *Penicillium* and *Aspergillus*. One important aspect of the patulin toxicity *in vivo* is an injury of the gastrointestinal tract including ulceration and inflammation of the stomach and intestine. Recently, patulin has been shown to be genotoxic by causing oxidative damage to the DNA, and oxidative DNA base modifications have been considered to play a role in mutagenesis and cancer initiation. Conventional analytical methods for patulin detection involve chromatographic analyses, such as High Pressure Liquid Chromatography (HPLC), GC, and, more recently, techniques such as Liquid Chromatography/Mass Spectrometry (LC/MS) and Gass Chromatography/Mass Spectrometry (GC/MS). All of these methods require the use of extensive protocols and the use of expensive analytical instrumentation.

The conjugation of a new derivative of patulin to the bovine serum albumin for the production of polyclonal antibodies was described by Pennacchio *et al.* (2014), and an innovative competitive immune assay for detection of patulin is presented. Experimentally, an important part of the detection method is based on the optical technique called SPR. Laser beam-induced interactions between probe and target molecules in the vicinity of gold surface of the biochip lead to the shift in resonance conditions and consequently to slight but easily detectable change of reflectivity.

Sensors are often organized in multidimensional systems or networks for particular applications. This is facilitated by the large improvements in the miniaturization process, power consumption reduction, and data analysis techniques nowadays possible. Such sensors are frequently organized in multidimensional arrays oriented to the realization of artificial sensorial systems mimicking the mechanisms of human senses. Instruments that make use of these sensors are frequently employed in the fields of medicine and food science. Among them, the so-called electronic nose and tongue are becoming more and more popular. Santonico *et al.* (2013) illustrated an innovative multisensorial system based on sensing materials of biological origin. Anthocyanins are exploited here as chemical interactive materials for both quartz microbalance (QMB) transducers used as gas sensors and for electrodes used as liquid electrochemical sensors. The optical properties of anthocyanins are well established and widely used, but they have never been exploited as sensing materials for both gas and liquid sensors in non-optical applications. By using the same set of selected anthocyanins an integrated system has been realized, which includes a gas sensor array based on QMB and a sensor array for liquids made up of suitable ion-sensitive electrodes (ISEs). The arrays are also monitored from an optical point of view. This embedded system, is intended to mimic the working principles of the nose, tongue and eyes. They called this setup BIONOTE

(for BIOsensor-based multisensorial system for mimicking NOse, Tongue and Eyes). The complete design, fabrication and calibration processes of the BIONOTE system are described herein, and a number of preliminary results are discussed. These results are relative to (a) the characterization of the optical properties of the tested materials; (b) the performance of the whole system as gas sensor array with respect to ethanol, hexane and isopropyl alcohol detection (concentration range 0.1–7 ppm) and as a liquid sensor array (concentration range 73–98 μM (Santonico *et al*., 2013).

In recent years, CNTs have received widespread attention as promising carbon-based nanoelectronic devices. Due to their exceptional physical, chemical, and electrical properties, namely a high surface-to-volume ratio, their enhanced electron transfer properties, and their high thermal conductivity, CNTs can be used effectively as electrochemical sensors. The integration of CNTs with a functional group provides a good and solid support for the immobilization of enzymes. The determination of glucose levels using biosensors, particularly in the medical diagnostics and food industries, is gaining mass appeal. Glucose biosensors detect the glucose molecule by catalyzing glucose to gluconic acid and hydrogen peroxide in the presence of oxygen. This action provides high accuracy and a quick detection rate. Pourasl *et al*. (2014) studied and analytically modeled a single-walled CNT field-effect transistor biosensor for glucose detection. In the proposed model, the glucose concentration is presented as a function of gate voltage. Subsequently, the proposed model is compared with existing experimental data. A good consensus between the model and the experimental data is reported. The simulated data demonstrate that the analytical model can be employed with an electrochemical glucose sensor to predict the behavior of the sensing mechanism in biosensors.

The non-specific binding of non-target species to functionalized surfaces of biosensors continues to be challenge for biosensing in real-world media. Three different low-fouling and functionalizable surface platforms were employed to study the effect of functionalization on fouling resistance from several types of undiluted media including blood plasma and food media. The surface platforms investigated by Vaisocherova *et al*. (2014) included two polymer brushes: hydroxy-functional poly(2-hydroxyethylmethacrylate) (pHEMA) and carboxy-functional poly(carboxybetaineacrylamide) (pCBAA), and a standard OEG-based carboxy-functional alkanethiolate SAM (AT-SAM). The wet and dry polymer brushes were analyzed by AFM, ellipsometry, Fourier transform infrared reflection absorption (FT-IRRAS), and SPR. The surfaces were functionalized by the covalent attachment of antibodies, streptavidin, and oligonucleotides and the binding and biorecognition characteristics of the coatings were compared. They found that

functionalization did not substantially affect the ultra-low fouling properties of pCBAA (plasma fouling of ~20 ng/cm^2), a finding in contrast with pHEMA that completely lost its resistance to fouling after the activation of hydroxyl groups. Blocking a functionalized AT-SAM covalently with BSA decreased fouling down to the level comparable to unblocked pCBAA. However, the biorecognition capability of blocked functionalized AT-SAM was poor in comparison with functionalized pCBAA. Limits of detection of *Escherichia coli* O157:H7 in undiluted milk were determined to be 6×10^4, 8×10^5, and 6×10^5 cells/ml for pCBAA, pHEMA, and AT-SAM-blocked, respectively. Effect of analyte size on biorecognition activity of functionalized coatings was investigated and it was shown that the best performance in terms of overall fouling resistance and biorecognition capability is provided by pCBAA.

10.3 Aptamers

The presence of pathogenic bacteria is a major health risk factor in food samples and the commercial food supply chain is susceptible to bacterial contamination. Thus, rapid and sensitive identification methods are in demand for the food industry. Quantitative PCR is one of the reliable specific methods with reasonably fast assay times. However, many constituents in food samples interfere with PCR, resulting in false results and thus hindering the usability of the method. Therefore, Ozalp *et al.* (2014) aimed to develop an aptamer-based MS system as a sample preparation method for subsequent identification and quantification of the contaminant bacteria by real-time PCR. To achieve this goal, MBs were prepared via suspension polymerization and grafted with glycidylmethacrylate (GMA) brushes that were modified into high quantities of amino groups. The MBs were decorated with two different aptamer sequences binding specifically to *E. coli* or *Salmonella typhimurium*. The results showed that even 1.0% milk inhibited PCR, but our magnetic affinity system capture of bacteria from 100% milk samples allowed accurate determination of bacterial contamination at less than 2.0 h with LOD around 100 CFU/mL for both bacteria in spiked-milk samples.

Aptamers are often described as nucleic acid antibodies. Aptamers are highly selective and sensitive bioaffinity agents. Additionally, aptamer-based technologies are often proposed as robust alternative biorecognition molecules with comparable specificity and affinity to antibodies (Schlecht *et al.*, 2006). These comparison studies showed that both antibodies and aptamers could have affinity constants at nanomolar levels. Compared to antibodies, aptamers have higher stability to environmental factors and low production costs.

Aptamers are selected by a combinatorial method completely *in vitro*, and therefore the selection technology can provide nucleic acid sequences binding to virtually any kind of targets. These advantages created great interest in aptamers as the preferred bioaffinity molecule in biosensor development research for a range of sensor platforms (Mairal *et al*., 2008).

The selective detection of ultra trace amounts of OTA is extremely important for food safety since it is one of the most toxic and widespread mycotoxin. Here, Chen *et al*. (2014) developed a signal-on fluorescent biosensor for detection of OTA based on fluorescent DNA-scaffolded silver nanocluster (AgNCs), structure switching of anti-OTA aptamer (Ap) and MBs, and demonstrate its feasibility in the application of detecting OTA in real samples of wheat. The method exhibits superior sensitivity with a detection limit as low as 2 pg/mL OTA with high specificity. To the best of our knowledge, this is the first attempt to detect OTA based on DNA-scaffolded AgNCs, which possesses relatively high-fluorescence quantum yield and photostability with regard to traditional organic dyes and QDs. Moreover, combined with the merits of MBs and aptamer, the proposed sensor has many advantages such as fabrication easiness, operation convenience, low cost, and being fast and portable, which may represent a promising path toward routine OTA control.

Convenient and sensitive point-of-care rapid diagnostic tests for foodborne pathogens have been a long-felt need of clinicians. Traditional approaches such as culture-based methods have good sensitivity and specificity, but they tend to be tedious and time consuming. Herein, Fang *et al*. (2014) presented a simple and sensitive aptamer-based biosensor for rapid detection of *Salmonella enteritidis*. One of the aptamers specific for the out membrane of *S. enteritidis* was used for MB enrichments. Another aptamer against *S. enteritidis* was used as a reporter for this pathogen, which was amplified by isothermal strand displacement amplification (SDA) and further detected by a lateral flow biosensor. As low as 10 colony forming units (CFU) of *S. enteritidis* was detected in this study. Without DNA extraction, the reduced handling and simpler equipment requirement render this assay a simple and rapid alternative to conventional methods.

10.4 Voltammetric Biosensors

Arrays of voltammetric electrodes chemically modified with electroactive materials (i.e., phthalocyanines) have demonstrated to be particularly interesting for the analysis of phenolic compounds (Gay *et al*., 2012; Ceto *et al*., 2012a; Parra *et al*., 2006).

Medina-Plaza *et al.* (2014) developed a multisensor system formed by nanostructured voltammetric biosensors based on phenol oxidases (tyrosinase and laccase). The enzymes have been incorporated into a biomimetic environment provided by a Langmuir–Blodgett (LB) film of arachidonic acid (AA). Lutetium bisphthalocyanine (LuPc2) has also been introduced in the films to act as electron mediator. The incorporation of the enzymes to the floating layers to form Tyr/AA/LuPc2 and Lac/AA/LuPc2 films has been confirmed by the expansion in the surface pressure isotherms and by the AFM images. The voltammetric response toward six phenolic compounds demonstrates the enhanced performance of the biosensors that resulted from a preserved activity of the tyrosinase and laccase combined with the electron transfer activity of LuPc2. Biosensors show improved detection limits in the range of 10^{-7} to 10^{-8} mol L^{-1}. An array formed by three sensors AA/LuPc2, Tyr/AA/LuPc2, and Lac/AA/LuPc2 has been employed to discriminate phenolic antioxidants of interest in the food industry. The principal component analysis scores plot has demonstrated that the multisensor system is able to discriminate phenols according to the number of phenolic groups attached to the structure. The system has also been able to discriminate grapes of different varieties according to their phenolic content. This good performance is due to the combination of four factors: the high functionality of the enzyme obtained using a biomimetic immobilization, the signal enhancement caused by the LuPc2 mediator, the improvement in the selectivity induced by the enzymes and the complementary activity of the enzymatic sensors demonstrated in the loading plots.

10.5 Amperometric Biosensors

An important step in several bioanalytical applications is the immobilization of biomolecules. Accordingly, this procedure must be carefully chosen to preserve their biological structure and fully explore their properties. For this purpose, Graca *et al.* (2014) combined the versatility of the layer-by-layer (LbL) method for the immobilization of biomolecules with the protective behavior of liposome-encapsulated systems to fabricate a novel amperometric glucose biosensor. To obtain the biosensing unit, an LbL film of the H_2O_2 catalyst polypeptide microperoxidase-11 (MP-11) was assembled onto an indium tin oxide (ITO) electrode followed by the deposition of a liposome encapsulated glucose oxidase (GOx) layer. The biosensor response toward glucose detection showed a sensitivity of 0.91 ± 0.09 ($\mu A/cm^2$)/mM and a LOD of 8.6 ± 1.1 μM, demonstrating an improved performance compared to similar biosensors with a single phospholipid

liposome or even containing a non-encapsulated GOx layer. Finally, glucose detection was also performed in a zero-lactose milk sample to demonstrate the potential of the biosensor for food analysis.

The LbL technique, a widely explored adsorption method, has been an effective approach for enzyme immobilization due to its simplicity and the mild conditions during the film formation (Ariga and Hill, 2010; Lee, 2008). Because most enzymes are water soluble and charged in solution, the LbL method is suitable for assembling different enzyme architectures with low denaturing effects (Ariga *et al*., 1997; Decher and Schlenoff, 2012).

Ferreira *et al*. (2004), for example, reported a successful strategy for glucose detection using LbL films of GOx and polyallylamine hydrochloride (PAH) on modified electrodes. Lee *et al*. (2011) developed a label-free immunoassay method using an LbL network of CNTs for detecting swine influenza H1N1 virus. Xiang *et al*. (2011) assembled multi-enzyme LbL films of CNTs for the electrochemical monitoring of important cancer biomarkers. An overview of LbL applications in biosensing and related fields has recently been published (Decher and Schlenoff, 2012).

10.6 Optical Biosensors

An optical biosensor assay utilizing a monoclonal antibody was developed by Indyk *et al*. (2014) for the quantitation of the biotin content of milk and pediatric formulae. The method provides a reliable estimate of total biotin accomplished by simple aqueous extraction, combined with heat treatment, prior to automated biosensor analysis. The binding assay was configured under inhibition conditions utilizing a sensor surface functionalized with biotin and was subjected to single-laboratory validation. Critical assay factors, including calibration parameters, cross-reactivity, non-specific binding and matrix interferences were evaluated systematically. Assay performance parameters including range, detection limits, precision, recovery, and bias were estimated. The method was applied to the routine compliance testing of pediatric formulae and the temporal change in the biotin content of early lactation milk and seasonal milk powder. The assay is an expedient alternative to current HPLC, microbiological and proprietary kit-based immunoassay methods for the determination of the biotin content of milk-based foods.

The most commonly applied biosensor system for the analysis of biotin in supplemented foods utilizes SPR optics and is routinely applied as a proprietary immunoaffinity-based kit assay, although other transducer detection principles have been exploited (Blake, 2007; Gao *et al*., 2008; Indyk *et al*., 2000; Indyk, 2011; Kalman *et al*., 2006; Kergaravat *et al*., 2012).

10.7 Magnetoelastic Biosensors

Magnetoelastic (ME) biosensors are one device that shows promise for *in situ*, real-time detection of pathogenic bacteria on food surfaces. The ME biosensor consists of a transducer (ME resonator) that is coated with a biomolecular recognition element for the specific capture and binding of a pathogenic target bacteria. ME resonators work on the principle of Joule magnetostriction, where the resonator experiences a change in its dimensions in the presence of a magnetic field (Ballantine *et al*., 1997; Kabos and Stalmachov, 1994). When subjected to a time-varying magnetic field in the direction of the resonator's length, the ME resonator longitudinally vibrates with a characteristic resonant frequency (Li *et al*., 2012).

Proof in principle of a new surface-scanning coil detector has been demonstrated. This new coil detector excites and measures the resonant frequency of free-standing ME biosensors that may now be placed outside the coil boundaries. With this coil design, the biosensors are no longer required to be placed inside the coil before frequency measurement (Chai *et al*., 2013). Hence, this new coil enables bacterial pathogens to be detected on fresh food surfaces in real time and *in situ*. The new coil measurement technique was demonstrated using an E2 phage-coated ME biosensor to detect *S. typhimurium* on tomato surfaces. Real-time, *in situ* detection was achieved with a LOD statistically determined to be lower than 1.5×10^3 CFU/mm^2 with a confidence level of difference higher than 95% ($p<0.05$).

10.8 Surface Acoustic Wave (SAW) Biosensors for Odor Detection

SAW sensors are based on the generation and detection of acoustic waves at the surface of a piezoelectric crystal. The acoustic energy is strongly confined at the surface of the device and is independent of the thickness of the substrate. SAWs are very sensitive to changes in mass, viscosity, or conductivity on the sensor's surface (Grate and Frye, 1996). Recently, a great interest is directed toward the development of SAW devices based on biological molecules as sensing material able to detect low concentrations of molecules in air (Lange *et al*., 2008). An interesting application is the use of SAW devices as odor sensors with odorant binding proteins (OBPs) as sensing element. OBPs are small extracellular proteins which belong to the lipocalin super-family (Marabotti *et al*., 2008; Bianchet *et al*., 1996). They have an important role in odor detection by carrying, deactivating, and/or selecting the odorant molecules.

Palla-Papavlu *et al.* (2014) presented the development of SAW biosensors for odor detection in the food industry. The SAW biosensors are coated by laser-induced forward transfer (LIFT) with wild-type bovine OBP (wtbOBP) solutions containing 20% and 50% glycerol. Optical microscopy investigations revealed that individual droplets could be printed from 50% glycerol solutions with a high resolution. Further investigations proved that despite the lower resolution of the 20% glycerol printed droplets it is possible to achieve higher uniformity in the coverage of the entire active area of the SAW biosensors. In addition, it is shown that the surface density of the wtbOBP LIFT-ed layer is four times higher than in the case of pipette deposition. Finally, the functionality of the SAW biosensors was investigated by testing the biosensors upon exposure to various concentrations of octenol vapors. A high sensitivity, i.e., of 5 Hz/ppm and detection limit in the low ppm range was obtained, lower that what has previously been reported with conventional methods.

Zhang *et al.* (2014) used a taste biosensor to measure and analyze different sweeteners, both natural and artificial sweeteners. Electrophysiological activities from taste epithelium were detected by the multi-channel biosensors and analyzed with spatiotemporal methods. The long-time signal result showed different temporal-frequency properties with stimulations of individual sweeteners such as glucose, sucrose, saccharin, and cyclamate, while the multi-channel results in their study revealed the spatial expression of taste epithelium to sweet stimuli. Furthermore, in the analysis of sweetener with different concentrations, the result showed obvious dose-dependent increases in signal responses of the taste epithelium, which indicated promising applications in sweetness evaluation. Besides, the mixture experiment of two natural sweeteners with a similar functional unit (glucose and sucrose) presented two signal patterns, which turned out to be similar with responses of each individual stimulus involved. The biosensor analysis of common sweeteners provided new approaches for both natural and artificial sweeteners evaluation.

10.9 Quorum Sensing and Toxoflavin Detection

Choi *et al.* (2013) developed a simple and sensitive biosensor for the determination of toxoflavin (which is toxic to various plants, fungi, animals, and bacteria) in natural samples based on β-galactosidase activity. The proposed toxoflavin detection method for toxin-producing bacteria or toxin-contaminated foods is simple and cost-effective. *Burkholderia glumae*, a species known to cause rice grain rot and wilt in various field

crops, produces toxoflavin under the control of a LysR-type transcriptional regulator ToxR and its ligand toxoflavin. As the expression of toxoflavin biosynthetic genes requires toxoflavin as a co-activator of ToxR, a novel biosensor stain was constructed based on lacZ reporter gene integration into the first gene of the toxoflavin biosynthesis operon, toxABCDE of *B. glumae*. ToxJ is controlled by quorum sensing and activates tox operon transcription. ToxR is also required to activate the tox operon with toxoflavin as a coinducer.

A biosensor was composed of a sensor strain (COK71), substrates (X-gal or ONPG), and culture medium, without any complex preparation process. They demonstrated that the biosensor strain is highly specific to toxoflavin, and can quantify relative amounts of toxoflavin compared with known concentrations of toxoflavin. The proposed method was reliable and simple; samples containing 50–500 nM of toxoflavin could be analyzed. More importantly, the proposed biosensor strain could identify toxoflavin-producing bacteria in real samples. The excellent performance of this biosensor is useful for diagnostic purposes, such as detecting toxoflavin-contaminated foods and environmental samples.

10.10 Xanthine Biosensors

Xanthine (3,7-dihydro-purine-2,6-dione) is generated from guanine by guanine deaminase and hypoxanthine by xanthine oxidase (XOD). The determination of xanthine in meat indicates its freshness, while its level in serum/urine provides valuable information about diagnosis and medical management of certain metabolic disorders such as xanthinuria, hyperurecemia, gout, and renal failure. Although chromatographic methods such a HPLC, capillary electrophoresis and mass spectrometry are available for quantification of xanthine in biological materials, these suffer from certain limitations such as complexity, time-consuming sample preparation and requirement of expensive apparatus and trained persons to operate. Immobilized XOD-based biosensors have emerged as simple, rapid, sensitive, and economic tools for determination of xanthine in food industries and clinical diagnosis. Pundir and Devi (2014) described the various immobilization methods of XOD and different matrices used for construction of xanthine biosensors, their classification, analytical performance, and applications along with their merits and demerits. The future perspectives for improvement of present xanthine biosensors are also discussed.

The most important step in the development of an enzyme sensor is the attachment of the enzyme onto the surface of the working electrode.

This process is governed by various interactions between the enzyme and the electrode material which affects the performance of a biosensor in term of its sensitivity, stability, response time, and reproducibility. A variety of methods have been employed for immobilization of XOD, ranging from physical adsorption and entrapment to covalent/chemical bonding, electropolymerization and cross-linking for construction of xanthine biosensors.

There are three 'generations' of xanthine biosensors based on binding of XOD onto transducer: biosensors based on support material used are membrane-based, polymeric matrices-based, and sol–gel-based xanthine biosensors.

Different biosensors are mentioned by Varzakas *et al*. (2014) involved in meat quality such as amperometric xanthine biosensors, use of novel biological components such as mammalian cells and bacteriophages for the detection of bacterial pathogens, Biacore assay kit, potentiometric sensors based on measuring the potential of an electrochemical cell while drawing negligible or no current with common examples the glass pH electrode and ion selective electrodes for ions such as K^+, Ca^{++}, Na^+, and Cl^-, optical fiber and a capillary-based biosensor for calpastatin detection in heated meat samples as well as immunological capacitive biosensors for calpastatin.

10.11 Conclusions and Future Prospects

The aim of this chapter is to bring into focus this important research area and advances of biosensors and more specifically to those related to the rapid detection of food toxicants and environmental pollutants. The scope is related to provide a comprehensive review of the research topics most pertinent to the advances of devices that can be used for the rapid real-time detections of food toxicants such as microbes, pathogens, toxins, nervous gases such as botulinum toxin, *E. coli, Klebsiella pneumoniae*, sarin, VX, *Listeria monocytogenes*, *Salmonella*, marine biotoxins, Staphylococcal enterotoxin B, saxitoxin, gonyautoxin (GTX5), francisella spore virus, *Bacillus subtilis*, ochratoxin, and even simple chemical compounds. Biosensors have found a large number of applications in the area of food analysis. Recent advances include portable devices for the rapid detection of insecticides, pesticides, food hormones, toxins, carcinogenic compounds in environment, such as polycyclic biphenols, etc.

Different categories of biosensors have been described such as electrochemical biosensors and more specifically nitrite electrochemical biosensing based on coupled GA and AuNPs, optical biosensors using monoclonal

antibodies or plasmonic biosensors for ochratoxin detection, biosensors for pesticide residue detection, SPR detectors, electronic tongues, DNA biosensors for detection of GMOs in food and feed, multi-channel biosensors for detection of natural and artificial sweeteners, biosensor strains for toxoflavin detection, xanthine biosensors, nanostructured voltammetric biosensors, and amperometric glucose biosensor.

Acknowledgments

The authors express their acknowledgements for the financial help of the Greek Ministry of Development, General Secretariat of Research and Technology and the European Commission (in particular the European Regional Development fund and National Resources) which co-funded the present research project in the framework of Greece–Slovakia bilateral projects (Contract 12SLO_ET30_1036).

References

1. Ahmed, M. U., Saito, M., Hossain, M. M., Rao, S. R., Furui, S., Hino, A., Takamura, Y., Takagi, M. and Tamiya, E. Electrochemical DNA biosensor using a disposable electrochemical printed (DEP) chip for the detection of SNPs from unpurified PCR amplicons, *Analyst* 134, 966–972, 2009.
2. Allen, M. J., Tung, V. C. and Kaner, R. B. Honeycomb carbon: a review of grapheme, *Chem. Rev.* 110, 132–145, 2010.
3. An, H. S., Kim, E. M., Lee, J. W., Dong, C. M., Lee, B. I. and Kim, Y. C. Novel polymorphicmicrosatellite loci for the Korean black scraper (*Thamnaconus modestus*), and their application to the genetic characterization of wild and farmed populations, *Int. J. Mol. Sci.* 12, 4104–4119, 2011.
4. Antiochia, R. and Gorton, L. A new osmium-polymer modified screen-printed graphene electrode for fructose detection, *Sen. Actuat. B* 195, 287–293, 2014.
5. Ariga, K., Onda, M., Lvov, Y. and Kunitake, T. Alternate layer-by-layer assembly of organic dyes and proteins is facilitated by pre-mixing with linear polyions, *Chem. Lett.* 26, 25–26, 1997.
6. Ariga, K., Ji, Q. and Hill, J. P. Enzyme-encapsulated layer-by-layer assemblies: current status and challenges toward ultimate nanodevices, in: F. Caruso (Ed.), *Modern Techniques for Nano- and Microreactors/-Reactions*, Springer: Berlin Heidelberg, 2010.
7. Arugula, M. A., Zhang, Y. and Simonian, A. L. Biosensors as 21st century technology for detecting genetically modified organisms in food and feed, *Anal. Chem.* 86, 119–129, 2014.

8. Bai, S., Zhang, J., Li, S., Chen, H., Terzaghi, W., Zhang, X., Chi, X., Tian, J., Luo, H., Huang, W., Chen, Y. and Zhang, Y. Detection of six genetically modified maize lines using optical thin-film biosensor chips, *J. Agric. Food Chem.* 58, 8490–8494, 2010.
9. Bai, S.-L., Zhong, X., Ma, L., Zheng, W., Fan, L.-M., Wei, N. and Deng, X. W. A simple and reliable assay for detecting specific nucleotide sequences in plants using optical thin-film biosensor chips, *Plant J.* 49(2), 354–366, 2007.
10. Ballantine, D. S., White, R. M., Martin, S. J., Ricco, A. J., Zellers, E. T., Frye, G. C. and Wohltjen, H. *Acoustic Wave Sensors*. San Diego: Academic Press, 1997.
11. Bano, F., Fruk, L., Sanavio, B., Glettenberg, M., Casalis, L., Niemeyer, C. M. and Scoles, G. Toward multiprotein nanoarrays using nanografting and DNA directed immobilization of proteins, *Nano. Lett.* 9, 2614–2618, 2009.
12. Bauch, M., Toma, K., Toma, M., Zhang Q. and Dostalek, J. Plasmon-enhanced fluorescence biosensors: a review, *Plasmonics* 9(4), 1–19, 2013.
13. Bianchet, M. A., Bains, G., Pelosi, P., Pevsner, J., Snyder, S. H., Monaco, H. L., Amzel, L. M. The three dimensional structure of bovine odorant binding protein and its mechanism of odor recognition, *Nat. Struct. Biol.* 3, 934–939, 1996.
14. Biscay, J., Cista Rama, E., Begona Gonzalez Garcia, M., Reviejo, A. J., Pingarron Carrazon, J. M. and Costa Garcia, A. Amperometric fructose sensor based on ferrocyanide modified screen-printed carbon electrode, *Talanta* 88, 432–438, 2012.
15. Blake, C. J. Analytical procedures for water-soluble vitamins in foods and dietary supplements: a review, *Anal. Bioanal. Chem.* 389, 63–76, 2007.
16. Bruchez, M. J., Moronne, M., Gin, P., Weiss, S. and Alivisatos, A. P. Semiconductor nanocrystals as fluorescent biological labels, *Science* 281, 2013–2016, 1998.
17. Ceto, X., Gutierrez, J. M., Gutierrez, M., Céspedes, F., Capdevila, J., Mínguez, S., Jimenez-Jorquera, C. and del Valle, M. Determination of total polyphenol index in wines employing a voltammetric electronic tongue, *Anal. Chim. Acta.* 732, 172–179, 2012.
18. Chai, Y., Horikawa, S., Li, S., Wikle, H. C. and Chin, B. A. A surface-scanning coil detector for real-time, in-situ detection of bacteria on fresh food surfaces, *Biosens. Bioelectron.* 50, 311–317, 2013.
19. Chen, H. and Yada, R. Nanotechnologies in agriculture: new tools for sustainable development, *Trends Food Sci. Technol.* 22(11), 585–594, 2011.
20. Chen, J., Zhang, X., Cai, S., Wu, D., Chen, M., Wang, S. and Zhang, J. A fluorescent aptasensor-based on DNA-scaffolded silver-nanocluster for ochratoxin A detection, *Biosens. Bioelectron.* 57, 226–231, 2014.
21. Choi, O., Lee, Y., Han, I., Kim, H., Goo, E., Kim, J., Hwang, I. A simple and sensitive biosensor strain for detecting toxoflavin using β-galactosidase activity, *Biosens. Bioelectron.* 50, 256–261, 2013.

22. Cushen, M., Kerry, J., Morris, M., Cruz-Romero, M. and Cummins, E. Nanotechnologies in the food industry and recent developments, risks and regulation, *Trends Food Sci. Technol.* 24(1), 30–46, 2012.
23. Decher, G. and Schlenoff, J. B. *Multilayer Thin Films: Sequential Assembly of Nanocomposite Materials*, Weinheim, Germany: John Wiley & Sons, 2012.
24. Dostalek, J. and Knoll, W. Biosensors based on surface plasmon-enhanced fluorescence spectroscopy, *Biointerphases* 3(3), FD12–FD22, 2008.
25. Duwensee, H., Mix, M., Broer, I. and Flechsig, G.-U. Electrochemical detection of modified maize gene sequences by multiplexed labeling with osmium tetroxide bipyridine, *Electrochem. Commun.* 11, 1487–1491, 2009.
26. Evtugyn, G., Porfireva, A., Stepanova, V., Sitdikov, R., Stoikov, I., Nikolelis, D. and Hianik, T. Electrochemical aptasensor based on polycarboxylic macrocycle modified with neutral red for Aflatoxin B1 detection, *Electroanalysis* 26(10), 2100–2109, 2014.
27. Fang, Z., Wu, W., Lu, X. and Zeng, L. Lateral flow biosensor for DNA extraction-free detection of salmonella based on aptamer mediated strand displacement amplification, *Biosens. Bioelectron.* 56, 192–197, 2014.
28. Feriotto, G., Borgatti, M., Mischiati, C., Bianchi, N. and Gambari, R. Biosensor technology and surface plasmon resonance for real time detection of genetically modified Roundup Ready soybean gene sequences, *J. Agric. Food Chem.* 50, 955–962, 2002.
29. Feriotto, G., Gardenghi, S. and Gambari, R. SPR-based assays for real-time detection of genetically modified organisms, *Biacore J.* 2, 5–8, 2003.
30. Ferreira, M., Fiorito, P. A., Oliveira, O. N. and de Torresi, S. I. C. Enzyme-mediated amperometric biosensors prepared with the layer-by-layer (LbL) adsorption technique, *Biosens. Bioelectron.* 19, 1611–1615, 2004.
31. Gao, Y., Guo, F., Gokavi, S., Chow, A., Sheng, Q. and Guo, M. Quantification of water-soluble vitamins in milk-based infant formulae using biosensor-based assays, *Food Chem.* 110, 769–776, 2008.
32. Gay, M., Muñoz, R., De Saja, J. A. and Rodriguez-Mendez, M. L. *Multisensor system based on bisphthalocyanine nanowires for the detection of antioxidants, Electrochim. Acta.* 68, 88–94, 2012.
33. Giljohann, D. A. and Mirkin, C. A. Drivers of biodiagnostic development, *Nature* 462, 461–464, 2009.
34. Goncalves, G., Marques, P. A. A. P., Granadeiro, C. M., Nogueira, H. I. S., Singh, M. K. and Grácio, J. Surface modification of graphene nanosheets with gold nanoparticles: the role of oxygen moieties at graphene surface on gold nucleation and growth, *Chem. Mater.* 21, 4796–4802, 2009.
35. Graça, J. S., de Oliveira, R. F., de Moraes, M. L. and Ferreira, M. Amperometric glucose biosensor based on layer-by-layer films of microperoxidase-11 and liposome-encapsulated glucose oxidase. *Bioelectrochemistry* 96, 37–42, 2014.
36. Grate, J. W. and Frye, G. C. Acoustic wave sensors, in: H. Baltes and G. J. Hesse (Eds.), *Sensors Update*, vol. 2, Weinheim: Wiley-VCH, 1996.

37. Guo, S. J., Wen, D., Zhai, Y. M., Dong, S. J. and Wang, E. K. Platinum nanoparticle ensemble-on-graphene hybrid nanosheet: one-pot, rapid synthesis, and used as new electrode material for electrochemical sensing, *ACS Nano* 4, 3959–3968, 2010.
38. Guven, B., Boyacı, İ. H., Tamer, U. and Çalık, P. A rapid method for detection of genetically modified organisms based on magnetic separation and surface-enhanced Raman scattering, *Analyst* 137, 202–208, 2012.
39. Hoppener, C. and Novotny, L. Exploiting the light-metal interaction for biomolecular sensing and imaging, *Q. Rev. Biophys.* 45(2), 209–255, 2012.
40. Indyk, H. E. An optical biosensor assay for the determination of folate in milk and nutritional products, *Int. Dairy J.* 21, 783–789, 2011.
41. Indyk, H. E., Gill, B. D. and Woollard, D. C. Biotin content of paediatric formulae, early lactation milk and seasonal bovine milk powders by biosensor immunoassay, *Int. Dairy J.* 35, 25–31, 2014.
42. Indyk, H. E., Evans, E. A., Boström Caselunghe, M. C., Persson, B. S., Finglas, P. M., Woollard, D. C., *et al.* Determination of biotin and folate in infant formula and milk by optical biosensor-based immunoassay, *J. AOAC Int.* 83, 1141–1148, 2000.
43. Jang, H.-J., Cho, I.-H., Kim, H.-S., Jeon, J.-W., Hwang, S.-Y. and Paek, S.-H. Development of a chemiluminometric immunosensor array for on-site monitoring of genetically modified organisms, *Sens. Actuat. B* 155, 598–605, 2011.
44. Jiang, J., Fan, W. and Du, X. Nitrite electrochemical biosensing based on coupled graphene and gold nanoparticles, *Biosens. Bioelectron.* 51, 343–348, 2014.
45. Kabos, P. and Stalmachov, V. S. *Magnetostatic Waves and Their Application*. London: Chapman & Hall, 1994.
46. Kalman, A., Caelen, I. and Svorc, J. Vitamin and pseudovitamin analysis with biosensors in food products: a review. *J. AOAC Int.* 89, 819–825, 2006.
47. Kergaravat, S. V., Gómez, G. A., Fabiano, S. N., Laube Chávez, T. I., Pividori, M. I. and Hernández, S. R. Biotin determination in food supplements by an electrochemical magneto biosensor, *Talanta* 97, 484–490, 2012.
48. Kubant, R., Malinski, C., Burewicz, A. and Malinski, T. Peroxynitrite/nitric oxide balance in ischemia/reperfusion injury-nanomedical approach, *Electroanalysis* 18(4), 410–416, 2006.
49. Kumar, P., Roy, A. S. and Ramamurthy, P. C. The design of polyaniline based sensor for the qualitative estimation of malonaldehyde, *Measurement* 47, 1–4, 2014.
50. Kumari, A. and Yadav, S. K. Nanotechnology in agri-food sector, *Crit. Rev. Food Sci. Nutr.* 54, 975–984, 2014.
51. Lakowicz, J. R., Ray, K., Chowdhury, M., Szmacinski, H., Fu, Y., Zhang, J. and Nowaczyk, K. Plasmon-controlled fluorescence: a new paradigm in fluorescence spectroscopy, *Analyst* 133(10), 1308–1346, 2008.

52. Lal, S., Grady, N. K., Kundu, J., Levin, C. S., Lassiter, J. B. and Halas, N. J. Tailoring plasmonic substrates for surface enhanced spectroscopies, *Chem. Soc. Rev.* 37(5), 898–911, 2008.
53. Länge, K., Rapp, B. E. and Rapp, M. Surface acoustic biosensors: a review, *Anal. Bioanal. Chem.* 391, 1509–1519, 2008.
54. Lazcka, O., Del Campo, F. J. and Munoz, F. X. Pathogen detection: a perspective of traditional methods and biosensors, *Biosens. Bioelectron.* 22(7), 1205–1217, 2007.
55. Lee, D., Chander, Y., Goyal, S. M. and Cui, T. Carbon nanotube electric immunoassay for the detection of swine influenza virus H1N1, *Biosens. Bioelectron.* 26, 3482–3487, 2011.
56. Lee, Y. S. *Self-Assembly and Nanotechnology: A Force Balance Approach*, Hoboken, NJ: John Wiley & Sons, 2008.
57. Li, S., Horikawa, S., Park, M., Chai, Y., Vodyanoy, V. J. and Chin, B. A. Amorphous metallic glass biosensors, *Intermetallics* 30, 80–85, 2012.
58. Li, Y. and G. Han. Ionic liquid-functionalized graphene for fabricating an amperometric acetylcholinesterase biosensor, *Analyst* 137, 3160–3165, 2012.
59. Ligaj, M., Tichoniuk, M., Gwiazdowska, D. and Filipiak, M. Electrochemical DNA biosensor for the detection of pathogenic bacteria *Aeromonas hydrophila, Electrochim. Acta* 128, 67–74, 2014.
60. Liu, J. B., Fu, S. H., Yuan, B., Li, Y. L. and Deng, Z. X. Toward a universal "adhesive nanosheet" for the assembly of multiple nanoparticles based on a protein-induced reduction/decoration of graphene oxide, *J. Am. Chem. Soc.* 132, 7279–7281, 2010.
61. Liu, T., Su, H., Qu, X., Ju, P., Cui, L. and Ai, S. Acetylcholinesterase biosensor based on 3-carboxyphenylboronic acid/reduced graphene oxide–gold nanocomposites modified electrode for amperometric detection of organophosphorus and carbamate pesticides, *Sens. Actuat. B Chem.* 160, 1255–1261, 2011.
62. Liu, T., Tang, J., Zhao, H., Deng, Y. and Jiang, L. Particle size effect of the DNA sensor amplified with gold nanoparticles, *Langmuir* 18, 5624–5626, 2002.
63. Magnuson, B. A., Jonatis, T. S. and Card, J. W. A brief review of the occurrence, use, and safety of food-related nanomaterials, *J. Food Sci.* 76(6), 126–133, 2011.
64. Mairal, T., Ozalp, V. C., Lozano, P., Sanchez, M., Mir, I., Katakis, M., O'Sullivan, C. K. Aptamers: molecular tools for analytical applications, *Anal. Bioanal. Chem.* 390, 989–1007, 2008.
65. Marabotti, A., Lefèvre, T., Staiano, M., Crescenzo, R., Varriale, A., Rossi, M., Pézo-let, M. and D'Auria, S. Mutant bovine odorant-binding protein: temperature affects the protein stability and dynamics as revealed by infrared spectroscopy and molecular dynamics simulations, *Proteins* 72, 769–778, 2008.

66. Mariotti, E., Minunni, M. and Mascini, M. Surface plasmon resonance biosensor for genetically modified organisms detection, *Anal. Chim. Acta* 453, 165–172, 2002.
67. Medina-Plaza, C., de Saja, J. A. and Rodriguez-Mendez, M. L. Bioelectronic tongue-based on lipidic nanostructured layers containing phenol oxidases and lutetium bisphthalocyanine for the analysis of grapes, *Biosens. Bioelectron.* 57, 276–283, 2014.
68. Medintz, I. L., Uyeda, H. T., Goldman, E. R. and Mattoussi, H. Quantum dot bioconjugates for imaging, labelling and sensing, *Nat. Biotechnol.* 4, 435–446, 2005.
69. Meng, H., Yang, Y., Chen, Y., Zhou, Y., Liu, Y., Chen, X., Ma, H., Tang, Z., Liu, D. and Jiang, L. Photoelectric conversion switch based on quantum dots with i-motif DNA scaffolds, *Chem. Commun*., 2293–2295, 2009.
70. Merkoci, Nanoparticles-based strategies for DNA, protein and cell sensors, *Biosens. Bioelectron.* 26, 1164–1177, 2010.
71. Nica, A. G., Mascini, M. and Ciucu, A. A. DNA-based biosensor for detection of genetically-modified organisms, *Anal. U. B. Chim.* 23, 84–94, 2004.
72. Ozalp, V. C., Bayramoglu, G., Kavruk, M., Keskin, B. B., Oktem, H. A. and Arica, M. Y. Pathogen detection by core–shell type aptamer-magnetic preconcentration coupled to real-time PCR, *Anal. Biochem.* 447, 119–125, 2014.
73. Paek, S. M., Yoo, E. and Honma, I. Enhanced cyclic performance and lithium storage capacity of SnO_2/graphene nanoporous electrodes with three-dimensionally delaminated flexible structure, *Nano Lett.* 9, 72–75, 2009.
74. Palla-Papavlu, A., Patrascioiu, A., Di Pietrantonio, F., Fernández-Pradas, J-M., Cannatà, D., Benetti, M., D'Auria, S., Verona, E. and Serra, P. Preparation of surface acoustic wave odor sensors by laser-induced forward transfer, *Sens. Actuat. B* 192, 369–377, 2014.
75. Parra, V., Arrieta, A., Fernández-Escudero, J. A., García, H., Apetrei, C., Rodriguez- Mendez, M. L. and de Saja, J. A. E-tongue based on a hybrid array of voltammetric sensors based on phthalocyanines, perylene derivatives and conducting polymers: discrimination capability towards red wines elaborated with different varieties of grapes, *Sens. Actuat. B* 115(1), 54–61, 2006.
76. Pennacchio, A., Ruggiero, G., Staiano, M., Piccialli, G., Oliviero, G., Lewkowicz, A., Synak, A., Bojarski, P., D'Auria, S. A surface plasmon resonance based biochip for the detection of patulin toxin. *Opt. Mater.*, http://dx.doi.org/10.1016/j.optmat.2013.12.045, 2014.
77. Peteu, S. F., Boukherroub, R. and Szunerits, S. Nitro-oxidative species in vivo biosensing: challenges and advances with focus on peroxynitrite quantification, *Biosens. Bioelectron.* 58, 359–373, 2014.
78. Pourasl, A. H., Ahmadi, M. T., Rahmani, M., Chin, H. C., Lim, C. S., Ismail, R. and Tan, M. L. P. Analytical modeling of glucose biosensors based on carbon nanotubes, *Nanoscale Res. Lett.* 9, 33, 2014.

79. Pundir, C. S. and Devi, R. Biosensing methods for xanthine determination: a review, *Enzyme Microb. Technol.* 57, 55–62, 2014.
80. Raghu, P., Reddy, T. M., Reddaiah, K., Kumara Swamy, B. E. and Sreedhar, M. Acetylcholinesterase based biosensor for monitoring of Malathion and Acephate in food samples: a voltammetric study, *Food Chem.* 142, 188–196, 2014.
81. Raynes, J. K., Carver, J. A., Gras S. L. and Gerrard, J. A. Protein nanostructures in food – should we be worried? *Trends Food Sci. Technol.* 37, 42–50, 2014.
82. Sandoval Cortes, J., Gutierrez Grabados, S., Alatorre, A., Lopez Jiminez, J. A., Griveau, S. and Bedioui, F. Electropolymerized manganese tetraaminophthalocyanine thin films onto platinum ultramicroelectrode for the electrochemical detection of peroxynitrite in solution, *Electroanalysis* 19, 61, 2007.
83. Santonico, M., Pennazza, G., Grasso, S., D'Amico, A. and Bizzarri, M. Design and test of a biosensor-based multisensorial system: a proof of concept study, *Sensors* 13, 16625–16640. 2013.
84. Sassolas, A., Leca-Bouvier, B. D. and Blum, L. J. DNA biosensors and microarrays, *Chem. Rev.* 108, 109–139, 2008.
85. Schlecht, U., Malave, A., Gronewold, T., Tewes, M. and Lohndorf, M. Comparison of antibody and aptamer receptors for the specific detection of thrombin with a nanometer gap-sized impedance biosensor, *Anal. Chim. Acta* 573–574, 65–68, 2006.
86. Shan, C. S., Yang, H. F., Han, D. X., Zhang, Q. X., Ivaska, A. and Niu, L. Graphene/AuNPs/chitosan nanocomposites film for glucose biosensing, *Biosens. Bioelectron.* 25, 1070–1074, 2010.
87. Sharma, B., Frontiera, R. R., Henry, A. I., Ringe, E. and Van Duyne, R. P. SERS: materials, applications, and the future, *Mater. Today* 15(1–2), 16–25, 2012.
88. Somers, R. C., Bawendi, M. G. and Nocera, D. G. CdSe nanocrystal based chem/bio sensors, *Chem. Soc. Rev.* 36, 579–591, 2007.
89. Song, H., Ni, Y. and Kokot, S. Investigations of an electrochemical platform based on the layered MoS_2–graphene and horseradish peroxidase nanocomposite for direct electrochemistry and electrocatalysis, *Biosens. Bioelectron.* 56, 137–143, 2014.
90. Spadavecchia, J., Manera, M. G., Quaranta, F., Siciliano, P. and Rella, R. Surface plamon resonance imaging of DNA based biosensors for potential applications in food analysis, *Biosens. Bioelectron.* 21, 894–900, 2005.
91. Sundaram, R. S., Gómez-Navarro, C., Balasubramanian, K., Burghard, M. and Kern, K. Electrochemical modification of graphene, *Adv. Mater.* 20(16), 3050–3053, 2008.
92. Tichoniuk, M., Ligaj, M. and Filipiak, M. Application of DNA hybridization biosensor as a screening method for the detection of genetically modified food components, *Sensors* 8, 2118–2135, 2008.

93. Todescato, F., Antognoli, A., Meneghello, A., Cretaio, E., Signorini, R. and Bozio, R. Sensitive detection of ochratoxin A in food and drinks using metal-enhanced fluorescence, *Biosens. Bioelectron.* 57, 125–132, 2014.
94. Truong, T. N. L., Tran, D. L., Vu, T. H. A., Tran, V. H., Duong, T. Q., Dinh, Q. K., Tsukahara, T., Lee, Y. H. and Kim, J. S. Multi-wall carbon nanotubes (MWCNTs)-doped polypyrrole DNA biosensor for label-free detection of genetically modified organisms by QCM and EIS, *Talanta* 80, 1164–1169, 2010.
95. Tung, V. C., Chen, L. M., Allen, M. J., Wassei, J. K., Nelson, K., Kaner, R. B. and Yang, Y. Low-temperature solution processing of graphene–carbon nanotube hybrid materials for high-performance transparent conductors, *Nano Lett.* 9, 1949–1955, 2009.
96. Ulianas, A., Heng, L. Y., Ahmad, M., Lauc, H-Y., Ishak, Z. and Ling, T. L. A regenerable screen-printed DNA biosensor based on acrylic microsphere–gold nanoparticle composite for genetically modified soybean determination, *Sens. Actuat. B* 190, 694–701, 2014.
97. Vaisocherová, H., Ševců, V., Adam, P., Špačková, B., Hegnerová, K., de los Santos Pereira, A., Rodriguez-Emmenegger, C., Riedel, T., Houska, M., Brynda, E. and Homola, J. Functionalized ultra-low fouling carboxy-and hydroxy-functional surface platforms: functionalization capacity, biorecognition capability and resistance to fouling from undiluted biological media, *Biosens. Bioelectron.* 51, 150–157, 2014.
98. Varzakas, T., Nikoleli, G.-P. and Nikolelis. D. P. Biosensors in quality of meat products, in: D. Nikolelis, T. Varzakas, E. Arzum and G. P. Nikoleli, eds., *Portable Biosensing of Food Toxicants and Environmental Pollutants (A Volume in the Series in Sensors)*, USA: CRC Press, Taylor and Francis, 2014.
99. Wang, K., Li, H.-N., Wu, J., Ju, C., Yan, J.-J., Liu, Q. and Qiu, B. TiO_2-decorated graphene nanohybrids for fabricating an amperometric acetylcholinesterase biosensor, *Analyst* 136, 3349–3354, 2011.
100. Wang, Y., Zhang, S., Du, D., Shao, Y., Li, Z., Wang, J., Engelhard, M. H., Li, J. and Lin, Y. Self assembly of acetylcholinesterase on a gold nanoparticles-graphene nanosheet hybrid for organophosphate pesticide detection using polyelectrolyte as a linker, *J. Mater. Chem.* 21, 5319–5325, 2011.
101. Williams, G., Seger, B. and Kamat, P. V. TiO_2-graphene nanocomposites. UV-assisted photocatalytic reduction of graphene oxide, *ACS Nano* 2(7), 1487–1491, 2008.
102. Xiang, Y., Zhang, H., Jiang, B., Chai, Y. and Yuan, R. Quantum dot layer-by-layer assemblies as signal amplification labels for ultrasensitive electronic detection of uropathogens, *Anal. Chem.* 83, 4302–4306, 2011.
103. Xue, J., Ying, X., Chen, J., Xian, Y. and Jin, J. Amperometric ultramicrosensors for peroxynitrite detection and its application toward single myocardial cells, *Anal. Chem.* 72(21), 5313–5321, 2000.

104. Zhang, F., Zhang, Q., Zhang, D., Lu, Y., Liu, Q. and Wang, P. Biosensor analysis of natural and artificial sweeteners in intact taste epithelium, *Biosens. Bioelectron.* 54, 385–392, 2014.
105. Zhang, H., Li, Z-f., Snyder, A., Xie, J. and Stanciu, L. A. Functionalized graphene oxide for the fabrication of paraoxon biosensors, *Anal. Chim. Acta* 827, 86–94, 2014.
106. Zhang, J., Song, S., Wang, L., Pan, D. and Fan, C. A gold nanoparticle-based chrono-coulometric DNA sensor for amplified detection of DNA, *Nat. Protoc.* 2, 2888–2895, 2007.
107. Zhou, H., Dong, J., Deo, V. K., Park, E. Y. and Lee, J. Detection of anti-Neospora antibodies in bovine serum by using spiky Au–Cd Te nanocomplexes, *Sens. Actuat. B* 178 (2013a) 192–199.
108. Zhou, H., Kim, J., Zou, F., Koh, K., Park, J. Y. and Lee, J. Rapid detection of DNA by magnetophoretic assay, *Sens. Actuat. B* 198, 77–81, 2014.
109. Zhou, H., Lee, J., Park, T. J., Lee, S. J., Park, J. Y. and Lee, J. Ultrasensitive DNA monitoring by Au–Fe_3O_4 nanocomplex, *Sens. Actuat. B* 163, 224–232, 2012.
110. Zhou, H., Kim, J.-P., Bahng, J. H., Kotov, N. A. and Lee, J. Self-assembly mechanism of spiky magnetoplasmonic supraparticles, *Adv. Funct. Mater.* (2013b), http://dx.doi.org/10.1002/adfm.201302405.
111. Zhu, D., Liu, J., Tang, Y. and Xing, D. A reusable DNA biosensor for the detection of genetically modified organism using magnetic bead-based electrochemiluminescence, *Sens. Actuat. B* 149, 221–225, 2010.

11

Numerical Modeling and Calculation of Sensing Parameters of DNA Sensors

Hediyeh Karimi[1], Farzaneh Sabbagh[2], Mohammad Eslami[3], Hamid sheikhveisi[4], Hossein Samadyar[5], and Omid Talaee[6]

[1]Malaysia Japan International Ins. of Technology, Universiti Teknologi Malaysia, Kuala Lumpur, Malaysia
[2]Department of Bioprocess Engineering, Faculty of Chemical Engineering, University Technology Malaysia, Johor, Malaysia
[3]Department of Electrical & Computer, College of Engineering, Islamic Azad University, Zahedan Branch, Zahedan, Iran
[4]Department Of Computer Engineering, Payame Noor University, IR. Iran
[5]Young Researchers and Elites club, Science and Research Branch, Islamic Azad University, Tehran, Iran
[6]Department of Nuclear and Heat Power Engineering, Faculty of Energy and Transport System, Peter the Great Saint Petersburg Polytechnic University, Saint-Petersburg, Russia

Abstract

These days, construction and operation of label-free DNA biosensors are the definitive factors for achieving trustworthy laboratory tests. Hence, detection systems or sensors using new emerging nanomaterials are considered as powerful tools for the genetic researchers to understand the progression and early screening of diseases, routine walk-in medical checkups, which make the controlled design of these sensors vital. Nanotechnology has devoted itself for the purpose of producing very sensitive and reliable biosensors. Despite these efforts, the sensing mechanism in label-free field-effect-based DNA sensors has aroused a great deal of controversy among scientists. In order to find an answer for these questions, developing the analytical model of these sensors expected to help. In addition, just computational calculations can allow designers to evaluate the importance of several parameters involved in the fabrication and provide a framework to which experimental results can be compared. In this chapter, we present a numerical model for the current–voltage characteristic of graphene-based liquid-gated field

*Corresponding author: h.karimifeizabadi.2013@ieee.org

Ashutosh Tiwari, Hirak K. Patra and Anthony P.F. Turner (eds.) Advanced Bioelectronic Materials, (389–412) © 2015 Scrivener Publishing LLC

effect transistors (FETs), which include the calculation of the conductance changes in the sensor's response during DNA hybridization. The results are compared with the experimental work and an acceptable agreement is observed.

Keywords: Graphene, graphene-based transistors, DNA hybridization, DNA concentration, I-V characteristics

11.1 Introduction to Graphene

The nanomaterials of graphene (sp^2 aromatic)-based carbon have been widely used for biosensing, and they have been the subject of much interest, even though it has been a relatively short period since discovery of them. Graphene and its derivatives such as the graphene oxide (GO), reduced graphene oxide (rGO), and n-doped graphene are reported to be used successfully in biosensing applications [1]. An oxidized form of graphene, GO, created in solution with highly negative charges and hydrophilicity characteristic has been used as a template for DNA hybridization studies [2]. The fabrication process of GO has a strong influence on the electrical possessions of GO films which have been employed in sensor configuration. On the other hand, the sensitivity of these sensors produced from GO are dependent on some factors such as size, shape, presence of wrinkles, defects, and oxidation degree of GO sheets. Therefore, from the point of fabrication, more studies and supervision are required to control the quality of fabrication of GO sheets [3–5]. In contradiction of GO, large-size graphene layers are claimed as more reliable and beneficial nanomaterials in biosensing experiments from the device fabrication viewpoint.

Graphene provides a two-dimensional (2D) honeycomb structure consisting of a thin layer of single carbon atoms. The reason for that being the idiosyncratic physical and chemical characteristics like exceptional strength [6], and its great thermal conductivity plus biocompatibility that it possess [7]. Graphene, as a nearly perfect 2D crystal free of the structural defects [8–9], presents surprisingly ballistic transport due to its significant high electron mobility at low temperatures that can reach up to 200 000 cm^2/Vs with typical carrier concentration of 2×10^{11} cm^{-2} [10, 11]. Graphene and nanotubes have been utilized as an essential element in several electronic devices, e.g., biosensors [12, 13]. There has been major evidence indicating biosensing applications shown in graphene and its by-products [14]. Due to the biocompatibility and extreme environmental distress affectability of thin graphene plates, it provides an essential biosensing application for them. Meaning that they are greatly sensitive to variables such as electronic doping [15–18] and molecule adsorption [3,14,19–20]. In addition, it is considerable

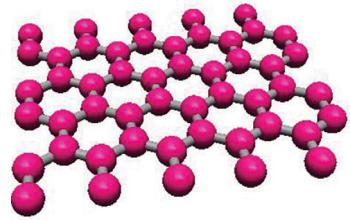

Figure 11.1 Schematic of graphene as a sensing layer.

that, because of easier contact, the surface structure of graphene (displayed in Figure 11.1) in comparison to other carbon derivatives ensures a higher adsorption of DNA molecules [21]. This resulted in the selection of graphene as the DNA detection sensory framework in this study.

11.1.1 Electronic Structure of Graphene

Understanding the electronic structure of graphene is the starting point for pursuing the electronic properties of graphene. Intrinsic graphene is known as a semimetal with zero bandgap [22]. It is widely claimed that its valence and conduction bands are cone shaped and meet at the K points of the Brillouin zone [22, 23]. Because the bandgap is zero, devices with channels made of large-area graphene cannot be switched off and therefore are not suitable for logic applications. However, bandgap can be induced in these materials with two demonstrated ways [22]. Firstly, narrowing the graphene to nanoribbon, by which its bandgap has a reverse relation with the width of nanoribbon in this method [24]. Secondly, by applying a perpendicular electric field to bilayer graphene (BLG) that results a potential difference between layers which opens the bandgap in BLG [25, 26]. Although the physical simulation is accurate enough, there are still many controversies about their ability to compute the potential model of the device. Analytical modeling possibly will facilitate this challenge. But, it needs serious improvement due to the lack of effective mass effect on the vertical electric field proposed by Ref. [27].

11.1.2 Graphene as a Sensing Element

Maximum surface-to-volume ratio for sensing application would be provided by employing graphene with its unique 2D structure, exposing every atom of graphene to the environment. Furthermore, graphene shows no distinction between surface sites and the bulk material, which is the major motivation behind implementation of other nanostructured materials. Exceptional electronic structure and interesting properties of graphene

resulted in the adaptability of graphene as a basic sensing element in sensor application. The ambipolarity can be mentioned as one of the important characteristic of graphene, meaning that "chemical gating" of the material can be achieved by adsorption of either electron withdrawing or donating groups, which can be easily monitored in a resistive-type sensor setup. In other words, a graphene-based field effect transistor (FET) is an ambipolar device. It can operate via both electron and hole branches where the conductivity changes as a function of the electron or hole concentration and is proportional to the gate voltage [28]. Any molecular disruption on the graphene can be easily detected due to its ultrahigh surface area combing with its specific electronic features. Our expectations from graphene-oriented sensors for detection of individual molecules on and off its surface have become high because of its unique structures. The availability of 2D graphene will open up possibilities for designing and preparing graphene-oriented electrodes for a wide range of liquid-sensing and biosensing applications ranging from amperometric sensors to amperometric enzyme biosensors and label-free DNA biosensors. With the help of the study and molecular analysis of nucleic acids, almost 400 and increasing genetic conditions are diagnosable now [29].

11.1.3 DNA Molecules

A diagram of the DNA molecule is drawn in Figure 11.2 [30], where it is shown that the DNA molecule is a polyelectrolyte comprised of two helically wound sugar–phosphate backbones, joined in the middle by nucleobases (adenine, thymine, cytosine, and guanine). The strong hydrogen bonds between matching nucleobases keep the two strands together (AT and CG), as well as with dispersion forces that occur between the stacked flat nucleobases [31]. The phosphate groups are negatively charged in biologically relevant conditions (25 °C, 1 mM–1 M monovalent salt concentration, pH 7). It is strongly believed that the signal changes in a BioFET would occur because of the negative charges of phosphate groups either directly or indirectly, as DNA molecules attached to the surface [32].

11.1.4 DNA Hybridization

The process of establishing a non-covalent, sequence-specific interaction between two or more complementary strands of nucleic acids into a single complex is known as a hybridization phenomenon which in the case of the two strands is referred to as a duplex. The detection of DNA hybridization has been a topic of central importance owing to a wide variety of

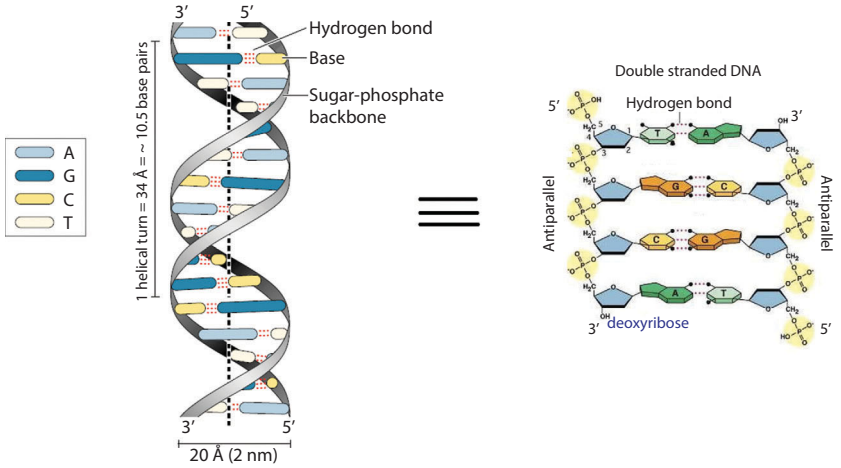

Figure 11.2 Helical and detailed structure of DNA molecules.

applications such as diagnosis of pathogenic and genetic disease, gene expression analysis, and the genotyping of mutations and polymorphisms [33, 34]. Technologies in DNA biosensing [35] have received special appeal not only for their low cost and simplicity, but for their ultimate capabilities in detecting single-nucleotide polymorphisms (SNP) which have been correlated to several diseases and genetic disorders such as Alzheimer's and Parkinson's diseases.

The DNA hybridization event is the basis of many existing DNA detection techniques. In DNA hybridization as depicted in Figure 11.3, the target, unknown single-stranded DNA (ssDNA), is identified and formed by a probe ssDNA and a double-stranded (dsDNA) helix structure with two complementary strands. It is believed that, in the presence of a mixture of diverse non-complementary nucleic acids, the hybridization reaction is known to be extremely efficient and specific. The basis for the high specificity of the biorecognition process is the uniqueness of the complementary nature of this binding reaction between the base pairs, i.e., adenine–thymine and cytosine–guanine.

In a graphene-based FETs (GFETs) with DNA application, the DNA molecules used as probes are short (typically 20–30 bases long). ssDNA probes could be captured on a surface through long-range electrostatic forces or by chemical combination with an activated (or functionalized) surface. The success of a DNA sensor depends on the high specificity of capturing only the exact complementary target, allowing DNA sensors to detect SNP. For this purpose, the DNA probes should be made short such

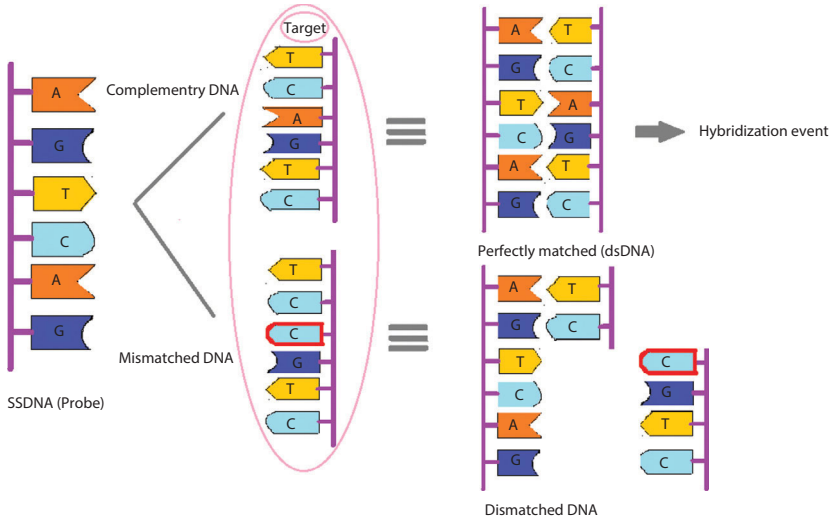

Figure 11.3 Schematic of DNA hybridization event.

that the energy of binding is severely changed with a single mismatch, prohibiting nonspecific pairing. Therefore, faster and more precise hybridization rate would obtained by choosing the shorter probes (oligonucleotides). It is noteworthy that the density of capture probes should be high to avoid targets absorbing and attaching to vacant sites on the surface. Also, there is another way to deactivate the vacant sites by a chemical step, but such processes are not perfect, and active sites can still exist.

The hybridization experiment should be carried out in a buffer solution with precisely selected ionic concentration (often a saturated or near-saturated monovalent salt). In all DNA biosensor experiments, the biochemical hybridization reaction occurs in an electrolytic aqueous medium. The biological recognition will only proceed under specific conditions of ionic strength, solution's pH, and temperature. The molecular electrostatics and chemistry of the DNA molecule are very important in dictating the interaction of the DNA with its surroundings. Specificity is obtained by the unique affinity of binding between the probe and target.

11.1.5 Graphene-Based Field Effect Transistors

GFETs as breakthrough results were reported by Manchester Group in 2004 [36]. Since that time, large numbers of attempts have also been made to use graphene as a novel channel material in FETs for electronics [37–42]. As shown in Figure 11.4, GFET structure consists of a 300-nm SiO_2 layer as a

back-gate dielectric and a doped silicon substrate as the back-gate has been proposed [43]. The graphene is sandwiched between the source and drain electrodes controlled by the gate through the gate voltage applied. The most interesting feature of graphene in transistors is providing the possibility of having channels that are just one atomic layer thick [22]. Plus the rewarding experiments on electronic, peripherals such as FET [44] made with the application of thin graphene plates [31] by nano-microlithographic fabrication [33]. This suggests and justifies the call for action and the necessity of further DNA detection studies [34] as well as understanding the high sensitivity of the transport carriers in graphene plates and the conductance response to environmental distress [35].

In the process of observing the conductance variations of fabricated device base carbon materials, electrical and label-free DNA detection hybridization was possible to attain [1]. Graphene conductive characteristic as a channel in the FETs was considered as a seminal electronic features in the material [45]. Presently, the attention has moved toward been a focus on the exploratory capabilities in single-layer graphene [46]. Besides, single-electron transistor base on monolayer graphene was discovered in an experiment as well [47]. Among the bonuses in the incorporation of graphene as an FETs' channel material is a great electrostatics control capability. Therefore, the reduction of short channel effect is anticipated [48].

11.1.6 DNA Sensor Structure

As shown in Figure 11.4, large graphene film has incorporated to be DNA detection template constructed of multi-layer and single-layer graphene with a ratio of 40 to 60 percent. These graphene films are made using the chemical vapor deposition (CVD) method [4, 49]. As a notable fact, transference of the graphene film from nickel to glass substrate results in the possibility of the fabrication of FET transistor based on large graphene [50]. The result of producing a DNA detection solution chamber was achieved through incorporating silver paint as source and drain electrodes and polydimethylsiloxanes (PDMS) as an insulator. The conductance between source and drain varies in response to the surface electric potential of graphene, and the gate electrode coupled through the liquid electrolytes is used to control the on and off switching of the devices. The configuration of the liquid-gated FETs (LGFETs) is possible with the incorporation of graphene films (Figure 11.4) which have the DNA molecule detection sensitivity of 0.01nM [51]. Another one of the abilities in this device is the detection of target DNA hybridization to the probe DNAs that are pre-fixated on graphene. Plus, it has the capability of differentiating

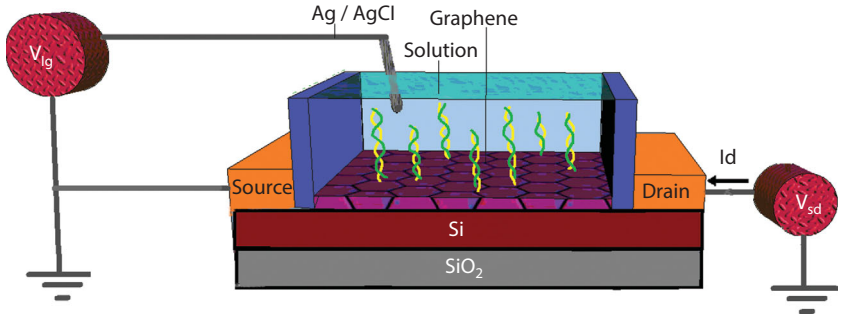

Figure 11.4 Proposed structure of graphene-based DNA sensor with liquid gate for DNA sensing.

single-based incompatibility. Additionally, the harmonious DNA and the one-base incompatible DNA can be simply distinguished considering that $V_{g,min}$ is less sensitive to the incompatible DNA, which was responsible for 20 meV alteration at a high concentration (500 nM).

Ag/AgCl is used as a reference electrode in this experiment. The most significant reaction which plays a crucial role in determining the potential of the solution is the electron transfer reaction for electrodes. Three types of electrodes from electrochemical point are defined as: ideally polarizable, non-polarizable, and partially polarizable. This categorization differentiates electrode boundaries in terms of their capability to carry out current. A non-polarizable electrode is one which can freely allow electron transfer reactions without any hindrance. It is noteworthy that typically a reference electrode is anticipated to be non-polarizable; if not it could weaken the sensitivity of the biosensor. The reference electrode sets the potential of the solution by achieving electrochemical equilibrium with the solution via electron transfer reactions.

11.1.7 Sensing Mechanism

The (π–π) reactions among the carbon plane and the DNA molecules strongly affect the device conductivity of device by the means of different mechanisms like electronic doping [1] and electrostatic gating [2, 52]. Both the DNA and graphene are negative in charges; hence, the considerable role of buffer in ssDNA hybridizing sensing of graphene [53] is significant. Phosphate buffer saline (PBS) or sodium chloride solution has recurrently been incorporated in the form of a buffer for charge screening [54, 55]. The outcome of which is DNA adsorption due to both van Der Waals and electrical attraction [55, 56]. Meaning, the detection process could be defined as a transference of the electron between DNA and graphene films [5].

Built on the detection process, a DNA hybridization kinetic model was suggested with kinetic coefficients for surface-bound DNA probes [57]. Here in this research, the concentration of DNA in the form of a gate voltage is replicated and DNA sensing factor (α) is suggested. Eventually, the collation study between suggested model, and the data attained from the experiments are reported.

11.2 Numerical Modeling

Modeling and simulation incorporating partial differential equations (PDE) are an essential factor in the process of current–voltage characteristics, sensitivity, and the performance of the sensory peripherals that DNA molecules are exposed to. The proposed model here possesses the electrical detection of DNA hybridization performance capability by the means of simulating the conductance of the graphene plates. Built on the sensing process derived from the experiment to study the factors at lay in the absorption of DNA in relation to graphene, the function of gate voltage is presumed to be the DNA concentration with the implication of sensing factor (α). In this study, the selection of conductance in the form of a calculable sensory factor has taken place based on the fact of graphene nanomaterial's sensitivity to the presence of DNA molecules. Also, it can be argued that that the initiation of modeling from graphene conductance is valid.

11.2.1 Modeling of the Sensing Parameter (Conductance)

The conductivity of the graphene might show a discrepancy due to the variations of carrier density, carrier concentration, type of electron scattering at the edges, Fermi level, and chirality width [58]. Naeemi and Meindl [25] suggested that each conduction channel in graphene contributes one quantum. A district of the lowest G regards to gate voltage as a basic constant proportional to Planck's constant and electron charge in bulk graphene is defined and calculates for the minimum conductivity by the

$$G_0 = \frac{2e^2}{h} \tag{11.1}$$

Two factors make possible the conductance output in large channels, resulting in the capability of adhering to the Ohmic scaling law built upon the Landauer formula. The first is the self-sufficiency of the interface resistance length. The second would be a result of the nonlinearity relation

between the conductance and width that does rely on the quantity of modes in the conductor. Hence, the Landauer formula conductance would extend as the form of Equation (11.2) at the same time as these quantized parameters are taken into consideration.

$$G = \frac{2q2}{h}\int_{0}^{+\infty} M(E)T(E)\left(-\frac{df(E)}{dE}\right)dE \tag{11.2}$$

where q is the electron charge, h is Planck's constant, E is the energy band structure, $T(E)$ is the transmission probability, $M(E)$ is the number of modes at an applied energy near the wave vector which is dependent on the sub band's position, and $f(E)$ is the Fermi–Dirac distribution function. Without scattering, electrons in ballistic transport behave according to second law of Newton for motion of particle at non-relativistic speeds; so, the electrical resistivity can be neglected in a ballistic channel of graphene due to lack of scattering for electron transport [46, 59]. So, T would be defined as the probability of one injected electron at one end that can be transmitted to other end is considered equal to one ($T(E)$ =1) [60]. Additionally, $f(E)$ is the likelihood of the Fermi level, occupation with electrons that is defined as the Fermi–Dirac distribution function [61–63].

$$f(E) = \frac{1}{e^{\frac{E-EF}{k_BT}} + 1} \tag{11.3}$$

where E_F is the Fermi energy, k_B is the Boltzmann constant, and T is temperature. By applying the Maxwell–Boltzmann approximation, the distribution function can be expressed as

$$f(E) \approx \frac{1}{e^{\frac{E-E_F}{k_BT}}} = e^{-\frac{E-E_F}{k_BT}} \tag{11.4}$$

The graphene length has a seminal part in the definition of conductivity equation [64]. By the substitution of sub-bands (mode numbers) quantity in addition to the Fermi–Dirac distribution function in Equation (11.2), it is possible to obtain conductance as

$$G = \frac{3q^2}{h}\cdot\frac{a_{CC}t}{L}\cdot(3a_{CC}t)^{\frac{1}{2}}\cdot\left(\int_{0}^{+\infty}\left(E-\frac{2\beta 2}{3a_{CC}t}\right)^{\frac{1}{2}}\cdot d\left(-\frac{1}{1+e^{(E-E_F)/K_BT}}\right)\right) \tag{11.5}$$

By making the substitution of $x = (E–E_g)/K_BT$, the boundary of integral changes as follows. Equation (11.5) becomes

$$G = \frac{3q^2}{hL}\left(3\pi a_{CC}{}^3 t^3 K_B T\right)^{\frac{1}{2}} \cdot \left(\int_0^{+\infty} \frac{x^{\frac{1}{2}}}{\left(1+e^{x-\eta}\right)} dx + \int_0^{+\infty} \frac{x^{-\frac{1}{2}}}{\left(1+e^{x+\eta}\right)} dx \right) \tag{11.6}$$

where the normalized Fermi energy is defined as $\eta=(E_F–E_g)/K_BT$. The incorporation of the Fermi–Dirac integral (FDI) form of conductance will prove to be beneficial in order to comprehend the function of degenerate and non-degenerate regimes. It is noted that the FDI of an order i is defined as

$$\Im_i(\eta) = \frac{1}{\Gamma(i+1)} \int_0^{\infty} \frac{x^i}{1+e^{x-\eta}} dx \tag{11.7}$$

In general, $\Gamma(i+1) = \int_0^{\infty} e^{-x} x^i dx = i!$ if i is an integer applicable to gamma function, $\Gamma(1/2) = \sqrt{\pi}$ and $\Gamma(3/2) = (1/2)\,\Gamma(1/2) = \sqrt{\pi}/2$. A notable matter of observation is the common characteristics of the FDI in the non-degenerate and the heavily degenerate limits. Therefore, attaining the typical mode of graphene is similar to that of silicon as suggested by Gunlycke [65].

$$G = \frac{3q^2}{hL}\left(3\pi a_{CC}^3 t^3 K_B T\right)^{\frac{1}{2}} \left(\Im_{-\frac{1}{2}}(\eta) + \Im_{-\frac{1}{2}}(-\eta) \right) \tag{11.8}$$

where $\Im_{-\frac{1}{2}}(\eta)$ is the FDI of order $(-\frac{1}{2})$. The distribution function of Fermi–Dirac is ascribed to degenerate and non-degenerate states with the quantity of $(\eta >> 0)$ and $(\eta \ll 0)$ each. During the non-degenerate state, the approximation of FDI is possible using Maxwell–Boltzmann distribution factor of $(E)=\exp(\eta^{\eta})$. Therefore, in the nondegenerate limit, graphene's general conductance model can be transformed into the exponential equation as [66, 67].

$$G = \frac{3q^2}{hL}\left(3\pi a_{CC}{}^3 t^3 K_B T\right)^{\frac{1}{2}} \left(e^{(\eta)} + e^{(-\eta)}\right) \tag{11.9}$$

As normalized Fermi energy derived as $\eta = (E–E_g)/K_BT$, and the band-gap energy is $E_g = q.v_g$; then, the normalized Fermi energy is calculated

as $\eta = (V_t - V_g)/K_B Tq$ which correspond to a function of V_g. Employing η in Equation (11.9), the conductance expresses as

$$G = \mp \frac{3q^2}{hL}\left(3a_{CC}{}^3 t^3 \pi K_B T\right)^{\frac{1}{2}}\left(e^{\left(V_t - V_g/K_B Tq\right)} + e^{\left(-V_t + V_g/K_B Tq\right)}\right) \tag{11.10}$$

which represents conductance (G) as a function of gate voltage (V_g). Figure 11.3 would display graphene-based DNA sensor conductance model in comparison to the gate voltage prior to the addition of a DNA molecule. Based on the data gathered from the experiment, the suggested model can meet the major expectation of graphene-based DNA sensor [1].

The simulation results demonstrated that the conductance in graphene is minimum at the Dirac point, suggesting that the resistance is higher at the point closest to the charge neutrality point.

11.2.2 Current–Voltage (I_d–V_g) Characteristics Modeling

The DNA sensor's performance built upon graphene nanostructure is assessed by the incorporation of its current–voltage properties [68]. Additionally, by replacing the FDI in Equation (11.10), the general conductance model of single-layer graphene would be obtained as

$$\mathrm{I_d} = \frac{3q^2\left(3\pi a^3 t^3 k_{BT}\right)^{\frac{1}{2}}}{hL}\left[\Im_{-\frac{1}{2}}(\eta) + \Im_{-\frac{1}{2}}(-\eta)\right]\left(V_{gs} - V_t\right) \tag{11.11}$$

where V_{gs} is the gate-source voltage, and V_t is the threshold voltage. As shown in Figure 11.4, prior to the addition of the probe DNA, pure PBS (40 μL) has been added to the chamber in order to calculate the transfer curve, in other words, drain current (I_d) in comparison to the gate voltage [51]. A valid consensus is observable among the suggested model for DNA sensor and the outcome of the experiments obtained from the reference [51].

Since the DNA molecules need to saturate the graphene surface, high concentration of probe DNAs (1 μM) in 40 μL PBS buffer has been added to the chamber. As seen in Figure 11.5, the application of the gate voltage to the DNA solution will result in (graphene-based FETs) clear display of the ambipolar conductance behavior. The doping states of graphene have been controlled by the $V_{g,min}$ to calculate the graphene plate's lowest level of conductance as determined by transfer characteristic curve.

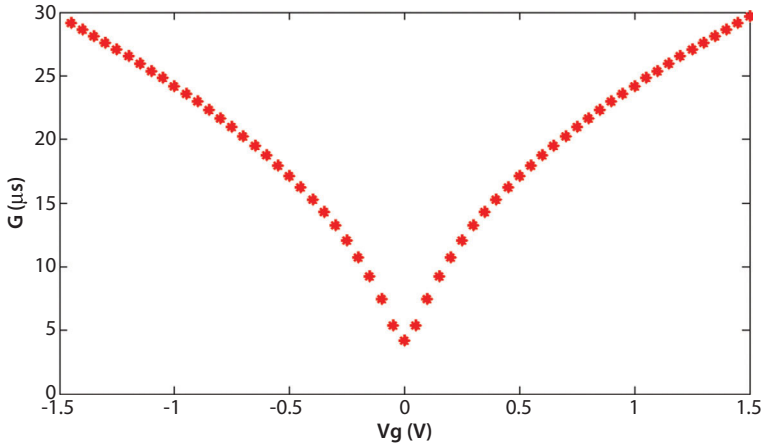

Figure 11.5 Conductance model of graphene-based LGFETs prior to addition of DNA molecules.

11.2.3 Proposed Alpha Model

The considerable left shift of $V_{g,min}$ is a result of the fixation of probe DNA upon on the graphene surface, then is dramatically left shifted. Based on this, it is reasonable to conclude that $V_{g,min}$ is greatly sensitive to the probe DNA and hybridization and fixation of harmonious target DNAs. In order to support this conclusion, the observation of gate voltage change toward left as a result of DNA molecules doping the graphene film is helpful [3, 69]. However, the increased number of carriers affects the conductivity of the (graphene) FET devices in the channel. The attachment among graphene and nucleotides was experimented and researched [42, 69, 70]. Commonly, $V_{g,min}$ turn is to be considered as a legitimate hint toward DNA detection. Ultimately, the harmonious DNAs with concentration of 40 **μL** were appended to the device made for hybridization using probe-DNA-fixated graphene [51]. It can be seen in Figure 11.6 that, during the expansion of concentrated harmonious DNAs from 0.01 to 500 nM, additional DNA molecules will be adsorbed and the attraction of additional molecules would be possible, resulting in alteration of $V_{g,min}$ on the properties which relies on and will calculate the location of the Fermi level respective to the conduction band border.

Inspired by this fact, the gate voltage is simulated as a function of DNA concentration and DNA immobilization factor (α) is recommended. Eventually, the variation in the gate voltage can be modeled by DNA

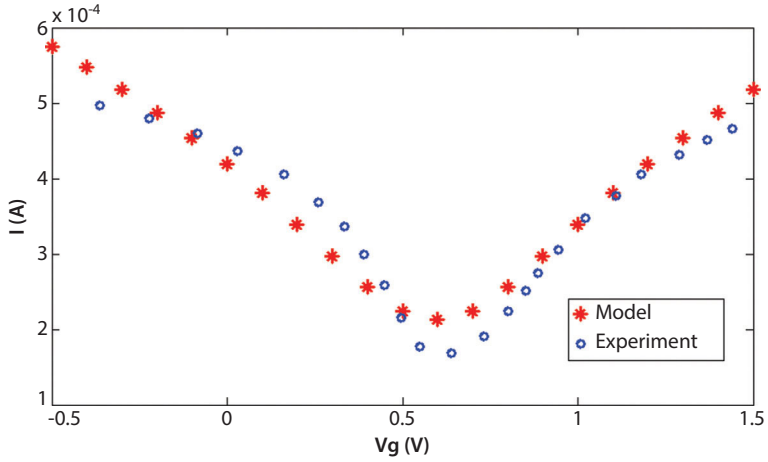

Figure 11.6 Comparison of the proposed numerical model (starred line) with experiment (circle line) for bare sensor.

concentration factor (F), i.e., V_g after hybridization is assumed as a function of DNA concentration and gate voltage without DNA molecules, as follows:

$$V_{gs(DNA)} = \frac{a(F)}{1} V_{gs(withoutDNA)} \tag{11.12}$$

In the nonsaturation region, the DNA concentration model is employed as a function of gate voltage, and the ideal current–voltage relation for the n-channel FET from Equations (11.11 and 11.12) is customized as

$$I_d = \frac{3q^2\left(3\pi a^3 t^3 k_{BT}\right)^{\frac{1}{2}}}{hL}\left[\Im_{-\frac{1}{2}}(\eta) + \Im_{-\frac{1}{2}}(-\eta)\right]\left(aV_{gs(withoutDNA)} - V_t\right) \tag{11.13}$$

where q is the electron charge, a = 1.42 Å defines carbon–carbon (C–C) bond length, t=2.7 (eV)is the nearest neighbor C–C tight binding overlap energy, K_B is the Boltzmann's constant, T represents temperature, h is Planck's constant, and L denotes the length of conducting channel. V_{gs} presents the gate-source voltage, and refers to the threshold voltage. Furthermore, $\Im_{-\frac{1}{2}}(\eta)$, and $\Im_{-\frac{1}{2}}(-\eta)$ are the FDIs of orders $-\frac{1}{2}$, which can be solved numerically. Its value depends on which measures the location of the Fermi level with respect to the conduction band edge. The Fermi–Dirac

distribution function has divergent manifestations in degenerate and non-degenerate states which are ascribed to ($\eta >> 0$) each.

In order to validate this hypothesis, the models of I_d–V_g properties of LGFET for DNA concentration altering from 0.01 to 500 nM are represented. The Fermi–Dirac distribution function has different forms in degenerate and non-degenerate states which are attributed by ($\eta >> 0$), respectively [71, 72]. α is a DNA immobilization factor, and different concentrations of DNA molecules are presented in the form of F parameter. Thus, the DNA molecules are adsorbed on graphene surface by iteration method was modeled as

$$\alpha = \left(aF^2 + bF + c\right)/F \tag{11.14}$$

A=13, B=50, and C=4070parameters are calculated based on iteration method. The current–voltage characteristic of LGFET according to the proposed model of DNA sensor using nanostructured graphene layer is obtained as

$$I_d = \frac{3q^2\left(3\pi a^3 t^3 k_{BT}\right)^{\frac{1}{2}}}{hL}\left[\Im_{-\frac{1}{2}}(\eta) + \Im_{\frac{1}{2}}(-\eta)\right]\left(\frac{13F^2 + 50F + 4070}{F}V_{gs(withoutDNA)} - V_t\right) \tag{11.15}$$

As discussed here, the drain source current of the LGFET as a function of gate voltage is simulated; moreover, DNA immobilization factor as a function of DNA concentration factor (F) is suggested. In order to

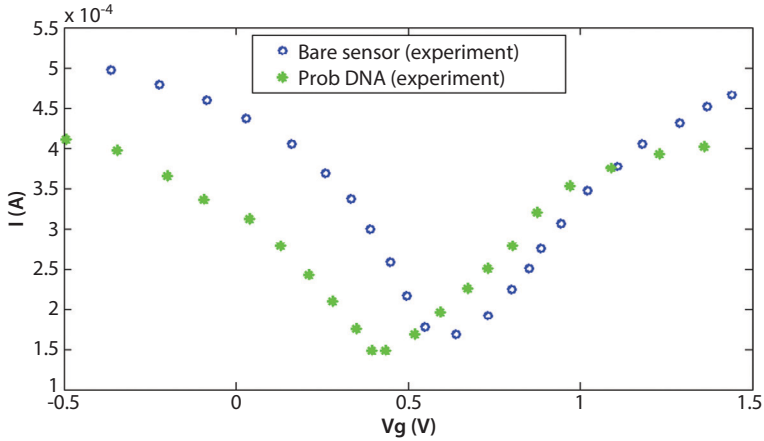

Figure 11.7 The current–voltage characteristic of graphene-based FET with the presence of probe DNAs (1 μM).

validate this hypothesis, the models of I_d–V_g properties of LGFET for DNA concentration altering from 0.01 to 500 nM are represented in Figure 11.7. The comparison of the experiment outcome with the theoretical modeling [73], it would be a legitimate statement that the sensor model based on the proposed parameters stipulates the directions that have been outlined by the data gathered from the experiments.

11.2.4 Comparison of the Proposed Numerical Model with Experiment

As shown in Figure 11.7, the suggested model indicates the cogent concentration reliance on current–voltage property, displaying the influence of the concentration increment effect on the minimum voltage conductance. Meaning that, the $V_{g,min}$, as mentioned in the data gathered from the experiments, will be moved towards left and the quantity of movement escalates with the growing concentration of the harmonious DNA from 0.01 to 10 nM as stated by experimental results [73]. Figures 11.9 and 11.10 describe the I_d–V_g characteristic of the proposed numerical model with the experimental data for different concentrations of complementary DNA. As shown in Figures 10a-c that each diagram depicts specific concentration of DNA molecules as F=0.01 nM, F=0.1 nM, and F=10 nM, respectively.

Another observation made in the experiment is that, the variation of, I_d–V_g property is a result of DNA concentration made possible by the DNA immobilization factor (Figure 11.10). Furthermore, the proposed model presents strongly approximate results compared with experimental data. According to Figures 11.10a and b, the amount of $V_{g,min}$ shift remains unchanged by increasing the DNA concentration from 10 to 500nM, holding the fact that the number of DNA molecules is limited and the graphene surface has become saturated. The electron transfer from DNA molecules (electron rich) to graphene have been explored experimentally in Ref. [51]. Also, as shown in Figure 11.9a and b, each diagram depicts specific concentration of DNA molecules. For example, when concentration value is F=100 nM, the model is closer to the blue line; in the same manner we can compare other concentrations as well (Figure11.11).

The proposed numerical model with coupled with experimental data is shown in this work to confirm that the conductivity of the graphene-based DNA sensor is decreased by the introduction of DNA molecules.

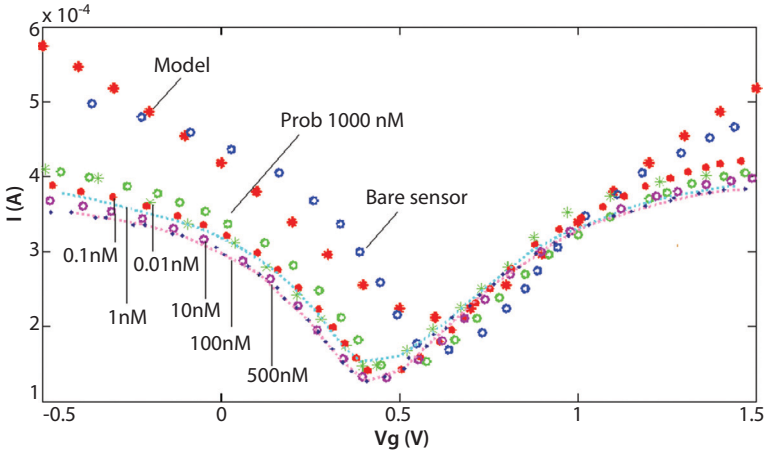

Figure 11.8 The current–voltage characteristic of LGFET applied to different concentration of DNA molecules (0.01–500 nM).

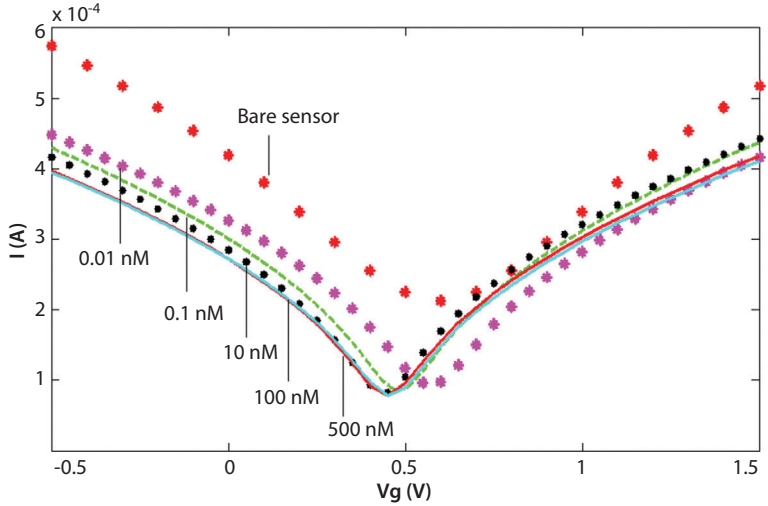

Figure 11.9 All numerical models of I_d–V_g characteristics altering from 0.01 to 500 nM.

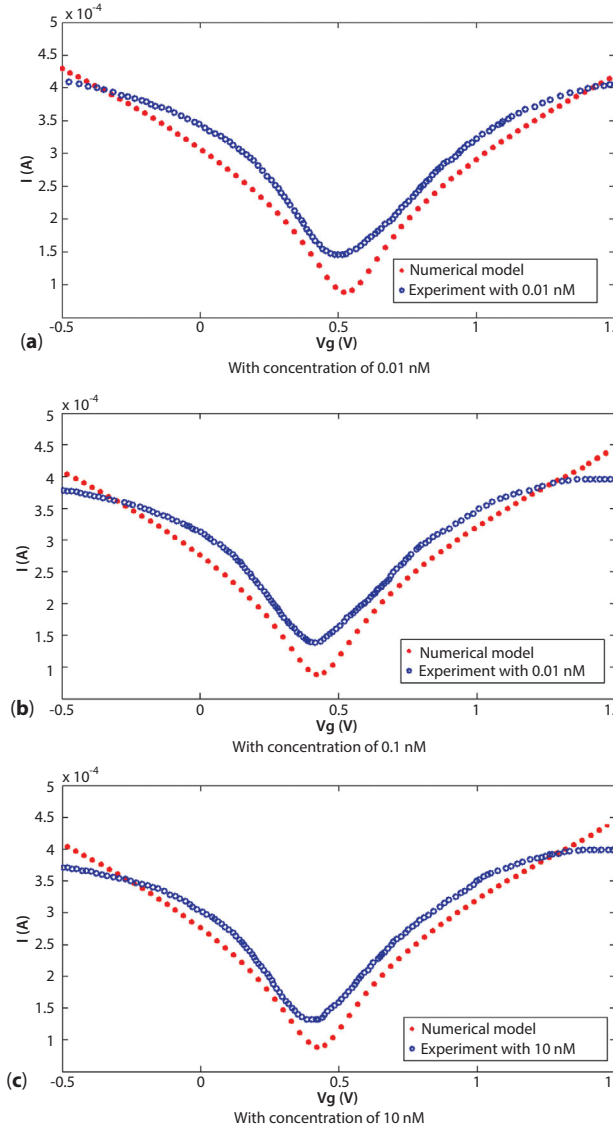

Figure 11.10 The I_d–V_g characteristic of the proposed alpha model comparing with the extracted experimental data for the specific DNA concentration of (a) F=0. 01 nM, (b) F=0. 1 nM, and (c) F=10 nM.

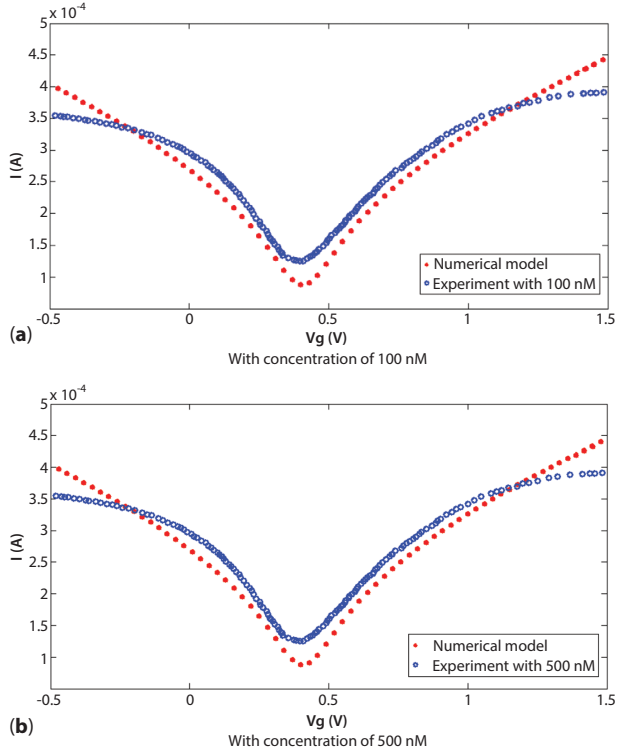

Figure 11.11 The I_d–V_g characteristics of the proposed alpha model with the experimental data for DNA concentration of (a) F=100 nM and (b) F=500 nM.

References

1. A. Star, *et al.*, "Label-free detection of DNA hybridization using carbon nanotube network field-effect transistors," *Proceedings of the National Academy of Sciences of the United States of America,* vol. 103, p. 921, 2006.
2. D. Fu and L. J. Li, "Label-free electrical detection of DNA hybridization using carbon nanotubes and graphene," *Nano Reviews,* vol. 1, 2010.
3. N. Mohanty and V. Berry, "Graphene-based single-bacterium resolution biodevice and DNA transistor: interfacing graphene derivatives with nanoscale and microscale biocomponents," *Nano Letters,* vol. 8, pp. 4469–4476, 2008.
4. A. Reina, *et al.*, "Large area, few-layer graphene films on arbitrary substrates by chemical vapor deposition," *Nano Letters,* vol. 9, pp. 30–35, 2008.

5. Y. Wen, *et al.*, "A graphene-based fluorescent nanoprobe for silver (I) ions detection by using graphene oxide and a silver-specific oligonucleotide," *Chemical Communications,* vol. 46, pp. 2596–2598, 2010.
6. K. S. Novoselov, *et al.*, "Electric field effect in atomically thin carbon films," *Science,* vol. 306, pp. 666–669, 2004.
7. K. S. Novoselov, *et al.*, "Two-dimensional atomic crystals," *Proceedings of the National Academy of Sciences of the United States of America,* vol. 102, pp. 10451–10453, 2005.
8. R. Grassi, *et al.*, "Graphene nanoribbons FETs for high-performance logic applications: perspectives and challenges," *9th International Conference on Solid-State and Integrated-Circuit Technology,* vol. 1, pp. 365–368, 2008.
9. G. C. Liang, *et al.*, "Performance projections for ballistic graphene nanoribbon field-effect transistors," *IEEE Transactions on Electron Devices,* vol. 54, pp. 677–682, 2007.
10. K. I. Bolotin, *et al.*, "Ultrahigh electron mobility in suspended graphene," *Solid State Communications* vol. 146, pp. 351–355, 2008.
11. K. S. Novoselov, *et al.*, "Electric field effect in atomically thin carbon films," *Science,* vol. 306, pp. 666–669, 2004.
12. F. Schedin, *et al.*, "Detection of individual gas molecules adsorbed on graphene," *Nature Materials,* vol. 6, pp. 652–655, 2007.
13. K. Welsher, *et al.*, "Selective probing and imaging of cells with single walled carbon nanotubes as near-infrared fluorescent molecules," *Nano Letters,* vol. 8, pp. 586–590, 2008.
14. Y. Shi, *et al.*, "Effective doping of single-layer graphene from underlying SiO_2 substrates," *Physical Review B,* vol. 79, p. 115402, 2009.
15. J. Kong, *et al.*, "Nanotube molecular wires as chemical sensors," *Science,* vol. 287, p. 622, 2000.
16. P. G. Collins, *et al.*, "Extreme oxygen sensitivity of electronic properties of carbon nanotubes," *Science,* vol. 287, p. 1801, 2000.
17. E. Snow, *et al.*, "Chemical detection with a single-walled carbon nanotube capacitor," *Science,* vol. 307, p. 1942, 2005.
18. Y. B. Shi, *et al.*, "Binary channel SAW mustard gas sensor based on PdPc(0.3) PANI(0.7)hybrid sensitive film," in *4th International Symposium on Instrumentation Science and Technology*. vol. 48, J. Tan, ed., 2006, pp. 292–297.
19. T. Wehling, *et al.*, "Molecular doping of graphene," *Nano Letters,* vol. 8, pp. 173–177, 2008.
20. X. Dong, *et al.*, "Doping single-layer graphene with aromatic molecules," *Small,* vol. 5, pp. 1422–1426, 2009.
21. M. Zheng, *et al.*, "DNA-assisted dispersion and separation of carbon nanotubes," *Nature Material,* vol. 2, pp. 338–342, 2003.
22. F. Schwierz, "Graphene transistors," *Nature Nanotechnology,* vol. 5, pp. 487–496, 2010.
23. Y.-J. Kang, *et al.*, "Electronic structure of graphene and doping effect on SiO_2," *Physical Review B,* vol. 78, p. 115404, 2008.

24. Y.-W. Son, *et al.*, "Energy Gaps in Graphene Nanoribbons," *Physical Review Letters,* vol. 97, p. 216803, 2006.
25. W. Zhang, *et al.*, "Opening an electrical band gap of bilayer graphene with molecular doping," *ACS Nano,* vol. 5, pp. 7517–7524, 2011.
26. Y. Zhang, *et al.*, "Direct observation of a widely tunable bandgap in bilayer graphene," *Nature,* vol. 459, pp. 820–823, 2009.
27. V. Ryzhii, *et al.*, "Device model for graphene bilayer field-effect transistor," *Journal of Applied Physics,* vol. 105, p. 4510, 2009.
28. Y. Ouyang, *et al.*, "Analysis of ballistic monolayer and bilayer graphene field-effect transistors," *Applied Physics Letters,* vol. 92, p. 063120, 2008.
29. C. Mastrangelo, "DNA analysis systems on a chip," *Advances in Science and Technology,* vol. 26, pp. 465–476, 1999.
30. M. W. Shinwari, "Static and dynamic modeling of DNA biosensors for biomedical applications," 2011.
31. K. S. Novoselov, *et al.*, "Two-dimensional gas of massless Dirac fermions in graphene," *Nature,* vol. 438, pp. 197–200, 2005.
32. N. Varghese, *et al.*, "Binding of DNA nucleobases and nucleosides with graphene," *Chemphyschem,* vol. 10, pp. 206–210, 2009.
33. L. X. Dong and Q. Chen, "Properties, synthesis, and characterization of graphene," *Frontiers of Materials Science in China,* vol. 4, pp. 45–51, 2010.
34. T. G. Drummond, *et al.*, "Electrochemical DNA sensors," *Nature biotechnology,* vol. 21, pp. 1192–1199, 2003.
35. Y. Huang, *et al.*, "Graphene-based biosensors for detection of bacteria and their metabolic activities," *Journal of Materials Chemistry,* vol. 21, pp. 12358–12362, 2011.
36. K. Novoselov, *et al.*, "Electric field effect in atomically thin carbon films," *Science,* vol. 306, p. 666, 2004.
37. F. Karimi, *et al.*, "Analytical modeling of graphene-based DNA sensor," *Science of Advanced Materials,* vol. 4, pp. 1142–1147, 2012.
38. K. Xu, *et al.*, "Graphene-based FET structure: modeling FET characteristics for an aptamer-based analyte sensor," in *Computational Electronics (IWCE), 2012 15th International Workshop on*, pp. 1–4, 2012.
39. D. Chen, *et al.*, "Graphene-based materials in electrochemistry," *Chemical Society Reviews,* vol. 39, pp. 3157–3180, 2010.
40. H. K. F. Abadi, *et al.*, "Semi analytical modeling of quantum capacitance of graphene-based ion sensitive field effect transistor," *Journal of Computational and Theoretical Nanoscience,* vol. 11, pp. 596–600, 2014.
41. H. Karimi, *et al.*, "Analytical prediction of liquid-gated graphene nanoscroll biosensor performance," *RSC Advances,* vol. 4, pp. 16153–16162, 2014.
42. L.-J. Wang, *et al.*, "A graphene quantum dot with a single electron transistor as an integrated charge sensor," *Applied Physics Letters,* vol. 97, 262113, 2010.
43. X. Dong, *et al.*, "Synthesis and application of graphene nanoribbons," *Current Physical Chemistry,* vol. 3, pp. 291–301, 2013.

44. J. Nilsson, *et al.*, "Transmission through a biased graphene bilayer barrier," *Physical Review B (Condensed Matter and Materials Physics),* vol. 76, pp. 165416-10, 2007.
45. M. Dankerl, *et al.*, "Graphene solution-gated field-effect transistor array for sensing applications," *Advanced Functional Materials,* vol. 20, pp. 3117–3124, 2010.
46. D. S. L. Abergel, *et al.*, "Properties of graphene: a theoretical perspective," *Advances in Physics,* vol. 59, pp. 261–482, 2010.
47. T. Cohen-Karni, *et al.*, "Graphene and nanowire transistors for cellular interfaces and electrical recording," *Nano Letters,* vol. 10, pp. 1098–1102, 2010.
48. J. Choi, *et al.*, "Graphene used for device and graphene sheet, comprises etched edge portion comprising functional group of carbonyl, carboxy, hydroxy, formyl and/or oxycarbonyl," US2010178464-A1; KR2010083954-A.
49. A. Reina, *et al.*, "Growth of large-area single-and bi-layer graphene by controlled carbon precipitation on polycrystalline Ni surfaces," *Nano Research,* vol. 2, pp. 509-516, 2009.
50. C.-A. Di, *et al.*, "Interface engineering: an effective approach toward high-performance organic field-effect transistors," *Accounts of Chemical Research,* vol. 42, pp. 1573–1583, 2009.
51. X. Dong, *et al.*, "Electrical detection of DNA hybridization with single-base specificity using transistors based on CVD-grown graphene sheets," *Advanced Materials,* vol. 22, pp. 1649, 2010.
52. A. T. Johnson Jr, *et al.*, "Single walled carbon nanotubes functionally adsorbed to biopolymers for use as chemical sensors," ed: Google Patents, 2011.
53. R. Tel-Vered, *et al.*, "Biohybrid electrochemical devices," *Electrochemistry of Functional Supramolecular Systems,* vol. 6, p. 333, 2010.
54. J. H. Chen, *et al.*, "Charged-impurity scattering in graphene," *Nature Physics,* vol. 4, pp. 377–381, 2008.
55. X. Dong, *et al.*, "Electrical detection of DNA hybridization with single-base specificity using transistors based on CVD-grown graphene sheets," *Advanced Materials,* vol. 22, pp. 1649–1653, 2010.
56. W. Wang and S. He, "Theoretical analysis on response mechanism of polymer-coated chemical sensor based Love wave in viscoelastic media," *Sensors and Actuators B-Chemical,* vol. 138, pp. 432–440, 2009.
57. D. Erickson, *et al.*, "Modeling of DNA hybridization kinetics for spatially resolved biochips," *Analytical Biochemistry,* vol. 317, pp. 186–200, 2003.
58. Y. Wu and P. A. Childs, "Conductance of graphene nanoribbon junctions and the tight binding model," *Nanoscale Research Letters,* vol. 6, 1–5, 2011.
59. A. F. Avila, *et al.*, "Hybrid nanocomposites for mid-range ballistic protection," *International Journal of Impact Engineering,* vol. 38, pp. 669–676, 2011.
60. S. Datta, *Electronic Transport in Mesoscopic Systems*. Cambridge, UK: Cambridge University Press, 2002.

61. B. Polash and H. F. Huq, "Analytical model of carbon nanotube field effect transistors for NEMS applications," *2008 51st Midwest Symposium on Circuits and Systems,* Vols. 1 and 2, pp. 61–64, 2008.
62. M. T. Ahmadi, *et al.*, "Numerical study of Fermi energy for P-type silicon nanowire," *Nanoscience and Nanotechnology,* vol. 1136, pp. 98–102, 2009.
63. J. Karamdel, *et al.*, "Formulation and simulation for electrical properties of a (5,3) single wall carbon nanotube," *ICSE: 2008 IEEE International Conference on Semiconductor Electronics, Proceedings,* pp. 545–548, 2008.
64. N. Peres, *et al.*, "Conductance quantization in mesoscopic graphene," *Physical Review B,* vol. 73, p. 195411, 2006.
65. D. Gunlycke, *et al.*, "Semiconducting graphene nanostrips with edge disorder," *Applied Physics Letters,* vol. 90, p. 142104, 2007.
66. R. B. Dingle and R. Dingle, *Asymptotic expansions: their derivation and interpretation*. London: Academic Press, 1973.
67. J. Zaharah, *et al.*, "Modelling of graphene nanoribbon Fermi energy," *Journal of Nanomaterials,* vol. 2010, 14, 2010.
68. M. Passlack, "III-V Metal-oxide-semiconductor technology," *2008 IEEE 20th International Conference on Indium Phosphide and Related Materials (IPRM),* 59, 2008.
69. Z. Liu, *et al.*, "PEGylated nanographene oxide for delivery of water-insoluble cancer drugs," *Journal of the American Chemical Society,* vol. 130, pp. 10876–10877, 2008.
70. S. Manohar, *et al.*, "Peeling single-stranded DNA from graphite surface to determine oligonucleotide binding energy by force spectroscopy," *Nano Letters,* vol. 8, pp. 4365–4372, 2008.
71. M. J. Kiani, *et al.*, "Analytical modelling of monolayer graphene-based ion-sensitive FET to pH changes," *Nanoscale Research Letters,* vol. 8, pp. 1–9, 2013.
72. H. K. F. Abadi, *et al.*, "Current–voltage modeling of graphene-based DNA sensor," *Neural Computing and Applications,* 24(1), 85–89, 2014
73. N. Varghese, *et al.*, "Binding of DNA nucleobases and nucleosides with graphene," *ChemPhysChem,* vol. 10, pp. 206–210, 2009.

12

Carbon Nanotubes and Cellulose Acetate Composite for Biomolecular Sensing

Padmaker Pandey[1], Anamika Pandey[1], O. P. Pandey[2], and N. K. Shukla*[1]

[1]Department of Chemistry, Mahatma Gandhi P. G. College, Gorakhpur, India
[2]Department of Chemistry, D. D. U. Gorakhpur University, Gorakhpur, India

Abstract

In this chapter we present general instructions for the preparations of CNTs-mixed cellulose acetate (CA)-based membranous support for the potentiometric biosensing of glucose. The data obtained by measurements with CA membrane and CNTs-mixed CA membranous supports, respectively, that the CNTs-mixed CA membrane assures superior performances of the biosensor for low glucose concentrations determination. The results were also supported by the decrease in pH value at similar concentrations of glucose solution used.

The diffusion through the CNTs-mixed CA membrane support was enhanced to a larger extent and the enzymatic reaction was starting immediately than with CA membrane alone. This leads to a significant decrease of the response time of the biosensor with CNTs-mixed CA membrane. The general concept of this body of work is to open a new area of enzyme immobilisation and its supported membrane technique in the fabrication of potentiometric biosensor. In the future, efforts will need to be directed towards the development of biosensor with eco-friendly substances and advanced materials.

Keywords: Cellulose acetate, carbon nanotubes, glucose oxidase, glucose, glutaraldehyde, potentiometric biosensor

12.1 Introduction

Being an efficient component of nanotechnology, carbon nanotubes (CNTs) are tending to revolutionise maximum fields in science. Before ventilating

**Corresponding author*: drnkshukla@gmail.com

Ashutosh Tiwari, Hirak K. Patra and Anthony P.F. Turner (eds.) Advanced Bioelectronic Materials, (413–426)

into its application and property mainly its electrochemical property, it is very important and genuine too, to consider the basics of CNTs. CNTs are seamless cylinder of one or multiple layers of graphene sheets with open or closed end [1,2]. Depending upon the mode of carbon–carbon bonding, length, thickness and in the type of helicity and number of layers of graphene sheets there are many different structures of CNTs. Although they are formed from essentially the same graphene sheet, their electrical properties differ depending on these variations, acting either as metals or as semiconductors [3–5].

CNTs are divided into two classes single-walled CNT (SWNT) and multiwalled CNT (MWNT). SWNT as the name suggests consists of single layer of graphene sheet with diameter between 0.4 and 2 nm, whereas MWNTs are composed of multiple concentric layers of graphene sheets 0.34 nm apart and its final diameter is in between the range of 2 and 100 nm [6,7].

The different structures, morphologies and properties of CNTs depend on the method from which they are prepared and further processed. A wide variety of synthetic methods have been developed to synthesise CNTs of desired shape, size and properties that is fit for further scientific studies and for various technological applications. Arc electric discharge, laser ablation and chemical vapour deposition (CVD) are quintessential ways for the production of CNTs. Arc discharge and laser ablation are early process of CNT production. They allow the synthesis of single-walled nanotubes in large amount; both these methods rely on the condensation of carbon atom generated from evaporation of solid carbon source. Both the method arc discharge and laser ablation provides a good quality of CNTs with little defect. Nevertheless, the requirement and large amount of energy consumption of both the equipments make them less favourable for nanotube production. In spite of these, they usually produce highly entangled CNTs bundle which are difficult to manipulate in order to assemble for building an addressable structure. The third last method based on CVD has been emerged as widely accepted method for producing CNTs in recent year. This method uses thermal decomposition of liquid or gas phase carbon source such as carbon mono oxide or hydrocarbons (CH_4, C_2H_4) catalysed by metallic particle. The growing interest in the CVD process lies on greater possibilities of this method for successful synthesis of well separated individual SWNTs and also aligned SWNTs or MWNTs with more controlled diameter and length. It has also the advantage of being the only technique that allows synthesis of CNT directly on a substrate or wafer, thus facilitating device integration [8,9].

Due to the nano structural properties of CNT, it has appeared as wonder material of this new era of nanotechnology. There is no any field remains

untouched by this overriding material. It has a huge range of unexplored potential applications in various technological areas such as aerospace, energy, automobile, medicine or chemical industry, in which they can be used as gas adsorbents, templates, actuators, composite reinforcements, catalysts supports, probes, chemical sensors, nano pipes, nano-reactors, etc. [10].

Most importantly, CNTs hold a lot of potential for medical applications due to its small dimension**.** The practical uses of CNTs in biomedical include their use as channels for biosensors, delivery of drugs, and sheathe for enzymes and transfection of DNA [11,12]. Within this new field of nanotechnology, the area of biosensor is the most developed and the one which has the highest potential. Biosensor based on electrochemical principles stand out due to their marked advantage in terms of simplicity, robust and low cost. These sensors are becoming very attractive for rapid and simple diagnosis in clinical, non-clinical, and environmental research. Among all platforms with the interest for biosensor CNT composites are presenting as a groundbreaking material that offers novel possibilities in biosensing approach.

There are many CNTs composites employed for biosensing of different biomolecules in biological samples. But among all, glucose biosensor has its own valuable space in biosensor field. Glucose biosensors alone account for about 85% of the entire biosensor market [13]. Glucose biosensors are so much important because it stands for most battling disease called diabetes mellitus. Diabetes mellitus is one of the commonest long-term disorders and is a chronic disease that has no cure. Despite of recent decrease in the rates of cardio vascular disease, it still remains as the most common cause of mortality in the whole world. It can only be reduced and controlled by regular tight monitoring of blood glucose level which can be only accompanied by a glucose biosensor.

There are various composites used in development of glucose biosensor they are SWNT and polypyrrole composites for amperometric glucose biosensor [14], MWNT zinc oxide composites for enzymatic glucose biosensor [15], studies of glucose oxidase (GOx)-immobilised MWNT polyaniline composites [16], glucose biosensor of platinum nanospheres connected by CNTs [17], glucose biosensor based on immobilisation of GOx in platinum nanoparticles/graphene/chitosan nanocomposite film [18], etc.

Keeping in view the above wide range of work anyone may easily conclude that CNTs are frequently used in composites for the development of different biosensors. This becomes possible only because of its excellent electrochemical properties. It has large length-to-diameter aspect ratios which provide high surface-to-volume ratios. Moreover, CNTs have an outstanding ability to mediate fast electron transfer kinetics for a wide

range of electroactive species [19–21]. Incorporation of functionalised CNTs in polymeric substances is preferred because of its easy solubility in them than the pristine form [22]. Chemical functionalisation of CNTs, makes them soluble and biocompatible, is helpful to attach any desired chemical species to them. Use of CNTs as a major component of biosensor has resulted into the development of novel biomaterials like functional polymers, sol–gel materials, and other such materials which have given an upsurge to the ongoing researches in this field.

12.2 Background of the Work

Nowadays, there is a little change in the fundamentals of glucose biosensor. The first blood glucose meter was not a biosensor. It was the Ames reflectance meter (ARM) (Miles Laboratories, Elkhart, IN, USA) based on a reflectometer. That ARM automatically assessed the colour change of enzyme-based reagent strips. That enzyme strips was Dextrostix introduced in 1971. It was the first blood glucose strip. Then, after a period of time ARM was succeeded by Ames eyestone. It can be concluded that medieval history of blood glucose meter was totally based on reflectometer [23,24].

The concept of biosensors came into light in 1962 with the pioneering work of Clark and Lyons of Cincinnati Children's Hospital. First glucose enzyme electrode relied on a thin layer of GOx entrapped over an oxygen electrode via a semipermeable dialysis membrane. The first enzyme-based glucose sensor commenced by Updike and Hicks in 1967. In 1979, the first glucose analyser using biomolecule for the detection of blood glucose was commercialised by Yellow Springs Instruments Co., USA [24–26]. All the aforementioned biosensors represent the first-generation glucose biosensor. The first-generation glucose biosensor used natural oxygen as substrate and measured hydrogen peroxide produced. The amperometric measurement of hydrogen peroxide required a high operation potential for high selectivity which was the main disadvantage of this biosensor. These drawbacks of first-generation glucose biosensor were overcome by second-generation glucose biosensors. Introduction of non-physiological electron acceptor instead of oxygen removed the limitations of this biosensor. These non-physiological electron acceptors were able to conduct electron from enzyme to the surface of working electrode. The various electron mediators are ferrocene, ferricyanide, quinines, tetrathialfulvalene (TTF) and tetracyanoquinodimethane (TCNQ). The third-generation glucose biosensor was reagentless and was based on direct transfer of electron between the enzyme and the electrode without mediators. We are continuing with this third-generation glucose biosensor.

An extensive research is being done on the various aspects for the development of an efficient glucose biosensor using different techniques like amperometry, potentiometry and impedimetry or conductometry. These electrochemical techniques show lower detection limit, faster response time, better long-term stability and inexpensiveness because of their unbeaten sensitivity and selectivity. The most important thing is that the electrodes can sense the materials which are present over the host without doing any damage to the host system.

In the present study, we have characterised a suitable membranous support for the development of a pH-based potentiometric glucose biosensor. It is very challenging to choose an appropriate membranous support because all the prerequisite and desired features for an efficient and successful glucose biosensor only depend on it. It is the target reason for a biosensor to being on top among other rivals in sprinter.

For the accomplishment of and giving a successful vision to an endeavoured task, there are various hurdles which we have to cross one by one. The first and the foremost part of this work is the selection and preparation of a suitable membranous support. Various conducting polymeric membranes are there which can be used as a membranous support. In the present work, we have used cellulose acetate (CA) membrane, an eco-friendly polymeric material as a membranous support. Cellulose acetate is generally recognised as biodegradable polymer within the scientific community, although CA membrane shows low chemical, mechanical, and thermal resistance. It is not affected by mineral acid but is sensitive towards oxidising agent except hypochlorite and peroxide solution [27]. In the present work, we have prepared two different membranes CA membrane and SWNTs-mixed CA membrane (CA-CNT). The second most important step is immobilisation of an oxidoreductase GOx enzyme over the membrane. Enzyme that are physically confined or localised with retention of their catalytic activity is known as immobilised enzyme. The immobilisation of enzyme is a crucial step which is done by either of the methods known like adsorption, covalent binding, cross-linking and entrapment.

The term immobilised enzyme was adopted in 1971 at the first Enzyme Conference [28]. An immobilised molecule is one whose movement in space has been restricted either completely or to a small limited region [29]. The cardinal needs and targeted point that can be reached through immobilisation are the repetitive use of enzyme about 10 times which affects the cost of enzyme in a colossal manner and also in enhancement of enzyme stability against pH, temperature, solvents, contaminants and impurities.

Adsorption is a very simple and old method of immobilisation. This method is simply placing of aqueous enzyme solution in contact with solid

support for a fixed span of time and enzyme gets attached to membranous support either by van der Walls' forces, ionic bonding, hydrogen bonding or by hydrophobic interactions. The main disadvantage of this method is that enzyme gets easily desorbed by the factors like change in temperature, pressure or concentration.

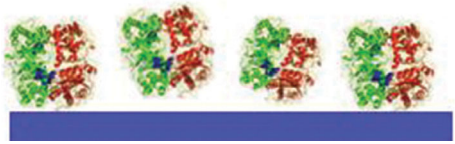

Adsorption

Entrapment is the method based on the localisation of enzyme in the lattice of the support material like a natural or synthetic polymer matrice, a gel like structure, natural or polymer fibre and does not contain a direct link between the matrice and the enzyme. This method is mainly used for the immobilisation of microbial, animal and plant cells in which calcium alginate is widely used.

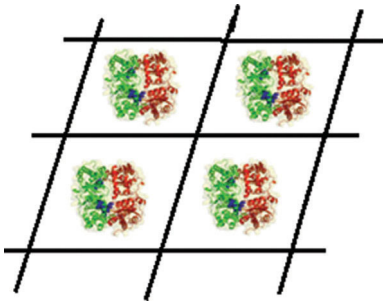

Entrapment

Covalent binding is the method in which the enzyme is linked to the support through the functional groups in the enzyme which are not essential for catalytic activity through covalent bond.

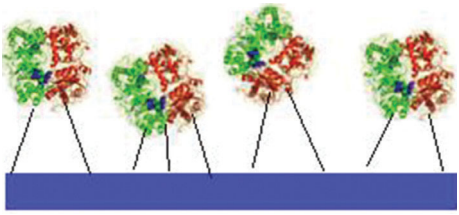

Covalent binding

The method of cross-linking is an extended form of covalent binding. In this method a bifunctional or polyfunctional coupling agent, i.e. cross-linker is used which provides an intermolecular binding to enzyme and membranous support. This intermolecular binding provides a better

attachment and proper interaction between the two. Common coupling agents that may be used for this purpose are glutaraldehyde, bisisocyanate derivative, bisbenzidine derivative and succinyldisalicylate. Glutaraldehyde which exists in various isomeric forms is used as cross-linker in the present work. It is a homobifunctional reagent, and it works in ambient conditions and in wide range of pH. It is expected that with one functional end glutaraldehyde couple with functional moiety present in membranous support and with other end it binds the functional group of enzyme. The exact mechanism of immobilisation via glutaraldehyde is yet in debate [28–32].

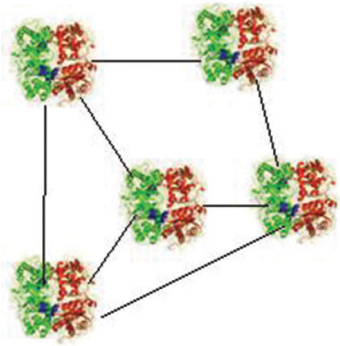

Crosslinking

In last, pH measurement is carried out using CA and cellulose acetate carbon nanotubes (CA-CNT) membrane un-immobilised and immobilised followed by comparison of the activity of all the four membranes in terms of increase or decrease in pH, sensitivity and data reproducibility to obtain the benign host for the pH based potentiometric glucose biosensor.

12.3 Materials and Methodology

Cellulose acetate, CNTs, glutaraldehyde, glucose, sodium dihydrogen phosphate, disodium hydrogen phosphate, sodium chloride, acetone and GOx were all purchased from Sigma Aldrich.

12.3.1 Preparation of Membranes

For the preparation of CA membrane, 0.15 gm of cellulose acetate powder was dissolved in 10 ml of acetone. For the preparation of CNTs composite, 10 µl of acid-functionalised CNT was added in the above solution. The solution was stirred continuously for 3–4 hours. Further, the solution was spread over three glass petriplates of 7 cm diameter in equal amount and kept overnight for drying at room temperature. The membranes were

removed from petriplates by using deionized (DI) water. It was stored between filter paper and kept pressed to avoid any wrinkles.

12.3.2 Immobilisation of Enzyme

For immobilisation of enzyme, both the CA and CA-CNT membranes were activated by introduction of cross-linker 30 µl 1% glutaraldehyde solution prepared in 1 M PBS, 100 µl enzymatic solution of GOx (500U GOx) were deposited over activated membranes. The membranes were further stored at 4°C.

12.3.3 Assay for Measurement of Enzymatic Reaction

The potentiometric detection of glucose is based on the measurement of change in pH due to the presence of enzymatic layer on the surface of pH electrode. The decrease in pH is due to the formation of gluconic acid produced by the enzymatic reaction of glucose and GOx.

$$\text{Glucose} + O_2 \xrightarrow{\text{GOx}} \text{Gluconic Acid} + H_2O_2$$

The potentiometric measurements were carried out with the help of pH meter using a two-electrode electrochemical cell system. The bioactive un-immobilised and immobilised membranes were fixed on the cylindrical tube. The glass electrode was placed in contact with the membrane with the help of a clamp which acted as working electrode. Another electrode, which is reference electrode, was placed inside the glucose solution prepared in 1 M PBS. The working electrode along with reference electrode (Ag/AgCl) was connected with pH meter. Working solution consist of different concentration of glucose (10^{-1}, 10^{-2}, 10^{-3}, 10^{-4}, 10^{-5} M) prepared in 1 M PBS, pH 7.2. The experimental set-up is shown in Figure 12.1.

12.4 Characterisation of Membranes

To study the morphology of pristine polymeric membrane and to assess the change occurred by the addition of acid functionalised CNTs, the different membranes (un-immobilised and immobilised) were examined by optical microscopy and scanning electron microscopy.

12.4.1 Optical Microscope Characterisation

Figure 12.2a shows optical micrograph of pristine CA membrane. Figure 12.2b shows appearance of SWNTs spreaded within the CA

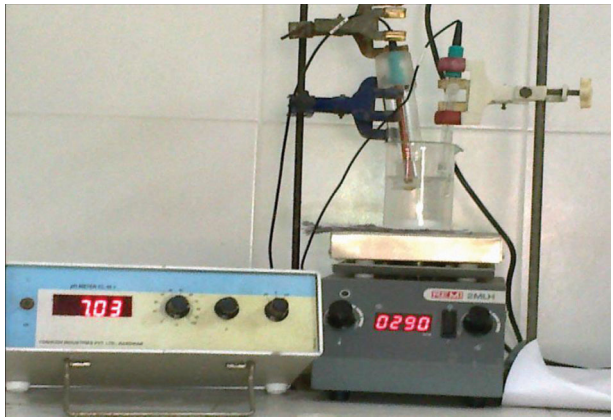

Figure 12.1 Experimental set-up.

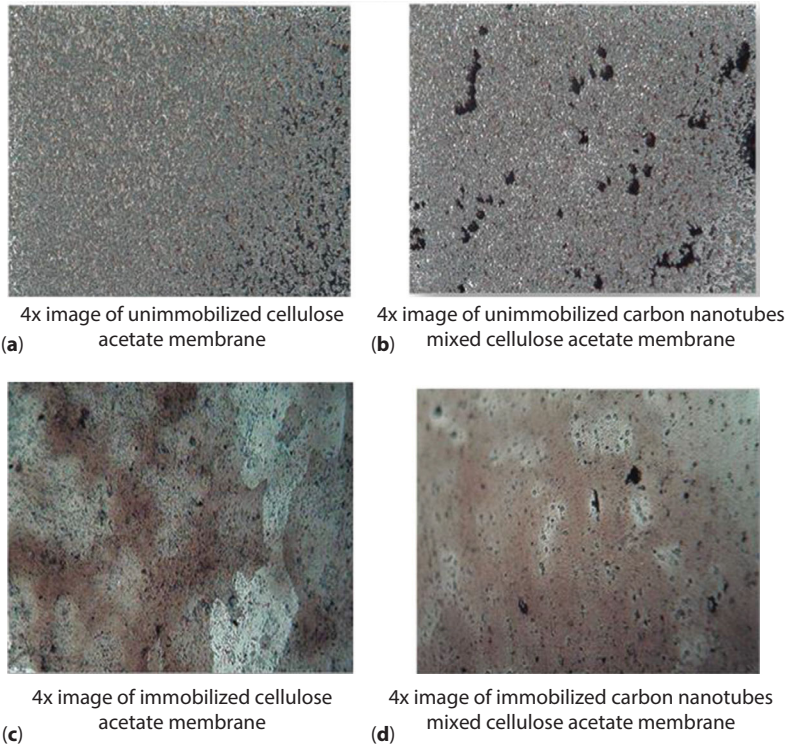

Figure 12.2 (a) 4× Image of un-immobilised cellulose acetate membrane, (b) 4× image of un-immobilised carbon nanotubes mixed cellulose acetate membrane, (c) 4× image of immobilised cellulose acetate membrane and (d) 4× image of immobilised carbon nanotubes mixed cellulose acetate membrane.

membrane matrix. Figure 12.2c and 12.2d shows a matted appearance of GOx enzyme appearing on the membrane matrix.

12.4.2 Scanning Electron Microscope Characterisation

The morphology of GOx un-immobilised and immobilised membranes were furthur characterised by using a LEO 430 scanning electron microscope (SEM), operating at EHT 15.00 kV with secondary electrons, in high vaccum mode. The scanning electron micrograph 12.3a and 12.3b of un-immobilised CA membrane and CA-CNT membrane show that the surface morphology of both the membranes is macro-porous (with the pore size 1.09 μm for cellulose aceate and 1.88 μm for celulose acetate CNT-mixed membrane), uniform with granular-like structure, which is suitable for immobilisation of biomolecule. The images show that the size of pore of the CA membrane is increased with the addition of carbon naotubes.

Figure 12.3c and d shows the surface topography of immobilised CA membrane and CNT-mixed CA membrane respectively. From Figure 12.3c, it is clear that GOx is spread allover the membrane surface in small circular form where as in Figure 12.3d immobilised GOx is spread uniformly in the form of interconnected bristle which is fit over the pore of membrane which was measured as 1.88 μm using bare CA-CNT membrane.

12.5 pH Measurements Using Different Membranes

12.5.1 For Un-immobilised Membranes

When un-immobilised CA membrane was used for potentiometric measurement it was observed that the pH increased for all the range of concentrations. This is because the glucose solution permeates to the pH electrode through the membrane and as there is no enzyme available, therefore no chemical reaction occurs. The values become steady for each range of concentration after 60 minutes (Figure 12.4a). Similar results were obtained by un-immobilised CA-CNTs-mixed membrane. Due to the electrochemical properties of CNTs, a remarkable increase in pH was observed (Figure 12.4b).

12.5.2 For Immobilised Membranes

When GOx-immobilised CA membrane (CA/GOx) and GOx-immobilised CNTs-mixed CA membrane (CA-CNT/GOx) were used for potentiometric

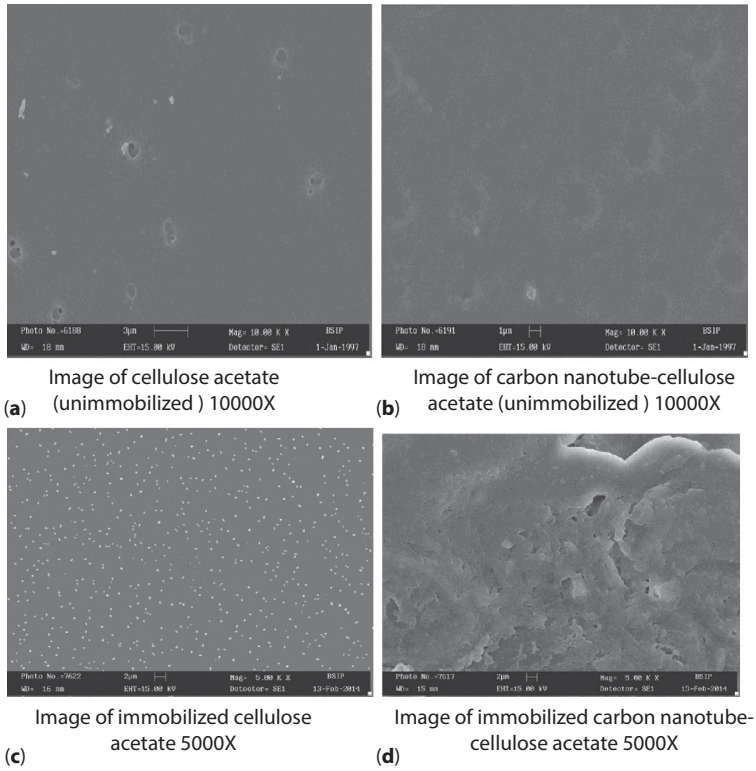

Figure 12.3 (a) Image of cellulose acetate (un-immobilised) 10000×, (b) image of carbon nanotube–cellulose acetate (un-immobilised) 10000×, (c) image of immobilised cellulose acetate 5000× and (d) image of immobilised carbon nanotube–cellulose acetate 5000×.

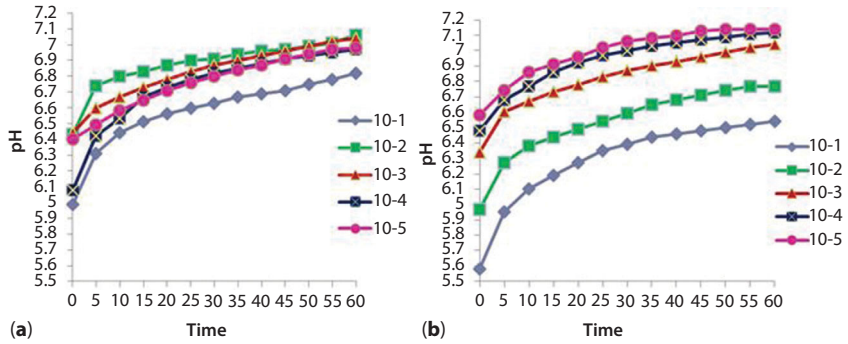

Figure 12.4 (a) pH versus time graph using un-immobilised cellulose acetate membrane and (b) pH versus time graph using un-immobilised carbon nanotubes mixed cellulose acetate membrane.

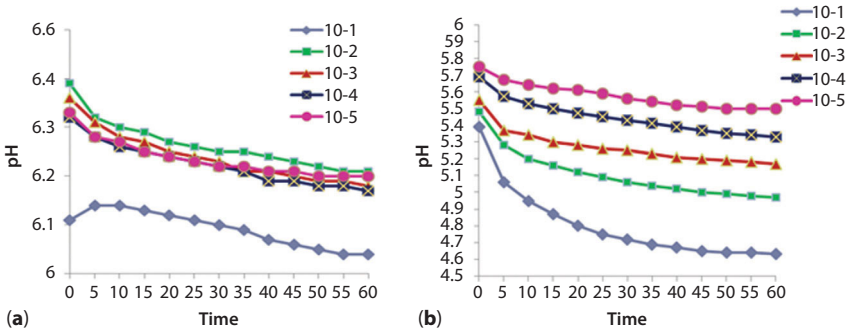

Figure 12.5 (a) pH versus time graph using immobilised cellulose acetate membrane and (b) pH versus time graph using immobilised carbon nanotubes mixed cellulose acetate membrane.

measurement a gradual decrease in pH was observed (Figure 12.5 a and b). This is due to the formation of gluconic acid by the reaction between analyte glucose solution and substrate immobilised GOx. The decrease in pH with the immobilised CA-CNT membrane is more than immobilised CA membrane alone. The reason for biosensor, CA-CNT/GOx matrix to exhibit a higher glucose response over CA/GOx matrix is due to the larger pore diameter in the former, which is in agreement with the data obtained through SEM. CNT plays dual role firstly by increasing the pore size which in turn increases the surface area that is compatible for enzyme immobilisation. Secondly, it facilitates enhanced electron transfer between enzyme and pH electrode.

12.6 Conclusion

The present work was carried out with a view to characterise CA and CA-CNTs-mixed membrane as a suitable support for enzyme immobilisation. The results obtained show that CNTs-mixed CA membrane proved to be a benign host for the immobilisation of GOX. The morphology of the membrane obtained through optical micrograph and SEM images also assured the immobilisation of enzyme. The CA-CNTs-mixed membrane is capable to sense the lower range of glucose concentration, i.e. up to 10^{-5} M. Hence, the novel membranous support system will become a leader that will be ready to lend a hand in the development of a rapid, economical and eco-friendly biosensor.

Reference

1. Michael F. L. De Volder, Sameh H. Tawfick, Ray H. Baughman, and A. John Hart, "Carbon Nanotubes: Present and Future Application", *Science*, Vol. 339, p. 535, 2013.
2. P. J. F. Harris, "*Carbon Nanotube Science – Synthesis, Properties, and Applications*", Cambridge University Press, New York, 2009.
3. Morinobu Endo, Takuya Hayashi, and Yoong-Ahm Kim, "Development and Application of Carbon Nanotubes", *Pure Appl. Chem.*, Vol. 78, No. 9, p. 1703, 2006.
4. M. S. Dresselhaus, G. Dresselhaus, and P. C. Eklund (Eds.). "*Science of Fullerene and Carbon Nanotubes*", Academic Press, Tokyo, 1995.
5. R. Saito, G. Dresselhaus, and M. S. Dresselhaus (Eds.). "*Physical Properties of Carbon Nanotubes*", Imperial College Press, London, 1998.
6. S. Niyogi, M. A. Hamon, H. Hu, B. Zhao, P. Bhowmik, R. Sen, M. E. Itkis, and R. C. Haddon, "Chemistry of Single-Walled Carbon Nanotubes", *Acc. Chem. Res.*, Vol. 35, p. 1105, 2002.
7. Pulickel M. Ajayan and Otto Z. Zhou, "Applications of Carbon Nanotubes", *Topics Appl. Phys.*, Vol. 80, p. 391, 2001.
8. Muhammad Musaddique Ali Rafique, and Javed Iqbal, „Production of Carbon Nanotubes by Different Routes", *J. Encapsulation Adsorpt. Sci.*, Vol. 1, p. 29, 2011.
9. Andrea Szabó, Caterina Perri, Anita Csató, Girolamo Giordano, Danilo Vuono, and János B. Nagy, "Synthesis Methods of Carbon Nanotubes and Related Materials", *Materials*, Vol. 3, p. 3092, 2010.
10. G. Udupa, Shrikantha Rao, and K. V. Gangadharan, "Future Application of Carbon Nanotubes Reinforced Functionally Graded Composite Materials", *Adv. Eng. Sci. Manag.*, IEEE Conference Publications, pp. 399–404, 2012.
11. Geoffrey S. Simate and Clarence S. Yah, "The Use of Carbon Nanotubes in Medical Applications—Is It a Success Story?", *Occup. Med. Health Aff.*, Vol. 2(1), 2014.
12. A. R. Harutyunyan, B. K. Pradhan, G. U. Sumanasekera, E. Yu. Korobko, and A. A. Kuznetsov, "Carbon Nanotubes for Medical Applications", *Eur. Cells Mater.*, Vol. 3. Suppl. 2, p. 84, 2002.
13. Joseph Wang, "Electrochemical Glucose Biosensors", *Chem. Rev.*, Vol. 108, p. 814, 2008.
14. Matei Raicopol, Alina Prună, Celina Damian, and Luisa Pilan, "Functionalised Single-Walled Carbon Nanotubes/Polypyrrole Composites for Amperometric Glucose Biosensors", *Nanoscale Res. Lett.*, Vol. 8(1), p. 316, 2013.
15. Selvakumar Palanisamy, Srikanth Cheemalapati, and Shen-Ming Chen, "Enzymatic Glucose Biosensors based on Multiwalled Carbon Nanotubes-Zinc Oxide Composite", *Int. J. Electrochem. Sci.*, Vol. 7, No. 9, p. 8394, 2012.
16. Özlem Çolak, Halit Arslan, Hüseyin Zengin, and Gülay Zengin, "Amperometric Detection of Glucose by Polyaniline-Activated Carbon Composite Carbon Paste Electrode", *Int. J. Electrochem. Sci.*, Vol. 7, No. 8, p. 6988, 2012.

17. Jonathan C. Claussen, Sungwon S. Kim, Aeraj ul Haque, Mayra S. Artiles, Marshall Porterfield, and Timothy S. Fisher, "Electrochemical Glucose Biosensor of Platinum Nanosphere Connected by Carbon Nanotubes", *J. Diabetes Sci. Technol.*, Vol. 4(2), p. 312, 2010.
18. HongWua, Jun Wanga, Xinhuang Kanga, Chongmin Wanga, Donghai Wanga, Jun Liua, Ilhan A. Aksayb, and Yuehe Lin, "Glucose Biosensor Based on Immobilization of Glucose Oxidase in Platinum Nanoparticle/Graphene/Chitosan Nanocomposite Film", *Talanta*, Vol. 80(1), p. 403, 2009.
19. Kannan Balasubramanian and Marko Burghard, "Biosensors Based on Carbon Nanotubes", *Anal. Bioanal. Chem.*, Vol. 385, p. 452, 2006.
20. Archana Pandey, Abhishek Prasad, Jason Moscatello, and Yoke Khin Yap, "Glucose Biosensor Based on Vertically-Aligned Multi-Walled Carbon Nanotubes", *Mater. Res. Soc. Symp. Proc.*, Vol. 1204, 181–186, 2010.
21. Anthony Guiseppi-Elie, Abdur Rub Abdur Rahman, and Nikhil K. Shukla, "SAM-Modified Microdisc Electrode Array (MDEAs) with Functionalised Carbon Nanotubes", *Electrochim. Acta*, Vol. 55, No. 14, p. 4247, 2010.
22. Matthew W. Marshall, Simina Popa-Nita, and Joseph G. Shapter, "Measurement of Functionalised Carbon Nanotubes Carboxylic Acid Groups Using a Simple Chemical Process", *Carbon*, Vol. 44, p. 1137, 2006.
23. N. S. Oliver, C. Toumazou, A. E. G. Cass, and D. G. Johnston, "Glucose Sensors: A Review of Current and Emerging Technology", *Diabetes Med.*, Vol. 26(3), pp. 197–210, 2009.
24. E.-H. Yoo and S.-Y. Lee, "Glucose Biosensors: An Overview of Use in Clinical Practice", *Sensors*, Vol. *10*, p. 4558, 2010.
25. Joseph Wang, "Glucose Biosensors: 40 Years Advances and Challenges", *Electroanalysis*, Vol. 13, No. 12, p. 983, 2001.
26. Steven J. Setford and Jeffrey D. Newman, "Enzyme Biosensors", *Microb. Enzymes Biotransform. Methods Biotechnol.*, Vol. 17, p. 29, 2005.
27. Juergen Puls, Steven A. Wilson, and Dirk Holter, "Degradation of Cellulose Acetate-Based Materials", *J. Polym. Environ.*, Vol. 19, No. 1, p. 152, 2011.
28. T. Tosa and T. Sato, "*Enzymes Immobilization Methods*", Wiley, Wiley Online Library, 2002.
29. Magdy M. M. Elnashar, "Immobilized Molecules Using Biomaterials and Nanobiotechnology", *J. Biomat. Nanobiotechnol.*, Vol. 1, No. 1, p. 61, 2010.
30. Wenshan Li, Liang Wang, and Rongrong Jiang, "Specific Enzyme Immobilization Approaches and Their Application with Nanomaterial", *Topics Catal.*, Vol. 55, Nos. 16–18, p. 1146, 2012.
31. M. D. Gouda, M. Thakur, and N. G. Karanth, "Stability Studies on Immobilised Glucose Oxidase Using an Amperometric Biosensor – Effect of Protein Based Stabilizing Agents", *Electroanalysis*, Vol. 13, No. 10, p. 849, 2001.
32. P. C. Ashly, "A Study on the Immobilization of Enzyme on Polymeric Support", Thesis, Cochin University, 2009.

13

Review of the Green Synthesis of Metal/Graphene Composites for Energy Conversion, Sensor, Environmental, and Bioelectronic Applications

Shude Liu[1], K.S. Hui*[2], and K.N. Hui*[1,3]

[1]*School of Materials Science and Engineering, Pusan National University, Republic of Korea*
[2]*Department of Mechanical Convergence Engineering, Hanyang University, Republic of Korea*
[3]*Institute of Applied Physics and Materials Engineering, Faculty of Science and Technology, University of Macau, Macao SAR, China*

Abstract

Green reduction has almost emerged as a separate branch in the synthesis of nanomaterial in terms of the urgent needs of energy saving and environment. In favor of constituting a green alternative to the use of hazardous chemicals in the production of graphene, metal/graphene green composites are materials having ecofriendly attributes that are technically and economically feasible while minimizing the generation of pollution. The synthesis, modification, and the performance of metal/graphene developed during the past decade and the latest developments are comprehensively summarized, especially a focus on different environmentally friendly routes toward practical applications in electrochemical energy storage and conversion, electrochemical sensors, heterogeneous catalysis, and bioelectronics. However, apart from use of less toxic chemicals, other notable features of green technology are that most operates at mild conditions such as room temperature, visible light, and atmospheric pressure making it affordable, environmental, and cost effective for future researches.

Keywords: Metal/graphene composites, green synthesis, energy storage and conversion, electrochemical sensors, heterogeneous catalysis, bioelectronics

**Corresponding authors*: kshui@hanyang.ac.kr; bizhui@umac.mo; bizhui@pusan.ac.kr

Ashutosh Tiwari, Hirak K. Patra and Anthony P.F. Turner (eds.) Advanced Bioelectronic Materials, (427–466)

13.1 Introduction

This chapter presents a summary of environmentally friendly ways to synthesize metal/graphene composites for use in energy, detection, and environmental remediation. The increasing need for environmental protection and energy production in modern society has prompted significant advances in materials science and engineering. In particular, metal/graphene composites have many profound applications compared to traditional material systems. In this chapter, the following three main routes to the synthesis of graphene are summarized: (1) processing of graphite and graphite derivatives in the liquid phase by chemical methods, (2) epitaxial growth via the high-temperature treatment of silicon carbide (SiC), and (3) chemical vapor deposition (CVD) of hydrocarbons on transition metal substrates. Among these, the reduction of graphene oxide chemically is currently the only feasible means of mass-scale production. On the other hand, the preparation of graphene from graphite oxide typically involves the use of hazardous reducing agents such as sodium borohydride, formaldehyde, and hydrazine posing environmental issues. The focus of this chapter is on the green synthesis of graphene and metal/graphene composites as well as their applications in energy storage and conversion, electrochemical sensors, and heterogeneous catalysis. Four major green synthesis routes are discussed: microwave-assisted method, non-toxic reducing agents, *in situ* sonication method, and photocatalytic reduction method. Finally, the applications of these materials in energy and environmental areas are described.

13.2 Metal/Graphene Composites

Graphene not only exhibits fascinating electrical conductivity (10^3–10^4 S/m) but also has a high specific surface area (2600 m^2/g), excellent mechanical strength, and various unique features for the design of tailored composite materials [1–4]. Currently, the hybridization of graphene with metal nanoparticles (NPs) has become an emerging material for many potential applications in the areas of efficient catalysis, energy conversion and storage, and environmental remediation [5]. The next-generation metal/graphene composite systems are expected to possess extraordinary capability to integrate conversion and storage of solar energy, detection, multistep heterogeneous catalysis, and specific decomposition of trace environmental contaminants.

13.3 Synthesis Routes of Graphene

Graphene, a two-dimensional nanoscale allotrope of carbon with a honeycomb structure, is a promising material with many intriguing properties, including fast electron mobility, high optical transparency, excellent thermal property, high chemical stability and tensile strength, high elasticity, room temperature quantum Hall effect, peculiar electronic band structure, and electromechanical modulation [6–9]. These remarkable features of graphene have been adopted as promising catalyst supports for tremendous potential applications such as energy storage, wastewater treatment, and hydrogen production. Any technological application, however, demands a reliable source of large-area, high-quality mono-/multilayer graphene films. Although the mechanical exfoliation of graphene produces high-quality graphene in terms of the electrical and mechanical properties [10], obtaining single-layer graphene or few-layer graphene (FLG) via adhesive tape or mechanical exfoliation methods is impractical in mass-scale production because the process yield is low and the graphene flake size is comparatively small [11]. The ability to synthesize and place large-scale graphene films on a variety of substrates using methods compatible with current industrial technology is very important for future applications. Regarding the challenge of producing mass-scale graphene for industrial applications, over the past few years, the number of studies on the development of facile graphene approaches has increased dramatically. A range of methods have been explored to synthesize graphene for mass production, such as the chemical exfoliation of graphene [12], epitaxial growth of graphene [13], and CVD [14]. Figure 13.1 summarizes the four main categories of the synthesis methods for graphene.

13.3.1 CVD Synthesis of Graphene

CVD synthesis of graphene on catalytic transition metal surfaces, such as nickel and copper [15], has emerged as an important method for the preparation and production of graphene for a range of applications because of the large area and superior structural, electrical, optical, and mechanical properties. In CVD growth, reactant gas species are fed into the reactor and pass through a hot zone, where hydrocarbon precursors decompose to carbon radicals on the metal substrate surface, and then form single-layer graphene and FLG depending on the reaction gases flow rate, reaction time and temperature, pressure of synthesis, and cooling rate [16]. Previous reviews [17–19] focused on the synthetic methods of graphene

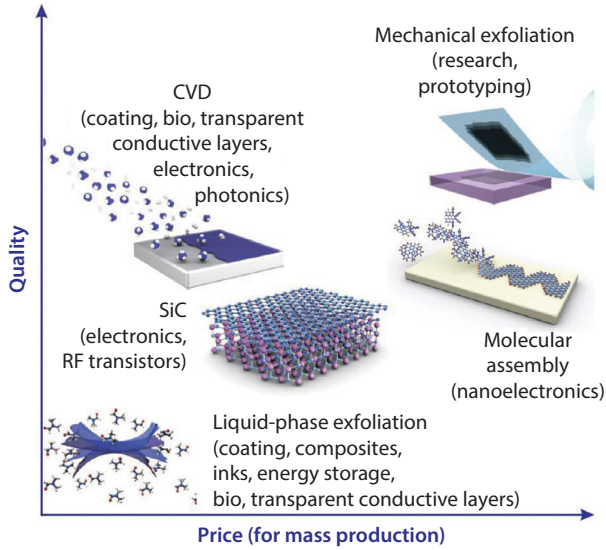

Figure 13.1 There are several methods of mass production of graphene, which allow a wide choice in terms of size, quality, and price for any particular application. (Adapted with permission from Ref. [1]. Copyright 2012 Nature.)

with novel architectures for potential applications in energy production and storage, electrochemical sensors, and biosensors. This section focuses mainly on the gas-phase synthesis of graphene on catalytic transition metal surfaces; specifically, metal nickel and copper.

In a typical gas-phase synthetic route, gaseous hydrocarbons as the carbon source are introduced at elevated temperatures (~1050 °C) together with a suitable metal substrate working as a catalyst to lower the energy barrier of the reaction. These reagents are reacted at a certain temperature and reaction time under high pressure. By varying the cooling rates, growth time and hydrocarbon concentration, the thickness and morphology of graphene can be controlled.

Guermoune *et al.* [20] reported a method to synthesize graphene on copper foils in a tube furnace using different liquid alcohols. The field-effect mobility of large-area graphene transistors was measured at room temperature to be in the range of 1800–2100 cm^2/V s, at carrier densities between 10^{11} and 10^{12} cm^{-2}, exhibiting high carrier mobility. This result paves the way for using low-purity carbon sources to grow high-purity, large-area graphene films. Maria *et al.* [21] examined in real time, the CVD kinetics using CH_4–H_2 precursors on both polycrystalline copper and nickel foils. The results showed that hydrogen acts as an inhibitor of CH_4 dehydrogenation on copper, helping suppress deposition onto the

copper substrate, and degrades the quality of graphene. In the case of Ni, however, the resurfacing recombination of hydrogen aids CH_4 decomposition. Recently, there has been a shift in the research focus in the field from developing techniques for graphene synthesis to designing strategies for transferring a high-quality, transferable, large-area graphene films to various substrates [22, 23]. For example, Liu *et al.* [24] reported that uniform large area (>100 μm^2) single-layer graphene could be produced on an annealed nickel catalyst of predominantly (111) oriented grains within 50 s using a hot-wall CVD system followed by a rapid cooling (7–25 °C/min). Zhao *et al.* [25] reported the low-pressure alcohol catalytic CVD growth of graphene to synthesize graphene films with high surface coverage (>80%) in less than 30 s growth time. In their study, they used isotopically labeled ^{13}C ethanol as the precursor to examine the growth mechanism of graphene on Ni substrates. The results showed that both ^{12}C-graphene and ^{13}C-graphene flakes can form independently, even at high temperatures (900 °C). Alternatively, Huang *et al.* [26] reported that high-quality graphene films on Ni foils can be obtained using a cold-wall reactor by rapid thermal CVD, as shown in Figure 13.2(a). The high-quality graphene films were produced by reducing the growth time to 10 s, suggesting that a direct growth mechanism may play a larger role rather than a precipitation mechanism [27]. The results showed that a lower H_2 flow rate is favorable for the growth of high-quality graphene films, and graphene films prepared in the absence of H_2 achieved a sheet resistance as low as 367 Ω per square

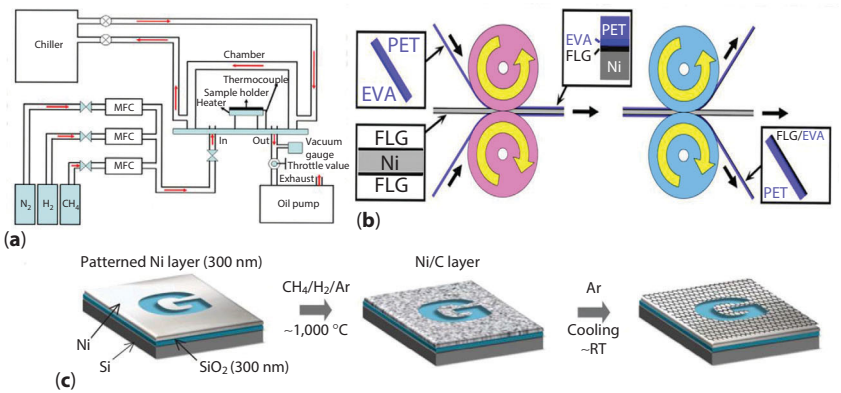

Figure 13.2 (a) Diagram of the cold-wall CVD system (adapted with permission from Ref. [2]. Copyright 2012 Elsevier). (b) A diagram to show the roll-to-roll process for the transfer of FLG from nickel foil to EVA/PET substrates (adapted with permission from Ref. [3]. Copyright 2010 Elsevier). (c) Synthesis of patterned graphene films on thin nickel layers (adapted with permission from Ref [4]. Copyright 2009 Nature).

coupled with 97.3% optical transmittance at 550 nm, which is much better than for those grown by hot-wall CVD systems [28].

Kim *et al.* [10] reported a simple roll-to-roll method to grow a $Ni/SiO_2/Si$ substrate and transfer high-quality stretchable graphene films on a large scale by CVD on thin nickel layers, as shown in Figure 13.2(b). The resulting patterned films can be transferred easily to stretchable substrates using simple contact methods, which showed a very low sheet resistance of ~280 Ω per square, with ~80 % optical transparency. In such an approach, monolayer graphene can be transferred easily to silicon dioxide substrates at low temperatures (~25 °C), showing an electron mobility greater than 3700 $cm^2 V^{-1} s^{-1}$ and exhibiting a half-integer quantum Hall effect. Moreover, the number of graphene layers can be controlled by varying the thickness of the catalytic metals, the growth time and/or the ultraviolet treatment time; scaling up can be readily achieved, and the outstanding properties of the graphene films enable numerous applications [29, 30].

Although a low-pressure CVD approach was shown to be scalable for large-area graphene film fabrication, it does not appear to be as appealing as ambient pressure deposition for the continuous high-quality 'roll-to-roll' [31] mass production of graphene. Juang *et al.* [22] synthesized FLG films by CVD using Ni foil as a substrate. The results obtained proved that controlling the cooling rate of the CVD process may not be suitable parameter for controlling the thickness of the graphene films, mainly because deposition and precipitation mechanisms can occur simultaneously during graphene growth. In addition, they transferred FLG to transparent flexible polyethylene terephthalate (PET) substrates via an efficient 'roll-to-roll' process, as shown in Figure 13.2(c) and found that the thickness of the graphene films on PET is dependent on their initial thickness on the Ni surface. Recently, Vlassiouk *et al.* [32] reported graphene growth on copper foils by CVD at atmospheric pressure using a mixed flow of stock gases (H_2 and CH_4) as the methane source, which is significant advantage over low-pressure CVD. The results suggested that the atmospheric CVD approach eliminates the difficulties associated with the low-pressure CVD approach while allowing the straightforward employment of this technology in roll-to-roll industrial-scale graphene production. According to their study, a 40" single-layer graphene with graphene domains generally larger than 100 μm was obtained successfully and then transferred on transparent PET substrates, using a roll-to-roll approach, highlighting the potential for many commercial and research applications. In another important comprehensive study, Zhang *et al.* [33] reported the formation of graphene on single crystal Ni (111) and polycrystalline Ni substrates by CVD. The results showed that the preferential formation of monolayer/bilayer graphene on

the single crystal surface can be attributed to an atomically smooth surface and the absence of grain boundaries. In contrast, CVD graphene formed on polycrystalline Ni leads to a higher percentage of multilayer graphene, surface mapping showed that the area percentage of monolayer/bilayer graphene are 91.4% for a Ni (111) substrate and 72.8% for a polycrystalline Ni substrate. Pristine large-area graphene films produced by CVD are always polycrystalline and contain grain boundaries that can potentially weaken the material. Lee *et al.* [34] examined the mechanical properties of CVD graphene films with different grain sizes. The results showed that the elastic stiffness of CVD graphene is identical to that of pristine graphene if the post processing steps can avoid damage or rippling.

Despite the significant progress reviewed in this section, there are a number of important challenges, as discussed in the following. The synthesis of graphene with a large and controlled grain size with a precisely controlled thicknesses and spatial structures is very important for a range of electronic applications. The growth of wafer-sized graphene single crystals to further facilitate the fabrication of graphene-based devices and low-temperature graphene growth will be attractive for reducing the cost and may enable direct growth on flexible polymer-based substrates [16, 35].

13.3.2 Liquid-Phase Production of Graphene

The liquid-phase production of graphene involves dispersing graphite in a solvent, whose surface energy matches that of graphene, with a surface tension that favors an increase in the total area of graphite crystallites [36]. Typically, the solvent is non-aqueous, but aqueous solutions with a surfactant can also be applied successfully [37]. Figure 13.3 presents the liquid-phase exfoliation (LPE) process of graphite. During the process, graphite splits into individual platelets with the aid of sonication for several hours [38] and yields a significant fraction of monolayer flakes in the suspension, which can be enriched further by centrifugation [12]. The extensive technique has been applied for the oxidation and subsequent exfoliation of graphite to produce graphene oxide. The high quality of the graphene flakes obtained is comparable to micromechanical exfoliation [36].

Zhang *et al.* [39] reported the synthesis of FLG sheets with a controlled number of layers (3 or 4) on a large scale by the chemical reduction of few-layered graphene oxide (FGO) using hydrazine vapor reduction for chemical reduction and examined the effects of various chemical and thermal reduction treatments on the electrical conductivity of FLG transparent films. The results showed that the reduced FGO has much better electrical conductivity of 108 S/cm, which is two orders of magnitude higher

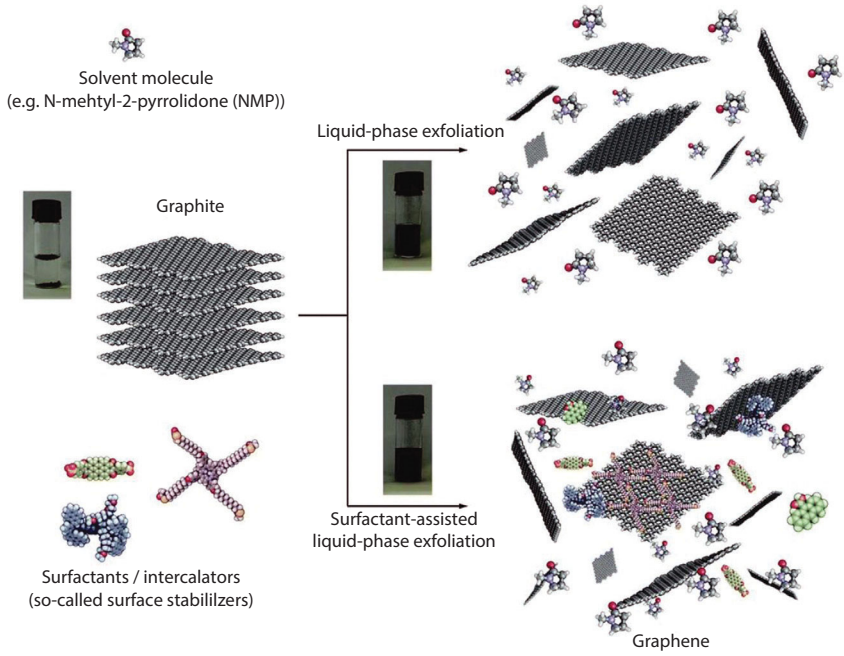

Figure 13.3 Schematic representation of the LPE process of graphite in the absence (top right) and presence (bottom right) of surfactant molecules. (Adapted with permission from Ref [5]. Copyright 2014 Royal Chemical Society.)

than that of reduced GO after the reduction treatments under the same conditions as that used for GO. The excellent conductivity of the reduced films indicated that it has great potential for large-scale and low-cost applications compared to its single-layered counterpart. Following the work reported by Zhang *et al.* [39], Stankovich *et al.* [40] reported the reduction of exfoliated graphene oxide sheets in water with hydrazine. The preparative carbon-based nanoplatelet consisted of thin graphene-based sheets (30–100 nm) and had a high specific surface area (466 m^2/g). This result provided evidence to support the claim that GO can be exfoliated completely into individual graphene oxide sheets and that the chemical reduction of such sheets can furnish graphene-like sheets. Recently, Liu *et al.* [41] reported a facile method for improving the efficiency of the liquid exfoliation of graphene using organic solvent cyclohexanone. The yield of graphene sheets in solvents was increased significantly (up to 20 times) due to NaOH intercalation into graphite; expandable graphite augments the graphite intercalating space of the adjacent graphite layers. Although previous studies [42–44] described the dispersion and exfoliation of graphene oxide, these techniques also suffer from the formation of structural defects

during the oxidation process. These defects continue to disrupt the electronic structure of graphene to render it semiconducting [13]. Therefore, a non-covalent, solution-phase method to produce significant quantities of defect-free, unoxidized graphene is urgently needed. Recently, Hernandez *et al.* [12] produced high-quality unoxidized monolayer graphene in significant yield by the non-chemical, solution-phase exfoliation of graphite in organic solvents, such as N-methyl-pyrrolidone. Graphene obtained without significant structural defects can be dispersed at concentrations of up to 0.01 mg/ml. Their method resulted in a monolayer yield of ~1 wt%, which could potentially be improved to 7–12 wt% with further processing. Some groups [45, 46] reported a significant breakthrough in that graphite could be exfoliated in certain solvents to provide defect-free monolayer graphene using particular solvents, such as N-methyl-pyrrolidone [47], whose surface energy is so well matched to that of graphene that exfoliation occurs freely. On the other hand, N-methyl-pyrrolidone solvents are expensive and require special care when handling. Moreover, this type of solvent tends to have a high boiling point, making it difficult to deposit individual monolayers on the surfaces. Taking these factors into consideration, it is logical to develop an alternative liquid-phase process that results in the exfoliation of graphite to provide graphene in reasonably high yield. With regard to this, Lotya *et al.* [48] developed a method to disperse graphite in surfactant–water solutions with the aid of ultrasound. Although the exfoliated graphene flakes have a relatively large potential barrier, which originates from the coulomb repulsion between the surfactant-coated sheets, they are stabilized against re-aggregation by the negative surface charge. Compared to other chemical reduction methods reported, Rio-Castillo *et al.* [49] reported the ball-milling exfoliation of graphitic into single-layer graphene by adding small amounts of solvent. They showed that it is feasible to discriminate between monolayer graphene and poorly exfoliated fibers selectively by simply taking advantage of the Hansen solubility parameters. This technique may permit an inexpensive and scalable means of producing monolayer graphene in suspension. Parvez *et al.* [50] reported another breakthrough; the exfoliation of graphite into graphene using aqueous solutions of inorganic salts. They obtained graphene in high yield (>85%, ≤3 layers), large lateral size (up to 44 μm), and a remarkable hole mobility of 310 $cm^2\ V^{-1}\ s^{-1}$. The efficient exfoliation of graphene was achieved by coupling gas-producing thermal decomposition and mechanical exfoliation on a macroscale with non-covalent exfoliation and preservation of graphene properties on a molecular scale. Xia *et al.* [51] comprehensively presented different exfoliation routes of graphite to produce graphene by sonication in a solvent, chemical oxidation and

electrochemical oxidation. Compared to the previous reports, they chose as a starting substrate the flat surface of highly oriented pyrolytic graphite (HOPG), rather than using graphite powder or microscopic flakes. They showed that chemical oxidation and electrochemical oxidation methods are very effective ways but the process results in defective graphene. On the other hand, the sonication of HOPG in organic solvents can produce the best quality graphene but acts only on the uppermost few nanometers of the surface, requiring a lengthy treatment time. On the other hand, prolonged sonication leads to the undesirable fragmentation of exfoliated graphene sheets, which results in small-sized graphene sheets of lateral dimension ~1 mm [52].

In summary, the liquid exfoliation of graphene has been shown to produce pristine graphene and its derivatives exhibit highly desirable properties and performance in many applications. On the other hand, a significant challenge in the large-scale production of FLG is to select or design proper exfoliating reagents, including the appropriate solvents and assistants. An ideal exfoliation system should involve the use of a commonly available solvent, an assistant that can be removed easily, and low-cost natural graphite powder. A deep understanding of the mechanisms of the exfoliation of graphite will be essential to the design and discovery of new molecules with enhanced affinity for the basal plane of graphene, thereby boosting the LPE and enhancing the average size of the crystal while retaining good solubility in organic media, such as chloroform or ethanol [53, 54].

13.3.3 Epitaxial Growth of Graphene

The epitaxial growth of graphene is a commonly used technique for creating high-quality monolayer graphene [55]. Originally, epitaxial graphene was grown from SiC by simply heating and cooling. Generally, single- or bilayer graphene forms on the Si face of the crystal, whereas FLG grows on the C face [56]. Molecular beam epitaxy has been used to grow epitaxial graphene layer on SiC substrate at temperatures ranging from 1000 to 1100 °C [57]. The molecular beam epitaxy (MBE) process, however, requires an ultra-high vacuum, which makes the process tedious and impractical for mass production. The typical epitaxial growth of graphene can be described in Figure 13.4(a–f). Graphene with the desired quality can be obtained through the use of this method by optimizing the growth parameters, such as temperature, heating rate, and pressure. The details of this process as well as the characterization of epitaxial graphene on SiC and its manipulation according to its technological relevance are discussed in the following part.

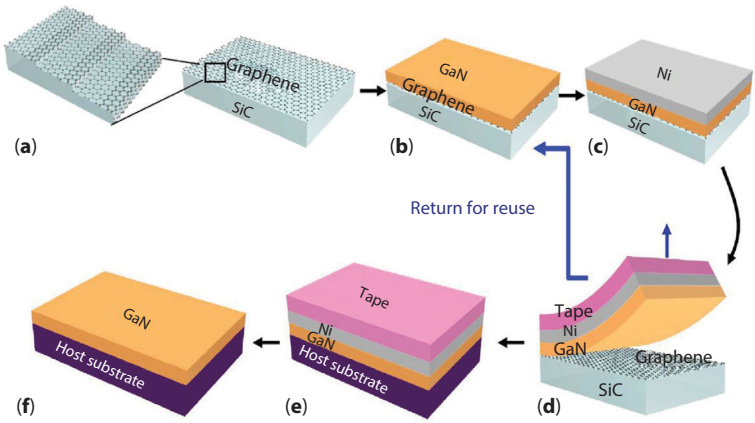

Figure 13.4 (a) Graphitization of SiC substrate to form epitaxial graphene. (b) Epitaxial growth of GaN on graphene. (c) Deposition of a stressor layer (Ni). (d) Release of GaN from the substrate with a handling tape. (e) Transfer of the released GaN/Ni/tape stack on a host substrate. (f) Removal of the tape and Ni by thermal release and wet etching, leaving a GaN film on the host substrate. (Adapted with permission from Ref. [6]. Copyright 2014 Nature.)

An understanding of the epitaxial graphene growth mechanisms at the atomic level plays a crucial role in the synthesis of high-quality graphene [58]. Recently, Kara *et al.* [59] observed silicon nanowires self-aligned in a massively parallel array on Ag(110) by scanning tunneling microscopy. They proved by density functional theory (DFT) that Si atoms tend to form hexagons on top of the Ag substrate in a honeycomb, graphene-like arrangement. Özçelik *et al.* [60] performed atomic structure optimization and ab initio finite temperature molecular dynamics (MD) calculations within DFT using VASP software. They found that the growth of graphene is under the control of two mechanisms. The first is the formation of large carbon rings at the edges that eventually collapse to form a honeycomb structure with defects. The second mechanism is the formation of pentagon–heptagon defects near the edge followed by their healing.

The factors influencing graphene growth were also examined using different substrates such as Ru(0001), Ni(111), Cu(111), and Pd(111) [61–63]. For example, Gao *et al.* [64] reported the epitaxial growth of graphene on a Pt(111) surface. The result showed that the proportion of different rotational domains varies with the growth temperature and the graphene quality can be improved by adjusting both the growth temperature and ethylene exposure. The prepared graphene was grown by exposing the Pt(111) substrate to high-purity (99.995%) ethylene, whereas the substrate temperature was varied from 773 to 1073 K. Moreover, the interaction between

graphene and the Pt surface is quite weak, and the electronic structure is similar to that of free-standing graphene. Hu *et al.* [65] reported the atmospheric pressure growth of single-layer graphene over a crystalline Cu (111) film deposited heteroepitaxially on a *c*-plane sapphire substrate. The temperature was found to affect the quality and orientation of graphene grown on the substrates. Moreover, the method indicated rapid exchange of the surface-adsorbed and gas-supplied carbon atoms at higher temperatures, resulting in highly crystallized graphene with energetically the most stable orientation consistent with the underlying Cu (111) lattice. De Heer *et al.* [56] used the near-equilibrium, confinement-controlled sublimation method to produce epitaxial graphene (mono and multi) layers on a SiC wafer. The method allows good control of the graphitization temperatures in the case of producing defective graphene layers at low temperatures. In addition, it allows further control of the graphitization rates by introducing inert gasses to instantly inhibit graphene growth. The synthesis of graphene via the decomposition of SiC has opened a promising route for the large-scale production of graphene. On the other hand, the almost perfectly ordered crystal SiC and the harsh process conditions, such as ultra-high vacuum, have limited the synthesis of graphene by the decomposition of SiC. Peng *et al.* [55], however, showed that amorphous TiC can be transformed to graphene nanosheets (GNS) with tunable layers by chlorination under ambient pressures. Hexagonal borazon (h-BN) has recently emerged as an excellent substrate for graphene nanodevices. Yang *et al.* [66] reported the epitaxial growth of a single-domain graphene on h-BN by the plasma-assisted deposition method. The scalable production graphene single crystals were grown successfully on h-BN with a fixed stacking orientation.

Although some significant progress has been made, enormous challenges still need to be overcome for the epitaxial growth of graphene to be achieved. One such limitation is that graphitization in a vacuum always transforms the ordered substrate surface to a rugged surface covered by small graphene domains with prominent thickness variations. Such disorder not only hinders further processing but also limits the device performance by scattering charge carriers flowing in the active graphene layer [67].

13.4 Green Synthesis Route of Metal/Graphene Composites

Metal/graphene composites exhibit novel dimension-dependent properties, leading to tremendous attractive applications in energy storage, catalysis, sensors, and environmental remediation [5, 68–70]. Metal/graphene

composites of specific sizes and morphologies can be synthesized feasibly using various chemical and physical methods. On the other hand, most of these methods use aggressive reducing agents, toxic solvents, and non-biodegradable stabilizing agents, or have high energy consumption, posing potential environmental and biological risks. A large number of research technologies [71, 72] have been used for the green synthesis of metal/graphene nanostructures in aqueous solutions, and the related experimental data has been well documented. This section reviews the recent main progress in the green synthesis of metal/graphene composites in aqueous solutions.

13.4.1 Microwave-Assisted Synthesis of Metal/Graphene Composites

The search for efficient heating methods to process reactions has led to the use of microwave radiation as an alternative power source to carry out chemical reactions [73]. Microwave chemistry has been a well-established technique in organic synthesis since the first reports in 1986 [74, 75]; its use in the synthesis of inorganic nanomaterials is still at the initial stages and is far from reaching its full potential [76]. The rapidly growing number of papers in this field suggests that microwave chemistry will play a vital role in the broad field of nanoscience and nanotechnology. Microwave-assisted synthesis methods not only reduce the chemical reaction times by several orders of magnitude but also create smaller particulate materials [77]. In particular, the synthesis of NPs and nanostructures, whose growth is quite sensitive to the reaction conditions, can benefit from efficient and controlled heating, as provided by microwave irradiation, thereby contributing to energy savings and satisfying the demands for environmentally friendlier synthetic nanotechnology. This section is not meant to give an exhaustive overview of all nanomaterials synthesized using the microwave technique but to discuss the principles, advantages, and limitations of microwave chemistry for metal/graphene composites along with its application in many areas of synthetic chemistry. Among the various methodologies for producing nanostructures of inorganic/inorganic nanocomposites, the microwave-assisted preparation of metal/graphene nanostructures has been investigated most intensively [78]. Metal/graphene composites have been developed by a facile and scalable chemical reduction method utilizing microwave irradiation with a variety of reducing agents in either aqueous or organic media [79]. Zhang *et al.* [80] reported the synthesis of graphene-supported Pd_1Pt_3 (Pd core/Pt shell) electrocatalysts by the simultaneous reduction of GO and metal salts, resulting in the dispersion of

metallic and bimetallic NPs supported on a large surface area of thermally stable 2D graphene sheets. The results showed that the introduction of graphene increases the electrochemically active surface area of the Pd_1Pt_3 nanostructures. Compared to the unsupported Pd_1Pt_3 electrocatalyst, the graphene-supported Pd_1Pt_3 electrocatalyst exhibited 80% enhancement of the electrocatalytic specific mass current for the oxidation of methanol. Siamaki *et al.* [81] reported highly active Pd NPs supported on graphene (Pd/G) by the microwave-assisted chemical reduction of the corresponding aqueous mixture of a palladium salt and dispersed graphite oxide (GO) sheets. The as-prepared Pd/G showed excellent catalytic activity for carbon–carbon cross-coupling reactions [82] with a wide range of utility under ligand-free ambient conditions in an environmental solvent system. This process also offers a remarkable turnover frequency (108,000 h^{-1}), as observed in microwave-assisted Suzuki cross-coupling reactions with easy removal from the reaction mixture, as well as recyclability with no loss of activity. Jen *et al.* [83] prepared the graphene nanosheet/polyethyleneimine/gold NP (GNS/PEI/AuNP) composite by microwave-assisted chemical reduction method, as is shown in Figure 13.5. The prepared GNS/PEI/AuNP composite film exhibited excellent sensitivity (0.2 μA μM^{-1} cm^{-2}) toward the selective determination of dopamine in the presence of ascorbic acid, which showed potential application in electrochemical sensors.

Graphene-supported monometallic composites have been studied extensively. Compared to individual NPs, bimetallic NPs exhibit enhanced

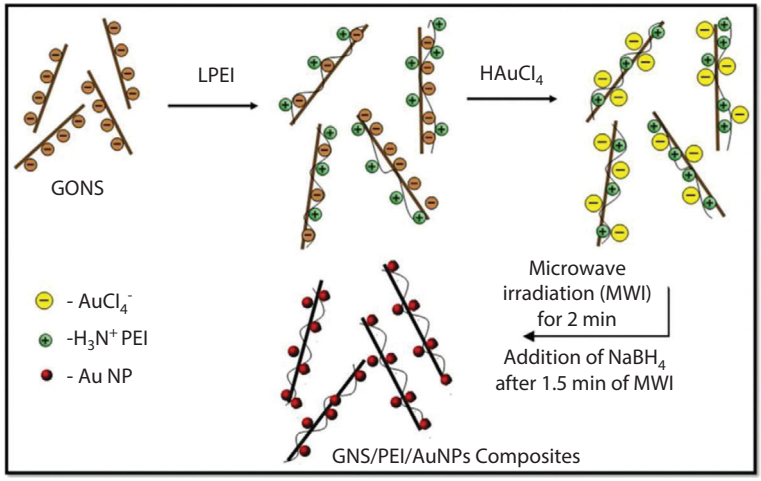

Figure 13.5 Schematic illustration of the preparation of GNS/PEI/AuNP composite. (Adapted with permission from Ref. [7]. Copyright 2014 Elsevier.)

catalytic properties. Bimetallic Au/Ag alloy–graphene hybrids were prepared using a one-step microwave-assisted method [84]. This is based on the fact that potential energy of Ag is smaller than that of Au [85], so electrons can transfer from Ag to Au, contributing to a synergistic effect for the catalytic activity of the hybrids. Microwave-based methods have been employed to synthesize inorganic nanostructures on a range of substrates. On the other hand, the mechanism for the rapid heating of a high dielectric loss solvent leading to the formation of nanostructures on the substrate is not fully understood. Kundu *et al.* [86] introduced the synthesis of catalytically active graphene/Pt nanohybrid via microwave-assisted route. They indicated a synergistic co-reduction mechanism because the presence of Pt ions leads to the faster reduction of GO and the presence of the defect sites on the reduced GO serves as anchor points for the heterogeneous nucleation of Pt on graphene. The resulting hybrid consists of ultra-fine NPs of Pt distributed uniformly over the reduced GO substrate. An exfoliation mechanism involves the spontaneous decomposition of an ammonia solution by microwave radiation to form gaseous NH_3 and H_2O, which perform the exfoliation [87].

Recently, Tian *et al.* [88] developed an environmentally friendly, one-pot strategy for the preparation of Ag NP-decorated reduced graphene oxide (AgNPs/rGO) composites without an extra reducing agent. The formation of AgNPs/rGO was accomplished by heating the mixture of GO and $AgNO_3$ aqueous solution directly in the presence of alkaline at 80 °C for 10 min with stirring. In the process, GO serves as a reducing agent and is converted to reduced graphene oxide (rGO) spontaneously under alkaline conditions. Hu *et al.* [89] dispersed minuscule amounts of graphene into a GO matrix and created an avalanche-like deoxygenating reaction of GO with local heating stimulated by graphene under microwave irradiation and graphene formation, which shows a high specific surface area (415 m^2/g) and specific capacitance (120 F/g). Guo *et al.* [90] proposed a one-step microwave-assisted heating procedure to synthesize a Pt NP ensemble-on-graphene hybrid nanosheet, and then dispersed it in a water/ethanol mixture with sonication to produce a colloidal suspension. The composite material obtained combined the unique and attractive electrocatalytic behavior of graphene particles with the good electronic and catalytic properties of Pt/graphene particles. In contrast to previous studies, Chen *et al.* [91] prepared tin–graphene nanocomposites using a combination of a microwave-assisted hydrothermal reaction and H_2 reduction. When applied as an anode material in lithium ion batteries, the obtained Sn–graphene nanocomposite exhibited a high lithium storage capacity of 1407 mAh g^{-1}. The Sn–graphene composite (weight ratio of 1:4) exhibited

a high initial reversible specific capacity of 946 mAh g^{-1} at a large current density of 1600 mA g^{-1}, and a high specific capacity of 542 mAh g^{-1} was maintained after 30 cycles. This showed that the electrode has excellent high rate capacity and stable cycle performance.

The use of microwave chemistry opens up remarkable opportunities for the eco-friendly synthesis of metal/graphene, which cannot be provided by other synthesis techniques. Although such time saving approaches are highly desirable, the influence of microwaves on the nucleation and growth of metal/graphene in the liquid phase under microwave irradiation remain to be answered [92, 93]. In conclusion, methods for measuring the local temperatures with high resolution need to be developed to understand the effects of selective heating and to take advantage of it in a rational way. The energy efficiency of microwave approaches and their scale-up to industrial quantities need to be addressed further.

13.4.2 Non-toxic Reducing Agent

Despite the distinctive advantages of the chemical route for the reduction of GO, this can be eliminated by the chemical modification of graphene using highly toxic reducing agents [94] (hydrazine, hydroquinone, sodium borohydride, etc.). The presence of trace amounts of such toxic agents might have a detrimental effect on humans and the environment. The use of green nanotechnology on the reduction of GO can overcome the above problem. From the literature, various phytochemicals obtained from different natural sources, such as [95] amino acid [96, 97], tea solution [97], wild carrot root [98], melatonin [99], and reducing sugar [100], have been used. The significant features of these phytochemicals are their abundance in nature and cost effectiveness along with their specific physicochemical properties [72]. More specifically, the negatively charged functional groups that exist on the surface of GO allow for the nucleation of positively charged non-toxic reducing agent in the presence of metallic salts, resulting in the growth of metal NPs on the GO surface and form rGO/metal NP composites.

Adhesive dopamine has been used successfully for the reduction of graphene oxide, which exhibits a controllable 2D morphology, reducing capability and aqueous stability [101]. The drug- and dye-loading tests showed that the resulting rGO presented high loading capacities as pristine GO. Wang *et al.* [102] confirmed the strong interactions between the reduced graphene and tea polyphenol (TP), which provides good dispersion of the reduced graphene for the synthesis of graphene. Similarly, the use of a carrot extract in the green synthesis of rGO was also studied. Vusa *et al.* [103] revealed the

potential of a wild carrot extract in the bio-reduction of GO. Raman spectroscopy showed that the I_d/I_g band ratio of 0.979 for GO increased to 1.198 after complete reduction, indicating the effective restoration of a carrot extract for the in-plane sp^2 domains in the resulting rGO. Interestingly, the reduction took place not because of the phytochemicals but due to the endophytic microorganism that are always present in the wild carrot extract and it was achieved at 90 °C in aqueous media. Recently, Hsu *et al.* [104] presented a green route for the formation of Ag NPs and the reduction of graphene oxide simultaneously using l-arginine as a reducing agent to yield a Ag/rGO nanocomposite. The detectable concentration of 4-aminothiophenol with the Ag/rGO nanocomposite as the Surface-enhanced Raman spectroscopy (SERS) substrate could be reduced to 10^{-10} M and the enhancement factor value could be increased to 1.27×10^{10}. Similarly, Song *et al.* [105] prepared high-quality graphene using oxalic acid as the reducing agent combining the advantages of low-toxicity, mild synthesis conditions and simple purification process. The as-prepared graphene deposited on platinum exhibited higher electrocatalytic activity for the methanol oxidation reaction.

Fernández-Merino *et al.* [94] compared the deoxygenation efficiency of graphene oxide suspensions using different reductants, such as vitamin C and hydrazine, as well as by heating the suspensions under alkaline conditions. They showed that vitamin C can yield highly reduced suspensions in a comparable manner to those provided by hydrazine. In addition, stable suspensions of vitamin C–rGO could be prepared not only in water but also in common organic solvents. As another example, Hsu *et al.* [106] reported a facile and rapid microwave-assisted green route for the uniform deposition of Ag NPs and the reduction of graphene oxide simultaneously with l-arginine as the reducing agent. The I_d/I_g ratios of the obtained rGO (1.07) and Ag/rGO (1.11) nanocomposite were larger than that of GO (0.78) because the conjugated graphene network would be re-established after chemical reduction of GO but the size of the re-established graphene network was usually smaller than the original graphite layer, leading to the increase in I_d/I_g ratio, which demonstrated that silver ions and GO were reduced simultaneously by l-arginine. In particular, a combination of two or more plant extracts was found to have more effective antioxidant properties than a single compound. This synergistic effect was more pronounced when lycopene or lutein was present in the mixture [103]. Gao *et al.* [107] produced graphene using vitamin C as the reducing agent and an amino acid as the stabilizer. They showed that graphene reduced by vitamin C exhibits a 10^6-fold increase in conductivity compared to that of graphite oxide. Tran *et al.* [108] prepared rGO nanosheets using non-aromatic and thiol-free amino acids as the reducing agent. Structural studies confirmed

the deoxygenation of GO from the loss of hydroxyl, carbonyl, and epoxy groups and that preparative graphene sheets between 20 and 70 nm are suitable for broad biomedical applications.

In the synthesis of rGO, one of the major drawbacks is the aggregation of graphene sheets because of the strong affinity between the two adjacent layers of graphene that lead to the formation of irreversible aggregates [109]. The decoration of metals on the rGO surface could prevent the direct π–π interactions between the layers and minimize aggregation [110]. Wang *et al.* [102] produced soluble graphene by reducing GO in a green tea solution. The polyphenols in the tea solution act as both a reducing agent and stabilizer, resulting in graphene with good solubility against aggregation in both aqueous solvents and a variety of organic solvents. Previous studies showed that the reduction of GO sheets by polyphenols in the presence of metal precursor ions resulted in better recovery of the graphitic structure of the sheets, which is in contrast to reduction by hydrazine. In a similar study by Akhavan *et al.* [111], graphene was synthesized using TP as a reducing and stabilizing agent at low temperatures in the presence of iron precursor ions. The results indicated that the reduction level and electrical conductivity of synthetic graphene in the presence of polyphenols and iron ions at 40 °C was much better than those of GO reduced by only polyphenols or iron ions at 80 °C.

Few studies have examined the implementation of green approaches in the preparation of graphene and graphene–metal NP hybrids with enhanced functionality from graphite oxide. In particular, the use of bioreductants and the testing of their relative efficacies are an emerging area of research. Fernández-Merino *et al.* [112] reported the use of biomolecules to prepare rGO–Ag NP hybrids. These hybrids displayed colloidal stability in water without the need for additional dispersants. Specifically, hybrids prepared with pyridoxamine exhibited a combination of long-term colloidal stability and exceptionally high catalytic activity among the Ag NP-based catalysts in the reduction of p-nitrophenol with $NaBH_4$. Similarly, Gnanaprakasam *et al.* [113] reported the eco-friendly biosynthesis of Ag nanowires on a rGO surface (Ag NWs–rGO) using an aqueous extract of Abelmoschus esculentus as a reducing and stabilizing agent. The size of the synthesized Ag NWs–rGO was approximately 92 nm in average thickness, and the length was in the range of a few micrometers.

13.4.3 *In Situ* Sonication Method

The chemical production of graphene from graphene oxide involves complicated processes, for which very strong oxidizing and reducing agents are

needed [114]. In addition, the graphene prepared under these harsh chemical conditions often contains a large number of defects even after reduction compared to graphene obtained from other methods [115]. Ultrasound, however, is a proven alternative to producing high-quality graphene in large quantities, and it is also environmentally friendly. Researchers have developed slightly different ways using ultrasound; but in general, the graphene production is a simple one-step process. Recently, Ag NPs–graphene oxide (AgNP–GO) was prepared by *in situ* sonication (~20 kHz) at room temperature with the assistance of vitamin C [116]. The results showed that Ag NPs with an average diameter of ~15 nm were uniformly dispersed over the surface of GO nanosheets by *in situ* ultrasonication with vitamin C for 1 min. Increasing the ultrasonication time resulted in the formation of Ag NPs with tunable dimensions ranging from 15 to 55 nm on the surface of the GO nanosheets. The key finding of this study is that the amount of silver nitrate and the ultrasonication time play key roles in controlling the dimensions of Ag NPs on GO. An Ostwald ripening mechanism was used to explain the tunable size of the as-prepared AgNP–GO composites. Sajini Vadukumpully *et al.* [117] reported the formation of highly ordered pyrolytic graphite by combination of high-frequency sonication and the presence of a cationic surfactant, cetyltrimethylammonium bromide, and acetic acid at room temperature, yielding graphene nanoflakes with a low defect concentration. The mean thickness of the obtained graphene flakes was found to be 1.18 nm. The nanoflakes showed a turn on voltage of 7.5 V/μm and emission current densities of 0.15 mA/cm^2 via field emission measurements. The surfactant-based methods are being investigated for large-scale production, but surfactant-based methods are currently limited by low concentrations of up to 0.05 mg/mL [118]. To improve the concentration and quality of surfactant-stabilized graphene dispersions, Smith *et al.* [119] prepared dispersions of graphene in a range of surfactants. They reported that the graphene concentration is controlled by the size of the potential barrier that stabilizes the surfactant-coated flakes against aggregation. Another example [120] was presented to produce graphene dispersions, which were stabilized in water by the surfactant sodium cholate with concentrations up to 0.3 mg/mL. The process employed sonication in a low-power sonic bath for 400 h followed by centrifugation to yield stable dispersions. The dispersed concentration increased with increasing sonication time, while the best quality dispersions were obtained for centrifugation rates between 500 and 2000 rpm. The method extends the scope for the scalable liquid-phase-assisted sonication processing of graphene for a wide range of applications.

Recently, Chabot *et al.* [121] demonstrated gum arabic as a green alternative for the exfoliation of graphite to produce graphene in water using a

sonication method. The fabricated film exhibited 20 times higher electrical conductivity than that of rGO. Moreover, the low-power bath sonication processing of graphite with environmentally approved biopolymers, such as gum arabic, opens up a scalable avenue for the production of inexpensive graphene. More recently, Hui *et al.* [122] reported the preparation of AgNPs/GO composites by *in situ* sonication (20 kHz ± 50 Hz) at room temperature and graphene oxide solutions with the assistance of vitamin C acting as an environmentally friendly reducing agent. In another study [123], they reported the lowest sheet resistance of 270 Ω/sq in an AgNPs/rGO film after 1 min of ultrasonication (~20 kHz), which is a 40 times lower resistivity than the film (10.93 kΩ/sq) [116]. This green synthesis approach for AgNPs/rGO hybrids is expected to lead to the further development of a broad new class of metal–graphene oxide composite films with enhanced properties to some extent.

Graphite can be exfoliated in the liquid phase using different chemical methods, such as electrochemical, chemical, and sonication-assisted techniques. Even if some of these techniques have been studied intensively in recent years [40, 124, 125], there are few reports of a comprehensive comparison of the different exfoliation mechanisms. In a recent study, Xia *et al.* [51] investigated the effects different approaches such as electrochemical, chemical, and sonication-assisted techniques (37kHz, 220 W) on the quality of graphene by graphite exfoliation. The results revealed the following: chemical oxidation is a very effective but disruptive way to exfoliate graphite; electrochemical oxidation allows a fast exfoliation and in-depth disruption of bulk quantities of graphite, but does yield defective graphene; and sonication in organic solvents produces graphene of high quality [126].

13.4.4 Photocatalytic Reduction Method

Recent studies have shown impurities and residual reductants in rGO dispersions during chemical exfoliation [127]. Furthermore, the reduction of water-dispersed GO nanosheets results in a significant decrease in their hydrophilic character, which leads to irreversible agglomeration and precipitation [128]. An environmentally friendly method for preparing rGO nanosheets based on the UV-irradiated reduction of exfoliated GO nanosheets was reported without the use of any photocatalyst or reducing agents because the typical chemical reducing agent, hydrazine, exhibits highly corrosive, explosive, and toxic properties [129]. The result revealed a sharp decrease in the absorbance peaks of oxygen functionalities after the UV reduction process. This is in contrast to the GO sheets reduced by hydrazine, which results in the formation of sp^3C–N bonds due to disorder

on the surface of the reduced sheets. Such disorders restrained the production of graphene sheets with high electrical conductivities [130]. Therefore, achieving an environmentally friendly and effective low-temperature method for the reduction of GO is essential.

Recently, chemically exfoliated GO sheets suspended in an ammonia solution (pH ~9) were found to reduce GO to rGO under room temperature conditions using nanosecond pulsed laser irradiation without the aggregation of reduced sheets in the solution [131]. The results showed that the O/C ratio of the GO sheets decreased from 49% to 21% after 10 min laser irradiation, which is comparable to that obtained using the common reducing agent, hydrazine, which resulted in an O/C ratio of 15% at 80 °C after 10 min. This is because rGO not only provides the nucleation sites but also prohibits the metal NPs from agglomeration [132] and photo-reduced phosphotungstates as well as electrons stored in rGO directly reduce the metal ions. Moon *et al.* [133] prepared a rGO suspension through the photocatalytic reduction of GO using phosphotungstate as the homogeneous photocatalyst under UV irradiation and deposited Ag, Au, and Pd NPs on the resulting rGO. Xing *et al.* [134] reported a photo reduction method for producing 3D photo-reduced graphene hydrogels (PRGHs) through the self-assembly of GO suspensions under photochemical reduction. The D band to G band (I_D/I_G) intensity ratio is 0.82 in GO and increases to 1.36 in PRGHs. Supercapacitors based on the PRGHs showed a high specific capacitance of 254 F/g at 1 A/g in KOH electrolyte, and 88% of its initial capacitance was retained after 4000 charge discharge cycles. In addition, the specific capacitance can still be maintained for 64% with an increase in the discharge current density to 4 A/g after the same charge and discharge laps.

13.5 Green Application of Metal/Graphene and Doped Graphene Composites

13.5.1 Energy Storage and Conversion Device

Metal/graphene nanocomposites are intriguing composites with the potential to improve the performance of fuel cells. Recently, Hui *et al.* [135] reported the facile synthesis of N-doped multilayer graphene (N-MLG) from milk powder using melamine as the nitrogen-doping source with Fe^{2+} ions as the catalytic growth agents. They reported a new method of using Fe ions as the catalytic growth agent to produce MLG without the need for toxic reducing agents. N-MLG also showed good electrocatalytic activity toward the oxygen reduction reaction (ORR) in an alkaline medium.

Liao *et al.* [136] reported Pt/GO nanocomposite electrocatalysts by microwave-polyol-water synthesis. The prepared Pt/GO had a maximum electrochemical active surface area (85.71 $m^2 g^{-1}$) for a reaction time of 5 min. This highlights the potential of Pt/GO nanocomposite electrocatalysts with high electrocatalytic activity for use as an anode material in electrochemical fuel cells. Xin *et al.* [4] prepared N-doped graphene (NG) by the microwave heating of the graphene in a NH_3 atmosphere as the supporting materials for fuel cell catalysts. They reported that the Pt/NG has better thermal stability than the Pt/G without doping nitrogen basing on thermogravimetric analysis (TGA) and differential scanning calorimetry (DSC). Moreover, the Pt/NG catalysts exhibited a higher electrochemical active surface area (80.45 $m^2 g^{-1}$), and tolerance to CO poisoning than those of the Pt/G under fuel cell conditions. They suggested that the prepared NG is a promising supporting material to improve the electrocatalytic activity of fuel cells. Alternatively, Bajpai *et al.* [137] reported the use of pulsed laser deposition to deposit Pt-NPs on chemically prepared GNS, and the lowest R_{ct} (2.36 Ω cm^2) of the Pt/G hybrid electrodes was obtained.

Many efforts have been made to either replace Pt with less expensive alternative materials or synthesize Pt/graphene composites at lower temperatures for commercial energy storage. For example, the Ag nanotriangle platelet-rGO pattern exhibited a low sheet resistance of 170 Ω/m with a transmittance of 90.2% [138]. Huang *et al.* [139] prepared a graphene composite foam with a Ni network. They produced a supercapacitor device based on the Ni/graphene composite foam that exhibited high rate capability of 100 Fg^{-1} at 0.5 A g^{-1} and 86.7 F g^{-1} at 62.5 A g^{-1}, good cycle stability with capacitance retention of 95% after 2000 cycles, low internal resistance (1.68 Ω), and a gravimetric capacitance as high as 40.9 F/g. Chu *et al.* [140] reported the chemical synthesis of rGO using the aqueous extract of *Hibiscus sabdariffa* L. as a reducing agent. The as-synthesized rGO was used as an electrode in the supercapacitor, which exhibited a good specific capacitance of 133.07 F g^{-1}, whereas the sheet resistance decreased significantly from 0.63 MΩ/sq to 36.50 Ω/sq. Wang *et al.* [141] reported a simple method to achieve a Sn/graphene nanocomposite with a 3D architecture that exhibited optimal electrochemical performance. The result showed that graphene plays a dual role as a support of Sn atoms to avoid aggregation and actively adsorbs lithium atoms. The observed storage capacity of Sn/graphene nanocomposites was up to 508 mAh g^{-1} in the 100^{th} cycle. Thakur *et al.* [72] reported the preparation of rGO using aqueous leaf extracts of *Colocasia esculenta* and *Mesua ferrea* Linn and an aqueous peel extract of orange (*Citrus sinensis*) for supercapacitor electrode materials. The rGO obtained as an electrode material exhibited good specific

capacitance (17–21 F g^{-1}) and high electrical conductivity (3032.6–4006 Sm^{-1}). Kim *et al.* [142] synthesized aqueous dispersible Pt/GNS nanohybrids as thin films using vitamin C for the co-reduction of GO and a Pt precursor (H_2PtCl_6) and without any binder using the electrospray method at room temperature. The results revealed the high electrocatalytic activity of the nanohybrids for the I^-/I_3^- redox couples in conventional Dye-sensitized solar cells (DSSCs) due to the semicircle with a small radius in the low frequency (Figure 13.6a). The lowest R_{CT} (27 Ωcm²) of the obtained GNS/Pt 20 (Pt loading levels were 20 wt%) could be delivered (Figure 13.6b).

To further increase the electrical contact between active materials and the current collector, binder-free electrodes have attracted considerable attention because of their convenience and binder-less features in various

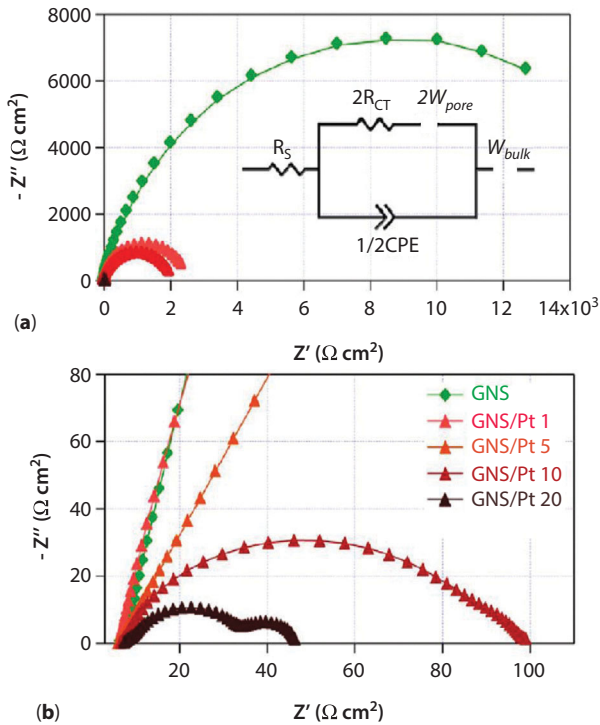

Figure 13.6 Nyquist plots of symmetrical cells. (a) Nyquist plot of entire frequency measured, and the equivalent circuit diagram (inserted figure: R_S is the series resistance, R_{CT} is the charge transfer resistance at the CE/electrolyte interface, W_{pore} is the Warburg impedance within CE layers, CPE is the constant phase element of one electrode, and W_{bulk} is the Warburg impedance between the two CEs. (b) Amplified Nyquist plot for the higher-frequency region. (Adapted with permission from Ref. [8]. Copyright 2013 American Chemical Society.)

electrochemical applications, such as lithium ion batteries and supercapacitors [143–145]. Recently, the one-step preparation of 3D graphene aerogel (GA) on a small piece of porous nickel foam (NF) was reported, which showed potential applications as a binder-free electrode for supercapacitors [146]. Tsang *et al.* [147] reported a simple and green method to prepare binder-free Pd/GA/NF electrodes with different Pd loadings for alcohol electro-oxidation. The Pd/GA/NF electrodes were formed through the self-assembly aggregation of Pd/GA on NF during the reduction of GO and Pd ions via a non-toxic reducing agent, vitamin C at 40 °C. The results showed that the catalytic performance of the electrodes increased with increasing Pd loading (Figure 13.7a–f). Cyclic voltammetry (CV) analysis showed that the 7.65 wt% Pd/GA/NF electrode had a maximum peak current density of 798.8 A /g [forward to backward peak current density ratio (I_f/I_b) of 3.11] and 874 A/g (I_f/I_b of 2.72) in methanol and ethanol electro-oxidation, respectively (Figure 13.7g and h). The proposed electrode preparation method showed great potential for the preparation of various binder-free catalytic electrodes, which would be beneficial to the development of fuel cell applications.

13.5.2 Electrochemical Sensors

Graphene offers a range of unique, versatile, and tunable properties that can be used creatively for electrochemical sensors. For example, the ambipolarity in graphene means that the adsorption of either electron withdrawing

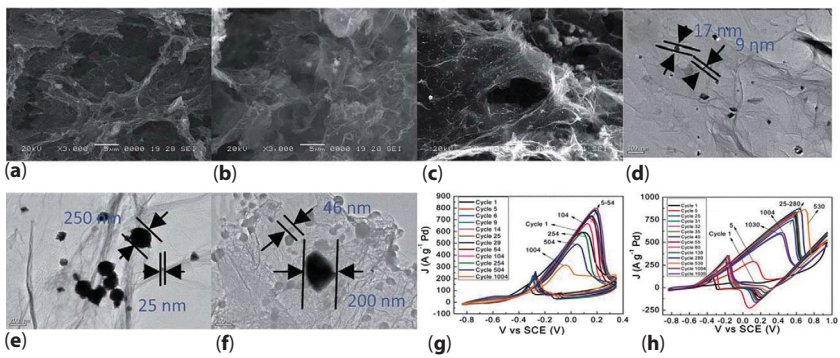

Figure 13.7 Scanning Electron Microscopy (SEM) images (scale bar: 5 mm) of (a) 0.8 wt% Pd/GA/NF, (b) 2.17 wt% Pd/GA/NF, (c) 7.65 wt% Pd/GA/NF, and Transmission Electron Microscopy (TEM) images of (d) 0.8 wt% Pd/GA/NF (scale bar: 100 nm), (e) 2.17 wt% Pd/GA/NF (scale bar: 200nm), (f) 7.65 wt%. Pd/GA/NF (scale bar: 200 nm), CV of 7.65 wt% Pd/GA/NF in (g) 1 M MeOH/1 M KOH solution (–0.845 to +0.355 V), and (h) 1 M EtOH/1 M KOH solution (–0.845 to +0.955 V) over 1000 scans. (Adapted with permission from Ref. [9]. Copyright 2014 Royal Society of Chemistry.)

or donating groups can lead to "chemical gating" of the material, which can be monitored easily in a resistive-type sensor setup [148]. Combining the high surface area with the specific electronic nature means that any molecular disruption on the graphene can be detected easily [149]. Therefore, graphene-oriented sensors can be expected to be highly sensitive for a wide range of fields. Recently, Gautam *et al.* [150] reported the NH_3 sensing behavior of the graphene surface decorated with gold (Au) NPs. The activation energy and heat of adsorption were estimated to be approximately 38 and 41 meV, respectively, at a NH_3 gas concentration of 58 ppm at room temperature. The dependence of the adsorption energies on the concentration of the target gas suggested inhomogeneous adsorption sites on the graphene surface. In a similar study, Ullah *et al.* [151] reported the synthesis Pt/graphene via a one-pot microwave-assisted method in an ethylene glycol solution within a short time (300 s). The visible-light photocatalytic activities of the Pt/graphene nanocomposites were tested by rhodamine B (RhB) and methylene blue (MB) as the model contaminants. Under visible-light irradiation, photo-generated active species (metal particle) [152] promoted the photo-catalytic degradation toward MB(RhB) molecules because of the extensive π-conjugation between the MB(RhB) molecule and the graphene domains. The nanocomposites obtained were found to be promising electrochemical sensors. GNS-Au nanocomposite was prepared in an aqueous medium assisted by microwave irradiation [144]. The results showed that the GNS–Au nanocomposite at the electrode surface could efficiently accelerate electron transfer and enhance the corresponding electrochemical performance due to Au NPs coated on the surface of the GNS, which disturbs the van der Waals interactions and prevents GNS from forming aggregates approaching each other. A green and facile strategy was developed to prepare metal/graphene hydrogel composites using a substrate-enhanced electroless deposition method [153]. The sensitivity of the hydrogel composite-modified glassy carbon electrode toward uric acid was 10.07 $\mu A\ \mu M^{-1}\ cm^{-2}$, which is higher than that of modified glassy carbon electrode toward glucose (2.47 $\mu A\ \mu M^{-1}\ cm^{-2}$) [154].

13.5.3 Wastewater Treatment

Pristine research achievements have been reviewed on the application of graphene-based metallic composites in environmental protection and detection. Graphene is a hydrophobic material that has less efficient contact with water molecules, resulting in the poor absorption of heavy ions in wastewater treatment. [155]. Kyzas *et al.* [156] reported that modified graphene exhibiting hydrophilic properties can adsorb heavy metal ions through this

mechanism. As graphene oxide with a high surface area has a mass of oxygen-containing groups on the surface, complexation reactions are caused by the combination of these oxygen-containing groups with heavy metals. The photodegradation of pollutants present in water is typically accomplished using UV-activated photo catalysts, mostly noble metals [157]. The mechanism of UV photodegradation is that electrons in the photocatalyst can be excited by UV radiation from the valence band to the conduction band to generate photo-generated electrons and holes in the valence band. These photo-generated electrons and holes diffuse to the surface of the catalyst and react with the different contaminants on the surface, resulting in the degradation of the contaminants [158]. The solubility and stability of the rGO suspension are a significant problem that needs to be solved because rGO easily precipitates from the suspensions [159]. Guo *et al.* [160] prepared Au (Ag) NP–rGO hybrids using chitosan as the reducing and stabilizing agent. The analysis showed that chitosan macromolecules can efficiently reduce GO at comparatively low temperatures and their adsorption onto the rGO nanosheets allowed the formation of a stable rGO aqueous dispersion. The stable RGO hybrids have potential applications for environmental protection. The photothermal degradation of RhB could in principle be possible with other sp^2-based carbon materials because the absorption of UV photons in the 280–450 nm wavelength range only requires the presence of C=C bonds in electronically conjugated structures [161]. Guardia *et al.* [162] reported the decomposition of RhB in the presence of only graphene oxide using intense UV irradiation through the photo-induced heating of the suspended graphene oxide sheets. The degradation rate of RhB involved the following process: (1) deoxygenation of the sheets in the absence of the photocatalysts, (2) selective nucleation and growth of metal NPs on the sheets to yield graphene-based hybrids, and (3) decomposition of the dye molecule RhB in the presence of only graphene oxide. Moreover, the graphene sheets in the hybrid material played a role as a catalyst but not as a reactant. Similarly, the adsorption of synthetic organic compounds by pristine GNS and GO was examined [163], and compared with carbon nanotubes in the presence of natural organic matters (dyes, phenanthrene, and biphenyl). The graphene produced exhibited comparable or better adsorption capacities than carbon nanotubes, which was attributed to a much less compact bundle structure. The results further indicated that graphene can serve as alternative adsorbents for the removal of organic compounds from water.

13.5.4 Bioelectronics

Recently, the emerging bioelectronics focus on exploiting biological materials in conjunction with and micro- and nano-electronics in an extensive

field encompassing, such as biological fuel cells, bionics, and biomaterials for information processing and storage. For example, there have been significant efforts to utilize graphene/metal composite materials for the development of biological energy storage and bioelectrocatalyst owing to the excellent sensitivity and catalytic activity of the nanomaterials and hydrophobic nature of graphene. By combining these two excellent and unique modalities, graphene/metal NP hybrids have demonstrated a number of bioelectronics applications.

Recently, growing Pt- or Pd-based NP catalysts directly on the graphene surface maximizes the contact between graphene and NP, resulting in high catalytic activity [164]. However, more efforts are needed to control the size, shape, and morphology of the NPs such that their catalytic potentials can fully be optimized. So far, the assembly of monodispersed NPs on the graphene surface has been demonstrated to optimize the catalytic performance of the graphene/metal composite. For example, Qiu *et al.* [165] reported that the monodispersed Pt NPs with ultra-fine particle size (~3 nm) are synthesized using ferritin protein nanocages as the template and subsequently self-assembled on the 3D graphene, resulting in a stable 3D graphene/Pt NP composite. The composite exhibited enhanced electrocatalytic activity (~2.5 mA cm^{-2}) for methanol oxidation as compared with both Pt/rGO (~1.6 mA cm^{-2}) and state-of-the-art Pt/C (~1.2 mA cm^{-2}) catalyst. Beside, Kim *et al.* [166] reported the charge transport behavior of protein-shelled Pt NPs combined with graphene for bionano-hybrid capacitor. In addition, field-effect transistor based on graphene/PepA-Pt NPs (PepA, a dodecameric bacterial aminopeptidase from *Streptococcus pneumonia*) has showed the modulation ability by varying the size and concentration of the Pt NPs encapsulated by the PepA, resulting in higher electron mobility than other well-known field-effect transistor devices [167, 168].

Since electrocatalytic activity and stability of metal NPs are strongly dependent on the exposed facets [169], Chen *et al.* [170] has demonstrated a high-sensitivity non-enzymatic H_2O_2 biosensor based on the *in situ* growth of surfactant-free Au(111)-like gold NPs (AuNPs) on nitrogen-doped graphene (NG) quantum dots (AuNPs–N-GQDs). The Au NPs–N-GQDs exhibited high sensitivity and selectivity for electrochemical detection of H_2O_2 with a low detection limit of 0.12 μM and sensitivity of 186.22 μA/μM cm^2.

Currently, organic and surfactant-assisted synthetic routes have been developed to enhance homogeneity and well-crystallized structure of metal particles [171]. For example, polypyrrole has been extensively studied owing to its high energy storage capacity, good electrical conductivity, good redox reversibility, and environmental stability [172]. Significantly, the presence of amine group (–NH–) on the pyrrole ring will contribute to

the enhancement of biomolecular sensing [173]. Shen *et al.* [172] reported the fabricated Au NPs decorated polypyrrole/rGO hybrid sheets electrode exhibit a remarkable sensitivity of 16.40 μA/μM in response to dopamine with a linear range of 0.1–5000 nM and limit of detection as low as 18.29 pM. Chen *et al.* [174] reported an innovative method to fabricate Poly(diallyldimethylammonium chloride) (PDDA)-capped gold NPs (AuNPs)-functionalized graphene (G)/multiwalled carbon nanotubes (MWCNTs) nanocomposites by an innovation method (Figure 13.8a). Specifically, the positively charged AuNPs can be absorbed onto the negatively charged G/MWCNTs hybrid electrode through electrostatic attraction, which was further decoded with glucose enzyme such as glucose oxidase. As shown in Figure 13.8(b) and (c), biosensor based on glucose oxidase anchored on AuNPs/G/MWCNTs electrode demonstrated a satisfactory analytical performance with high sensitivity (29.72 $\mu AM^{-1}\ cm^{-2}$) and low limit of detection (4.8 μM), indicating that the graphene–nanotube–NP composite hierarchical structure could be a promising architecture for immobilizing biomolecules for biosensor applications.

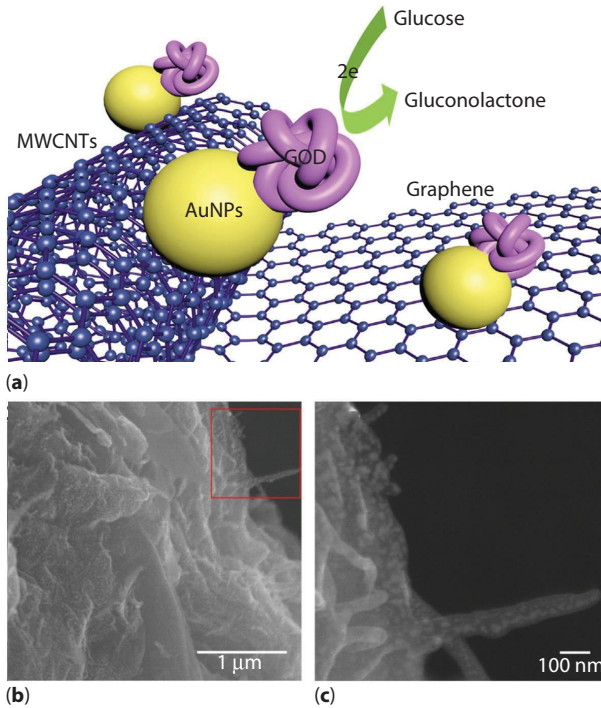

Figure 13.8 (a) Schematic illustration of construction of GOD/AuNPs/G/MWCNTs composites. (b) SEM image of AuNPs/G/MWCNTs. (c) Magnified SEM image of (b) marked in red box. (Adapted with permission from Ref. [10]. Copyright 2014 Elsevier.)

Compare with monometallic systems, bimetallic systems Pt M (M=Ru, Pd, Au, Ni, Pb, etc.) have a much higher intriguing catalytic behaviors, due to their rapid response, good stability, and high catalytic efficiency toward the targeted species by the electron coupling and ligand effects between the different components [175]. Zhao *et al.* [176] synthesized hollow AuPd (hAuPd) alloy NPs prepared through simultaneous reduction of $HAuCl_4$ and Na_2PdCl_4 using Co NPs as sacrificial template, and subsequently assembled on NG to prepare an NG–hAuPd hybrid film. The NG–hAuPd hybrid film showed a linear response to H_2O_2 in the range of 0.1–20 μM, with a sensitivity of 5095.5 μA μM^{-1} cm^{-2} and a comparable detection limit of 0.02 μM (S/N=3). Guo *et al.* [171] developed highly dispersed bimetallic PtPd alloy NPs anchored on reduced rGO with the assistance of ionic liquid (IL: [VEIM]BF4). The PtPd–IL–RGO-modified electrode can directly catalyze glucose oxidation and exhibited an enhanced current response within 3 s. The proposed electrode showed an excellent anti-interference to electroactive molecules and Cl^- with a good linear range from 0.1 to 22 μM at 0 V, long-term stability of at least 92.95% of the initial value was retained in the continuous tests after 1 month. Furthermore, NG sheet anchored with PtCo alloy NPs was demonstrated as a 3D bi-continuous spongy structures biosensor to capture antibody for detection of zearalenone [177]. The biosensor exhibited a highly sensitive response to zearalenone with a detection limit of 2.1 pg mL^{-1}. The greatly amplified properties were attributed to its abundant porous structures and bimetallic systems, which not only favors the linkage of antibody but also has admirable catalytic activity and super electron transfer properties. In addition, it is well known that clenbuterol (CLB), salbutamol (SAL), and ractopamine (RAC) are a family of β-adrenergic agonists with similar chemical structures and groups, originally used in the therapeutic treatment of asthma and preterm labor in humans [178]. Hence, a facile strategy was needed to achieve simultaneous detection of RAC, SAL, and CLB without cross talk between adjacent electrodes. Wei *et al.* [179] developed a multiplexed electrochemical biosensor for fast and sensitive detection of RAC, SAL, and CLB based on rGO and silver–palladium alloy NPs (AgPd NPs) without any other substrates. The designed strategy can simultaneously detect RAC, SAL, and CLB ranging from 0.01 to 100 ng mL^{-1} with detection limits of 1.52, 1.44, and 1.38 pg mL^{-1}, respectively. These strategies eliminate the possible negative effects of enzyme and mediator, reduce the cost, realize the simultaneous detection of three kinds of β-adrenergic agonists, and also ensure high sensitivity. Many works have revealed that the graphene/MWCNTs composite films can be used to develop novel types of highly sensitive and stable electrochemical sensors due to the distribution of graphene sheets in the MWCNTs bundles as well as the interfacial bonding between them

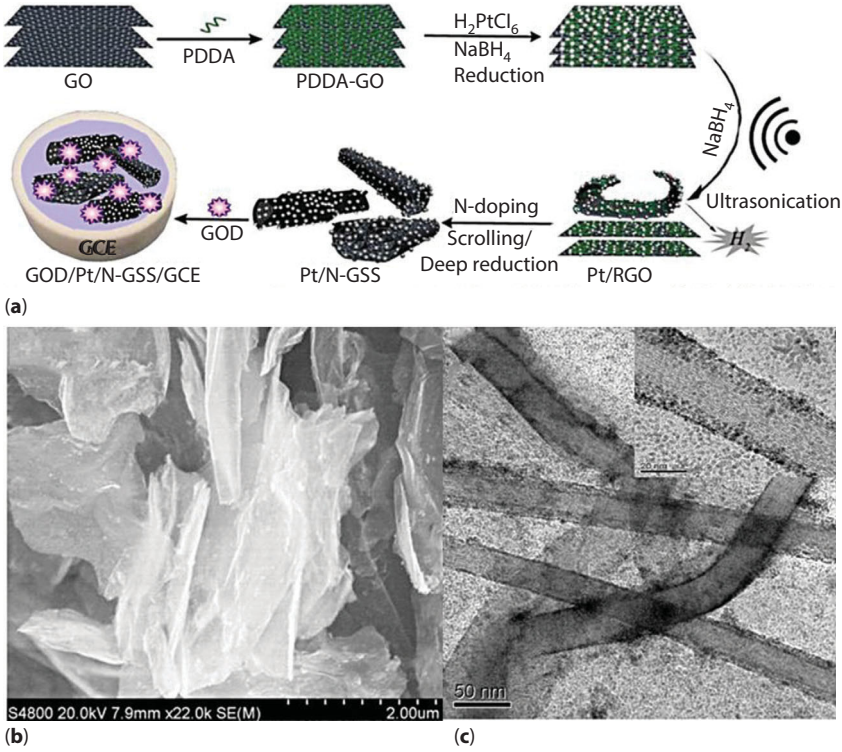

Figure 13.9 Schematic illustration for the fabrication of GOD/Pt/N-GSS. (b) SEM images of Pt/N-GSS. (c) TEM images of Pt/N-GSS, the inset image of (c) shows the magnified TEM of Pt/NGSS. (Adapted with permission from Ref. [11]. Copyright 2015 Elsevier.)

[180]. A hydrogen microexplosion method (Figure 13.9a) was adopted to prepare platinum NPs/nitrogen-doped graphene nanoscrolls (Pt/N-GSS) nanocomposites (Figure 13.9b and c) by Zhang *et al.* [181]. The composites exhibited an excellent electrocatalytic activity toward the oxidation of H_2O_2 with the sensitivity of 25.26 μA μM^{-1} and good linear response from 2 to 16.57 μM. Moreover, the resulting glucose amperometric biosensor toward glucose oxidase not only presents a wide linear range (10–12.55 μM) with a high sensitivity (6.36 μA μM^{-1}), but also possesses low detection limit of 1 μM and long-term stability for detection.

13.6 Conclusion and Future Perspective

Previous studies of the most recent progress in synthesis, modification, and the performance of graphene were reviewed comprehensively. Green

reduction has almost emerged as a separate branch in the synthesis of nanomaterials in terms of the urgent need for energy saving and environment. To identify a green alternative to the use of hazardous chemicals in the production of graphene, many of these reported approaches offer advantages, such as security, efficiency, versatility, and cost effectiveness of the material in different reagents, or easy scalability to the industrial level. These advances can eventually facilitate the use of graphene and metal/graphene materials in a number of commercial applications.

The chapter mainly discussed the different environmentally friendly routes that have been developed, mostly within the last year, toward the preparation of graphene from graphite oxide. Practical applications have been considered, including the use of composite materials as electrode materials for devices involved in electrochemical energy storage and conversion, as the electrode materials for electrochemical sensors, as absorbers for both gases and liquids, and as electrocatalyst and reducing agent for bioelectronics. On the other hand, apart from use of less toxic chemicals, other notable features of green technology are that most of these processes operate under mild conditions such as room temperature, visible light, and atmospheric pressure, making them affordable, environmental, and cost effective. In the near future, it will be exciting to see these promising integral green technologies in many technological applications of graphene and graphene composites.

Acknowledgments

This study was supported by the Basic Science Research Program through the National Research Foundation of Korea (NRF) funded by the Ministry of Education, Science and Technology (2013R1A1A2007365 and 2014R1A1A2055740).

References

1. H.J. Shin, K.K. Kim, A. Benayad, S.M. Yoon, H.K. Park, I.S. Jung, M.H. Jin, H.K. Jeong, J.M. Kim, J.Y. Choi, *Advanced Functional Materials*, 19, 1987–1992, 2009.
2. S. Stankovich, D.A. Dikin, G.H. Dommett, K.M. Kohlhaas, E.J. Zimney, E.A. Stach, R.D. Piner, S.T. Nguyen, R.S. Ruoff, *Nature*, 442, 282–286, 2006.
3. V.C. Tung, M.J. Allen, Y. Yang, R.B. Kaner, *Nature Nanotechnology*, 4, 25–29, 2008.

4. Y. Xin, J.-g. Liu, X. Jie, W. Liu, F. Liu, Y. Yin, J. Gu, Z. Zou, *Electrochimica Acta*, 60, 354–358, 2012.
5. I.V. Lightcap, P.V. Kamat, *Accounts of Chemical Research*, 46, 2235–2243, 2012.
6. K. Novoselov, A.K. Geim, S. Morozov, D. Jiang, M.K.I. Grigorieva, S. Dubonos, A. Firsov, *Nature*, 438, 197–200, 2005.
7. A.K. Geim, K.S. Novoselov, *Nature Materials*, 6, 183–191, 2007.
8. K.V. Emtsev, A. Bostwick, K. Horn, J. Jobst, G.L. Kellogg, L. Ley, J.L. McChesney, T. Ohta, S.A. Reshanov, J. Röhrl, *Nature Materials*, 8, 203–207, 2009.
9. S. Bae, H. Kim, Y. Lee, X. Xu, J.-S. Park, Y. Zheng, J. Balakrishnan, T. Lei, H.R. Kim, Y.I. Song, *Nature Nanotechnology*, 5, 574–578, 2010.
10. K.S. Kim, Y. Zhao, H. Jang, S.Y. Lee, J.M. Kim, K.S. Kim, J.-H. Ahn, P. Kim, J.-Y. Choi, B.H. Hong, *Nature*, 457, 706–710, 2009.
11. Y.H. Lee, X.Q. Zhang, W. Zhang, M.T. Chang, C.T. Lin, K.D. Chang, Y.C. Yu, J.T.W. Wang, C.S. Chang, L.J. Li, *Advanced Materials*, 24, 2320–2325, 2012.
12. Y. Hernandez, V. Nicolosi, M. Lotya, F.M. Blighe, Z. Sun, S. De, I. McGovern, B. Holland, M. Byrne, Y.K. Gun'Ko, *Nature Nanotechnology*, 3, 563–568, 2008.
13. A.K. Geim, *Science*, 324, 1530–1534, 2009.
14. Z. Chen, W. Ren, L. Gao, B. Liu, S. Pei, H.-M. Cheng, *Nature Materials*, 10, 424–428, 2011.
15. X. Li, W. Cai, J. An, S. Kim, J. Nah, D. Yang, R. Piner, A. Velamakanni, I. Jung, E. Tutuc, *Science*, 324, 1312–1314, 2009.
16. Y. Zhang, L. Zhang, C. Zhou, *Accounts of Chemical Research*, 46, 2329–2339, 2013.
17. Y. Shao, J. Wang, H. Wu, J. Liu, I.A. Aksay, Y. Lin, *Electroanalysis*, 22, 1027–1036, 2010.
18. M.J. Allen, V.C. Tung, R.B. Kaner, *Chemical Reviews*, 110, 132–145, 2009.
19. D.A. Brownson, D.K. Kampouris, C.E. Banks, *Journal of Power Sources*, 196, 4873–4885, 2011.
20. A. Guermoune, T. Chari, F. Popescu, S.S. Sabri, J. Guillemette, H.S. Skulason, T. Szkopek, M. Siaj, *Carbon*, 49, 4204–4210, 2011.
21. M. Losurdo, M.M. Giangregorio, P. Capezzuto, G. Bruno, *Physical Chemistry Chemical Physics*, 13, 20836–20843, 2011.
22. Z.-Y. Juang, C.-Y. Wu, A.-Y. Lu, C.-Y. Su, K.-C. Leou, F.-R. Chen, C.-H. Tsai, *Carbon*, 48, 3169–3174, 2010.
23. S.J. Chae, F. Güneş, K.K. Kim, E.S. Kim, G.H. Han, S.M. Kim, H.J. Shin, S.M. Yoon, J.Y. Choi, M.H. Park, *Advanced Materials*, 21, 2328–2333, 2009.
24. W. Liu, C.-H. Chung, C.-Q. Miao, Y.-J. Wang, B.-Y. Li, L.-Y. Ruan, K. Patel, Y.-J. Park, J. Woo, Y.-H. Xie, *Thin Solid Films*, 518, S128–S132, 2010.
25. P. Zhao, B. Hou, X. Chen, S. Kim, S. Chiashi, E. Einarsson, S. Maruyama, *Nanoscale*, 5, 6530–6537, 2013.
26. L. Huang, Q. Chang, G. Guo, Y. Liu, Y. Xie, T. Wang, B. Ling, H. Yang, *Carbon*, 50, 551–556, 2012.

27. R.S. Weatherup, B.C. Bayer, R. Blume, C. Baehtz, P.R. Kidambi, M. Fouquet, C.T. Wirth, R. Schlögl, S. Hofmann, *ChemPhysChem*, 13, 2544–2549, 2012.
28. O. Kordina, C. Hallin, A. Henry, J. Bergman, I. Ivanov, A. Ellison, N.T. Son, E. Janzén, *Physica Status Solidi (B)*, 202, 321–334, 1997.
29. J.W. Suk, A. Kitt, C.W. Magnuson, Y. Hao, S. Ahmed, J. An, A.K. Swan, B.B. Goldberg, R.S. Ruoff, *ACS Nano*, 5, 6916–6924, 2011.
30. F. Bonaccorso, Z. Sun, T. Hasan, A. Ferrari, *Nature Photonics*, 4, 611–622, 2010.
31. T. Kobayashi, M. Bando, N. Kimura, K. Shimizu, K. Kadono, N. Umezu, K. Miyahara, S. Hayazaki, S. Nagai, Y. Mizuguchi, *Applied Physics Letters*, 102, 023112, 2013.
32. I. Vlassiouk, P. Fulvio, H. Meyer, N. Lavrik, S. Dai, P. Datskos, S. Smirnov, *Carbon*, 54, 58–67, 2013.
33. Y. Zhang, L. Gomez, F.N. Ishikawa, A. Madaria, K. Ryu, C. Wang, A. Badmaev, C. Zhou, *The Journal of Physical Chemistry Letters*, 1, 3101–3107, 2010.
34. G.-H. Lee, R.C. Cooper, S.J. An, S. Lee, A. van der Zande, N. Petrone, A.G. Hammerberg, C. Lee, B. Crawford, W. Oliver, *Science*, 340, 1073–1076, 2013.
35. Z. Yan, Z. Peng, J.M. Tour, *Accounts of Chemical Research*, 47, 1327–1337, 2014.
36. U. Khan, H. Porwal, A. O'Neill, K. Nawaz, P. May, J.N. Coleman, *Langmuir*, 27, 9077–9082, 2011.
37. X. Zhao, B.M. Sánchez, P.J. Dobson, P.S. Grant, *Nanoscale*, 3, 839–855, 2011.
38. K.S. Novoselov, V. Fal, L. Colombo, P. Gellert, M. Schwab, K. Kim, *Nature*, 490, 192–200, 2012.
39. L. Zhang, X. Li, Y. Huang, Y. Ma, X. Wan, Y. Chen, *Carbon*, 48, 2367–2371, 2010.
40. S. Stankovich, D.A. Dikin, R.D. Piner, K.A. Kohlhaas, A. Kleinhammes, Y. Jia, Y. Wu, S.T. Nguyen, R.S. Ruoff, *Carbon*, 45, 1558–1565, 2007.
41. W. WeiáLiu, J. NongáWang, *Chemical Communications*, 47, 6888–6890, 2011.
42. V. Nicolosi, M. Chhowalla, M.G. Kanatzidis, M.S. Strano, J.N. Coleman, *Science*, 340 2013.
43. U. Khan, A. O'Neill, M. Lotya, S. De, J.N. Coleman, *Small*, 6, 864–871, 2010.
44. Y. Zhan, J. Wu, H. Xia, N. Yan, G. Fei, G. Yuan, *Macromolecular Materials and Engineering*, 296, 590–602, 2011.
45. J.N. Coleman, *Accounts of Chemical Research*, 46, 14–22, 2012.
46. S. De, P.J. King, M. Lotya, A. O'Neill, E.M. Doherty, Y. Hernandez, G.S. Duesberg, J.N. Coleman, *Small*, 6, 458–464, 2010.
47. A.A. Green, M.C. Hersam, *Nano Letters*, 9, 4031–4036, 2009.
48. M. Lotya, Y. Hernandez, P.J. King, R.J. Smith, V. Nicolosi, L.S. Karlsson, F.M. Blighe, S. De, Z. Wang, I. McGovern, *Journal of the American Chemical Society*, 131, 3611–3620, 2009.
49. A.E. Del Rio-Castillo, C. Merino, E. Díez-Barra, E. Vázquez, *Nano Research*, 7, 963–972, 2014.

50. K. Parvez, Z.-S. Wu, R. Li, X. Liu, R. Graf, X. Feng, K. Müllen, *Journal of the American Chemical Society*, 136, 6083–6091, 2014.
51. Z.Y. Xia, S. Pezzini, E. Treossi, G. Giambastiani, F. Corticelli, V. Morandi, A. Zanelli, V. Bellani, V. Palermo, *Advanced Functional Materials*, 23, 4684–4693, 2013.
52. K.P. Loh, Q. Bao, P.K. Ang, J. Yang, *Journal of Materials Chemistry*, 20, 2277–2289, 2010.
53. W. Du, X. Jiang, L. Zhu, *Journal of Materials Chemistry A*, 1, 10592–10606, 2013.
54. A. Ciesielski, P. Samorì, *Chemical Society Reviews*, 43, 381–398, 2014.
55. T. Peng, Z. Kou, H. Wu, S. Mu, *Scientific Reports*, 4 2014.
56. W.A. de Heer, C. Berger, M. Ruan, M. Sprinkle, X. Li, Y. Hu, B. Zhang, J. Hankinson, E. Conrad, *Proceedings of the National Academy of Sciences*, 108, 16900–16905, 2011.
57. E. Moreau, F. Ferrer, D. Vignaud, S. Godey, X. Wallart, *Physica Status Solidi (A)*, 207, 300–303, 2010.
58. L.B. Biedermann, M.L. Bolen, M.A. Capano, D. Zemlyanov, R.G. Reifenberger, *Physical Review B*, 79, 125411, 2009.
59. B. Aufray, A. Kara, S. Vizzini, H. Oughaddou, C. Leandri, B. Ealet and G. L. Lay, *Applied Physics Letters*, 96, 183102, 2010.
60. V.O. Özçelik, S. Cahangirov, S. Ciraci, *Physical Review B*, 85, 235456, 2012.
61. P.W. Sutter, J.-I. Flege, E.A. Sutter, *Nature Materials*, 7, 406–411, 2008.
62. X. Li, W. Cai, L. Colombo, R.S. Ruoff, *Nano Letters*, 9, 4268–4272, 2009.
63. B. Wang, X. Ma, M. Caffio, R. Schaub, W.-X. Li, *Nano Letters*, 11, 424–430, 2011.
64. M. Gao, Y. Pan, L. Huang, H. Hu, L. Zhang, H. Guo, S. Du, H.-J. Gao, *Applied Physics Letters*, 98, 033101, 2011.
65. B. Hu, H. Ago, Y. Ito, K. Kawahara, M. Tsuji, E. Magome, K. Sumitani, N. Mizuta, K.-i. Ikeda, S. Mizuno, *Carbon*, 50, 57–65, 2012.
66. W. Yang, G. Chen, Z. Shi, C.-C. Liu, L. Zhang, G. Xie, M. Cheng, D. Wang, R. Yang, D. Shi, *Nature Materials*, 12, 792–797, 2013.
67. P. Sutter, *Nature Materials*, 8, 171–172, 2009.
68. K. Lü, G. Zhao, X. Wang, *Chinese Science Bulletin*, 57, 1223–1234, 2012.
69. J. Huang, L. Zhang, B. Chen, N. Ji, F. Chen, Y. Zhang, Z. Zhang, *Nanoscale*, 2, 2733–2738, 2010.
70. M. Pumera, *Energy & Environmental Science*, 4, 668–674, 2011.
71. B. Li, H. Cao, J. Shao, G. Li, M. Qu, G. Yin, *Inorganic Chemistry*, 50, 1628–1632, 2011.
72. S. Thakur, N. Karak, *Carbon*, 50, 5331–5339, 2012.
73. P.T. Anastas, C.-J. Li, *Handbook of Green Chemistry, Green Processes, Green Synthesis*, John Wiley & Sons, 2014.
74. C. Qi, Y.J. Zhu, X.Y. Zhao, B.Q. Lu, Q.L. Tang, J. Zhao, F. Chen, *Chemistry-A European Journal*, 19, 981–987, 2013.
75. C. Qi, Y.J. Zhu, B.Q. Lu, X.Y. Zhao, J. Zhao, F. Chen, J. Wu, *Chemistry-A European Journal*, 19, 5332–5341, 2013.

76. S.L. Suib, N.E. Leadbeater, 2010, Microwave Heating as a Tool for Sustainable Chemistry, CRC Press, p. 207.
77. C. Yansheng, Z. Zhida, L. Changping, L. Qingshan, Y. Peifang, U. Welz-Biermann, *Green Chemistry*, 13, 666–670, 2011.
78. C. Tan, X. Huang, H. Zhang, *Materials Today*, 16, 29–36, 2013.
79. H.M. Hassan, V. Abdelsayed, S.K. Abd El Rahman, K.M. AbouZeid, J. Terner, M.S. El-Shall, S.I. Al-Resayes, A.A. El-Azhary, *Journal of Materials Chemistry*, 19, 3832–3837, 2009.
80. H. Zhang, X. Xu, P. Gu, C. Li, P. Wu, C. Cai, *Electrochimica Acta*, 56, 7064–7070, 2011.
81. A.R. Siamaki, A.E.R.S. Khder, V. Abdelsayed, M.S. El-Shall, B.F. Gupton, *Journal of Catalysis*, 279, 1–11, 2011.
82. L. Xue, Z. Lin, *Chemical Society Reviews*, 39, 1692–1705, 2010.
83. V.K. Ponnusamy, V. Mani, S.-M. Chen, W.-T. Huang, J.-F. Jen, *Talanta*, 120, 148–157, 2014.
84. H. Chen, X. Fan, J. Ma, G. Zhang, F. Zhang, Y. Li, *Industrial & Engineering Chemistry Research*, 53, 17976-17980, 2014.
85. Q. Zhang, J. Xie, J.Y. Lee, J. Zhang, C. Boothroyd, *Small*, 4, 1067–1071, 2008.
86. P. Kundu, C. Nethravathi, P.A. Deshpande, M. Rajamathi, G. Madras, N. Ravishankar, *Chemistry of Materials*, 23, 2772–2780, 2011.
87. I. Janowska, K. Chizari, O. Ersen, S. Zafeiratos, D. Soubane, V. Da Costa, V. Speisser, C. Boeglin, M. Houllé, D. Bégin, *Nano Research*, 3, 126–137, 2010.
88. J. Tian, S. Liu, Y. Zhang, H. Li, L. Wang, Y. Luo, A.M. Asiri, A.O. Al-Youbi, X. Sun, *Inorganic Chemistry*, 51, 4742–4746, 2012.
89. H. Hu, Z. Zhao, Q. Zhou, Y. Gogotsi, J. Qiu, *Carbon*, 50, 3267–3273, 2012.
90. S. Guo, D. Wen, Y. Zhai, S. Dong, E. Wang, *ACS Nano*, 4, 3959–3968, 2010.
91. S. Chen, Y. Wang, H. Ahn, G. Wang, *Journal of Power Sources*, 216, 22–27, 2012.
92. I. Bilecka, M. Niederberger, *Nanoscale*, 2, 1358–1374, 2010.
93. Y.-J. Zhu, F. Chen, *Chemical Reviews*, 114, 6462–6555, 2014.
94. M. Fernandez-Merino, L. Guardia, J. Paredes, S. Villar-Rodil, P. Solis-Fernandez, A. Martinez-Alonso, J. Tascon, *The Journal of Physical Chemistry C*, 114, 6426–6432, 2010.
95. M.M. Sk, C.Y. Yue, R.K. Jena, *Polymer*, 55, 798–805, 2014.
96. H. Ahn, T. Kim, H. Choi, C. Yoon, K. Um, J. Nam, K.H. Ahn, K. Lee, *Carbon*, 71, 229–237, 2014.
97. K. Kakaei, *Journal of Selcuk University Natural and Applied Science*, 2, 1021–1030, 2014.
98. T. Kuila, S. Bose, P. Khanra, A.K. Mishra, N.H. Kim, J.H. Lee, *Carbon*, 50, 914–921, 2012.
99. A. Esfandiar, O. Akhavan, A. Irajizad, *Journal of Materials Chemistry*, 21, 10907–10914, 2011.
100. C. Zhu, S. Guo, Y. Fang, S. Dong, *ACS Nano*, 4, 2429–2437, 2010.
101. C. Cheng, S. Li, S. Nie, W. Zhao, H. Yang, S. Sun, C. Zhao, *Biomacromolecules*, 13, 4236–4246, 2012.

102. Y. Wang, Z. Shi, J. Yin, *ACS Applied Materials & Interfaces*, 3, 1127–1133, 2011.
103. C.S.R. Vusa, S. Berchmans, S. Alwarappan, *RSC Advances*, 4, 22470–22475, 2014.
104. K.-C. Hsu, D.-H. Chen, *Nanoscale Research Letters*, 9, 1–9, 2014.
105. P. Song, X. Zhang, M. Sun, X. Cui, Y. Lin, *RSC Advances*, 2, 1168–1173, 2012.
106. K.-C. Hsu, D.-H. Chen, *Nanoscale Research Letters*, 9, 1–10, 2014.
107. J. Gao, F. Liu, Y. Liu, N. Ma, Z. Wang, X. Zhang, *Chemistry of Materials*, 22, 2213–2218, 2010.
108. D.N. Tran, S. Kabiri, D. Losic, *Carbon,* 76, 193-202, 2014.
109. J. Liu, S. Fu, B. Yuan, Y. Li, Z. Deng, *Journal of the American Chemical Society*, 132, 7279–7281, 2010.
110. J.A. Elemans, R.R. Slangen, A.E. Rowan, R.J. Nolte, *The Journal of Organic Chemistry*, 68, 9040–9049, 2003.
111. O. Akhavan, M. Kalaee, Z. Alavi, S. Ghiasi, A. Esfandiar, *Carbon*, 50, 3015–3025, 2012.
112. M. Fernández-Merino, S. Villar-Rodil, J. Paredes, P. Solís-Fernández, L. Guardia, R. García, A. Martínez-Alonso, J. Tascón, *Carbon*, 63, 30–44, 2013.
113. P. Gnanaprakasam, T. Selvaraju, *RSC Advances*, 4, 24518–24525, 2014.
114. K. Krishnamoorthy, Gui-Shik Kim, Sang Jae Kim, *Ultrasonics Sonochemistry*, 20, 644-649, 2013.
115. V. Datsyuk, M. Kalyva, K. Papagelis, J. Parthenios, D. Tasis, A. Siokou, I. Kallitsis, C. Galiotis, *Carbon*, 46, 833–840, 2008.
116. K. Hui, K. Hui, D. Dinh, C. Tsang, Y. Cho, W. Zhou, X. Hong, H.-H. Chun, *Acta Materialia*, 64, 326–332, 2014.
117. S. Vadukumpully, J. Paul, S. Valiyaveettil, *Carbon*, 47, 3288–3294, 2009.
118. K.R. Paton, E. Varrla, C. Backes, R.J. Smith, U. Khan, A. O'Neill, C. Boland, M. Lotya, O.M. Istrate, P. King, *Nature Materials*, 13, 624–630, 2014.
119. R.J. Smith, M. Lotya, J.N. Coleman, *New Journal of Physics*, 12, 125008, 2010.
120. M. Lotya, P.J. King, U. Khan, S. De, J.N. Coleman, *ACS Nano*, 4, 3155–3162, 2010.
121. V. Chabot, B. Kim, B. Sloper, C. Tzoganakis, A. Yu, *Scientific Reports*, 3, 1378, 2013.
122. D. Dinh, K. Hui, K. Hui, Y. Cho, W. Zhou, X. Hong, H.-H. Chun, *Applied Surface Science*, 298, 62–67, 2014.
123. J. Zhang, H. Yang, G. Shen, P. Cheng, J. Zhang, S. Guo, *Chemical Communications*, 46, 1112–1114, 2010.
124. N. Liu, F. Luo, H. Wu, Y. Liu, C. Zhang, J. Chen, *Advanced Functional Materials*, 18, 1518–1525, 2008.
125. G. Cravotto, P. Cintas, *Chemistry-A European Journal*, 16, 5246–5259, 2010.
126. C. Bendicho, I. De La Calle, F. Pena, M. Costas, N. Cabaleiro, I. Lavilla, *TrAC Trends in Analytical Chemistry*, 31, 50–60, 2012.
127. Y. Ding, P. Zhang, Q. Zhuo, H. Ren, Z. Yang, Y. Jiang, *Nanotechnology*, 22, 215601, 2011.

128. P. Wang, Z.-G. Liu, X. Chen, F.-L. Meng, J.-H. Liu, X.-J. Huang, *Journal of Materials Chemistry A*, 1, 9189–9195, 2013.
129. J.K. Niemeier, D.P. Kjell, *Organic Process Research & Development*, 17, 1580–1590, 2013.
130. H.A. Becerril, J. Mao, Z. Liu, R.M. Stoltenberg, Z. Bao, Y. Chen, *ACS Nano*, 2, 463–470, 2008.
131. E.E. Ghadim, N. Rashidi, S. Kimiagar, O. Akhavan, F. Manouchehri, E. Ghaderi, *Applied Surface Science*, 301, 183–188, 2014.
132. R. Pasricha, S. Gupta, A.K. Srivastava, *Small*, 5, 2253–2259, 2009.
133. G.-h. Moon, Y. Park, W. Kim, W. Choi, *Carbon*, 49, 3454–3462, 2011.
134. L.-B. Xing, S.-F. Hou, J. Zhou, S. Li, T. Zhu, Z. Li, W. Si, S. Zhuo, *The Journal of Physical Chemistry C*, 118, 25924–25930, 2014.
135. H. Zhao, K. Hui, K. Hui, *Carbon*, 76, 1–9, 2014.
136. C.-S. Liao, C.-T. Liao, C.-Y. Tso, H.-J. Shy, *Materials Chemistry and Physics*, 130, 270–274, 2011.
137. R. Bajpai, S. Roy, P. Kumar, P. Bajpai, N. Kulshrestha, J. Rafiee, N. Koratkar, D. Misra, *ACS Applied Materials & Interfaces*, 3, 3884–3889, 2011.
138. K. Xu, W. Li, Q. Liu, B. Li, X. Liu, L. An, Z. Chen, R. Zou, J. Hu, *Journal of Materials Chemistry A*, 2, 4795–4802, 2014.
139. G. Huang, S. Xu, Z. Xu, H. Sun, L. Li, *ACS Applied Materials & Interfaces*, 6, 21325–21334, 2014.
140. H.-J. Chu, C.-Y. Lee, N.-H. Tai, *Carbon*, 80, 725–733, 2014.
141. G. Wang, B. Wang, X. Wang, J. Park, S. Dou, H. Ahn, K. Kim, *Journal of Materials Chemistry*, 19, 8378–8384, 2009.
142. Y.-G. Kim, Z.A. Akbar, D.Y. Kim, S.M. Jo, S.-Y. Jang, *ACS Applied Materials & Interfaces*, 5, 2053–2061, 2013.
143. J. Gomez, E.E. Kalu, R. Nelson, M.H. Weatherspoon, J.P. Zheng, *Journal of Materials Chemistry A*, 1, 3287–3294, 2013.
144. J. Chen, K. Sheng, P. Luo, C. Li, G. Shi, *Advanced Materials*, 24, 4569–4573, 2012.
145. G.Q. Zhang, H.B. Wu, H.E. Hoster, M.B. Chan-Park, X.W.D. Lou, *Energy & Environmental Science*, 5, 9453–9456, 2012.
146. S. Ye, J. Feng, P. Wu, *ACS Applied Materials & Interfaces*, 5, 7122–7129, 2013.
147. C.-H.A. Tsang, K. Hui, K. Hui, L. Ren, *Journal of Materials Chemistry A*, 2, 17986–17993, 2014.
148. K. Kostarelos, K.S. Novoselov, *Nature Nanotechnology*, 9, 744–745, 2014.
149. D. Chen, L. Tang, J. Li, *Chemical Society Reviews*, 39, 3157–3180, 2010.
150. M. Gautam, A.H. Jayatissa, *Solid-State Electronics*, 78, 159–165, 2012.
151. K. Ullah, S. Ye, L. Zhu, Z.-D. Meng, S. Sarkar, W.-C. Oh, *Materials Science and Engineering: B*, 180, 20–26, 2014.
152. T. Ghosh, K. Ullah, V. Nikam, C.-Y. Park, Z.-D. Meng, W.-C. Oh, *Ultrasonics Sonochemistry*, 20, 768–776, 2013.
153. C. Du, Z. Yao, Y. Chen, H. Bai, L. Li, *RSC Advances*, 4, 9133–9138, 2014.

154. A.P. Periasamy, Y.-J. Chang, S.-M. Chen, *Bioelectrochemistry*, 80, 114–120, 2011.
155. Z. Li, Y. Wang, A. Kozbial, G. Shenoy, F. Zhou, R. McGinley, P. Ireland, B. Morganstein, A. Kunkel, S.P. Surwade, *Nature Materials*, 12, 925–931, 2013.
156. G.Z. Kyzas, E.A. Deliyanni, K.A. Matis, *Journal of Chemical Technology and Biotechnology*, 89, 196–205, 2014.
157. D. Ravelli, D. Dondi, M. Fagnoni, A. Albini, *Chemical Society Reviews*, 38, 1999–2011, 2009.
158. H.M. Sung-Suh, J.R. Choi, H.J. Hah, S.M. Koo, Y.C. Bae, *Journal of Photochemistry and Photobiology A: Chemistry*, 163, 37–44, 2004.
159. J. Paredes, S. Villar-Rodil, M. Fernandez-Merino, L. Guardia, A. Martínez-Alonso, J. Tascón, *Journal of Materials Chemistry*, 21, 298–306, 2011.
160. Y. Guo, X. Sun, Y. Liu, W. Wang, H. Qiu, J. Gao, *Carbon*, 50, 2513–2523, 2012.
161. D. Skoog, F. Holler, T. Nieman, There is no corresponding record for this reference.
162. L. Guardia, S. Villar-Rodil, J. Paredes, R. Rozada, A. Martínez-Alonso, J. Tascón, *Carbon*, 50, 1014–1024, 2012.
163. O.G. Apul, Q. Wang, Y. Zhou, T. Karanfil, *Water Research*, 47, 1648–1654, 2013.
164. G. Fu, K. Wu, J. Lin, Y. Tang, Y. Chen, Y. Zhou, T. Lu, *The Journal of Physical Chemistry C*, 117, 9826–9834, 2013.
165. H. Qiu, X. Dong, B. Sana, T. Peng, D. Paramelle, P. Chen, S. Lim, *ACS Applied Materials & Interfaces*, 5, 782–787, 2013.
166. B.-H. San, J.A. Kim, A. Kulkarni, S.H. Moh, S.R. Dugasani, V.K. Subramani, N.D. Thorat, H.H. Lee, S.H. Park, T. Kim, *ACS Nano*, ACS Nano, 8, 12120–12129, 2014.
167. F. Maddalena, M.J. Kuiper, B. Poolman, F. Brouwer, J.C. Hummelen, D.M. de Leeuw, B. De Boer, P.W. Blom, *Journal of Applied Physics*, 108, 124501, 2010.
168. S. Thiemann, M. Gruber, I. Lokteva, J. Hirschmann, M. Halik, J. Zaumseil, *ACS Applied Materials & Interfaces*, 5, 1656–1662, 2013.
169. H. Jing, Q. Zhang, N. Large, C. Yu, D.A. Blom, P. Nordlander, H. Wang, *Nano Letters*, 14, 3674–3682, 2014.
170. J. Ju, W. Chen, *Analytical Chemistry*, 87, 1903-1910, 2015.
171. M. Li, X. Bo, Y. Zhang, C. Han, L. Guo, *Biosensors and Bioelectronics*, 56, 223–230, 2014.
172. T. Qian, C. Yu, X. Zhou, S. Wu, J. Shen, *Sensors and Actuators B: Chemical*, 193, 759–763, 2014.
173. Ş. Ulubay, Z. Dursun, *Talanta*, 80, 1461–1466, 2010.
174. Y. Yu, Z. Chen, S. He, B. Zhang, X. Li, M. Yao, *Biosensors and Bioelectronics*, 52, 147–152, 2014.
175. X. Bo, J.C. Ndamanisha, J. Bai, L. Guo, *Talanta*, 82, 85–91, 2010.
176. L. Shang, B. Zeng, F. Zhao, *ACS Applied Materials & Interfaces*, 7, 122–128, 2015.

177. R. Feng, Y. Zhang, H. Ma, D. Wu, H. Fan, H. Wang, H. Li, B. Du, Q. Wei, *Electrochimica Acta*, 97, 105–111, 2013.
178. C. Li, Y.-L. Wu, T. Yang, Y. Zhang, W.-G. Huang-Fu, *Journal of Chromatography A*, 1217, 7873–7877, 2010.
179. H. Wang, Y. Zhang, H. Li, B. Du, H. Ma, D. Wu, Q. Wei, *Biosensors and Bioelectronics*, 49, 14–19, 2013.
180. S. Woo, Y.-R. Kim, T.D. Chung, Y. Piao, H. Kim, *Electrochimica Acta*, 59, 509–514, 2012.
181. L. Meng, Y. Xia, W. Liu, L. Zhang, P. Zou, Y. Zhang, *Electrochimica Acta*, 152, 330–337, 2015.

14

Ion Exchangers – An Open Window for the Development of Advanced Materials with Pharmaceutical and Medical Applications

Silvia Vasiliu*[1], Violeta Celan[1,2], Stefania Racovita[1], Cristina Doina Vlad[1], Maria-Andreea Lungan[3], and Marcel Popa[3]

[1]*"Petru Poni" Institute of Macromolecular Chemistry, Iasi, Romania*;
[2]*Collin County Community College, Plano, TX, USA;*
[3]*"Gheorghe Asachi" Technical University of Iasi, Faculty of Chemical Engineering and Environmental Protection Department of Natural and Synthetic Polymers, Iasi, Romania*

Abstract

The ion exchangers represent an important tool for the development of controlled or sustained release systems because of their excellent properties. The area of pharmaceutical applications of the ion exchangers is very large and includes: the isolation of chemicals, the masking of the unpleasant taste of a drug, the improvement of the dissolution of poorly soluble drugs, the improvement of the drugs stability, the delivery of anticancer drugs and chemosensitizers to multidrug resistant cells and solid tumors, the controlled drug release for oral, nasal, transdermal and ocular applications, the treatment of liver diseases, renal insufficiency, urolithic and skin diseases, as adsorbents of toxins, bile acid sequestrants or osmotic pump tablets. This chapter describes different strategies that have been developed in order to obtain the new advanced materials based on the ion exchangers as well as their medical applications where the materials have been used for the treatment of several diseases.

Keywords: Ion exchange resins, adsorbent, taste masking, controlled drug delivery, resinates, transdermal applications

**Corresponding authors*: vasisilv@yahoo.com and msilvia@icmpp.ro

Ashutosh Tiwari, Hirak K. Patra and Anthony P.F. Turner (eds.) Advanced Bioelectronic Materials, (467–502)

14.1 Introduction

The evolution and the amazing development in the field of polymer science and engineering have a great impact on the discovery and creation of new advanced materials that could be used in medical and pharmaceutical fields for the elaboration of modern therapeutic strategies. Because of their excellent properties such as, physico-chemical stability, inert nature, uniform size, spherical shape, presence of functional groups, high capacity of drug loading and prevention of dose dumping, the ion exchangers represent a huge opportunity to improve the old pharmaceutical forms or to develop new controlled or sustained release systems.

From the chemical point of view, an ion exchanger (IE_r) or ion exchange resin (IER) is defined as an insoluble matrix or crosslinked polymer network to which an ion is electrostatically bound [1]. Therefore these materials are insoluble polyelectrolytes with high molecular weights that can exchange their mobile ions with the surrounding medium (Figure 14.1).

IERs are used in reversible ion exchange process that involves two phases, an insoluble phase (IER) and an aqueous solution phase. When both phases are in contact an exchange can occur, the extend to which depends on the concentration of the ions in solution phase as well as their affinity for the insoluble phase [2].

Ion exchange resins are useful due to their insolubility in liquid phase that allows them to be separated by filtration. After filtration they could be regenerated by an ionic process that leads to their original ionic form. Therefore, they are used in continuous process involving columns and chromatographic separations [3].

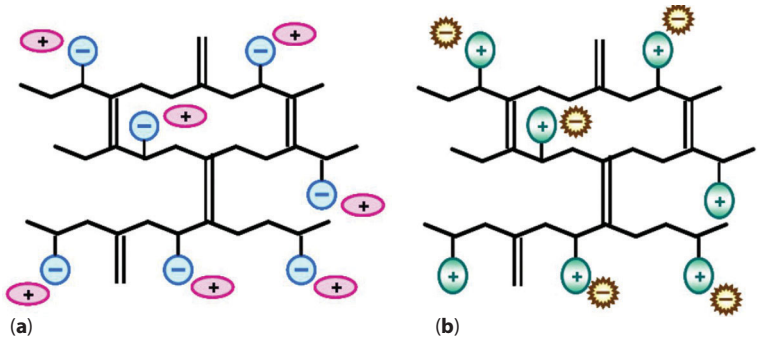

Figure 14.1 Schematic representation of a cation exchange resin (a) and an anion exchange resin (b)

IERs have many applications in different and various fields such as, water softening, removal of organic and inorganic pollutants from water, hydrometalurgy, biomolecular separations, biotechnology, catalysis, medicine and pharmacy [4-8].

14.1.1 Classification of IER

The various ion exchange resins can be classified as shown in Table 14.1 on the basis of nature of structural and functional components and ion exchange process.

Synthetic IER have been synthesized by two different methods namely polymerization and polycondensation and their classification is presented in Table 14.2.

A typical cation-exchange resin is prepared by the copolymerization of styrene and divinylbenzene. During the polymerization, polystyrene formed as linear chains become covalently bonded to each other by divinylbenzene crosslinks. If sulphuric acid is then allowed to react with this copolymer, sulfonic acid groups are introduced into most of the benzene rings of the styrene-divinylbenzene polymer, and the final substance formed is known as cation-exchange resin. A typical anion exchange resin is prepared initialy by a chloromethylation reaction of the benzene rings of the three dimensional styrene-divinylbenzene copolymers to attach $-CH_2Cl$ groups and then causing these to react with a tertiary amine, such as trimethylamine. This gives the chloride salt of strong-base exchanges.

Table 14.1 Classification of ion exchange resins

IER	1) Cation exchange resin	a) Inorganic	- Natural (e.g. clays) - Synthetic (e.g. zeolites)
		b) Organic	- Natural (e.g. lignite) - Semi synthetics (e.g. Sephadex Ion Exchangers) - Synthetic (e.G. Acrylic exchangers)
	2) Anion Exchangers	a) Inorganic	- Natural (e.g. Dolomite) - Synthetic (e.g. Silicates)
		b) Organic	- Natural (e.g. Soil humus) - Semi synthetic (e.g. Sephadex Ion Exchangers) - Synthetic (e.g. IRA 410)

Table 14.2 Classification of synthetic IER

Type	Name	Ionic Group	Commercial Resins
Anion Exchangers	Strong base	> N^+<; > S^+-; > P^+ <	Amberlite IRA 400; Duolite AP 143
	Weak base	-NH_2; > NH; > N -	Amberlite IR 48
	Intermediate	> N^+< and -NH_2	Dowex 2
Cation Exchangers	Strong acid	-SO_3H	Amberlite IR 120; Dowex 30
	Weak acid	-COOH; -C_6H_4OH	Amberlite IRC 50
	Intermediate	-$P(O)(OH)_2$; -O-P(O)(OH); -P(O)H(OH)	Dowex 50WX8
Amphoteric Exchangers	-	acid and base groups	Amberlite XAD-2

14.2 Characteristics of IER and Methods of Characterization

The characteristics of IER and some methods of characterization are presented in Figure 14.2.

14.2.1 Crosslinking Degree

Degree of crosslinking defined as the density of crosslinks between polymeric chains has a major influence on the structure of the matrix, elasticity, swelling ability as well as the mobility of the counterions inside the matrix of ion exchanger [9]. The materials characterized by a high crosslinking degree are harder and, in many cases, more stable. However, the diffusion in such materials is slow causing the reduction of the rate of all processes. Low crosslinked materials can be even jelly-like. Their stability could be low in benefit of fast kinetics of interactions. Conventionally, the crosslinking degree is expressed as percentage of the crosslinking reagent introduced in a reaction mixture at the synthesis stage.

For practical purposes the range of crosslinking degree is from 4% to 16%. IER with very low crosslinking degree tend to swell and change dimensions markedly.

The distribution of the polymeric chains, crosslinks, and functional groups in the bulk of ion exchange resin is random but it is sufficiently even to consider the material as homogeneous.

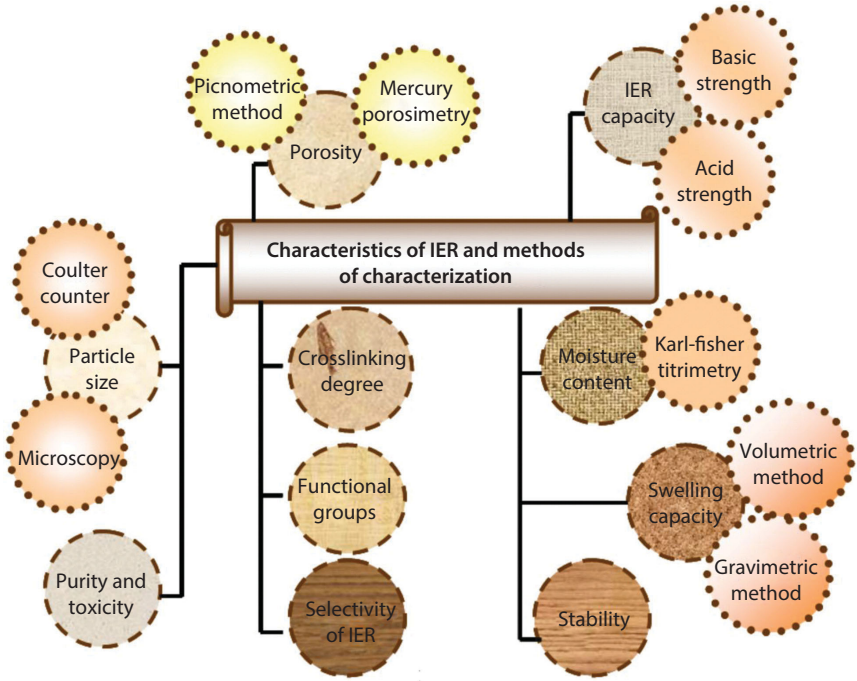

Figure 14.2 Characteristics of IER and methods of characterization

14.2.2 Moisture Content and Swelling Degree

Moisture content represents a physical property of the ion exchange resins that is directly proportional to the number of hydrophilic functional groups attached to the polymer matrix and inversely proportional to the degree of crosslinking degree. Also, the high moisture can cause a rapid exchange, low total capacity and good absorption capacity, while the low moisture can lead to higher total capacity, difficulty in resin regeneration, tendency to fouling and difficulty in removing of large ions. The moisture content can be determined by Karl Fisher titrimetry [10].

Water swelling of an ion exchanger is primarily a hydration of the fixed ionic groups and increases with an increase in capacity to the limits imposed by the polymer network. In order to determine the swelling degree two methods can be used: the gravimetric and the volumetric methods. Generally, the main factors which can affect the swelling of ion exchange resins are: (a) the nature of the polymer network and the solvent; (b) the types of the functional groups and the counterion, respectively; (c) the crosslinking degree; (d) the exchange capacity; (e) the macrostructure of the IER and (f) the composition, pH and temperature of the external solution [11]. The resin volumes change with the conversion to ionic forms

of different degrees of hydration; thus, for a cation exchanger, there is a volume change with the monovalent ion species, $Li^+ > Na^+ > K^+ > Cs^+ > Ag^+$.

With polyvalent ions, hydration is reduced by the crosslinking action; therefore, $Na^+ > Ca^{2+} > Al^{3+}$. In more concentrated solutions, less water is taken up owing to greater osmotic pressure.

14.2.3 Particle Size and Particle Size Distribution

Usually the IERs are prepared as spherical beads with diameter in the range of 0.5 mm to 1.0 mm. A series of ion exchange resins were prepared from polystyrene micropowders with a particle size of 0.5 μm to 1.5 μm. The results of their applications as materials incorporated into paper for removal of organic pollutants have revealed that ultrafine particles could limit the rates of the reaction [12]. It is known from literature, that the ion exchange rate is inversely proportional to the particle size of ion exchangers [13]. The particle size and the particle size distribution can be determined by microscopy, Coulter Counter and other techniques [14, 15].

14.2.4 Porosity

Porosity of IER is an important factor in ion exchange technology that depends on the crosslinking degree and represents a measure of limiting size of ions which can penetrate into a IER matrix.

Porosity can be classified as porosity in a swellen state and macroporosity. These types of porosity have been formed by the modification of the monomer phase used in the polymerization step by including a porogen – a compound in which the monomer was soluble and the polymer as it formed was soluble too (porosity in swelling state) or insoluble (macroporosity). The insolubility of the polymer resulted in a change of bead morphology so that it became permanently porous [16].

The advantages of macroporosity has been observed when the macroporous resins greatly outperform the conventional resins.

An important feature of the macroporous materials is the relative constancy of their shape. Macropores do not collapse when these materials lose water that is in contrary to pores of the gels which appear only in the swollen state (even their size is defined by the swelling degree).

Macroporous resins are highly advantageous if the performance of the process is limited by a slow diffusion of exchanged ions in the gel phase of the material. The diffusion is much faster when it takes place in the liquid phase filling the macropores (the solution in macropores is the same or, at least, similar to the solution surrounding the exchanger). Besides the

facilitation of the diffusion rates, the open-pore structure allows diffusion of large molecules. The exchange takes place on the surface of macropores or in close proximity to the surface, thus the molecules do not enter the dense gel regions. In addition to the faster process rates, macroporous ion exchange polymers exhibit better chemical stability, especially resistance to oxidation [17]. The porosity of IER can be determined by mercury porosimetry [18] or by the pycnometric methods [19].

Using the values of skeletal (r) and apparent (r_{ap}) densities determined by the pycnometric methods with n-heptane and mercury, respectively [20], two important characteristics of the macroporous ion exchangers can be calculate as follows:

1. Pore volume (PV) [21]:

$$PV = \frac{1}{\rho_{ap}} - \frac{1}{\rho} \text{ (mL/g)} \tag{14.1}$$

where ρ_{ap} is the apparent density (g/mL) and ρ is the skeletal density (g/mL).

2. Porosity (%P) [22]:

$$\%P = 100 \times \left(1 - \frac{\rho_{ap}}{\rho}\right) \tag{14.2}$$

Also, the scanning electron microscopy and atomic force microscopy (AFM) studies reveal important information about the internal and the surface pore structure.

14.2.5 Ion Exchange Capacity

The ion exchange capacity is the most important charateristic of IER and represents the total number of functional groups bearing ions per unit weight or unit volume of resin.

When the resins is highly crosslinked, the addition of the functional groups become more difficult and therefore the resin has a low ion exchange capacity value. In general terms, the capacity of an ion exchange resin can be expressed as the quantity of ions that can be taken up by a specific volume of the resin. This would be expressed in quantity per unit volume, such as milliequivalents per millilitr (meq/mL), which also equals equivalents per liter (eq/L).

Technically, resin capacity is a measurement of total capacity, as determined by a test performed in the lab by a titration methodology [23]. A

measured quantity of cation resin, for example, is fully converted to the hydrogen (H) form with an excess of strong acid and then well rinsed. A measured quantity of caustic soda (NaOH) is then passed through the resin in order to totally exhaust the resin. The effluent is captured. The NaOH that passed through the column represents the sodium (Na) ions that were not captured by the resin. This solution is then titrated with acid to neutralize it, and the amount of acid required is expressed in equivalents. The difference between the total equivalents of NaOH passed through the column and the NaOH exiting in the column represents the total equivalents of Na captured by the resin. Thus, the capacity of the resin is then determined.

Similarly, the anion resin would be fully regenerated with NaOH and exhausted with acid to make the capacity measurement. The total capacity can be expressed as meq/mL (volumetric) or meq/g (based on weight). Generally speaking, when we refer to the capacity of resin, we are referring to operating capacity that must specify the exact feed-water challenge and flow-rates as well as the endpoint. The operating capacity is a measure of the useful performance obtained with the ion exchange material when it is operating in a column under a prescribed set of conditions. It is dependent on a number of factors including the inherent (total) capacity of the resin, the level of regeneration, the composition of solution treated, the flow rates through the column, temperature and particle size and distribution.

14.2.6 Functional Groups

The main difference between polymeric ion exchangers and non-functional polymers is the presence of functional groups or functional sites in the structure, i.e. the presence of functional units is the main feature of the materials discussed. There is a wide diversity of functional groups that have been attached to polymeric networks to obtain ion exchange properties. Different examples are given in Table 14.2.

Chemical properties of functional groups define the type of a particular ion exchange material. The cation and anion exchangers are the two types bearing respectively the negatively and positively charged groups and, hence, being able to exchange cations or anions. Due to different dissociation properties of groups, strong and weak exchangers are recognized similar to that of strong and weak electrolytes. The most common cation exchangers are strongly acidic resins with sulfonic acid groups ($-SO_3H$) and weakly acid resins with carboxylic acid groups (–COOH). Different ion exchangers bearing the same groups can exhibit significantly different properties because the strengths of the groups depend on the nature of the supporting hydrocarbon structure. Most of the functional groups of anion

exchangers contain nitrogen as a proton-accepting atom. Similar to low molecular weight amines, weak-base ($-NH_3^+$, $>NH_2^+$) and strong-base (for example, $> N^+<$ or $-N^+(CH_3)_3$) anion exchangers are recognized.

14.2.7 Selectivity of the IER

Ion exchange reactions are reversible. By contacting an ion exchange resin with an excess of electrolyte (B^+), the resin can be converted entirely to the desired salt form according to the following reaction:

$$R\text{-}A^+ + B^+ \leftrightarrow R\text{-}B^+ + A^+$$

For the ion exchange to be efficient there must be a difference in affinity between the ion in the resin and the ion or ions from solution. The resin must have a higher affinity for the ion in solution compared to the ion in the resin [11]. The ion exchange technology is a perfect tool to remove or exchange contaminants present in low concentrations. In such a case the running time until the resin column is exhausted can be very long, ranging from a few hours to several months. When however the concentration of contaminants is high, the ion exchange cycles become exceedingly short and the quantity of regenerants increases to uneconomical levels. Based on the differences of affinity for different ions, common ion exchange resins can be used to remove selectively ions from water. One of the most obvious examples is softening. This works because the anion resin has more affinity for the nitrate or sulphate ion than for the chloride ion, the order of affinity being: $SO_4^{2-} > NO_3^- > Cl^- > HCO_3^- > OH^- > F^-$. For cation resins used in softeners, the affinity is $Pb^{2+} > Ca^{2+} > Mg^{2+} > Na^+ > H^+$.

14.2.8 Stability

The stability of ion exchangers can be influenced by a various forms of stress, such as physical, osmotic and thermal stress or organic fouling. Strong oxidizing agents, such as nitric or chromic acid, rapidly degrade ion exchange resins. Slower degradation with oxygen and chlorine may be induced catalytically. For this reason, certain metal ions, for example, iron, manganese and copper, should be minimized in an oxidizing solution. Highly crosslinked cation resins have an extended useful life because of the great number of sites that must be attacked before swelling reduces the useful volume capacity and produces unacceptable physical properties, for example, crush strength reduction and pressure drop increase. With anion exchangers, attack first occurs on the more susceptible functional groups, leading to the loss of total capacity and/or conversion

of strong base to weak base capacity. The limits of thermal stability are imposed by the strength of the carbon-nitrogen bond in the case of anion resins [24]. This strength is sensitive to pH and low pH enhances stability. A temperature limitation of 60 °C is recommended for hydroxide cycle operations. The cation resin stability also is dependent on pH: the stability to hydrolysis of the carbon-sulfur bond diminishes with a lowering of the pH. They are much more stable than anions and can be operated up to 150 °C.

14.2.9 Toxicity

For medical and pharmaceutical applications, the purification of the resin is necessary in order to remove the impurities that can cause severe toxicity. However, purified resins are nontoxic, but administrated in large quantities can cause harmful side effects and may seriously disturb the electrolyte balance in the gastrointestinal tract.

14.3 Resinate Preparation

Since 1920, when Folin and Withehorn [25, 26] used the ion exchange principle to solve some problems in the drug industry, the research has been directed towards finding the new materials based on ion exchangers to respond to the permanent requirements of the medical world. For the first time, Saunders and Chaudhary [27] have used the ion exchange resins as polymeric support in the manufacture of the sustained release system of charged drugs. The suitable selection of drugs and IER for resinate formulation should take into account many factors, which are presented in Table 14.3 [13, 28].

For example, if a rapid dissolution of drug in the gastrointestinal tract is necessary the IER must have the following requirements: weak cation or anion exchangers with low crosslinking degree, small particle size and high drug loading capacity, while for slow or sustained release and taste masking can be used strong cation and anion exchangers with high crosslinking degree, large particles size and lower drug loading capacity. Generally, resinates are obtained by mixing the resin with a drug solution for a few hours. Then, the esinate is separated by filtration and can be stored in dry form as free flowing powder or in liquid suspension according to later usage. In literature two main methods are known for loading the drug into ion exchange resin, such as: batch and column methods [29].

Table 14.3 Characteristics of drug and IER necessary to obtain resinate formulations

Characteristics of drugs	**Factors affecting IER performance**
Drug should be anionic, cationic or amphoteric	Crosslinking degree
The half –life of drugs must be 2-6 h	Particle size and size of exchanging ion
Should be stable in gastric juice	Swelling ratio
High bioavailability throughout the gastrointestinal tract	pH and temperature
pKa	Selectivity of counterion
	Stability and toxicity

In the batch method the drug solution is mixed with a known quantity of resin particles until the equilibrium is established, while in the column method the concentrated drug solution is passed through a fixed bed of resin. Also, the drug can be loaded onto resins by an ion exchange reaction, resulting in the formation of drug-resin complexes, better known as resinates. The amount of the drug loaded onto IER can be influenced by various factors such as: (a) concentration of drug solution; (b) selectivity of the ionic groups of resins for the drug; (c) type of solvent used; (d) molecular size of the drug; (e) resin: drug ratio; (f) contact and mixing time [30] The utility of ion exchange systems as carriers in the medical applications has some advantages, especially for drugs which can undergo an enzymatic degradation.

14.4 Pharmaceutical and Medical Applications

A major problem in medicine is represented by the increase of treatment efficiency as well as by the elimination of drug side effects, determined either by overdose, either by their aggressiveness sometimes not only against the cancerous cells, but also against healthy ones. In general, the purpose of drugs use consists in:

- prevention of illness through vaccinations;
- improvement of symptoms;
- cure of diseases with local action by application of solutions or unguents or diseases with general action through antibiotics.

The administration is mainly determined by the drug properties and therapeutic purposes. The drug administration can be achieved in two ways:

- natural ways which consist of a drug being absorbed through mucous (oral, conjunctival, nasal, rectal, auricular, vaginal) and through skin;
- artificial ways, known also as parenteral administrations (intramuscular, intravenous, subcutaneous).

Drugs administration under free form, no matter of its category: oral, parenteral or unguents has as effect the continuous change of drug concentrations in human body or at the affected area. Shortly after the administration, the concentration of the active element is higher than the one corresponding to the therapeutic domain, which at this point can become toxic. Then, the drug concentration drops rapidly under the therapeutic value, which imposes a new drug administration.

The administration of a drug immobilized on a polymeric support determines a variation of its concentration in the body based on different kinetics. The drug is gradually released from the macromolecular support maintaining in this way a constant concentration in the body at therapeutic value. It is obvious that the efficiency is increased in the second case. The controlled drug release has as objective not only having a sustained action, but also maintaining it constant, which would require a zero-order release rate in which the quantity of the drug released in the time frame towards the site of absorption remains constant for a long period.

The resinate can be obtained in various pharmaceutical forms, that are presented in Figure 14.3.

The area of pharmaceutical and medical applications of ion exchangers is very large and includes the following aspects:

1. pharmaceutical production (demineralization of water [31]; drug purification (cephalosporin-C, streptomycin sulfate, penicillin) [32]; treatment of fermentation products; extraction and purification of enzyme (lyzozyme), hormones, alkaloids (opium), amino acids, stabilization of vitamins [33]; separation of proteins, insulin and peptides [34]);
2. active pharmaceutical ingredients and excipients (taste and odor masking [35]; tablet disintegrants/superdisintegrant [36]; improve the dissolution of poorly soluble drugs [37]; improve the stability and physical characteristics of drugs

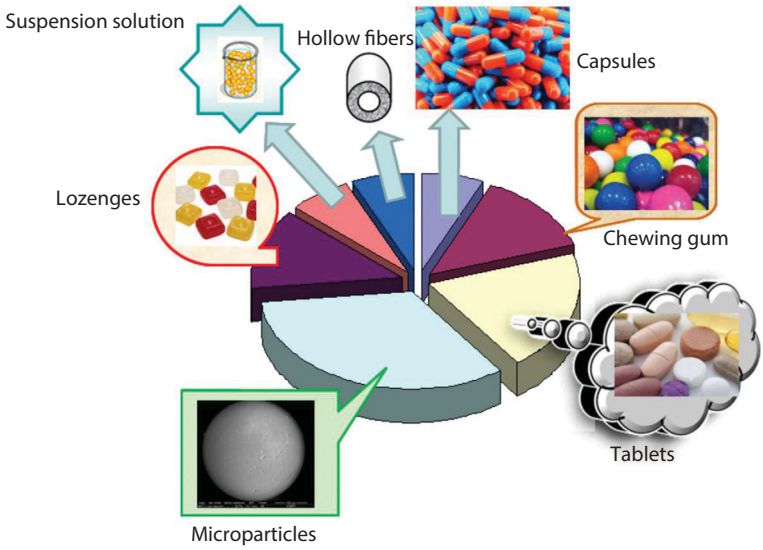

Figure 14.3 Pharmaceutical forms of resinate

[38]; solve the problem of deliquescence; eliminate polymorphism; powder processing aid [39]);

3. controlled drug delivery (delivery of anticancer drugs and chemosensitizers to multidrug resistant cells and solid tumors [40]; oral, nasal, transdermal and ophthalmic applications [41-44]; implantation devices [45]);
4. diagnosis and therapeutic applications (cholesterol reducer [46]; treatment of liver diseases; hiperkalemia and acute renal insufficiency [47]; urolithic and skin diseases; as adsorbents of toxins [48]; gastric acidity reducer [49]; bile acid sequestrants [46]; osmotic pump tablets [50]; regime of weight reduction; management of drug overdose; cardiac failure; pre-eclampsia; hemoperfussion [51]; chewing gum for smoking cessation program [42]; determination of sodium levels in blood and urine; removal of zinc and calcium ions from blood).

14.4.1 Taste and Odor Masking

Since the late 1950s, the IERs were used to mask the bitter taste of drugs for enhance patient compliance, especially for pediatric and geriatric purpose. Most of the bitter drugs have amine and amide functional groups and the

formation of an ionic complex with IER is a way to reduce drastically the bitterness of the drugs. The taste like the smell is a chemical sense that relies on the bonding of the chemical substance (tastants) from the food, drinks or drugs by the taste receptors from the mouth. In humans, in different regions of the tongue are located three types of papillae: filiform, fungiform, circumvallates and foliate papillae. The first type of papillae detect only the texture of the food, while the last three types of papillae contain the taste receptors clustered in a onion shaped cells namely taste buds [52]. These receptors take and then transmit the information to the brain via nerve, where they are perceived as tastes.

The history of the taste map started in the early 1900s, when the German researcher D.P Hanig published data on the taste sensitivity in various regions of the tongue. Also, in the same period of time in Japan, Professor Ikeda Kikunae discovered, while studying the taste of the Kombu broth, a new sense of taste called Umami, which has been accepted by the scientific world more recently. Umami or savory is a "good" taste and represents the sensitivity to aminoacids (glutamic acid) (Figure 14.4) [53]. Thus, some regions of the tongue are more sensitive to certain gustatory sensations as follows: tip of the tongue is most sensitive to sweet (indicates energy rich nutrients) and salty (modulate diet for electrolyte balance), the lateral sides are more sensitive to sour (taste of acids), bitter taste is perceived on the back of the tongue (taste of diverse natural toxins) and the whole tongue is sensitive to umami taste.

However, these gustatory sensations are not perfectly defined because most of taste buds can respond at two, three or all taste sensations. Thus,

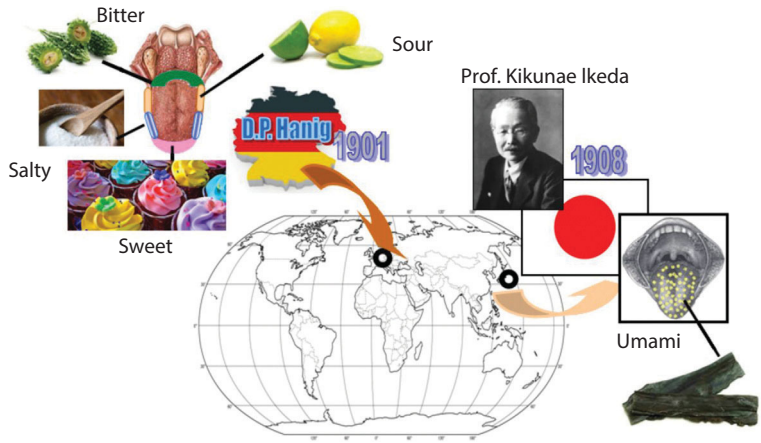

Figure 14.4 Taste sensations map and history

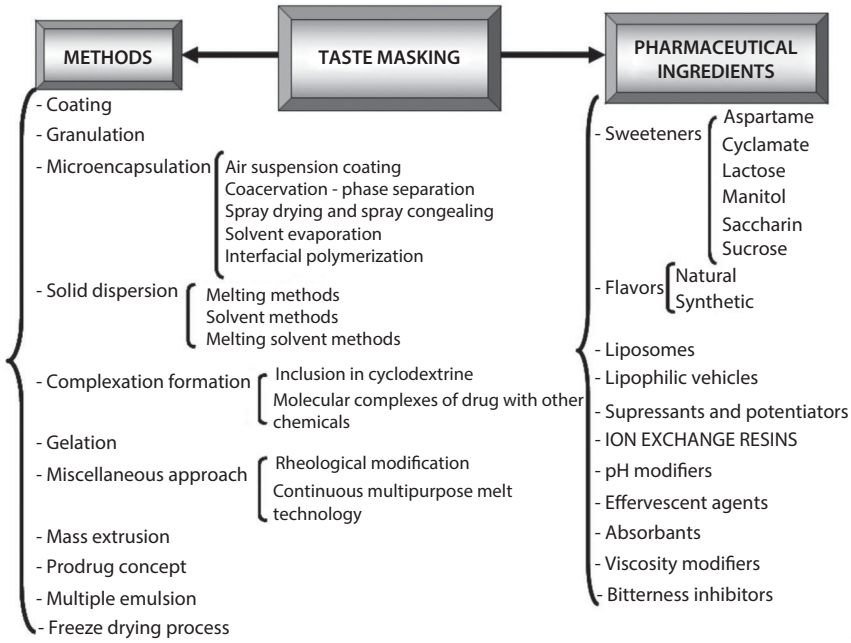

Figure 14.5 Methods used for taste masking of drug

certain substances seem to change their taste as they stay longer in the mouth. For example, at the beginning saccharin have a sweet taste, but over a period of time tends to become bitter. Generally, the bitterness is caused by two classes of substance such as, alkaloids and long chain organic substances with nitrogen in their structures. For bitter drugs [antibiotics (penicillin, levofloxacin), non steroidal anti inflammatory drugs] the taste can be masked by using either pharmaceutical ingredients like flavors, sweeteners, adsorbents, either various techniques as shown in Figure14.5 [54].

The selection of the taste masking methods can be affected by the following factors: (1) the quantity of active pharmaceutical ingredients; (2) the degree of bitterness of the drug; (3) the drug particle shape and drug solubility; (4) the dosage form; (5) the ionic characteristics of the drug molecules. Among these methods, ion exchange resins are a useful tool in taste masking of bitter drugs resulting in a better patient compliance. Thus, the strong acid cation exchangers and the strong anion exchangers can be used throughout entire pH range for taste masking of basic and acid bitter drugs, respectively. Weak acid cation exchangers can be used at pH values above 6, while the weak base anion exchangers function below pH = 7. Thus, to mask the bitter taste of drugs that contain in their structure amine or amide groups respectively, most of oral pharmaceutical preparations are

based on cation exchange resins [55]. In Table 14.4 are presented some examples of IER used in taste masking of bitter drugs.

14.4.2 Tablet Disintegrant and Rapid Dissolution of Drug

Disintegrants are excipients added to the tablets or capsules in order to achieve breakage of the tablets when these meet an aqueous medium.

The mechanisms of disintegrate action are: (1) swelling; (2) porosity and capillary action; (3) deformation; (4) particle/particle repulsive forces; (5) release of gases and (6) enzymatic route [74, 91]. Several types of ion exchange matrices are hydrophilic and have a high water retention capacity leading to the increase of the rate of drug dissolution and therefore their use as tablet disintegrant. For example, INDION 414 (ion exchange resin based on polyacrylic acid) used as tablet disintegrant present some advantages: (i) high swelling capacity; (ii) are compatible with various therapeutic agents and excipients; (iii) lack of adhesion tendency; (iv) are insoluble; (v) the tablet based on this resin has a good mechanical stability; (vi) don't lump [91].

Jeong and Park used the Amberlite IRP 69 for preparing dextromethorphan resinates, which are coated by various polymeric materials in order to obtain a sustained-release fast disintegrating tablets [92].

14.4.3 Controlled Drug Delivery

The low efficiency of drugs with small molecular weight in the treatment of severe diseases and the series of disadvantages, like: (1) the necessity of multiple drug doses in a short period of time in order to achieve the proper therapeutic dosage; (2) the possible fluctuation of the active principle concentration in the blood flow which may lead to low or toxic dosage and (3) intermittently and/or incomplete sorption of the active principle, lead to the necessity of finding new strategies in elaboration and improvement of controlled drug delivery systems or target systems.

In the last 30 years, the use of polymeric materials as transporters in biomedicine and biotechnology has made remarkable progress. As macromolecular supports for drug delivery, polymers can play two essential roles: protection of the bioactive molecules when it is transported through the body to the target organ, or to control the release of bioactive molecules in a pre-determined period of time.

The advantages presented by drug delivery systems are: maintenance of drug concentration in the therapeutic domain for a long period of time, prolongation of drug activity, elimination of local effects, low toxicity,

Table 14.4 IER used in taste masking of bitter drugs

Drug	Medical uses	Ion exchange resins	Ref.
Chlorpheniramine maleate	Symptoms of allergic conditions	Indion CRP-244	[56]
Pseudoephedrine hydrochloride	Bronchodilators	Indion CRP-244/254; Amberlite CG 50	[57]
Diphenhydramine hydrochloride	Allergic symptoms, itchiness, insomnia, motion sickness	Indion 234, Tulsion 343	[58]
Erythromycin	Antibiotics	Carbomer 934	[59]
Clarithromycin	Pharyngitis, tonsillitis, acute maxillary sinusitis, pneumonia	Carbomer 934	[59]
Ranitidine	Peptic ulcer disease, gastroesophageal reflux	Amberlite IRP 69	[60]
Paraxetine hydrochloride	Depression, obsessive compulsive disorders	Amberlite IRP 88	
Dextromethorphan	Cough suppressant	Amberlite IRP 69 Carbomer 934	[61]
Ciprofloxacin hydrochloride	Infections	Lewatit CNP, Indion 234	[62]
Chloroquinine	Malaria prevention	Indion 234	[63]
Norfloxacin	Urinary tract infection	Indion 204	[64]
Ofloxacin	Infections	Kyron T114, Indion 204	[65]
Levofloxacin	Respiratory, urinary tract, gastrointestinal, and abdominal infections	Amberlite IRP 69	[66]
Sparfloxacin	Treatment of bacterial infections	Cationic exchange resin	[67]
Azithromycin	Otitis, infections	Indion 214	[68]

(*Continued*)

Table 14.4 cont.

Drug	Medical uses	Ion exchange resins	Ref.
Cefpodoxime proxetil	Otitis media, sinusitis	Kyron T104	[69]
Metronidazole	Anaerobic infections, Crohn disease, giardisis	Kyron T134, Indion 234. Kyron T 114	[70]
Levamisole hydrochloride	Worm infestation, colon cancer, dermatologic diseases	Amberlite IRP 64/69	[71]
Rizatriptan benzoate	Headache, pain, migraine symptoms	Indion 204/214 Tulsion 339/335	[72]
Fexofenadine hydrochloride	Hay fever, allergy symptoms, urticaria	Indion 204, Indion 234, Indion 264	[73]
Orbifloxacin	Antibiotic for veterinary use	Amberlite IRP 64/69	[74]
Remacemide hydrochloride	Acute ischemic stroke, epilepsy, Huntington disease, Parkinson disease	Amberlite IRP 64	[52]
Buflomedil	Symptoms of peripheral arterial disease	Amberlite IRP 69	[74]
Lornoxicam	Osteoarthritis, surgery, sciatica, diseases of joints	Kyron 104	[75]
Thicolchicoside	Anti-inflammatory and analgesic effects	Kyron 104	
Itopride	Dyspepsia, anorexia, nausea and vomiting, bloating	Kyron 114	[76]
Tramadol HCl	Rheumatoid arthritis, restless legs syndrome, fybromyalgia	Kyron 114	[77]
Levocetirizine dyhidrochloride	Allergic rhinitis Chronic idiopathic urticaria	Kyron 114 Tulssion 335	[78]
Cefuroxime axetil	Infections caused by bacteria	Kyron 114	[79]

Cefaclor	Pneumonia, infections of ear, lung, skin, throat and urinary tract	Indion 464	[80]
Dicyclomine HCl	Intestine hypermotility, irritable bowel syndrome	Indion 464	[80]
Amodiaquine HCl	Malaria	Indion 464	[80]
Roxithromycin	Respiratory tract, urinary and soft tissue infections	Kyron T-134, Amberlite IRP-64, Indion 214	[81]
Erdosteine	Chronic obstructive bronchitis	Kyron T-134	[80]
Ondansetron HCl	Antiemetic drug	Kyron T-134 Indion 234	[82]
Artemether	Antimalarial, anthelmitic , anticancer	Kyron T-134	[83]
Melformin HCl	Diabetes mellitus	Indion 214	[84]
Ambroxol hydrochloride	Respiratory diseases	Indion 234 Tulsion 335	[85]
Etoricoxib	Arthritis, dysmenorrheal, acute dental surgery pain	Indion 214, Indion 234, Indion 414	[86]
Mefloquine	Malaria	Indion 234	[87]
Risperidone	Schizoaffective disorders	Amberlite IRP 64	[88]
Ephedrine Hydrochloride	Bronchodilators	Indion CRP 244/254	[89]
Metoclopramide Hydrochloride	Gastrointestinal disorders	Indion 234	[90]

target administration and release of a drug in a specific organ, coverage of the unpleasant taste and/or smell when necessary, diminution of a patient discomfort by eliminating repeat administration, optimization of the therapeutic process and efficiency improvement in the treatment (more uniform blood concentration and reduction in fluctuation in drug level and hence more uniform pharmacological response) and assurance of an optimal continuous treatment even in the night-time faze.

While the advantages of controlled drug release systems are significant, the potential limitations cannot be ignored, namely: potential toxicity of materials and methods of synthesis used, undesirable degradation products, poor *in vivo-in vitro* correlation, types of immobilization methods of drugs, the necessity for parenteral administration, limitation of the ability to cross the capillary endothelium, implantation and/or removal of the system is done by surgery, the controlled drug release systems can cause discomfort to the patients and cost of the preparation and processing of controlled drug release systems can be considerably higher compared with the traditional pharmaceutical formulations [93].

14.4.3.1 Oral Drug Delivery

The drug administration at the digestive tract level it is realized through the drug absorption at gastrointestinal tract by two ways: oral (sublingual, oral and gastrointestinal) and rectal. Comparing with the other ways of drugs administration the oral one has the highest rate due to the fact that it is easy and painless.

This method can have advantages, but also disadvantages.

A. Advantages:

- the easiest way for ambulatory therapy ;
- can be auto administrated painless and without stress ;
- the absorption may occur along gastrointestinal tract;
- the drugs administrated orally have a lower price compared with the ones administrated in different ways

B. Disadvantages:

- the slow therapeutic effect in case of unguents;
- irritation of the stomach lining leading to nausea and vomiting;
- sometimes the method is ineffective because only a part of the drug can be absorbed ;

- it can not be applied to the patients in coma, to the ones presenting vomiting syndrome, convulsions or psychotics [94].

Oral administration is done through the introduction of the system in oral cavity followed by swallowing. The oral administration can be done for:

- local treatment: gastroprotective treatment of the intestinal infections and parasitic diseases;
- general treatment, during which drug absorption occurs in the digestive mucosa followed by its diffusion into the body.

Gastric absorption of pharmaceutical systems can be affected by various factors, such as (1) size, shape and density of pharmaceutical dosage; (2) nature of food; (3) effect of gender, posture (upright position and supine position) and age of patients; (4) feeding regime.

Nowadays, technology offers the possibility to obtain controlled drug delivery systems in various presentation forms [95]:

- Floating drug delivery systems:
  - Single unit dosage forms (Non-effervescent systems and Gas generating systems)
  - Multiple unit dosage forms (Non-effervescent systems, Gas generating systems and Floating (hollow) microparticles);
  - Raft forming systems;
  - Low-density systems;
- Swelling and expandable systems;
- Bio/mucoadhesive systems;
- High-density systems;
- Modified systems.

Floating drug delivery represents one of the most promising buoyant approaches being used in the last period for the prolongation of the gastric residence times. A floating system based on ion exchange resin loaded with bicarbonate and theophylline was developed by Atyabi *et al.* [96, 97] When the system comes in contact with gastric fluid an ion exchange reaction between chloride and bicarbonate ions takes place, leading to CO_2 generation. The CO_2 is trapped on the surface of the microparticles and makes them to float. Yao *et al.* [98] immobilized riboflavin, a drug with limited adsorption window onto a strong anion exchange fibers based on poly(ethylene-g-styrene-trimethyl ammonium chloride) and

demonstrated that the drug-anion exchanger complexes provided good mucoadhesive properties and this system can be useful for the development of muchoadhesive oral drug delivery systems. Core-shell microparticles based on acrylic ion exchange resin as core and gellan or xanthan as shell were used for immobilization of cefotaxime sodium salt in order to obtain a suitable oral drug delivery system [99, 100]. Some examples of simple resinate used in oral controlled drug delivery are presented in Table 14.5.

In some cases the drug release can be very fast in the presence of an excess of ions and dose dumping can occur. This process can be prevented by coating the surface of resinates with different materials such as, waxes or natural and synthetic polymers. The coating acts as a diffusion barrier and its thickness can be adjusted by changing the synthesis parameters so as to provide a slow release of the drug in the gastrointestinal tract.

In Table 14.6 are presented some types of drug delivery systems based on ion exchangers coated with various polymers. For pediatric and gastric

Table 14.5 Examples of simple resinate used in oral controlled drug delivery

Drug	IER	Ref.
Dextromethorphan	Dowex 50WX Amberlite IRP-69	[92]
Propranolol HCl	Cationic exchangers based on calcium alginate Amberlite XE-364R, Amberlite IRP 69, Amberlite IR-120PLUS, Amberlite IR 122	[101]
Chlorpheniramine	Cationic exchangers based on sulfonated styrene-DVB copolymers	[102]
Tacrine	Smopex 101, Smopex 102	
Methylene blue	Indion 234, Indion 234S, Indion 254, Indion 294, Amberlite IRP 64, Amberlite IRP 69, Amberlite IRP 88	[41]
Diclofenac sodium	Duolite ATP 143	[103]
Sulfadiazine sodium	Dowex 1-X8	[104]
Diphenhydramine hydrochloride	Dowex 88, Amberlite IRP 64	[58]
Ranitidine	Amberlite IRP 69	[60]

Table 14.6 Some types of drug delivery systems based on coated ion exchangers [107-125]

Resin	Polymer coating	Drug
Amberlite IRP-69	Poly(methyl methacrylate)	Pseudo ephedrine HCl
	Kollicoat SR 30D	Dextromethorphan hydrobromide
	Methocel K4M	Diphenhydramine hydrochlroide
	Ethyl cellulose	Naproxen sodium
		Chlorpheniramine maleate
	Hydroxypropylmethyl cellulose	Propranolol HCl
	Eudragit RS 100	
	Eudragit RS 100	Venlafaxine HCl
Amberlite IP 88	Ethyl cellulose	Naproxen sodium
Amberlite IR-200	Ethyl cellulose	Phenyl propanolamine
Amberlite XE-69		Phenyl propanolamine
Dowex 2x10	Eudragit	Theophylline
Dowex	Paraffin, ethyl cellulose	Theophylline
Dowex 1-X4	Carbopol 934	Amoxicillin trihydrate
	Hydroxyl propyl methyl cellulose phtalate	Diclofenac sodium
Dowex 1-X8	Poly carbohil	Amoxicillin trihydrate
	Hydroxyl propyl methyl cellulose phtalate	Diclofenac sodium
Dowex 1-X2	Aquacoat	Diclofenac sodium
	Eudragit RS 30D	
Dowex 50Wx4-200	Kollicoat SR 30D	Dextromethorphan
Dowex 50Wx 4	Cellulose acetate butyrate, PVA	Diltiazem
	Eudragit RS, silicon, PVA	Terbutaline hemisulfate
	Ethocel Premium 20, 45, 100	Dextromethorphan hydrobromide monohydrate
Dowex 50Wx 8	Cellulose acetate butyrate	Diltiazem
Dowex 88	Eudragit RS 100	Chlorpheniramine maleate
Duolite AP 143	Eudragit RL	Naproxen sodium
Indion 244	Eudragit RS 100	Chlorpheniramine maleate
	HPMC	Verapamil HCl
Indion 254	HPMC	Verapamil HCl
	Poly ethylene imines, polystyrene	Propranolol HCl
	Polystyrene, methyl cellulose	Diltiazem HCl
Indion 234	Poly ethylene glycol	Ciprofloxacin
Tulsion 335	Hydroxypropyl cellulose-LF	Cetirizine HCl

patients were developed several oral controlled drug release liquid suspensions based on various resinates, such as: Delsym [105], Liquifer [13], Penntuss [106] and theophylline controlled release liquid [107].

Another approach for oral drug delivery system is represented by the elementary osmotic pump tablets that can be used in ulcerative colitis, asthma, heart diseases and arthritis. In this case, the driving force for delivery of active substance is osmotic pressure.

Wang *et al.* [50] have developed a novel time controlled system based on a combination between propranolol HCl-Amberlite IRP 69 complexes and osmotic pump tablet. The *in vitro - in vivo* experiments recommend these osmotic pump tablets as therapeutic agents in chronotherapy. The drug release mechanism from resinate in the gastrointestinal tract is presented in Figure 15. 6.

The release rate of drugs from resinates can be affected by various factors such as: selectivity of drug for the resin, ionic environment in the gastrointestinal tract and properties of resin [109].

Generally, the mathematical approaches to investigate the kinetics of drug release from drug delivery systems are presented in Table 14.7. Drug release from resinate can be controlled by two mechanisms: (1) diffusion of drug across the thin liquid film which is formed around the resinate particle; (2) diffusion of free drug in the resin matrix.

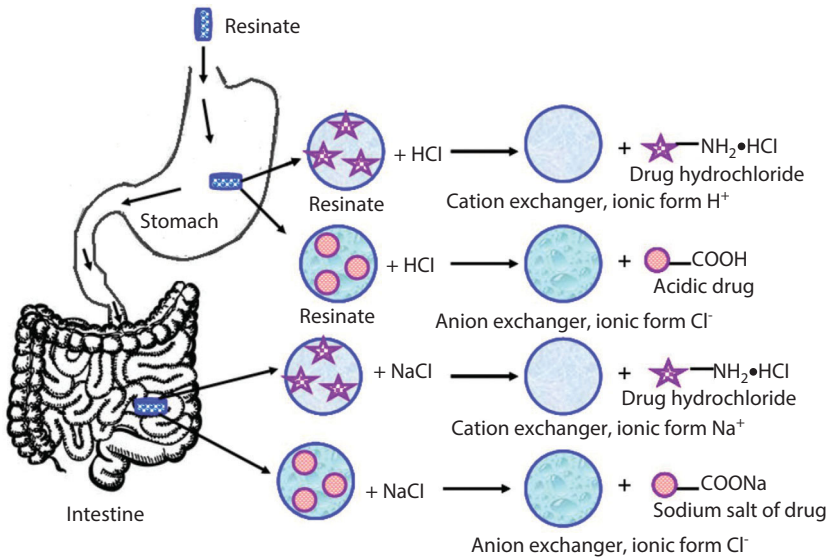

Figure 14.6 Drug release mechanism from resinate in the gastrointestinal tract

As suggested in the Boyd model [126] the fraction of drug released can be determined by the following equation:

$$F = \frac{M_t}{M_\infty} = 1 - \frac{6}{\pi^2}\sum_{n=1}^{\infty}\frac{e^{-n^2Bt}}{n^2} \qquad B = \frac{\pi^2 D_i}{r^2} \tag{14.3}$$

where: M_t = amount of drug released at time t; M_∞ = amount of drug released at infinite time; B = rate constant; D_i = effective diffusion coefficient; n = variable.

For F < 0.85 the equation is reduced to [127]:

$$Bt = 2\pi - \frac{\pi^2 F}{3} - 2\pi\left(1 - \frac{\pi F}{3}\right)^{1/2} \tag{14.4}$$

F > 0.85

$$Bt = -\ln(1 - F) - 0.04977 \tag{14.5}$$

The drug release profile of various resinates has been characterized by means of B and D values.

14.4.3.2 Ophthalmic Drug Delivery

The eye is a unique organ by means of which the information is transmitted in certain areas of occipital lobe of the brain, where the picture of the outer world that we see is formed. Over time, ophthalmology was a very important field with continuous progress that is based both on the discovery of new medical treatments specific to the etiology of each disease and a better understanding of the pathophysiology of the eye. The ocular drug delivery is a very important route of drug administration because the drug enters in systemic circulation avoiding the hepatic first pass effect [136]. According to route of administration the ocular drug delivery can be classified as follows: (1) topical; (2) intraocular and (3) systemic [137].

In Table 14.8 are presented some advantages and disadvantages of these drug delivery systems.

Because of their excellent properties the ion exchangers can be used successfully in the treatment of eye problems. Thus, the well-known sterile ophthalmic suspension Betoptic S, based on Amberlite IRP 69-betaxolol HCl (antiglaucoma drug) is the first ocular resinate produced and marketed in US since 1990, in order to lower elevated intraocular pressure [44]. Also, the treatment of eye infections can be realized with polystyrene sulfonate-ciprofloxacin complexes [138].

Table 14.7 Methods used in investigation of kinetics of drug release

Methods	Mathematical expression	Terms explanation	Applications	Ref.
Zero order	$Q_t = Q_0 + K_0 t$	Q_t = amount of drug dissolved at time t; Q_0 = initial amount of drug in solution; K_0 = zero order constant	transdermal systems; matrix tablets loaded with low soluble drugs; coated forms; osmotic systems	[128]
First order	$\log C = \log C_0 - kt / 2.303$	C_0 = initial concentration of drug; K = first order rate constant; t = time	water soluble drugs immobilized in porous matrices	[129]
Higuchi	$f_t = Q = K_H \cdot t^{1/2}$	K_H = Higuchi dissolution constant	transdermal systems	[130]
Hixson-Crowell	$W_0^{1/3} - W_t^{1/3} = kt$	W_0 = initial amount of drug in dosage form; W_t = remaining amount of drug in dosage form; k = constant	tablets	[131]
Korsomeyer-Peppas	$\frac{M_t}{M_\infty} = kt^n$	$M_t/M_¥$ = fraction of drug released; k = release rate constant; n = release exponent		[132]
Baker-Lousdale	$f_1 = \frac{3}{2}\left[1 - \left(1 - \frac{M_t}{M_\infty}\right)^{2/3}\right]$	$\frac{M_t}{M_\infty} = k$; k = release rate constant	microcapsules or microspheres	[133]
Weibull	$M = M_0\left[1 - e^{-\frac{\left(t - T^b\right)}{a}}\right]$	M = amount of drug dissolved as function of time; M_0 = total amount of drug released; T = lag time; a = scale parameter; b = shape parameter	matrix	[134]
Gompertz	$X(t) = X_{\max} \exp\left[-\alpha \cdot e^{\beta \log t}\right]$	X(t) = percent of drug dissolved at time t/100; X_{max} = maximum dissolution scale; a = scale parameter; b = shape parameter.	drugs having good solubility	[135]

Table 14.8 Advantages and disadvantages of ocular drug delivery systems

Advantages	**Disadvantages**
Increase of the corneal contact time	Is expensive
Ensure a better efficiency	Some operation technique (insertion) is difficult
Increase shelf life	Sometimes can occur a decrease in visual activity
Possibility of targeting within the ocular globe	Difficult to handle
Exclusion of preservatives	Occasional inadvertent loss
Improve therapeutic performance of drug	Foreign body sensation
Reduction of systemic side effect	

14.4.3.3 Ion Exchangers for Cancer Treatment

Nowadays, cancer is the second lethal disease after heart diseases, being the result of uncontrolled division of cells. The goal of all cancer treatments is to destroy or remove all tumors and cancer cells from the patient body. Cancer can attack anywhere and because of this, the treatment and prevention of disease represents a great challenge for the scientific world. Doxorubicin is a chemotherapeutic agent that can be used in the treatment of various forms of cancer: leukemia, multiple myeloma, Hodgkin's lymphoma and cancers of the breast, ovaries, lung, bladder, thyroid, stomach and soft tissue. Entrapment of ionic cancer drugs (vinblastine, doxorubicin) and chemosenziting agents (verapamil) within microspheres based on Sephadex SPC 25 can represented a new opportunity in cancer therapy [139].

Experiments have demonstrated that treatment with resinate leads to suppression of tumor growth and reduces the systemic toxicity compared with treatment based on injection of free doxorubicin solution [140]. Also, doxorubicin was immobilized by Sawaya *et al.* [141] onto ion exchange albumin microcapsules. Hydrophobically modified sulfopropylated dextran microspheres coated with Eudragit RL 100 or corn oil were used by Liu *et al* [23] as carrier supports for immobilization of anticancer drugs, namely verapamil. A promising method to reduce the immunogenicity of the virus as well as to increase gene delivery efficiency in a number of cell types is the use of ion exchange microparticles as carriers of liposomal-adenoviral conjugate [142].

14.4.4 Transdermal Drug Delivery Systems

In recent years iontophoresis and the combination with other approaches (electroporation, chemical enhancers, sonophoresis, microneedle and ion exchange material) have been investigated being used for delivery of macromolecules and poorly water soluble compounds [143]. Iontophoresis (electromotive drug administration) is a non-invasive method that uses a small electrical charge to deliver a bioactive substance (ionized and unionized molecules) through the skin [144]. This method is used for the application of anti-inflammatory drugs, in plantar fasciitis, bursitis and some types of hyperhidosis. Some advantages of iontophoresis are: (1) bypasses hepatic first past effect; (2) higher patient compliance; (3) continuous or pulsatile delivery of ionized or nonionized drugs; (4) can be used as systemic or topical release of drugs; (5) control the amount of drug released; (6) avoid severe skin irritations. Ion exchange fibers were designed as controlled transdermal delivery systems of some drugs such as ketoprofen [145], levodopa and metaraminol [38]. It was observed that iontophoretic enhancement permeation of the last two drugs across the skin was highly with metaraminol compared with the zwitterionic levodopa. Schwendeman *et al*. [146] have developed an iontophoretic implant based on heterogeneous cation-exchange membranes that are capable to deliver antiarrhytmic agents directly to the heart for treatment of cardiac arrhythmias.

14.4.5 Ion Exchangers as Therapeutics

Since the 1950s it was found that such polymers may have therapeutic application being used in the control of gastric acidity [147], treatment of cardiac edema [148], treatment of ulcer, cirrhosis of the liver [149], renal diseases [150] and toxemia in pregnancy. Moreover, the strong acid ion exchange resin sodium polystyrene sulfonate, namely Kayexalate or Kionex has been used as an adjuvant in treatment of hyperkalemia [151], while colestipole (weak base ion exchange resin) and cholestyramine (strong base ion exchangers) were used as bile acid sequestrants to treat or to control hypercholesterolemia [46].

A new resin Colestimide (2 methylimidazole epichlorohydrin polymer) was found to have double action: bile acid sequestrant to lower the high level of cholesterol, being four time more powerful than cholestyramine and reduces the level of plasma glucose in type 2 diabetes associated with hypercholesterolemia [152]. Tobacco is the second most important cause of death which can be prevented, The World Health Organization estimating that each year 5 million people die due to tobacco-related diseases like: lung cancer, chronic obstructive airways and ischemic heart diseases. The

nicotine, an alkaloid that is the main addictive agent can lead to the physical and psychological dependences as well as to the damage of various organs and systems of the human body, such as: circulatory system, lungs, heart, skin, eyes, teeth, stomach and respiratory system. Today the nicotine replacement therapy is one of the most widely used treatments to provide smoking cessation [42]. Products based on nicotine can be presented in different forms: chewing gum, nasal spray, adhesive transdermal patches, sublingual tablets and oral mucosal inhalers [153, 154]. For examples, a chewing gum called Nicorette contains nicotine adsorbed on a weakly acid ion exchanger [155]. Duromine (phentermine and ion exchanger resin complex) is indicated in the management of obesity as short-term adjuvant to weigh reduction in obese and overweight patients. Also, Biphetamine capsules that contain a mixture of amphetamine and dextroamphetamine sorbed onto sulfonic acid cation exchanger has been used for short period of time in order to control the children obesity [156].

14.5 Conclusions

Due to their excellent properties IERs are an open window for the development of advanced materials with pharmaceutical and medical applications. The efficiency of IERs as drug delivery systems depends on the same properties like: crosslinking degree, moisture content and swelling degree, particle size and particle size distribution, porosity, ion exchange capacity, functional groups, selectivity, stability and toxicity. Nowadays, various pharmaceutical formulations based on ion exchange resins are available in the market covering a wide range of applications such as: taste and odor masking, tablet disintegrants and rapid dissolution of drug, oral, ophthalmic and transdermal drug delivery, in cancer therapy and in therapeutic field (control of gastric acidity, treatment of cardiac edema, treatment of ulcer, cirrhosis, renal diseases, smoking cessation and bile acid sequestrants).

References

1. C. Luca, C.D. Vlad, and I. Bunia, *Revue Roumaine de Chimie*, Vol. 54, p. 107, 2009.
2. S.D. Alexandratos, *Industrial & Engineering Chemistry Research*, Vol. 48, p. 388, 2009.
3. W.A. Schroeder, R.T. Jones, J. Cromick, and K. McCalla, *Analytical Chemistry*, Vol. 34, p. 1570, 1962.

4. A.C.Q. Ladeira, and C.A. Morais, *Minerals Engineering*, Vol. 18, p. 1337, 2005.
5. V. Dulman, C. Simion, A. Barsanescu, I. Bunia, and V. Neagu, *Journal of Applied Polymer Science*, Vol. 113, p. 615, 2009.
6. G. Wojcik, V. Neagu, and I. Bunia, *Journal of Hazardous Materials*, Vol. 190, p. 544, 2011.
7. Y. Huang, J. Bi, L. Zhao, G. Ma, and Z. Su, *Protein Expression and Purification*, Vol. 74, p. 257, 2010.
8. A. Chakrabarti, and M.M. Sharma, *Reactive Polymers*, Vol. 20, p. 1, 1993.
9. M.B. Jackson, and N.H. Pilkington, *Journal of Chemical Technology and Biotechnology*, Vol. 36, p. 88, 1986.
10. V. Anand, R. Kandarapu, and S. Garg, *DDT*, Vol. 6, p. 905, 2001.
11. A.A. Zagorodni, *Ion Exchange Materials: Properties and Applications*, Amsterdam, Elsevier, 2007.
12. B.J. Schultz, and E.H. Crook, *Industrial & Engineering Chemistry Product Research and Development*, Vol. 7, p. 120, 1968.
13. X. Guo, R.K. Chang, and M.A. Hussain, *Journal of Pharmaceutical Sciences*, Vol. 98, p. 3886, 2009.
14. G.M. Burke, R.W. Mendes, and S.S. Jambhekar, *Drug Development and Industrial Pharmacy*, Vol. 12, p. 713, 1986.
15. D. Torres, L. Boado, D. Blanco, and J.L. Vila-Jato, *International Journal of Pharmaceutics*, Vol. 173, p. 171, 1998.
16. R. Kunin, E. Meitzner, and N. Bortnick, *Journal of the American Chemical Society*, Vol. 84, p.305, 1962.
17. M. Streat, *Chemistry & Industry*, Vol. 13, p.20, 2004.
18. N.P. Pavlenko, L.E. Lunin, L.I. Chemyshev, and A.G. Kostornov, *Powder Metallurgy and Metal Ceramics*, Vol. 27, p. 299, 1988.
19. Y. Pongpaibul, J.C. Price, and C.W. Whitworth, *Drug Development and Industrial Pharmacy*, Vol. 10, p. 1597, 1984.
20. C.D. Vlad, and S. Vasiliu, *Polimery*, Vol. 55, p. 17, 2010.
21. E. Erbay, and O. Okay, *Journal of Applied Polymer Sciences*, Vol. 71, p. 1055, 1999.
22. O. Okay, *Progress in Polymer Science*, Vol. 25, p. 711, 2000.
23. Z. Liu, X.Y. Wu, J.R. Ballinger, and R. Bendayan, *Journal of Pharmaceutical Sciences*, Vol. 89, p. 807, 2000.
24. N.G. Polyanskii, and P.E. Tulupov, *Russian Chemical Reviews*, Vol. 40, p. 1030, 1971.
25. O. Folin, *The Journal of Biological Chemistry*, Vol. 51, p. 377, 1922.
26. J.C. Whiterhorn, *The Journal of Biological Chemistry*, Vol. 56, p. 751, 1923.
27. N.C. Chaudhary, and L. Saunders, *Journal of Pharmacy and Pharmacology*, Vol. 8, p. 975, 1956.
28. M.V. Srikanth, S.A. Sunil, N.S. Rao, M.U. Uhumwangho, and K.V. Ramana Murthy, *Journal of Scientific Research*, Vol. 2, p. 597, 2010.

29. V. Sharma, and L. Singh, *International Journal of Pharmaceutical Sciences Review and Research*, Vol. 6, p. 10, 2011.
30. J.A. Plaizier-Vercammen, *International Journal of Pharmaceutics*, Vol. 85, p. 45, 1992.
31. E. Dejean, J. Sandeaux, R. Sandeaux, and C. Gavach, *Separation Science and Technoloy*, Vol. 33, p. 801, 1998.
32. P. Mishra, P. Srivastava, P.K. Mishra, and S. Kundu, *Indian Journal of Chemical Technology*, Vol. 14, p. 592, 2007.
33. J.A. Marques Pereira, P. de Tarso Vieira, E. Rosa, G.M. Pastore, and C.C. Santana, *Applied Biochemistry and Biotechnology*, Vol. 70-72, p. 779, 1998.
34. A. Porat, D. Winters, L. Cai, S. Smith, F. Abroson, L.T.T. Tam, Z. Shen, and R. Hecht, *Preparative Biochemistry and Biotechnology*, Vol. 42, p. 304, 2012.
35. Z. Ayenew, V. Puri, L. Kumar, and A.K. Bansal, *Recent Patents on Drug Delivery & Formulation*, Vol. 3, p. 26, 2009.
36. D. Bhowmik, B. Chiraujib, J. Yadav, R.M. Chndira, and K.P. Sampath Kumar, *Der Pharmacia Lettre*, Vol. 2, p. 495, 2010.
37. I. Singh, A.K. Rehni, R. Kalra, G. Joshi, M. Kumar, and H.Y. Aboul-Enein, *FABAD Journal of Pharmaceutical Sciences*, Vol. 32, p. 91, 2007.
38. T. Kankkunen, I. Huupponen, K. Lathinen, M. Sundell, K. Ekman, K. Kontturi, and J. Hirvonen, *European Journal of Pharmaceutical Sciences*, Vol. 16, p. 273, 2002.
39. M.V. Chaubal, *Drug Delivery Technology*, Vol. 3, p. 6, 2003.
40. W.J. Esdale, T.L. Walker, J. White, E.E. De Cruz, and M.A. Burton, *Clinical and Experimental Metastasis*, Vol. 15, p. 239, 1997.
41. F. Gut, W. Schick, W.E. Haefelli, I.W. Sack, and J. Burhenne, *European Journal of Pharmaceutics and Biopharmceutics*, Vol. 69, p. 582, 2008.
42. Y.H. Chen, P. Watts, M. Hinchcliffe, R. Hotchkiss, R. Nankervis, N.F. Faraj, A. Smith, S.S. Davis, and L. Illum, *Journal of Controlled Release*, Vol. 79, p. 243, 2002.
43. Q. Xu, S.A. Ibrahim, W.I. Higuhi, and S.K. Li, *International Journal of Pharmaceutics*, Vol. 369, p. 105, 2009.
44. R. Jani, O. Gan, Y. Ali, R. Rodstrom, and S. Handcock, *Journal of Ocular Pharmacology and Therapeutics*, Vol. 10, p. 57, 1994.
45. S.P. Schwendeman, V. Labhasetwar, and R.J. Levy, *Pharmaceutical Research*, Vol. 12, p. 790, 1995.
46. B. Angelin, and K. Einarsson, *Atherosclerosis*, Vol. 38, p. 33, 1981.
47. R.H. Sterns, M. Rojas, P. Bernstein , and S. Chennupati, J*ournal of the American Society of Nephrology*, Vol.21, p. 733, 2010.
48. R. Marangoni, *Giornale Italiano di Nefrologia*, Vol. 38, p. 92, 2007.
49. E.T. Schroeder, *Gastroenterology*, Vol. 56, p. 868, 1969.
50. C. Wang, F. Chen, P.W.S. Heng, J.Z. Li, X. Li, G.H. Ye, S.F. Nie, and W.S. Pan, *Chemical and Pharmaceutical Bulletin*, Vol. 56, p. 457, 2008.
51. R. Maini, *The International Journal of Artificial Organs*, Vol. 1, p. 196, 1978.
52. S. Sharma, and S. Lewis, *International Journal of Pharmacy and Pharmaceutical Sciences*, Vol. 2, p. 6, 2010.

53. K. Ikeda, *Tokyo Chemical Society*, Vol. 30, p. 820, 1909.
54. J.K. Sajal, S.R. Uday, and V. Surundra, *Journal of Pharmacy Research*, Vol. 1, p. 126, 2008.
55. S. Borodkin, and M.H. Yunker, *Journal of Pharmaceutical Sciences*, Vol. 59, p.481, 1970.
56. C.P. Yewale, M.N. Rathi, G.G. Kore, G.V. Jadhav, and M.P. Wagh, *Pharmaceutical Development and Technology*, Vol. 18, p. 367, 2013.
57. G.L. Radhika, Snehalatha, and B.S. Kumar, *American Journal of PharmTech Ressearh*, Vol. 2, p. 1, 2012.
58. K. Bhise, S. Shaikh, and D. Bora, *AAPS PharmSciTech*, Vol. 9, p. 557, 2008.
59. M.Y.F. Lu, S. Borodkin, L. Woodward, P. Li, C. Diesner, L. Hernandez, and M. Vadnere, *Pharmaceutical Research*, Vol. 8, p. 706, 1991.
60. S. Khan, A. Guha, P.G. Yeole, and P. Katariya, *Indian Journal of Pharmaceutical Sciences*, Vol. 69, p. 626, 2007.
61. M. Malladi, R. Jukanti, R. Nair, S. Wagh, H.S. Padakanti, and A Mateti, *Acta Pharmaceutica*, Vol. 60, p. 267, 2010.
62. S. Pisal, R. Zainnuddin, P. Nalowade, K. Mahadik, and S. Kadam, *AAPS PharmSciTech*, Vol. 5, p.84, 2004.
63. R. Agarwal, R. Mittal, and A. Singh, *Drug Development and Industrial Pharmacy*, Vol. 26, p. 773, 2000.
64. K.V. Chatap, K.D. Sharma, T.P. Deshmulth, and B.V. Gupta, *Pharma Time*, Vol. 40, p. 2008, 2008.
65. S.P. Dhamane, M.P. Wagh, G.P, Asnani, A.S. Kulkarni, B.S. Patil, and A.S. Gadekar, *International Journal of Pharmaceutical Sciences and Research*, Vol. 4, p. 1168, 2013.
66. X. Yu, H. Liu, C. Sun, S. Shi, X. Fu, and Y. He, *African Journal of Pharmacy and Pharmacology*, Vol. 6, p. 1617, 2012.
67. J.G. Avari, and M. Bhalekar, *Indian Drugs*, Vol. 4, p. 19, 2004.
68. L. Hu, J. Pan, C. Liu, H. Xu, and L. Luo, *Journal and Pharmacy and Pharmacology*, Vol. 61, p. 1631, 2009.
69. S. Saurabh, A.C. Rana, and B. Rajni, *International Research Journal of Pharmacy*, Vol. 3, p. 92, 2012.
70. A.M. Suthar, and M.M Patel, *International Journal of Applied Pharmaceutics*, Vol. 3, p. 16, 2011.
71. J.V. Cotterill, G. Massei, and D.P. Cowan, *Pest Management Science*, Vol. 62, p. 120, 2006.
72. P.D. Chaudhari, S.P. Chaudhari, S.R. Kolbe, K.V. Dave, and D.M. More, *Indian Drugs*, Vol.43, p.795, 2006.
73. S.J. Padya, T.Y. Pasha, A. Bhandari, J.K. Patel, T. Naitik, and T. Upama, *International Journal of Drug Formulation and Research*, Vol. 2, p. 134, 2011.
74. G.G. Gajare, S.R. Bakliwal, B.R. Rane, N.A. Gujrathi, and S.P. Pawar, *International Journal of Pharmaceutical Research and Development*, Vol. 3, p. 280, 2011.

75. S.K. Sheth, S.J. Patel, and B.J. Shukla, *International Journal of Pharma and Bio Sciences*, Vol. 1, p.1, 2010.
76. B.V. Akbari, B.P. Patel, R.B. Dholakiya, B.G. Shiyani, and D.J. Lodhiya, *International Journal of PharmTech Reserch*, Vol. 2, p. 240, 2010.
77. A.R. Madgulkar, M.R. Bhalekar, and R.R. Padalkar, *AAPS PharmSciTech*, Vol. 10, p.574, 2009.
78. V. Sharma, and H. Chopra, *Iranian Journal of Pharmaceutical Research*, Vol. 11, p. 457, 2012.
79. I. Singh, P. Kumar, M. Nagpal, and S. Arora, *Revista Cubana de Farmacia*, Vol. 45, p. 171, 2011.
80. V.K. Suhagiya, A.N. Gayani, and R.N. Gupta, *International Journal of Pharmaceutical Sciences and Research*, Vol. 1, p.22, 2010.
81. A.S. Mundada, D.R. Meshram, H.B. Banbale, M.R. Bhalekar, and J.G. Avari, *Asian Journal of Pharmaceutics*, Vol. 2, p. 116, 2008.
82. S. Shah, S. Pandya, and M.R. Bhalekar, *Journal of Young Pharmacists*, Vol.2, p.247, 2010.
83. R.G. Satapara, and V.P. Satapara, *International Journal of Pharmaceutical Research and Development*, Vol.4, p. 86, 2012.
84. P.K. Bhoyar, and Y.M. Amqaoukar, *Journal of Young Pharmacists*, Vol.3, p.112, 2011.
85. B.V. Jain, and S.D. Barhate, *International Journal of Advances Research in Pharmaceutical & Bio Sciences*, Vol. 3, p. 80, 2013.
86. I. Singh, B. Kaur, P. Kumar, and S. Arora, *Polimery w Medycynie*, Vol. T40, p.19, 2010.
87. S.J. Pandya, N. Kadam, S.J. Bidkar, N.H. Patel, and A. Patel, *The Pharma Review,* p. 135, 2008.
88. M.A. Tawakkul, R.B. Shah, A. Zidan, V.A. Sayeed, and M.A. Khan, *Pharmaceutical Development and Technology*, Vol. 14, p.409, 2009.
89. S.P. Manek, and V.S. Komat, *Indian Journal of Pharmaceutical Scie*nce, Vol. 43, p. 209, 1981.
90. J.G. Mahore, K.J. Wadher, and M.J. Umekar, *International Journal of PharmTech Research*, Vol. 2, p.1827, 2010.
91. G.P. Kumar, and R. Nirmala, *Journal of Global Pharma Technology*, Vol. 4, p. 1, 2012.
92. S.H. Jeong, and K. Park, *International Journal of Pharmaceutics*, Vol. 353, p. 195, 2008.
93. D.H. Robinson, and J.W. Mauger, *American Journal of Hospital Pharmacy*, Vol. 48, p.S14, 1991.
94. K.P.S. Kumar, D. Bhownik, Chiranjib, M. Chandira, and K.K. Tripathi, *Journal of Chemical and Pharmaceutical Research*, Vol. 2, p. 349, 2010.
95. P.L. Bardonnet, V. Faivre, W.J. Pugh, J.C. Piffaretti, and F. Falson, *Journal of Controlled Release*, Vol. 111, p. 1, 2006.

96. H.A.H. Mohammad, J.T. Fell, H.L. Sharma, and F. Atayabi, *Proceedings of the International Symposium on Controlled Release of Bioactive Materials*, Vol. 21, p.807, 1994.
97. F. Atyabi, H.L. Sharma, H.A.H. Mohammad, and J.T. Fell, *Journal of Controlled Release*, Vol. 42, p.25, 1996.
98. H. Yao, L. Xu, F. Han, X. Che, Y. Dong, M. Wei, J. Guan, X. Shi, and S. Li, *International Journal of Pharmaceutics*, Vol. 364, p.21, 2008.
99. S. Vasiliu, I. Bunia and V. Neagu, *Ion Exchange Letters*, Vol. 2, p. 31, 2009.
100. S. Vasiliu, I. Bunia, S. Racovita, V. Neagu, *Carbohydrate Polymers*, Vol. 85, p. 376, 2011.
101. S. Saxena, and S.K. Bajpai, *Journal of Macromolecular Science. Part A: Pure and Applied Chemistry*, Vol. 45, p. 387, 2008.
102. P. Akkaramongkolporn, T. Ngawhirunpat, and P. Opanasopit, *AAPS PharmSciTech*, Vol. 10, p. 641, 2009.
103. M. Kurowski, H, Menninger, and E. Pauli, *International Journal of Clinical Pharmacology and Therapeutics*, Vol. 32, p.433, 1994.
104. T. Kondo, E. Hafez, H. Abdel-Monem, M. Muramatsu, S. El-Haras, and I. El-Gibaly, *Powder Technology*, Vol. 88, p.101, 1996.
105. L.S. Lillenfield, and E.J. Zapolski, *Current Therapeutic Research*, Vol. 33, p. 692, 1983.
106. L.P. Amsel, D.N. Hinsvark, S. Rotenberg, and J.L. Sheumarker, *Pharmaceutical Technology*, Vol. 8, p. 28, 1984.
107. S. Motycka, C.J.L. Newth, and J.G. Nairn, *Journal of Pharmaceutical Sciences*, Vol. 74, p. 643, 1985.
108. M. Sriwongjanya, and R. Bodmaier, *International Journal of Pharmaceutics*, Vol. 158, p. 29, 1997.
109. S.H. Jeong, and K. Park, *International Journal of Pharmaceutics*, Vol. 361, p. 26, 2008.
110. P. Akkaramongkolporn, T. Ngawhirunpat, J. Nunthanid, and P. Opanasopit, *AAPS PharmSciTech*, Vol. 9, p. 899, 2008.
111. M. Sriwongjanya, and R. Bodmaier, *European Journal of Pharmaceutics and Biopharmaceutics*, Vol. 46, p. 321, 1998.
112. H.F. Liu, C.Y. Zhang, X. Li, X. Zhao, T.H. Sun, C.Y. Ju, N. Li, and W.S. Pan, *Indian Journal of Pharmaceutical Sciences*, Vol. 69, p. 550, 2007.
113. Y. Raghunathan, L. Amstel, O. Hinsvark, and W. Bryant, *Journal of Pharmaceutical Sciences*, Vol. 70, p. 379, 1981.
114. M. Cuna, M.J. Alonso, and D. Torres, *European Journal of Pharmaceutics and Biopharmaceutics*, Vol. 51, p. 199, 2001.
115. D. Torres, G. Garcia-Encina, B. Seijo, and J.L. Vila-Jato, *International Journal of Pharmaceutics*, Vol. 121, p. 239, 1995.
116. H. Ichikawa, K. Fujioka, M.C. Adeyeye, and Y. Fukumori, *International Journal of Pharmaceutics*, Vol. 216, p. 67, 2001.
117. N.H. Berhane, S.H. Jeong, K. Haghighi, and K. Park, *International Journal of Pharmaceutics*, Vol. 323, p. 64, 2006.

118. V.B. Junyapraset, and G. Manwiwattanakul, *International Journal of Pharmaceutics*, Vol. 352, p. 81, 2008.
119. M. Cuna, J.L. Vila-Jato, and D. Torres, *International Journal of Pharmaceutics*, Vol. 199, p. 151, 2000.
120. S.H. Jeong and K. Park, *Archives Pharmacal Research*, Vol. 33, p. 115, 2010.
121. T. Ngawhirunpat, S. Duangjit, E. Gocgebakan, P. Akkaramongkolporn, and M. Kumpugdee-Vollrath, *International Journal of Pharmacy and Pharmaceutical Sciences*, Vol. 2, p. 107, 2010.
122. S. Pisal, R. Zainnuddin, P. Nalowade, K. Mahadik, and S. Kadam, *AAPS PharmSciTech*, Vol. 5, p.101, 2004.
123. M.R. Bhalekar, J. Avari, and R.A. Umalkar, *Indian Journal of Pharmaceutical Science*, Vol. 69, p. 418, 2007.
124. A. Halder, and B. Sa, *Journal of Microencapsulation*, Vol. 23, p. 899, 2006.
125. R. Mishra, and A. Amin, *International Journal of Drug Formulation and Research*, Vol. 2, p. 314, 2011.
126. G.E. Boyd, A.W. Adamson, and L.S. Myers, *Journal of the American Chemical Society*, Vol. 69, p. 2836, 1947.
127. D. Reichenberg, *Journal of the American Chemical Society*, Vol. 75, p. 589, 1953.
128. L. Yang, and R. Fassihi, *Journal of Pharmaceutical Sciences*, Vol. 85, p. 170, 1996.
129. K. Vasanth Kumar, *Journal of Hazardous Materials*, Vol. 137, p. 1538, 2006.
130. T. Higuchi, *Journal of Pharmaceutical Sciences*, Vol. 52, p. 1145, 1963.
131. A.W. Hixson, and J.H. Crowell, *Industrial & Engineering Chemistry*, Vol 23, p. 923, 1931.
132. R.W. Korsmeyer, R. Gurny, E. Doelker, P. Buri, and N.A. Peppas, *International Journal of Pharmaceutics*, Vol. 15, p. 25, 1983.
133. F. S. Poletto, E. Jaeger. M.I. Re, S.S. Guteress, and A.R. Pohlmann, *International Journal of Pharmaceutics*, Vol. 345, p. 70, 2007.
134. S. Dash, P.N. Murthy, L. Nath, and P. Chowdhury, *Acta Poloniae Pharmaceutica-Drug Research*, Vol. 67, p. 217, 2010.
135. J. Siepmann, and N.A. Peppas, *Advanced Drug Delivery Reviews*, Vol. 48, p. 139, 2001.
136. R.D. Schoenwald, and V.F. Smolen, *Journal of Pharmaceutical Sciences*, Vol. 60, p. 1039, 1971.
137. K.S.G. Arul Kumaran, K. Karthika, and J. Padmapreetha, *International Journal of Pharmacy and Pharmaceutical Sciences*, Vol. 2, p. 1, 2010.
138. J.M. Moreau, L.C. Green, L.S. Engel, J.M. Hill and R.J. O'Callaghan, *Current Eye Research*, Vol. 17, p. 808, 1998.
139. Z. Liu, R. Cheung, X.Y. Wu, J.R. Ballinger, R. Bendayan, and A.M. Rauth, *Journal of Controlled Release*, Vol. 77, p. 213, 2001.
140. Z. Liu, X.Y. Wu, and R. Bendayan, *Journal of Pharmaceutical Sciences*, Vol. 88, p. 412, 1999.

141. A. Sawaya, J.P. Benoit, and S. Benita, *Journal of Pharmaceutical Sciences*, Vol. 76, p. 475, 1987.
142. J.C. Steel, H.M.A. Cavanagh, M.A. Burton, D. Dingwall, and W.H.J. Kalle, *Journal of Controlled Release*, Vol. 95, p. 601, 2004.
143. Y. Wang, R. Thakur, Q. Fan, and B. Michniak, *European Journal of Pharmaceutics and Biopharmaceutics*, Vol. 60, p. 179, 2005.
144. K. Malinovskaja, T. Laaksonen, K. Kontturi, and J. Hirvonen, *European Journal of Pharmaceutics and Biopharmaceutics*, Vol. 83, p. 477, 2013.
145. L. Yu, S. Li, Y. Yuan, Y. Dai, and H. Liu, *International Journal of Pharmaceutics*, Vol. 319, p. 107, 2006.
146. S.P. Schwendeman, G.L. Amidon, V. Labhasetwar, and R.J. Levy, *Journal of Pharmaceutical Sciences*, Vol. 83, p. 1482, 1994.
147. B.H. Bass, *British Medical Journal*, Vol. 1, p. 1406, 1956.
148. A.W. Feinderg, and B. Rosenberg, *American Heart Journal*, Vol. 42, p. 698, 1951.
149. K.Z. Minima, E.P. Kurapov, W. Goncharov, I.A. Leikin, T.I. Tarasova, and N.I. Trenshnikova, *Anesteziologiia I Reanimatologiia*, Vol. 4, p. 40, 1989.
150. A.G. Spencer, and H.G.L. Lloyd-Thomas, *British Medical Journal*, Vol. 1, p. 597, 1954.
151. H. Yaseen, M. Khalaf, A. Dana, N. Yaseen, and M. Darwich, *American Journal of Perinatology*, Vol. 25, p. 193, 2008.
152. T. Suzuki, K. Oba, Y. Igari, N. Matsumura, K. Watanabe, S. Futami-Suda, H. Yasuoka, M. Ouchi, K. Suzuki, Y. Kigawa, and H. Nakano, *Journal of Nippon Medical School*, Vol. 74, p. 338, 2007.
153. O.M. Conaghy, J. Corish, and O.I. Corrigan, *International Journal of Pharmaceutics*, Vol. 170, p. 225, 1998.
154. J.E. Rose, *Annual Review of Medicine*, Vol. 47, p.493, 1996.
155. K.O. Fagerstrom, *Preventive Medicine*, Vol. 13, p.517, 1984.
156. E.A. De Felice, A. Cohen, P.L. Schmitz, K.G. Rothwell, and A.P. Truant, *The Journal of Clinical Pharmacology and The Journal of New Drugs*, Vol. 8, p. 360, 1968.

Index

Also of Interest

Check out these published volumes in the Advanced Materials Series

Advanced Bioelectronic Materials
Edited by Ashutosh Tiwari, Hirak K. Patra and Anthony P.F. Turner
Published 2015. ISBN 9781118998304

Graphene
An Introduction to the Fundamentals and Industrial Applications
By Madhuri Sharon and Maheswar Sharon
Published 2015. ISBN 9781118842560

Advanced Theranostic Materials
Edited by Ashutosh Tiwari, Hirak K. Patra and Jeong-Woo Choi
Published 2015. ISBN: 978-1-118-99829-8

Advanced Functional Materials
Edited by Ashutosh Tiwari and Lokman Uzun
Published 2015. ISBN 978-1-118-99827-4

Advanced Catalytic Materials
Edited by Ashutosh Tiwari and Salam Titinchi
Published 2015. ISBN 978-1-118-99828-1

Graphene Materials
Fundamentals and Emerging Applications
Edited by Ashutosh Tiwari and Mikael Syväjärvi
Published 2015. ISBN 978-1-118-99837-3

DNA Engineered Noble Metal Nanoparticles
Fundamentals and State-of-the-Art-of Nanobiotechnology
By Ignác Capek
Published 2015. ISBN 978-1-118-07214-1

Advanced Electrical and Electronics Materials
Process and Applications
By K.M. Gupta and Nishu Gupta
Published 2015. ISBN: 978-1-118-99835-9

Advanced Materials for Agriculture, Food and Environmental Safety
Edited by Ashutosh Tiwari and Mikael Syväjärvi
Published 2014. ISBN: 978-1-118-77343-7

Advanced Biomaterials and Biodevices
Edited by Ashutosh Tiwari and Anis N. Nordin
Published 2014. ISBN 978-1-118-77363-5

Biosensors Nanotechnology
Edited by Ashutosh Tiwari and Anthony P. F. Turner
Published 2014. ISBN 978-1-118-77351-2

Advanced Sensor and Detection Materials
Edited by Ashutosh Tiwari and Mustafa M. Demir
Published 2014. ISBN 978-1-118-77348-2

Advanced Healthcare Materials
Edited by Ashutosh Tiwari
Published 2014. ISBN 978-1-118-77359-8

Advanced Energy Materials
Edited by Ashutosh Tiwari and Sergiy Valyukh
Published 2014. ISBN 978-1-118-68629-4

Advanced Carbon Materials and Technology
Edited by Ashutosh Tiwari and S.K. Shukla
Published 2014. ISBN 978-1-118-68623-2

Responsive Materials and Methods
State-of-the-Art Stimuli-Responsive Materials and Their Applications
Edited by Ashutosh Tiwari and Hisatoshi Kobayashi
Published 2013. ISBN 978-1-118-68622-5

Other Scrivener books edited by Ashutosh Tiwari

Nanomaterials in Drug Delivery, Imaging, and Tissue Engineering
Edited by Ashutosh Tiwari and Atul Tiwari
Published 2013. ISBN 978-1-118-29032-3

Biomedical Materials and Diagnostic Devices Devices
Edited by Ashutosh Tiwari, Murugan Ramalingam, Hisatoshi Kobayashi and Anthony P.F. Turner
Published 2012. ISBN 978-1-118-03014-1

Intelligent Nanomaterials
Processes, Properties, and Applications
Edited by Ashutosh Tiwari Ajay K. Mishra, Hisatoshi Kobayashi and Anthony P.F. Turner
Published 2012. ISBN 978-0-470-93879-9

Integrated Biomaterials for Biomedical Technology
Edited by Murugan Ramalingam, Ashutosh Tiwari, Seeram Ramakrishna and Hisatoshi Kobayashi
Published 2012. ISBN 978-1-118-42385-1

WILEY END USER LICENSE AGREEMENT

Go to www.wiley.com/go/eula to access Wiley’s ebook EULA.